PERFORMANCE COMPARISON OF FEW SELECTED ALGORITHMS FOR STATE AND PARAMETER ESTIMATION OF MULTI-STOREYED BUILDINGS

Thesis Submitted in Partial Fulfilment of the Requirements

for the Degree of

DOCTOR OF PHILOSOPHY

By

PRODIP KUMAR PAUL

DEPARTMENT OF CIVIL ENGINEERING

INDIAN INSTITUTE OF TECHNOLOGY GUWAHATI

GUWAHATI-781039, INDIA

APRIL 2021

To the loving memory

of

my father Late Probodh Chandra Paul

CANDIDATE'S DECLARATION

I hereby declare that the work presented in the thesis entitled "Performance Comparison of few Selected Algorithms for State and Parameter Estimation of Multi-Storey Buildings" in fulfilment of the requirement for the award of the degree of Doctor of Philosophy is an authentic record of my own work carried out in Department of Civil Engineering of the Institute. The work has been carried out under guidance of Prof. A. Dutta and Prof. S.K.Deb.

The content presented in this thesis has not been submitted by me for the award of any other degree of this or any other Institute.

Prodip kumar Paul

(PRODIP KUMAR PAUL)

This is to clarify that the above statement made by the candidate is correct to the best of our knowledge.

Dr. Sajal Kanti Deb
Professor
Department of Civil Engineering
Indian Institute of Technology Guwahati
Guwahati-781039
India

Dr. Anjan Dutta
Professor
Department of Civil Engineering
Indian Institute of Technology Guwahati
Guwahati-781039
India

ACKNOWLEDGEMENT

This thesis is the outcome of analytical studies using simulated and experimental data obtained from the department of civil engineering at Indian Institute of Technology (IIT) Guwahati, Assam, India. At the outset, I would like to express my sincere gratitude to the great human being, guide and philosopher Prof. Anjan Dutta and Prof. S. K. Deb for initiating an interesting and innovative research topic and for their unconditional support, valuable advices and continuous guidance.

The data of the experimental studies which has been used in the present work is the contribution from previous researchers specially Dr. Animesh Das, Dr. Arun Chandra Borsaikia and Mr. Rupam Jyoti Nath of the department of Civil Engineering, IIT Guwahati. Therefore, I express my gratitude to them for their great effort in conducting the various experimentation and data acquisition.

I would like to thank the members of my doctoral committee, Prof. Debabrata Chakraborty (Chairman), Dr. Arunasis Chakraborty and Dr. Sandip Das for their remarks and valuable suggestions during the entire course of my research.

This thesis I am going to dedicate to my beloved deceased father Late Probodh Chandra Paul. He expired while I just started my PhD work. The thesis dedicated to him when he was alive. He was a great philosopher and guide for me. He taught me the values and principles of life and he is still my inspiration in my quest for achieving higher studies. I also express my affection to my mother, relatives and in laws, whom I have deprived without meeting them for a long time due to busy schedule work and research.

I extend my thanks to my beloved wife Parijat for providing me mental support and encouragement to complete my PhD work. I remember those days of my struggle when I was going through tremendous work load combined with severe illness of my almost bed-ridden mother. During those difficult times, she provided me mental support to continue with my research. I deeply express my apology for depriving her in many things of life by not spending time with her in various family and social occasions.

I have also deprived my beloved sweet daughter Prachita who is nine years old now. I have not spent sufficient time with her in playing with her and helping her in her studies.

I am also very grateful to my undergraduate college friends Prof. Amaresh Dalal and Dr. Swarup Bag of Department of Mechanical Engineering, IIT Guwahati for the providing me

with all their unconditional support and personal help during my periodic stays at IIT Guwahati campus and from the very beginning of my research work.

I am also grateful to Mr. Subranshu Tewary (Ex. M.Tech student), Mr. Kamal Jyoti Nath and Mr. Subhra Pal (research scholar) for all their technical or personal support.

I am very much grateful to my dear colleague and friends for their support in my official as well as personal life. I also thank superiors of my office for allowing me occasional leaves for my PhD works. Without their support this precious work would not have been completed. The list is never ending to include in this page. The last but not the least, I acknowledge the permission given by my organization Public Works Department, Government of West Bengal to carry out this research work.

Prodip kumar Paul

Prodip Kumar Paul

TABLE OF CONTENTS

ABSTRACT

The health of a structure may deteriorate as the structure experiences repeated earthquake. There may be cases of rupture of reinforcement or deterioration of bond between reinforcement bar and surrounding concrete in RC structures, loosening of bolts or rivets, tearing of joints in case of steel structures. The damages may or may not be visible externally. Even if damages are visible from outside or even if internal damages are assessed by any available non-destructive testing such X-ray images etc., proper quantification of damages may not be possible. Therefore, future load carrying capacity of the structure cannot be evaluated appropriately. If severity of damage can be identified as well as quantified, then the extent of rehabilitation can be ascertained for restoration of original capacity. This is where, system identification (SI) comes into play. SI uses output responses from a structure experiencing vibration either due to seismic excitation, wind induced excitation, or due to passing vehicles in case of bridges etc. Using the output response like accelerations, input excitation such as earthquake excitation and a mathematical model, the SI techniques are utilized to identify the state (displacement, velocity etc) and the parameters (stiffness, damping) of structure with quite appreciable degree of accuracy. Hence, SI is recognized as an advanced technique for assessment of structural system.

There are various SI techniques in literature. However, in the present study a few of them have been considered. The SI techniques that are considered in the present study are primarily based on least square estimate (LSE) and Kalman filter based techniques. An improved form of LSE is Recursive Least Square Estimate (RLSE). Further, there is Sequential Non-Linear least Square Estimate (SNLSE) and its variants to handle limited input and output called Sequential Non-Linear least Square Estimate with unknown input and output (SNLSE-UI-UO). Kalman filter based techniques which are discussed in this work are Extended Kalman Filter (EKF), Two-Stage Extended Kalman Filter and Unscented Kalman Filter (UKF) techniques.

The Kalman filter based algorithms are much more advanced and computationally less cumbersome than LSE based techniques, especially in handling noisy responses from structures and also in cases with limited sensors. Despite the above mentioned limitations of LSE based algorithms, this technique and its subsequent developed form like RLSE is considered as the basic initial approach to SI. Thus, in the present work, these algorithms have also been explored to understand the applicability for building structures.

As observed from the review of literature, a few numbers of comparative studies have been carried out by researchers on fixed base buildings by considering some of these algorithms. Comparative study on the performance between EKF and UKF has been reported, but there are no literatures which takes into account all these algorithms such as SNLSE-UI-UO, EKF, Two-Stage EKF and UKF together. Moreover, studies on influence of different noise level on the performance of these algorithms are also missing. In the present work, the influence of increasing amount of added noise in the simulated response used for identifying the state and parameters of the fixed base multi-storey building has also been evaluated. The SNLSE-UI-UO algorithm has been found to be performing well in case of noise-free responses, but the performance of the algorithm deteriorates with slight increase in amount of added noise. The performance of KF based algorithms such as EKF, Two-Stage EKF and UKF are observed to be comparable in case of noisy response data.

Literature review reveals the lack of comparative study based on these algorithms in limited sensor environment. In the present work an effort has been made to study the impact of missing sensors on the performance of these algorithms on real life structures such as standard multi-storey building as well as base-isolated building. Studies have been performed using both simulated responses and acquired seismic induced responses from some of the existing buildings. The performance of EKF, Two-Stage EKF and UKF are observed to be comparable in the limited sensor environment.

As observed from literature, the performance of SNLSE-UI-UO with regard to identification problems has been generally good, though a very limited work has been presented, where there is only one number of sensors is missing. Study with multiple missing sensors using this algorithm is not reported. In the present work, a simulated example has been shown, illustrating the performance of SNLSE-UI-UO where more than one missing sensor is considered. It is observed that while the algorithm performs well with one missing sensor, the performance drastically degrades with increase in the number of missing sensors. Observing the poor performance of the SNLSE-UI-UO algorithm with both noise corrupted responses and multiple missing sensors, this algorithm has not been utilized further in the problems dealing with multiple missing sensors of both fixed base as well as base-isolated building systems considered in the present investigation.

From review of literature, it is observed that examples cited so far for SI, generally deals with responses due to input earthquake excitation of large magnitude such as that of El Centro, Koyna or Victoria etc. All these earthquakes are of large magnitude and obviously the

responses from the building system excited by these earthquakes are also large. The SI algorithms such as EKF, Two-Stage EKF and UKF function well for high intensity responses, but it has been observed that if the responses are of very low intensities due to low intensity input base excitation, a drift in identified displacement has been observed. Drift in identified displacement due to response corrupted with low frequency component is a very common phenomenon. Occurrence of such drifts is very often discussed in literatures. Adoption of a technique to correct such drift has been reported in one of the literatures by resorting to a method in which artificial white noise of insignificant magnitude has been used as additional input. This technique of drift correction has been adopted in the present work and has yielded an excellent result. Identification of the base-isolated building system with low amplitude excitation has been performed with all the considered algorithms and UKF is found to be producing a consistent result in state identification, although in few instances of simulation study, EKF is observed to perform well. In respect of state identification, the performances of all these algorithms are quite comparable.

Further, SI based studies in a base-isolated multi-storey building with missing sensor at floor level just above the isolator has never been dealt so far. Formulation has been specifically made to handle such case and SI has been carried out using response data from simulation based studies.

For base-isolation of multi-storey buildings, Steel Reinforced Elastomeric Isolator (SREI) are commonly used. SREIs are heavy and expensive, since elastomer / rubber layers are interleaved with thin steel reinforcing plates. The Steel plates and elastomeric layers are placed in alternate layers. A recent development took place in this field with the advent of Fibre Reinforced Elastomeric Isolator (FREI). In FREI, the steel plates are replaced by bi-directionally oriented fibres, thereby reducing the weight and cost of the isolators. FREIs can also be cut into desired sizes. FREI has been found to be cost effective substitute of SREI especially for low-rise buildings. Similar to other types of base isolators, FREIs are also susceptible to damaging effect of earthquake. So, it becomes necessary to assess the health of FREIs directly from the measured responses from the BI structure. There are literatures on FREI which deals with seismic vulnerability assessment and 3D FEM modelling aspect of FREI. There is however, no literature on SI based approaches for FREI supported structural system utilizing measured vibration data.

In this work, different variants of Kalman filter based algorithms like EKF, Two-Stage EKF and UKF are used to estimate and compare the performance of these algorithms in identifying

the state and parameters of un-bonded Fibre Reinforced Elastomeric Isolator (U-FREI). The test model comprises of a two-storey masonry building supported on U-FREI. Recorded response from the test model, subjected to different earthquake excitations have been considered for the identification study. Since the hysteretic behaviour of U-FREI is somewhat different from that of SREI, emphasis has been put to select an appropriate model for representing U-FREI and extended Bouc-Wen model has been observed to be appropriate. A rough estimate of the model parameters of U-FREI are obtained using force displacement hysteresis behaviour of the test model. These parameter values are considered as initial guess in the identification process. The mathematical model representing FREI comprises of many parameters and the results of identified parameters vary across different algorithms and also for different considered earthquakes. Therefore, percentage error index (PEI) has been introduced to compare the performance of these algorithms. PEI is evaluated using the parameter weights obtained from parameter sensitivity analysis represented in the form of spider diagram. It has been observed that the selected model is suitable for identification of FREIs. The state and parameters of the U-FREI model are identified using recorded response of the test model as well as from noise corrupted response from analytical model. In the analytical study, the response is contaminated with varying level of artificially added Gaussian white noise. The effect of these added noise on the identification of state and parameters are investigated. It is observed that these algorithms are quite stable and the identified results are comparable with that assumed in the analytical study.

There are literatures which deal with comparative studies of the performances of the EKF and UKF algorithms, but no literature has been found towards holistic approach to SI based studies for fixed-base and base-isolated building using algorithms like SNLSE-UI-UO, EKF, Two-Stage EKF and UKF.

Thus, the present work is an attempt to holistically study some of the commonly used well known algorithms and apply it to different building systems encountered in general. Formulation of each of these algorithms for each of the varied specific cases of structural system has been covered in detail starting from the very basic principles. The derivations are shown in very simple steps and can be readily applied. Further, the identification approach of the newly developed FREI isolators has also been covered.

LIST OF FIGURES

LIST OF TABLES

NOTATIONS

Nomenclature		Meaning
a_0	=	Amplitude of acceleration
a_1 to a_5	=	Stiffness parameters of the nonlinear spring
α	=	Ratio of post yield stiffness to pre-yield stiffness
$\tilde{\alpha}$	=	A constant that determines the spread of the sigma points in UKF algorithm
$\hat{\alpha}$	=	Rayleigh damping coefficient
$\breve{\boldsymbol{A}}$	=	Matrix of input
$\boldsymbol{\mathcal{A}}$	=	State transition matrix
$\mathbb{A}, B, \beta, \gamma, Y$	=	Parameters of Bouc-Wen hysteresis model that control the characteristics of resulting hysteresis loop
$\boldsymbol{B_1}$ and $\boldsymbol{B_2}$	=	Matrices defined in Newmark's method
$\bar{\beta}$	=	Parameter in Newmark's method
$\hat{\beta}$	=	Rayleigh damping coefficient
$\tilde{\beta}$	=	A parameter in UKF algorithm
c, c_b	=	Coefficient of viscous damping of isolator
c_1, c_2 and c_3	=	Viscous damping coefficient of 1st, 2nd and 3rd floor
$\mathbf{C}$	=	Damping matrix
γ	=	Parameter of Bouc-Wen hysteresis model
$\bar{\gamma}$	=	Parameter in Newmark's method
$\breve{\boldsymbol{d}}$	=	Desired output sequence vector
δ	=	Direct delta function
$\boldsymbol{e}$	=	Error vector
$\mathbf{E}$	=	Expectation
E_f	=	Young's modulus of fibre reinforcement
$\boldsymbol{\varepsilon}(t)$	=	Vector of model noises
$\mathbf{f}$	=	Nonlinear system function
f_s	=	Spring force
f_d	=	Damping force
$\mathbf{F}_\mathrm{c}$	=	Damping force vector
$\mathbf{F}_\mathrm{s}$	=	Stiffness force vector
$\mathbf{F}$	=	Force excitation vector
F_r	=	Hysteric restoring force

Nomenclature		Meaning
$\mathbb{F}$	=	State transition matrix
$\boldsymbol{\mathcal{F}}$	=	A function representing damping force and stiffness force
$F(t)$	=	Restoring force at time instant t
$\boldsymbol{\Phi}$	=	State transition matrix of linearized system
$\boldsymbol{g}$	=	A function of state vector, parametric vector and forcing function when the state vector or extended state vector is represented in state space form
g	=	Acceleration due to gravity
G	=	Shear modulus of elastomer
$\mathbf{h}$	=	A function used to compute the predicted measurement from the predicted state
$\breve{\boldsymbol{h}}$	=	A vector of filter coefficients
$\breve{\boldsymbol{h}}^*$	=	Best estimate of $\breve{\boldsymbol{h}}^*$
$\hat{h}_1, \hat{h}_2, \hat{h}_3$ and $\hat{h}_4$	=	Storey height
$\mathbf{H}$	=	Jacobian matrix of measurement equation
$\mathbf{H}_\theta$	=	Partial differential of measurement function with respect to parametric vector
$\mathbf{H}_X$	=	Partial differential of measurement function with respect to state vector
$\mathbf{X}_\theta$	=	Partial differential of state vector with respect to parametric vector
$\mathbf{I}$	=	Identity matrix
$\boldsymbol{\mathcal{J}}$	=	Objective function
k	=	Time step
k_i	=	Pre-yield stiffness
k_b	=	Stiffness of the isolator
k_1, k_2, k_3 and k_4	=	Storey stiffness of 1st, 2nd, 3rd and 4th floor
$\mathbf{K}$	=	Stiffness matrix
$\mathbf{K}_g$	=	The Gain matrix used in RLSE algorithm
$\boldsymbol{\mathcal{K}}$	=	The Kalman Gain matrix
$\mathcal{L}$	=	Laplace operator
m	=	Mass
m_b	=	Mass at isolator top
m_1, m_2, m_3 and m_4	=	Mass at 1st, 2nd, 3rd and 4th floor level
$\boldsymbol{M}$	=	Mass matrix

Nomenclature		Meaning
$\bar{\mathbf{M}}$	=	Mass matrix corresponding to known degrees of freedom
$\mathbf{M}^*$	=	Mass matrix corresponding to unknown degrees of freedom
n, m	=	Number of degrees of freedom
$\bar{m}$	=	Number of known or measured excitation input
$\breve{n}$	=	Total number of input parameter
$\breve{n}_e$	=	Number of error terms considered
$\breve{n}_f$	=	Filter length
p_1 *to* p_6	=	Coefficients of polynomial
$\bar{p}$	=	Number of stiffness parameter
$\mathbf{P_x}$	=	Error covariance matrix of state
$\mathbf{P_\theta}$	=	Error covariance matrix of parameter
$\widehat{\boldsymbol{P}}_0$	=	Initially assumed error covariance matrix for state vector
$\widehat{\boldsymbol{P}}_{\theta,0}$	=	Initially assumed error covariance matrix for structural parameters
$\boldsymbol{P}_{m\|n}$	=	Predicted error covariance at time *m* with given observation upto and including time *n*, where *m*>*n*
$\mathbf{Q}$	=	Process noise covariance matrix
r	=	Number of unknown or unmeasured excitation input
$\mathbf{R}$	=	Measurement noise covariance matrix
$\mathfrak{s}$	=	Number of unknown or unmeasured acceleration response
$\mathbf{S}_1$, $\mathbf{S}_2$,..	=	Stiffness matrix without stiffness coefficient
t_e	=	Thickness of single layer of elastomer
t_f	=	Thickness of single layer of fibre reinforcement
Δt	=	Time interval
T	=	Time period
T_b	=	Time period for base isolated system
T_f	=	Time period for fixed base system
u_1, u_2 and u_3	=	Inter-storey drift
x	=	Displacement
x_b	=	Horizontal displacement of isolator top
$\boldsymbol{x}[n]$	=	Input sequence
x_y	=	Horizontal displacement of isolator top
x_1, x_2, x_3 and x_4	=	Horizontal displacement at 1st, 2nd, 3rd and 4th floor level
$\dot{x}$	=	Velocity
$\ddot{x}$	=	Acceleration

Nomenclature		Meaning
$\ddot{\bar{x}}$	=	Acceleration response corresponding to known degrees of freedom
$\ddot{x}^*$	=	Acceleration response corresponding to unknown degrees of freedom
$\ddot{x}_b$	=	Horizontal acceleration at isolator top
$\ddot{x}_g$	=	Horizontal component of ground acceleration
$\ddot{x}_1, \ddot{x}_2$ and $\ddot{x}_3$	=	Horizontal acceleration at 1st, 2nd and 3rd floor level
$\mathbf{X}$	=	State vector
$\boldsymbol{X}_1$	=	Vector of displacement
$\boldsymbol{X}_2$	=	Vector of velocity
$\boldsymbol{X}_3$	=	Vector of parameters such as stiffness, damping or hysteretic parameters
$\mathbf{X}_e$	=	Extended state vector
$\widehat{\boldsymbol{X}}_0$	=	Initially assumed state vector
$\widehat{\boldsymbol{X}}_{\theta,0}$	=	Initially assumed sensitivity matrix
$\widehat{\boldsymbol{X}}_{m\|n}$	=	Predicted **X** at time *m* with given observation upto and including time *n*, where *m*>*n*
$\mathfrak{X}$	=	Sigma point matrix
$\boldsymbol{\eta}, \boldsymbol{\eta}'$	=	Excitation influence matrix
$\boldsymbol{\theta}$	=	Parametric vector
$\widehat{\boldsymbol{\theta}}_0$	=	Initially assumed structural parametric vector
$\boldsymbol{v}_k$	=	Zero mean Gaussian measurement noise vector
υ_f	=	Poisson's ratio of fibre reinforcement
$\boldsymbol{w}_k$	=	Zero mean Gaussian process noise vector
ω_b	=	Frequency of base isolated system
$W_i^{(m)}$	=	Weight for the mean
$W_i^{(c)}$	=	Weight for the covariance
$\boldsymbol{\Lambda}$	=	Sensor location matrix
κ	=	A secondary scaling parameter used in Unscented Kalman Filter algorithm
λ	=	A scaling parameter used in Unscented Kalman Filter algorithm
$\boldsymbol{\mathcal{Y}}$	=	Predicted measurement vector using transformed sigma points
z	=	Non-observable dimensionless nonlinear hysteretic Bouc-Wen parameter
$\bar{\boldsymbol{z}}$	=	Measurement vector
$\mathbf{0}$	=	Zero Matrix

ABBREVIATIONS

Abbreviation		Meaning
ACM	=	Accelerometer
BI	=	Base Isolated
dof or DOF	=	Degrees of Freedom
EKF	=	Extended Kalman Filter
FREI	=	Fibre Reinforced Elastomeric Isolator
KF	=	Kalman Filter
LSE	=	Least Square Estimate
LVDT	=	Linear Variable Differential Transducer
PEI	=	Percentage Error Index
RLSE	=	Recursive Least Square Estimate
RMSE	=	Root Mean Square Error
SNLSE	=	Sequential Nonlinear Least Square Estimate
SNLSE-UI-UO	=	Sequential Nonlinear Least Square Estimate with Unknown Input and Unknown Output
SREI	=	Steel Reinforced Elastomeric Isolator
B-FREI		Bonded Fibre Reinforced Elastomeric Isolator
SU-FREI		Stable Unbonded Fibre Reinforced Elastomeric Isolator
Two-Stage EKF	=	Two Stage Extended Kalman Filter
U-FREI		Unbonded Fibre Reinforced Elastomeric Isolator
UKF	=	Unscented Kalman Filter

Chapter 1

Introduction

1.1 Background

Civil Engineering structures, like buildings, bridges, towers etc can be modelled using a mathematical formulation. If the structure is excited by external forces such as ground excitation, wind etc, the responses of these structures at any location due to the external excitation can be obtained from the mathematical model which is based on the governing dynamic equation of motion. The response components can be acceleration, velocity or displacement. To obtain these responses, prior knowledge is required for structural masses, stiffness and damping. System identification (SI) is an inverse problem wherein the state of the structural system and its parameters such as stiffness and damping are identified from the measured response of the structure experiencing vibration due to external excitation. SI can also be reckoned as a process of identifying unknown parameters of the considered mathematical model of the structural system by using the measured input and output signal of the system. A *model* is a mathematical relationship between a system's input and output responses.

Since few decades, there is a tremendous effort going on towards the research and development in the direction of system identification techniques. After any major earthquake, it becomes necessary to examine the structural health of any important structure like bridges or buildings. By simple observation of any externally visible damage or cracks one cannot assess the amount and severity of damage in a structure as there may be presence of serious internal damage also. In such situation, SI plays a major role in rapid assessment of structural damages of important structure and thereby helps in the emergency management of the situation.

Structural system identification techniques can be classified into strategies based on: 1) frequency domain, 2) time-domain and 3) time-frequency domain analysis. Examples of frequency domain based analysis are Frequency Domain decomposition (FDD), Enhanced Frequency Domain Decomposition (EFDD), Maximum Likelihood Estimate (MLE). Examples of time-domain analysis are algorithm for sub-space identification (N4SID), Natural Excitation Technique (NExT), eigen value realization algorithm (ERA), least square estimation (LSE), recursive least square estimation (RLSE) and among filter based approaches are Kalman Filter (KF), Extended Kalman Filter (EKF), Two-Stage Extended

Kalman filter (Two-Stage EKF) and Unscented Kalman Filter (UKF), H_∞ filter and Monte-Carlo filter etc. Examples of time-frequency analysis are wavelet transforms Hilbert-Huang transform etc.

The research for system identification of linear structural system is quite established and there is lots of frequency and time-domain based identification schemes which can easily carry out accurate evaluation of system parameters. However, it is well known fact that nothing is fully linear in the real world. Almost every structure exhibits some form of nonlinearity in some magnitude or other. Nonlinearity may develop in any structure, experiencing vibration due to formation of cracks. Further, nonlinearity is also exhibited by the isolators used in base-isolated structural systems. Structures exhibit inelastic behaviour under severe cyclic loads associated with earthquakes, high winds, etc. When the restoring force is plotted against the structural deformation, inelastic behaviour often manifests itself in the form of hysteresis loops. The area enclosed by each loop is a measure of the energy dissipated over a complete cycle. In general terms, hysteresis refers to the hereditary and the memory nature of an inelastic system, in which the restoring force depends not only on the instantaneous deformation but also on the past history of deformation. Mechanical and structural systems capable of dissipating appreciable energy tend to possess large hysteresis loops. Hysteresis is thus particularly important in depicting the damping characteristics of inelastic systems.

Response measurement from all dynamic degrees of freedom is desirable for efficient functioning of the SI algorithms. However, there may be situations where limited number of sensor data may be available. This may be due to inaccessibility of sensor placement location or due to financial constraints etc. Hence, it can be concluded that the selected SI needs to be able to handle nonlinearity and perform in limited sensor scenario.

In the field of nonlinear structural dynamics, the problem which is commonly encountered is the modelling of the nonlinear system and its identification. Therefore, proper mathematical model is required which can represent the nonlinear behaviour of the structural system.

In the present thesis work, attempt is made to make a comparative study of few selected nonlinear system identification schemes with regard to their applicability, performance and robustness. Out of the huge domain of system identification schemes available till date, it will be impractical or rather confusing if all the available schemes are considered together for such comparative study. In the current study a few algorithms based on LSE and KE are

considered for SI. Among the LSE based identification schemes, RLSE, Sequential Nonlinear Least Square Estimate (SNLSE), Sequential Nonlinear Least Square Estimate with Unknown Input and Unknown Output (SNLSE-UI-UO) are taken into consideration. Similarly EKF, Two-Stage EKF and UKF are considered for KF based identification schemes. Brief discussion about the evolution of these algorithms and their pros and cons are detailed in section-1.2 and section-1.3.

Till date, research work on nonlinear structural system identification using all the above mentioned schemes were carried out by utilizing data from simulation and experimental work. However, limited works are observed for comparative study regarding the performance of identifications of states as well as parameters involving only EKF and UKF. However, no such comparative studies are available considering limited sensors as well as involving base isolated system. Thus, it is felt necessary to carry out studies to propose recommendation for selection of identification algorithms in the system identification of some existing structures, generally encountered in civil engineering field.

Using the considered SI algorithms, identification studies on both fixed base and base-isolated multi-storey building have been carried out. The study has been conducted considering data from both simulated model as well as existing structures. The impact on identification by all the different algorithms due to limited number of sensors and response corrupted with varying degrees of Gaussian white noise have also been carried out.

Using the selected algorithms, identification of state and parameters has also been carried out for Fibre Reinforced Elastomeric Isolator (FREI) supporting structures. FREI isolator is relatively new in the field of rubber based isolator and is a cost effective alternative to conventional laminated Steel Reinforced Elastomeric Isolator (SREI). State and parameter identification of FREI using the available system identification schemes is not reported till date. In this thesis, an attempt has been carried out to perform a comparative study of the state and parameter identification using the above mentioned selected algorithms.

1.2 Overview of different identification scheme based on Least Square Estimate Technique

LSE can be regarded as one of the first approaches towards time-domain based identification scheme. Any identification scheme is associated with 1) a governing dynamic equation of motion, 2) unknown state vector such as displacement, velocity, 3) unknown parametric vector containing unknown stiffness and damping parameter and 4) issue related to

availability of sensors to output. Apart from measured acceleration data, there may be additional available data such as displacement and velocity as well. In such cases displacement sensors are also supposed to be available at the site under study. Observation equation is the theoretical relative acceleration that is obtained from the equation of motion, expressed in terms of unknown stiffness and damping. The error in observation is the difference between the observed acceleration and the theoretical acceleration. The essence of the scheme is minimization of sum of squares of this observation error by tuning the model parameters considering full time history analysis. LSE is applicable in cases of over-determined system, where number of equations are more that the number of unknown parameters to be determined.

LSE appears to be rudimentary identification technique from the point of view of advancement achieved in the techniques of SI till date. However, LSE still needs mentioning as it appears somewhere in some form in most of the present day techniques. To achieve the desired objective, progressive modifications were introduced on LSE after its drawbacks were determined.

Drawbacks of LSE scheme are as follows

- If any new observation needs to be incorporated in the analysis, the analysis has to be started from beginning. There is no provision of updating the identification scheme with new observation.
- Therefore, online identification of state and parameter using LSE scheme is time consuming as the analysis has to be started from beginning for processing any new observation in each forward step.
- Handling the case of limited sensor is not possible with LSE scheme.

RLSE is the next updated version of LSE, wherein the drawbacks of LSE are partly overcome. In RLSE technique, the gain matrix gets updated with every new observation and therefore the analysis need not be run from beginning of time history as is done in LSE. There were further subsequent developments towards this direction with the advent of SNLSE, which is a modification of RLSE. In SNLSE scheme, the state and parameters are identified separately wherein, state is first identified followed by parameters. This is in contrary to RLSE wherein, identification of state and parameter are done simultaneously.

As the state and parameters are interdependent of each other, these are identified in sequential manner in SNLSE. First, the parameters are identified on the assumption that the state is known using RLSE. Secondly, the state is identified from the identified parameters of first step using RLSE. The state is determined on the basis of numerical integration scheme. In the third step, the parameter is revised with the identified state. These three steps are repeated in every time step and thus state and parameter are identified.

A slight improvement or modification was made in the SNLSE algorithm to enable it to function in situations, where limited numbers of sensor measurements are available. This modified algorithm is known as SNLSE-UI-UO. SNLSE-UI-UO is further updated version of SNLSE, which proposes to identify unknown input as well as unknown output or responses apart from state and parameter. This algorithm evolved due to the fact that SNLSE has the inability to handle limited sensor cases. However, there is every possibility of limited sensor measurement due to either economic constraint or inaccessibility to fix sensors at desired location or may be due faulty sensor etc.

1.3 Overview of different identification scheme based on Kalman Filter Techniques

One of the popular SI techniques is the KF based approach. These KF based algorithms can handle noise corrupted responses efficiently. The algorithm works in two steps; 1) the prediction step and 2) the correction step. In the prediction step, the unknown parameters and state are predicted from the dynamic model and in the correction step, this prediction of state and parameter are corrected or updated using current measurement. Updating is done using the Kalman Gain matrix, in which more weights are given to estimate with higher certainty. The algorithm is recursive. It runs in real time, using only the current input measurements, no additional past information is required. There is various application of KF which includes target tracking of ballistic missiles, robotic motion planning and control, trajectory optimization, navigational guidance and control of vehicles, particularly aircraft and space craft etc.

The KF is applicable only for linear systems and it works with Gaussian noise. In order to apply KF to non-linear systems, the non-linearity in the system is locally linearized using Taylor series. Thus, Jacobian needs to be evaluated for linearising a nonlinear system. Such techniques of using KF after linearization are called the EKF. In EKF, the state vector and the parametric vector to be identified are arranged in a single vector called the extended state vector. The EKF is applicable to time invariant system. The EKF containing both the state

vector and the parametric vector is quite cumbersome and a lot of computational effort is required for its evaluation and sometimes the filter diverges. To overcome this issue, Two-Stage EKF was developed in which state vector and parametric vector are handled separately. The computation of Jacobians is a cumbersome process and sometimes it may not be possible to evaluate. In such cases EKF algorithm cannot be used.

To overcome this lacuna in EKF, the UKF came into picture. Jeffrey Uhlmann [1997a] proposed UKF. In UKF, the mean and covariance of the state and parametric vector for the next updated time step is not evaluated directly. The mean and covariance of some predetermined salient points called sigma points are evaluated. From this transformed sigma points, the mean and covariance of state and parametric vector are evaluated. By doing this, the process of evaluation of Jacobians is bypassed, thus the error involved in Jacobian determination are avoided. The error involved by not considering the higher order terms while using Taylor series expansion is thus avoided. Therefore, UKF is a better option of all the above mentioned KF based techniques.

1.4 Basic differences and similarities between the identification scheme based on Least Square Estimate Technique and Kalman Filter based Techniques

- The KF is an algorithm in which state of a system can be estimated using the available observation data.
- The KF requires a mathematical model of the system under consideration. It requires input excitation as well as response of the structure. It also requires process noise matrix **[Q]** and measurement noise matrix **[R]**. The process noise represents the deficiencies of the model in form of inaccurate parameter estimation and the measurement noise is the noise corrupted observation signal like noise from instruments.
- The KF works in two steps: 1) the prediction step and 2) updating step. In the prediction step the unknown future state of the system is predicted using the equation of the model. In the updating step, the predicted future step is updated using the current measurement.
- In RLSE based techniques, there is only updating step using the current measurement data and there is no prediction step, unlike KF.

- Both RLSE and KF have an error covariance matrix of state and parameter. Both are based on minimization of sum of square of the diagonal terms of the error covariance matrix. Both the approaches assume zero-mean Gaussian errors.
- Both RLSE and KF have similar final formulation but the approaches for detailed derivation are different.
- Both RLSE and KF have the same form of expression:

  Updated estimate = Previous Estimate + Gain * Innovation (error).

  The difference between RLSE and KF is in the expression of *gain* matrix. In KF the gain matrix is associated with [**Q**] and [**R**] terms.

Notable Differences:

Some notable differences between LSE, RLSE based algorithm and KF based algorithm are given in Table 1.1.

Table 1.1: Difference between LSE, RLSE and KF based technique

Sl No	LSE and RLSE based algorithm	KF based algorithm
1	Faster than KF	Slower than LSE or RLSE
2	Less accurate	More accurate
3	Easier to implement	Comparatively difficult to implement
4	Not necessary to model in state-space form	System needs to be modelled in state-space form
5	There is no existence of any noise covariance matrix	The process noise and measurement noise covariance matrix needs tuning

1.5 Multi-storey buildings for identification

Multi-storey buildings have been considered for both state and parameter identification. The considered buildings may be of conventional foundation system and idealised as fixed base or supported on seismic isolators. In any conventional fixed base multi-storey building under seismic excitation, the inter-storey drifts are the major threat to the structural system. Inter-storey drifts create bending in beams and columns, leading to damage in extreme cases, if the intensity of excitation is higher than the design values. Such cases arise due to transmission of ground excitation to upper storey. Base isolation is one of the ways to reduce the seismic transmissibility. This is achieved by introducing base isolators in between the foundation and

superstructure. These isolators will act like a fuse in electrical system. The base isolators will allow a certain amount of vibration arising due to ambient wind etc. to pass and will start functioning if vibrations are beyond a limit. The primary idea is to reduce the inter-storey drift effect. This may be achieved if the structure above the isolators behaves like a rigid body so that the floors of entire building move in unison under seismic excitation, thereby creating lesser inter-storey drifts.

Fig-1(a) shows a fixed base building with storey stiffness *k*, damping *c* and floor mass *m*. The natural frequency of the system is $\omega_f = \sqrt{\frac{k}{m}}$ and fundamental time period is $T_f = \frac{2\pi}{\omega_f} = 2\pi\sqrt{\frac{m}{k}}$.

Fig-1(b) shows a base-isolated building with storey stiffness *k*, damping *c* and floor mass *m*. The mass of base slab mounted directly on the isolator is m_b, stiffness of the isolator is k_b and damping of the isolator is c_b. The natural frequency of the system is $\omega_b = \sqrt{\frac{k_b}{m+m_b}}$ and fundamental time period is $T_b = \frac{2\pi}{\omega_b} = 2\pi\sqrt{\frac{m+m_b}{k_b}}$. The ratio $\frac{T_b}{T_f} = \sqrt{\frac{m+m_b}{m}} * \sqrt{\frac{k}{k_b}}$ is always greater than one as the horizontal stiffness of isolator is always much lesser than storey stiffness. Thus, it is evident that the fundamental time period of the structure is lengthened, if base-isolation is adopted. As shown by the elastic design spectrum of Fig-2, this lengthening of period can reduce the pseudo-acceleration and hence the earthquake-induced force in the structure.

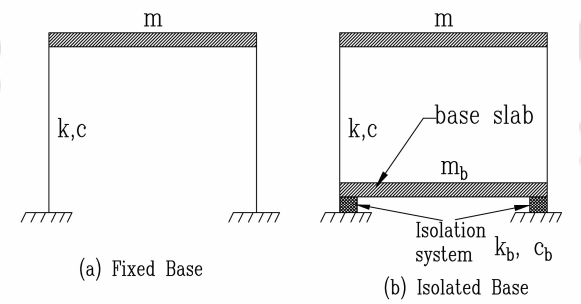

Fig-1.1: (a) Fixed-base structure; (b) isolated structure

The most common type of available bearing is SREI, which is comprised of elastomer layers interleaved with thin steel reinforcing plates (Fig-1.3). The Steel plates and elastomeric layers are placed in alternate layers. These laminated bearings are strong and stiff under vertical loads, but very flexible under horizontal force.

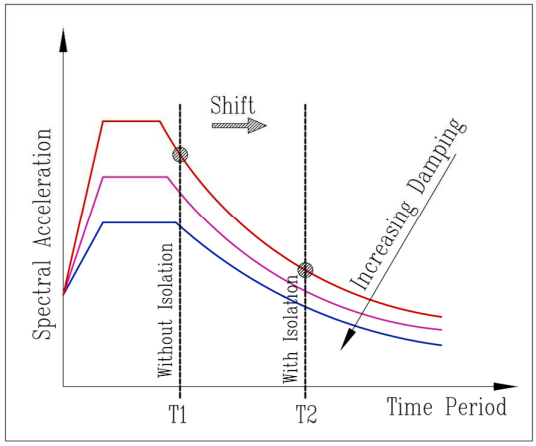

Fig-1.2: Elastic Design Spectrum

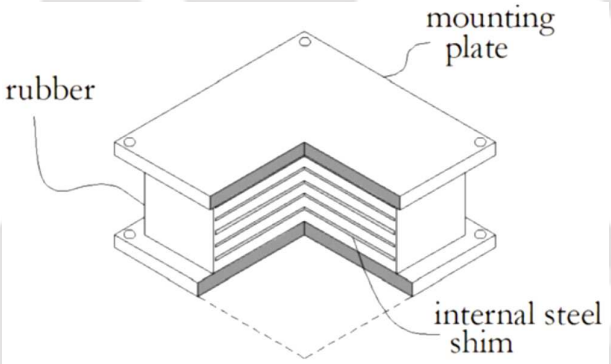

Fig-1.3: Steel Reinforced Elastomeric Isolator (SREI).

Another type of bearing gaining popularity is the FREI in which steel plates of SREI are replaced by bi-directionally oriented carbon or glass fibres, thereby reducing the weight and cost of the isolators. It can be effectively used for base isolation of low-rise masonry building. The bearing is stiff in vertical direction, but very flexible under horizontal force. FREI has another implementation advantage over conventional SREI. The advantage is that it can be cut into desired shape and size from a long sheet of the bearing. There are two types of FREI on the basis of the methodology adopted while placing them between sub and superstructure. These are Bonded FREI (B-FREI) and Unbonded FREI (U-FREI) (Fig-4). In B-FREI, the top and bottom surfaces in contact with the support are bonded together such that the isolators don't lose contact during its service life. In U-FREI, the top and bottom surfaces of the isolator may lose contact with the supports, if the horizontal applied force on

the bearing top exceeds certain threshold limit. A roll over deformation takes place, which reduces the stiffness of the bearing further, thereby enhancing the effectiveness of better isolation.

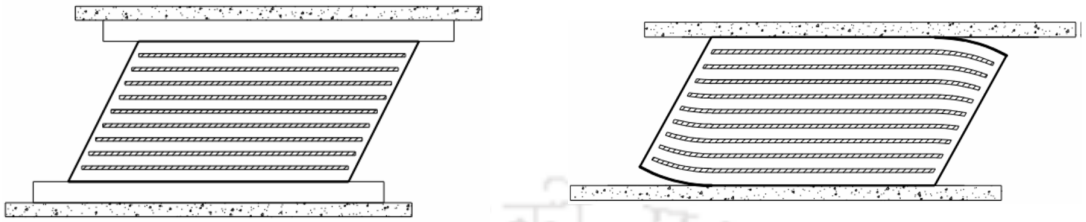

Bonded FREI Un-bonded FREI

Fig-1.4: Bonded FREI and Un-bonded FREI.

1.6 Problem Identification

Literature survey on nonlinear structural system identification reveals that various identification schemes have been suggested by different researchers. These algorithms were adopted using responses from numerically simulated model as well as experimental investigation on different types of structural systems. Works on comparative study of identification results obtained from various identification schemes, especially in an environment with limited sensor data are however very few.

Further literature related to studies on SREI supported structures as well as identification of parameters of SREI are available. However, FREI is a relatively newer concept and research works on identification of parameters of FREI isolator from available response measurement and comparative study using different identification schemes are not available till date. Thus, it is felt that further studies should be conducted to have some idea about the applicability of the selected system identification schemes for assessment of some typical real time existing structures in civil engineering field. The present study is an attempt to provide some insight to problem wise selection of algorithm.

After any major earthquake, it becomes necessary to assess the health of any important structure such as a bridge or building etc. By mere visible observation, assessment of any severe damage, which may be detrimental to the service condition of the structure, may not be feasible. One cannot guarantee the effectiveness of reuse of the structure or suggest any remedial measure to make it fit to serve the community. Wrong assessment of damage may lead to further calamity as the structure may fail, hindering relief and rescue activity in post earthquake scenario. So, it becomes imperative to proceed with more scientific approach

involving NDT and system identification technique to identify the extent of damage and suggest any remedial measures for its retrofitting. However, the pertinent issue is to select an appropriate identification schemes out of so many available schemes for the structural system in question. One would get confused as each identification scheme is performance wise better than the other in some respect or other. In order to tackle such type of situation, a comprehensive study should be made to characterize various schemes on the basis of performance, computational complexity, effectiveness in handling noise, effectiveness with respect to the extent of missing sensor data availability.

1.7 Research Objective

Data from numerically simulated building structures and previously carried out experimental investigations at IIT Guwahati are utilized. The major objectives of the research work are as follows.

I. To assess the performance of different SI strategies for evaluation of system parameters of fixed base building.

II. To assess the performance of different SI strategies for evaluation of system parameters for SREI supported BI building.

III. To select appropriate model for representation of hysteretic behaviour of FREI.

IV. To identify the state as well as parameters of model representing FREI in BI building using the selected algorithms and to assess the comparative performance of these different SI schemes.

V. To evaluate the influence of noise and limited sensors on the performance of all the considered algorithms.

1.8 Scope of Study

Major scopes of study in the present research comprise of application of different system identification strategies by utilizing data obtained from 1) numerically simulated model of prototype structures, 2) recorded responses of existing buildings and 3) experimental laboratory test models.

Two different categories of algorithm are considered in this thesis. One is the LSE based algorithm and the other is KF based algorithm. In the LSE based algorithm, SLNSE-UI-UO and in KF based algorithm EKF, Two-Stage EKF and UKF algorithm have been considered.

Thus, a total of four algorithms i.e. SNLSE-UI-UO, EKF, Two-Stage EKF and UKF have been considered. These selected algorithms are used for state and parameter identification of different types of structural systems. The performance of these algorithms in identifying the state and parameters of the considered structural systems are evaluated. Structural system considered in the present study consists of fixed base as well as SREI supported base isolated multi-storey buildings. Additionally, state and parameter identification of FREI supporting a model masonry building is also carried out.

1.8.1 Fixed base building

I. To simulate a three-storey shear frame building with fixed base and to analyse under different considered earthquake excitations. The floor responses obtained from simulation are corrupted with Gaussian noise with 1%, 2% and 5% noise levels. All the four selected identification schemes namely SNLSE, EKF, Two-Stage EKF and UKF are to be utilized to make a comparative study on the identification abilities of these algorithms in respect to evaluation of state and parameter of the structural system.

II. To make a comparative study on the performance of the considered algorithms with limited sensor data. From the simulated responses, the measurement records of different floor levels are manually omitted to represent a condition of missing sensor and identification is to be carried out. The impacts of limited number of sensors on the performance of different algorithms are to be examined.

III. The study is also extended to two numbers of identical existing three-storey RCC framed building with brick masonry in-fill walls with one having fixed base and the other supported on SREI isolators. This sample structure is located in the campus of Indian Institute of Technology, Guwahati. The acceleration response of the building and ground accelerations records are available from past earthquakes. Sensors are installed only at ground floor level (floor slab just above the isolator) and roof level and a separate sensor to record ground excitation. State and structural parameters of the building are to be identified using all the considered algorithms. A comparative study on the effectiveness of the algorithms in identifying the state and structural parameters are also to be carried out.

IV. The study is further extended to an existing multi-storey building situated at Guwahati city, Assam. Measured sensor data for two different earthquakes are

available for a (G+8) multi-storey RCC building with fixed base. The building is equipped with limited number of accelerometers. State and structural parameters of the building are to be identified using all the considered algorithms and carry out a comparative study of the effectiveness of the algorithms in identifying the state and structural parameters. The building is having large numbers of degrees of freedom with only limited numbers of available sensor data and hence is also an ideal case for the present study.

1.8.2 Base isolated building

I. To develop formulation for base-isolated structure that will have the ability to fit into the identification algorithm.

II. To simulate a three-storey shear frame building with isolated base and obtain responses at all the floor levels under different sample earthquake excitations.

III. To carry out a comparative study on the performance of the identification algorithms with missing sensor data at floor level just above the isolator. Modification is to be performed on the existing formulation to make it suitable to carry out this identification.

IV. To carry out a comparative study on the performance of the identification algorithms with limited sensor data. Simulated responses of specific floor levels are utilised by the identification algorithms to represent a condition of missing sensor. The impacts of missing sensors on the performance of the different algorithms are studied.

V. The study is also extended to identification of state and parameter of the existing base isolated structure of the twin building located at IIT Guwahati as mentioned before. This is an ideal case of structures with different support conditions and having limited number of available sensor data and thus it represents an appropriate case for comparative study.

1.8.3 FREI supporting a scaled model masonry building

I. To select a suitable model to simulate the behaviour of FREI.

II. To validate the selected mathematical model with that of force-displacement laboratory test result of FREI.

III. To carryout identification of both state and model parameters of FREI using EKF, Two-stage EKF and UKF algorithm using experimental test results of FREI supported masonry building (test model).

IV. To access the performance of the selected algorithms due to varying levels of added noise in the simulated response of the FREI supported structural system.

V. To assess the performance of these algorithms in evaluating the state and parameter of the model representing FREI, supporting building structure.

1.9 Outline of the Thesis

In this thesis, a comparative study is made using well established identification algorithms like SNLSE-UI-UO, EKF, Two-Stage EKF and UKF on identification of state and parameters of multi-storey shear buildings, both fixed base and base isolated, which are excited by ground acceleration. Both simulation based results as well as data from instrumented existing buildings are utilized. A comparative study is carried out to study the effect of response corrupted with varying level of added noise on the performance of the algorithms. Study is also made on the effectiveness of the algorithm in identifying the state and parameter due to limited availability of sensors placed in the building for acquisition of data.

For the case of FREI isolator, a suitable model is selected to represent the hysteretic behaviour of the isolator. The parameters of the selected model is determined by trial and error to best fit the experimental hysteresis curve obtained from available force-displacement test results. A sensitivity analysis is performed for each of the parameters and is represented in the form of *spider diagram*. Detailed study are conducted for identification of state and parameter of these type of isolators using the algorithm EKF, Two-Stage EKF and UKF on the basis of simulated responses. The effect of varying degree of noise on the identification result carried out using the algorithms is conducted. The study is finally extended to identification of state and parameter of the FREI using the available shake table based experimental data and a performance comparison of the algorithms is therefore made.

In Chapter 1, general description of the different identification schemes, structural systems, scopes and detailed objectives of the study are presented.

Chapter 2 provides the brief review of the existing literature on identification scheme starting from LSE to other variants of LSE like RLSE, SNLSE and SNLSE-UI-UO. Brief literature review has also been presented for KF based identification scheme starting from simple KF

for linear systems to EKF for identification of nonlinear systems using local linearization of the nonlinear function using Taylor series expansion and then preceded with Two-Stage EKF. Further, literature review of UKF and its application on civil structure is also carried out. Lastly, literature review of some relevant literatures of FREI is presented.

In chapter-3, detailed formulations of different considered identification schemes are presented.

Chapter 4 deals with the evaluation of state and parameter of fixed base multi-storey building system. The algorithms such as SNLSE-UI-UO, EKF, Two-Stage EKF and UKF are used for state and parameter identification of buildings. First, the study is made using responses from simulated building and then the study is extended by utilizing field data from existing buildings. Using simulated responses, a comparative study is made on the effect of varying degree of noise and limited availability of sensor measurements.

Chapter 5 is based on the evaluation of state and parameter of multi-storey building supported on base-isolators. The algorithms such as EKF, Two-Stage EKF and UKF are used for state and parameter identification of base isolated building. First, the study is made using simulated responses and then the study is carried out by using data obtained from existing sample buildings under seismic excitations. Using simulated responses, a comparative study is also made on the effect of varying degree of noise and limited availability of sensor measurements.

Chapter 6 is based on the evaluation of state and parameter of FREI from the response data available from shake table test and other laboratory investigations. The algorithms namely, EKF, Two-Stage EKF and UKF are used for state and parameter identification of the FREI supported masonry building system. A comparison is made on the performance of different algorithms.

Chapter 7 presents the summary and conclusion of research work undertaken. Major finding from the present research work and scopes of future work have also been presented in this chapter.

Chapter 2

Literature Review

2.1 Introduction

In section 1.1 of chapter-1, various existing SI schemes based on algorithms such as frequency domain, time domain and time-frequency domain are mentioned. Amongst the various schemes for SI techniques, algorithms those have been considered in present study comprises of Least Square Estimation (LSE), Recursive Least Square Estimate (RLSE), which is a modified form of LSE, Sequential Non-Linear Least Square Estimate (SNLSE), Sequential Non-Linear Least Square Estimate with Unknown Input and Unknown Output (SNLSE-UI-UO), Kalman Filter (KF), Extended Kalman Filter (EKF), Two-Stage EKF, Unscented Kalman Filter (UKF). There are various advantages and disadvantages of all these identification techniques which have been briefly described under section 1.2 and 1.3 of chapter-1.

In any SI of a structural system, states and parameters are coupled. In the considered LSE based scheme, SNLSE is an identification technique based on RLSE, which evolved from LSE. In SNLSE states and parameters are identified one after the other and in sequence; thereby chances of divergence of results are reduced. For the online identification of state and parameter, KF based algorithms have been popular choices. However, the basic drawback of KF is that it is applicable only for linear problem. However, many civil engineering structures like base isolated buildings may exhibit some form of nonlinearity under seismic excitation of appreciable intensity.

To extend the applicability of KF to nonlinear problems, EKF evolved. In EKF, the nonlinear function is linearized by Taylor series expansion. The nonlinear function is approximated by considering only up to the 1st order derivative in the Taylor series expansion while the higher order terms are neglected due to computational complexity. This linearization process involves Jacobian to be evaluated at each time instant. The derivation of Jacobian involves complex calculation and sometimes it cannot be calculated for certain nonlinear functions, thus leading to implementation difficulties.

The extended state vector in EKF algorithm contains both the state vector and structural parameters. The state and parameters are interdependent which may lead to difficulties in computational convergence especially when the extended state vector is large or in case of limited available sensors. In order to overcome this problem, the state and parameters are

identified separately and in sequence one after the other. This led to the evolution of Two-Stage EKF. In the first step, the state vector is considered as an implicit function of the parametric vector and so, the parametric vector is identified by KF, assuming the state vector to be known. In the second step, the state vector is identified based on the identified parametric vector of the first step using the KF.

Initially EKF was extensively used for tracking and estimation problem, since it was simple and quick. However, it was found that EKF can be used only for low level of nonlinearity. In case of highly nonlinear systems, there was difficulty in tuning the EKF. Further, noise source are assumed to be having Gaussian distribution. To overcome these problems, the unscented Kalman filter (UKF) came in to picture.

In UKF method the noise sources need not be Gaussian and linearization of nonlinear function is also not required and thus the algorithm is superior to EKF. Some salient points called sigma points and its corresponding weights are selected and evaluated using the nonlinear function. KF is then applied to the current measurement and transformed sigma points to estimate the future state.

Using algorithms namely SNLSE-UO-UO, EKF, Two-Stage EKF and UKF, identification of state and parameters of different structural systems has been carried out. The responses used for the identification are either from simulated model or recorded response from existing and experimental structures experiencing vibration under different earthquake excitations.

A brief review of literature containing simulation, analysis, experimentation and application to laboratory based test model as well as real life structures using LSE and KF based algorithms are presented in the following sections.

2.2 Recursive Least Square based Estimation Technique

Quite a number of works have been reported on identification techniques based on RLSE and its variants such as SNLSE or SNLSE-UI-UO. Many analytical and experimental studies were performed on base isolated structures as well as linear structures using this technique of identification. Studies related to identification of damage in structure are also reported in the literature. The present study is limited only to identification of state and parameters of structures without any introduction of damage. A brief review of literatures on this approach is presented in the following paragraphs.

Chen and Li [2004] proposed a scheme by which the structural parameters as well as input ground excitation were identified simultaneously. It is an iterative method using the LSE.

Raleigh damping was considered in the scheme. The governing dynamic equation of motion was represented by forming two sets of equations. The two equations were solved iteratively. Stiffness was identified from one equation and damping from the second. Iterations were continued till it satisfied the specified convergence criteria. This is simply a LSE technique, wherein for processing every forward step, one has to start from the very initial step. Further, there is a high chance of drift in the determination of displacement and velocity from the direct integration of acceleration measurement.

Yang and Lin [2004] used RLSE technique to identify structural parameters for nonlinear hysteretic structures. Acceleration as well as velocity responses are needed to be supplied to the algorithm. Solutions were obtained using constraint optimization algorithm. The effectiveness of the algorithm was demonstrated through numerically simulated SDOF and MDOF hysteretic structure. To simulate field condition, artificial white noise with 2% RMS was superimposed with the measured acceleration and then the velocity was calculated using numerical integration. A low pass filter was used to filter out noisy acceleration prior to identification.

Yang and Lin [2005] proposed an adaptive tracking technique using LSE to identify the time varying structural parameters due to the occurrence of damage. Solution was presented using the minimum variation principle leading to the constrained optimization algorithm. The advantage of the proposed technique was demonstrated using simulated SDOF linear system and a nonlinear elastic structure. The major drawback of this system is that the velocity and displacement have to be obtained from integration of acceleration measurement, which may produce severe drift in displacement and therefore solution may not converge.

Yang *et al.* [2006] proposed a scheme called SNLSE, which is a modified form of RLSE for online identification of structural parameters as well as state vectors such as displacement and velocity. The identification was carried out in two steps and in sequential manner. First, the parametric vector was identified on the consideration that structural parameters would not change with time considering time invariant system and based on the assumption that state vector was known. The state vector was then identified based on identified parametric vector. Further, the revised parametric vector was identified by replacing the identified state vector. In each time step, this procedure was followed. This procedure has an advantage over the earlier technique proposed by Yang and Lin [2004] in terms of convergence since integration is avoided to evaluate displacement. As generally measurement of acceleration data is convenient, direct integration on acceleration to get velocity and displacement sometimes

may result in drift in displacement and often spikes are observed in case of measured field data. Hence, processing the unknown structural parameters and state vector separately in a sequential manner eliminates the problem of convergence. Effectiveness of the proposed algorithm was demonstrated on 2-DOF nonlinear elastic structure and 5-DOF hysteretic structure.

SNLSE algorithm as was proposed by Yang *et al.* [2006] was modified as SNLSE-UI-UO by Yang *et al.* [2007] in order to make the SNLSE algorithms perform with missing sensor as well as with unknown input ground excitation or external force. Similarly, the adaptive version of the scheme was used to identify the time-varying structural parameters in case of occurrence of any damage. The accuracy and effectiveness of the proposed algorithm was demonstrated using a 5-DOF non-linear hysteretic building model and a 3-storey steel frame finite-element model.

In this sub-section on literature review on LSE based identification approach, it is observed that numerous research works were carried out using different variants of the algorithm. It is observed that online tracking based on only LSE is not practical as all data starting from beginning should be under consideration as the analysis proceeds. This is not only a cumbersome task but also time consuming. Hence, an improved version of LSE came in to picture and is called RLSE in which one does not have to start the analysis from scratch, instead the algorithm gets updated with current sets of measurement data at each forward time step. Further, it is observed that SNLSE has been performing well in identifying the state and parameters of linear as well as nonlinear structure. For tracking the changes in the value of parameters of the structure due to the onset of damage, an adaptive tracking technique was also proposed. Both state and parameters can be identified with the SNLSE scheme along with identification of time-varying parameters using adaptive variant of the scheme. The major drawback of this scheme lies in its inability to handle missing sensor data. This drawback was overcome by a modified version of this scheme known as the SNLSE-UI-UO. Further, the adaptive variant of this scheme has the ability to track time varying parameters online due to occurrence of damage. By the word sequential, it is meant that state and parameters are identified sequentially, one after the other under the assumption that one is known when the other is being identified.

From the review of literature, it is observed that the effectiveness of the different variants of the LSE based algorithm is demonstrated using analytical and laboratory based scaled models. These algorithms were applied for identification of state and parameters of different

types of idealised building models like linear SDOF and MDOF fixed base buildings as well as nonlinear hysteretic multi-storey buildings. It is also observed that the literatures involving missing sensor are very scanty. A detailed literature review demonstrated the performance of SNLSE-UO-UO algorithm was so far studied with only one missing sensor. Therefore, more extensive studies involving the algorithm with more missing sensors are needed.

2.3 Kalman Filter based Estimation Technique

The literature review on KF based technique is divided into two sub-sections. In one sub-section, literatures related to EKF and Two-Stage EKF are reviewed, while in another sub-section literature related to UKF is reviewed. The literatures related to applications of EKF, Two-Stage EKF and UKF in identification of state and parameters of different types of buildings are included.

2.3.1 The Extended Kalman Filter and Two-Stage Extended Kalman Filter

In the last few decades, the KF or specially the EKF gained a huge popularity amongst researchers. The EKF has the ability to identify both the state and parameter simultaneously from recorded time histories. There were extensive uses of this identification scheme for the evaluation of state and parameter of conventional fixed base multi-storeyed buildings, base isolated buildings as well as isolators itself. However, as the dimension of the structure increases, issues such as divergence of results crept up. An alternative approach was introduced in which state and parameters were identified separately and in sequence, which is called as Two-Stage EKF. A brief literature review about the EKF and Two-Stage EKF is furnished below.

Hoshiya and Saito [1984] applied EKF to the SI of structural systems under the influence of seismic excitation. In order to obtain the stable and convergent solutions, a weighted global iterative procedure with an objective function was proposed, which was incorporated into the EKF algorithm. For the effectiveness of this proposal, the identification problems were investigated for linear multiple DOF systems, bilinear hysteretic systems and equivalent linearization of bilinear hysteretic systems.

Tan and Chen [1988] used EKF for both state and parameter estimation of a nonlinear three-storey shear building. To identify the system, a two-stage iterative procedure was used. The filtering technique was introduced on an equivalent linear system to estimate certain parameters. Using those estimated parameter values, the filtering technique was further extended to hysteretic system.

Hoshiya and Sutoh [1992] proposed an algorithm which is known as weighted local iteration method for structural SI using EKF. In this algorithm, the state vectors were identified iteratively for a fixed number of loops. An initial estimate of state vector, covariance and noise covariance matrix were assumed. EKF was used to find the updated state and covariance matrix at the end of specified number of iteration loops. To achieve good convergence, the updated covariance matrix was weighted with arbitrary weighing factor in order to disturb the covariance. There is however no guidelines provided in choosing the weighing factor, except that it should be greater than one. After the end of iteration, a test of convergence was carried out in order to minimize a selected objective function. The objective function was defined as the ratio of sum of squares of errors in observation, which is the ratio of sum of squares of differences between the observed values and predicted values to the sum of squares of observed values for fix numbers of observation data. Identification of a linear SDOF system was carried out using this method. The performance of the algorithm in respect of its capability of identifying parameters and also the stability of algorithm is doubtful since 1) initial conditions were arbitrarily assigned and 2) use of Taylor's series expansion for linearization.

Yang *et al.* [2006a] proposed an adaptive scheme using EKF to track the damage in a structure. Analytical studies were conducted using simulated output response to validate the adaptive algorithm. An adaptive factor matrix was used to track the variation of parameters when the structure sustained damages. The solution of the adaptive factor matrix was determined using constraint optimization technique. Studies were carried out to identify simulated damage on a SDOF nonlinear hysteretic structure, two-storey hysteretic structure and five-storey linear structure.

Yang *et al.* [2007a] developed an algorithm using EKF to identify the unknown input excitation with known output responses. The unknown input could be either ground excitation or any external excitation on any part of the structure. The adaptive part of the algorithm has the ability to identify the changes in structural parameters like degradation of stiffness etc., whenever damage occurs. The algorithm was verified by simulation result obtained from 3-DOF nonlinear elastic building, 3-DOF hysteretic building and ASCE phase I benchmark structure. The derivation of the equations to take into account the unknown input is however quite cumbersome and complex.

Yang *et al.* [2008] made an attempt to experimentally validate the adaptive EKF, as proposed by Yang *et al.* [2006a] for identification of structural damage. A three-storey shear frame

building was created in the laboratory and fitted with an innovative device which could reduce the storey stiffness at a predefined time during the experiment, thus experimentally simulating structural damage during experiment. The algorithm was used using the output response from all the floors and known input ground excitation and good results were obtained.

In EKF, a single vector called the extended state vector, which is a combination of both unknown state and parameter, is evaluated. It was observed that due its large size, there is computational convergence difficulty while handling large number of nonlinear structural parameters in limited sensor scenario. In order to overcome this problem, Lei and Jiang [2011] proposed an algorithm by separately identifying the state and parameter at each step using EKF. This approach reduced the execution time of the algorithm. To demonstrate the effectiveness of the proposed approach, state and parameters identification of a numerically simulated 6-storey hysteretic shear building was carried out. It was observed that the proposed scheme has the ability to handle large number of nonlinear structural parameters.

Ying *et al.*[2012] proposed an algorithm for identification of nonlinear time invariant structural parameters under limited input and output measurement. The algorithm is based on the implementation of EKF for identification of nonlinear structural parameters. LSE was used for identification of unknown input excitation. The conditions under which this scheme is applicable are: (i) the number of output measurements is larger than that of unknown excitation; (ii) measurement sensors are available at the DOF's where external excitation acts. The algorithm was also extended to identify large size nonlinear structural system using sub-structure approach. The force at the interface of the substructure was treated as additional unknown input. The additional unknown input can be estimated even when responses of the DOF's at substructure interfaces were not available. The capability of the algorithm in identifying the nonlinear structural parameters under limited input and output measurement was demonstrated using numerical examples of 4-storey and 8-storey hysteretic shear buildings.

The traditional EKF contains the unknown state vector and parametric vector, thus the extended unknown vector becomes quite large which possess difficulty in convergence for large scale structure with many DOF's. To simplify the process, Lei et al. [2015] proposed a Two-Stage EKF to identify the nonlinear structural parameters as well as the unknown state vector in two steps. In the first step, the unknown parametric vectors are identified using EKF and under the assumption that the state vectors are known. In the second step, the state

vectors are identified from the identified parametric vector of first step and using EKF approach. The second time step starts with the identified parameters and state vector of previous step. The advantage of the Two-Stage Kalman filter is that the number of unknown parameters gets reduced. The algorithm is applicable for 1) time-invariant system, 2) known external excitation and 3) low level of non-linearity.

From the literature review on KF based techniques, it is observed that EKF has been extensively used by research community for identifying both state and parameter of structures. Initially researchers faced the problem of convergence related issues. To solve this, weighted iteration techniques were employed by many researchers. However, there was the problem of selection of weight as there were no guidelines in this matter. Other technique employed was that the parameter was identified separately by modifying the governing equation of motion. However, this did not produce any fruitful results as velocity and displacement had to be found out by direct integration which resulted in drift of identified displacement. Due to the issues related to computational convergence in handling large data, two-stage Kalman Filter came into existence.

Literature review shows that various studies on identification of state and parameters using EKF and Two-Stage EKF have been performed on linear SDOF, MDOF as well as nonlinear hysteretic fixed base building systems. However, elaborate studies related to lack of missing sensors cases are not observed.

2.3.2 The Unscented Kalman Filter

KF was extensively used for various purposes such as target tracking and estimation. The algorithm is simple, robust and demonstrated optimal performance and thus became a popular choice. However, Kalman Filer is applicable only for linear systems. In order to apply KF for nonlinear systems, the nonlinearity is locally linearized using Taylor's series expansion of the nonlinear function. This modified version of linear KF for nonlinear systems is called the EKF. In EKF, only the first order derivative of Taylor's series expansion is considered while second and higher order derivatives are ignored. During evaluation of Taylor's series, Jacobian matrix needs to be derived and hence it is a cumbersome process. Sometimes, the nonlinear function may not be differentiable at certain points leading to errors or issues related to convergence. Further, convergence issues may also arise in case of large dimension of a problem. To overcome these problems, UKF came into picture. UKF was introduced by Julier and Uhlmann [1997a].

The UKF is superior to EKF as in UKF linearization is avoided and therefore Jacobians are not required. Further, the noise source need not be Gaussian. The fundamental idea of UKF lies in Unscented Transforms (UT). UT and KF are combined to form UKF. A brief literature review of evolution of unscented transform and its gradual intervention into the identification of civil engineering structures is furnished in the following paragraphs.

In the UT, a set of sample points called sigma point are created for each of the parameters of the extended state vector containing the state and parameters to be identified. The sigma points are selected deterministically and some specific weights are assigned to them. This sigma point matrix is passed through the nonlinear function and thereby, transformed sigma points matrix is created and finally the mean and covariance of the transformed parameters of the vector are calculated from the specified weights of the sigma points. The critical issues regarding the number of sigma points to be selected, or their assigned weights were addressed using a criteria that the points should be so chosen that it should capture the most important or desired property of the parameter under consideration. To capture the moment upto n^{th} order is something like matching the Taylor's series expansion upto n^{th} order. The literature discusses about the distribution of sigma points to capture the 2^{nd} and 4^{th} order moment by showing the example of coordinate transformation from polar to Cartesian coordinate system. Further, the 4^{th} order filter was used to demonstrate a navigation problem and results were compared to show the better performance of 4^{th} order filter. The use of 2^{nd} and 4^{th} order in UT was intended to capture certain specific property of a random distribution. However, the 3^{rd} order or skew is missed out.

Julier [1998] proposed a procedure to determine sigma points so that skew or asymmetry of the distribution gets captured. The example problem considered was that of tracking a body re-entering the earth's atmosphere at a very high altitude and at high velocity. For this re-entry problem, the nonlinearity is very high due to the huge amount of drag force encountered by the falling body as it penetrates the progressively denser air media of the earth's atmosphere. The drag force is proportional to square of the velocity. It was stated that as the nonlinearity was sufficiently large, the EKF algorithm could not be used. It was stressed that the prediction of both the mean and covariance must be accurate to the second order and this could be achieved by using UT. The uncertainty in both the ballistic coefficient and velocity led to a highly non-symmetric distribution. To capture the skew in unscented transform algorithm, three different types of sigma shapes were introduced. The effectiveness of using the skew to capture information about the asymmetry was examined. The UT was devised to

capture the mean, covariance and skew. It was found that by introduction of skew capturing method, there was little change in performance as the skew was extremely small.

Merwe and Wan [2001] introduced the square-root UKF (SR-UKF) to overcome the drawbacks of EKF approach. This approach results in third order (Taylor's series) approximation for Gaussian inputs and at least second order accuracy for non-Gaussian inputs. The performances of EKF, UKF and SR-UKF were compared and it was found that SR-UKF is about 20% faster than UKF and about 10% faster than EKF.

Julier and Uhlmann [2002a] introduced the scaled UT. As the dimension of the state space increases, the spread of the sigma points increases as well, this introduces error in capturing mean and covariance. The conventional UT overcame this problem by using weights having values which are positive, zero or negative. When the weight is zero, it causes the sigma point to scale to origin, so the mean is evaluated up to second order accuracy, but negative weight can lead to non-positive semi definite covariance matrix. A correction term was used to tackle this problem. However, use of this modified covariance matrix lacks physical intuition and is applicable only for symmetric unscented transform and its applicability to other sigma points are not explored. This problem is tackled by introducing additional scaling parameter. The algorithm is superior to conventional UT in all respects. It is able to retain second order accuracy in both the mean and covariance. It was observed that this method is superior to conventional UT for all systems whose dimensionality is greater than three.

Julier and Uhlmann [2002b] proposed a reduced sigma point filter for the UT. The numbers of sigma points were reduced from $(2n+1)$ to $(n+2)$ for problem with n^{th} dimension. The need for reducing the number of sigma points is to achieve high computational speed. The computational cost of UT is directly proportional to the number of sigma points used. The resulting algorithm has the same capacity as that of truncated 2^{nd} order filter, but the derivatives are not required to be calculated. The algorithm also takes into account the skew of the sigma point distribution.

The unscented filter by Julier and Uhlmann [1997a] matches up to the fifth order moment of the input variable, whereas the transformed covariance introduces errors at the fourth and higher orders of a Taylor series expansion. To match any desirable higher order input moment, Tenne and Singh [2003] proposed a modified σ-set. The HOUF consists of an augmented σ-set with separate weights. This results in higher order approximation of the transformed covariance. This was demonstrated by an example with varied degree of

nonlinearity. The 2-σ HOUF can match up to eighth central moment and 3-σ HOUF can match up to 12^{th} order moment.

Wu and Smyth [2007] made a comparative study by identifying the nonlinear structural parameters using EKF and UKF algorithm. Comparisons of results obtained from both the algorithms were done using three case studies. A single degree of freedom nonlinear hysteretic system, a 2-DOF linear structural system and a 2-DOF nonlinear structural system were considered. Percentage estimation error for structural parameters were evaluated and compared with both UKF and EKF for 1%, 2% and 5% noise level. It was found that the performance of both UKF and EKF were equally good in case of weak nonlinearity. In case of high nonlinearity, the UKF was observed to be performing better than EKF. It was also found that UKF was more robust to handle measurement noise than EKF. The UKF procedure has the advantage that it is applicable to non-differential functions.

Xie and Feng [2012] proposed a new technique for identification of nonlinear structural parameters using UKF. The new technique was named as iterated unscented KF (IUKF). The IUKF is same as UKF, but iterations are performed in each step to meet certain convergence criteria. Studies were conducted on a single DOF nonlinear hysteretic system, 2-DOF linear structural system and two-storey nonlinear elastic system. It was concluded that the performance of IUKF is comparable to UKF in weak nonlinearity, while in highly nonlinear cases, IUKF performed better than UKF. Further, IUKF was found to be robust in handling noises.

Bisht and Singh [2014] proposed a technique to track sudden changes in parameters during identification procedure. For achieving this objective of parameter tracking, a modification was carried out in the conventional UKF. The algorithm first detects the sudden changes and then quickly adapts to track parameter values. As the UKF tracking nears convergence, the error in the estimated measurements, also referred to as the innovation and its covariance successively become small. However, any sudden change in parameters causes the value of innovation to increase. To capture this change, a parameter β was used. A threshold value was selected. Any value of β greater than the threshold would raise an alarm indicating sudden changes in the structural parameter. Once a sudden change is identified, the diagonal value of the covariance matrix is increased by certain amount only for the corresponding structural parameter which has shown a sudden change. This was done to indicate reduced confidence in the estimated value.

In this sub-section on the literature review of UKF, it is observed that UKF is superior to EKF as higher order terms due to linearization are included within the UKF algorithm. The superiority of the algorithm can also be observed in its less computational burden, since no Jacobians are needed to be evaluated. Some of the initial literatures were concerned about the incorporation of 2^{nd} and higher order terms of Taylor series expansion and various comparative results were demonstrated related to the inclusion or exclusion of higher order terms and skew terms. These were mainly concerned with the unscented transformation part. UKF is a combination of unscented transform with that of KF. UKF has been applied by various researchers for structural identification problem. Comparative study of EKF and UKF in identifying the state and parameter of SDOF nonlinear hysteretic structure, 2-DOF linear and nonlinear structure using different noise level were reported in literature. Some literature used iterative schemes combined with UKF for better convergence. Adaptive version of UKF is applied by various researchers to track time-varying parameter to detect occurrence of damage. There are also literatures which used modified version of UKF called CUKF to constrain the parameters of UKF or their corresponding sigma point within a bounded limit. However, there is no literature which deals with the comparative study of all the considered algorithms applied to fixed base building combined with impact of varying noise levels and influence of missing sensors.

2.4 Application of identification techniques for evaluation of parameters of mathematical model representing seismic base isolation system

Base isolators are used to reduce the transfer of seismic effects to the superstructure. Base isolators are placed in between the foundation and superstructure. Generally, SREI are used as base isolators in base isolated buildings. A mathematical model is a primary requirement for SI of either the isolator or base isolated building system. There are various literatures which deal with identification of state and parameter of base isolated system. Application of the identification algorithms like SNLSE-UI-UO, EKF, Two Stage EKF and UKF on simulated or experimental model of base isolated building system using SREI has been reported in literature. A brief review of literature is presented in this section.

Zhang *et al.* [2003] carried out an extensive study on the parameter identification of Bouc-Wen model. The classical Bouc-Wen model contains only five loop parameters. The generalized differential model contains thirteen parameters and it can account for strength degradation, stiffness degradation and even pinching characteristics of an inelastic structure. It was found that some parameters of the model were functionally redundant. Transformation

was performed in parameter space to reduce the number of parameters for simplifying the model. Parameter sensitivity analysis, which includes local and global sensitivity analysis, was performed using a large parameter set and Monte-Carlo simulation to determine the parameters which were highly sensitive. The sensitivity analysis was performed by repeatedly varying one parameter at a time keeping other parameter at chosen nominal value. Thus during identification process, these non-sensitive parameters was fixed as a constant value and sensitive parameters were identified.

Yang and Huang [2006] used SNLSE-UI-UO for damage tracking and identification of base isolated structure. This technique was used to identify the damage in the inelastic rubber-bearing isolation system. The accuracy and effectiveness of the proposed scheme were demonstrated using an 8-story base-isolated building using simulation results. Bouc-Wen model was used to model the nonlinear behaviour of the rubber base isolator.

Yin *et al.* [2010] used SNLSE technique to identify both the state and parameter of rubber bearing isolator. Standard Bouc-Wen model was used to model the rubber isolator. Due to the involvement of large number of parameters to be identified including the structural parameters like damping, stiffness as well as hysteretic parameter β and γ, the process becomes cumbersome. A simplified approach was adopted wherein parameter sensitivity analysis was performed. The error obtained by varying a particular parameter, keeping other parameters constant was obtained in the form of *spider diagram.* The parameter which is insensitive was kept constant and the parameter which is highly sensitive was identified using SNLSE, by the procedure as suggested by Yang *et al.* [2006] for time invariant case. The effectiveness of the procedure was demonstrated by considering SDOF system with the rubber isolator. The system was excited by seismic ground acceleration for identification and response corrupted with white noise was used.

Yang [2014] proposed an improved adaptive SNLSE algorithm (ASNLSE-UI) with unknown input applied to real-time tracking of any changes in structural parameters during base excitation. The effectiveness of the algorithm was demonstrated using a laboratory based 3-storey base isolated building. The base isolator was modelled using standard Bouc-Wen model. Degradation and pinching were not considered and the building was modelled as shear frame building. Online damage or change in stiffness during the time history was simulated by using a special device fitted within the building.

Zhang and Lin [1994] made an extensive study on the effect of identification of parameter of nonlinear hysteretic SDOF system by adopting different initial estimates, noise covariance and the weighing factor using the weighted iteration scheme based on EKF algorithm as proposed by Hoshiya and Sutoh [1992]. As no guidelines were available in selection of the weighing parameter, different arbitrary values were randomly selected and their effects in identification were determined. Similarly, for noise covariance matrix, a diagonal covariance matrix was selected with the diagonal terms containing a scaled variance of the state vector.

Recently, FREI has evolved to be a low cost viable alternative to SREI, especially for low-rise masonry building. Both SREI and FREI have a common material and that is the elastomer. In order to provide adequate vertical stiffness to soft elastomer in SREI, elastomer / rubber layers are interleaved with thin steel reinforcing plates. Thus, the weight of the bearing is increased due to the presence of steel plates and the manufacturing process is also costlier. In FREI, steel plates of SREI are replaced by bi-directionally oriented fibres, thereby reducing the weight and cost of the isolators. The fibre reinforcements are lighter and have similar mechanical properties in tension, thereby retaining large vertical stiffness. FREI can be further classified into two categories depending upon whether two ends of FREI's are connected to sub-structure and super-structure and are named as Bonded FREI (B-FREI) and Un-bonded FREI (U-FREI). In bonded application, the top and bottom surfaces of the bearing are attached or bonded to the top super-structure and bottom sub-structure and such FREI's never lose contact, whereas in un-bonded application the top and bottom surfaces of the bearing may lose contact with super and sub-structure depending on the severity of excitation. Masonry buildings are very vulnerable to seismic activities and often we hear about the devastating effects of earthquakes on such types of building located in high seismic zones. In developing countries, low-rise masonry structures are quite common and earthquake induced calamities indirectly affect the life and economic progress in a big way. FREI is a very pertinent low-cost substitute for base isolation of such types of low-rise masonry buildings. Considering its advantages and area of application, a number of researches are being carried out worldwide to study the different aspects of these isolators. Base isolation, especially by using FREI has recently received attention in spite of the fact that base-isolation technology using convention or other methods is in vogue for the last three decades.

Further, a brief review of existing literature on effectiveness of FREI in seismic isolation of FREI supported structures are presented.

Toopchi-Nezhad *et al.* [2008a] made an extensive experimental study on carbon fibre based FREIs from which the mechanical properties of the bearings, including displacement characteristics and damping values were evaluated. FREIs have significant potential of application in generally low rise buildings for seismic mitigation. FREIs have several advantages over traditional SREIs including superior damping properties, lower manufacturing cost, light weight, and the possibility of being produced in long rectangular strips with individual isolators cut to the required size. From the results of the experimental test conducted, it was suggested that the FREI can be viable alternative for the base isolation of ordinary low-rise buildings.

Das *et al.* [2014] performed an analysis of the square FREI by modelling the FREI using 3D finite element model subjected to cyclic horizontal displacement under constant vertical loading. Both bonded and Un-Bonded FREI was considered in the model. Investigation was made regarding effectiveness of FREI's in mitigating seismic effects. It was observed that at high displacement level un-bonded FREI performed better that bonded FREI in respect of seismic isolation. Study was also conducted to evaluate the performance of the isolators placed at 0 degree and 45 degrees. It was observed that FREI's placed at 45 degrees to horizontal loading direction had higher initial stiffness than that placed at 0 degree. The result obtained from the FEM model was in good agreement with that of experimental results.

Das *et al.* [2016a] performed a shake table test of a $1/5^{th}$ scaled masonry building for both fixed base and base isolated system. For fixed base system the base of the building was directly attached to the shake table and for base isolated system, four numbers of FREI isolators were placed in between the shake table and base of the building. The test was conducted for unbounded condition of FREI. A comparative study of the dynamic responses of the structure was carried out for both fixed base and base isolated system. It was observed that the FREI isolators are very effective in reducing the base excitation and it was concluded that FREI is a suitable alternative to tradition SREI. Further, FREI can also be treated as a cheap viable substitute to costly SREI and applicable to low rise masonry building.

Das *et al.* [2016b] made a comparative study on the seismic responses obtained from experimental and numerical model of an unreinforced brick masonry building supported on unbounded FREI isolators which was of in-house design. The experimental building was fully instrumented to measure accelerations and displacements at different floor levels. The FREI was modelled as multi-linear pivot hysteretic plasticity model and plate element were used for the masonry building walls. The analysis was carried out using SAP2000 software.

The parameters of the FREI model was evaluated from the force-displacement test results. It was observed that the simulated responses from the numerical model agreed well with that of experimental model and it was concluded that the numerical model can be used to evaluate responses with quite reasonable degree of accuracy.

Thuyet *et al.* [2017b] evaluated the horizontal stiffness of FREI for both the cases of bonded and unbonded application. Experimental, numerical as well as analytical studies were conducted on three different sizes of FREIs. For numerical studies, 3D FE model for the FREIs were developed. Experimental studies were conducted by subjecting the FREIs to cyclic horizontal displacement. In the numerical study, the cyclic displacement was continued beyond rollover deformation. The stiffness was evaluated using analytical formula on the basis of the results obtained from both numerical and experimental studies and was found to be in good agreement. It was concluded that stiffness can be evaluated with reasonable accuracy using a numerical model of FREI.

Thuyet *et al.* [2018] performed a seismic vulnerability assessment on a numerically simulated two-storeyed stone masonry building supported on U-FREIs. The numerical model of the prototype building, which is located in Tawang, India, was modelled using SAP2000 software. Isolators were modelled as bilinear model using link elements. The properties of the isolator model were obtained from the backbone curve obtained from cyclic force-displacement tests. Using the numerical analysis, the effectiveness of the FREIs in reducing the seismic vulnerability of stone masonry building was established.

Additionally, literature related to modelling strategies of FREI for FREI supported structures are briefly reviewed and presented.

Chen and Ahmadi [1992] studied the sensitivity of base-isolated structures due to the effect of wind. 3rd order polynomial was adopted to model the hysteretic behaviour of high damping rubber bearing.

Toopchi-Nezhad *et al.* [2008b] performed time-history analysis on a two storey masonry shear wall type structure, supported on fixed base and another on U-FREI bearing. A 5th order polynomial combined with Bouc-Wen hysteresis was used to model the isolator. Simulations were performed to compare with the experimentally evaluated lateral load displacement properties of the bearing. Analytical results indicated that the SU-FREI bearings can effectively decrease the seismic demand on typical low-rise buildings constructed in high seismic risk region.

Sireteanu *et al.* [2010] proposed a Genetic Algorithm scheme to identify the parameters of extended Bouc-Wen model from experimental hysteretic loops obtained from laboratory force-displacement test. Since conventional Bouc-Wen model has the inability to take into account the softening regime followed by stiffening regime exhibited by FREIs, the extended Bouc-Wen model was to match the properties of experimental hysteretic loops. Illustrative demonstration of the approach was made on two types of seismic protection devices with hysteretic characteristics: 1) elastomeric base isolators and 2) buckling restrained dissipative braces. Numerical simulation of a three storey building was performed using this model and efficiency of the base isolators using FREIs was highlighted in reducing the seismic response of the structure.

Love *et al.* [2011] investigated the use of a tuned liquid damper as a cost effective method to reduce the wind induced vibrations of base isolated structures. FREI was used to model the base isolated structure containing the Tuned liquid damper. To model the softening behaviour of SU-FREI the cubic polynomial model as proposed by Chen and Ahmadi [1992] was initially adopted. However, the SU-FREIs, were shown to experience softening followed by hardening. To accommodate this isolator behaviour, a fifth order polynomial to model was proposed.

Manzoori and Nezhad [2017] developed an extended Bouc-Wen model to model the SU-FREI. The Extended Bouc-Wen model was used to characterize the gradual softening followed by stiffening. The presented model is a modified version of that suggested by Chen and Ahmadi [1992]. Under shear load, unbounded-FREI exhibited rollover deformation. It is a condition in which some part of top and bottom contact surface looses contact from support. Rollover deformation occurs due to unbounded boundary condition. As a result of rollover deformation, the effective lateral stiffness of isolator is decreased. At ultimate rollover deformation, the vertical surface completely comes in contact with the top and bottom support and thus exhibits stiffening regime. The third order polynomial equation as proposed by Chen and Ahmadi [1992] could not capture the stiffening regime following the gradual softening regime. A fifth order polynomial as proposed by Love *et al.* [2011] was used to replace the 3rd order polynomial. The constant coefficients of the model were determined by global fitting of the model to the experimental hysteresis loop of the isolator. To validate the proposed model, responses was simulated for a base-isolated building and compared with result of previous shake table test results. It was concluded that the proposed Extended Bouc-Wen model is robust and reasonably accurate for seismic analysis of U-FREIs.

It has been observed from the review of literature that there exist several studies towards SI on base isolated structures, using the two variants of RLSE such as SNLSE and SNLSE-UI-UO. In all the studies, SREI has been used as base isolator. Further, it has been observed that SREI has been modelled using Bouc-Wen hysteresis model. The effectiveness of the identification scheme was demonstrated using simulated and experimental base isolated building systems.

From the above section on literature review of LSE and KF based estimation technique, it has been observed that the application of SI algorithms were only limited to base-isolated building supported on SREI. No such literature is found which dealt with the identification of base-isolated structural system supported on FREI. Available literatures on FREIs mainly deal with its effectiveness in seismic mitigation. The isolation capacity of the FREIs has been demonstrated using different analytical and 3D FEM modelling strategies. In the present work, the most appropriate model for representation of behaviour of FREI is considered from existing, since in any SI algorithm, a mathematical model is the primary requirement. Amongst the analytical models, 1) modified form of Bouc-Wen model, 2) bilinear link model and 3) multi-linear pivot hysteretic plasticity model have been found in literature. The standard Bouc-Wen model has been observed to be suitable for representing the hysteretic behaviour of SREI. The hysteretic behaviour of FREIs has been found to be different from that of SREIs. Literature survey reveals the existence of different models based on modified version of standard Bouc-Wen model for representing the FREIs. The parameters of the model have been found to be obtained by using curve fitting method from the laboratory based force displacement test. Use of genetic algorithms towards parameter evaluation has also been reported in literature.

There are various other researches based on finite element modelling and analysis of FREI for both bonded and unbounded cases, design aspect consideration of FREI, impact of loading direction of FREI etc; but extensive literature survey considering these aspects is not carried out over here as they are not relevant to this present study.

2.5 Concluding Remarks

Literature review of LSE based algorithms reveals that although experimental or analytical studies were performed considering limited sensor, but the study with more than one missing sensor is not reported. Further, studies on influence of varying level of noise on the performance of these algorithms are also missing. Applications of these algorithms of SI on

real life buildings under service condition combined with missing sensors are not available in literatures.

Literature survey reveals the absence of comparative study using EKF, Two-Stage EKF and UKF, taken together, on state and parameter identification of fixed-base and base-isolated building systems supported on SREI.

There are literatures which deal with comparative studies on the performances of the EKF and UKF algorithms but no literature has been found towards holistic approach to SI using algorithms like SNLSE-UI-UO, EKF, Two-Stage EKF and UKF.

There are literatures which deal with the evaluation of parameters of model representing FREI using curve fitting technique with the data obtained from laboratory based force displacement test. However, no literature has been found which evaluates states and parameters of FREI using vibration response from FREI supported build.

Chapter 3

Review of formulation of different considered existing identification schemes

3.1 Introduction

In this section, detailed discussions on some of the considered existing identification schemes are made. The mathematical background, advantages and disadvantages of different such schemes are presented. The considered identification schemes essentially belong to two categories as least square based identification scheme and Kalman Filter based identification schemes.

Detailed and complete step by step derivation of these considered algorithms are presented in this thesis so that a better understanding can be achieved regarding the underlying principles of each scheme and how does each scheme differ from the other. The derivation of Least Square Estimate (LSE) is shown by starting the derivation from scratch and presented in a form which is quite intuitive. The derivation of Recursive Least Square Estimate (RLSE) is based on the derivation of LSE and therefore continuity is observed in deriving the RLSE. The Sequential Nonlinear Least Square Estimate (SNLSE), in which state and parameter of the structure are obtained separately and sequentially, was developed by Yang *et al.* (2006). In the present study, the SNLSE algorithm is derived in a different manner by bringing parity between RLSE and SNLSE so that the formulation is intuitively appealing and simplified.

Similarly, the derivation of the Kalman Filter (KF) based techniques such as Extended Kalman Filter (EKF), Two-Stage EKF and Unscented Kalman Filter (UKF) are reviewed from different related literatures and presented in a step-by-step simplified form, keeping continuity between each steps. In this work, an attempt is made to present the derivations of all the above mentioned KF based identification schemes in a simplified and lucid manner so that it becomes easily comprehendible. Specific relevant portions of the derivations has been collected from different literatures and presented here in a concise format. These formulations are a step forward towards the problem-specific derivation undertaken for the entire considered problem in this thesis. The different problems considered are: 1) fixed base multi-storeyed building, 2) base isolated multi-storeyed building supported on Steel Reinforced Elastomeric Isolator (SREI) and 3) Fibre Reinforced Elastomeric Isolator (FREI) supported building.

3.2 Least Square Estimation based Approach

Under the Least Square based identification scheme, the following algorithm will be considered in the present study

a) LSE Algorithm.

b) RLSE Algorithm.

c) SNLSE Algorithm.

d) SNLSE-UI-UO Algorithm.

3.2.1 Least Square Estimation (LSE) Algorithm

The LSE is a technique of solving a linear system of equation of the form given by Eq. (3.1). The unknown vector $\boldsymbol{x}$ is solved by minimizing the sum of squares of errors. The formulations shown here have been adopted from the Sayed Ali H. and Kailath Thomas (2000).

$$\breve{\boldsymbol{A}}\boldsymbol{x} = \breve{\boldsymbol{b}} \tag{3.1}$$

The problem is primarily a filter design problem, wherein the filter $\breve{\boldsymbol{h}}$ is needed to be determined from given input sequence $\boldsymbol{x}$ to get the desired output sequence $\breve{\boldsymbol{d}}$ by minimizing the error $\boldsymbol{e}$.

The model is given by Eq.(3.2).

$$\breve{\boldsymbol{d}}[\breve{n}] = \sum_{k=0}^{\breve{n}_f - 1} \breve{\boldsymbol{h}}[k]\boldsymbol{x}[\breve{n} - k] + \boldsymbol{e}[\breve{n}] \tag{3.2}$$

where, $\breve{n}$ is the total number of input parameters under consideration and $\breve{n}_f$ is the filter length. Thus it is seen that the output is a linear combination of input. Eq. (3.2) and can be rewritten as

$$\begin{aligned}\breve{\boldsymbol{d}}[\breve{n}] = \breve{h}[0].x[\breve{n}] + \breve{h}[1].x[\breve{n}-1] + \breve{h}[2].x[\breve{n}-2] \\ + \cdots \ldots + \breve{h}\left[\breve{n}_f - 1\right].x\left[\breve{n} - \breve{n}_f + 1\right] + e[\breve{n}]\end{aligned} \tag{3.3}$$

In the above equation, Eq. (3.3), the model is known, the input sequence, $\breve{\boldsymbol{x}}[\breve{n}]$ and the desired output sequence, $\breve{\boldsymbol{d}}[\breve{n}]$ are also known. Hence, the problem is to find out the filter vector $\breve{\boldsymbol{h}}[\breve{n}]$ so that the error $\boldsymbol{e}[\breve{n}]$ is minimized.

Re-arranging Eq. (3.2), the error term can be expressed as given in Eq.(3.4).

$$\boldsymbol{e}[\breve{n}] = \breve{\boldsymbol{d}}[\breve{n}] - \sum_{k=0}^{\breve{n}_f - 1} \breve{\boldsymbol{h}}[k]\boldsymbol{x}[\breve{n} - k] \tag{3.4}$$

If the first $\breve{n}_e$ errors are only considered, then n_1=0 and $n_2 = \breve{n}_e - 1$, $\breve{n}_f$ is the filter length.

$$\begin{Bmatrix} e[0] \\ e[1] \\ e[2] \\ \vdots \\ e[\breve{n}_e - 1] \end{Bmatrix} = \begin{Bmatrix} \breve{d}[0] \\ \breve{d}[1] \\ \breve{d}[2] \\ \vdots \\ \breve{d}[\breve{n}_e - 1] \end{Bmatrix} - \begin{bmatrix} x[0] & x[-1] & x[-2] & \dots & x[-\breve{n}_f + 1] \\ x[1] & x[0] & x[-1] & \cdots & x[-\breve{n}_f + 2] \\ x[2] & x[1] & x[0] & \cdots & x[-\breve{n}_f + 3] \\ \vdots & \vdots & \vdots & \dots & \vdots \\ x[\breve{n}_e - 1] & x[\breve{n}_e - 2] & x[\breve{n}_e - 3] & \dots & x[\breve{n}_e - \breve{n}_f] \end{bmatrix} \begin{Bmatrix} \breve{h}[0] \\ \breve{h}[1] \\ \breve{h}[2] \\ \vdots \\ \breve{h}[\breve{n}_f - 1] \end{Bmatrix} \tag{3.5}$$

Eq. (3.5) is of the form shown in Eq. (3.6).

$$\boldsymbol{e} = \breve{\boldsymbol{d}} - \breve{\boldsymbol{A}}\, x\, \breve{\boldsymbol{h}} \tag{3.6}$$

where, $\boldsymbol{e} = \breve{n}_e\, x\, 1$ vector, $\breve{\boldsymbol{d}} = \breve{n}_e\, x\, 1$ vector, $\breve{\boldsymbol{A}} = \breve{n}_f\, x\, \breve{n}_e$ matrix and $\breve{\boldsymbol{h}} = \breve{n}_f x 1$ vector. Minimizing the square of the error or norm-2 is obtained as

$$\begin{aligned} \|\boldsymbol{e}\|_2^2 = \left\|\breve{\boldsymbol{d}} - \breve{\boldsymbol{A}}\breve{\boldsymbol{h}}\right\|_2^2 &= \left(\breve{\boldsymbol{d}} - \breve{\boldsymbol{A}}\breve{\boldsymbol{h}}\right)^T \left(\breve{\boldsymbol{d}} - \breve{\boldsymbol{A}}\breve{\boldsymbol{h}}\right) \\ &= \breve{\boldsymbol{d}}^T\breve{\boldsymbol{d}} - \breve{\boldsymbol{h}}^T\breve{\boldsymbol{A}}^T\breve{\boldsymbol{d}} - \breve{\boldsymbol{d}}^T\breve{\boldsymbol{A}}\breve{\boldsymbol{h}} + \breve{\boldsymbol{h}}^T\breve{\boldsymbol{A}}^T\breve{\boldsymbol{A}}\breve{\boldsymbol{h}} \end{aligned} \tag{3.7}$$

Eq. (3.8) is obtained by putting $\frac{d\|\boldsymbol{e}\|_2^2}{d\breve{\boldsymbol{h}}} = 0$, in Eq. (3.7),

$$\frac{d\|\boldsymbol{e}\|_2^2}{d\breve{\boldsymbol{h}}} = -2\breve{\boldsymbol{A}}^T\breve{\boldsymbol{d}} + 2\breve{\boldsymbol{A}}^T\breve{\boldsymbol{A}}\breve{\boldsymbol{h}} = 0 \tag{3.8}$$

$$\Rightarrow \breve{\boldsymbol{A}}^T\breve{\boldsymbol{A}}\breve{\boldsymbol{h}} = \breve{\boldsymbol{A}}^T\breve{\boldsymbol{d}}$$

$$\Rightarrow \breve{\boldsymbol{h}}^* = \left(\breve{\boldsymbol{A}}^T\breve{\boldsymbol{A}}\right)^{-1}\breve{\boldsymbol{A}}^T\breve{\boldsymbol{d}} = \breve{\boldsymbol{A}}^+\breve{\boldsymbol{d}} \tag{3.9}$$

where, $\breve{\boldsymbol{h}}^*$ is the best estimate of $\breve{\boldsymbol{h}}$ and $\breve{\boldsymbol{A}}^+$ is the pseudo inverse of $\breve{\boldsymbol{A}}$. The error $\left(\breve{\boldsymbol{d}} - \breve{\boldsymbol{A}}\breve{\boldsymbol{h}}\right)$is orthogonal to the column spaces of $\breve{\boldsymbol{A}}$ and is shown in Fig. 3.1.

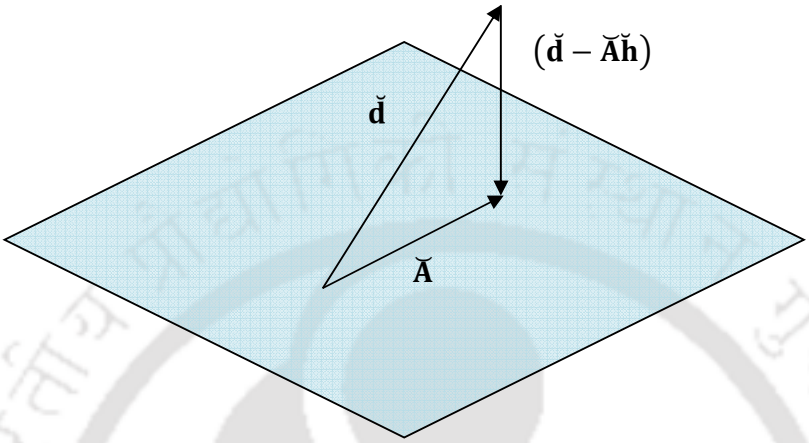

Fig. 3.1: Representation of Least Square Estimate

From the above formulation it is clear that LSE is a procedure in which sum of the squares of the error in observation is minimized to get the desired output. In order to achieve this, a coefficient vector, also known as filter, is evaluated.

3.2.2 Recursive Least Square Estimation (RLSE) Algorithm

RLSE is a continuation of LSE but the two techniques differ in their approach. In LSE, for every future time step, solution has to be performed by taking all the input measurements from beginning of time and up to current time step. Whereas, RLSE is solved by considering only the current input measurement. The sequence of formulation that leads to final solution of RLSE is performed by continuing from LSE formulation as shown below. The formulations are in line with that presented by Sayed Ali H. and Kailath Thomas (2000).

The matrix $\boldsymbol{A}$ is obtained from Eq. (3.5) and Eq. (3.6)

$$\breve{\boldsymbol{A}}^T\breve{\boldsymbol{A}} = \begin{bmatrix} x[0] & x[1] & x[2] & \dots & x[\breve{n}_e - 1] \\ x[-1] & x[0] & x[1] & \cdots & x[\breve{n}_e - 2] \\ x[-2] & x[-1] & x[0] & \cdots & x[\breve{n}_e - 3] \\ \vdots & \vdots & \vdots & \dots & \vdots \\ x[-\breve{n}_e + 1] & x[-\breve{n}_e + 2] & x[-\breve{n}_e + 3] & \dots & x[\breve{n}_e - \breve{n}_f] \end{bmatrix}$$

$$* \begin{bmatrix} x[0] & x[-1] & x[-2] & \dots & x[-\breve{n}_f + 1] \\ x[1] & x[0] & x[-1] & \cdots & x[-\breve{n}_f + 2] \\ x[2] & x[1] & x[0] & \cdots & x[-\breve{n}_f + 3] \\ \vdots & \vdots & \vdots & \dots & \vdots \\ x[\breve{n}_e - 1] & x[\breve{n}_e - 2] & x[\breve{n}_e - 3] & \dots & x[\breve{n}_e - \breve{n}_f] \end{bmatrix}$$

$$= \sum_{i=0}^{\breve{n}_e - 1} \hat{\boldsymbol{u}}_i \hat{\boldsymbol{u}}_i^T \tag{3.10}$$

Therefore,

$$\breve{\boldsymbol{A}}^T\breve{\boldsymbol{A}} = \begin{bmatrix} x(0)^2 + x(1)^2 + \dots . + x(\breve{n}_e - 1)^2 \approx \breve{n}_e \boldsymbol{r}(0) \\ x(-1)x(0) + x(0)x(1) + \cdots + x(\breve{n}_e - 2)x(\breve{n}_e - 1) \approx \breve{n}_e \boldsymbol{r}(1) \\ x(-2)x(0) + x(-1)x(1) + \cdots + x(\breve{n}_e - 3)x(\breve{n}_e - 1) \approx \breve{n}_e \boldsymbol{r}(2) \\ \vdots \end{bmatrix} \tag{3.11}$$

where, $\boldsymbol{r}(0)$ is auto correlation with lag zero, $\boldsymbol{r}(1)$ is auto correlation with lag one and $\boldsymbol{r}(2)$ is auto correlation with lag two and so on. From Eq. (3.11) it is observed that this is an underlying auto regressive process.

Eq. (3.12) is obtained from the least square formulation (LSE) of Eq. (3.9) as

$$\breve{\boldsymbol{h}}_k^* = \left(\breve{\boldsymbol{A}}_k^T\breve{\boldsymbol{A}}_k\right)^{-1}\breve{\boldsymbol{A}}_k^T\breve{\boldsymbol{d}}_k \tag{3.12}$$

Eq. (3.12) is the equation for LSE up to time step k

$$\breve{\boldsymbol{h}}_{k+1}^* = \left(\breve{\boldsymbol{A}}_{k+1}^T\breve{\boldsymbol{A}}_{k+1}\right)^{-1}\breve{\boldsymbol{A}}_{k+1}^T\breve{\boldsymbol{d}}_{k+1} \tag{3.13}$$

Eq. (3.13) is the equation for least square estimation up to time step (k+1), that is Eq. (3.13) is the updated least square estimation equation after incorporating the input at time step (k+1). Thus, $\breve{\boldsymbol{h}}_{k+1}^*$ is obtained from $\breve{\boldsymbol{h}}_k^*$ without having to solve the problem from scratch and this is called RLSE.

For the optimal problem at time step (k-1), Eq. (3.12) can be expressed in the form as given below

$$\breve{\boldsymbol{h}}_{k-1}^{*} = \left(\breve{\boldsymbol{A}}_{k-1}^{T}\breve{\boldsymbol{A}}_{k-1}\right)^{-1}\breve{\boldsymbol{A}}_{k-1}^{T}\breve{\boldsymbol{d}}_{k-1} \tag{3.14}$$

or,

$$\breve{\boldsymbol{h}}_{k-1}^{*} = \breve{\boldsymbol{\varphi}}_{k-1}^{-1}\breve{\boldsymbol{z}}_{k-1} \tag{3.15}$$

where, $\breve{\boldsymbol{\varphi}}_{k-1} = \breve{\boldsymbol{A}}_{k-1}^{T}\breve{\boldsymbol{A}}_{k-1}$ and $\breve{\boldsymbol{z}}_{k-1} = \breve{\boldsymbol{A}}_{k-1}^{T}\breve{\boldsymbol{d}}_{k-1}$

Let $\hat{\boldsymbol{u}}_i = \breve{\boldsymbol{A}}_{k-1}^{T}$ and $\hat{\boldsymbol{u}}_i^{T} = \breve{\boldsymbol{A}}_{k-1}$

where, for $\breve{n}_e$ recent inputs, $\hat{\boldsymbol{u}}_i$ is expressed as

$$\hat{\boldsymbol{u}}_i = [x(i) \quad x(i-1) \quad \ldots \quad x(i-(\breve{n}_e-1))] \tag{3.16}$$

Therefore, $\breve{\boldsymbol{\varphi}}_{k-1} = \breve{\boldsymbol{A}}_{k-1}^{T}\breve{\boldsymbol{A}}_{k-1} = \sum_{i=0}^{k-1}\hat{\boldsymbol{u}}_i\hat{\boldsymbol{u}}_i^{T}$ (3.17)

$$\breve{\boldsymbol{z}}_{k-1} = \breve{\boldsymbol{A}}_{k-1}^{T}\breve{\boldsymbol{d}}_{k-1} = \sum_{i=0}^{k-1}\hat{\boldsymbol{u}}_i\breve{\boldsymbol{d}}[i] \tag{3.18}$$

For the optimal problem at time step *k*, Eq. (3.15) can be expressed in the form as given below

$$\breve{\boldsymbol{h}}_{k}^{*} = \breve{\boldsymbol{\varphi}}_{k}^{-1}\breve{\boldsymbol{z}}_{k} \tag{3.19}$$

and Eq. (3.17) and Eq. (3.18) becomes

$$\breve{\boldsymbol{\varphi}}_{k} = \sum_{i=0}^{k}\hat{\boldsymbol{u}}_i\hat{\boldsymbol{u}}_i^{T} \tag{3.20}$$

$$\breve{\boldsymbol{z}}_{k} = \sum_{i=0}^{k}\hat{\boldsymbol{u}}_i\breve{\boldsymbol{d}}[i] \tag{3.21}$$

Eq. (3.20) can be expressed as

$$\breve{\boldsymbol{\varphi}}_{k} = \sum_{i=0}^{k-1}\hat{\boldsymbol{u}}_i\hat{\boldsymbol{u}}_i^{T} + \hat{\boldsymbol{u}}_k\hat{\boldsymbol{u}}_k^{T} \tag{3.22}$$

It is seen in Eq. (3.22) that fundamentally a new data is added at time step *k*.

$$\breve{\boldsymbol{\varphi}}_k = \sum_{i=0}^{k-1} \hat{\boldsymbol{u}}_i \hat{\boldsymbol{u}}_i^T + \hat{\boldsymbol{u}}_k . \{1\} . \hat{\boldsymbol{u}}_k^T \tag{3.23}$$

$$\breve{\boldsymbol{\varphi}}_k = \breve{\boldsymbol{\varphi}}_{k-1} + \hat{\boldsymbol{u}}_k . \{1\} . \hat{\boldsymbol{u}}_k^T \tag{3.24}$$

The inversion of the matrix $\breve{\boldsymbol{\varphi}}_k$ is done using matrix inversion lemma, the detail of which is as follows:

Matrix Inversion Lemma [Haykin Simon (2014),]

Let $\hat{\boldsymbol{A}}, \hat{\boldsymbol{B}}$ be positive definitive matrix of size $\hat{m}\ x\ \hat{m}$ and $\hat{\boldsymbol{C}}$ is $\hat{m}\ x\ \hat{n}$ matrix also $\hat{\boldsymbol{D}}$ is positive definitive matrix of size $\hat{n}\ x\ \hat{n}$.

If $\hat{\boldsymbol{A}} = \hat{\boldsymbol{B}}^{-1} + \hat{\boldsymbol{C}}\hat{\boldsymbol{D}}^{-1}\hat{\boldsymbol{C}}^T$ then

$$\hat{\boldsymbol{A}}^{-1} = \hat{\boldsymbol{B}} - \hat{\boldsymbol{B}}\hat{\boldsymbol{C}}\left(\hat{\boldsymbol{D}} + \hat{\boldsymbol{C}}^T\hat{\boldsymbol{B}}\hat{\boldsymbol{C}}\right)^{-1}\hat{\boldsymbol{C}}^T\hat{\boldsymbol{B}} \tag{3.25}$$

The inverse of the $\breve{\boldsymbol{\varphi}}_k$ matrix is obtained using Eq. (3.24) and Eq. (3.25) as

$$\breve{\boldsymbol{\varphi}}_k^{-1} = \breve{\boldsymbol{\varphi}}_{k-1}^{-1} - \frac{\breve{\boldsymbol{\varphi}}_{k-1}^{-1}\hat{\boldsymbol{u}}_k . \hat{\boldsymbol{u}}_k^T \breve{\boldsymbol{\varphi}}_{k-1}^{-1}}{\{1\} + \hat{\boldsymbol{u}}_k^T \breve{\boldsymbol{\varphi}}_{k-1}^{-1} \hat{\boldsymbol{u}}_k} \tag{3.26}$$

Let $\boldsymbol{P}_k = \breve{\boldsymbol{\varphi}}_k^{-1}$, therefore Eq. (3.26) can be expressed as

$$\boldsymbol{P}_k = \boldsymbol{P}_{k-1} - \frac{\boldsymbol{P}_{k-1}\hat{\boldsymbol{u}}_k . \hat{\boldsymbol{u}}_k^T \boldsymbol{P}_{k-1}}{\boldsymbol{I} + \hat{\boldsymbol{u}}_k^T \boldsymbol{P}_{k-1} \hat{\boldsymbol{u}}_k} \tag{3.27}$$

$$\boldsymbol{K}_g = \frac{\boldsymbol{P}_{k-1}\hat{\boldsymbol{u}}_k}{\boldsymbol{I} + \hat{\boldsymbol{u}}_k^T \boldsymbol{P}_{k-1} \hat{\boldsymbol{u}}_k} \tag{3.28}$$

$\boldsymbol{K}_g$ = the Gain matrix. Then Eq. (3.27) can be expressed as

$$\boldsymbol{P}_k = \boldsymbol{P}_{k-1} - \boldsymbol{K}_g \hat{\boldsymbol{u}}_k^T \boldsymbol{P}_{k-1} = \boldsymbol{P}_{k-1}(\boldsymbol{I} - \boldsymbol{K}_k \hat{\boldsymbol{u}}_k^T) \tag{3.29}$$

Now, Eq. (3.21) can be expressed as

$$\check{\boldsymbol{z}}_k = \sum_{i=0}^{k} \hat{\boldsymbol{u}}_i \breve{\boldsymbol{d}}[i] = \sum_{i=0}^{k-1} \hat{\boldsymbol{u}}_i \breve{\boldsymbol{d}}[i] + \hat{\boldsymbol{u}}_k \breve{\boldsymbol{d}}[k] = \check{\boldsymbol{z}}_{k-1} + \hat{\boldsymbol{u}}_k \breve{\boldsymbol{d}}[k] \tag{3.30}$$

Recalling Eq. (3.19)

$$\breve{\boldsymbol{h}}_k^* = \breve{\boldsymbol{\varphi}}_k^{-1}\breve{\boldsymbol{z}}_k = \boldsymbol{P}_k\breve{\boldsymbol{z}}_k = \boldsymbol{P}_k\left(\breve{\boldsymbol{z}}_{k-1} + \hat{\boldsymbol{u}}_k\breve{\boldsymbol{d}}[k]\right) = \boldsymbol{P}_k\breve{\boldsymbol{z}}_{k-1} + \boldsymbol{P}_k\hat{\boldsymbol{u}}_k\breve{\boldsymbol{d}}[k] \tag{3.31}$$

Eq. (3.32) is obtained by substituting $\boldsymbol{P}_k$ from Eq. (3.29) into Eq. (3.31) as

$$\begin{aligned}\breve{\boldsymbol{h}}_k^* &= \left(\boldsymbol{P}_{k-1} - \boldsymbol{K}_g\hat{\boldsymbol{u}}_k^T\boldsymbol{P}_{k-1}\right)\breve{\boldsymbol{z}}_{k-1} + \boldsymbol{P}_k\hat{\boldsymbol{u}}_k\breve{\boldsymbol{d}}[k] \\ &= \boldsymbol{P}_{k-1}\breve{\boldsymbol{z}}_{k-1} - \boldsymbol{K}_g\hat{\boldsymbol{u}}_k^T\boldsymbol{P}_{k-1}\breve{\boldsymbol{z}}_{k-1} + \boldsymbol{P}_k\hat{\boldsymbol{u}}_k\breve{\boldsymbol{d}}[k]\end{aligned}$$

$$\text{or, } \breve{\boldsymbol{h}}_k^* = \breve{\boldsymbol{h}}_{k-1}^* - \boldsymbol{K}_g\hat{\boldsymbol{u}}_k^T\breve{\boldsymbol{h}}_{k-1}^* + \boldsymbol{K}_g\breve{\boldsymbol{d}}[k] \tag{3.32}$$

where, $\breve{\boldsymbol{h}}_{k-1}^* = \boldsymbol{P}_{k-1}\breve{\boldsymbol{z}}_{k-1}$ = best estimate at previous time step (k-1) and $\boldsymbol{P}_k\hat{\boldsymbol{u}}_k = \boldsymbol{K}_g$ (using Eq. (3.36) to Eq. (3.38).On simplification of Eq. (3.32), gives

$$\breve{\boldsymbol{h}}_k^* = \breve{\boldsymbol{h}}_{k-1}^* - \boldsymbol{K}_g\left(\hat{\boldsymbol{u}}_k^T\breve{\boldsymbol{h}}_{k-1}^* - \breve{\boldsymbol{d}}[k]\right) \tag{3.33}$$

$$\text{or, } \breve{\boldsymbol{h}}_k^* = \breve{\boldsymbol{h}}_{k-1}^* + \boldsymbol{K}_g\boldsymbol{\xi}_k \tag{3.34}$$

$$\text{where, } \boldsymbol{\xi}_k = \breve{\boldsymbol{d}}[k] - \hat{\boldsymbol{u}}_k^T\breve{\boldsymbol{h}}_{k-1}^* \tag{3.35}$$

From Eq. (3.28), the gain matrix $\boldsymbol{K}_g$ is obtained as

$$\boldsymbol{K}_g = \frac{\boldsymbol{P}_{k-1}\hat{\boldsymbol{u}}_k}{1 + \hat{\boldsymbol{u}}_k^T\boldsymbol{P}_{k-1}\hat{\boldsymbol{u}}_k} \tag{3.36}$$

on rearranging Eq. (3.36) in the following manner, Eq. (3.37) is obtained.

$$\boldsymbol{K}_g(1 + \hat{\boldsymbol{u}}_k^T\boldsymbol{P}_{k-1}\hat{\boldsymbol{u}}_k) = \boldsymbol{P}_{k-1}\hat{\boldsymbol{u}}_k$$

$$\text{or, } \boldsymbol{K}_g + \boldsymbol{K}_g\hat{\boldsymbol{u}}_k^T\boldsymbol{P}_{k-1}\hat{\boldsymbol{u}}_k = \boldsymbol{P}_{k-1}\hat{\boldsymbol{u}}_k$$

$$\text{or, } \boldsymbol{K}_g = \boldsymbol{P}_{k-1}\hat{\boldsymbol{u}}_k - \boldsymbol{K}_g\hat{\boldsymbol{u}}_k^T\boldsymbol{P}_{k-1}\hat{\boldsymbol{u}}_k$$

$$\text{or, } \boldsymbol{K}_g = \left(\boldsymbol{P}_{k-1} - \boldsymbol{K}_g\hat{\boldsymbol{u}}_k^T\boldsymbol{P}_{k-1}\right)\hat{\boldsymbol{u}}_k \tag{3.37}$$

Using Eq. (3.29) in Eq. (3.37), the following Eq. (3.38) is obtained.

$$\text{or, } \boldsymbol{K}_g = \boldsymbol{P}_k\hat{\boldsymbol{u}}_k \tag{3.38}$$

A brief summary of all the steps of the algorithm is given below.

Summary of Recursive Least Square estimate (RLSE)

Step 1: Estimate the Gain Matrix, $\boldsymbol{K}_g$

$$\boldsymbol{K}_g = \frac{\boldsymbol{P}_{k-1}\hat{\boldsymbol{u}}_k}{\boldsymbol{I} + \hat{\boldsymbol{u}}_k^T \boldsymbol{P}_{k-1}\hat{\boldsymbol{u}}_k} \tag{3.39}$$

Step 2: Estimate the error in measurement, $\boldsymbol{\xi}_k$ from previous estimation and current measurement

$$\boldsymbol{\xi}_k = \breve{\boldsymbol{d}}[k] - \hat{\boldsymbol{u}}_k^T \breve{\boldsymbol{h}}_{k-1}^* \tag{3.40}$$

Step 3: Update the filter

$$\breve{\boldsymbol{h}}_k^* = \breve{\boldsymbol{h}}_{k-1}^* + \boldsymbol{K}_g \boldsymbol{\xi}_k \tag{3.41}$$

Step 4: Update the $\boldsymbol{P}_{k-1}$ matrix

$$\boldsymbol{P}_k = \boldsymbol{P}_{k-1}\left(\boldsymbol{I} - \boldsymbol{K}_g \hat{\boldsymbol{u}}_k^T\right) \tag{3.42}$$

The error in observation $\boldsymbol{\xi}_k$ is obtained from the current measurement $\breve{\boldsymbol{d}}[k]$ and the predicted measurement $\hat{\boldsymbol{u}}_k^T \breve{\boldsymbol{h}}_{k-1}^*$ as shown in Eq. (3.40). The predicted measurement is evaluated using the current input and past filter coefficient. From the gain matrix $\boldsymbol{K}_g$, the filter gets updated as shown in (3.41). The error covariance matrix gets updated as shown in (3.42). All the above steps are executed recursively to obtain the filter coefficients.

3.2.3 Sequential Nonlinear Least Square Estimate (SNLSE) Algorithm

Yang *et al.* (2006) showed how RLSE can be further extended for system identification of structural system and named the suggested approach as Sequential non-linear least square estimation (SNLSE).Both single step approach and two step approaches towards RLSE was carried out to overcome divergence issues of the highly non-linear filtering problem. As in any other filtering problem, there is an observation equation through which structural responses are captured. In this approach also, the structural acceleration responses are utilized.

The equation of motion of a multi-degree of freedom (MDOF) non-linear structure subjected to external excitation can be written as

$$\boldsymbol{M}\ddot{\boldsymbol{x}}(t) + \boldsymbol{F}_c[\dot{\boldsymbol{x}}(t)] + \boldsymbol{F}_s[\boldsymbol{x}(t)] = \boldsymbol{\eta}\boldsymbol{F}(t) \tag{3.43}$$

In which **M** is *n* x *n* mass matrix; $\boldsymbol{x}(t) = \{x_1 \quad x_2 \quad \dots \quad x_n\}^T$ is *n*-displacement vector; $\boldsymbol{F}_c[\dot{\boldsymbol{x}}(t)]$ is *n*-damping force vector; $\boldsymbol{F}_s[\boldsymbol{x}(t)]$ is *n*-stiffness force vector; $\boldsymbol{F}(t)$ =excitation

vector; and $\boldsymbol{\eta}$ is excitation influence matrix. The acceleration responses $\ddot{\boldsymbol{x}}(t)$ and the excitation forces $\boldsymbol{F}(t)$ are known measured quantities. The unknown to be identified are the state vector $\boldsymbol{X} = \{\boldsymbol{x}^T, \dot{\boldsymbol{x}}^T\}^T$, including displacement and velocity vectors and the parametric vector $\boldsymbol{\theta} = \{\theta_1, \theta_2, \ldots, \theta_n\}^T$, involving n unknown parameters, such as stiffness, damping and non-linear parameters.

Re-arranging Eq. (3.43), the observation equation as shown in Eq. (3.44) is obtained. The left hand side of the equation consists of the unknown damping force and stiffness force and right hand side consists of known forcing function and measured acceleration.

$$\boldsymbol{F}_c[\dot{\boldsymbol{x}}(t)] + \boldsymbol{F}_s[\boldsymbol{x}(t)] = \boldsymbol{\eta}\boldsymbol{F}(t) - \boldsymbol{M}\ddot{\boldsymbol{x}}(t) \tag{3.44}$$

The observation equation associated with the equation of motion, Eq. (3.44) can be written as

$$\boldsymbol{\varphi}[\boldsymbol{X}; t]\boldsymbol{\theta} + \boldsymbol{\varepsilon}(t) = \boldsymbol{y}(t) \tag{3.45}$$

where, $\boldsymbol{y}(t) = \boldsymbol{\eta}\boldsymbol{F}(t) - \boldsymbol{M}\ddot{\boldsymbol{x}}(t)$ is known and $\boldsymbol{\varepsilon}(t)$ is the model noise. Eq. (3.45) can be discretized at $t = t_k = k\Delta t$ as

$$\boldsymbol{\varphi}_k(\boldsymbol{X}_k)\boldsymbol{\theta}_k + \boldsymbol{\varepsilon}_k = \boldsymbol{y}_k \tag{3.46}$$

In Eq. (3.46), $\boldsymbol{\varphi}_k(\boldsymbol{X}_k) = \boldsymbol{\varphi}[\boldsymbol{X}(t_k); t_k]$, $\boldsymbol{\theta}_k = \boldsymbol{\theta}(t_k)$, $\boldsymbol{\varepsilon}_k = \boldsymbol{\varepsilon}(t_k)$ and $\boldsymbol{y}_k = \boldsymbol{y}(t_k)$. It is noted that $\boldsymbol{\theta}$ and $\boldsymbol{X}$ in Eq. (3.45) or $\boldsymbol{\theta}_k$ and $\boldsymbol{X}_k$ in Eq. (3.46) are unknown quantities to be estimated. Hence, Eq. (3.45) and Eq. (3.46) are nonlinear equations to be solved for unknowns' $\boldsymbol{\theta}_k$ and $\boldsymbol{X}_k$.

Instead of solving $\boldsymbol{\theta}_k$ and $\boldsymbol{X}_k$ together as in EKF, $\boldsymbol{\theta}_k$ and $\boldsymbol{X}_k$ are solved in two steps. The first step is to determine $\boldsymbol{\theta}_k$ by assuming (or under the condition) that $\boldsymbol{X}_k$ is given using the LSE solution. The second step is to determine $\boldsymbol{X}_k$ through a nonlinear LSE approach, referred to as SNLSE.

3.2.3.1 The Parametric Vector (Step-1)

Suppose the state vector $\boldsymbol{X}_k$ is known and the parametric vector $\boldsymbol{\theta}_k$ is constant, such that $\boldsymbol{\theta} = \boldsymbol{\theta}_1 = \boldsymbol{\theta}_2 = \ldots = \boldsymbol{\theta}_k$.

The error in the estimate is given by Eq. (3.47).

$$\boldsymbol{e} = (\boldsymbol{y}_i - \boldsymbol{\varphi}_i(\boldsymbol{X}_i)\boldsymbol{\theta}_i) \tag{3.47}$$

which is of the form of Eq. (3.6). Comparing Eq. (3.6) and Eq. (3.47), it is observed that vector $\breve{\boldsymbol{d}}$ of Eq. (3.6) corresponds to vector $\boldsymbol{y}_i$ of Eq. (3.47). Matrix $\breve{\boldsymbol{A}}$ of Eq. (3.6) corresponds to matrix $\boldsymbol{\varphi}_i(\boldsymbol{X}_i)$ of Eq. (3.47) and vector $\breve{\boldsymbol{h}}$ of Eq. (3.6) corresponds to vector $\boldsymbol{\theta}_i$ of Eq. (3.47). In Eq. (3.6) $\breve{\boldsymbol{h}}$ is unknown, similarly in Eq. (3.47) $\boldsymbol{\theta}_i$ is unknown. The objective function is given by the square of the error function as given in Eq. (3.48).

$$\begin{aligned}\boldsymbol{J}(\theta) &= \|\boldsymbol{e}\|_2^2 = \|\boldsymbol{y}_i - \boldsymbol{\varphi}_i(\boldsymbol{X}_i)\boldsymbol{\theta}_i\|_2^2 \\ &= \sum_{i=1}^{k+1}[(\boldsymbol{y}_i - \boldsymbol{\varphi}_i(\boldsymbol{X}_i)\boldsymbol{\theta}_i)^T(\boldsymbol{y}_i - \boldsymbol{\varphi}_i(\boldsymbol{X}_i)\boldsymbol{\theta}_i)]\end{aligned} \tag{3.48}$$

Minimizing the objective function (sum square errors) one obtains the classical LSE recursive solution $\widehat{\boldsymbol{\theta}}_{k+1}$ in the given following equations.

The derivation to the solutions of recursive least square estimate (RLSE) is already obtained vide Eq. (3.28) to Eq. (3.38). Just by comparing the notations used in the equation, the solution of the LSE is obtained as given by Eq. (3.47).

In Eq. (3.33), if $\widehat{\boldsymbol{u}}_i$ is denoted as $\widehat{\boldsymbol{u}}_i = \breve{\boldsymbol{A}}_{k-1}^T$ and $\widehat{\boldsymbol{u}}_i^T = \breve{\boldsymbol{A}}_{k-1}$ and if the following notations are replaced as $\breve{\boldsymbol{h}}_k^* = \widehat{\boldsymbol{\theta}}_k$, $\breve{\boldsymbol{h}}_{k-1}^* = \widehat{\boldsymbol{\theta}}_{k-1}$, $\widehat{\boldsymbol{u}}_k^T = \breve{\boldsymbol{A}}_{k-1} = \boldsymbol{\varphi}_k(\boldsymbol{X}_k)$, $\boldsymbol{K}_{g,k} = \boldsymbol{K}_g(\boldsymbol{X}_k)$ and $\breve{\boldsymbol{d}}[k] = \boldsymbol{y}_k$, then Eq. (3.49) is obtained as

$$\begin{aligned}\widehat{\boldsymbol{\theta}}_k &= \widehat{\boldsymbol{\theta}}_{k-1} - \boldsymbol{K}_{g,k}(\boldsymbol{X}_k)\left[\boldsymbol{\varphi}_k(\boldsymbol{X}_k)\widehat{\boldsymbol{\theta}}_{k-1} - \boldsymbol{y}_k\right] \\ &= \widehat{\boldsymbol{\theta}}_{k-1} + \boldsymbol{K}_{g,k}(\boldsymbol{X}_k)\left[\boldsymbol{y}_k - \boldsymbol{\varphi}_k(\boldsymbol{X}_k)\widehat{\boldsymbol{\theta}}_{k-1}\right]\end{aligned} \tag{3.49}$$

Eq. (3.50) is obtained by replacing k with k+1 in Eq. (3.49)

$$\widehat{\boldsymbol{\theta}}_{k+1} = \widehat{\boldsymbol{\theta}}_k + \boldsymbol{K}_{g,k+1}(\boldsymbol{X}_{k+1})\left[\boldsymbol{y}_{k+1} - \boldsymbol{\varphi}_{k+1}(\boldsymbol{X}_{k+1})\widehat{\boldsymbol{\theta}}_k\right] \tag{3.50}$$

Eq. (3.28) gives $\boldsymbol{K}_{g,k} = \frac{\boldsymbol{P}_{k-1}\widehat{\boldsymbol{u}}_k}{\boldsymbol{I}+\widehat{\boldsymbol{u}}_k^T\boldsymbol{P}_{k-1}\widehat{\boldsymbol{u}}_k}$

$$\boldsymbol{K}_{g,k+1}(\boldsymbol{X}_{k+1}) = \boldsymbol{P}_k\boldsymbol{\varphi}_{k+1}^T(\boldsymbol{X}_{k+1})[\boldsymbol{I} + \boldsymbol{\varphi}_{k+1}(\boldsymbol{X}_{k+1})\boldsymbol{P}_k\boldsymbol{\varphi}_{k+1}^T(\boldsymbol{X}_{k+1})]^{-1} \tag{3.51}$$

Eq. (3.51) is obtained, by changing the notations and replacing k by k+1.

Eq. (3.29) gives $\boldsymbol{P}_k = \boldsymbol{P}_{k-1} - \boldsymbol{K}_k\widehat{\boldsymbol{u}}_k^T\boldsymbol{P}_{k-1} = \boldsymbol{P}_{k-1}(\boldsymbol{I} - \boldsymbol{K}_k\widehat{\boldsymbol{u}}_k^T)$

By changing the notations in the above Equation, Eq. (3.52) is obtained.

$$\boldsymbol{P}_k = \boldsymbol{P}_{k-1} - \boldsymbol{K}_{g,k}(\boldsymbol{X}_k)\boldsymbol{\varphi}_k(\boldsymbol{X}_k)\boldsymbol{P}_{k-1} = \boldsymbol{P}_{k-1}\left(\boldsymbol{I} - \boldsymbol{K}_{g,k}(\boldsymbol{X}_k)\boldsymbol{\varphi}_k(\boldsymbol{X}_k)\right) \tag{3.52}$$

Therefore, Eq. (3.50), Eq. (3.51) and Eq. (3.52) give the RLSE estimate of $\widehat{\boldsymbol{\theta}}_{k+1}$ in which $\boldsymbol{K}_{g,k+1}(\boldsymbol{X}_{k+1})$ is the LSE gain matrix.

The State Vector (Step-2)

The formulation of state vector is similar for both SNLSE and SNLSE-UI-UO (sub-section:3.2.4), therefore sub-section 3.2.4.3 may be referred.

3.2.4 Sequential Nonlinear Least Square Estimate with unknown input and unknown output (SNLSE-UI-UO) Algorithm

SNLSE-UI-UO is an extension of SNLSE with a modification in the algorithm to handle limited sensor information and work with unknown input excitation. An excerpt of the formulation by Yang and Hongwei (2007) is presented below.

The observation equation

Displacement vector is represented as

$$\boldsymbol{x}(t) = \{x_1(t), x_2(t), \dots, x_m(t)\}^T \tag{3.53}$$

Velocity vector is represented as

$$\dot{\boldsymbol{x}}(t) = \{\dot{x}_1(t), \dot{x}_2(t), \dots, \dot{x}_m(t)\}^T \tag{3.54}$$

and the acceleration vector is represented as

$$\ddot{\boldsymbol{x}}(t) = \{\ddot{x}_1(t), \ddot{x}_2(t), \dots, \ddot{x}_m(t)\}^T \tag{3.55}$$

m corresponds to degrees of freedom.

The equation of motion of multi degree of freedom (MDOF) non-linear structural system can be expressed as

$$\boldsymbol{M}\ddot{\boldsymbol{x}}(t) + \boldsymbol{F_c}[\dot{x}(t), \theta] + \boldsymbol{F_s}[x(t), \theta] = \boldsymbol{\eta F}(t) \tag{3.56}$$

The acceleration vector $\ddot{\boldsymbol{x}}(t)$is divided into two parts $\begin{Bmatrix} \ddot{\boldsymbol{x}}^*(t) \\ \ddot{\bar{\boldsymbol{x}}}(t) \end{Bmatrix}$

where,

$$\ddot{\boldsymbol{x}}^*(t) = \{\ddot{x}_1^*(t), \ddot{x}_2^*(t), \dots, \ddot{x}_s^*(t)\}^T \tag{3.57}$$

corresponds to s unknown, unmeasured acceleration responses.

$$\ddot{\bar{\boldsymbol{x}}}(t) = \{\ddot{\bar{x}}_1^*(t), \bar{x}_2^*(t), \dots, \ddot{\bar{x}}_{m-s}^*(t)\}^T \tag{3.58}$$

corresponds to $(m - s)$ known, measured acceleration responses.

Similarly, the excitation vector $\boldsymbol{F}(t)$ is divided into two parts $\begin{Bmatrix}\boldsymbol{F}^*(t)\\ \widetilde{\boldsymbol{F}}(t)\end{Bmatrix}$

$$\boldsymbol{F}^*(t) = \{f_1^*(t), f_2^*(t) \dots, f_r^*(t)\}^T \tag{3.59}$$

corresponds to *r* unknown, unmeasured excitation input.

$$\widetilde{\boldsymbol{F}}(t) = \{f_1(t), f_2(t), \dots, f_{\bar{m}}(t)\}^T \tag{3.60}$$

corresponds to $\bar{m}$ known, measured excitation input.

Therefore, Eq. (3.56) can be written as shown in Eq. (3.61).

$$[\boldsymbol{M}^*\bar{\boldsymbol{M}}]\begin{Bmatrix}\ddot{\boldsymbol{x}}^*(t)\\ \ddot{\bar{\boldsymbol{x}}}(t)\end{Bmatrix} + \boldsymbol{F_c}[\dot{x}(t), \theta] + \boldsymbol{F_s}[x(t), \theta] = [\boldsymbol{\eta}^*\widetilde{\boldsymbol{\eta}}]\begin{Bmatrix}\boldsymbol{F}^*(t)\\ \widetilde{\boldsymbol{F}}(t)\end{Bmatrix} \tag{3.61}$$

Expanding Eq. (3.61) as

$$\boldsymbol{M}^*\ddot{\boldsymbol{x}}^*(t) + \bar{\boldsymbol{M}}\ddot{\bar{\boldsymbol{x}}}(t) + \boldsymbol{F_c}[\dot{x}(t), \theta] + \boldsymbol{F_s}[x(t), \theta] = \boldsymbol{\eta}^*\boldsymbol{F}^*(t) + \widetilde{\boldsymbol{\eta}}\widetilde{\boldsymbol{F}}(t) \tag{3.62}$$

$\bar{\mathbf{M}}$ is $m\ x\ (m - s)$ mass matrix corresponds to $(n - s)$ known or measured acceleration response vector $\ddot{\bar{\boldsymbol{x}}}(t)$.

$\mathbf{M}^*$is $(m$ x $s)$ mass matrix corresponds to *s*-unknown or unknown acceleration response vector $\ddot{\boldsymbol{x}}^*(t)$.

$\boldsymbol{F_c}[\dot{x}(t), \theta]$is *n*-damping force vector and $\boldsymbol{F_s}[x(t), \theta]$ = *n*-stiffness force vector.

$\widetilde{\boldsymbol{\eta}} = m$ x $\bar{m}$ excitation influence matrix corresponding to $\widetilde{\boldsymbol{F}}(t)$

$\boldsymbol{\eta}^* = m$ x r excitation influence matrix corresponding to $\boldsymbol{F}^*(t)$

$\boldsymbol{\theta} = \{\theta_1, \theta_2, \dots, \theta_n\}^T$is the unknown parametric vector of the structure, involving n unknown parameters such as stiffness, damping and non-linear parameters.

Eq. (3.62) is re-arranged as follows,

$$\boldsymbol{F_c}[\dot{x}(t),\theta] + \boldsymbol{F_s}[x(t),\theta] = \boldsymbol{\eta}^*\boldsymbol{F}^*(t) - \boldsymbol{M}^*\ddot{\boldsymbol{x}}^*(t) + \widetilde{\boldsymbol{\eta}}\widetilde{\boldsymbol{F}}(t) - \bar{\boldsymbol{M}}\ddot{\bar{\boldsymbol{x}}}(t) \tag{3.63}$$

$$=> \boldsymbol{F_c}[\dot{x}(t),\theta] + \boldsymbol{F_s}[x(t),\theta] = \left(\boldsymbol{\eta}^*\boldsymbol{F}^*(t) - \boldsymbol{M}^*\ddot{\boldsymbol{x}}^*(t)\right) + \left(\widetilde{\boldsymbol{\eta}}\widetilde{\boldsymbol{F}}(t) - \bar{\boldsymbol{M}}\ddot{\bar{\boldsymbol{x}}}(t)\right) \tag{3.64}$$

$$\boldsymbol{\varphi}(\boldsymbol{X})\boldsymbol{\theta} + \boldsymbol{\epsilon} = [\boldsymbol{\eta}^*, -\boldsymbol{M}^*]\begin{Bmatrix}\boldsymbol{F}^*(t)\\ \ddot{\boldsymbol{x}}^*(t)\end{Bmatrix} + \left(\widetilde{\boldsymbol{\eta}}\widetilde{\boldsymbol{F}}(t) - \bar{\boldsymbol{M}}\ddot{\bar{\boldsymbol{x}}}(t)\right) \tag{3.65}$$

$$\boldsymbol{\varphi}(\boldsymbol{X})\boldsymbol{\theta} + \boldsymbol{\epsilon} = [\boldsymbol{\eta}^*, -\boldsymbol{M}^*]\left[\boldsymbol{F}^{*T}, \ddot{\boldsymbol{x}}^{*\boldsymbol{T}}\right]^T + \left(\widetilde{\boldsymbol{\eta}}\widetilde{\boldsymbol{F}} - \bar{\boldsymbol{M}}\ddot{\bar{\boldsymbol{x}}}\right) = \bar{\boldsymbol{\eta}}\bar{\boldsymbol{f}} + \boldsymbol{y} \tag{3.66}$$

where, $\boldsymbol{y} = \widetilde{\boldsymbol{\eta}}\widetilde{\boldsymbol{F}} - \bar{\boldsymbol{M}}\ddot{\bar{\boldsymbol{x}}}$ is known

$\bar{\boldsymbol{f}} = \left[\boldsymbol{F}^{*T}, \ddot{\boldsymbol{x}}^{*\boldsymbol{T}}\right]^T$ is unknown input − output vector,

$\boldsymbol{F}^*$ is unknown input vector and $\ddot{\boldsymbol{x}}^*$ is unknown output vector. The vector $\bar{\boldsymbol{\eta}} = [\boldsymbol{\eta}^*, -\boldsymbol{M}^*]$, is known.

Therefore the observation equation becomes $\boldsymbol{\varphi}(\boldsymbol{X})\boldsymbol{\theta} + \boldsymbol{\varepsilon} = \bar{\boldsymbol{\eta}}\bar{\boldsymbol{f}} + \boldsymbol{y}$ (3.67)

where $\boldsymbol{\varepsilon}(t)$ is the model uncertainty vector.
Eq. (3.67) can be discretized at $t = t_k = k\Delta t$ as

$$\boldsymbol{\varphi}_k(\boldsymbol{X}_k)\boldsymbol{\theta}_k + \boldsymbol{\varepsilon}_k - \bar{\boldsymbol{\eta}}\bar{\boldsymbol{f}}_k = \boldsymbol{y}_k \tag{3.68}$$

In which $\boldsymbol{X}_k = \boldsymbol{X}(t_k)$, $\boldsymbol{\varphi}_k(\boldsymbol{X}_k) = \boldsymbol{\varphi}[\boldsymbol{X}(t_k); t_k]$, $\boldsymbol{\theta}_k = \boldsymbol{\theta}(t_k)\boldsymbol{\epsilon}_k = \boldsymbol{\epsilon}(t_k), \bar{\boldsymbol{f}}_k = \bar{\boldsymbol{f}}(t_k)$ *and* $\boldsymbol{y}_k = \boldsymbol{y}(t_k)$
An $(n + r + s)$ extended unknown vector $\boldsymbol{\theta}_{e,k}$ at t_k is defined as

$$\boldsymbol{\theta}_{e,k} = \begin{Bmatrix}\boldsymbol{\theta}_k\\ \bar{\boldsymbol{f}}_k\end{Bmatrix} \tag{3.69}$$

Then Eq. (3.69) can be expressed as

$$\boldsymbol{\varphi}_{e,k}(\boldsymbol{X}_k)\boldsymbol{\theta}_{e,k} + \boldsymbol{\epsilon}_k = \boldsymbol{y}_k \tag{3.70}$$

In which $\boldsymbol{\varphi}_{e,k}(\boldsymbol{X}_k) = [\boldsymbol{\varphi}_k(\boldsymbol{X}_k) - \bar{\boldsymbol{\eta}}]$. Note that $\boldsymbol{X}_k$ and $\boldsymbol{\theta}_k$ in Eq. (3.70) are the unknowns to be estimated. Hence, Eq. (3.70) is a non-linear vector equation to be solved for unknowns $\boldsymbol{X}_k$ and $\boldsymbol{\theta}_{e,k}$.

Instead of solving $\boldsymbol{X}_k$ and $\boldsymbol{\theta}_{e,k}$ simultaneously, it is solved in two steps. The first step is to determine $\boldsymbol{\theta}_{e,k}$ by assuming or under the condition that $\boldsymbol{X}_k$ is known and the second step is to determine $\boldsymbol{X}_k$ through a non-linear LSE approach referred to as SNLSE-UI-UO.

3.2.4.1 The Parametric Vector (Step-1)

Determination of recursive solution for $\boldsymbol{\theta}_{k+1}(\boldsymbol{X}_{k+1})$ and $\bar{\boldsymbol{f}}_{\boldsymbol{k+1}}$ given $\mathbf{X_{k+1}}$.

Here, it is considered that the state vector $\boldsymbol{X_{k+1}}$is known and parametric vector $\boldsymbol{\theta}_k$is constant, i.e. $\theta = \theta_1 = \theta_2 = \cdots = \theta_{k+1}$

Combining all equations in Eq. (3.70) for k =1, 2,…, k+1 one obtains

$$\boldsymbol{\Phi}_{e,k+1}\boldsymbol{\Theta}_{e,k+1} + \boldsymbol{E}_{k+1} = \bar{\boldsymbol{y}}_{k+1} \tag{3.71}$$

In which

$$\boldsymbol{\Theta}_{e,k+1} = \{\theta_{k+1} \quad \bar{f}_1 \quad \bar{f}_2 \quad \dots \quad \bar{f}_{k+1}\}^T \tag{3.72}$$

$$\boldsymbol{E}_{k+1} = \{\varepsilon_1 \quad \varepsilon_2 \quad \dots \quad \varepsilon_{k+1}\}^T \tag{3.73}$$

$$\bar{\boldsymbol{y}}_{k+1} = \{y_1 \quad y_2 \quad \dots \quad y_{k+1}\}^T \tag{3.74}$$

$$\boldsymbol{\Phi}_{e,k+1} = \begin{bmatrix} \varphi_1 & -\bar{\eta} & 0 & 0 & \dots & 0 \\ \varphi_2 & 0 & -\bar{\eta} & 0 & \dots & 0 \\ \varphi_3 & 0 & 0 & -\bar{\eta} & \dots & 0 \\ \vdots & \vdots & \vdots & \vdots & \ddots & \vdots \\ \varphi_{k+1} & 0 & 0 & 0 & 0 & -\bar{\eta} \end{bmatrix} \tag{3.75}$$

Where $\boldsymbol{\Theta}_{e,k+1}$ is an $[n + (r+s)(k+1)]$ unknown vector, $\bar{\boldsymbol{y}}_{k+1}$ is a $(k+1)m$ known(measured) vector, $\boldsymbol{E}_{k+1}$ is a $(k+1)m$ model noise vector, and $\boldsymbol{\Phi}_{e,k+1}$ is a $\{(k+1)m\text{x}[n + (r+\text{ऽ})(k+1)]\}$ known(measured) data matrix.

Based on Eq. (3.68) to Eq. (3.71), the sum-square error can be expressed as a quadratic function of the extended unknown vector $\boldsymbol{\Theta}_{e,k+1}$:

$$\mathcal{J}_{k+1}\boldsymbol{\theta}_{e,k+1} = \sum_{i=1}^{k+1}\left[y_i - \varphi_i(X_i)\theta + \bar{\eta}\bar{f}_i\right]^T\left[y_i - \varphi_i(X_i)\theta + \bar{\eta}\bar{f}_i\right]$$
$$= \sum_{i=1}^{k+1}\left[y_i - \varphi_{e,i}(X_i)\theta_{e,i}\right]^T\left[y_i - \varphi_{e,i}(X_i)\theta_{e,i}\right]$$
$$= \sum_{i=1}^{k+1}\left[\bar{y}_{k+1} - \Phi_{e,k+1}\Theta_{e,k+1}\right]^T\left[\bar{y}_{k+1} - \Phi_{e,k+1}\Theta_{e,k+1}\right] \quad (3.76)$$

The final solution is presented below

3.2.4.2 The Data Matrix $\boldsymbol{\varphi}$

Re-arranging Eq. (3.62), the following is obtained

$$\boldsymbol{F_c}[\dot{x}(t),\theta] + \boldsymbol{F_s}[x(t),\theta] = \left(\boldsymbol{\eta}^*\boldsymbol{F}^*(t) - \boldsymbol{M}^*\ddot{\boldsymbol{x}}^*(t)\right) + \left(\tilde{\boldsymbol{\eta}}\tilde{\boldsymbol{f}}(t) - \bar{\boldsymbol{M}}\ddot{\bar{\boldsymbol{x}}}(t)\right)$$

where, $\boldsymbol{F_c}[\dot{x}(t),\theta] + \boldsymbol{F_s}[x(t),\theta]$ may be written as $\boldsymbol{C\dot{x}} + \boldsymbol{Kx}$

where, $\boldsymbol{F_c}[\dot{x}(t),\theta] = \boldsymbol{C\dot{x}}$ and $\boldsymbol{F_s}[x(t),\theta] = \boldsymbol{Kx}$

which when re-arranged takes the form as $\boldsymbol{Kx} + \boldsymbol{C\dot{x}}$

$$=> [\boldsymbol{K}]\{\boldsymbol{x}\} + \left(\hat{\beta}[\boldsymbol{K}] + \hat{\alpha}[\boldsymbol{M}]\right)\{\dot{\boldsymbol{x}}\}$$

$$=> [\boldsymbol{K}_1 + \boldsymbol{K}_2 + \boldsymbol{K}_3 + \ldots\ldots + \boldsymbol{K}_{\bar{p}}]\{\boldsymbol{x}\} + \left(\hat{\beta}[\boldsymbol{K}_1 + \boldsymbol{K}_2 + \boldsymbol{K}_3 + \ldots\ldots + \boldsymbol{K}_{\bar{p}}] + \hat{\alpha}[\boldsymbol{M}]\right)\{\dot{\boldsymbol{x}}\}$$

$$=> [\boldsymbol{K}_1]\{\boldsymbol{x}\} + [\boldsymbol{K}_2]\{\boldsymbol{x}\} + [\boldsymbol{K}_3]\{\boldsymbol{x}\} + \cdots\left[\boldsymbol{K}_{\bar{p}}\right]\{\boldsymbol{x}\} + \hat{\beta}[\boldsymbol{K}_1]\{\dot{\boldsymbol{x}}\} + \hat{\beta}[\boldsymbol{K}_2]\{\dot{\boldsymbol{x}}\} + \hat{\beta}[\boldsymbol{K}_3]\{\dot{\boldsymbol{x}}\} + \cdots + \hat{\beta}\left[\boldsymbol{K}_{\bar{p}}\right]\{\dot{\boldsymbol{x}}\} + \hat{\alpha}[\boldsymbol{M}]\{\dot{\boldsymbol{x}}\}$$

$$=> [k_1\boldsymbol{S}_1]\{\boldsymbol{x}\} + [k_2\boldsymbol{S}_2]\{\boldsymbol{x}\} + [k_3\boldsymbol{S}_3]\{\boldsymbol{x}\} + \cdots\left[k_{\bar{p}}\boldsymbol{S}_{\bar{p}}\right]\{\boldsymbol{x}\} + \hat{\beta}[k_1\boldsymbol{S}_1]\{\dot{\boldsymbol{x}}\} + \hat{\beta}[k_2\boldsymbol{S}_2]\{\dot{\boldsymbol{x}}\} + \hat{\beta}[k_3\boldsymbol{S}_3]\{\dot{\boldsymbol{x}}\} + \cdots + \hat{\beta}\left[k_{\bar{p}}\boldsymbol{S}_{\bar{p}}\right]\{\dot{\boldsymbol{x}}\} + \hat{\alpha}[\boldsymbol{M}]\{\dot{\boldsymbol{x}}\}$$

$$=> \Big[[\boldsymbol{S}_1]\{\boldsymbol{x}\} + [\boldsymbol{S}_2]\{\boldsymbol{x}\} + [\boldsymbol{S}_3]\{\boldsymbol{x}\} + \cdots\left[\boldsymbol{S}_{\bar{p}}\right]\{\boldsymbol{x}\} + [\boldsymbol{S}_1]\{\dot{\boldsymbol{x}}\} + [\boldsymbol{S}_2]\{\dot{\boldsymbol{x}}\} + [\boldsymbol{S}_3]\{\dot{\boldsymbol{x}}\} + \cdots + \left[\boldsymbol{S}_{\bar{p}}\right]\{\dot{\boldsymbol{x}}\} + [\boldsymbol{M}]\{\dot{\boldsymbol{x}}\}\Big]$$
$$* \left\{k_1 \quad k_2 \quad k_3 \quad \ldots \quad k_{\bar{p}} \quad \hat{\beta}k_1 \quad \hat{\beta}k_2 \quad \hat{\beta}k_3 \quad \ldots \quad \hat{\beta}k_{\bar{p}} \quad \hat{\alpha}\right\}^{\boldsymbol{T}} \quad (3.77)$$
$$= \varphi(\boldsymbol{X})\boldsymbol{\theta}$$

where the data matrix $\boldsymbol{\varphi}(\boldsymbol{X})$is given as

$$\boldsymbol{\varphi}(\boldsymbol{X}) = \Big[[\boldsymbol{S}_1]\{\boldsymbol{x}\} + [\boldsymbol{S}_2]\{\boldsymbol{x}\} + [\boldsymbol{S}_3]\{\boldsymbol{x}\} + \cdots [\boldsymbol{S}_{\bar{p}}]\{\boldsymbol{x}\} + [\boldsymbol{S}_1]\{\dot{\boldsymbol{x}}\} + [\boldsymbol{S}_2]\{\dot{\boldsymbol{x}}\} + [\boldsymbol{S}_3]\{\dot{\boldsymbol{x}}\} + \cdots + [\boldsymbol{S}_{\bar{p}}]\{\dot{\boldsymbol{x}}\} + [\boldsymbol{M}]\,\{\dot{\boldsymbol{x}}\}\Big] \tag{3.78}$$

and the parametric vector

$$\boldsymbol{\theta} = \{k_1 \quad k_2 \quad k_3 \quad \ldots \quad k_{\bar{p}} \quad \hat{\beta}k_1 \quad \hat{\beta}k_2 \quad \hat{\beta}k_3 \quad \ldots \quad \hat{\beta}k_{\bar{p}} \quad \hat{\alpha}\}^{\boldsymbol{T}} \tag{3.79}$$

$$\boldsymbol{\theta} = \{k_1 \quad k_2 \quad k_3 \quad \ldots \quad k_{\bar{p}} \quad c_1^* \quad c_2^* \quad c_3^* \quad \ldots \quad c_{\bar{p}}^* \quad \hat{\alpha}\}^{\boldsymbol{T}} \tag{3.80}$$

where $c_1^* = \hat{\beta}k_1,\ c_2^* = \hat{\beta}k_2,\ \ldots c_{\bar{p}}^* = \hat{\beta}k_{\bar{p}}$

$$\widehat{\boldsymbol{\theta}}_{k+1}(\boldsymbol{X}_{k+1}) = \widehat{\boldsymbol{\theta}}_k + \boldsymbol{K}_{\theta,k+1}(\boldsymbol{X}_{k+1})\left[\boldsymbol{y}_{k+1} - \boldsymbol{\varphi}_{k+1}(\boldsymbol{X}_{k+1})\widehat{\boldsymbol{\theta}}_k + \overline{\boldsymbol{\eta}}\hat{\bar{\mathbf{f}}}_{\mathrm{k+1|k+1}}\right] \tag{3.81}$$

$$\hat{\bar{\mathbf{f}}}_{\mathrm{k+1|k+1}} = -\mathbf{S}_{\mathrm{k+1}}(\boldsymbol{X}_{k+1})\overline{\boldsymbol{\eta}}^{\mathrm{T}}\left[\mathbf{I} - \varphi_{\mathrm{k+1}}(\boldsymbol{X}_{k+1})\mathbf{K}_{\theta,\mathrm{k+1}}(\boldsymbol{X}_{k+1})\right]\left(\mathbf{y}_{\mathrm{k+1}} - \boldsymbol{\varphi}_{\mathrm{k+1}}(\boldsymbol{X}_{k+1})\widehat{\boldsymbol{\theta}}_{\mathrm{k}}\right) \tag{3.82}$$

In which

$$\boldsymbol{K}_{\theta,k+1}(\boldsymbol{X}_{k+1}) = \mathbf{P}_{\theta,\mathrm{k}}\boldsymbol{\varphi}_{\mathrm{k+1}}^{\mathrm{T}}(X_{k+1})\left[\mathbf{I} + \boldsymbol{\varphi}_{\mathrm{k+1}}(\boldsymbol{X}_{k+1})\mathbf{P}_{\theta,\mathrm{k}}\boldsymbol{\varphi}_{\mathrm{k+1}}^{\mathrm{T}}(\boldsymbol{X}_{k+1})\right]^{-1} \tag{3.83}$$

$$\boldsymbol{S}_{k+1}(\boldsymbol{X}_{k+1}) = \left[\overline{\boldsymbol{\eta}}^{T}\left(\boldsymbol{I} - \boldsymbol{\varphi}_{k+1}(\boldsymbol{X}_{k+1})\boldsymbol{K}_{\theta,k+1}(\boldsymbol{X}_{k+1})\right)\overline{\boldsymbol{\eta}}\right]^{-1} \tag{3.84}$$

$$\mathbf{P}_{\boldsymbol{\theta},\mathbf{k}} = \left(\boldsymbol{I} + \boldsymbol{K}_{\boldsymbol{\theta},\boldsymbol{k}}(X_k)\overline{\boldsymbol{\eta}}\boldsymbol{S}_{\boldsymbol{k}}(X_k)\overline{\boldsymbol{\eta}}^{\boldsymbol{T}}\boldsymbol{\varphi}_{\boldsymbol{k}}(X_k)\right)\left(\boldsymbol{I} - \boldsymbol{K}_{\boldsymbol{\theta},\boldsymbol{k}}(X_k)\boldsymbol{\varphi}_{\boldsymbol{k}}(X_k)\right)\mathbf{P}_{\boldsymbol{\theta},\mathbf{k-1}} \tag{3.85}$$

3.2.4.3 The State Vector (Step-2)

Determination of the estimate of $\widehat{\boldsymbol{X}}_{k+1|k+1}$ for $\mathbf{X}_{\mathrm{k+1}}$ based on non-linear LSE.Since, $\boldsymbol{\theta}_{k+1}$ and $\mathbf{X}_{\mathrm{k+1}}$ are interrelated, the estimation $\widehat{\boldsymbol{\theta}}_{k+1}$ is a function of the unknown state vector $\boldsymbol{X}_{k+1}$, i.e. $\widehat{\boldsymbol{\theta}}_{k+1} = \widehat{\boldsymbol{\theta}}_{k+1}(\mathbf{X}_{\mathrm{k+1}})$, as shown in Eq. (3.81). It follows from Eq. (3.23) that the general objective function (sum-square error) can be expressed as

$$\boldsymbol{\mathcal{J}}_{k+1}(\boldsymbol{X}_{k+1}) = \sum_{i=1}^{k+1}\left\{\boldsymbol{y}_i - \boldsymbol{\varphi}_i(\boldsymbol{X}_i)\widehat{\boldsymbol{\theta}}_i(\boldsymbol{X}_i) + \overline{\boldsymbol{\eta}}\hat{\bar{\mathbf{f}}}_{\mathrm{i|i}}\right\}^{T}\left\{\boldsymbol{y}_i - \boldsymbol{\varphi}_i(\boldsymbol{X}_i)\widehat{\boldsymbol{\theta}}_i(\boldsymbol{X}_i) + \overline{\boldsymbol{\eta}}\hat{\bar{\mathbf{f}}}_{\mathrm{i|i}}\right\} \tag{3.86}$$

And the unknown state vector $\boldsymbol{X}_{k+1}$ will be estimated by further minimizing the general objective function in Eq. (3.86) that is highly non-linear in unknown state vector $\boldsymbol{X}_{k+1}$.To

minimize the objective function in Eq. (3.86) $\boldsymbol{X}_i$ will be expressed in terms of $\boldsymbol{X}_{k+1}$ through the following transformation. The Newmark-β method will be used to derive the state transition relation as follows:

$$x_{k+1} = x_k + (\Delta t)\dot{x}_k + \left(0.5 - \bar{\beta}\right)(\Delta t)^2\ddot{x}_k + \bar{\beta}(\Delta t)^2\ddot{x}_{k+1} \tag{3.87}$$

$$\dot{x}_{k+1} = \dot{x}_k + (1 - \bar{\gamma})(\Delta t)\ddot{x}_k + \bar{\gamma}(\Delta t)\ddot{x}_{k+1} \tag{3.88}$$

The state vector is defined as $\boldsymbol{X}_{k+1} = \begin{Bmatrix} x_{k+1} \\ \dot{x}_{k+1} \end{Bmatrix}$

Re-writing Eq. (3.87) & Eq. (3.88)

$$\begin{bmatrix} x_{k+1} \\ \dot{x}_{k+1} \end{bmatrix} = \begin{bmatrix} x_k + (\Delta t)\dot{x}_k \\ 0 \quad + \quad \dot{x}_k \end{bmatrix} + \begin{bmatrix} \left(0.5 - \bar{\beta}\right)(\Delta t)^2\ddot{x}_k \\ (1 - \bar{\gamma})(\Delta t)\ddot{x}_k \end{bmatrix} + \begin{bmatrix} \bar{\beta}(\Delta t)^2 \\ \bar{\gamma}(\Delta t) \end{bmatrix} \begin{Bmatrix} \ddot{x}_{k+1} \\ \ddot{x}_{k+1} \end{Bmatrix} \tag{3.89}$$

$$=> \begin{bmatrix} x_{k+1} \\ \dot{x}_{k+1} \end{bmatrix} = \begin{bmatrix} I & (\Delta t)I \\ 0 & I \end{bmatrix} \begin{Bmatrix} x_k \\ \dot{x}_k \end{Bmatrix} + \begin{bmatrix} \left(0.5 - \bar{\beta}\right)(\Delta t)^2 \\ (1 - \bar{\gamma})(\Delta t) \end{bmatrix} \{\ddot{x}_k\} + \begin{bmatrix} \bar{\beta}(\Delta t)^2 \\ \bar{\gamma}(\Delta t) \end{bmatrix} \{\ddot{x}_{k+1}\} \tag{3.90}$$

Therefore, the transition relation is obtained as follows

$$\boldsymbol{X}_{k+1} = \boldsymbol{\varphi}_{k+1,k}\boldsymbol{X}_k + \boldsymbol{B_1}\ddot{\boldsymbol{x}}_{\boldsymbol{k}} + \boldsymbol{B_2}\ddot{\boldsymbol{x}}_{\boldsymbol{k+1}} \tag{3.91}$$

where, $\bar{\beta}$=0.25 and $\bar{\gamma}$=0.5, $\boldsymbol{\varphi}_{k+1,k}$ is the transition matrix for the state vector from k to k+1 and

$$\boldsymbol{B_1} = \begin{bmatrix} \left(0.5 - \bar{\beta}\right)(\Delta t)^2 \\ (1 - \bar{\gamma})(\Delta t) \end{bmatrix} \tag{3.92}$$

$$\boldsymbol{B_2} = \begin{bmatrix} \bar{\beta}(\Delta t)^2 \\ \bar{\gamma}(\Delta t) \end{bmatrix} \tag{3.93}$$

Eq. (3.91) can be re-written as

$$\boldsymbol{X}_k = \boldsymbol{\varphi}_{k,k+1}\boldsymbol{X}_{k+1} - \boldsymbol{\varphi}_{k,k+1}(\boldsymbol{B_1}\ddot{\boldsymbol{x}}_{\boldsymbol{k}} + \boldsymbol{B_2}\ddot{\boldsymbol{x}}_{\boldsymbol{k+1}}) \tag{3.94}$$

where,

$$\boldsymbol{\varphi}_{k,k+1} = \boldsymbol{\varphi}_{k+1,k}^{-1} = \begin{bmatrix} \boldsymbol{I} & -(\Delta t)I \\ \boldsymbol{0} & \boldsymbol{I} \end{bmatrix} \tag{3.95}$$

Hence, using the above transition relation, $\boldsymbol{X}_i$ may be expressed in terms of $\boldsymbol{X}_{k+1}$, as

$$\boldsymbol{X}_i = \boldsymbol{\varphi}_{i,k+1}\boldsymbol{X}_{k+1} - \sum_{j=1}^{k+1-i} \boldsymbol{\varphi}_{i,j+1}\left(\boldsymbol{B_1}\ddot{\boldsymbol{x}}_{j+i-1} + \boldsymbol{B_2}\ddot{\boldsymbol{x}}_{j+i}\right), \quad i = k, k-1, \ldots 1 \tag{3.96}$$

where $\boldsymbol{\varphi}_{i,j} = \boldsymbol{\varphi}_{k,k+1}^{j-i}$for any *j*>*i*. Based on Eq. (3.91), the estimation of $\boldsymbol{X}_{k+1}$ at $k\Delta t$, denoted by $\widehat{\boldsymbol{X}}_{k+1,k}$, is given byEq. (3.97), in which $\widehat{\boldsymbol{X}}_{k,k}$ is the estimation of $\widehat{\boldsymbol{X}}_k$ estimated at at $k\Delta t$.

$$\widehat{\boldsymbol{X}}_{k+1,k} = \boldsymbol{\varphi}_{k+1,k}\widehat{\boldsymbol{X}}_{k,k} + \boldsymbol{B_1}\ddot{\boldsymbol{x}}_{\boldsymbol{k}} + \boldsymbol{B_2}\ddot{\boldsymbol{x}}_{\boldsymbol{k+1}} \tag{3.97}$$

Eq. (3.87) & Eq. (3.88) is referred to as the Newmark-β method with linear acceleration in$[\mathrm{k}\Delta\mathrm{t},\ (\mathrm{k}+1)\Delta\mathrm{t}]$. At time $t_{k+1} = (k+1)\Delta\mathrm{t}$, *s* elements in $\ddot{\boldsymbol{x}}_{k+1}$ belong to the elements of $\ddot{\boldsymbol{x}}_{k+1}^*$, which are not measured and hence are unknown. However, at $t_k = k\Delta t$ all elements of $\ddot{\boldsymbol{x}}_k^*$ are known quantities, since unmeasured quantities in $\ddot{\boldsymbol{x}}_k^*$ have been estimated from Eq. (3.82). With a reasonable approximation, the Newmark- β method with a constant acceleration in $[k\Delta t,\ (k+1)\Delta t]$ can be used for those elements in $\ddot{\boldsymbol{x}}_{k+1}^*$ (unmeasured acceleration), $\ddot{\boldsymbol{x}}_{k+1}^* \approx \ddot{\boldsymbol{x}}_k^*$ and $\bar{\gamma} = 0$ in Eq. (3.87) and Eq. (3.88).

With the transition relation between $\boldsymbol{X}_{k+1}$ and $\boldsymbol{X}_i$ in Eq. (3.96) the sum-square error objective function in Eq. (3.86) can now be expressed as a function of $\boldsymbol{X}_{k+1}$ and is given by Eq. (3.98), in which $\widehat{\boldsymbol{y}}_i[\boldsymbol{X}_i(\boldsymbol{X}_{k+1})]$ is given by Eq. (3.99).

$$\boldsymbol{\mathcal{J}}_{k+1}(\boldsymbol{X}_{k+1}) = \sum_{i=1}^{k+1} \{\boldsymbol{y}_i - \widehat{\boldsymbol{y}}_i[\boldsymbol{X}_i(\boldsymbol{X}_{k+1})]\}^T \{\boldsymbol{y}_i - \widehat{\boldsymbol{y}}_i[\boldsymbol{X}_i(\boldsymbol{X}_{k+1})]\} \tag{3.98}$$

$$\widehat{\boldsymbol{y}}_i[\boldsymbol{X}_i(\boldsymbol{X}_{k+1})] \cong \boldsymbol{\varphi}_i(\boldsymbol{X}_i)\widehat{\boldsymbol{\theta}}_i(\boldsymbol{X}_i) - \overline{\boldsymbol{\eta}}\widehat{\overline{\boldsymbol{f}}}_{i|i} = \boldsymbol{\varphi}_i[\boldsymbol{X}_i(\boldsymbol{X}_{k+1})]\widehat{\boldsymbol{\theta}}_i[\boldsymbol{X}_i(\boldsymbol{X}_{k+1})] - \overline{\boldsymbol{\eta}}\widehat{\overline{\boldsymbol{f}}}_{i|i} \tag{3.99}$$

The objective function in Eq. (3.98) is highly non-linear function of unknown state vector $\boldsymbol{X}_{k+1}$. To minimize the objective function, the nonlinear function $\hat{y}_i[\boldsymbol{X}_i(\boldsymbol{X}_{k+1})]$ inEq. (3.99) is linearized using the first-order Taylor's series expansion around $\widehat{\boldsymbol{X}}_{k+1,k}$ as follows:

$$\widehat{\boldsymbol{y}}_i\left(\boldsymbol{X}_i(\boldsymbol{X}_{k+1})\right) \approx \widehat{\boldsymbol{y}}_i\left(\widehat{\mathbf{X}}_{\mathrm{k+1,k}}\right) + \boldsymbol{\Psi}_{\mathrm{i,k+1}}\left(\boldsymbol{X}_{k+1} - \widehat{\boldsymbol{X}}_{k+1|k}\right) \tag{3.100}$$

in which $\widehat{\boldsymbol{X}}_{k+1|k}$ is the estimate of $\boldsymbol{X}_{k+1}$ at $k\Delta t$ given by

$$\hat{\boldsymbol{y}}_i[\hat{\boldsymbol{X}}_{k+1,k}] = \boldsymbol{\varphi}_i[\boldsymbol{X}_i(\hat{\boldsymbol{X}}_{k+1,k})]\hat{\boldsymbol{\theta}}_i[\boldsymbol{X}_i(\hat{\boldsymbol{X}}_{k+1,k})] - \overline{\boldsymbol{\eta}}\hat{\bar{\boldsymbol{f}}}_{i|i} \tag{3.101}$$

$$\boldsymbol{\Psi}_{\mathrm{i,k+1}} = \left[\frac{\partial \hat{\boldsymbol{y}}_i(\boldsymbol{X}_i)}{\partial \boldsymbol{X}_i} \quad \frac{\partial \boldsymbol{X}_i}{\partial \boldsymbol{X}_{k+1}}\right]_{\mathrm{X_i}=\boldsymbol{X}_i(\hat{\boldsymbol{X}}_{k+1|k})} = \left.\frac{\partial \hat{\boldsymbol{y}}_i(\boldsymbol{X}_i)}{\partial \boldsymbol{X}_i}\right|_{\mathrm{X_i}=\boldsymbol{X}_i(\hat{\boldsymbol{X}}_{k+1|k})} \boldsymbol{\varphi}_{\mathrm{i,k+1}} \tag{3.102}$$

In Eq. (3.102), $\frac{\partial \boldsymbol{X}_i}{\partial \boldsymbol{X}_{k+1}}$ follows from Eq. (3.96). Substituting Eq. (3.100) into Eq. (3.98), one obtains the following objective function given by Eq. (3.103).

$$\mathcal{J}_{k+1}(\boldsymbol{X}_{k+1}) \approx \sum_{i=1}^{k+1} \left(\overline{\boldsymbol{y}}_{i,k+1} - \boldsymbol{\Psi}_{\mathrm{i,k+1}}\boldsymbol{X}_{k+1}\right)^T \left(\overline{\boldsymbol{y}}_{i,k+1} - \boldsymbol{\Psi}_{\mathrm{i,k+1}}\boldsymbol{X}_{k+1}\right) \tag{3.103}$$

where $\overline{\boldsymbol{y}}_{i,k+1}$ is known,

$$\overline{\boldsymbol{y}}_{i,k+1} = y_i - \hat{y}_i[\boldsymbol{X}_i(\boldsymbol{X}_{k+1})] + \boldsymbol{\Psi}_{\mathrm{i,k+1}}\hat{\boldsymbol{X}}_{k+1|k} \tag{3.104}$$

Now Eq. (3.103) is a quadratic function of $\boldsymbol{X}_{k+1}$. Minimizing the quadratic objective function in Eq. (3.103), the recursive solution $\hat{\boldsymbol{X}}_{k+1|k+1}$ that is the estimation of $\hat{\boldsymbol{X}}_{k+1}$ at $(k+1)\Delta t$ is obtained as follows:

$$\hat{\boldsymbol{X}}_{k+1|k+1} = \hat{\boldsymbol{X}}_{k+1|k} + \overline{\boldsymbol{K}}_{k+1}\left[\boldsymbol{y}_{k+1} - \hat{\boldsymbol{y}}_{k+1}\left(\hat{\boldsymbol{X}}_{k+1|k}\right)\right] \tag{3.105}$$

where,

$$\hat{\mathbf{X}}_{\mathrm{k+1|k}} = \boldsymbol{\varphi}_{\mathrm{k+1,k}}\hat{\mathbf{X}}_{\mathrm{k|k}} + \mathbf{B_1}\ddot{\mathbf{x}}_{\mathbf{k}} + \mathbf{B_2}\ddot{\mathbf{x}}_{\mathbf{k+1}} \tag{3.106}$$

$$\overline{\boldsymbol{K}}_{k+1} = \overline{\boldsymbol{P}}_{k+1|k}\boldsymbol{\Psi}^{\mathrm{T}}{}_{\mathrm{k+1,k+1}}\left[\mathrm{I} + \boldsymbol{\Psi}_{\mathrm{k+1,k+1}}\overline{\boldsymbol{P}}_{k+1|k}\boldsymbol{\Psi}^{\mathrm{T}}{}_{\mathrm{k+1,k+1}}\right]^{\mathrm{T}} \tag{3.107}$$

$$\overline{\boldsymbol{P}}_{k+1|k} = \boldsymbol{\varphi}_{\mathrm{k+1,k}}\overline{\boldsymbol{P}}_{k|k}\boldsymbol{\varphi}^T_{\mathrm{k+1,k}} \tag{3.108}$$

$$\overline{\boldsymbol{P}}_{k|k} = \overline{\boldsymbol{P}}_{k|k-1} - \overline{\boldsymbol{K}}_k\boldsymbol{\Psi}_{\mathrm{k,k}}\overline{\boldsymbol{P}}_{k|k-1} = \left(I - \overline{\boldsymbol{K}}_k\boldsymbol{\Psi}_{\mathrm{k,k}}\right)\overline{\boldsymbol{P}}_{k|k-1} \tag{3.109}$$

It is to be noted that $\hat{\boldsymbol{y}}_{k+1}\left(\hat{\boldsymbol{X}}_{k+1|k}\right)$ in Eq. (3.105) is obtained from Eq. (3.101) in which i is replaced by k+1. This results in a term $\hat{\bar{\boldsymbol{f}}}_{k+1|k+1}$ that will be approximated by $\hat{\bar{\boldsymbol{f}}}_{k|k}$. Thus the estimation $\hat{\boldsymbol{X}}_{k+1|k+1}$ obtained from Eq. (3.105) to Eq.(3.109) will be used to replace $\boldsymbol{X}_{k+1}$ in Eq. (3.81) to Eq. (3.85).

3.3 The Kalman Filter Based Approach

Under the Kalman Filter based identification scheme, the following algorithms are considered in the present study

a) Kalman Filter (KF) algorithm.

b) Extended Kalman Filter (EKF) algorithm.

c) Two-Stage Extended Kalman Filter (2-Stage EKF) algorithm.

d) Unscented Kalman Filter (UKF) algorithm.

3.3.1 The Kalman Filter Algorithm

The Kalman Filter is a recursive estimator. This means that only the estimated state from the previous time step and the current measurement are needed to compute the estimate for the current state. In contrast to purely LSE techniques, no histories of observation and or estimates are required. The notation $\hat{\boldsymbol{X}}_{k+1|k}$ represents the estimate of $\boldsymbol{X}$ at time $k+1$ given observations up to and including at time k.

The Kalman filter has two distinct phases: *Predict* and *Update*

The predict phase: The predict phase uses the state estimate from the previous time-step to produce an estimate of the state at the current time-step. This predicted state estimate is also known as a prior state estimate because, although it is an estimate of the state at the current time-step, it does not include observation information from the current time-step.

The update phase: In the update phase, the current a prior prediction is combined with current observation information to refine the state estimate. This improved estimate is termed a posterior state estimate.

The process equation is given as

$$\boldsymbol{x}_k = \mathbb{F}\boldsymbol{x}_{k-1} + \boldsymbol{w}_k \tag{3.110}$$

where, $\boldsymbol{x}_k$ is the state vector of the process at time k; $\mathbb{F}$ is the state transition matrix of the process from state $k-1$ to state k and is assumed stationary over time. $\boldsymbol{w}_k$ is the associated white noise process with known covariance. The measurement or observation equation is given by Eq. (3.111) as

$$\bar{\boldsymbol{z}}_k = \boldsymbol{H}\boldsymbol{x}_k + \boldsymbol{v}_k \tag{3.111}$$

where, $\bar{\boldsymbol{z}}_k$ is the actual measurement of x at time k.

$\boldsymbol{H}$ is a relation between the state vector and the measurement vector and is assumed stationary over time. $\boldsymbol{e}_k$ is the associated measurement error and assumed to be a white noise process. The covariance of the two noise models are assumed stationary over time.

Stationary process

In mathematics and statistics, a stationary is a process whose unconditional joint probability distribution does not change when shifted in time. Consequently, parameters such as mean and variance also do not change over time.

The derivation has been adopted from Lacey A.J. and Thacker N.A. (1998).

The following assumptions are made

$$\boldsymbol{E}[\boldsymbol{w}_k] = 0 \; \forall \; k \tag{3.112}$$

$$\boldsymbol{E}[\boldsymbol{v}_k] = 0 \; \forall \; k \tag{3.113}$$

as $\mathbf{w}_k$ and $\mathbf{e}_k$ are assumed to be a white noise process with zero mean

$$Cov\{\boldsymbol{w}_k, \boldsymbol{w}_j\} = \boldsymbol{Q}_k \delta_{kj} \tag{3.114}$$

or, $$\boldsymbol{Q} = \boldsymbol{E}[\boldsymbol{w}_k \boldsymbol{w}_k^T] \tag{3.115}$$

Similarly, $$Cov\{\boldsymbol{v}_k, \boldsymbol{v}_j\} = \boldsymbol{R}_k \delta_{kj} \tag{3.116}$$

or, $$\boldsymbol{R} = \boldsymbol{E}[\boldsymbol{v}_k \boldsymbol{v}_k^T] \tag{3.117}$$

where, δ is direct delta function and is equal to 1 if $k=j$, else zero.

$$Cov\{\boldsymbol{w}_k, \boldsymbol{v}_j\} = 0 \; \forall \; k \tag{3.118}$$

The overall objective is to estimate $\boldsymbol{x}_k$. The error in the estimate is defined by the difference between the estimate $\hat{\boldsymbol{x}}_{k|k}$ and original $\boldsymbol{x}_k$ given by Eq. (3.119).

$$\boldsymbol{f}(\boldsymbol{e}_k) = \boldsymbol{f}\left(\boldsymbol{x}_k - \hat{\boldsymbol{x}}_{k|k}\right) \tag{3.119}$$

The particular shape of the function depends upon the application and should be positive and increases monotonically. The squared error function exhibits these characteristics.

$$f(\boldsymbol{e}_k) = \left(\boldsymbol{x}_k - \hat{\boldsymbol{x}}_{k|k}\right)^2 \tag{3.120}$$

or, the mean squared error function

$$\epsilon(t) = \boldsymbol{E}(\boldsymbol{e}_k^2) \tag{3.121}$$

This is equivalent to

$$\boldsymbol{E}[\boldsymbol{e}_k \boldsymbol{e}_k^T] = \boldsymbol{P}_{k|k} \tag{3.122}$$

where, $\boldsymbol{P}_{k|k}$is the error covariance matrix at time *k*. Substituting $\boldsymbol{e}_k = \left(\boldsymbol{x}_k - \widehat{\boldsymbol{x}}_{k|k}\right)$ into Eq. (3.122)

$$\boldsymbol{P}_{k|k} = \boldsymbol{E}[\boldsymbol{e}_k \boldsymbol{e}_k^T] = \boldsymbol{E}\left[\left(\boldsymbol{x}_k - \widehat{\boldsymbol{x}}_{k|k}\right)\left(\boldsymbol{x}_k - \hat{x}_{k|k}\right)^T\right] = cov\left(\boldsymbol{x}_k - \widehat{\boldsymbol{x}}_{k|k}\right) \tag{3.123}$$

The prior estimate of $\widehat{\boldsymbol{x}}_{k|k}$ is denoted as $\widehat{\boldsymbol{x}}_{k|k-1}$

$\widehat{\boldsymbol{x}}_{k|k-1}$ is the predicted prior state estimate

$$\widehat{\boldsymbol{x}}_{k|k-1} = \mathbb{F}_k \widehat{\boldsymbol{x}}_{k-1|k-1} + \boldsymbol{w}_k \tag{3.124}$$

It is possible to write an update equation for the new estimate, combining the old estimate with measurement data.

$$\widehat{\boldsymbol{x}}_{k|k} = \widehat{\boldsymbol{x}}_{k|k-1} + \boldsymbol{\mathcal{K}}_k\left(\bar{\boldsymbol{z}}_k - \boldsymbol{H}\widehat{\boldsymbol{x}}_{k|k-1}\right) \tag{3.125}$$

$$\widehat{\boldsymbol{y}}_k = \bar{\boldsymbol{z}}_k - \boldsymbol{H}\widehat{\boldsymbol{x}}_{k|k-1} \tag{3.126}$$

$\widehat{\boldsymbol{y}}_k$ is known as the innovation or measurement residual.

Substituting Eq. (3.111) into Eq. (3.125) gives the updated posterior state estimate

$$\widehat{\boldsymbol{x}}_{k|k} = \widehat{\boldsymbol{x}}_{k|k-1} + \boldsymbol{\mathcal{K}}_k\left(\boldsymbol{H}\boldsymbol{x}_k + \boldsymbol{v}_k - \boldsymbol{H}\widehat{\boldsymbol{x}}_{k|k-1}\right) \tag{3.127}$$

Substituting Eq. (3.127) into Eq. (3.123) gives

$$\begin{aligned}\boldsymbol{P}_{k|k} = \boldsymbol{E}\Big[&\left[(\boldsymbol{I} - \boldsymbol{\mathcal{K}}_k\boldsymbol{H})\left(\boldsymbol{x}_k - \widehat{\boldsymbol{x}}_{k|k-1}\right)\right.\\ &\left.- \boldsymbol{\mathcal{K}}_k\boldsymbol{v}_k\right]\left[(\boldsymbol{I} - \boldsymbol{\mathcal{K}}_k\boldsymbol{H})\left(\boldsymbol{x}_k - \widehat{\boldsymbol{x}}_{k|k-1}\right) - \boldsymbol{\mathcal{K}}_k\boldsymbol{v}_k\right]^T\Big]\end{aligned} \tag{3.128}$$

$$\begin{aligned}\boldsymbol{P}_{k|k} = (\boldsymbol{I} - \boldsymbol{\mathcal{K}}_k\boldsymbol{H})\boldsymbol{E}\left[\left(\boldsymbol{x}_k - \widehat{\boldsymbol{x}}_{k|k-1}\right)\left(\boldsymbol{x}_k - \widehat{\boldsymbol{x}}_{k|k-1}\right)^T\right](\boldsymbol{I} - \boldsymbol{\mathcal{K}}_k\boldsymbol{H})^T\\ + \boldsymbol{\mathcal{K}}_k\boldsymbol{E}[\boldsymbol{v}_k{\boldsymbol{v}_k}^T]\boldsymbol{\mathcal{K}}_k^T\end{aligned} \tag{3.129}$$

Substituting Eq. (3.117) and Eq. (3.123) into Eq. (3.128) gives

$$\boldsymbol{P}_{k|k} = (\boldsymbol{I} - \boldsymbol{\mathcal{K}}_k\boldsymbol{H})\boldsymbol{P}_{k|k-1}(\boldsymbol{I} - \boldsymbol{\mathcal{K}}_k\boldsymbol{H})^T + \boldsymbol{\mathcal{K}}_k\boldsymbol{R}\boldsymbol{\mathcal{K}}_k^T \tag{3.130}$$

Where $\boldsymbol{P}_{k|k-1}$ is the prior estimate of $\boldsymbol{P}_{k|k}$.

Eq. (3.130) is the error covariance update equation. The diagonal of the covariance matrix contains the mean squared error as

$$\boldsymbol{P}_{kk} = \begin{bmatrix} E[\boldsymbol{e}_{k-1}\boldsymbol{e}_{k-1}^T] & E[\boldsymbol{e}_k\boldsymbol{e}_{k-1}^T] & E[\boldsymbol{e}_{k+1}\boldsymbol{e}_{k-1}^T] \\ E[\boldsymbol{e}_{k-1}\boldsymbol{e}_k^T] & E[\boldsymbol{e}_k\boldsymbol{e}_k^T] & E[\boldsymbol{e}_{k+1}\boldsymbol{e}_k^T] \\ E[\boldsymbol{e}_{k-1}\boldsymbol{e}_{k+1}^T] & E[\boldsymbol{e}_k\boldsymbol{e}_{k+1}^T] & E[\boldsymbol{e}_{k+1}\boldsymbol{e}_{k+1}^T] \end{bmatrix} \tag{3.131}$$

The sum of the diagonal elements of a matrix is the trace of a matrix. In the case of the error covariance matrix, the trace is the sum of the mean squared errors. Therefore, the mean squared error may be minimized by minimizing the trace of $\boldsymbol{P}_{k|k}$.

The trace of $\boldsymbol{P}_{k|k}$ is first differentiated with respect to $\boldsymbol{\mathcal{K}}_k$ and the result is set to zero in order to find the condition of this minimum.

Expansion of Eq. (3.130) gives

$$\boldsymbol{P}_{k|k} = \boldsymbol{P}_{k|k-1} - \boldsymbol{\mathcal{K}}_k\boldsymbol{H}\boldsymbol{P}_{k|k-1} - \boldsymbol{P}_{k|k-1}\boldsymbol{H}^T\boldsymbol{\mathcal{K}}_k^T + \boldsymbol{\mathcal{K}}_k\left(\boldsymbol{H}\boldsymbol{P}_{k|k-1}\boldsymbol{H}^T + \boldsymbol{R}\right)\boldsymbol{\mathcal{K}}_k^T \tag{3.132}$$

Note that the trace of a matrix is equal to the trace of its transpose. Therefore it may be written as

$$\boldsymbol{T}\left[\boldsymbol{P}_{k|k}\right] = \boldsymbol{T}\left[\boldsymbol{P}_{k|k-1}\right] - 2\boldsymbol{T}\left[\boldsymbol{\mathcal{K}}_k\boldsymbol{H}\boldsymbol{P}_{k|k-1}\right] + \boldsymbol{T}\left[\boldsymbol{\mathcal{K}}_k\left(\boldsymbol{H}\boldsymbol{P}_{k|k-1}\boldsymbol{H}^T + \boldsymbol{R}\right)\boldsymbol{\mathcal{K}}_k^T\right] \tag{3.133}$$

where, $\boldsymbol{T}\left[\boldsymbol{P}_{k|k}\right]$ is the trace of a matrix $\boldsymbol{P}_{k|k}$.

Differentiating with respect to $\boldsymbol{\mathcal{K}}_k$ gives

$$\frac{d\boldsymbol{T}\left[\boldsymbol{P}_{k|k}\right]}{d\boldsymbol{\mathcal{K}}_k} = -2\left(\boldsymbol{H}\boldsymbol{P}_{k|k-1}\right)^T + 2\boldsymbol{\mathcal{K}}_k\left(\boldsymbol{H}\boldsymbol{P}_{k|k-1}\boldsymbol{H}^T + \boldsymbol{R}\right) \tag{3.134}$$

Setting to zero and rearranging gives;

$$\left(\boldsymbol{H}\boldsymbol{P}_{k|k-1}\right)^T = \boldsymbol{\mathcal{K}}_k\left(\boldsymbol{H}\boldsymbol{P}_{k|k-1}\boldsymbol{H}^T + \boldsymbol{R}\right) \tag{3.135}$$

$$\boldsymbol{\mathcal{K}}_k = \boldsymbol{P}_{k|k-1}\boldsymbol{H}^T\left(\boldsymbol{H}\boldsymbol{P}_{k|k-1}\boldsymbol{H}^T + \boldsymbol{R}\right)^{-1} \tag{3.136}$$

Eq. (3.136) is the Kalman gain equation.

Substituting Eq. (3.136) into Eq. (3.132) gives updated posterior estimate covariance

$$\begin{aligned} \boldsymbol{P}_{k|k} &= \boldsymbol{P}_{k|k-1} - \boldsymbol{P}_{k|k-1}\boldsymbol{H}^T\left(\boldsymbol{H}\boldsymbol{P}_{k|k-1}\boldsymbol{H}^T + \boldsymbol{R}\right)^{-1}\boldsymbol{H}\boldsymbol{P}_{k|k-1} \\ &= \boldsymbol{P}_{k|k-1} - \boldsymbol{\mathcal{K}}_k\boldsymbol{H}\boldsymbol{P}_{k|k-1} = (\boldsymbol{I} - \boldsymbol{\mathcal{K}}_k\boldsymbol{H})\boldsymbol{P}_{k|k-1} \end{aligned} \tag{3.137}$$

Eq. (3.137) is the update equation for the error covariance matrix with optimal gain.

$$\hat{\boldsymbol{x}}_{k+1|k} = \mathbb{F}\hat{x}_{k|k} \tag{3.138}$$

To complete the recursion, it is necessary to find an equation which projects the error covariance matrix into the next time interval, k+1. This is achieved by first forming an expression for the prior error as

$$\boldsymbol{e}'_{k+1} = \boldsymbol{x}_{k+1} - \hat{\boldsymbol{x}}_{k+1|k} = (\mathbb{F}\boldsymbol{x}_k + \boldsymbol{w}_k) - \mathbb{F}\hat{\boldsymbol{x}}_{k|k} = \mathbb{F}\boldsymbol{e}_k + \boldsymbol{w}_k \tag{3.139}$$

Extending Eq. (3.123) to time k+1;

$$\boldsymbol{P}_{k|k+1} = \boldsymbol{E}\left[e'_{k+1}{\boldsymbol{e}'_{k+1}}^{T}\right] = \boldsymbol{E}[(\mathbb{F}\boldsymbol{e}_k + \boldsymbol{w}_k)(\mathbb{F}\boldsymbol{e}_k + \boldsymbol{w}_k)^T] \tag{3.140}$$

It may be noted that $\boldsymbol{e}_k$ and w_k have zero cross-correlation because the noise w_k actually accumulates between k and k+1, whereas the error $\boldsymbol{e}_k$ is the error upto time k. Therefore,

$$\boldsymbol{P}_{k|k+1} = \boldsymbol{E}\left[\boldsymbol{e}'_{k+1}{\boldsymbol{e}'_{k+1}}^{T}\right] = \boldsymbol{E}[\mathbb{F}\boldsymbol{e}_k(\mathbb{F}\boldsymbol{e}_k)^T] + \boldsymbol{E}[\boldsymbol{w}_k{\boldsymbol{w}_k}^T] = \mathbb{F}\boldsymbol{P}_{k|k}\mathbb{F}^T + \boldsymbol{Q} \tag{3.141}$$

The above formulations of Kalman Filter algorithm can be summarized as follows.

Summary of the Kalman Filter

The above steps of Kalman Filter are summarized as given below.

The Predict Phase

Predicted prior state estimate

$$\hat{\boldsymbol{x}}_{k|k-1} = \mathbb{F}_k\hat{\boldsymbol{x}}_{k-1|k-1} + \boldsymbol{w}_k \tag{3.142}$$

$\hat{\boldsymbol{x}}_{k|k-1}$ is an estimate of the state at current time step k, it does not include observation information from the current time step.

Predicted prior estimate covariance $\boldsymbol{P}_{k|k-1} = \mathbb{F}\boldsymbol{P}_{k-1|k-1}\mathbb{F}^T + \boldsymbol{Q}$ (3.143)

The update Phase

Innovation or measurement residual

$$\hat{\boldsymbol{y}}_k = \bar{\boldsymbol{z}}_k - \boldsymbol{H}\hat{\boldsymbol{x}}_{k|k-1} \tag{3.144}$$

$\bar{\boldsymbol{z}}_k$ is the actual measurement of x at time k, $\hat{\boldsymbol{x}}_{k|k-1}$ the predicted state estimate using state transformation matrix $\mathbb{F}$ and updated state estimate of previous step. $\boldsymbol{H}$ is a transformation

matrix which converts the state vector to measurement vector equivalent. Optimal Kalman gain is given by

$$\boldsymbol{\mathcal{K}}_k = \boldsymbol{P}_{k|k-1}\boldsymbol{H}^T\left(\boldsymbol{H}\boldsymbol{P}_{k|k-1}\boldsymbol{H}^T + \boldsymbol{R}\right)^{-1} \tag{3.145}$$

where, $\boldsymbol{P}_{k|k-1}$ is the predicted prior estimate covariance

$$\boldsymbol{P}_{k|k-1} = \mathbb{F}\boldsymbol{P}_{k-1|k-1}\mathbb{F}^T + \boldsymbol{Q} \tag{3.146}$$

where, $\boldsymbol{P}_{k-1|k-1}$ is the posterior estimate covariance of last time step (k-1)

Updated posterior state estimate at current time k,

$$\hat{\boldsymbol{x}}_{k|k} = \hat{\boldsymbol{x}}_{k|k-1} + \boldsymbol{\mathcal{K}}_k\hat{\boldsymbol{y}}_k \tag{3.147}$$

Updated posterior estimate covariance for current step k is given as

$$\boldsymbol{P}_{k|k} = (\boldsymbol{I} - \boldsymbol{\mathcal{K}}_k\boldsymbol{H})\boldsymbol{P}_{k|k-1} \tag{3.148}$$

Using the above formulation, the KF cannot be applied directly to evaluate state and parameter of the structural system under consideration. Problem specific formulation and their derivation as well as implementation issues are covered in detail in the relevant chapters. Detailed derivation has been carried out for different structural systems consisting of fixed base; base isolated buildings supported on SREI as well as FREI supported structures along with missing sensor cases.

In-spite of several advantages of KF, there are various limitations which are as follows.

3.3.1.1 Limitations of Kalman Filter (KF)

One of the limitations of KF is that it is unable to predict or estimate the state vector of nonlinear model accurately and in such cases the KF breaks down. The improved form of KF, known as the EKF can handle nonlinearity through a linearization procedure by making use of Taylor series Expansion of the nonlinear model. Once a linear model is obtained, the KF equations are then applied to obtain the estimate.

The two assumptions regarding KF are-:

1. Kalman Filter will always work with *Gaussian distribution.*
2. Kalman Filter will always work with *Linear Functions*.

The main reason behind this is that if a Gaussian is fed with a linear function then the output is also a Gaussian. If Gaussian distributed signal is fed into a nonlinear function, then the output is not a Gaussian. Nonlinear functions lead to Non Gaussian Distributions (Fig. 3.2).

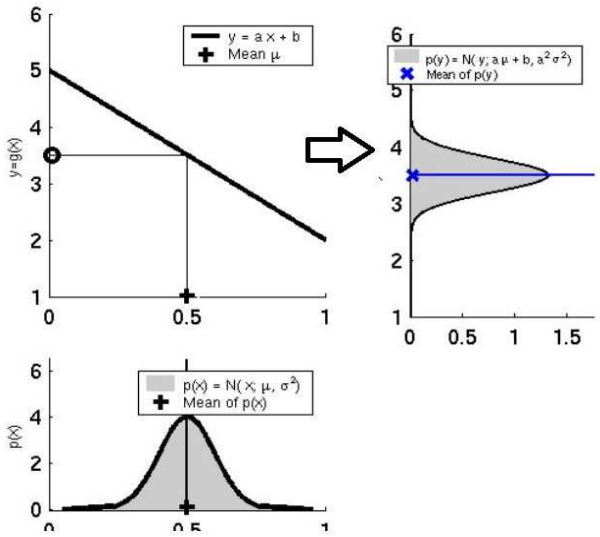

Fig. 3.2: Gaussian + Linear Function = Gaussian (Source) [*figure courtesy: internet*]

So, if a nonlinear function is fed with Gaussian, it will not end up as a Gaussian distribution on which Kalman Filter cannot be applied anymore. Nonlinearity destroys the Gaussian distribution upon nonlinear transformation and it does not make sense to compute the mean and variances (Fig. 3.3).

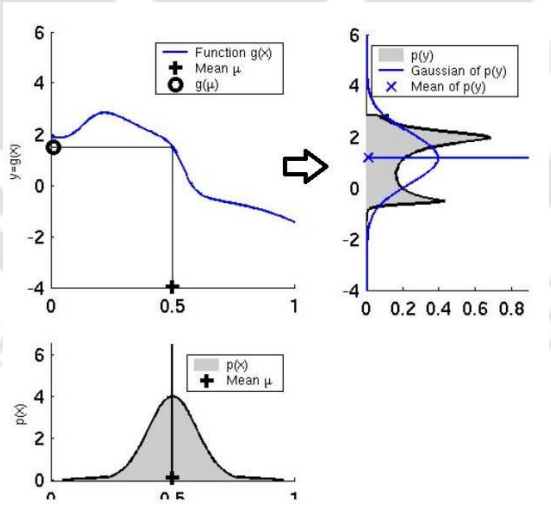

Fig. 3.3: Gaussian + Nonlinear Function = Non Gaussian (Source) [*figure courtesy: internet*]

To apply Kalman Filter for nonlinear functions, the nonlinear function is linearized and used for Kalman filtering. A powerful tool called Taylor Series expansion helps to get a linear

approximation of the nonlinear function. After applying the approximation, what one gets is an EKF.

3.3.2 The Extended Kalman Filter (EKF) Algorithm

This method extends the Kalman filtering through a procedure of linearization by making use of the Taylor series expansion of the nonlinear model. Once a linear model is obtained the KF equations are then applied to obtain the estimate.

Assuming the process has a state vector $\boldsymbol{x}$, but the process is now governed by the nonlinear stochastic difference equation

$$\boldsymbol{x}_k = \boldsymbol{f}(\boldsymbol{x}_{k-1}, \boldsymbol{w}_{k-1}) \tag{3.149}$$

with a measurement $\bar{\mathbf{z}}$, whose equation is given by

$$\bar{\boldsymbol{z}}_k = \boldsymbol{h}(\boldsymbol{x}_k, \boldsymbol{v}_k) \tag{3.150}$$

The random variable w_k and v_k again represent the process and measurement noises respectively which are still white Gaussian. Their covariances are respectively $\boldsymbol{Q}_k$ and $\boldsymbol{R}_k$. The function $\boldsymbol{f}$ is used to compute the prior state from the previous estimate and the function $\boldsymbol{h}$ is also used to compute the predicted measurement from the predicted state. The two functions cannot be applied to the covariance directly. Instead, a matrix of partial derivatives or Jacobian is computed using Taylor series expansion.

The details of the formulations as presented in this sub-section have been adopted from various literatures like Darryl Morrell (1997), Brown Robert Grover and Hwang Patrick Y.C. and Gelb Arthur (2001).

The state transition and observation matrices are defined as below

$$\mathbb{F}_{k-1} = \frac{\partial f}{\partial x}|_{\hat{\boldsymbol{x}}_{k-1|k-1}} \tag{3.151}$$

$$\boldsymbol{H}_k = \frac{\partial h}{\partial x}|_{\hat{\boldsymbol{x}}_{k|k-1}} \tag{3.152}$$

The extended Kalman filter has its time update equations given by

$$\hat{\boldsymbol{x}}_{k|k-1} = \boldsymbol{f}(\boldsymbol{x}_{k-1}, \boldsymbol{w}_{k-1}) \tag{3.153}$$

and that of the measurement updates are

$$\boldsymbol{\mathcal{K}}_k = \boldsymbol{P}_{k|k-1}\boldsymbol{H}_k^T\left(\boldsymbol{H}_k\boldsymbol{P}_{k|k-1}\boldsymbol{H}_k^T + \boldsymbol{R}_k\right)^{-1} \tag{3.154}$$

where, $\boldsymbol{P}_{k|k-1}$ is the predicted prior estimate covariance.

$$\boldsymbol{P}_{k|k-1} = \mathbb{F}_{k-1}\boldsymbol{P}_{k-1|k-1|k-1}\mathbb{F}_{k-1|k-1}^{T} + \boldsymbol{Q}_{k-1} \tag{3.155}$$

where, $\boldsymbol{P}_{k-1|k-1}$ is the posterior estimate covariance of last time step (k-1)

Updated posterior state estimate at current time k,

$$\hat{\boldsymbol{x}}_{k|k} = \hat{\boldsymbol{x}}_{k|k-1} + \boldsymbol{\mathcal{K}}_k \left(\bar{\boldsymbol{z}}_k - \boldsymbol{h}\left(\hat{\boldsymbol{x}}_{k|k-1}\right)\right) \tag{3.156}$$

Updated posterior estimate covariance for current step k is given as

$$\boldsymbol{P}_{k|k} = (\boldsymbol{I} - \boldsymbol{\mathcal{K}}_k\boldsymbol{H}_k)\boldsymbol{P}_{k|k-1} \tag{3.157}$$

The Mathematical approach to Extended Kalman Filter (EKF)

Consider the following nonlinear system, described by the difference equation Eq. (3.158) and the observation model Eq. (3.159) with additive noise:

$$\boldsymbol{x}_k = \boldsymbol{f}(x_{k-1}) + \boldsymbol{w}_k \tag{3.158}$$

$$\bar{\boldsymbol{z}}_k = \boldsymbol{h}(x_k) + \boldsymbol{v}_k \tag{3.159}$$

The following assumptions are made

$$E[\boldsymbol{w}_k] = 0 \;\forall\; k \tag{3.160}$$

$$E[\boldsymbol{v}_k] = 0 \;\forall\; k \tag{3.161}$$

As $\boldsymbol{w}_k$ and $\boldsymbol{v}_k$ are assumed to be a white noise process with zero mean

$$Cov\{w_k, w_j\} = \boldsymbol{Q}_k\delta_{kj} \tag{3.162}$$

or, $\boldsymbol{Q} = E[w_k w_k^T]$ (3.163)

Similarly, $Cov\{v_k, v_j\} = \boldsymbol{R}_k\delta_{kj}$ (3.164)

Where δ is direct delta function and is equal to 1 if k=j else zero.

$$Cov\{\boldsymbol{w}_k, \boldsymbol{v}_j\} = 0 \;\forall\; k \tag{3.165}$$

The error in the estimate is defined by the difference between the estimate $\hat{\boldsymbol{x}}_{k|k}$ and original$\boldsymbol{x}_k$.

$$\boldsymbol{f}(\boldsymbol{e}_k) = \boldsymbol{f}\left(\boldsymbol{x}_k - \hat{\boldsymbol{x}}_{k|k}\right) \tag{3.166}$$

The particular shape of the function depends upon the application and should be positive and increase monotonically. The squared error function exhibits these characteristics.

$$\boldsymbol{f}(\boldsymbol{e}_k) = \left(\boldsymbol{x}_k - \hat{\boldsymbol{x}}_{k|k}\right)^2 \tag{3.167}$$

or, the mean squared error function

$$\boldsymbol{\epsilon}(t) = \boldsymbol{E}(\boldsymbol{e}_k^2) \tag{3.168}$$

This is equivalent to

$$E[\boldsymbol{e}_k \boldsymbol{e}_k^T] = \boldsymbol{P}_{k|k} \tag{3.169}$$

where, $\boldsymbol{P}_{k|k}$ is the error covariance matrix at time k

Substituting $\boldsymbol{e}_k = \left(\boldsymbol{x}_k - \hat{\boldsymbol{x}}_{k|k}\right)$ into Eq. (3.169) gives

$$\boldsymbol{P}_{k|k} = E[\boldsymbol{e}_k \boldsymbol{e}_k^T] = E\left[\left(\boldsymbol{x}_k - \hat{\boldsymbol{x}}_{k|k}\right)\left(\boldsymbol{x}_k - \hat{\boldsymbol{x}}_{k|k}\right)^T\right] = cov\left(\boldsymbol{x}_k - \hat{\boldsymbol{x}}_{k|k}\right) \tag{3.170}$$

Assuming the prior estimate of $\hat{\boldsymbol{x}}_{k|k}$ is called $\hat{\boldsymbol{x}}_{k|k-1}$

$\hat{\boldsymbol{x}}_{k|k-1}$ is the predicted prior state estimate

$$\hat{\boldsymbol{x}}_{k|k-1} = \boldsymbol{f}\left(\hat{\boldsymbol{x}}_{k-1|k-1}\right) + \boldsymbol{w}_{k-1} \tag{3.171}$$

It is possible to write an update equation for the new estimate, combining the old estimate with measurement data Thus,

$$\hat{\boldsymbol{x}}_{k|k} = \hat{\boldsymbol{x}}_{k|k-1} + \boldsymbol{\mathcal{K}}_k\left(\bar{\boldsymbol{z}}_k - \boldsymbol{h}\left(\hat{\boldsymbol{x}}_{k|k-1}\right)\right) \tag{3.172}$$

$$\hat{\boldsymbol{y}}_k = \bar{\boldsymbol{z}}_k - \boldsymbol{h}\left(\hat{\boldsymbol{x}}_{k|k-1}\right) \tag{3.173}$$

$\hat{\boldsymbol{y}}_k$is known as the innovation or measurement residual.

Substituting Eq.(3.159) into Eq. (3.172) gives the updated posterior state estimate

$$\hat{\boldsymbol{x}}_{k|k} = \hat{\boldsymbol{x}}_{k|k-1} + \boldsymbol{\mathcal{K}}_k\left(\boldsymbol{h}(\boldsymbol{x}_k) + \boldsymbol{v}_k - \boldsymbol{h}\left(\hat{\boldsymbol{x}}_{k|k-1}\right)\right) \tag{3.174}$$

Eq. (3.175) is obtained by expanding $\boldsymbol{h}$(.) at $\hat{\boldsymbol{x}}_{k|k-1}$in Taylor series as

$$\boldsymbol{h}(\boldsymbol{x}_k) \equiv \boldsymbol{h}\left(\hat{\boldsymbol{x}}_{k|k-1}\right) + \boldsymbol{H}\left(\hat{\boldsymbol{x}}_{k|k-1}\right)\left(\boldsymbol{x}_k - \hat{\boldsymbol{x}}_{k|k-1}\right) + H.O.T. \tag{3.175}$$

where, $\boldsymbol{H}$ is the Jacobian of $\boldsymbol{h}$(.) and higher order terms (H.O.T.) are considered negligible. The Jacobian of $\boldsymbol{h}$(.) is defined as

$$\boldsymbol{H} \equiv \begin{bmatrix} \frac{\partial h_1}{\partial x_1} & \frac{\partial h_1}{\partial x_2} & \cdots & \frac{\partial h_1}{\partial x_n} \\ \vdots & \vdots & \ddots & \vdots \\ \frac{\partial h_m}{\partial x_1} & \frac{\partial h_m}{\partial x_2} & \cdots & \frac{\partial h_m}{\partial x_n} \end{bmatrix} \tag{3.176}$$

where, $\boldsymbol{h}(x)= (\boldsymbol{h}_1(x), \boldsymbol{h}_2(x), \ldots\ldots, \boldsymbol{h}_m(x),)^T$ and $\boldsymbol{x}=(\boldsymbol{x}_1, \boldsymbol{x}_2, \ldots\ldots..\boldsymbol{x}_n)^T$

Substituting $\boldsymbol{h}(\boldsymbol{x}_k)$ from Eq. (3.175) into Eq. (3.174) gives Eq. (3.178) and neglecting H.O.T.

$$\begin{aligned} \hat{\boldsymbol{x}}_{k|k} = \hat{\boldsymbol{x}}_{k|k-1} + \boldsymbol{\mathcal{K}}_k \Big(& \boldsymbol{h}\big(\hat{\boldsymbol{x}}_{k|k-1}\big) + \boldsymbol{H}\big(\hat{\boldsymbol{x}}_{k|k-1}\big)\big(\boldsymbol{x}_k - \hat{\boldsymbol{x}}_{k|k-1}\big) + \boldsymbol{v}_k \\ & - \boldsymbol{h}\big(\hat{\boldsymbol{x}}_{k|k-1}\big)\Big) \end{aligned} \tag{3.177}$$

$$\hat{\boldsymbol{x}}_{k|k} = \hat{\boldsymbol{x}}_{k|k-1} + \boldsymbol{\mathcal{K}}_k\big(\boldsymbol{H}\big(\hat{\boldsymbol{x}}_{k|k-1}\big)\big(\boldsymbol{x}_k - \hat{\boldsymbol{x}}_{k|k-1}\big) + \boldsymbol{v}_k\big) \tag{3.178}$$

Eq. (3.179) is obtained from Eq. (3.170) as

$$\boldsymbol{P}_{k|k} = E[\boldsymbol{e}_k \boldsymbol{e}_k^T] = E\left[\big(\boldsymbol{x}_k - \hat{\boldsymbol{x}}_{k|k}\big)\big(\boldsymbol{x}_k - \hat{\boldsymbol{x}}_{k|k}\big)^T\right] \tag{3.179}$$

Substituting $\hat{\boldsymbol{x}}_{k|k}$ from Eq. (3.178) into Eq. (3.170), the following is obtained

$$\begin{aligned} \boldsymbol{P}_{k|k} = E\Big[\Big(\boldsymbol{x}_k - \hat{\boldsymbol{x}}_{k|k-1} & \\ & - \boldsymbol{\mathcal{K}}_k\big(\boldsymbol{H}\big(\hat{\boldsymbol{x}}_{k|k-1}\big)\big(\boldsymbol{x}_k - \hat{\boldsymbol{x}}_{k|k-1}\big) + \boldsymbol{v}_k\big)\Big)\Big(\boldsymbol{x}_k - \hat{\boldsymbol{x}}_{k|k-1} \\ & - \boldsymbol{\mathcal{K}}_k\big(\boldsymbol{H}\big(\hat{\boldsymbol{x}}_{k|k-1}\big)\big(\boldsymbol{x}_k - \hat{\boldsymbol{x}}_{k|k-1}\big) + \boldsymbol{v}_k\big)\Big)^T\Big] \end{aligned}$$

$$\begin{aligned} = E\Big[\Big\{\big(\boldsymbol{x}_k - \hat{\boldsymbol{x}}_{k|k-1}\big)\Big(I - \boldsymbol{\mathcal{K}}_k\boldsymbol{H}\big(\hat{\boldsymbol{x}}_{k|k-1}\big)\Big) & \\ - \boldsymbol{\mathcal{K}}_k\boldsymbol{v}_k\Big\}\Big\{\big(\boldsymbol{x}_k - \hat{\boldsymbol{x}}_{k|k-1}\big)\Big(I - \boldsymbol{\mathcal{K}}_k\boldsymbol{H}\big(\hat{\boldsymbol{x}}_{k|k-1}\big)\Big) - \boldsymbol{\mathcal{K}}_k\boldsymbol{v}_k\Big\}^T\Big] & \end{aligned}$$

$$\begin{aligned} = \Big(\boldsymbol{I} - \boldsymbol{\mathcal{K}}_k\boldsymbol{H}\big(\hat{\boldsymbol{x}}_{k|k-1}\big)\Big) E\Big[\big(\boldsymbol{x}_k - \hat{\boldsymbol{x}}_{k|k-1}\big)\big(\boldsymbol{x}_k - \hat{\boldsymbol{x}}_{k|k-1}\big)^T\Big]\Big(\boldsymbol{I} & \\ - \boldsymbol{\mathcal{K}}_k\boldsymbol{H}\big(\hat{\boldsymbol{x}}_{k|k-1}\big)\Big)^T + \boldsymbol{\mathcal{K}}_k E[\boldsymbol{v}_k \boldsymbol{v}_k{}^T]\boldsymbol{\mathcal{K}}_k{}^T & \end{aligned} \tag{3.180}$$

Representing $\boldsymbol{H}\big(\hat{\boldsymbol{x}}_{k|k-1}\big)$ by $\boldsymbol{H}$ by dropping the term $\big(\hat{\boldsymbol{x}}_{k|k-1}\big)$, the following is obtained

$$\boldsymbol{P}_{k|k} = (\boldsymbol{I} - \boldsymbol{\mathcal{K}}_k\boldsymbol{H})\boldsymbol{P}_{k|k-1}(\boldsymbol{I} - \boldsymbol{\mathcal{K}}_k\boldsymbol{H})^T + \boldsymbol{\mathcal{K}}_k\boldsymbol{R}\boldsymbol{\mathcal{K}}_k{}^T \tag{3.181}$$

where, prior estimate of $\boldsymbol{P}_{k|k} = \boldsymbol{P}_{k|k-1} = \boldsymbol{E}\left[\big(\boldsymbol{x}_k - \hat{\boldsymbol{x}}_{k|k-1}\big)\big(\boldsymbol{x}_k - \hat{\boldsymbol{x}}_{k|k-1}\big)^T\right]$

Eq. (3.181) is the error covariance update equation. The diagonal of the covariance matrix contains the mean squared error as shown;

$$\boldsymbol{P}_{k|k} = \begin{bmatrix} E[e_{k-1}e_{k-1}^T] & E[e_k e_{k-1}^T] & E[e_{k+1}e_{k-1}^T] \\ E[e_{k-1}e_k^T] & E[e_k e_k^T] & E[e_{k+1}e_k^T] \\ E[e_{k-1}e_{k+1}^T] & E[e_k e_{k+1}^T] & E[e_{k+1}e_{k+1}^T] \end{bmatrix} \tag{3.182}$$

The sum of the diagonal elements of a matrix is the trace of a matrix. In the case of the error covariance matrix the trace is the sum of the mean squared errors. Therefore, the mean squared error may be minimized by minimizing the trace of $\boldsymbol{P}_{k|k}$ which in turn will minimize the trace of $\boldsymbol{P}_{k|k}$.

The trace of $\boldsymbol{P}_{k|k}$ is first differentiated with respect to $\boldsymbol{\mathcal{K}}_k$ and the result set to zero in order to find the condition of this minimum.

Expansion of Eq. (3.181) gives

$$\begin{aligned} \boldsymbol{P}_{k|k} = \boldsymbol{P}_{k|k-1} - \boldsymbol{\mathcal{K}}_k \boldsymbol{H} \boldsymbol{P}_{k|k-1} - \boldsymbol{P}_{k|k-1} \boldsymbol{H}^T \boldsymbol{\mathcal{K}}_k^T \\ + \boldsymbol{\mathcal{K}}_k \left(\boldsymbol{H} \boldsymbol{P}_{k|k-1} \boldsymbol{H}^T + \boldsymbol{R} \right) \boldsymbol{\mathcal{K}}_k^T \end{aligned} \tag{3.183}$$

Note that the trace of a matrix is equal to the trace of its transpose; therefore it may be written as

$$T\left[\boldsymbol{P}_{k|k}\right] = T\left[\boldsymbol{P}_{k|k-1}\right] - 2T\left[\boldsymbol{\mathcal{K}}_k \boldsymbol{H} \boldsymbol{P}_{k|k-1}\right] + T\left[\boldsymbol{\mathcal{K}}_k \left(\boldsymbol{H} \boldsymbol{P}_{k|k-1} \boldsymbol{H}^T + \boldsymbol{R} \right) \boldsymbol{\mathcal{K}}_k^T\right] \tag{3.184}$$

where $T\left[\boldsymbol{P}_{k|k}\right]$ is the trace of matrix $\boldsymbol{P}_{k|k}$.

Differentiating with respect to $\boldsymbol{\mathcal{K}}_k$ gives

$$\frac{dT\left[\boldsymbol{P}_{k|k}\right]}{d\boldsymbol{\mathcal{K}}_k} = -2\left(\boldsymbol{H} \boldsymbol{P}_{k|k-1}\right)^T + 2\boldsymbol{\mathcal{K}}_k \left(\boldsymbol{H} \boldsymbol{P}_{k|k-1} \boldsymbol{H}^T + \boldsymbol{R} \right) \tag{3.185}$$

Setting to zero and rearranging gives;

$$\left(\boldsymbol{H} \boldsymbol{P}_{k|k-1}\right)^T = \boldsymbol{\mathcal{K}}_k \left(\boldsymbol{H} \boldsymbol{P}_{k|k-1} \boldsymbol{H}^T + \boldsymbol{R} \right) \tag{3.186}$$

$$\boldsymbol{\mathcal{K}}_k = \boldsymbol{P}_{k|k-1} \boldsymbol{H}^T \left(\boldsymbol{H} \boldsymbol{P}_{k|k-1} \boldsymbol{H}^T + \boldsymbol{R} \right)^{-1} \tag{3.187}$$

Eq. (3.187) is the Kalman gain equation.

Substituting Eq. (3.187) into Eq. (3.183) gives updated posterior estimate covariance

$$\begin{aligned} \boldsymbol{P}_{k|k} &= \boldsymbol{P}_{k|k-1} - \boldsymbol{P}_{k|k-1}\boldsymbol{H}^T\left(\boldsymbol{H}\boldsymbol{P}_{k|k-1}\boldsymbol{H}^T + \boldsymbol{R}\right)^{-1}\boldsymbol{H}\boldsymbol{P}_{k|k-1} \\ &= \boldsymbol{P}_{k|k-1} - \boldsymbol{\mathcal{K}}_k\boldsymbol{H}\boldsymbol{P}_{k|k-1} = (\boldsymbol{I} - \boldsymbol{\mathcal{K}}_k\boldsymbol{H})\boldsymbol{P}_{k|k-1} \end{aligned} \tag{3.188}$$

To complete the recursion it is necessary to find an equation which projects the error covariance matrix into the next time interval, k+1. This is achieved by first forming an expression for the prior error.

Eq. (3.158) is re-written as

$$\boldsymbol{x}_k = \boldsymbol{f}(x_{k-1}) + \boldsymbol{w}_k \tag{3.189}$$

Therefore, for next time interval, k+1, $\boldsymbol{x}_{k+1}$ is given by Eq. (3.189) as

$$\boldsymbol{x}_{k+1} = \boldsymbol{f}(x_k) + \boldsymbol{w}_{k+1} \tag{3.190}$$

The, error, $\boldsymbol{e}'_{k+1}$ for next time interval, k +1, is given by Eq. (3.191) as

$$\boldsymbol{e}'_{k+1} = \boldsymbol{x}_{k+1|k} - \hat{\boldsymbol{x}}_{k+1|k} = (\boldsymbol{f}(x_k) + \boldsymbol{w}_{k+1}) - \boldsymbol{f}(\hat{x}_{k|k}) \tag{3.191}$$

Eq. (3.192) is obtained by expanding $\boldsymbol{f}$(.) in Taylor series about $\hat{\boldsymbol{x}}_{k|k}$ as

$$\boldsymbol{f}(\boldsymbol{x}_k) \equiv \boldsymbol{f}(\hat{\boldsymbol{x}}_{k|k}) + \mathbb{F}(\hat{\boldsymbol{x}}_{k|k})(\boldsymbol{x}_{k|k} - \hat{\boldsymbol{x}}_{k|k}) + H.O.T. \tag{3.192}$$

$$\boldsymbol{f}(\boldsymbol{x}_k) \equiv \boldsymbol{f}(\hat{\boldsymbol{x}}_{k|k}) + \mathbb{F}(\hat{\boldsymbol{x}}_{k|k})e_k + H.O.T. \tag{3.193}$$

where, $\mathbb{F}$ is the Jacobian of $\boldsymbol{f}$(.) and higher order terms (H.O.T.) are considered negligible. The Jacobian of $\boldsymbol{f}$(.) is defined as

$$\mathbb{F} \equiv \begin{bmatrix} \frac{\partial f_1}{\partial x_1} & \frac{\partial f_1}{\partial x_2} & \cdots & \frac{\partial f_1}{\partial x_n} \\ \vdots & \vdots & \ddots & \vdots \\ \frac{\partial f_m}{\partial x_1} & \frac{\partial f_m}{\partial x_2} & \cdots & \frac{\partial f_m}{\partial x_n} \end{bmatrix} \tag{3.194}$$

where, $\boldsymbol{f}$(x)= ($\boldsymbol{f}_1$(x), $\boldsymbol{f}_2$(x), ……, $\boldsymbol{f}_m$(x),)^T and $\boldsymbol{x}$=($\boldsymbol{x}_1$, $\boldsymbol{x}_2$, ……..$\boldsymbol{x}_n$)^T

Eq. (3.195) is obtained from Eq. (3.191) and Eq. (3.193) as

$$\boldsymbol{e}'_{k+1} = \boldsymbol{f}(\hat{\boldsymbol{x}}_{k|k}) + \mathbb{F}(\hat{\boldsymbol{x}}_{k|k})e_k - \boldsymbol{f}(\hat{x}_{k|k}) \tag{3.195}$$

$$or, \qquad \boldsymbol{e}'_{k+1} = \mathbb{F}(\hat{\boldsymbol{x}}_{k|k})e_k = \mathbb{F}e_k \tag{3.196}$$

Representing $\mathbb{F}(\hat{\boldsymbol{x}}_{k|k})$ by $\mathbb{F}$ by dropping the term $(\hat{\boldsymbol{x}}_{k|k})$

Extending Eq. (3.170) to time k+1;

$$P_{k|k+1} = E\left[\boldsymbol{e}'_{k+1}{e'_{k+1}}^{T}\right] = E[(\mathbb{F}\boldsymbol{e}_k + \boldsymbol{w}_{k+1})(\mathbb{F}\boldsymbol{e}_k + \boldsymbol{w}_{k+1})^T] \tag{3.197}$$

Note that $\boldsymbol{e}_k$ and $\boldsymbol{w}_k$ have zero cross-correlation because the noise $\boldsymbol{w}_k$ actually accumulates between *k* and *k*+1 where the error $\mathbf{e}_k$ is the error upto time k. Therefore,

$$\begin{aligned}\boldsymbol{P}_{k|k+1} = E\left[e'_{k+1}{e'_{k+1}}^{T}\right] &= E[\mathbb{F}e_k(\mathbb{F}\boldsymbol{e_k})^T] + E[\boldsymbol{w}_{k+1}{w_{k+1}}^T] \\ &= \mathbb{F}\boldsymbol{P}_{k|k}\mathbb{F}^T + \boldsymbol{Q_{k+1}}\end{aligned} \tag{3.198}$$

The above formulations of the EKF algorithm can be summarized as follows.

Summary of Extended Kalman Filter

The above formulation of EKF can be summarized as given below.

The Predict Phase

Predicted prior state estimate

$$\hat{\boldsymbol{x}}_{k|k-1} = \boldsymbol{f}(x_{k-1}) + \boldsymbol{w}_k \tag{3.199}$$

$\hat{\boldsymbol{x}}_{k|k-1}$ is an estimate of the state at current time step *k*, it does not include observation information from the current time step.

Defining the state transition and observation matrices by the following Jacobians

$$\mathbb{F} = \frac{\partial f}{\partial x}|_{\hat{x}_{k|k}} \tag{3.200}$$

$$\boldsymbol{H} = \frac{\partial h}{\partial x}|_{\hat{x}_{k|k-1}} \tag{3.201}$$

Predicted prior estimate covariance $\boldsymbol{P}_{k|k-1} = \mathbb{F}\boldsymbol{P}_{k-1|k-1}\mathbb{F}^T + \boldsymbol{Q}$ (3.202)

The update Phase

Innovation or measurement residual

$$\hat{\boldsymbol{y}}_k = \bar{\boldsymbol{z}}_k - \boldsymbol{h}\left(\hat{\boldsymbol{x}}_{k|k-1}\right) \tag{3.203}$$

$\bar{\boldsymbol{z}}_k$ is the actual measurement of *x* at time *k*,

$\hat{\boldsymbol{x}}_{k|k-1}$ the predicted state estimate using state transformation matrix $\mathbb{F}$ and updated state estimate of previous step.

Optimal Kalman gain is given by

$$\boldsymbol{\mathcal{K}}_k = \boldsymbol{P}_{k|k-1}\boldsymbol{H}^T\left(\boldsymbol{H}\boldsymbol{P}_{k|k-1}\boldsymbol{H}^T + \boldsymbol{R}\right)^{-1} \tag{3.204}$$

where, $\boldsymbol{P}_{k|k-1}$ is the predicted prior estimate covariance

$$\boldsymbol{P}_{k|k-1} = \mathbb{F}\boldsymbol{P}_{k-1|k-1}\mathbb{F}^T + \boldsymbol{Q_k} \tag{3.205}$$

where, $\boldsymbol{P}_{k-1|k-1}$ is the posterior estimate covariance of last time step (k-1)

Updated posterior state estimate at current time k,

$$\hat{\boldsymbol{x}}_{k|k} = \hat{\boldsymbol{x}}_{k|k-1} + \boldsymbol{\mathcal{K}}_k\hat{\boldsymbol{y}}_k \tag{3.206}$$

Updated posterior estimate covariance for current step k is given as

$$\boldsymbol{P}_{k|k} = (\boldsymbol{I} - \boldsymbol{\mathcal{K}}_k\boldsymbol{H})\boldsymbol{P}_{k|k-1} \tag{3.207}$$

The formulation of the state transfer matrix is given below.

The formulation of State Transfer Matrix

If the Eq. (3.158) above is represented in the following general non-linear differential state equation as

$$\dot{\boldsymbol{X}} = \boldsymbol{g}(X, f, f^u, t) \tag{3.208}$$

which is of the form $\dot{x}(t) = \boldsymbol{\mathcal{A}}x(t)$, for homogeneous solution, Laplace Transform is applied on both sides as

$$s\boldsymbol{X}(s) - \boldsymbol{x}(0) = \boldsymbol{\mathcal{A}}\boldsymbol{X}(s)$$

or, $$\boldsymbol{X}(s) = (s\boldsymbol{I} - \boldsymbol{\mathcal{A}})^{-1}x(0) \tag{3.209}$$

By taking inverse Laplace Transform, Eq. (3.210) is obtained as

$$\boldsymbol{x}(t) = \mathcal{L}^{-1}[(s\boldsymbol{I} - \boldsymbol{\mathcal{A}})^{-1}]\boldsymbol{x}(0) = e^{\boldsymbol{\mathcal{A}}t}\boldsymbol{x}(0) \ldots \tag{3.210}$$

Or, the State Transition Matrix for Eq. (3.208) is given by Eq. (3.211)

$$\boldsymbol{\Phi}(t) \triangleq e^{\boldsymbol{\mathcal{A}}t} = \mathcal{L}^{-1}[(s\boldsymbol{I} - \boldsymbol{\mathcal{A}})^{-1}] \tag{3.211}$$

$$\boldsymbol{\Phi}_{k-1|k-1} = e^{\boldsymbol{\mathcal{A}}(\hat{\boldsymbol{X}}_{k-1|k-1})\Delta t} \approx \boldsymbol{I} + \Delta t.\boldsymbol{\mathcal{A}}\left(\hat{\boldsymbol{X}}_{k-1|k-1}\right) \tag{3.212}$$

Replacing $\mathbb{F}$ by $\boldsymbol{\Phi}_{\mathrm{k-1|k-1}}$ in Eq.(3.207) gives the predicted prior estimate covariance

$$\boldsymbol{P}_{k|k-1} = \boldsymbol{\Phi}_{\mathrm{k-1|k-1}}\boldsymbol{P}_{k-1|k-1}\boldsymbol{\Phi}_{k-1|k-1}^T + \boldsymbol{Q_k} \tag{3.213}$$

Other equations remain same.

3.3.3 The Two-Stage Extended Kalman Filter Algorithm.

The Mathematical approach to Two-Stage Kalman Filter Algorithm

In EKF algorithm, the parametric vector or the structural parameters represented as $\boldsymbol{X}_3 = \{\theta_1, \theta_2, \ldots\ldots, \theta_m, \}^T$, where $\theta_1, \theta_2, \ldots\ldots, \theta_m$ represents stiffness, damping or hysteretic parameters etc, are included within the unknown extended state vector along with state vector $\boldsymbol{X}_1 = \boldsymbol{x}^T$; $\boldsymbol{X}_2 = \dot{\boldsymbol{x}}^T$, where $\boldsymbol{x}$ is displacement and $\dot{\boldsymbol{x}}$ the velocity. Together, the extended state vector is represented as $\boldsymbol{X_e} = \{\boldsymbol{X}_1^T, \boldsymbol{X}_2^T, \boldsymbol{X}_3^T\}^T$. The extended state vector is unknown and it is needed to be evaluated. The extended state vector becomes quite large with lot of unknown parameters and therefore, there is a high chance that the filter may diverge and consequently fail. To overcome this issue, Lei and Jiang (2011) suggested two-stage EKF algorithm. In the 1st step of two-stage EKF, the state vector is identified on the presumption that parametric vector is known. In the 2nd step, the parametric vector is identified with the help of evaluated state vector of 1st step. The detailed derivation of two-stage EKF as was proposed by Lei and Jiang (2011) is shown below.

The equation of motion of an MDOF structure can be expressed as follows:

$$\boldsymbol{M}\ddot{\boldsymbol{x}} + \boldsymbol{F}_c[\dot{\boldsymbol{x}}, \boldsymbol{\theta}] + \boldsymbol{F}_s[\boldsymbol{x}, \boldsymbol{\theta}] = \boldsymbol{\eta F} \tag{3.214}$$

where, $\boldsymbol{x}, \dot{\boldsymbol{x}}$ and $\ddot{\boldsymbol{x}}$ are the vectors of structural displacement, velocity and acceleration, respectively; $\boldsymbol{\theta}$ is the unknown parameter of the structure, including damping, stiffness, nonlinear parameter; $\boldsymbol{F}_c[\dot{\boldsymbol{x}}, \boldsymbol{\theta}]$ is the damping force vector; $\boldsymbol{F}_s[\boldsymbol{x}, \boldsymbol{\theta}]$ is the stiffness force vector; $\boldsymbol{F}$ is the external excitation vector; and $\boldsymbol{\eta}$ is the influence matrix associated with $\boldsymbol{F}$. As in most cases mass of a structure can be estimated accurately, so $\boldsymbol{M}$ is assumed to be known here.

The extended state vector of the structure is defined as $\boldsymbol{X_e} = \{\boldsymbol{X}_1^T, \boldsymbol{X}_2^T, \boldsymbol{X}_3^T\}^T$ in which $\boldsymbol{X}_1 = \boldsymbol{x}^T$; $\boldsymbol{X}_2 = \dot{\boldsymbol{x}}^T$; and $\boldsymbol{X}_3 = \{\theta_1, \theta_2, \ldots\ldots, \theta_m, \}^T$. $\{\boldsymbol{X}_1^T, \boldsymbol{X}_2^T\}^T$ is the state vector of the structure; $\boldsymbol{X}_3^T$ is a m-dimension unknown parametric vector of $\boldsymbol{\theta}_i$ (i=1,2,.., m)

As the unknown structural parameters are constant, which implies $\dot{\boldsymbol{\theta}}_i = \boldsymbol{0}$, Eq. (3.214) can be written into the following extended state equation for the extended state vector as

$$\dot{\boldsymbol{X}}_{\boldsymbol{e}} = \begin{Bmatrix} \dot{\boldsymbol{X}}_1 \\ \dot{\boldsymbol{X}}_2 \\ \dot{\boldsymbol{X}}_3 \end{Bmatrix} = \begin{Bmatrix} \boldsymbol{X}_2 \\ \boldsymbol{M}^{-1}\{\boldsymbol{\eta F} - \boldsymbol{\mathcal{F}}[\boldsymbol{X}_1, \boldsymbol{X}_2, \boldsymbol{X}_3]\} \\ 0 \end{Bmatrix} = \boldsymbol{g}(\boldsymbol{X}, \boldsymbol{F}) \tag{3.215}$$

where, $\boldsymbol{\mathcal{F}}[\boldsymbol{X}_1, \boldsymbol{X}_2, \boldsymbol{X}_3] = \boldsymbol{F}_c[\dot{\boldsymbol{x}}, \boldsymbol{\theta}] + \boldsymbol{F}_s[\boldsymbol{x}, \boldsymbol{\theta}]$

The discretized observation equation can be represented in the following Eq. (3.216) on the assumption that few accelerometers have been attached to the structure to measure structural acceleration responses.

$$\boldsymbol{y}_k = \boldsymbol{\Lambda M}^{-1}(\boldsymbol{\eta F}_k - \boldsymbol{\mathcal{F}}[\boldsymbol{X}_1, \boldsymbol{X}_2, \boldsymbol{X}_3]) + \boldsymbol{v}_k = \boldsymbol{h}(\boldsymbol{X}_k, \boldsymbol{f}_k) + \boldsymbol{v}_k \tag{3.216}$$

where, $\boldsymbol{y}_k$ is the measured acceleration responses at time $t = k \times \Delta t$ with Δt being the sampling time step. $\boldsymbol{\Lambda}$ denotes the matrix associated with the location of accelerometers, and $\boldsymbol{v}_k$ is the measurement noise vector of a Gaussian white noise vector with zero mean and a covariance matrix $\boldsymbol{E}[\boldsymbol{v}_i \boldsymbol{v}_j] = \boldsymbol{R}_{ij}, \delta_{ij}$ where δ_{ij} is the Kronecker delta.

In what follows, the notation $\widehat{\boldsymbol{X}}_{k+1|k}$ represents the estimate of $\boldsymbol{X}_{\boldsymbol{e}}$ at time $k+1$ given observations up to and including at time k.

The extended state vector can be written based on the traditional EKF as

$$\widehat{\boldsymbol{X}}_{k+1|k+1} = \widetilde{\boldsymbol{X}}_{k+1|k} + \boldsymbol{\mathcal{K}}_{k+1}[\boldsymbol{y}_{k+1} - \boldsymbol{h}(\widetilde{\boldsymbol{X}}_{k+1|k}, \boldsymbol{F}_{k+1})] \tag{3.217}$$

$$\widetilde{\boldsymbol{X}}_{k+1|k} = \widehat{\boldsymbol{X}}_{k|k} + \int_k^{(k+1)} \boldsymbol{g}(\widehat{\boldsymbol{X}}_{t|k}, \boldsymbol{F}, t)dt \tag{3.218}$$

where, $\boldsymbol{\mathcal{K}}_{k+1}$ is the Kalman gain matrix at time $t = k \times \Delta t$.

Therefore, structural state vector and unknown parameters are identified simultaneously by forming an extended state vector in the traditional EKF algorithm. In two-step Kalman filter, state vector of the structure is defined as

$\boldsymbol{X} = \{\boldsymbol{X}_1^T, \boldsymbol{X}_2^T\}^T$ in which $\boldsymbol{X}_1 = \boldsymbol{x}^T$; $\boldsymbol{X}_2 = \dot{\boldsymbol{x}}^T$; and Eq. (3.215) can be written as

$$\dot{\boldsymbol{X}} = \begin{Bmatrix} \dot{\boldsymbol{X}}_1 \\ \dot{\boldsymbol{X}}_2 \end{Bmatrix} = \begin{Bmatrix} \boldsymbol{X}_2 \\ \boldsymbol{M}^{-1}\{\boldsymbol{\eta F} - \boldsymbol{\mathcal{F}}[\boldsymbol{x}, \dot{\boldsymbol{x}}, \boldsymbol{\theta}]\} \end{Bmatrix} + \boldsymbol{w} = \boldsymbol{g}(\boldsymbol{X}, \boldsymbol{\theta}, \boldsymbol{F}) + \boldsymbol{w} \tag{3.219}$$

Also, the discretized observation equation of the acceleration responses can be expressed as follows:

$$\boldsymbol{y}_k = \boldsymbol{\Lambda M}^{-1}(\boldsymbol{\eta F}_k - \boldsymbol{\mathcal{F}}[\boldsymbol{x}, \dot{\boldsymbol{x}}, \boldsymbol{\theta}]) + \boldsymbol{v}_k = \boldsymbol{h}(\boldsymbol{X}_k, \boldsymbol{\theta}_k, \boldsymbol{F}_k) + \boldsymbol{v}_k \tag{3.220}$$

Step 1:*In two-step Kalman Filter*

Supposing that structural parametric vector $\boldsymbol{\theta}_{k+1}$ is known, recursive solution for structural state vector at time $t = (k + 1) \times \Delta t$, denoted by $\widehat{\boldsymbol{X}}_{k+1|k+1}$ can be derived by the traditional

Kalman filter based on thestate equation of Eq.(3.219) and the observation equation of Eq.(3.220) as

$$\widehat{\boldsymbol{X}}_{k+1|k+1}(\boldsymbol{\theta}_{k+1}) = \widetilde{\boldsymbol{X}}_{k+1|k} + \boldsymbol{\mathcal{K}}_{X,k+1}\left[\boldsymbol{y}_{k+1} - \boldsymbol{h}\left(\widetilde{\boldsymbol{X}}_{k+1|k}, \boldsymbol{\theta}_{k+1}, \boldsymbol{F}_{k+1}\right)\right] \tag{3.221}$$

where, $\widetilde{\boldsymbol{X}}_{k+1|k}$ are the predicted estimate of state $\boldsymbol{X}_{k+1}$ at time $t=k\times\Delta t$, which can be obtained from Eq. (3.219) by integration as

$$\widetilde{\boldsymbol{X}}_{k+1|k} = \widehat{\boldsymbol{X}}_{k|k} + \int_{k\Delta t}^{(k+1)\Delta t} \boldsymbol{g}\left(\widehat{\boldsymbol{X}}_{t|k}, \boldsymbol{\theta}, \boldsymbol{F}, t\right) dt \tag{3.222}$$

$\boldsymbol{\mathcal{K}}_{X,k+1}$ is the Kalman gain matrix for state $\boldsymbol{X}$ given by

$$\boldsymbol{\mathcal{K}}_{X,k+1} = \boldsymbol{P}_{k+1|k}\boldsymbol{H}_{X,k+1}^{T}\left(\boldsymbol{H}_{X,k+1}\boldsymbol{P}_{k+1|k}\boldsymbol{H}_{X,k+1}^{T} + \boldsymbol{R}_{k+1}\right)^{-1} \tag{3.223}$$

$$\boldsymbol{H}_{X,k+1} = \left[\frac{\partial \boldsymbol{h}(\boldsymbol{x}, \boldsymbol{\theta}, \boldsymbol{f})}{\partial \boldsymbol{X}}\right]_{\boldsymbol{X}=\widetilde{\boldsymbol{X}}_{k+1|k}, \boldsymbol{\theta}=\boldsymbol{\theta}_{k+1}} \tag{3.224}$$

and the error covariance matrix $\boldsymbol{P}_{k+1|k}$ can be derived as

$$\boldsymbol{P}_{k+1|k} = \boldsymbol{\Phi}_k \boldsymbol{P}_{k|k} \boldsymbol{\Phi}_k^{T} + \boldsymbol{Q}_k \tag{3.225}$$

$\boldsymbol{\Phi}_k$is the state transition matrix of the linearized system in Eq. (3.219), that is

$$\boldsymbol{\Phi}_{\mathrm{k}} = \mathrm{e}^{\boldsymbol{\mathcal{A}}(\widehat{\mathbf{X}}_{\mathrm{k|k}})\Delta \mathrm{t}} \approx \mathbf{I} + \Delta \mathrm{t}.\boldsymbol{\mathcal{A}}\left(\widehat{\mathbf{X}}_{\mathrm{k|k}}\right) \tag{3.226}$$

$$\text{State Transition matrix, } \boldsymbol{\mathcal{A}} = \left[\frac{\partial \boldsymbol{g}(\boldsymbol{x}, \boldsymbol{\theta}, \boldsymbol{F})}{\partial \boldsymbol{X}}\right]_{\boldsymbol{X}=\widetilde{\boldsymbol{X}}_{k|k}, \boldsymbol{\theta}=\widehat{\boldsymbol{\theta}}_k} \tag{3.227}$$

In which $\boldsymbol{I}$ is the unit matrix and the recursive estimation of the error covariance matrix $\boldsymbol{P}_{k+1|k+1}$ is given as

$$\boldsymbol{P}_{k+1|k+1} = \left(\boldsymbol{I} - \boldsymbol{\mathcal{K}}_{X,k+1}\boldsymbol{H}_{X,k+1}\right)\boldsymbol{P}_{k+1|k} \tag{3.228}$$

Thus it is observed that the recursive solutions for identification of structural state vector are derived using the traditional Kalman filter under the assumption that in the first step of the two-step Kalman filter approach the structural parameters are given or assumed.

Step 2: *In two-step Kalman Filter*

As shown by Eqs. (3.221)-(3.222), structural state vector is a function of its structural parametric vector. Then, the observation equation at time t = (k+1) × Δt is a nonlinear

function of unknown parametric vector $\boldsymbol{\theta}_{k+1}$ and can be linearized via Taylor expansion, that is,

$$\boldsymbol{h}(\boldsymbol{X}_{k+1}, \boldsymbol{\theta}_{k+1}, \boldsymbol{F}_{k+1}) = \boldsymbol{h}\left(\widehat{\boldsymbol{X}}_{k+1|k}, \widehat{\boldsymbol{\theta}}_k, \boldsymbol{F}_{k+1}\right) + \boldsymbol{H}_{k+1}\left(\boldsymbol{\theta}_{k+1} - \widehat{\boldsymbol{\theta}}_k\right) \tag{3.229}$$

where, $\boldsymbol{H}_{k+1}$ is obtained based on the chain rule of partial differential with respect to the parametric vector $\boldsymbol{\theta}_{k+1}$ as follows

$$\boldsymbol{H}_{k+1} = \boldsymbol{H}_{\theta,k+1} + \boldsymbol{H}_{X,k+1}\boldsymbol{X}_{\theta,k+1} \tag{3.230}$$

In which,

$$\boldsymbol{H}_{\theta,k+1} = \left[\frac{\partial \boldsymbol{h}(\boldsymbol{X}, \boldsymbol{\theta}, \boldsymbol{F})}{\partial \boldsymbol{\theta}}\right]_{\boldsymbol{X}=\widehat{\boldsymbol{X}}_{k+1|k}, \boldsymbol{\theta}=\widehat{\boldsymbol{\theta}}_k} \tag{3.231}$$

$$\boldsymbol{H}_{X,k+1} = \left[\frac{\partial \boldsymbol{h}(\boldsymbol{X}, \boldsymbol{\theta}, \boldsymbol{F})}{\partial \boldsymbol{X}}\right]_{\boldsymbol{X}=\widehat{\boldsymbol{X}}_{k+1|k}, \boldsymbol{\theta}=\widehat{\boldsymbol{\theta}}_k} \tag{3.232}$$

$$\boldsymbol{X}_{\theta,k+1} = \left[\frac{\partial \boldsymbol{X}(\boldsymbol{X}, \boldsymbol{\theta}, \boldsymbol{F})}{\partial \boldsymbol{\theta}}\right]_{\boldsymbol{\theta}=\widehat{\boldsymbol{\theta}}_k} \tag{3.233}$$

From Eqs. (3.219) and (3.222), $\boldsymbol{X}_{\theta,k+1}$ can be derived as

$$\begin{aligned}\boldsymbol{X}_{\theta,k+1} &= \boldsymbol{X}_{\theta,k} + \int_{k\Delta t}^{(k+1)\Delta t} \frac{\partial \boldsymbol{g}(\boldsymbol{X}, \boldsymbol{\theta}, \boldsymbol{F})}{\partial \boldsymbol{\theta}} dt \\ &= \boldsymbol{X}_{\theta,k} + \int_{k\Delta t}^{(k+1)\Delta t} \overline{\boldsymbol{g}}\left(X_{\theta,t|k}, \widehat{\boldsymbol{\theta}}_{\boldsymbol{k}}, \boldsymbol{F}\right) dt\end{aligned} \tag{3.234}$$

Here, the structural parameters are assumed as time invariant. So, the structural parameters can be estimated by the classical Kalman filter as

$$\widehat{\boldsymbol{\theta}}_{k+1} = \widehat{\boldsymbol{\theta}}_k + \boldsymbol{\mathcal{K}}_{\theta,k+1}\left[\boldsymbol{y}_{k+1} - \boldsymbol{h}\left(\widehat{\boldsymbol{X}}_{k+1|k}\left(\widehat{\boldsymbol{\theta}}_k\right), \boldsymbol{F}_{k+1}\right)\right] \tag{3.235}$$

where $\widehat{\boldsymbol{\theta}}_{k+1}$ and $\widehat{\boldsymbol{\theta}}_k$ are the estimated values of structural parameter vector at time $t=(k+1)\Delta t$ and $t=k$ x Δt, respectively; $\boldsymbol{\mathcal{K}}_{\theta,k+1}$ is the Kalman gain matrix for θ given by

$$\boldsymbol{\mathcal{K}}_{\theta,k+1} = \boldsymbol{P}_{\theta,k}\boldsymbol{H}_{k+1}^T\left(\boldsymbol{H}_{k+1}\boldsymbol{P}_{\theta,k}\boldsymbol{H}_{k+1}^T + \boldsymbol{R}_{k+1}\right)^{-1} \tag{3.236}$$

In which $\boldsymbol{P}_{\theta,k}$is the error covariance for parametric vector

$$\boldsymbol{P}_{\theta,k+1} = \left(\boldsymbol{I} - \boldsymbol{\mathcal{K}}_{\theta,k+1}\boldsymbol{H}_{k+1}\right)\boldsymbol{P}_{\theta,k} \tag{3.237}$$

The assumed $\widehat{\boldsymbol{\theta}}_{k+1}$ in Eq. (3.219)-(3.224) is replaced by the estimated $\widehat{\boldsymbol{\theta}}_{k+1}$ of Eq. (3.235) in the first step to update the recursive solution for structural state vector $\widehat{\boldsymbol{X}}_{k+1|k+1}$.

Determination of the Sensitivity matrix $\boldsymbol{X}_{\boldsymbol{\theta},\boldsymbol{k+1}}$

The matrix $\boldsymbol{X}_{\boldsymbol{\theta},\boldsymbol{k+1}}$is determined as given in Eq.(3.238). The equation of motion of a structure under external excitation is given as

$$\boldsymbol{M}\ddot{\boldsymbol{x}}(t) + \boldsymbol{F}_c[\dot{\boldsymbol{x}}(t), \boldsymbol{\theta}] + \boldsymbol{F}_s[\boldsymbol{x}(t), \boldsymbol{\theta}] = \boldsymbol{\eta F}(t) \tag{3.238}$$

Eq. (3.238) can be represented as given in Eq. (3.239)

$$\boldsymbol{M}\frac{d^2\boldsymbol{x}}{dt^2} + \boldsymbol{F}_c\left[\frac{d\boldsymbol{x}}{dt}, \boldsymbol{\theta}\right] + \boldsymbol{F}_s[\boldsymbol{x}, \boldsymbol{\theta}] = \boldsymbol{\eta F}(t) \tag{3.239}$$

Differentiating both sides of Eq. (3.239)with respect to $\boldsymbol{\theta}$ using chain rule, Eq. (3.240) is obtained.

$$\boldsymbol{M}\frac{d^2\left(\frac{d\boldsymbol{x}}{d\boldsymbol{\theta}}\right)}{dt^2} + \frac{d\boldsymbol{F}_c\left[\frac{d\boldsymbol{x}}{dt}, \boldsymbol{\theta}\right]}{d\theta} + \frac{d\boldsymbol{F}_s[\boldsymbol{x}, \boldsymbol{\theta}]}{d\theta} = \frac{d\boldsymbol{\eta F}(t)}{d\theta} \tag{3.240}$$

Let,$\frac{d\boldsymbol{x}}{d\boldsymbol{\theta}}$ be replaced as$\frac{d\boldsymbol{x}}{d\boldsymbol{\theta}} = \boldsymbol{x}_\theta$ in the above Eq. (3.240); then

$$\boldsymbol{M}\frac{d^2\boldsymbol{x}_\theta}{dt^2} + \frac{d\boldsymbol{F}_c[\dot{\boldsymbol{x}}, \boldsymbol{\theta}]}{d\theta} + \frac{d\boldsymbol{F}_s[\boldsymbol{x}, \boldsymbol{\theta}]}{d\theta} = 0 \tag{3.241}$$

$$\boldsymbol{M}\frac{d^2\boldsymbol{x}_\theta}{dt^2} + \left(\frac{\partial\boldsymbol{F}_c[\dot{\boldsymbol{x}}, \boldsymbol{\theta}]}{\partial\dot{\boldsymbol{x}}}.\frac{\partial\dot{\boldsymbol{x}}}{\partial\boldsymbol{\theta}} + \frac{\partial\boldsymbol{F}_c[\dot{\boldsymbol{x}}, \boldsymbol{\theta}]}{\partial\theta}\right) + \left(\frac{\partial\boldsymbol{F}_s[\boldsymbol{x}, \boldsymbol{\theta}]}{\partial\boldsymbol{x}}.\frac{\partial\boldsymbol{x}}{\partial\boldsymbol{\theta}} + \frac{\partial\boldsymbol{F}_s[\boldsymbol{x}, \boldsymbol{\theta}]}{\partial\boldsymbol{\theta}}\right) = 0 \tag{3.242}$$

$$\boldsymbol{M}\frac{d^2\boldsymbol{x}_\theta}{dt^2} + \left(\frac{\partial\boldsymbol{F}_c[\dot{\boldsymbol{x}}, \boldsymbol{\theta}]}{\partial\dot{\boldsymbol{x}}}.\frac{d\left(\frac{\partial\boldsymbol{x}}{\partial\boldsymbol{\theta}}\right)}{dt} + \frac{\partial\boldsymbol{F}_c[\dot{\boldsymbol{x}}, \boldsymbol{\theta}]}{\partial\theta}\right) + \left(\frac{\partial\boldsymbol{F}_s[\boldsymbol{x}, \boldsymbol{\theta}]}{\partial\boldsymbol{x}}.\frac{\partial\boldsymbol{x}}{\partial\boldsymbol{\theta}} + \frac{\partial\boldsymbol{F}_s[\boldsymbol{x}, \boldsymbol{\theta}]}{\partial\boldsymbol{\theta}}\right) = 0 \tag{3.243}$$

Dropping the terms within the square bracket for ease of representation and on further simplification the following equation is obtained.

$$\boldsymbol{M}\frac{d^2\boldsymbol{x}_\theta}{dt^2} + \left(\frac{\partial\boldsymbol{F}_c}{\partial\dot{\boldsymbol{x}}}.\frac{d\boldsymbol{x}_\theta}{dt} + \frac{\partial\boldsymbol{F}_c}{\partial\theta}\right) + \left(\frac{\partial\boldsymbol{F}_s}{\partial\boldsymbol{x}}.\boldsymbol{x}_\theta + \frac{\partial\boldsymbol{F}_s}{\partial\boldsymbol{\theta}}\right) = 0 \tag{3.244}$$

Further simplification of Eq. (3.244) gives the following

$$\boldsymbol{M}\frac{d^2\boldsymbol{x}_\theta}{dt^2} + \left[\frac{\partial\boldsymbol{F}_c}{\partial\dot{\boldsymbol{x}}}\right].\frac{d\boldsymbol{x}_\theta}{dt} + \left[\frac{\partial\boldsymbol{F}_s}{\partial\boldsymbol{x}}\right].\boldsymbol{x}_\theta = -\frac{\partial\boldsymbol{F}_c}{\partial\theta} - \frac{\partial\boldsymbol{F}_s}{\partial\boldsymbol{\theta}} = \boldsymbol{\mathcal{F}}(\boldsymbol{x}, \dot{\boldsymbol{x}}, \boldsymbol{\theta}) \tag{3.245}$$

Introducing a state vector $\boldsymbol{X}_\theta(\theta)$ which contains $\boldsymbol{x}_\theta$ and $d\boldsymbol{x}_\theta/dt$

$$\boldsymbol{X}_\theta(\theta) = \begin{bmatrix} \boldsymbol{x}_\theta \\ d\boldsymbol{x}_\theta/dt \end{bmatrix} \tag{3.246}$$

Eq. (3.245) can be transformed into a state equation as

$$\begin{aligned} \frac{d\boldsymbol{X}_\theta(\theta)}{dt} &= \begin{bmatrix} \dot{\boldsymbol{x}}_\theta \\ \dfrac{d^2\boldsymbol{x}_\theta}{dt^2} \end{bmatrix} \\ &= \begin{bmatrix} 0 & I \\ -M^{-1}\dfrac{\partial \boldsymbol{F}_s}{\partial \boldsymbol{x}} & -M^{-1}\dfrac{\partial \boldsymbol{F}_c}{\partial \dot{\boldsymbol{x}}} \end{bmatrix} \cdot \begin{Bmatrix} \boldsymbol{x}_\theta \\ \dot{\boldsymbol{x}}_\theta \end{Bmatrix} + \begin{bmatrix} 0 \\ M^{-1}\left(-\dfrac{\partial \boldsymbol{F}_c}{\partial \theta} - \dfrac{\partial \boldsymbol{F}_s}{\partial \boldsymbol{\theta}}\right) \end{bmatrix} \\ &= \overline{\boldsymbol{g}}(X_\theta, \boldsymbol{\theta}, \boldsymbol{F}) \end{aligned} \tag{3.247}$$

Consequently, Eq. (3.248) is obtained as

$$\boldsymbol{X}_{\theta,k+1} = \boldsymbol{X}_{\theta,k} + \int_{k\Delta t}^{(k+1)\Delta t} \overline{\boldsymbol{g}}(X_\theta, \boldsymbol{\theta}, \boldsymbol{F}) dt \tag{3.248}$$

The above formulation of two-stage EKF can be summarized as shown below.

Summary of Two-Stage Kalman Filter Algorithm

To start the two-stage EKF as like any other algorithms considered in this thesis, some initialization is required for state vector, its error covariance matrix, parametric vector, its error covariance matrix and sensitivity matrix.

i. Initialization of state vector, parametric vector and their error covariance matrix as well as sensitivity matrix.
ii. Step-1: recursive estimate for structural state vector is done by Kalman filter under the condition that structural parametric vector is given.
    a) Predict the state vector for time time $t=(k+1)\times\Delta t$, by numerical integration say by Runga-Kutta 4th order integration scheme

    $$\widetilde{\boldsymbol{X}}_{k+1|k} = \widehat{\boldsymbol{X}}_{k|k} + \int_{k\Delta t}^{(k+1)\Delta t} \boldsymbol{g}\left(\widehat{\boldsymbol{X}}_{t|k}, \boldsymbol{\theta}, \boldsymbol{F}, t\right) dt$$

    b) Find the Kalman gain $\boldsymbol{\mathcal{K}}_{X,k+1}$ using Eq. (3.223)-(3.224).
    c) Estimate the state vector error covariance matrix $\boldsymbol{P}_{k+1|k}$ for current time step using Eq. (3.225).

d) Estimate the state vector $\widehat{\boldsymbol{X}}_{k+1|k+1}(\boldsymbol{\theta}_{k+1})$ for next time step $(k+1)\times\Delta t$, using Eq. (3.221).

e) Estimate the state vector error covariance matrix $\boldsymbol{P}_{k+1|k+1}$ for next time step using Eq. (3.228).

iii. Step-2: recursive estimate for structural parametric vector are obtained by Kalman filter. The state vector is an implicit function of parametric vector and is obtained in step-1.

a) The nonlinear observation matrix, $\boldsymbol{h}(\boldsymbol{X}_{k+1}, \boldsymbol{\theta}_{k+1}, \boldsymbol{F}_{k+1})$ is linearized using Taylor series expansion and using chain rule of partial differentiation using Eqs. (3.229)-(3.231) at point $\boldsymbol{X} = \widehat{\boldsymbol{X}}_{k+1|k}, \boldsymbol{\theta} = \widehat{\boldsymbol{\theta}}_k$.

b) Find the Kalman gain $\boldsymbol{\mathcal{K}}_{\theta,k+1}$ using Eq. (3.236).

c) Estimate the parametric vector $\widehat{\boldsymbol{\theta}}_{k+1}$ for next time step $(k+1)\times\Delta t$, using Eq. (3.235). Estimate the parametric vector error covariance matrix $\boldsymbol{P}_{\theta,k+1}$ for next time step using Eq. (3.237).

iv. Recursive estimation of structural state vector is updated based on the estimation of structural parameters in (iii) of the second step.

v. Repeat (i)-(iv) for the next time segment. The values derived at the previous time segment are taken as the initial values for the next time segment.

There are various advantage and drawback of two-stage EKF which are as follows.

The Advantage of Two-Stage Kalman Filter Algorithm.

The main advantage of this algorithm is that it reduces the number of unknown parameters in each time step

The Drawback of Two-Stage Kalman Filter Algorithm.

i. It has similar applicable condition as that of traditional extended Kalman filter.

ii. It is applicable for time invariant systems.

iii. The excitation is assumed known (measured).

iv. The nonlinearity of the identification system is not so strong.

The above formulation of two-stage EKF covers the generalized derivation of the algorithm. More detailed derivations are required for its implementation to the structural system under consideration such as: 1) fixed base multi-storey building system, 2) base isolated multi-storey building system, 3) fixed base and base isolated multi-storey building with missing

sensors and 4) FREI supported structural system. The problem specific derivation has been taken up in the respective chapters.

3.3.4 The Unscented Kalman Filter (UKF) Algorithm

UKF algorithm is based on the concept of Unscented Transform (UT). UKF algorithm is the combination of UT and Kalman Filter. The UT was proposed by Jeffrey Uhlmann in the year 1997. The word *unscented* was an arbitrary name that was adopted to avoid it being referred to as the *Uhlmann filter*.

The state of a system can be represented in the form of a mean vector and an associated error covariance matrix. As an example, the estimated 2-dimensional position of an object of interest might be represented by a mean position vector, [*x, y*]. The uncertainty of the mean position vector is given in the form of a 2x2 covariance matrix giving the variance in *x*, the variance in *y*, and the cross covariance between the two. A covariance that is zero implies that there is no uncertainty or error and that the position of the object is exactly what is specified by the mean vector (*www.wikipedia.com*).

The Kalman Filter is a linear filter. In order to apply Kalman Filter to nonlinear systems, the nonlinearity needs to be linearized. This linearization is performed locally by using Taylor's series expansion. The Extended Kalman Filter (EKF) is the algorithm which is based on this linearization concept and is extensively used as a filtering tool for non-linear filtering application. The EKF uses only the 1st order derivative of Taylor's series expansion. This 1st order derivative is also called the Jacobian matrix. The computation of Jacobian is a complex process. To overcome the drawbacks of EKF, the UKF came to picture. The advantage of UKF is that it is easier to implement as it does not require to evaluate Jacobian to linearise a non-linear function and also because some nonlinear functions is not differentiable at some points. Therefore, the well-known drawbacks of EKF:

1) Linearization can produce filter instability.
2) The derivation of the Jacobian matrices in some cases can be extremely difficult and error-prone to derive.

In UKF algorithm, a weighted set of samples called sigma points are chosen so that they capture certain properties of the distribution of $\boldsymbol{x}$. The nonlinear function is applied to each of these sigma points to yield transformed sigma points. Finally, the mean and covariance of the transformed sigma points are evaluated by using specific weights. This method somewhat resembles Monte Carlo-type methods however, there is an extremely important and

fundamental difference. The samples are not drawn at random but rather according to a specific, deterministic algorithm. Thus, in UKF algorithm with only a very small number of points, high order information about the distribution can be captured.

The formulation of the UKF algorithm has been shown below. The following formulation has been adopted from Smyth Andrew W. and Wu Meiliang (2007).

The set of sigma points, σ consists of p+1 vectors and their appropriate weights, $\sigma = \{i = 0,1, \ldots., p: \chi_i, W_i\}$. The weights W_i can be positive or negative, but must obey the normalized condition $\sum_{i=0}^{p} W_i = 1$. Given these points, $\tilde{y}$ and P_y are calculated using the following procedure:

1. Instantiate each point through the function to yield the set of transformed sigma points,

Consider a general dynamic system described by a nonlinear continuous state-space equation as

$$\dot{\boldsymbol{X}} = \mathcal{F}\big(\boldsymbol{X}(t), \boldsymbol{u}(t), \boldsymbol{w}(t)\big) \tag{3.249}$$

with the measurement equation

$$\boldsymbol{Y}(t) = \boldsymbol{h}\big(\boldsymbol{X}(t), \boldsymbol{v}(t)\big) \tag{3.250}$$

where, **u**(t) is the known system input, **w**(t) is the system process noise vector, and **v**(t) is the measurement noise.

To implement the UKF method for the system identification problem, Eq. (3.249) and Eq.(3.250) is re-written in discrete time to obtain the discrete nonlinear difference state space equation as (3.251) and Eq. (3.252).

$$\boldsymbol{X}_{k+1} = \mathbb{F}(\boldsymbol{X}_k, \boldsymbol{u}_k, \boldsymbol{w}_k) \tag{3.251}$$

$$\boldsymbol{Y}_k = \boldsymbol{H}(\boldsymbol{X}_k, \boldsymbol{v}_k) \tag{3.252}$$

in which $\mathbf{w_k}$ is the discrete process noise assumed to be a Gaussian white noise with zero mean and a covariance matrix Q; and $\mathbf{v_k}$ is the measurement noise also assumed to be a Gaussian white noise with zero mean and a covariance matrix **R**. Function $\mathbb{F}$ is obtained from the function *f* in Eq. (3.249) as

$$\mathbb{F}(\boldsymbol{X}_k, \boldsymbol{u}_k, \boldsymbol{w}_k) = \boldsymbol{X}_k + \int_{k\Delta t}^{(k+1)\Delta t} \boldsymbol{\mathcal{F}}\big(\boldsymbol{X}(t), \boldsymbol{u}(t), \boldsymbol{w}(t)\big) dt \tag{3.253}$$

The integration in Eq. (3.253)can be evaluated by using numerical methods such as fourth order Runge–Kutta method. To implement the UKF algorithm, the state vector is redefined as the concatenation of the original state vector and noise variables as in Eq. (3.254).

$$\boldsymbol{X}_k^a = [\boldsymbol{X}_k^T, \boldsymbol{w}_k^T, \boldsymbol{v}_k^T] \tag{3.254}$$

The initialization is started with Eq. (3.255) and (3.256).

$$\widehat{\boldsymbol{X}}_0 = \boldsymbol{E}[\boldsymbol{X}_0] \tag{3.255}$$

$$\boldsymbol{P}_0 = \boldsymbol{E}\left[(\boldsymbol{X}_0 - \widehat{\boldsymbol{X}}_0)(\boldsymbol{X}_0 - \widehat{\boldsymbol{X}}_0)^T\right] \tag{3.256}$$

where, $\mathbf{P}_0$is the initial error covariance matrix.

$$\widehat{\boldsymbol{X}}_0^a = \boldsymbol{E}[\boldsymbol{X}^a] = \left[\widehat{\boldsymbol{X}}_0^T \mathbf{0}\ \mathbf{0}\right]^T \tag{3.257}$$

$$\boldsymbol{P}_0^a = \boldsymbol{E}\left[(\boldsymbol{X}_0^a - \widehat{\boldsymbol{X}}_0^a)(\boldsymbol{X}_0^a - \widehat{\boldsymbol{X}}_0^a)^T\right] = \begin{bmatrix} \boldsymbol{P}_0 & 0 & 0 \\ 0 & \boldsymbol{Q} & 0 \\ 0 & 0 & \boldsymbol{R} \end{bmatrix} \tag{3.258}$$

At time step *k*, the sample points or so-called sigma points are then computed by using Eq. (3.257).

$$\mathfrak{X}_k^a = \left[\widehat{\boldsymbol{X}}_k^a \widehat{\boldsymbol{X}}_k^a + \sqrt{(L+\lambda)\boldsymbol{P}_k^a}\widehat{\boldsymbol{X}}_k^a - \sqrt{(L+\lambda)\boldsymbol{P}_k^a}\right] \tag{3.259}$$

where, λ is a scaling parameter which is defined by

$$\lambda = \alpha^2(l_x + \kappa) - l_x \tag{3.260}$$

L is the dimension of the augmented state vector $\mathbf{X}^a$ and l_x is the dimension of the original state vector **X;** The constant parameter α determines the spread of the sigma points and should be a small positive number$0 \leq \alpha \leq 1$: κ is a secondary scaling parameter, which is usually set to (3-l_x): Once the $\mathfrak{X}_a^k$is computed, the time update step is then performed. The predicted state vector $\boldsymbol{X}_{k+1}^-$ and its predicted covariance $\boldsymbol{P}_{k+1}^-$ are computed by using Eq. (3.262) and Eq. (3.263).

$$\mathfrak{X}_{k+1/k}^X = \boldsymbol{F}(\mathfrak{X}_k^X, u_k, \mathfrak{X}_k^w) \tag{3.261}$$

$$\widehat{\boldsymbol{X}}_{k+1}^- = \sum_{i=0}^{2L} W_i^{(m)}\, \mathfrak{X}_{i,k+1/k}^X \tag{3.262}$$

$$\boldsymbol{P}_{k+1}^- = \sum_{i=0}^{2L} W_i^{(c)}\left[\mathfrak{X}_{i,k+1/k}^X - \widehat{\boldsymbol{X}}_{k+1}^-\right]\left[\mathfrak{X}_{i,k+1/k}^X - \widehat{\boldsymbol{X}}_{k+1}^-\right]^T \tag{3.263}$$

Similarly, the predicted measurement vector $\widehat{\boldsymbol{Y}}_{k+1}^{-}$ and its predicted $\boldsymbol{P}_{k+1}^{YY}$ are also calculated as given in Eq. (3.265) and (3.266).

$$\boldsymbol{\mathcal{Y}}_{k+1/k} = \boldsymbol{H}\left(\boldsymbol{\mathfrak{X}}_{k+1/k}^{X}, \boldsymbol{\mathfrak{X}}_{k}^{v}\right) \tag{3.264}$$

$$\widehat{\boldsymbol{Y}}_{k+1}^{-} = \sum_{i=0}^{2L} W_i^{(m)} \boldsymbol{\mathcal{Y}}_{i,k+1,k} \tag{3.265}$$

$$\boldsymbol{P}_{k+1}^{YY} = \sum_{i=0}^{2L} W_i^{(c)} \left[\boldsymbol{\mathcal{Y}}_{i,k+1,k} - \widehat{\boldsymbol{Y}}_{k+1}^{-}\right]\left[\boldsymbol{\mathcal{Y}}_{i,k+1,k} - \widehat{\boldsymbol{Y}}_{k+1}^{-}\right]^{T} \tag{3.266}$$

where, $W_i^{(m)}$ is the weight for the mean and $W_i^{(c)}$ is the weight for the covariance given by

$$W_0^{(m)} = \frac{\lambda}{l_x + \lambda} \tag{3.267}$$

$$W_0^{(c)} = \frac{\lambda}{l_x + \lambda} + \left(1 - \tilde{\alpha}^2 + \tilde{\beta}\right) \tag{3.268}$$

$$W_i^{(m)} = W_i^{(c)} = \frac{1}{2(l_x + \lambda)}, i = 1, \ldots., 2l_x \tag{3.269}$$

where $\tilde{\beta}$ is a parameter that makes further higher order effects to be incorporated by adding the weighting of the zeroth sigma point of the calculation of the covariance, and $\tilde{\beta} = 2$ is the optimal for Gaussian distribution. The measurement update step is given by Eq. (3.270) to Eq. (3.273).

$$\boldsymbol{P}_{k+1}^{XY} = \sum_{i=0}^{2L} W_i^{(c)} \left[\boldsymbol{\mathfrak{X}}_{i,k+1/k}^{X} - \widehat{\boldsymbol{X}}_{k+1}^{-}\right]\left[\boldsymbol{\mathcal{Y}}_{i,k+1,k} - \widehat{\boldsymbol{Y}}_{k+1}^{-}\right]^{T} \tag{3.270}$$

$$\boldsymbol{\mathcal{K}}_{k+1} = \boldsymbol{P}_{k+1}^{XY}(\boldsymbol{P}_{k+1}^{YY})^{-1} \tag{3.271}$$

$$\widehat{\boldsymbol{X}}_{k+1} = \widehat{\boldsymbol{X}}_{k+1}^{-} + \boldsymbol{\mathcal{K}}_{k+1}\left(\boldsymbol{Y}_{k+1} - \widehat{\boldsymbol{Y}}_{k+1}^{-}\right) \tag{3.272}$$

$$\boldsymbol{P}_{k+1} = P_{k+1}^{-} - \boldsymbol{\mathcal{K}}_{k+1}\boldsymbol{P}_{k+1}^{YY}\boldsymbol{\mathcal{K}}_{k+1}^{T} \tag{3.273}$$

The above formulation of UKF is a generalized derivation and a forward step towards implementation to the structural system considered in this thesis. The structural system considered in this thesis are: 1) fixed base multi-storey building system, 2) base isolated multi-storey building system, 3) fixed base and base isolated multi-storey building with missing sensors and 4) FREI supported structural system. The formulation to apply UKF to

each of the structural system under consideration has been taken up in the relevant chapters of this thesis.

3.4 Concluding Remarks

In this chapter, a detail formulation has been presented for all the algorithms under consideration such as SNLSE, SNLSE-UI-UO, EKF, Two-Stage EKF and UKF algorithms. The gradual development of LSE based technique from LSE to RLSE and then to SNLSE and finally SNLSE-UO-UO. The various modifications applied on the basic formulations are also shown. On the other hand, a parallel technique based on Kalman Filter also evolved. The fundamentals behind Kalman Filter are also covered in this chapter. The modified Kalman Filter to handle nonlinearity is also presented. The modified form of Kalman Filter with capability to handle nonlinearity is the EKF algorithm. To resolve the issue of instability of EKF while handling a large system, Two-Stage Kalman Filter evolved. All the modifications in formulations applied to Kalman Filter to transform it to EKF have been presented. Further, the modifications applied to EKF to transform it to Two-Stage EKF are also presented. The UKF algorithm came in existence to overcome all the drawbacks of Kalman Filter, EKF and Two-Stage EKF. The formulation of UKF is different than that of Kalman Filter, EKF and Two-Stage EKF algorithms.

General formulations of different algorithms are presented in this chapter. The formulations and theory behind each of the algorithms already exists in various literatures in piece-meal forms. In this chapter an attempt has been carried out to bring under one umbrella all the existing formulation of the different algorithms which are scattered in different literature. The primary objective is to arrange the algorithms in a manner as they evolved so as to have a better understanding on their working principle and the basic changes that were carried out during their transformation to advanced form. This type of exercise perhaps had never been performed earlier.

Chapter 4

Evaluation of state and structural parameters of multi-storey fixed base building system

4.1 Introduction

In this chapter, identification of state and structural parameters of multi-storey shear frame building system with fixed base is carried out using the different identification algorithms such as SNLSE-UI-UO, EKF, Two-Stage EKF and UKF. The building is idealized as a shear frame building. One horizontal degree-of-freedom (dof) is considered at each storey level. Different problem types are considered in this study as described in Table 4.1. Identification of state and parameters are carried out on a simulated model of three-storey building and then the study is extended to two numbers of existing buildings having different number of storey. Influence of added noise and availability of limited sensors on the performance of these algorithms has also been carried out. Finally, a comparative study of the performance of the identification algorithms has been presented. In Problem Type-IIIa, influence of noise is not considered, instead influence of missing sensor on identification of the structural system has been considered. The difference between Problem Type-I and IIIa is that the in the former all sensors are present and in the later sensors are missing at different floors. Further, Problem Type-IIIa bears structural properties resembling the existing building IIIb.

Table 4.1: Different types of problems considered

Problem Type	Description	Sensor Location	Noise consideration
I	Simulated three-storey	Sensor in all floors	0%, 1%, 2% and 5% added Gaussian white noise
IIa	Simulated nine-storey	Sensor in different floors as per Fig. 4.3	No noise considered
IIb	Existing nine-storey		Field data
IIIa	Simulated three-storey	Sensor in roof and basement	Noise not considered
IIIb	Existing three-storey		Field data

4.2 Description of an analytical model of fixed base three-storey building (Problem Type-I)

The building is idealized as 2D shear building in which the floor slab is considered to be behaving like a rigid diaphragm. There is only one dof at each storey level with lumped masses m_1, m_2, m_3 and m_4 as shown in Fig. 4.1. The storey stiffnesses are designated ask_1, k_2, k_3 and k_4. The storey heights are designated as $\hat{h}_1, \hat{h}_2, \hat{h}_3and\hat{h}_4$ .Rayleigh damping is considered for this model with mass coefficient $\hat{\alpha}$ and stiffness coefficient $\hat{\beta}$.

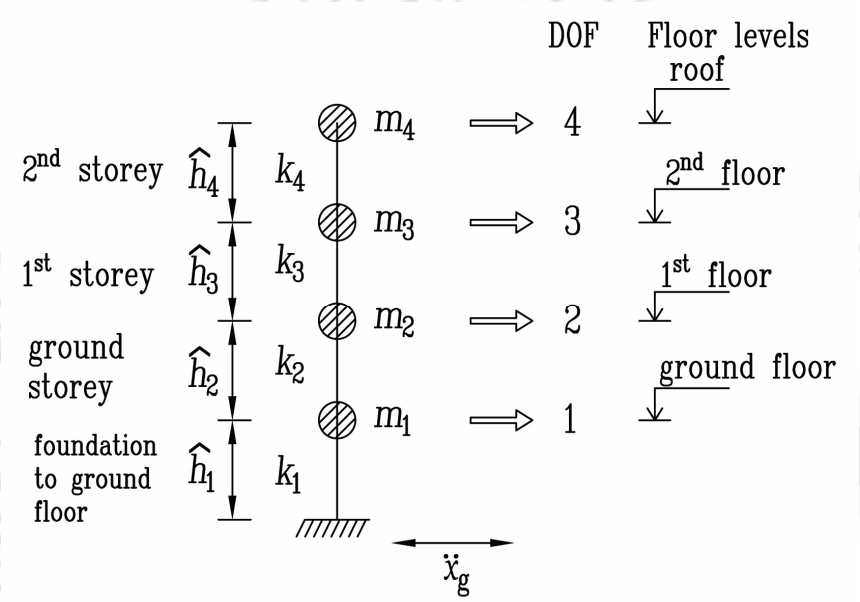

Fig. 4.1: Analytical model of the three-storey shear frame building

The governing equation of motion is given by

$$\boldsymbol{M\ddot{x} + C\dot{x} + Kx = -\eta M\ddot{x}_g = F} \tag{4.1}$$

The Eq.(4.1) may be represented in state-space form as given by

$$\begin{Bmatrix}\dot{\boldsymbol{x}}\\ \ddot{\boldsymbol{x}}\end{Bmatrix} = \frac{d}{dt}\begin{Bmatrix}\boldsymbol{x}\\ \dot{\boldsymbol{x}}\end{Bmatrix} = \begin{Bmatrix}\dot{\boldsymbol{x}}\\ \left(-\boldsymbol{\eta M\ddot{x}_g - Kx - C\dot{x}}\right)/\boldsymbol{M}\end{Bmatrix} = \begin{Bmatrix}\dot{\boldsymbol{x}}\\ -\boldsymbol{\eta\ddot{x}_g - Kx/M - C\dot{x}/M}\end{Bmatrix} \tag{4.2}$$

Eq. (4.2) is of the form $\boldsymbol{y}'=\boldsymbol{f}(x)$, and is solved by Runga-Kutta 4th order integration scheme.

The global stiffness matrix is expressed as

$$\boldsymbol{K} = \begin{bmatrix} k_1+k_2 & -k_2 & 0 & 0 \\ -k_2 & k_2+k_3 & -k_3 & 0 \\ 0 & -k_3 & k_3+k_4 & -k_4 \\ 0 & 0 & -k_4 & k_4 \end{bmatrix} \tag{4.3}$$

Global mass matrix is expressed as

$$\boldsymbol{M} = \begin{bmatrix} m_1 & 0 & 0 & 0 \\ 0 & m_2 & 0 & 0 \\ 0 & 0 & m_3 & 0 \\ 0 & 0 & 0 & m_4 \end{bmatrix} \tag{4.4}$$

Global damping matrix is expressed as

$$\boldsymbol{C} = \hat{\beta} * \boldsymbol{K} + \hat{\alpha} * \boldsymbol{M} \tag{4.5}$$

Study is carried out using three different ground excitations as given in Table 4.2. The structural parameters considered for the simulation model are given in Table 4.3.

Table 4.2: Characteristics of selected earthquake records for Problem Type-I

Earthquake Components	**Peak Ground Acceleration (g)**	**Frequency Range (radian/sec)**
El Centro (1940): Comp - 180	0.32	0-65
Koyna (167): Comp - Longitudinal	0.63	0-12
Victoria (1980): Comp – CPE045	0.62	0-160

Table 4.3: Parameters considered for Problem Type-I

Storey	**Storey Stiffness (kN/m)**		**Storey Height (m)**		**Mass (M.T.)**	
Foundation to ground floor	k_1	1.35E+005	$\hat{h}_1$	1.93	m_1	16.582
Ground storey	k_2	3.0E+005	$\hat{h}_2$	3.00	m_2	22.641
1st storey	k_3	3.0E+005	$\hat{h}_3$	3.00	m_3	22.641
2nd storey	k_4	3.0E+005	$\hat{h}_4$	3.00	m_4	20.907

The numerical model is used to generate acceleration, velocity and displacement response at all floor levels subjected to ground excitation as furnished in Table 4.2. These acceleration responses have been used for identification of structural parameters by the identification algorithms, the details of which are presented in this chapter.

4.3 Description of fixed base nine-storey existing building (Problem Type-II)

The structure considered for this study is a nine-storey (G+8) building having ground plus eight floors. The building is situated in Guwahati city, Assam, India. This multi-storey building considered in the study is located in the seismic Zone-V (zone with highest seismicity) of seismic zone map of India. The storey height of the building is 3m with infill walls, except the ground storey which has height of 2.75m and without any infill walls. Thus, the distribution of stiffness and mass is not uniform along the height. A photograph of the building is shown in Fig. 4.2.

Fig. 4.2: Photograph of nine-storey building (photo courtesy Borsakia *et al.*(2010))

Instrumentation of the building and acquisition of its acceleration response, following seismic events were carried out by Borsakia *et al.* (2010). Accelerometers were fixed at different floor levels (Fig. 4.3) to acquire earthquake responses. To record ground motion in three orthogonal directions, X, Y and vertical Z direction, a tri-axial accelerometer was installed at

the ground floor level. Similarly, another tri-axial accelerometer was fixed at the roof of the building. Uni-axial accelerometers were fixed on selected floors in both X (longitudinal) and Y (transverse) directions of the building. Detail of placement of accelerometers is shown in Fig. 4.3and further mentioned in Table 4.4. All the accelerometers at different floor levels were fixed in the same vertical line. The sampling frequency of adopted for data collection was 200Hz.The recorded earthquake data is furnished in Table 4.5.

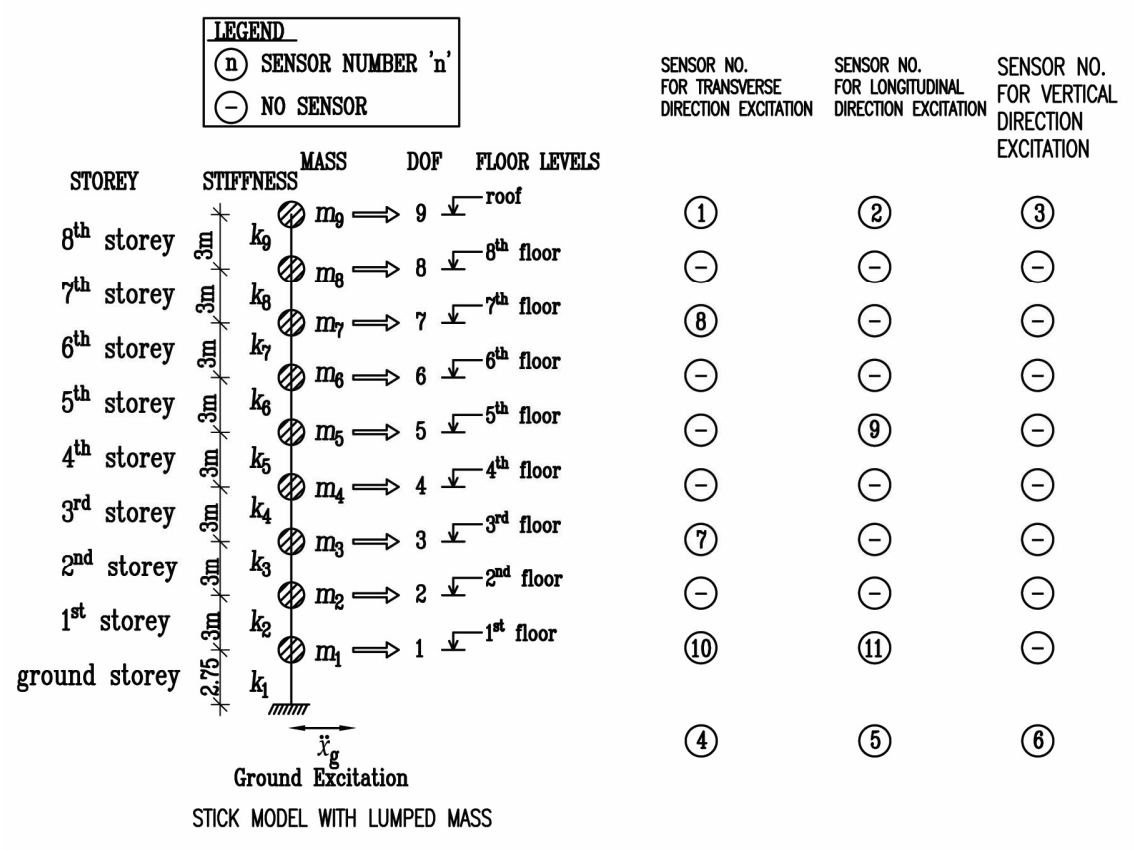

Fig. 4.3: Modelling and instrumentation details of nine-storey sample building (Problem Type-II)

Table 4.4: Sensor location at different floors of the sample building

Floors	Longer Direction	Shorter Direction
Ground	Triaxial	
First	Uni-axial	Uni-axial
Third	Uni-axial	-----
Fifth	-----	Uni-axial
Seventh	Uni-axial	----
Roof	Triaxial	

Table 4.5: Characteristics of selected earthquake records for nine-storey building

Earthquake Components	Date	Peak Ground Acceleration (g)	Frequency Range (radian/sec)
NE EQ-1: Comp-transverse	14th February 2006	0.0067	0-189
NE EQ-1: Comp-longitudinal	14th February 2006	0.0045	0-189
NE EQ-2: Comp-transverse	12th August 2006	0.0030	0-140
NE EQ-2: Comp-longitudinal	12th August 2006	0.0026	0-140

Before taking up the system identification of the building using field measured response, a simulation study has been carried out using the structural properties obtained from the physical dimensions of the building. The parameters considered for the simulated model are furnished in Table 4.6. The results from the simulated study is found to be helpful in the comparative study using different identification schemes as described in relevant section of this chapter. This simulated model is categorized as Problem Type-IIa as described in Table 4.1.

Table 4.6: Parameters considered for the nine-storey simulated model

Storey	Storey Stiffness (N/m)			Storey Height (m)		Mass (kg)	
		Transverse direction	Longitudinal direction				
Ground	k_1	3.30E+009	4.49E+009	$\hat{h}_1$	2.75	m_1	511770
1st	k_2	2.56E+009	4.15 E+009	$\hat{h}_2$	3.00	m_2	515930
2nd	k_3	2.56E+009	4.15 E+009	$\hat{h}_3$	3.00	m_3	515580
3rd	k_4	2.56E+009	4.15 E+009	$\hat{h}_4$	3.00	m_4	515580
4th	k_5	2.56E+009	4.15 E+009	$\hat{h}_5$	3.00	m_5	515570
5th	k_6	2.56E+009	4.15 E+009	$\hat{h}_6$	3.00	m_6	515570
6th	k_7	2.56E+009	4.15 E+009	$\hat{h}_7$	3.00	m_7	515570
7th	k_8	2.56E+009	4.15 E+009	$\hat{h}_8$	3.00	m_8	511080
8th	k_9	2.56E+009	4.15 E+009	$\hat{h}_9$	3.00	m_9	362710

4.4 Description of fixed base three-storey existing building (Problem Type-III)

Two numbers of three-storey reinforced concrete framed prototype buildings located at IIT Guwahati is considered for the present study. Both the buildings are identical in plan, elevation and have identical structural details with the exception that one is a base-isolated building while other is conventional fixed base building. The base-isolated building is supported on lead plug bearings, comprising of alternate layers of rubber and steel shims with

a central lead core. Detailed study of base-isolated building is presented in chapter-5. The fixed base building is supported on conventional isolated footing. In this chapter only the fixed base building will be considered. The photograph of the building along with instrumentation and floor plan detail are shown in Fig. 4.4 and Fig. 4.5.Instrumentation of the building and acquisition of its acceleration response, following different seismic events were carried out by Nath R.J. *et al.* (2013).

(a) View of conventional building to the left and isolated building to the right

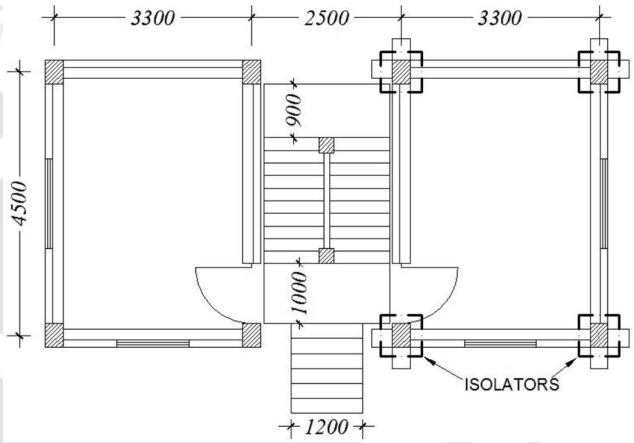

(b) Plan of conventional and isolated building showing position of isolators

Fig. 4.4: (a) Photograph of the twin three-storey sample building and (b) its ground floor plan

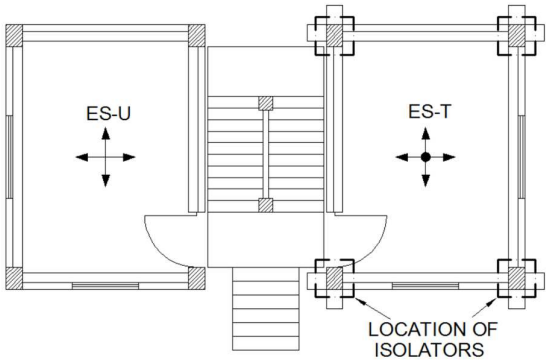

(a) Position of accelerometers in the prototype conventional and isolated buildings- ground floor level.

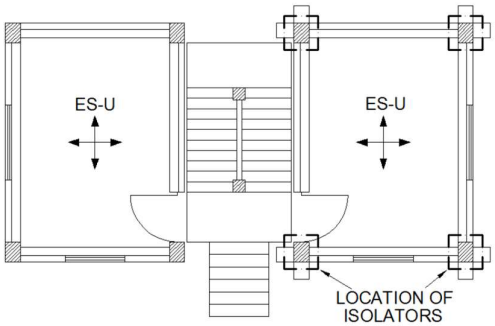

(b) Position of accelerometers in the prototype conventional and isolated buildings- Roof level.

Fig. 4.5: Plan of twin three-storey sample building at (a) ground floor and (b) roof level

The placements of sensors at different floor levels are shown in Table 4.7 and Fig. 4.4 to Fig. 4.6.

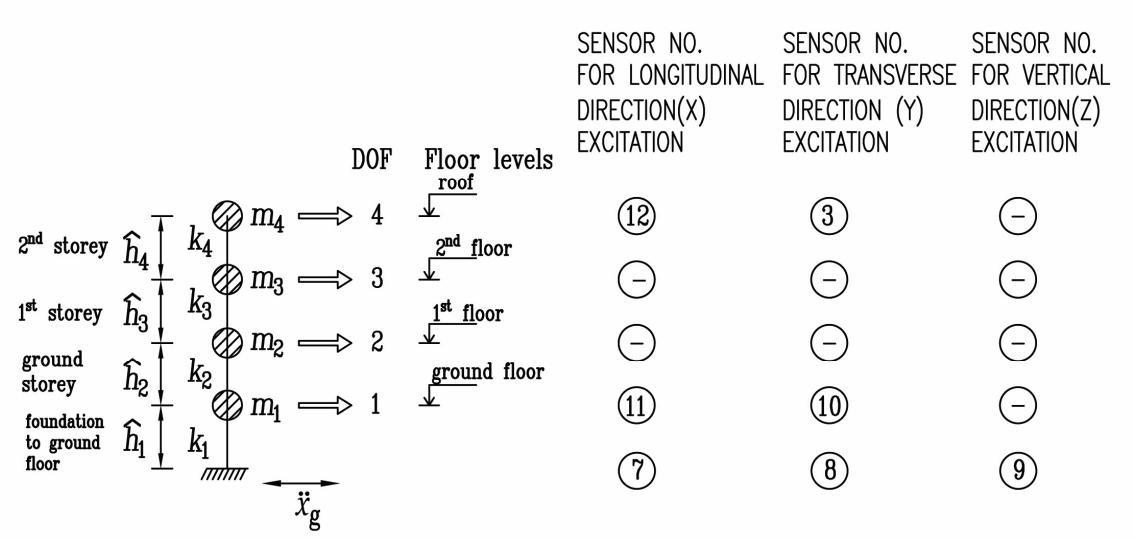

Fig. 4.6: Modelling and instrumentation details of three-storey conventional fixed base existing building

Table 4.7: Sensor location at different floors of the three-storey conventional building

Conventional Building			Base-isolated Building	
Floor	Sensor		Floor	Sensor
Ground Floor	*x, y*		Ground Floor	*x, y, z*
1st Floor	No sensor		1st Floor	No sensor
2nd Floor	No sensor		2nd Floor	No sensor
Roof	*x, y*		Roof	*x, y*

where, *x*-direction is the longitudinal direction. Amongst the collected response data, the 1st floor *x*-direction acceleration response data is not available due to faulty accelerometer.

NE EQ-3 (Comp: transverse) earthquake excitation dated 10th September, 2006 with PGA of 0.003g and frequency range of 0-170 radian/sec is considered for the identification study of Problem Type-IIIa and IIIb. The structural parameters assumed for the simulation study using Problem Type-IIIa are furnished in Table 4.8.

Table 4.8: Parameters considered for the three-storey conventional fixed base simulated model (Problem Type-IIIa)

Storey No.	**Storey Height (m)**		**Mass (M.T.)**	
Ground	$\hat{h}_1$	1.93	m_1	16.582
1st	$\hat{h}_2$	3.00	m_2	22.641
2nd	$\hat{h}_3$	3.00	m_3	22.641
3rd	$\hat{h}_4$	3.00	m_4	20.907

4.5 Evaluation of state and parameter using different algorithms

In this section, EKF, Two-Stage EKF, UKF and SNLSE-UI-UO algorithms are used for the evaluation of state and parameters of the structural systems as furnished in Table 4.1 and described in sections 1.2 to4.4.

All the three types of structures under consideration have been modelled as shear building. Mass and stiffness proportional damping has been considered for all the three types of structures under consideration. The formulation of each of these algorithms that are specific to the considered structural system has been described in the following sub-sections.

4.5.1 EKF for four-DOF fixed base shear frame building

In this section, mathematical formulations of EKF for four-DOF fixed base shear building (Fig. 4.1) is presented. This formulation can be easily extended to develop EKF for similar system with higher numbers of DOFs.

4.5.1.1 Detailed formulation of EKF for four-DOF Fixed base shear building

Matrices such as stiffness, damping and Jacobian etc. which are required for EKF implementation are derived first. The global stiffness, mass and damping matrices are given by Eqs. (4.3) to Eq. (4.5).

The governing equation of motion is given by

$$\boldsymbol{M\ddot{x} + C\dot{x} + Kx = -\eta M\ddot{x}_g = F} \tag{4.6}$$

The process equation is expressed in state-space form as given by Eq. (4.7)

$$\dot{\boldsymbol{X}}_e = \begin{Bmatrix} \dot{\boldsymbol{x}}_i \\ \ddot{\boldsymbol{x}}_i \\ \dot{\boldsymbol{k}}_i \\ \dot{\hat{\beta}} \\ \dot{\hat{\alpha}} \end{Bmatrix} = \frac{d}{dt}\begin{Bmatrix} \boldsymbol{x}_i \\ \dot{\boldsymbol{x}}_i \\ \boldsymbol{k}_i \\ \hat{\beta} \\ \hat{\alpha} \end{Bmatrix} = \frac{d\boldsymbol{X}_e}{dt} = \begin{Bmatrix} \dot{\boldsymbol{x}}_i \\ -\boldsymbol{\eta}\ddot{x}_g - \boldsymbol{K}\boldsymbol{x}_i/\boldsymbol{M} - \boldsymbol{C}\dot{\boldsymbol{x}}_i/M \\ 0 \\ 0 \\ 0 \end{Bmatrix} \tag{4.7}$$

Expanding Eq. (4.7) as

$$\dot{\boldsymbol{X}}_e = \frac{d}{dt}\{x_1 \quad x_2 \quad x_3 \quad x_4 \quad \dot{x}_1 \quad \dot{x}_2 \quad \dot{x}_3 \quad \dot{x}_4 \quad k_1 \quad k_2 \quad k_3 \quad k_4 \quad \hat{\beta} \quad \hat{\alpha}\}^{\boldsymbol{T}}$$
$$= \boldsymbol{g}(\boldsymbol{X}_e, \boldsymbol{\theta}, \boldsymbol{F})$$
$$= \{\dot{x}_1 \quad \dot{x}_2 \quad \dot{x}_3 \quad \dot{x}_4 \quad \ddot{x}_1 \quad \ddot{x}_2 \quad \ddot{x}_3 \quad \ddot{x}_4 \quad \dot{k}_1 \quad \dot{k}_2 \quad \dot{k}_3 \quad \dot{k}_4 \quad \dot{\hat{\beta}} \quad \dot{\hat{\alpha}}\}^{\boldsymbol{T}}$$

$$\boldsymbol{g}(\boldsymbol{X}_e, \boldsymbol{\theta}, \boldsymbol{F}) = \begin{bmatrix} \{\dot{x}_i\} \\ \{\eta\}\ddot{x}_g - [M^{-1}]\big[[K]\{x_i\} + [C]\{\dot{x}_i\}\big] \\ [0]_{6x1} \end{bmatrix} = \{g_j\} \tag{4.8}$$

where, $\{\eta\} = \{-1 \quad -1 \quad -1 \quad -1\}^T$, $\{\dot{x}_i\} = \{\dot{x}_1 \quad \dot{x}_2 \quad \dot{x}_3 \quad \dot{x}_4\}^T$ and

$\{g_j\} = \{g_1 \quad g_2 \quad \cdots \quad g_{14}\}^T$

Replacing damping matrix $[C] = \hat{\beta}[K] + \hat{\alpha}[M]$ in Eq.(4.8) and expanding the matrix [K] and [M],

$$[K]\{x\} = [K]\begin{Bmatrix} x_1 \\ x_2 \\ x_3 \\ x_4 \end{Bmatrix} = \begin{bmatrix} k_1 + k_2 & -k_2 & 0 & 0 \\ -k_2 & k_2 + k_3 & -k_3 & 0 \\ 0 & -k_3 & k_3 + k_4 & -k_4 \\ 0 & 0 & -k_4 & k_4 \end{bmatrix}\begin{Bmatrix} x_1 \\ x_2 \\ x_3 \\ x_4 \end{Bmatrix}$$
$$= \begin{Bmatrix} k_1x_1 + k_2x_1 - k_2x_2 \\ -k_2x_1 + k_2x_2 + k_3x_2 - k_3x_3 \\ -k_3x_2 + k_3x_3 + k_4x_3 - k_4x_4 \\ -k_4x_3 + k_4x_4 \end{Bmatrix} \tag{4.9}$$

Expanding the damping matrix [C] as

$$[C]\{\dot{x}\} = \left[\hat{\beta}[K] + \hat{\alpha}[M]\right]\begin{Bmatrix} \dot{x}_1 \\ \dot{x}_2 \\ \dot{x}_3 \\ \dot{x}_4 \end{Bmatrix}$$
$$= \begin{Bmatrix} \hat{\beta}k_1\dot{x}_1 + \hat{\beta}k_2\dot{x}_1 - \hat{\beta}k_2\dot{x}_2 + \hat{\alpha}m_1\dot{x}_1 \\ -\hat{\beta}k_2\dot{x}_1 + \hat{\beta}k_2\dot{x}_2 + \hat{\beta}k_3\dot{x}_2 - \hat{\beta}k_3\dot{x}_3 + \hat{\alpha}m_2\dot{x}_2 \\ -\hat{\beta}k_3\dot{x}_2 + \hat{\beta}k_3\dot{x}_3 + \hat{\beta}k_4\dot{x}_3 - \hat{\beta}k_4\dot{x}_4 + \hat{\alpha}m_3\dot{x}_3 \\ -\hat{\beta}k_4\dot{x}_3 + \hat{\beta}k_4\dot{x}_4 + \hat{\alpha}m_4\dot{x}_4 \end{Bmatrix} \tag{4.10}$$

Differentiating $[K]\{x_i\}$with respect to$\{x_i\}$

$$\frac{\partial}{\partial x_i}[K]\{x_i\} = \begin{bmatrix} k_1 + k_2 & -k_2 & 0 & 0 \\ -k_2 & k_2 + k_3 & -k_3 & 0 \\ 0 & -k_3 & k_3 + k_4 & -k_4 \\ 0 & 0 & -k_4 & k_4 \end{bmatrix} = [K] \tag{4.11}$$

where, $i = 1,2,3,4$

Differentiating $[K]\{x_i\}$with respect to$\{k_i\}$

$$\frac{\partial}{\partial k_i}[K]\{x_i\} = \begin{bmatrix} x_1 & (x_1 - x_2) & 0 & 0 \\ 0 & -(x_1 - x_2) & (x_2 - x_3) & 0 \\ 0 & 0 & -(x_2 - x_3) & (x_3 - x_4) \\ 0 & 0 & 0 & -(x_2 - x_3) \end{bmatrix} = [KK] \tag{4.12}$$

Differentiating $[K]\{x_i\}$with respect to$\{\dot{x}_i\}$,$\hat{\beta}$ and $\hat{\alpha}$

$$\frac{\partial}{\partial \dot{x}_i}[K]\{x_i\} = 0 \qquad \frac{\partial}{\partial \beta}[K]\{x_i\} = 0 \qquad \frac{\partial}{\partial \alpha}[K]\{x_i\} = 0 \tag{4.13}$$

Differentiating $[C]\{\dot{x}_i\}$with respect to$\{\dot{x}_i\}$

$$\frac{\partial}{\partial \dot{x}_i}[C]\{\dot{x}_i\} = \frac{\partial}{\partial \dot{x}_i}\left[\hat{\beta}[K] + \hat{\alpha}[M]\right]\{\dot{x}_i\} = \left[\hat{\beta}[K] + \hat{\alpha}[M]\right] \tag{4.14}$$

Differentiating $[C]\{\dot{x}_i\}$with respect to$\{k_i\}$

$$\frac{\partial}{\partial k_i}[C]\{\dot{x}_i\} = \frac{\partial}{\partial k_i}\left[\hat{\beta}[K] + \hat{\alpha}[M]\right]\{\dot{x}_i\} = \left[\hat{\beta}\frac{\partial}{\partial k_i}[K] + [0]\right]\{\dot{x}_i\}$$

$$= \hat{\beta}\frac{\partial}{\partial k_i}[K]\{\dot{x}_i\} = \hat{\beta}\begin{bmatrix} \dot{x}_1 & (\dot{x}_1 - \dot{x}_2) & 0 & 0 \\ 0 & -(\dot{x}_1 - \dot{x}_2) & (\dot{x}_2 - \dot{x}_3) & 0 \\ 0 & 0 & -(\dot{x}_2 - \dot{x}_3) & (\dot{x}_3 - \dot{x}_4) \\ 0 & 0 & 0 & -(\dot{x}_2 - \dot{x}_3) \end{bmatrix} = \hat{\beta}[VV] \tag{4.15}$$

Differentiating $[C]\{\dot{x}_i\}$with respect to$\hat{\beta}$

$$\frac{\partial}{\partial \hat{\beta}}[C]\{\dot{x}_i\} = \frac{\partial}{\partial \hat{\beta}}\left[\hat{\beta}[K] + \hat{\alpha}[M]\right]\{\dot{x}_i\} = \left[[K] + [0]\right]\{\dot{x}_i\} = [K]\{\dot{x}_i\} \tag{4.16}$$

Differentiating $[C]\{\dot{x}_i\}$with respect to$\hat{\alpha}$

$$\frac{\partial}{\partial \hat{\alpha}}[C]\{\dot{x}_i\} = \frac{\partial}{\partial \hat{\alpha}}\left[\hat{\beta}[K] + \hat{\alpha}[M]\right]\{\dot{x}_i\} = \left[[0] + [M]\right]\{\dot{x}_i\} = [M]\{\dot{x}_i\} \tag{4.17}$$

Jacobian of Matrix $\boldsymbol{g}$ is$\boldsymbol{A} = \frac{\partial \boldsymbol{g}}{\partial \boldsymbol{x_e}}$.

$$\frac{\partial g}{\partial X_e} = \begin{bmatrix} \frac{\partial g_1}{\partial x_1} & \frac{\partial g_1}{\partial x_2} & \frac{\partial g_1}{\partial x_3} & \frac{\partial g_1}{\partial x_4} & \frac{\partial g_1}{\partial \dot{x}_1} & \frac{\partial g_1}{\partial \dot{x}_2} & \frac{\partial g_1}{\partial \dot{x}_3} & \frac{\partial g_1}{\partial \dot{x}_4} & \frac{\partial g_1}{\partial k_1} & \frac{\partial g_1}{\partial k_2} & \frac{\partial g_1}{\partial k_3} & \frac{\partial g_1}{\partial k_4} & \frac{\partial g_1}{\partial \hat{\beta}} \\ \frac{\partial g_2}{\partial x_1} & \frac{\partial g_2}{\partial x_2} & \frac{\partial g_2}{\partial x_3} & \frac{\partial g_2}{\partial x_4} & \frac{\partial g_2}{\partial \dot{x}_1} & \frac{\partial g_2}{\partial \dot{x}_2} & \frac{\partial g_2}{\partial \dot{x}_3} & \frac{\partial g_2}{\partial \dot{x}_4} & \frac{\partial g_2}{\partial k_1} & \frac{\partial g_2}{\partial k_2} & \frac{\partial g_2}{\partial k_3} & \frac{\partial g_2}{\partial k_4} & \frac{\partial g_2}{\partial \hat{\beta}} \\ \vdots & \vdots & \vdots & \vdots & \vdots & \vdots & \vdots & \vdots & \vdots & \vdots & \vdots & \vdots & \vdots \\ \frac{\partial g_{14}}{\partial x_1} & \frac{\partial g_{14}}{\partial x_2} & \frac{\partial g_{14}}{\partial x_3} & \frac{\partial g_{14}}{\partial x_4} & \frac{\partial g_{14}}{\partial \dot{x}_1} & \frac{\partial g_{14}}{\partial \dot{x}_2} & \frac{\partial g_{14}}{\partial \dot{x}_3} & \frac{\partial g_{14}}{\partial \dot{x}_4} & \frac{\partial g_{14}}{\partial k_1} & \frac{\partial g_{14}}{\partial k_2} & \frac{\partial g_{14}}{\partial k_3} & \frac{\partial g_{14}}{\partial k_4} & \frac{\partial g_{14}}{\partial \hat{\beta}} \end{bmatrix} \tag{4.18}$$

where, the extended unknown state vector is represented by $\boldsymbol{X_e}$ and is given by Eq. (4.19)

$$\boldsymbol{X}_e = \{x_1 \quad x_2 \quad x_2 \quad x_4 \quad \dot{x}_1 \quad \dot{x}_2 \quad \dot{x}_3 \quad \dot{x}_4 \quad k_1 \quad k_2 \quad k_3 \quad k_4 \quad \hat{\beta} \quad \hat{\alpha}\}^T \tag{4.19}$$

The vector $\boldsymbol{X_e}$ is called the extended state vector because apart from state vector $\{X\} = \{x_i, \dot{x}_i\}^T$, the vector $\boldsymbol{X_e}$ is also appended with parameters of the model under consideration, called as the parametric vector $\{\theta\} = \{k_i, \hat{\beta}, \hat{\alpha}\}^T$, where, i =1,2,3,4.

The Jacobian is evaluated and is shown as

$$\boldsymbol{A} = \frac{\partial \boldsymbol{g}}{\partial \boldsymbol{X_e}} = \begin{bmatrix} \frac{\partial \dot{x}_i}{\partial x_i} & \frac{\partial \dot{x}_i}{\partial \dot{x}_i} & \frac{\partial \dot{x}_i}{\partial k_i} & \frac{\partial \dot{x}_i}{\partial \hat{\beta}} & \frac{\partial \dot{x}_i}{\partial \hat{\alpha}} \\ \boldsymbol{M}^{-1}\frac{\partial(\boldsymbol{K}x_i + \boldsymbol{C}\dot{x}_i)}{\partial x_i} & \boldsymbol{M}^{-1}\frac{\partial(\boldsymbol{K}x_i + \boldsymbol{C}\dot{x}_i)}{\partial \dot{x}_i} & M^{-1}\frac{\partial(\boldsymbol{K}x_i + \boldsymbol{C}\dot{x}_i)}{\partial k_i} & \boldsymbol{M}^{-1}\frac{\partial(\boldsymbol{K}x_i + \boldsymbol{C}\dot{x}_i)}{\partial \hat{\beta}} & \boldsymbol{M}^{-1}\frac{\partial(\boldsymbol{K}x_i + \boldsymbol{C}\dot{x}_i)}{\partial \hat{\alpha}} \\ [0]_{6x4} & [0]_{6x4} & [0]_{6x4} & [0]_{6x1} & [0]_{6x1} \end{bmatrix} \quad (4.20)$$

Substituting the differentials from Eq. (4.11) to Eq. (4.16) into Eq. (4.20)

$$\boldsymbol{A} = \begin{bmatrix} [0]_{4x4} & [I]_{4x4} & [0]_{4x4} & [0]_{4x1} & [0]_{4x1} \\ \boldsymbol{M}^{-1}[K] & \boldsymbol{M}^{-1}[C] & \boldsymbol{M}^{-1}\left([KK] + \hat{\beta}[VV]\right) & \boldsymbol{M}^{-1}[K]\{\dot{x}_i\} & \boldsymbol{M}^{-1}[M]\{\dot{x}_i\} \\ [0]_{6x4} & [0]_{6x4} & [0]_{6x4} & [0]_{6x1} & [0]_{6x1} \end{bmatrix}$$

$$= \begin{bmatrix} [0]_{4x4} & [I]_{4x4} & [0]_{4x4} & [0]_{4x1} & [0]_{4x1} \\ \boldsymbol{M}^{-1}[[K] & [C] & \left([KK] + \hat{\beta}[VV]\right) & [K]\{\dot{x}_i\} & [M]\{\dot{x}_i\}] \\ [0]_{4x4} & [0]_{4x4} & [0]_{4x4} & [0]_{4x1} & [0]_{4x1} \end{bmatrix} \quad (4.21)$$

where,

$$[0]_{4x4} = \begin{bmatrix} 0 & 0 & 0 & 0 \\ 0 & 0 & 0 & 0 \\ 0 & 0 & 0 & 0 \\ 0 & 0 & 0 & 0 \end{bmatrix} \quad [I]_{4x4} = \begin{bmatrix} 1 & 0 & 0 & 0 \\ 0 & 1 & 0 & 0 \\ 0 & 0 & 1 & 0 \\ 0 & 0 & 0 & 1 \end{bmatrix} \quad [0]_{4x1} = \begin{bmatrix} 0 \\ 0 \\ 0 \\ 0 \end{bmatrix} \quad (4.22)$$

Using the above formulation, the implementation in MATLAB software is as follows.

4.5.1.2 Implementation of EKF formulation in MATLAB platform

Mathematical formulations of EKF developed in the previous section are implemented in MATLAB platform using following four steps.

Step-1: Initialization Step.

Initialization is done by assuming the initial value of

a) The extended state vector, $\boldsymbol{X_e}$.
b) Error covariance matrix of $\boldsymbol{X_e}$, which is $\boldsymbol{P}$.
c) Process error covariance matrix, $\boldsymbol{Q}$.
d) Measurement error covariance matrix, $\boldsymbol{R}$.

Step-2: Evaluation of state transfer matrix

The state transition matrix is determined by evaluating the Jacobian of the process equation and is given by Eq(4.21).

Step-3: Prediction Step

Prediction of unknown extended state vector is made for current time step using the input information and state information of previous time step. This is done by integrating the Eq. (4.7) by 4th order Runga-Kutta integration scheme.

Upon integration of Eq. (4.7), the predicted value of extended state vector $\boldsymbol{X_e}$is obtained, using which the measurement equation is generated as

$$\ddot{\hat{\boldsymbol{x}}}_i = \boldsymbol{\Lambda}\left(-\boldsymbol{\eta}\ddot{x}_g - \boldsymbol{Kx/M} - \boldsymbol{C\dot{x}/M}\right) \tag{4.23}$$

where, $\boldsymbol{\Lambda}$ is a matrix expressing the sensor location. Suppose, sensor at dof-2 is missing, then the sensor location matrix is expressed as

$$\boldsymbol{\Lambda} = \begin{bmatrix} 1 & 0 & 0 & 0 \\ 0 & 0 & 1 & 0 \\ 0 & 0 & 0 & 1 \end{bmatrix} \tag{4.24}$$

The rows denote the sensor numbers and the columns denote the dofs. The dofs where sensor is present is having value of one. In case where all sensor data are available, $\boldsymbol{\Lambda}$ is an identity matrix having the dimension of total number of dof.The predicted state vector is expressed as$\widehat{\boldsymbol{X}}_{k|k}$.

Step-4: Updating Step

The measurement information at current time step is used to correct the estimate to get more accurate state information. This is accomplished by Kalman Filtering which is described in the following steps.

The state transition matrix $\boldsymbol{\Phi}_{\mathrm{k-1|k-1}}$is determined as

$$\boldsymbol{\Phi}_{\mathrm{k-1|k-1}} = \boldsymbol{I}_{14x14} + \Delta t.\boldsymbol{A}\left(\widehat{\boldsymbol{X}}_{k-1|k-1}\right) \tag{4.25}$$

Using the state transition matrix, the predicted apriori estimate covariance is determined

$$\mathbf{P}_{\mathrm{k|k-1}} = \boldsymbol{\Phi}_{\mathrm{k-1|k-1}}\mathbf{P}_{\mathrm{k-1|k-1}}\boldsymbol{\Phi}^{\mathbf{T}}{}_{\mathrm{k-1|k-1}} + \mathbf{Q}_{\mathrm{k}} \tag{4.26}$$

The Kalman Gain matrix is determined as

$$\mathcal{K}_{\mathrm{k}} = \frac{\mathbf{P}_{\mathrm{k|k-1}}\mathbf{H}^{\mathrm{T}}}{\mathbf{H}\mathbf{P}_{\mathrm{k|k-1}}\mathbf{H}^{\mathrm{T}} + \mathbf{R}} \tag{4.27}$$

where, [H] is the Jacobian of the measurement equation

$$[H] = [\Lambda]\left([M]^{-1}\left([K] \quad [C] \quad \left([KK] + \hat{\beta}[KK]\right) \quad [K]\{\dot{x}_i\} \quad [M]\{\dot{x}_i\}\right)\right) \tag{4.28}$$

If the current measured acceleration from the system is denoted as $\ddot{\boldsymbol{x}}_i$, then the difference between current measurement and estimated measurement (Eq.(4.23)), also known as innovation is given as

$$\hat{\boldsymbol{y}}_{\boldsymbol{k}} = \left(\boldsymbol{\Lambda}\ddot{\boldsymbol{x}}_i - \hat{\ddot{\boldsymbol{x}}}_i\right) \tag{4.29}$$

The updated posterior estimate of the extended state vector is given as

$$\hat{\boldsymbol{X}}_{e,k|k} = \hat{\boldsymbol{X}}_{e,k|k-1} + \mathcal{K}_{\mathrm{k}}\hat{\boldsymbol{y}}_{\boldsymbol{k}} \tag{4.30}$$

In this way the steps are run recursively to obtain the extended state vector.

4.5.2 Two-Stage EKF for four-DOF fixed base shear frame building

The general formulation of Two-Stage EKF is presented in chapter-3. In this section, mathematical formulations of Two-Stage EKF for four-DOF fixed base shear building (Fig. 4.1) is presented. This formulation can be easily extended to develop Two-Stage EKF for similar system with higher numbers of DOFs.

4.5.2.1 Detail formulation of Two-Stage EKF for four-DOF Fixed base shear building

In this sub-section, the matrices such as stiffness, damping and Jacobian etc. required for Two-Stage EKF implementation are derived.

The unknown extended state vector, $\boldsymbol{X}_e$, given by Eq.(4.31) contains both state vector $\boldsymbol{X}$ and parametric vector $\boldsymbol{\theta}$. The vector $\boldsymbol{X}_e$ is partitioned into state and parametric vector denoted by **X** and **θ** respectively.

$$\boldsymbol{X}_e = \begin{Bmatrix} \boldsymbol{x}_i \\ \dot{\boldsymbol{x}}_i \\ \boldsymbol{k}_i \\ \hat{\beta} \\ \hat{\alpha} \end{Bmatrix} = \begin{Bmatrix} \boldsymbol{X} \\ \boldsymbol{\theta} \end{Bmatrix} \tag{4.31}$$

where, $\boldsymbol{X} = \{x_1 \quad x_2 \quad x_3 \quad x_4 \quad \dot{x}_1 \quad \dot{x}_2 \quad \dot{x}_3 \quad \dot{x}_4\}^T$ and $\boldsymbol{\theta} = \{k_1 \quad k_2 \quad k_3 \quad k_4 \quad \hat{\beta} \quad \hat{\alpha}\}^T$

The state-space form of the governing differential equation is given by

$$\dot{\boldsymbol{X}} = \begin{Bmatrix} \dot{\boldsymbol{x}}_i \\ \ddot{\boldsymbol{x}}_i \end{Bmatrix} = \frac{d}{dt}\begin{Bmatrix} \boldsymbol{x}_i \\ \dot{\boldsymbol{x}}_i \end{Bmatrix} = \frac{d\boldsymbol{X}}{dt} = \begin{Bmatrix} \dot{\boldsymbol{x}}_i \\ -\boldsymbol{\eta}\ddot{x}_g - \boldsymbol{M}^{-1}\boldsymbol{K}\boldsymbol{x}_i - \boldsymbol{M}^{-1}\boldsymbol{C}\dot{\boldsymbol{x}}_i \end{Bmatrix} \tag{4.32}$$

The observation equation is given by

$$\boldsymbol{h} = \boldsymbol{\Lambda}\left(-\boldsymbol{\eta}\ddot{x}_g - \boldsymbol{M}^{-1}\boldsymbol{K}\boldsymbol{x} - \boldsymbol{M}^{-1}\boldsymbol{C}\dot{\boldsymbol{x}}\right) \tag{4.33}$$

where, $\boldsymbol{x} = \{ \quad _1 \quad x_2 \quad x_3 \quad x_4\}^T$, $\dot{\boldsymbol{x}} = \{\dot{x}_1 \quad \dot{x}_2 \quad \dot{x}_3 \quad \dot{x}_4\}^T$, the sensor location matrix $\boldsymbol{\Lambda}$ is defined in Eq. (4.24) and the stiffness matrix **K** is given as

$$\boldsymbol{K} = \begin{bmatrix} k_1 + k_2 & -k_2 & 0 & 0 \\ -k_2 & k_2 + k_3 & -k_3 & 0 \\ 0 & -k_3 & k_3 + k_4 & -k_4 \\ 0 & 0 & -k_4 & k_4 \end{bmatrix} \tag{4.34}$$

The mass matrix **M** is given as

$$\boldsymbol{M} = \begin{bmatrix} m_1 & 0 & 0 & 0 \\ 0 & m_2 & 0 & 0 \\ 0 & 0 & m_3 & 0 \\ 0 & 0 & 0 & m_4 \end{bmatrix} \tag{4.35}$$

And the damping matrix **C** is expressed as Raleigh damping, which is mass and stiffness proportional damping

$$\boldsymbol{C} = \hat{\beta} * \boldsymbol{K} + \hat{\alpha} * \boldsymbol{M} \tag{4.36}$$

The observation equation at time $t = k \times \Delta t$ is a nonlinear function of unknown parametric vector $\boldsymbol{\theta}_k$ and can be linearized via Taylor series expansion. Then,

$$\boldsymbol{h}(\boldsymbol{X}_k, \boldsymbol{\theta}_k, \boldsymbol{F}_k) = \boldsymbol{h}\left(\widehat{\boldsymbol{X}}_{k|k-1}, \widehat{\boldsymbol{\theta}}_{k-1}, \boldsymbol{F}_k\right) + \boldsymbol{H}_k\left(\boldsymbol{\theta}_k - \widehat{\boldsymbol{\theta}}_{k-1}\right) \tag{4.37}$$

where, $\boldsymbol{H}_k$ is obtained based on the chain rule of partial differential with respect to the parametric vector $\boldsymbol{\theta}_k$ as follows

$$\boldsymbol{H}_k = \boldsymbol{\Lambda}\left(\boldsymbol{H}_{\theta,k} + \boldsymbol{H}_{X,k}\boldsymbol{X}_{\theta,k}\right) \tag{4.38}$$

In which,

$$\boldsymbol{H}_{\theta,k} = \boldsymbol{\Lambda}\left[\frac{\partial \boldsymbol{h}(\boldsymbol{X}, \boldsymbol{\theta}, \boldsymbol{F})}{\partial \boldsymbol{\theta}}\right]_{\boldsymbol{X}=\widehat{\boldsymbol{X}}_{k|k-1}, \boldsymbol{\theta}=\widehat{\boldsymbol{\theta}}_{k-1}}$$

$$\boldsymbol{H}_{X,k} = \boldsymbol{\Lambda}\left[\frac{\partial \boldsymbol{h}(\boldsymbol{X}, \boldsymbol{\theta}, \boldsymbol{F})}{\partial \boldsymbol{X}}\right]_{\boldsymbol{X}=\widehat{\boldsymbol{X}}_{k|k-1}, \boldsymbol{\theta}=\widehat{\boldsymbol{\theta}}_{k-1}} ; \boldsymbol{X}_{\theta,k} = \left[\frac{\partial \boldsymbol{X}(\boldsymbol{X}, \boldsymbol{\theta}, \boldsymbol{F})}{\partial \boldsymbol{\theta}}\right]_{\boldsymbol{\theta}=\widehat{\boldsymbol{\theta}}_{k-1}} \tag{4.39}$$

The details of Eqs.(4.37) to (4.39) are given in Chapter-3 of this thesis, wherein the matrix $\boldsymbol{\Lambda}$is not shown for simplicity of expression.The partial derivative of the observation equation, Eq. (4.33) with respect to state vector $\boldsymbol{X}$ is given by

$$\boldsymbol{H}_{X,k} = \boldsymbol{\Lambda}\frac{\partial \boldsymbol{h}}{\partial \boldsymbol{X}} = \boldsymbol{\Lambda}\frac{\partial}{\partial \boldsymbol{X}}\left(-\boldsymbol{\eta}\ddot{x}_g - \boldsymbol{M}^{-1}\boldsymbol{K}\boldsymbol{x} - \boldsymbol{M}^{-1}\boldsymbol{C}\dot{\boldsymbol{x}}\right)$$
$$= \boldsymbol{\Lambda}\left(-\boldsymbol{M}^{-1}\frac{\partial}{\partial \boldsymbol{X}}(\boldsymbol{K}\boldsymbol{x}) - \boldsymbol{M}^{-1}\frac{\partial}{\partial \boldsymbol{X}}(\boldsymbol{C}\dot{\boldsymbol{x}})\right) \tag{4.40}$$

Evaluating $\frac{\partial}{\partial \boldsymbol{X}}(\boldsymbol{K}\boldsymbol{x})$as

$$\frac{\partial}{\partial \boldsymbol{X}}(\boldsymbol{K}\boldsymbol{x}) = [K]\frac{\partial \boldsymbol{x}}{\partial \boldsymbol{X}} = [K]\begin{bmatrix} \frac{\partial x_1}{\partial x_1} & \frac{\partial x_1}{\partial x_2} & \frac{\partial x_1}{\partial x_3} & \frac{\partial x_1}{\partial x_4} & \frac{\partial x_1}{\partial \dot{x}_1} & \frac{\partial x_1}{\partial \dot{x}_2} & \frac{\partial x_1}{\partial \dot{x}_3} & \frac{\partial x_1}{\partial \dot{x}_4} \\ \frac{\partial x_2}{\partial x_1} & \frac{\partial x_2}{\partial x_2} & \frac{\partial x_2}{\partial x_3} & \frac{\partial x_2}{\partial x_4} & \frac{\partial x_2}{\partial \dot{x}_1} & \frac{\partial x_2}{\partial \dot{x}_2} & \frac{\partial x_2}{\partial \dot{x}_3} & \frac{\partial x_2}{\partial \dot{x}_4} \\ \frac{\partial x_3}{\partial x_1} & \frac{\partial x_3}{\partial x_2} & \frac{\partial x_3}{\partial x_3} & \frac{\partial x_3}{\partial x_4} & \frac{\partial x_3}{\partial \dot{x}_1} & \frac{\partial x_3}{\partial \dot{x}_2} & \frac{\partial x_3}{\partial \dot{x}_3} & \frac{\partial x_3}{\partial \dot{x}_4} \\ \frac{\partial x_4}{\partial x_1} & \frac{\partial x_4}{\partial x_2} & \frac{\partial x_4}{\partial x_3} & \frac{\partial x_4}{\partial x_4} & \frac{\partial x_4}{\partial \dot{x}_1} & \frac{\partial x_4}{\partial \dot{x}_2} & \frac{\partial x_4}{\partial \dot{x}_3} & \frac{\partial x_4}{\partial \dot{x}_4} \end{bmatrix} \tag{4.41}$$

$$\frac{\partial}{\partial \boldsymbol{X}}(\boldsymbol{K}\boldsymbol{x}) = [K]\left[\begin{array}{cccc:cccc} 1 & 0 & 0 & 0 & 0 & 0 & 0 & 0 \\ 0 & 1 & 0 & 0 & 0 & 0 & 0 & 0 \\ 0 & 0 & 1 & 0 & 0 & 0 & 0 & 0 \\ 0 & 0 & 0 & 1 & 0 & 0 & 0 & 0 \end{array}\right] = [K][\boldsymbol{I}_{4x4} \quad \boldsymbol{0}_{4x4}] = [K] \tag{4.42}$$

Evaluating $\frac{\partial}{\partial \boldsymbol{X}}(\boldsymbol{C}\dot{\boldsymbol{x}})$ as

$$\frac{\partial}{\partial \boldsymbol{X}}(\boldsymbol{C}\dot{\boldsymbol{x}}) = \frac{\partial}{\partial \boldsymbol{X}}\left[\hat{\beta}\boldsymbol{K} + \hat{\alpha}\boldsymbol{M}\right]\{\dot{x}\} = \left[\hat{\beta}\boldsymbol{K} + \hat{\alpha}\boldsymbol{M}\right]\frac{\partial \dot{\boldsymbol{x}}}{\partial \boldsymbol{X}} \tag{4.43}$$

$$= \left[\hat{\beta}\boldsymbol{K} + \hat{\alpha}\boldsymbol{M}\right]\begin{bmatrix} \frac{\partial \dot{x}_1}{\partial x_1} & \frac{\partial \dot{x}_1}{\partial x_2} & \frac{\partial \dot{x}_1}{\partial x_3} & \frac{\partial \dot{x}_1}{\partial x_4} & \frac{\partial \dot{x}_1}{\partial \dot{x}_1} & \frac{\partial \dot{x}_1}{\partial \dot{x}_2} & \frac{\partial \dot{x}_1}{\partial \dot{x}_3} & \frac{\partial \dot{x}_1}{\partial \dot{x}_4} \\ \frac{\partial \dot{x}_2}{\partial x_1} & \frac{\partial \dot{x}_2}{\partial x_2} & \frac{\partial \dot{x}_2}{\partial x_3} & \frac{\partial \dot{x}_2}{\partial x_4} & \frac{\partial \dot{x}_2}{\partial \dot{x}_1} & \frac{\partial \dot{x}_2}{\partial \dot{x}_2} & \frac{\partial \dot{x}_2}{\partial \dot{x}_3} & \frac{\partial \dot{x}_2}{\partial \dot{x}_4} \\ \frac{\partial \dot{x}_3}{\partial x_1} & \frac{\partial \dot{x}_3}{\partial x_2} & \frac{\partial \dot{x}_3}{\partial x_3} & \frac{\partial \dot{x}_3}{\partial x_4} & \frac{\partial \dot{x}_3}{\partial \dot{x}_1} & \frac{\partial \dot{x}_3}{\partial \dot{x}_2} & \frac{\partial \dot{x}_3}{\partial \dot{x}_3} & \frac{\partial \dot{x}_3}{\partial \dot{x}_4} \\ \frac{\partial \dot{x}_4}{\partial x_1} & \frac{\partial \dot{x}_4}{\partial x_2} & \frac{\partial \dot{x}_4}{\partial x_3} & \frac{\partial \dot{x}_4}{\partial x_4} & \frac{\partial \dot{x}_4}{\partial \dot{x}_1} & \frac{\partial \dot{x}_4}{\partial \dot{x}_2} & \frac{\partial \dot{x}_4}{\partial \dot{x}_3} & \frac{\partial \dot{x}_4}{\partial \dot{x}_4} \end{bmatrix} \tag{4.44}$$

$$\frac{\partial}{\partial \boldsymbol{X}}(\boldsymbol{C}\dot{\boldsymbol{x}}) = \left[\hat{\beta}\boldsymbol{K} + \hat{\alpha}\boldsymbol{M}\right]\left[\begin{array}{cccc:cccc} 0 & 0 & 0 & 0 & 1 & 0 & 0 & 0 \\ 0 & 0 & 0 & 0 & 0 & 1 & 0 & 0 \\ 0 & 0 & 0 & 0 & 0 & 0 & 1 & 0 \\ 0 & 0 & 0 & 0 & 0 & 0 & 0 & 1 \end{array}\right]$$
$$= \left[\hat{\beta}\boldsymbol{K} + \hat{\alpha}\boldsymbol{M}\right][\boldsymbol{0}_{4x4} \quad \boldsymbol{I}_{4x4}] = \left[\hat{\beta}\boldsymbol{K} + \hat{\alpha}\boldsymbol{M}\right] \tag{4.45}$$

Therefore, from Eq. (4.40), (4.42) and (4.45), $\boldsymbol{H}_{X,k}$ is obtained as

$$\boldsymbol{H}_{X,k} = \boldsymbol{\Lambda}\left(-\boldsymbol{M}^{-1}\frac{\partial}{\partial \boldsymbol{X}}(\boldsymbol{K}\boldsymbol{x}) - \boldsymbol{M}^{-1}\frac{\partial}{\partial \boldsymbol{X}}(\boldsymbol{C}\dot{\boldsymbol{x}})\right) = \boldsymbol{\Lambda}\left(-\boldsymbol{M}^{-1}\left[\boldsymbol{K} \quad \left(\hat{\beta}\boldsymbol{K} + \hat{\alpha}\boldsymbol{M}\right)\right]\right) \tag{4.46}$$

The partial derivative of the observation equation, Eq. (4.33) with respect to parametric vector $\boldsymbol{\theta}$ is

$$\boldsymbol{H}_{\theta,k} = \boldsymbol{\Lambda}\frac{\partial \boldsymbol{h}}{\partial \boldsymbol{\theta}} = \boldsymbol{\Lambda}\frac{\partial}{\partial \boldsymbol{\theta}}\left(-\boldsymbol{\eta}\ddot{x}_g - \boldsymbol{M}^{-1}\boldsymbol{K}\boldsymbol{x} - \boldsymbol{M}^{-1}\boldsymbol{C}\dot{\boldsymbol{x}}\right)$$
$$= \boldsymbol{\Lambda}\left(-\boldsymbol{M}^{-1}\left(\frac{\partial}{\partial \boldsymbol{\theta}}(\boldsymbol{K}\boldsymbol{x}) + \frac{\partial}{\partial \boldsymbol{\theta}}(\boldsymbol{C}\dot{\boldsymbol{x}})\right)\right) \tag{4.47}$$

Evaluating $\frac{\partial}{\partial \boldsymbol{\theta}}(\boldsymbol{K}\boldsymbol{x})$ as

$$\frac{\partial(\boldsymbol{K}\boldsymbol{x})}{\partial \boldsymbol{\theta}} = \left[\frac{\partial(\boldsymbol{K}\boldsymbol{x})}{\partial k_1} \quad \frac{\partial(\boldsymbol{K}\boldsymbol{x})}{\partial k_2} \quad \frac{\partial(\boldsymbol{K}\boldsymbol{x})}{\partial k_3} \quad \frac{\partial(\boldsymbol{K}\boldsymbol{x})}{\partial k_4} \quad \frac{\partial(\boldsymbol{K}\boldsymbol{x})}{\partial \hat{\beta}} \quad \frac{\partial(\boldsymbol{K}\boldsymbol{x})}{\partial \hat{\alpha}}\right] \tag{4.48}$$

Recalling Eq. (4.9)

$$\boldsymbol{K}\boldsymbol{x} = \begin{Bmatrix} k_1x_1 + k_2x_1 - k_2x_2 \\ -k_2x_1 + k_2x_2 + k_3x_2 - k_3x_3 \\ -k_3x_2 + k_3x_3 + k_4x_3 - k_4x_4 \\ -k_4x_3 + k_4x_4 \end{Bmatrix} \tag{4.49}$$

Differentiating [K]{x} with respect to {θ},

$$\frac{\partial(\boldsymbol{K}\boldsymbol{x})}{\partial \boldsymbol{\theta}} = \begin{bmatrix} x_1 & (x_1 - x_2) & 0 & 0 & 0 & 0 \\ 0 & -(x_1 - x_2) & (x_2 - x_3) & 0 & 0 & 0 \\ 0 & 0 & -(x_2 - x_3) & (x_3 - x_4) & 0 & 0 \\ 0 & 0 & 0 & -(x_3 - x_4) & 0 & 0 \end{bmatrix}$$
$$= [\boldsymbol{K}\boldsymbol{K} \quad \boldsymbol{0}_{4x2}] = [\boldsymbol{K}\boldsymbol{K} \quad \boldsymbol{0}_{4x1} \quad \boldsymbol{0}_{4x1}] \tag{4.50}$$

Evaluating $\frac{\partial}{\partial \boldsymbol{\theta}}(\boldsymbol{C}\dot{\boldsymbol{x}})$ as

$$\frac{\partial(\boldsymbol{C}\dot{\boldsymbol{x}})}{\partial\boldsymbol{\theta}} = \frac{\partial\left(\hat{\beta}\boldsymbol{K} + \hat{\alpha}\boldsymbol{M}\right)\dot{\boldsymbol{x}}}{\partial\boldsymbol{\theta}} = \frac{\partial\left(\hat{\beta}\boldsymbol{K}\dot{\boldsymbol{x}}\right)}{\partial\boldsymbol{\theta}} + \frac{\partial(\hat{\alpha}\boldsymbol{M}\dot{\boldsymbol{x}})}{\partial\boldsymbol{\theta}} \tag{4.51}$$

Evaluating $\frac{\partial(\boldsymbol{K}\dot{\boldsymbol{x}})}{\partial\boldsymbol{\theta}}$as

$$\frac{\partial\left(\hat{\beta}\boldsymbol{K}\dot{\boldsymbol{x}}\right)}{\partial\boldsymbol{\theta}} = \frac{\partial}{\partial\boldsymbol{\theta}}\begin{Bmatrix}\hat{\beta}(k_1\dot{x}_1 + k_2\dot{x}_1 - k_2\dot{x}_2)\\ \hat{\beta}(-k_2\dot{x}_1 + k_2\dot{x}_2 + k_3\dot{x}_2 - k_3\dot{x}_3)\\ \hat{\beta}(-k_3\dot{x}_2 + k_3\dot{x}_3 + k_4\dot{x}_3 - k_4\dot{x}_4)\\ \hat{\beta}(-k_4\dot{x}_3 + k_4\dot{x}_4)\end{Bmatrix}$$

$$= \begin{bmatrix}\hat{\beta}\dot{x}_1 & \hat{\beta}(\dot{x}_1 - \dot{x}_2) & 0 & 0 & (k_1\dot{x}_1 + k_2\dot{x}_1 - k_2\dot{x}_2) & 0\\ 0 & -\hat{\beta}(\dot{x}_1 - \dot{x}_2) & \hat{\beta}(\dot{x}_2 - \dot{x}_3) & 0 & (-k_2\dot{x}_1 + k_2\dot{x}_2 + k_3\dot{x}_2 - k_3\dot{x}_3) & 0\\ 0 & 0 & -\hat{\beta}(\dot{x}_2 - \dot{x}_3) & \hat{\beta}(\dot{x}_3 - \dot{x}_4) & (-k_3\dot{x}_2 + k_3\dot{x}_3 + k_4\dot{x}_3 - k_4\dot{x}_4) & 0\\ 0 & 0 & 0 & -\hat{\beta}(\dot{x}_3 - \dot{x}_4) & (-k_4\dot{x}_3 + k_4\dot{x}_4) & 0\end{bmatrix}$$

$$= [\hat{\beta} * \boldsymbol{VV} \quad \boldsymbol{K}\dot{\boldsymbol{x}} \quad \boldsymbol{0}_{4x1}] \tag{4.52}$$

where,

$$[VV] = \begin{bmatrix}\dot{x}_1 & (\dot{x}_1 - \dot{x}_2) & 0 & 0\\ 0 & -(\dot{x}_1 - \dot{x}_2) & (\dot{x}_2 - \dot{x}_3) & 0\\ 0 & 0 & -(\dot{x}_2 - \dot{x}_3) & (\dot{x}_3 - \dot{x}_4)\\ 0 & 0 & 0 & -(\dot{x}_2 - \dot{x}_3)\end{bmatrix} \quad \{0\}_{4x1} = \begin{Bmatrix}0\\0\\0\\0\end{Bmatrix}$$

Evaluating $\frac{\partial(\hat{\alpha}\boldsymbol{M}\dot{\boldsymbol{x}})}{\partial\boldsymbol{\theta}}$as

$$\frac{\partial(\hat{\alpha}\boldsymbol{M}\dot{\boldsymbol{x}})}{\partial\boldsymbol{\theta}} = \frac{\partial}{\partial\boldsymbol{\theta}}\hat{\alpha}\begin{bmatrix}m_1 & 0 & 0 & 0\\ 0 & m_2 & 0 & 0\\ 0 & 0 & m_3 & 0\\ 0 & 0 & 0 & m_4\end{bmatrix}\begin{Bmatrix}\dot{x}_1\\ \dot{x}_2\\ \dot{x}_3\\ \dot{x}_4\end{Bmatrix} = \frac{\partial}{\partial\boldsymbol{\theta}}\begin{Bmatrix}\hat{\alpha}m_1\dot{x}_1\\ \hat{\alpha}m_2\dot{x}_2\\ \hat{\alpha}m_3\dot{x}_3\\ \hat{\alpha}m_4\dot{x}_4\end{Bmatrix}$$

$$= \begin{bmatrix}\frac{\partial(\hat{\alpha}m_1\dot{x}_1)}{\partial k_1} & \frac{\partial(\hat{\alpha}m_1\dot{x}_1)}{\partial k_2} & \frac{\partial(\hat{\alpha}m_1\dot{x}_1)}{\partial k_3} & \frac{\partial(\hat{\alpha}m_1\dot{x}_1)}{\partial k_4} & \frac{\partial(\hat{\alpha}m_1\dot{x}_1)}{\partial\hat{\beta}} & \frac{\partial(\hat{\alpha}m_1\dot{x}_1)}{\partial\hat{\alpha}}\\ \frac{\partial(\hat{\alpha}m_2\dot{x}_2)}{\partial k_1} & \frac{\partial(\hat{\alpha}m_2\dot{x}_2)}{\partial k_2} & \frac{\partial(\hat{\alpha}m_2\dot{x}_2)}{\partial k_3} & \frac{\partial(\hat{\alpha}m_2\dot{x}_2)}{\partial k_4} & \frac{\partial(\hat{\alpha}m_2\dot{x}_2)}{\partial\hat{\beta}} & \frac{\partial(\hat{\alpha}m_2\dot{x}_2)}{\partial\hat{\alpha}}\\ \frac{\partial(\hat{\alpha}m_3\dot{x}_3)}{\partial k_1} & \frac{\partial(\hat{\alpha}m_3\dot{x}_3)}{\partial k_2} & \frac{\partial(\hat{\alpha}m_3\dot{x}_3)}{\partial k_3} & \frac{\partial(\hat{\alpha}m_3\dot{x}_3)}{\partial k_4} & \frac{\partial(\hat{\alpha}m_3\dot{x}_3)}{\partial\hat{\beta}} & \frac{\partial(\hat{\alpha}m_3\dot{x}_3)}{\partial\hat{\alpha}}\\ \frac{\partial(\hat{\alpha}m_4\dot{x}_4)}{\partial k_1} & \frac{\partial(\hat{\alpha}m_4\dot{x}_4)}{\partial k_2} & \frac{\partial(\hat{\alpha}m_4\dot{x}_4)}{\partial k_3} & \frac{\partial(\hat{\alpha}m_4\dot{x}_4)}{\partial k_4} & \frac{\partial(\hat{\alpha}m_4\dot{x}_4)}{\partial\hat{\beta}} & \frac{\partial(\hat{\alpha}m_4\dot{x}_4)}{\partial\hat{\alpha}}\end{bmatrix}$$

$$= \begin{bmatrix}0 & 0 & 0 & 0 & 0 & m_1\dot{x}_1\\ 0 & 0 & 0 & 0 & 0 & m_2\dot{x}_2\\ 0 & 0 & 0 & 0 & 0 & m_3\dot{x}_3\\ 0 & 0 & 0 & 0 & 0 & m_4\dot{x}_4\end{bmatrix} = [\boldsymbol{0}_{4x4} \quad \boldsymbol{0}_{4x1} \quad \boldsymbol{M}\dot{\boldsymbol{x}}] \tag{4.53}$$

Substituting $\frac{\partial(\hat{\beta}\boldsymbol{K}\dot{\boldsymbol{x}})}{\partial\boldsymbol{\theta}}$ from Eq. (4.52) and $\frac{\partial(\hat{\alpha}\boldsymbol{M}\dot{\boldsymbol{x}})}{\partial\boldsymbol{\theta}}$from Eq. (4.53) into Eq. (4.51), $\frac{\partial(\boldsymbol{C}\dot{\boldsymbol{x}})}{\partial\boldsymbol{\theta}}$ is obtained as

$$\frac{\partial(\boldsymbol{C}\dot{\boldsymbol{x}})}{\partial\boldsymbol{\theta}} = \frac{\partial\left(\hat{\beta}\boldsymbol{K} + \hat{\alpha}\boldsymbol{M}\right)\dot{\boldsymbol{x}}}{\partial\boldsymbol{\theta}} = \frac{\partial\left(\hat{\beta}\boldsymbol{K}\dot{\boldsymbol{x}}\right)}{\partial\boldsymbol{\theta}} + \frac{\partial(\hat{\alpha}\boldsymbol{M}\dot{\boldsymbol{x}})}{\partial\boldsymbol{\theta}}$$
$$= [\hat{\beta} * \boldsymbol{VV} \quad \boldsymbol{K}\dot{\boldsymbol{x}} \quad \boldsymbol{0}_{4x1}] + [\boldsymbol{0}_{4x4} \quad \boldsymbol{0}_{4x1} \quad \boldsymbol{M}\dot{\boldsymbol{x}}]$$
$$= [\hat{\beta} * \boldsymbol{VV} \quad \boldsymbol{K}\dot{\boldsymbol{x}} \quad \boldsymbol{M}\dot{\boldsymbol{x}}] \tag{4.54}$$

Substituting $\frac{\partial}{\partial\boldsymbol{\theta}}(\boldsymbol{Kx})$ and $\frac{\partial}{\partial\boldsymbol{\theta}}(\boldsymbol{C}\dot{\boldsymbol{x}})$ from Eq. (4.50) and Eq. (4.54) respectively into Eq. (4.47)

$$\boldsymbol{H}_{\theta,k} = \boldsymbol{\Lambda}\left(-\boldsymbol{M}^{-1}\left(\frac{\partial}{\partial\boldsymbol{\theta}}(\boldsymbol{Kx}) + \frac{\partial}{\partial\boldsymbol{\theta}}(\boldsymbol{C}\dot{\boldsymbol{x}})\right)\right)$$
$$= \boldsymbol{\Lambda}\left(-\boldsymbol{M}^{-1}([\boldsymbol{KK} \quad \boldsymbol{0}_{4x1} \quad \boldsymbol{0}_{4x1}] + [\hat{\beta} * \boldsymbol{VV} \quad \boldsymbol{K}\dot{\boldsymbol{x}} \quad \boldsymbol{M}\dot{\boldsymbol{x}}])\right) =$$
$$= \boldsymbol{\Lambda}\left(-\boldsymbol{M}^{-1}\left[\left(\boldsymbol{KK} + \hat{\beta} * \boldsymbol{VV}\right) \quad \boldsymbol{K}\dot{\boldsymbol{x}} \quad \boldsymbol{M}\dot{\boldsymbol{x}}\right]\right) \tag{4.55}$$

The partial derivative of the state vector $\boldsymbol{X}$ with respect to parametric vector $\boldsymbol{\theta}$ is $\frac{\partial\boldsymbol{X}}{\partial\boldsymbol{\theta}}$and is derived as follows:

The governing equation of motion is given by

$$\boldsymbol{M}\ddot{\boldsymbol{x}} + \boldsymbol{C}\dot{\boldsymbol{x}} + \boldsymbol{Kx} = -\eta\boldsymbol{M}\ddot{x}_g = \boldsymbol{F} \tag{4.56}$$

In the following derivation also $\boldsymbol{\Lambda}$has been omitted and has been incorporated in the final steps.

Expressing the equation, Eq. (4.56) in state-space form as

$$\dot{\boldsymbol{X}} = \begin{Bmatrix}\dot{\boldsymbol{x}}_i \\ \ddot{\boldsymbol{x}}_i\end{Bmatrix} = \frac{d\boldsymbol{X}}{dt} = \frac{d}{dt}\begin{Bmatrix}\boldsymbol{x}_i \\ \dot{\boldsymbol{x}}_i\end{Bmatrix} = \begin{Bmatrix}\dot{\boldsymbol{x}}_i \\ -\boldsymbol{\eta}\ddot{x}_g - \boldsymbol{M}^{-1}\boldsymbol{Kx}_i - \boldsymbol{M}^{-1}\boldsymbol{C}\dot{\boldsymbol{x}}_i\end{Bmatrix}$$
$$= \begin{Bmatrix}\dot{\boldsymbol{x}}_i \\ -\boldsymbol{\eta}\ddot{x}_g - \boldsymbol{M}^{-1}\boldsymbol{F}_s(\boldsymbol{x},\boldsymbol{\theta}) - \boldsymbol{M}^{-1}\boldsymbol{F}_c(\dot{\boldsymbol{x}},\boldsymbol{\theta})\end{Bmatrix} \tag{4.57}$$

where, $\boldsymbol{F}_s(\boldsymbol{x},\boldsymbol{\theta}) = \boldsymbol{Kx}_i$ and $\boldsymbol{F}_c(\dot{\boldsymbol{x}},\boldsymbol{\theta}) = \boldsymbol{C}\dot{\boldsymbol{x}}_i$

Differentiating both side of Eq. (4.57) by $\boldsymbol{\theta}$ and denoting $\frac{d\boldsymbol{x}_i}{d\boldsymbol{\theta}} = \boldsymbol{x}_{\theta,i}$

$$\frac{d\dot{\boldsymbol{X}}}{d\boldsymbol{\theta}} = \begin{Bmatrix} \frac{d\dot{\boldsymbol{x}}_i}{d\boldsymbol{\theta}} \\ \frac{d\ddot{\boldsymbol{x}}_i}{d\boldsymbol{\theta}} \end{Bmatrix} = \begin{Bmatrix} \dot{\boldsymbol{x}}_{\theta,i} \\ \ddot{\boldsymbol{x}}_{\theta,i} \end{Bmatrix} = \dot{\boldsymbol{X}}_{\theta,i} = \frac{d}{dt}\begin{Bmatrix} \boldsymbol{x}_{\theta,i} \\ \dot{\boldsymbol{x}}_{\theta,i} \end{Bmatrix}$$

$$= \begin{Bmatrix} \frac{d\dot{\boldsymbol{x}}_i}{d\boldsymbol{\theta}} \\ \frac{d}{d\boldsymbol{\theta}}\left(-\boldsymbol{\eta}\ddot{x}_g - \boldsymbol{M}^{-1}\boldsymbol{F}_s(\boldsymbol{x},\boldsymbol{\theta}) - \boldsymbol{M}^{-1}\boldsymbol{F}_c(\dot{\boldsymbol{x}},\boldsymbol{\theta})\right) \end{Bmatrix}$$

$$= \begin{Bmatrix} \dot{\boldsymbol{x}}_{\theta,i} \\ -\boldsymbol{M}^{-1}\frac{d\boldsymbol{F}_s(\boldsymbol{x},\boldsymbol{\theta})}{d\boldsymbol{\theta}} - \boldsymbol{M}^{-1}\frac{d\boldsymbol{F}_c(\dot{\boldsymbol{x}},\boldsymbol{\theta})}{d\boldsymbol{\theta}} \end{Bmatrix} \tag{4.58}$$

Applying chain rule of differentiation into Eq. (4.58)

$$\frac{d\boldsymbol{F}_s(\boldsymbol{x},\boldsymbol{\theta})}{d\boldsymbol{\theta}} = \frac{\partial \boldsymbol{F}_s}{\partial \boldsymbol{x}}\frac{d\boldsymbol{x}}{d\boldsymbol{\theta}} + \frac{\partial \boldsymbol{F}_s}{\partial \boldsymbol{\theta}}\frac{d\boldsymbol{\theta}}{d\boldsymbol{\theta}} = \frac{\partial \boldsymbol{F}_s}{\partial \boldsymbol{x}}\frac{d\boldsymbol{x}}{d\boldsymbol{\theta}} + \frac{\partial \boldsymbol{F}_s}{\partial \boldsymbol{\theta}} \tag{4.59}$$

$$\frac{d\boldsymbol{F}_c(\dot{\boldsymbol{x}},\boldsymbol{\theta})}{d\boldsymbol{\theta}} = \frac{\partial \boldsymbol{F}_c}{\partial \dot{\boldsymbol{x}}}\frac{d\dot{\boldsymbol{x}}}{d\boldsymbol{\theta}} + \frac{\partial \boldsymbol{F}_c}{\partial \boldsymbol{\theta}}\frac{d\boldsymbol{\theta}}{d\boldsymbol{\theta}} = \frac{\partial \boldsymbol{F}_c}{\partial \dot{\boldsymbol{x}}}\frac{d\dot{\boldsymbol{x}}}{d\boldsymbol{\theta}} + \frac{\partial \boldsymbol{F}_c}{\partial \boldsymbol{\theta}} \tag{4.60}$$

Substituting $\frac{d\boldsymbol{F}_s}{d\boldsymbol{\theta}}$ and $\frac{d\boldsymbol{F}_c}{d\boldsymbol{\theta}}$ obtained from Eq.(4.59) and (4.60) into Eq. (4.58)

$$\dot{\boldsymbol{X}}_{\theta,i} = \frac{d}{dt}\begin{Bmatrix} \boldsymbol{x}_{\theta,i} \\ \dot{\boldsymbol{x}}_{\theta,i} \end{Bmatrix} = \begin{Bmatrix} \dot{\boldsymbol{x}}_{\theta,i} \\ -\boldsymbol{M}^{-1}\left(\frac{\partial \boldsymbol{F}_s}{\partial \boldsymbol{x}}\frac{d\boldsymbol{x}}{d\boldsymbol{\theta}} + \frac{\partial \boldsymbol{F}_s}{\partial \boldsymbol{\theta}}\right) - \boldsymbol{M}^{-1}\left(\frac{\partial \boldsymbol{F}_c}{\partial \dot{\boldsymbol{x}}}\frac{d\dot{\boldsymbol{x}}}{d\boldsymbol{\theta}} + \frac{\partial \boldsymbol{F}_c}{\partial \boldsymbol{\theta}}\right) \end{Bmatrix}$$

$$= \begin{Bmatrix} \dot{\boldsymbol{x}}_{\theta,i} \\ -\boldsymbol{M}^{-1}\left(\frac{\partial \boldsymbol{F}_s}{\partial \boldsymbol{x}}\boldsymbol{x}_{\theta,i} + \frac{\partial \boldsymbol{F}_s}{\partial \boldsymbol{\theta}}\right) - \boldsymbol{M}^{-1}\left(\frac{\partial \boldsymbol{F}_c}{\partial \dot{\boldsymbol{x}}}\dot{\boldsymbol{x}}_{\theta,i} + \frac{\partial \boldsymbol{F}_c}{\partial \boldsymbol{\theta}}\right) \end{Bmatrix}$$

$$= \begin{Bmatrix} \dot{\boldsymbol{x}}_{\theta,i} \\ -\boldsymbol{M}^{-1}\frac{\partial \boldsymbol{F}_s}{\partial \boldsymbol{x}}\boldsymbol{x}_{\theta,i} - \boldsymbol{M}^{-1}\frac{\partial \boldsymbol{F}_c}{\partial \dot{\boldsymbol{x}}}\dot{\boldsymbol{x}}_{\theta,i} - \boldsymbol{M}^{-1}\frac{\partial \boldsymbol{F}_s}{\partial \boldsymbol{\theta}} - \boldsymbol{M}^{-1}\frac{\partial \boldsymbol{F}_c}{\partial \boldsymbol{\theta}} \end{Bmatrix}$$

$$= \begin{bmatrix} \boldsymbol{0} & \boldsymbol{I} \\ -\boldsymbol{M}^{-1}\frac{\partial \boldsymbol{F}_s}{\partial \boldsymbol{x}} & -\boldsymbol{M}^{-1}\frac{\partial \boldsymbol{F}_c}{\partial \dot{\boldsymbol{x}}} \end{bmatrix}\begin{Bmatrix} \boldsymbol{x}_{\theta,i} \\ \dot{\boldsymbol{x}}_{\theta,i} \end{Bmatrix} + \boldsymbol{\Lambda}\begin{bmatrix} \boldsymbol{0} \\ -\boldsymbol{M}^{-1}\frac{\partial \boldsymbol{F}_s}{\partial \boldsymbol{\theta}} - \boldsymbol{M}^{-1}\frac{\partial \boldsymbol{F}_c}{\partial \boldsymbol{\theta}} \end{bmatrix} \tag{4.61}$$

Equation (4.61) can be simplified as

$$\dot{\boldsymbol{X}}_{\theta,i} = \begin{bmatrix} \boldsymbol{0}_{4x4} & \boldsymbol{I}_{4x4} \\ -\boldsymbol{M}^{-1}\frac{\partial \boldsymbol{F}_s}{\partial \boldsymbol{x}} & -\boldsymbol{M}^{-1}\frac{\partial \boldsymbol{F}_c}{\partial \dot{\boldsymbol{x}}} \end{bmatrix}\boldsymbol{X}_{\theta,i} + \begin{bmatrix} \boldsymbol{0}_{4x6} \\ -\boldsymbol{M}^{-1}\frac{\partial \boldsymbol{F}_s}{\partial \boldsymbol{\theta}} - \boldsymbol{M}^{-1}\frac{\partial \boldsymbol{F}_c}{\partial \boldsymbol{\theta}} \end{bmatrix} \tag{4.62}$$

where,

$$\frac{\partial \boldsymbol{F}_s}{\partial \boldsymbol{x}} = \frac{\partial(\boldsymbol{K}\boldsymbol{x})}{\partial \boldsymbol{x}} = \boldsymbol{K} \qquad \frac{\partial \boldsymbol{F}_c}{\partial \dot{\boldsymbol{x}}} = \frac{\partial(\boldsymbol{C}\dot{\boldsymbol{x}})}{\partial \dot{\boldsymbol{x}}} = \boldsymbol{C} = \hat{\beta}\boldsymbol{K} + \hat{\alpha}\boldsymbol{M} \tag{4.63}$$

Using Eq. (4.50) and Eq. (4.54)

$$\frac{\partial \boldsymbol{F_s}}{\partial \boldsymbol{\theta}} = \frac{\partial (\boldsymbol{Kx})}{\partial \boldsymbol{\theta}} = [\boldsymbol{KK} \quad \boldsymbol{0}_{4x1} \quad \boldsymbol{0}_{4x1}] \quad \frac{\partial \boldsymbol{F_c}}{\partial \boldsymbol{\theta}} = \frac{\partial (\boldsymbol{C\dot{x}})}{\partial \boldsymbol{\theta}} = [\hat{\beta} * \boldsymbol{VV} \quad \boldsymbol{K\dot{x}} \quad \boldsymbol{M\dot{x}}] \tag{4.64}$$

Therefore, in Eq. (4.62)

$$-\boldsymbol{M}^{-1}\frac{\partial \boldsymbol{F_s}}{\partial \boldsymbol{\theta}} - \boldsymbol{M}^{-1}\frac{\partial \boldsymbol{F_c}}{\partial \boldsymbol{\theta}} = -\boldsymbol{M}^{-1}[\boldsymbol{KK} \quad \boldsymbol{0}_{4x1} \quad \boldsymbol{0}_{4x1}] - \boldsymbol{M}^{-1}[\hat{\beta} * \boldsymbol{VV} \quad \boldsymbol{K\dot{x}} \quad \boldsymbol{M\dot{x}}]$$

$$= -\boldsymbol{M}^{-1}\left[\left(\boldsymbol{KK} + \hat{\beta} * \boldsymbol{VV}\right) \quad \boldsymbol{K\dot{x}} \quad \boldsymbol{M\dot{x}}\right] = \boldsymbol{H}_{\theta,k} \tag{4.65}$$

Where, the expression for $\boldsymbol{H}_{\theta,k}$ is obtained from Eq. (4.55).

Eq. (4.62) is simplified by replacing the terms obtained from Eq. (4.63), (4.64) and (4.65) as

$$\dot{\boldsymbol{X}}_{\theta,i} = \begin{bmatrix} \boldsymbol{0}_{4x4} & \boldsymbol{I}_{4x4} \\ -\boldsymbol{M}^{-1}\boldsymbol{K} & -\boldsymbol{M}^{-1}\boldsymbol{C} \end{bmatrix} \boldsymbol{X}_{\theta,i} + \begin{bmatrix} \boldsymbol{0}_{4x6} \\ \boldsymbol{H}_{\theta,k} \end{bmatrix} \tag{4.66}$$

Expanding $\boldsymbol{X}_{\theta,i}$ gives

$$\boldsymbol{X}_{\theta,i} = \begin{Bmatrix} \frac{\partial x_1}{\partial \boldsymbol{\theta}} \\ \frac{\partial x_2}{\partial \boldsymbol{\theta}} \\ \frac{\partial x_3}{\partial \boldsymbol{\theta}} \\ \frac{\partial x_4}{\partial \boldsymbol{\theta}} \\ \frac{\partial \dot{x}_1}{\partial \boldsymbol{\theta}} \\ \frac{\partial \dot{x}_2}{\partial \boldsymbol{\theta}} \\ \frac{\partial \dot{x}_3}{\partial \boldsymbol{\theta}} \\ \frac{\partial \dot{x}_4}{\partial \boldsymbol{\theta}} \end{Bmatrix} = \begin{bmatrix} \frac{\partial x_1}{\partial k_1} & \frac{\partial x_1}{\partial k_2} & \frac{\partial x_1}{\partial k_3} & \frac{\partial x_1}{\partial k_4} & \frac{\partial x_1}{\partial \hat{\beta}} & \frac{\partial x_1}{\partial \hat{\alpha}} \\ \vdots & \vdots & \vdots & \vdots & \vdots & \vdots \\ \vdots & \vdots & \vdots & \vdots & \vdots & \vdots \\ \frac{\partial x_4}{\partial k_1} & \frac{\partial x_4}{\partial k_2} & \frac{\partial x_4}{\partial k_3} & \frac{\partial x_4}{\partial k_4} & \frac{\partial x_4}{\partial \hat{\beta}} & \frac{\partial x_4}{\partial \hat{\alpha}} \\ \frac{\partial \dot{x}_1}{\partial k_1} & \frac{\partial \dot{x}_1}{\partial k_2} & \frac{\partial \dot{x}_1}{\partial k_3} & \frac{\partial \dot{x}_1}{\partial k_4} & \frac{\partial \dot{x}_1}{\partial \hat{\beta}} & \frac{\partial \dot{x}_1}{\partial \hat{\alpha}} \\ \vdots & \vdots & \vdots & \vdots & \vdots & \vdots \\ \vdots & \vdots & \vdots & \vdots & \vdots & \vdots \\ \frac{\partial \dot{x}_4}{\partial k_1} & \frac{\partial \dot{x}_4}{\partial k_2} & \frac{\partial \dot{x}_4}{\partial k_3} & \frac{\partial \dot{x}_4}{\partial k_4} & \frac{\partial \dot{x}_4}{\partial \hat{\beta}} & \frac{\partial \dot{x}_4}{\partial \hat{\alpha}} \end{bmatrix} \tag{4.67}$$

Integrating Eq. (4.66) using 4th order Runga-Kutta integration scheme, gives $\boldsymbol{X}_{\theta}$ or $\frac{d\boldsymbol{X}}{d\boldsymbol{\theta}}$.

Therefore, $\boldsymbol{H}_k$ of Eq. (4.38) is obtained by substituting $\boldsymbol{H}_{\theta,k}, \boldsymbol{H}_{X,k}, \boldsymbol{X}_{\theta,k}$ obtained from Eqs.(4.55), (4.46) and integrating Eq.(4.66) respectively. Using the formulation as derived above, the implementation procedure in MATLAB software is as follows.

4.5.2.2 Implementation ofTwo-Stage EKF formulation in MATLAB platform

Mathematical formulations of Two-Stage EKF developed in the previous section are implemented in MATLAB platform using following four steps.

Step-1: Initialization Step.

Initialization is done by assuming the initial value of

a) The state vector, $\boldsymbol{X}$.
b) Error covariance matrix of $\boldsymbol{X}$, which is $\boldsymbol{P}_x$.
c) The parametric vector, $\boldsymbol{\theta}$.
d) Error covariance matrix of $\boldsymbol{\theta}$ is $\boldsymbol{P}_\theta$.
e) The matrix $\boldsymbol{X}_\theta$ or $\frac{d\boldsymbol{X}}{d\boldsymbol{\theta}}$.
f) Process error covariance matrix, $\boldsymbol{Q}$.
g) Measurement error covariance matrix, $\boldsymbol{R}$.

Step-2: Evaluation of state transfer matrix

The linearized observation equation matrix, $\boldsymbol{H}_k$ is evaluated using Eq. (4.38).

Step-3a: Prediction of State Vector

With the state and parametric vector of previous step, the stiffness and damping matrix of current step is evaluated. The predicted state vector is evaluated by integration of the state space equation, Eq. (4.32), using 4th order Runga-Kutta integration scheme.

Step-3b: Updating of State Vector

The measurement information at current time step is used to correct the estimate to get more accurate state information. This is accomplished by Kalman Filtering which is described in the following steps.

The state transition matrix $\boldsymbol{\Phi}_{\mathrm{k-1|k-1}}$ is determined as

$$\boldsymbol{\Phi}_{\mathrm{k-1|k-1}} = \boldsymbol{I}_{8x8} + \Delta t.\, \boldsymbol{A2}\left(\widehat{\boldsymbol{X}}_{k-1|k-1}\right) \tag{4.68}$$

where,

$$\boldsymbol{A2}\left(\widehat{\boldsymbol{X}}_{k-1|k-1}\right) = -M^{-1}[\boldsymbol{K} \quad \boldsymbol{C}] \tag{4.69}$$

The Kalman Gain matrix is determined as

$$\mathcal{K}_{\mathrm{k}} = \frac{\mathbf{\Phi}_{\mathrm{k-1|k-1}}\mathbf{P}_{\mathrm{k|k-1}}\mathbf{H}_{\mathrm{x,k}}{}^{\mathrm{T}}}{\mathbf{H}_{\mathrm{x,k}}\mathbf{P}_{\mathrm{k|k-1}}\mathbf{H}_{\mathrm{x,k}}{}^{\mathrm{T}} + \mathbf{R}} \tag{4.70}$$

where, $\mathbf{H}_{\mathrm{x,k}}$is obtained from Eq.(4.40)

From the measurement equation, Eq. (4.71), the predicted measurement (in the present case: acceleration) is evaluated as

$$\ddot{\hat{\boldsymbol{x}}}_i = \boldsymbol{\Lambda}\left(-\boldsymbol{\eta}\ddot{x}_g - \boldsymbol{M}^{-1}\boldsymbol{K}\boldsymbol{x} - \boldsymbol{M}^{-1}\boldsymbol{C}\dot{\boldsymbol{x}}\right) \tag{4.71}$$

where, the state $\boldsymbol{x}, \dot{\boldsymbol{x}}$ are the predicted states obtained from Eq. (4.32). The predicted stiffness and damping matrices are obtained from the parametric vector of previous step. If the current measured acceleration from the system is denoted as $\ddot{\boldsymbol{x}}_i$, then the difference between current measurement and estimated measurement (Eq. (4.71)), also known as innovation is given as

$$\hat{\boldsymbol{y}}_{\boldsymbol{k}} = \left(\boldsymbol{\Lambda}\ddot{\boldsymbol{x}}_i - \ddot{\hat{\boldsymbol{x}}}_i\right) \tag{4.72}$$

The updated posterior estimate of the state vector is given as

$$\hat{\boldsymbol{X}}_{k|k} = \hat{\boldsymbol{X}}_{k|k-1} + \mathcal{K}_{\mathrm{k}}\hat{\boldsymbol{y}}_{\boldsymbol{k}} \tag{4.73}$$

and the updated error covariance matrix of $\boldsymbol{X}$, which is $\boldsymbol{P}_X$, is obtained as

$$\boldsymbol{P}_{X,k|k+1} = \mathbf{\Phi}_{\mathrm{k-1|k-1}}\boldsymbol{P}_{X,k|k}\mathbf{\Phi}^{\mathbf{T}}_{\mathrm{k-1|k-1}} - \mathcal{K}_{\mathrm{k}}\mathbf{H}_{\mathrm{x,k}}\boldsymbol{P}_{X,k|k}\mathbf{\Phi}^{\mathbf{T}}_{\mathrm{k-1|k-1}} \tag{4.74}$$

Step-3c: Updating Parametric Vector

The Kalman Gain matrix is determined as

$$\mathcal{K}_{\mathrm{k}} = \frac{\mathbf{I}_{6\mathrm{x}6}\mathbf{P}_{\mathrm{k|k-1}}\mathbf{H}_{\mathrm{k}}{}^{\mathrm{T}}}{\mathbf{H}_{\mathrm{k}}\mathbf{P}_{\mathrm{k|k-1}}\mathbf{H}_{\mathrm{k}}{}^{\mathrm{T}} + \mathbf{R}} \tag{4.75}$$

where, $\mathbf{H}_{\mathrm{k}}$ is the linearized measurement equation obtained from Eq.(4.38)

The updated posterior estimate of the parametric vector is evaluated as

$$\boldsymbol{\theta}_{k|k} = \boldsymbol{\theta}_{k|k-1} + \mathcal{K}_{\mathrm{k}}\hat{\boldsymbol{y}}_{\boldsymbol{k}} \tag{4.76}$$

and the updated error covariance matrix of $\boldsymbol{\theta}$, which is $\boldsymbol{P}_\theta$, is obtained as

$$\boldsymbol{P}_{\theta,k|k+1} = \boldsymbol{I}_{6x6}\boldsymbol{P}_{\theta,k|k}\boldsymbol{I}^T_{6x6} - \mathcal{K}_{\mathrm{k}}\mathbf{H}_{\mathrm{k}}\boldsymbol{P}_{\theta,k|k}\boldsymbol{I}^T_{6x6} \tag{4.77}$$

Step-4: Prediction Step of matrix $\boldsymbol{X}_\theta$ or $\frac{d\boldsymbol{X}}{d\boldsymbol{\theta}}$ *for next time step*

The predicted matrix $\boldsymbol{X}_{\theta}$, which is required for the evaluation of the linearized measurement equation given by Eq. (4.38) is obtained by integration of the differential equation, Eq. (4.61) by using 4th order Runga-Kutta integration scheme.

4.5.3 Formulation of UKF for four-DOF fixed base shear frame building

In UKF, there is no need to evaluate the complex Jacobian matrices. The process of implementation is relatively simpler. The details of formulation are presented in chapter-3. In this section, mathematical formulations of UKF for four-DOF fixed base shear building (Fig. 4.1) is presented. This formulation can be easily extended to develop UKF for similar system with higher numbers of DOFs.

4.5.3.1 Implementation of UKF formulation in MATLAB platform

The identification of state and parameter of a sample four storey shear building using UKF technique is described in detail in this sub-section. In this case state and parameters are arranged in a single vector or extended state vector similar to EKF identification.

The unknown extended state vector to be identified is

$$\boldsymbol{X}_e = \{x_1 \quad x_2 \quad x_3 \quad x_4 \quad \dot{x}_1 \quad \dot{x}_2 \quad \dot{x}_3 \quad \dot{x}_4 \quad k_1 \quad k_2 \quad k_3 \quad k_4 \quad \hat{\beta} \quad \hat{\alpha}\}^T \tag{4.78}$$

The dimension of the extended state vector, L=14.

The process equation is expressed in state-space form as given by Eq. (4.79)

$$\dot{\boldsymbol{X}}_e = \begin{Bmatrix} \dot{\boldsymbol{x}}_i \\ \ddot{\boldsymbol{x}}_i \\ \dot{\boldsymbol{k}}_i \\ \dot{\hat{\beta}} \\ \dot{\hat{\alpha}} \end{Bmatrix} = \frac{d}{dt}\begin{Bmatrix} \boldsymbol{x}_i \\ \dot{\boldsymbol{x}}_i \\ \boldsymbol{k}_i \\ \hat{\beta} \\ \hat{\alpha} \end{Bmatrix} = \frac{d\boldsymbol{X}_e}{dt} = \begin{Bmatrix} \dot{\boldsymbol{x}}_i \\ -\boldsymbol{\eta}\ddot{x}_g - \boldsymbol{K}\boldsymbol{x}_i/\boldsymbol{M} - \boldsymbol{C}\dot{\boldsymbol{x}}_i/M \\ 0 \\ 0 \\ 0 \end{Bmatrix} \tag{4.79}$$

Step-1: Initialization Step.

Initialization is done by assuming the initial value of

a) The extended state vector, $\boldsymbol{X}_e$containing both state and parameter.
b) Error covariance matrix of $\boldsymbol{X}_e$, which is $\boldsymbol{P}$.
c) Process error covariance matrix, $\boldsymbol{Q}$.
d) Measurement error covariance matrix, $\boldsymbol{R}$.

Step-2: Generation of Sigma point.

If the total number of elements in the extended state vector is n, then for each element in the extended state vector $(2n+1)$ sigma points are generated. So, a matrix of sigma points of size n x $(2n + 1)$ is created.

Step-3: Passing the Sigma Points through Process equation.

The sigma points are passed through the process equation. The process equation is expressed in state-space form. Using the input ground excitation and one set of sigma point vector, the predicted transformed sigma point vector is generated by integration of the process equation using 4^{th} order Runga-Kutta integration scheme. Similarly, other sigma points are passed through the process equation and $(2n+1)$ transformed sigma point vectors are generated. All the $(2n+1)$ sigma point vectors are combined using specified weights to get the predicted transformed sigma point and its error covariance matrix.

Step-4: Passing the Sigma Points through measurement equation.

The predicted observation is generated from the transformed sigma points obtained from step-3 and using input ground acceleration. All the sigma point vectors are combined using specified weights to get the predicted transformed observation and its error covariance matrix.

Step-5: Evaluation of cross covariance matrix, Kalman Gain and updated state and parameter

Cross covariance matrix and Kalman Gain matrix is evaluated. From the Kalman gain and current measurement, the updated extended state vector and its error covariance is evaluated.

4.5.3.2 Formulation of SNLSE-UI-UO for four-DOF Fixed base shear building

The governing equation of motion of a four storey fixed base sample building is given by

$$\boldsymbol{M\ddot{x} + C\dot{x} + Kx = -\eta M\ddot{x}_g = \eta F} \tag{4.80}$$

Let the measured acceleration response at 2^{nd}floor level be missing. The mass matrix is segregated into known and unknown masses corresponding to known and unknown acceleration measurement and Eq. (4.80) is written as

$$\boldsymbol{\bar{M}\ddot{\bar{x}} + M^{*}\ddot{x}^{*} + C\dot{x} + Kx = \eta F} \tag{4.81}$$

The process of transition from Eq. (4.80) to Eq. (4.81) using matrix form is shown below

$$\begin{bmatrix} m_1 & 0 & 0 & 0 \\ 0 & m_2 & 0 & 0 \\ 0 & 0 & m_3 & 0 \\ 0 & 0 & 0 & m_4 \end{bmatrix} \begin{Bmatrix} \ddot{x}_1 \\ \ddot{x}_2 \\ \ddot{x}_3 \\ \ddot{x}_4 \end{Bmatrix} + \boldsymbol{\varphi}(\boldsymbol{X})\boldsymbol{\theta} = \boldsymbol{\eta F} \tag{4.82}$$

where, $\boldsymbol{\varphi}(\boldsymbol{X})\boldsymbol{\theta} = \boldsymbol{C\dot{x}} + \boldsymbol{Kx}$, $\boldsymbol{\varphi}(\boldsymbol{X})$ is called the data matrix and $\boldsymbol{\theta}$is the parametric vector. The Eq. (4.81) is represented in matrix form as

$$\bar{\boldsymbol{M}}\ddot{\bar{x}} + \boldsymbol{M}^*\ddot{x}^* + \boldsymbol{C\dot{x}} + \boldsymbol{Kx} = \begin{bmatrix} m_1 & 0 & 0 \\ 0 & 0 & 0 \\ 0 & m_3 & 0 \\ 0 & 0 & m_4 \end{bmatrix} \begin{Bmatrix} \ddot{x}_1 \\ \ddot{x}_3 \\ \ddot{x}_4 \end{Bmatrix} + \begin{bmatrix} 0 \\ m_2 \\ 0 \\ 0 \end{bmatrix} \{\ddot{x}_2\} + \boldsymbol{\varphi}(\boldsymbol{X})\boldsymbol{\theta} = \boldsymbol{\eta F}$$

$$\text{or, } \boldsymbol{\varphi}(\boldsymbol{X})\boldsymbol{\theta} = \boldsymbol{\eta F} - \begin{bmatrix} m_1 & 0 & 0 \\ 0 & 0 & 0 \\ 0 & m_3 & 0 \\ 0 & 0 & m_4 \end{bmatrix} \begin{Bmatrix} \ddot{x}_1 \\ \ddot{x}_3 \\ \ddot{x}_4 \end{Bmatrix} + \begin{bmatrix} 0 \\ m_2 \\ 0 \\ 0 \end{bmatrix} \{\ddot{x}_2\}$$

$$= (\boldsymbol{\eta F} - \bar{\boldsymbol{M}}\ddot{\bar{x}}) - \boldsymbol{M}^*\ddot{x}^* = \boldsymbol{y} + \bar{\boldsymbol{\eta}}\bar{\boldsymbol{F}} \tag{4.83}$$

where,$\boldsymbol{y} = (\boldsymbol{\eta F} - \bar{\boldsymbol{M}}\ddot{\bar{x}})$ and $\bar{\boldsymbol{\eta}} = [-M^*]$are known and $\bar{\boldsymbol{F}} = \{\ddot{x}_2\}$ is unknown and needs to be determined.

The formulation of the data matrix and the parametric vector is described below

$$\boldsymbol{\varphi}(\boldsymbol{X})\boldsymbol{\theta} = \boldsymbol{Kx} + \boldsymbol{C\dot{x}} = \boldsymbol{Kx} + \left(\hat{\beta}\boldsymbol{K} + \hat{\alpha}\boldsymbol{M}\right)\dot{\boldsymbol{x}} \tag{4.84}$$

$$\boldsymbol{Kx} = \begin{bmatrix} k_1 + k_2 & -k_2 & 0 & 0 \\ -k_2 & k_2 + k_3 & -k_3 & 0 \\ 0 & -k_3 & k_3 + k_4 & -k_4 \\ 0 & 0 & -k_4 & k_4 \end{bmatrix} \begin{Bmatrix} x_1 \\ x_2 \\ x_3 \\ x_4 \end{Bmatrix}$$

$$= \begin{bmatrix} x_1 & (x_1 - x_2) & 0 & 0 \\ 0 & -(x_1 - x_2) & (x_2 - x_3) & 0 \\ 0 & 0 & -(x_2 - x_3) & (x_3 - x_4) \\ 0 & 0 & 0 & -(x_3 - x_4) \end{bmatrix} \begin{Bmatrix} k_1 \\ k_2 \\ k_3 \\ k_4 \end{Bmatrix}$$

$$\boldsymbol{C\dot{x}} = \left(\hat{\beta}\boldsymbol{K} + \hat{\alpha}\boldsymbol{M}\right)\dot{\boldsymbol{x}} = \hat{\beta}\boldsymbol{K\dot{x}} + \hat{\alpha}\boldsymbol{M\dot{x}} \tag{4.85}$$

$$= \hat{\beta}\begin{bmatrix} k_1 + k_2 & -k_2 & 0 & 0 \\ -k_2 & k_2 + k_3 & -k_3 & 0 \\ 0 & -k_3 & k_3 + k_4 & -k_4 \\ 0 & 0 & -k_4 & k_4 \end{bmatrix} \begin{Bmatrix} \dot{x}_1 \\ \dot{x}_2 \\ \dot{x}_3 \\ \dot{x}_4 \end{Bmatrix} + \hat{\alpha}\begin{bmatrix} m_1 & 0 & 0 & 0 \\ 0 & m_2 & 0 & 0 \\ 0 & 0 & m_3 & 0 \\ 0 & 0 & 0 & m_4 \end{bmatrix} \begin{Bmatrix} \dot{x}_1 \\ \dot{x}_2 \\ \dot{x}_3 \\ \dot{x}_4 \end{Bmatrix}$$

$$= \hat{\beta}\begin{bmatrix} \dot{x}_1 & (\dot{x}_1 - \dot{x}_2) & 0 & 0 \\ 0 & -(\dot{x}_1 - \dot{x}_2) & (\dot{x}_2 - \dot{x}_3) & 0 \\ 0 & 0 & -(\dot{x}_2 - \dot{x}_3) & (\dot{x}_3 - \dot{x}_4) \\ 0 & 0 & 0 & -(\dot{x}_2 - \dot{x}_3) \end{bmatrix} \begin{Bmatrix} k_1 \\ k_2 \\ k_3 \\ k_4 \end{Bmatrix} + \begin{Bmatrix} m_1\dot{x}_1 \\ m_2\dot{x}_2 \\ m_3\dot{x}_3 \\ m_4\dot{x}_4 \end{Bmatrix} \{\hat{\alpha}\} \tag{4.86}$$

$$= \begin{bmatrix} \dot{x}_1 & (\dot{x}_1 - \dot{x}_2) & 0 & 0 \\ 0 & -(\dot{x}_1 - \dot{x}_2) & (\dot{x}_2 - \dot{x}_3) & 0 \\ 0 & 0 & -(\dot{x}_2 - \dot{x}_3) & (\dot{x}_3 - \dot{x}_4) \\ 0 & 0 & 0 & -(\dot{x}_2 - \dot{x}_3) \end{bmatrix} \begin{Bmatrix} \hat{\beta} k_1 \\ \hat{\beta} k_2 \\ \hat{\beta} k_3 \\ \hat{\beta} k_4 \end{Bmatrix} + \begin{Bmatrix} m_1 \dot{x}_1 \\ m_2 \dot{x}_2 \\ m_3 \dot{x}_3 \\ m_4 \dot{x}_4 \end{Bmatrix} \{\hat{\alpha}\} \tag{4.87}$$

Therefore, substituting the expanded form of the matrices from Eq. (4.86) and Eq. (4.87) into Eq. (4.84) gives

$$\begin{aligned} \boldsymbol{\varphi}(\boldsymbol{X})\boldsymbol{\theta} = & \begin{bmatrix} x_1 & (x_1 - x_2) & 0 & 0 \\ 0 & -(x_1 - x_2) & (x_2 - x_3) & 0 \\ 0 & 0 & -(x_2 - x_3) & (x_3 - x_4) \\ 0 & 0 & 0 & -(x_3 - x_4) \end{bmatrix} \begin{Bmatrix} k_1 \\ k_2 \\ k_3 \\ k_4 \end{Bmatrix} \\ & + \begin{bmatrix} \dot{x}_1 & (\dot{x}_1 - \dot{x}_2) & 0 & 0 \\ 0 & -(\dot{x}_1 - \dot{x}_2) & (\dot{x}_2 - \dot{x}_3) & 0 \\ 0 & 0 & -(\dot{x}_2 - \dot{x}_3) & (\dot{x}_3 - \dot{x}_4) \\ 0 & 0 & 0 & -(\dot{x}_3 - \dot{x}_4) \end{bmatrix} \begin{Bmatrix} \hat{\beta} k_1 \\ \hat{\beta} k_2 \\ \hat{\beta} k_3 \\ \hat{\beta} k_4 \end{Bmatrix} \\ & + \begin{Bmatrix} m_1 \dot{x}_1 \\ m_2 \dot{x}_2 \\ m_3 \dot{x}_3 \\ m_4 \dot{x}_4 \end{Bmatrix} \{\hat{\alpha}\} \end{aligned} \tag{4.88}$$

$$\boldsymbol{\varphi}(\boldsymbol{X})\boldsymbol{\theta} = [KK] \begin{Bmatrix} k_1 \\ k_2 \\ k_3 \\ k_4 \end{Bmatrix} + [VV] \begin{Bmatrix} \hat{\beta} k_1 \\ \hat{\beta} k_2 \\ \hat{\beta} k_3 \\ \hat{\beta} k_4 \end{Bmatrix} + [M]\{\dot{x}_i\}\{\hat{\alpha}\}$$

$$= [\boldsymbol{KK} \quad \boldsymbol{VV} \quad \boldsymbol{M\dot{x}_i}] * \{k_1 \quad k_2 \quad k_3 \quad k_4 \quad \hat{\beta} k_1 \quad \hat{\beta} k_2 \quad \hat{\beta} k_3 \quad \hat{\beta} k_4 \quad \hat{\alpha}\}^{\boldsymbol{T}} \tag{4.89}$$

From Eq. (4.89), it is observed that data matrix $\boldsymbol{\varphi}(\boldsymbol{X}) = [\boldsymbol{KK} \quad \boldsymbol{VV} \quad \boldsymbol{M\dot{x}_i}]$ and the unknown parametric vector, which is to be identified, is

$\boldsymbol{\theta} = \{k_1 \quad k_2 \quad k_3 \quad k_4 \quad \hat{\beta} k_1 \quad \hat{\beta} k_2 \quad \hat{\beta} k_3 \quad \hat{\beta} k_4 \quad \hat{\alpha}\}^{\boldsymbol{T}}$ which is shown in Eq. (4.89).

Differentiating $\boldsymbol{\varphi}(\boldsymbol{X})\boldsymbol{\theta}$ given in Eq. (4.84) with respect to the state vector $\boldsymbol{X}$ is derived as

$$\begin{aligned} \frac{\partial}{\partial \boldsymbol{X}}(\boldsymbol{\varphi}(\boldsymbol{X})\boldsymbol{\theta}) = \frac{\partial}{\partial \boldsymbol{X}}(\boldsymbol{Kx} + \boldsymbol{C\dot{x}}) &= \frac{\partial}{\partial \boldsymbol{X}}\left(\boldsymbol{Kx} + \left(\hat{\beta}\boldsymbol{K} + \hat{\alpha}\boldsymbol{M}\right)\dot{\boldsymbol{x}}\right) \\ &= \frac{\partial}{\partial \boldsymbol{X}}\left(\left[\boldsymbol{K} \quad \left(\hat{\beta}\boldsymbol{K} + \hat{\alpha}\boldsymbol{M}\right)\right]\begin{Bmatrix} \boldsymbol{x} \\ \dot{\boldsymbol{x}} \end{Bmatrix}\right) = \frac{\partial}{\partial \boldsymbol{X}}\left(\left[\boldsymbol{K} \quad \left(\hat{\beta}\boldsymbol{K} + \hat{\alpha}\boldsymbol{M}\right)\right]\boldsymbol{X}\right) \\ &= \left[\boldsymbol{K} \quad \left(\hat{\beta}\boldsymbol{K} + \hat{\alpha}\boldsymbol{M}\right)\right] \end{aligned} \tag{4.90}$$

From the state transition relation as given in Eq. (3.91) and using the formula as given in Eq. (3.95) of Chapter-3, the formula of $\boldsymbol{\Phi}_{k,k+1}$ is re-written as

$$\boldsymbol{\Phi}_{k,k+1} = \boldsymbol{\Phi}_{k+1,k}^{-1} = \begin{bmatrix} \mathbf{I} & -(\Delta t)\mathrm{I} \\ \mathbf{0} & \mathbf{I} \end{bmatrix} \tag{4.91}$$

The $\boldsymbol{\Psi}$ matrix is formed by using the relation given in Eq. (3.102), which is re-written here as

$$_{i,k+1} = \left[\frac{\partial \hat{\boldsymbol{y}}_i(\boldsymbol{X}_i)}{\partial \boldsymbol{X}_i} \quad \frac{\partial \boldsymbol{X}_i}{\partial \boldsymbol{X}_{k+1}}\right]_{X_i = \boldsymbol{X}_i(\hat{\boldsymbol{X}}_{k+1|k})} = \left.\frac{\partial \hat{\boldsymbol{y}}_i(\boldsymbol{X}_i)}{\partial \boldsymbol{X}_i}\right|_{X_i = \boldsymbol{X}_i(\hat{\boldsymbol{X}}_{k+1|k})} \boldsymbol{\Phi}_{i,k+1} \tag{4.92}$$

where, $\hat{\boldsymbol{y}}_i(\boldsymbol{X}_i)$ is given as

$$\hat{\boldsymbol{y}}_i[\hat{\mathbf{X}}_{k+1,k}] = \boldsymbol{\varphi}_i[\mathbf{X}_i(\hat{\mathbf{X}}_{k+1,k})]\hat{\boldsymbol{\theta}}_i[\mathbf{X}_i(\hat{\mathbf{X}}_{k+1,k})] - \bar{\boldsymbol{\eta}}\hat{\bar{\mathbf{f}}}_{i|i} \tag{4.93}$$

$$\text{and } \frac{\partial}{\partial \boldsymbol{X}}(\hat{\boldsymbol{y}}_i[\hat{\mathbf{X}}_{k+1,k}]) = \frac{\partial}{\partial \boldsymbol{X}}\left(\boldsymbol{\varphi}_i[\mathbf{X}_i(\hat{\mathbf{X}}_{k+1,k})]\hat{\boldsymbol{\theta}}_i[\mathbf{X}_i(\hat{\mathbf{X}}_{k+1,k})] - \bar{\boldsymbol{\eta}}\hat{\bar{\mathbf{f}}}_{i|i}\right) = \frac{\partial}{\partial \boldsymbol{X}}(\boldsymbol{\varphi}_i\hat{\boldsymbol{\theta}}_i) \tag{4.94}$$

By substituting $\frac{\partial}{\partial \boldsymbol{X}}(\boldsymbol{\varphi}(\boldsymbol{X})\boldsymbol{\theta})$ from Eq.(4.90) and $\boldsymbol{\Phi}_{k,k+1}$ from Eq. (4.91) into Eq. (4.92),

$$\boldsymbol{\Psi}_{i,k+1} = \left[\boldsymbol{K} \quad (\hat{\beta}\boldsymbol{K} + \hat{\alpha}\boldsymbol{M})\right]\begin{bmatrix} \mathbf{I} & -(\Delta t)\mathbf{I} \\ \mathbf{0} & \mathbf{I} \end{bmatrix} \tag{4.95}$$

Using the relation $\boldsymbol{\Psi}$ and $\boldsymbol{\varphi}$ matrices as detailed in chapter-3, the unknown parametric vector, state vector and unmeasured acceleration are obtained.

4.6 Performance evaluation of different identification strategies for the evaluation of state and parameter of multi-storey shear frame building system with fixed support

In this section, a comparative study has been conducted based on the identification of states and parameters using EKF, Two-Stage EKF, UKF and SNLSE algorithms. Three different problems are considered for the comparative study, which are presented in the following paragraphs.

1) Problem Type-I: This is a simulated three-storey fixed base shear building. A numerical model of the building has been developed in MATLAB. The assumed structural properties are described in section-1.2. The structure is subjected to excitation mentioned in Table 4.2. The acceleration response from the structure is corrupted by addition of white Gaussian noises with noise to signal ratio of 0%, 1%, 2% and 5%. These noise corrupted responses are used as inputs in the identification algorithms to identify the state and structural parameters. The prime focus in this study is to assess the performance of each of these algorithms under gradual increase in measurement noise level. The responses obtained from all the floor levels are used in this study and hence this problem is not concerned with any missing sensor.

2) Problem Type-II: In this study, two types of problems are considered. One is an existing sample building (Problem Type-IIb) and other is the simulated model of the existing sample building (Problem Type-IIa). Problem Type-IIa deals with the identification study using simulated responses. Problem Type-IIb deals with identification study using acquired field responses from an existing building. For the existing building, measured acceleration responses are available corresponding to two orthogonal (in plan) directions. The plan dimension of the building is rectangular. These directions are categorized as longitudinal direction having larger stiffness and transverse direction or direction having smaller stiffness. The placement of sensors has been shown in Fig. 4.3. The building is a Nine-storey building modelled as a shear frame building with 9 numbers of dof in two orthogonal directions. In the simulated building (Problem Type-IIa), no added noise is considered, but the sensor availability similar to existing building has been replicated. The total numbers of floors are nine, out of which three sensors (at floor 1, 5 and 9) are placed in longitudinal direction and four sensors (at floor 1, 3, 7 and 9) are placed in transverse direction. Therefore, the number of missing sensors in longitudinal direction is more than that of transverse direction. Floor-1 and floor-9 corresponds to first floor and roof respectively. The structure is subjected to excitation as mentioned in Table 4.5. The geometrical properties of the simulated building have been described under section-4.3. The acceleration responses obtained from simulation are used for identification of state and parameter for Problem Type-IIa using different algorithms. The identified state and parameters are compared with that of simulated one.

3) Problem Type-III: This building is further categorised as Problem Type-IIIa and IIIb. In Problem Type-IIIa, identification is carried out using simulated responses whereas in Problem Type-IIIb, the same is carried out using acquired response from an existing building. Problem Type-IIIa and Problem Type-I are same building with only difference is that in Problem Type-I, sensors are available in all floor levels, whereas in Problem Type-IIIa, there are missing sensors at 1st and 2nd floor levels. Problem Type-IIIb is an existing three-storey conventional fixed base building, which is one of the twin buildings of the block. Sensors are missing along transverse direction corresponding to dof-2 (1st floor level) and dof-3 (2nd floor level). The numerical model of the building is developed from the geometry and material property of the building and this model has been used for detailed comparative study for the evaluation of performance of the identification algorithm. The details of the building model are described under section-4.4. The structure is subjected to NE EQ-3: Comp-transverse ground excitation. Further, the same

building with isolated base (which is the part of the twin building) has been considered in chapter-5.

The results of identification of building systems have been analyzed in two different ways as described below.

a) The first part is concerned with identification of state of the system. In the present study only measured acceleration data are considered. The RMSE of the identified displacement has been evaluated by considering the simulated displacement of the numerical model as the reference. The lower the RMSE, the better is the performance of the algorithm. RMSE of identified displacement is used as a measure of accuracy of state identification. RMSE of identified displacement is evaluated by considering a reference displacement time-history. In case of identification using data from simulated model, the simulated displacement time-history acts as a reference displacement for RMSE evaluation. However, in the study involving data from existing building, this is not possible since the reference displacement is not available. Therefore, performance evaluation of these algorithms is not carried out for the case involving data from existing building

b) The second part is concerned with the identification of parameters (stiffness) of the structures. To make a comparative study of the efficiency of these algorithms for identification of parameters, error in identified stiffnesses are evaluated w.r.t. assumed parameters in the simulation study. The identified parameters as well as the error in identification using each of these algorithms and for each of the ground motions are plotted in bar chart format. This is possible only for simulation based studies using Problem Type-I, IIa and IIIa. In case of study using acquired field responses for Problem Type-IIb and IIIb, this is not possible as the actual stiffness of the field building is unknown.

The details of the results obtained for each case study are presented in the subsequent sub-sections. State identification of all the three problem cases is discussed first followed by identification of parameters.

4.6.1 Results of state identification

Within the state identification only displacement identification is considered. Each of the Problem Types I, II and III are undertaken one after the other. The detailed investigations of the problems have been carried out as given.

4.6.1.1 Results of state identification for Problem Type-I

Fig. 4.7 to Fig. 4.12 show the plot of identified displacement time-history along with simulated displacement time-history obtained using different algorithms and ground motions under consideration. The acceleration response measurement used is noise-free. From the identified displacement plots, it is observed that all these algorithms are performing well. The measure of its performance is represented in 3D RMSE plot as shown in Fig. 4.13. The RMSE values are furnished in Table 4.9 to Table 4.11.The RMSE values are different for different floor levels and for different algorithms for any particular ground motions under consideration. So, it becomes difficult to compare the performance of these algorithms. Therefore, average of RMSE has been performed for the floor levels. The average RMSE values are furnished in Table 4.12 and presented in the form of 2D Bar Chart in Fig. 4.24. From the average RMSE, it is observed that SNLSE-UI-UO has the highest value; therefore, its performance is least. From among the rest three, EKF has the least value, so its performance is the best followed by Two-Stage EKF and then UKF.

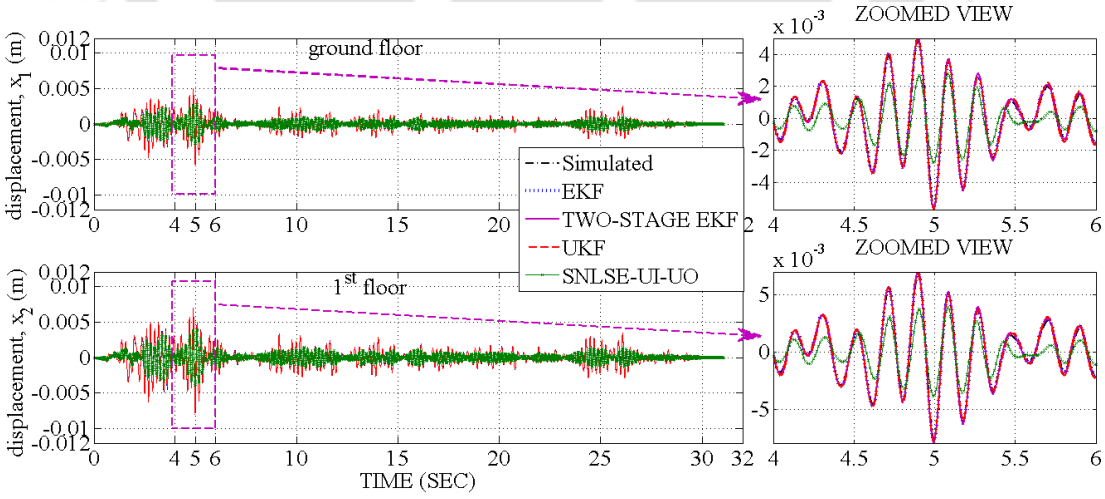

Fig. 4.7: Comparison of identified displacement time-history and simulated displacement time-history at ground floor (x_1) and 1st floor (x_2) level for Problem Type-I (using simulated response with 0% added noise) under excitation El Centro(1940):Comp-180

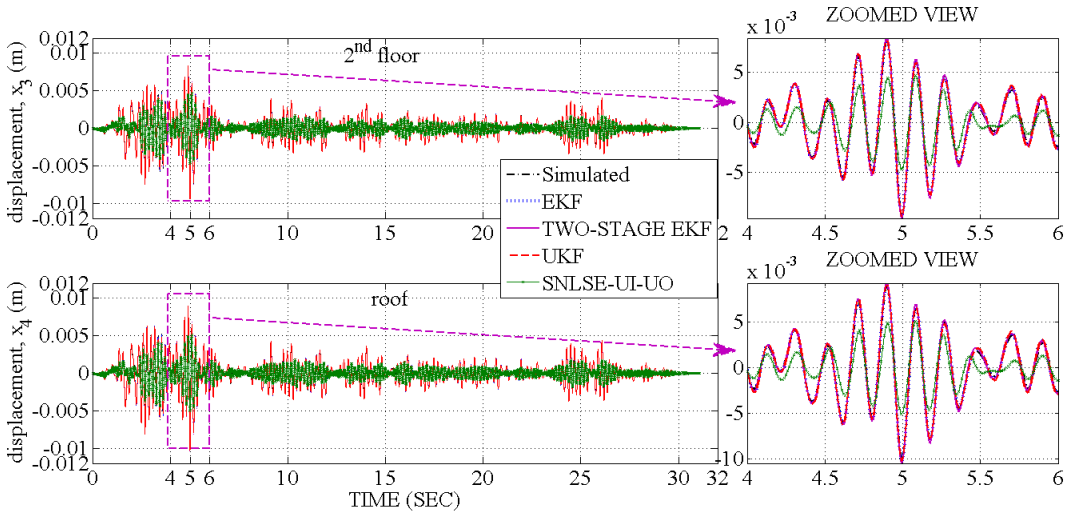

Fig. 4.8: Comparison of identified displacement time-history and simulated displacement time-history at 2nd floor (x_3) and roof (x_4) level for Problem Type-I (using simulated response with 0% added noise) under excitation El Centro (1940):Comp-180

Similarly, Fig. 4.17 to Fig. 4.22 show the plot of identified displacement obtained using acceleration response measurement corrupted with 5% noise. 3D plot of RMSE of identified displacements is given in Fig. 4.23. The plots against 1% and 2% noise level have been skipped intentionally, instead a higher noise level of 5% plot has been presented. However, the performances have been shown in RMSE plots against 1% and 2% noise level in Fig. 4.15 and Fig. 4.16 respectively.

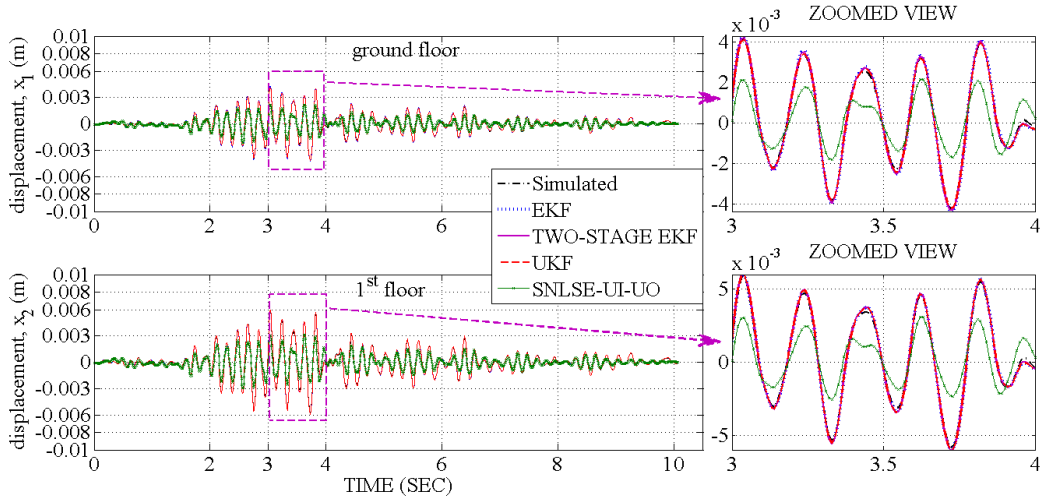

Fig. 4.9: Comparison of identified displacement time-history and simulated displacement time-history at ground floor (x_1) and 1st floor (x_2) level for Problem Type-I (using simulated response with 0% added noise) under excitation Koyna (1967): Comp-Longitudinal

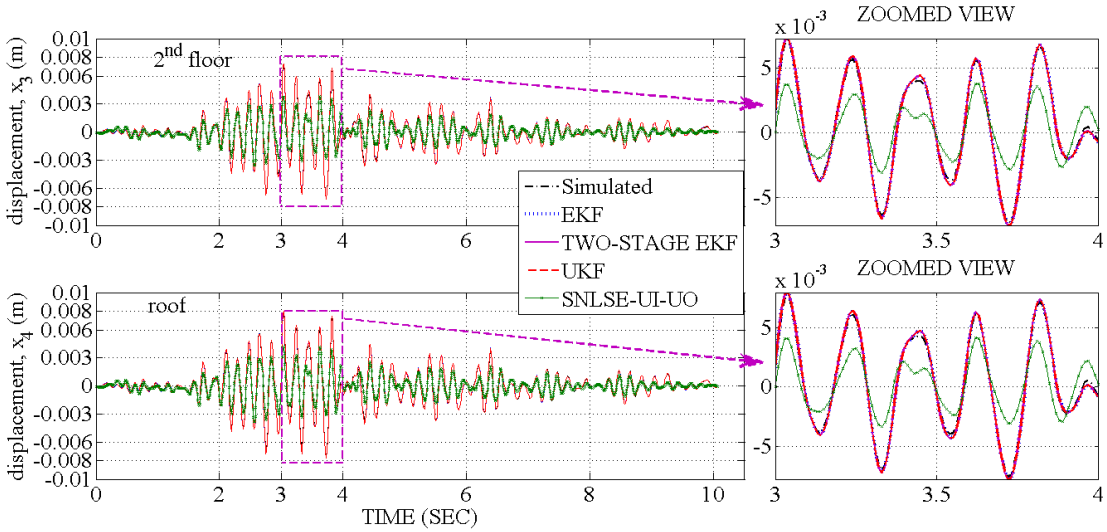

Fig. 4.10: Comparison of identified displacement time-history and simulated displacement time-history at 2nd floor (x_3) and roof (x_4) level for Problem Type-I (using simulated response with 0% added noise) under excitation Koyna (1967): Comp-Longitudinal

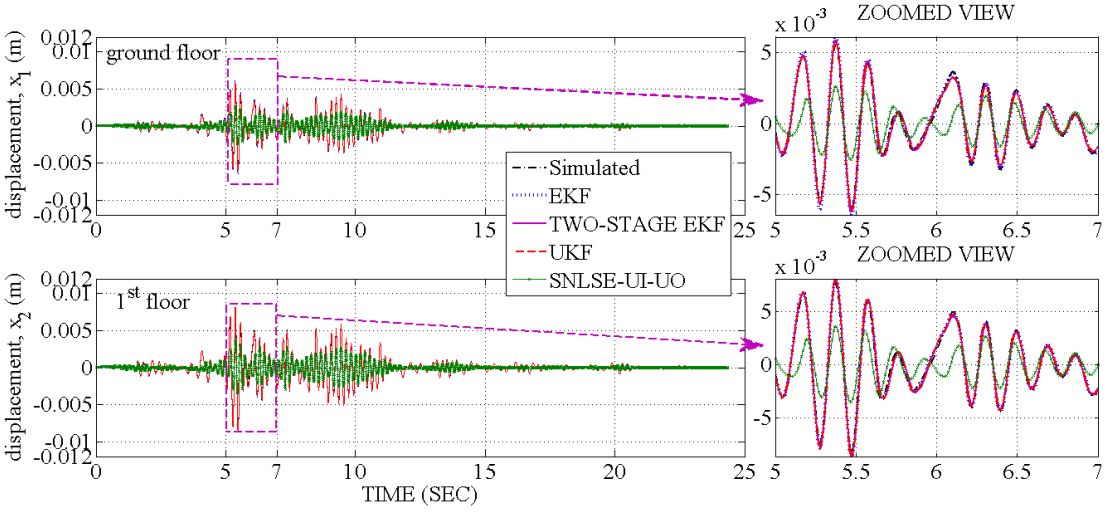

Fig. 4.11: Comparison of identified displacement time-history and simulated displacement time-history at ground floor (x_1) and 1st floor (x_2) level for Problem Type-I (using simulated response with 0% added noise) under excitation Victoria (1980): Comp-CPE045

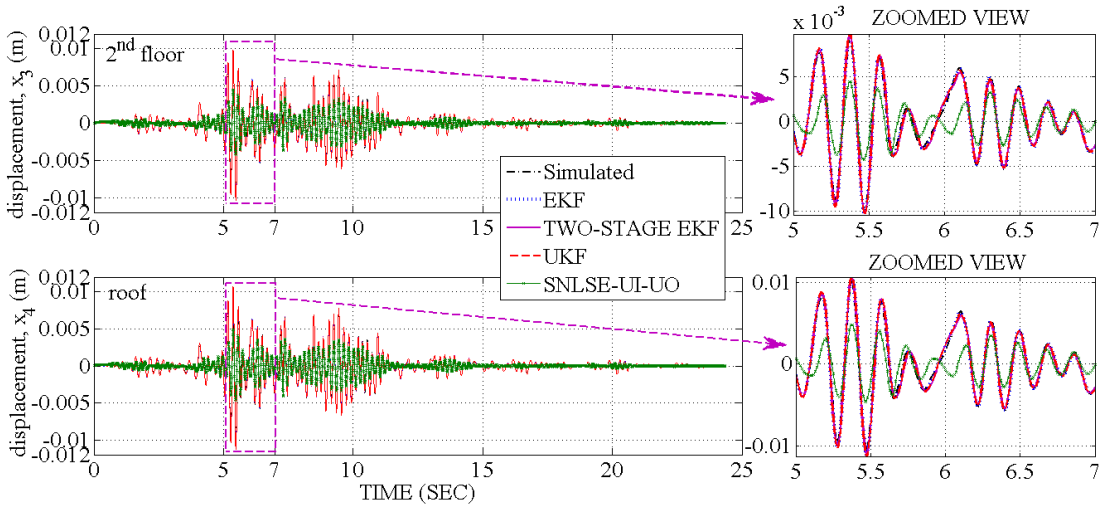

Fig. 4.12: Comparison of identified displacement time-history and simulated displacement time-history at 2nd floor (x_3) and roof (x_4) level for Problem Type-I (using simulated response with 0% added noise) under excitation Victoria (1980): Comp-CPE045

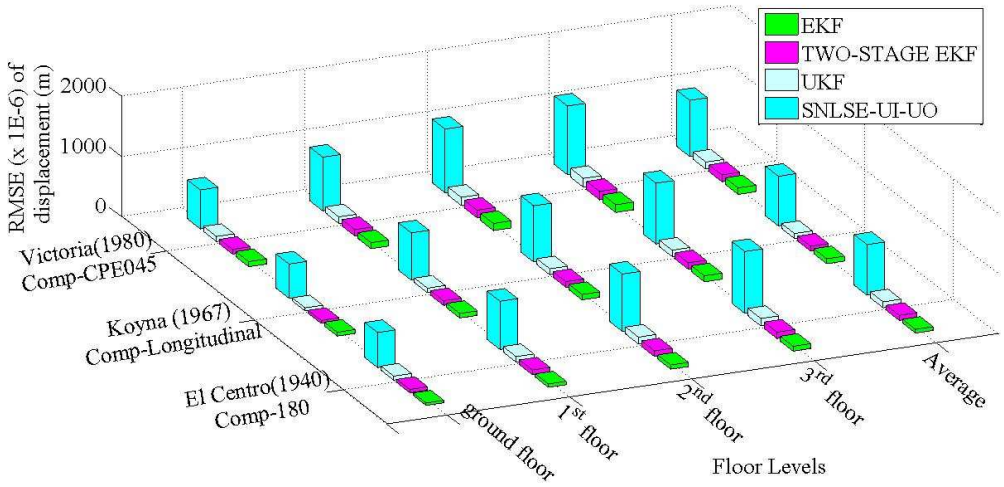

Fig. 4.13: 3D Bar Chart showing RMSE of identified displacement at all floor levels for Problem Type-I (using simulated response with 0% added noise) under all considered earthquake excitations

In the case of Kalman Filter based algorithms such as EKF, Two-Stage EKF and UKF, the identifications are carried out successfully using the noise contaminated responses. However, in the case of identification using SNLSE-UI-UO algorithm, if the same noise contaminated responses are used, the identified displacement shows a drift as shown in Fig. 4.14.

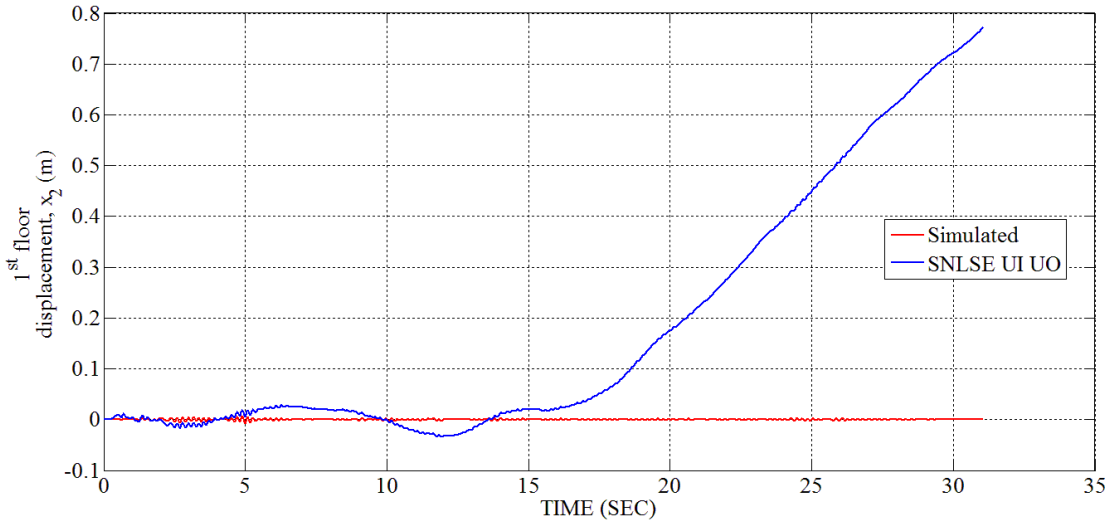

Fig. 4.14: Comparison of identified displacement time-history (using SNLSE-UI-UO algorithm) and simulated displacement time-history at 1st floor (x_1) level for Problem Type-I (using simulated response with 1% added noise) under excitation El Centro (1940): Comp-180

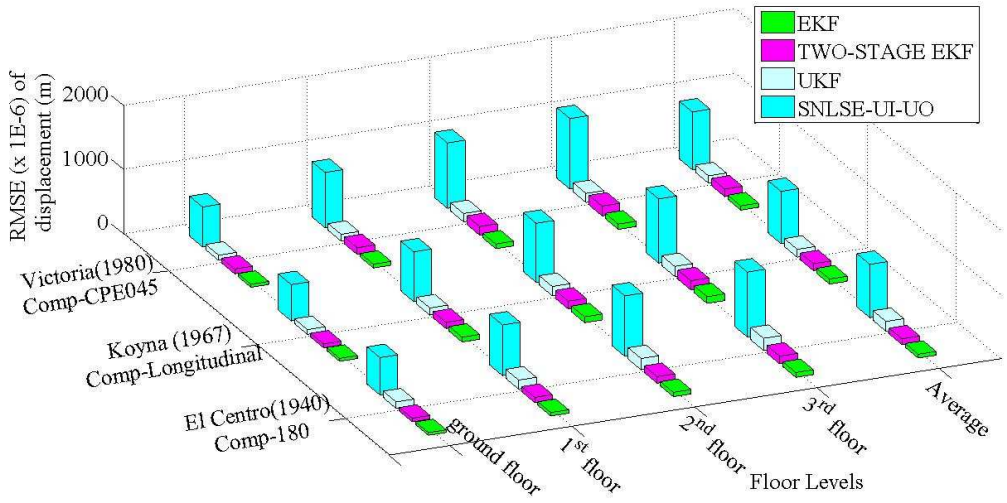

Fig. 4.15: 3D Bar Chart showing RMSE of identified displacement at all floor levels for Problem Type-I (using simulated response with 1% added noise) under all considered earthquake excitations

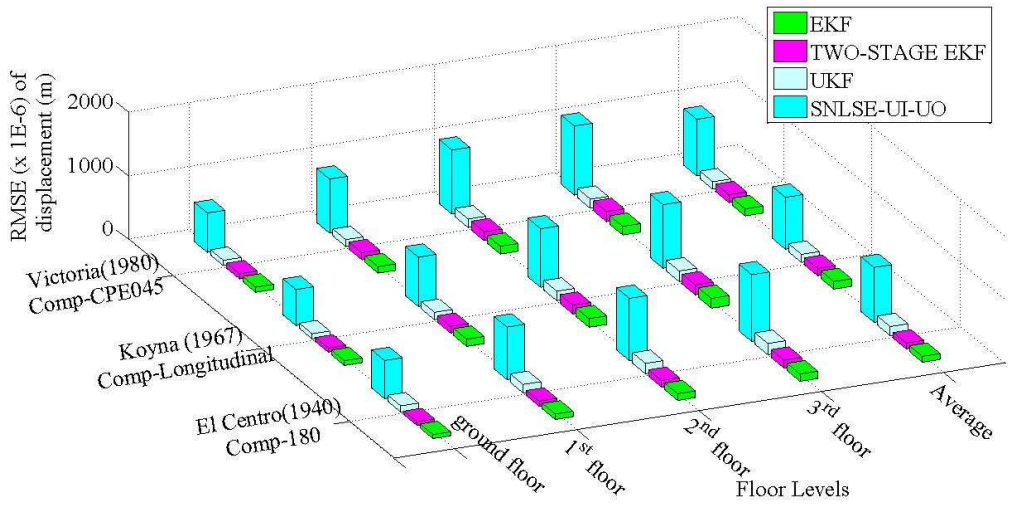

Fig. 4.16: 3D Bar Chart showing RMSE of identified displacement at all floor levels for Problem Type-I (using simulated response with 2% added noise) under all considered earthquake excitations

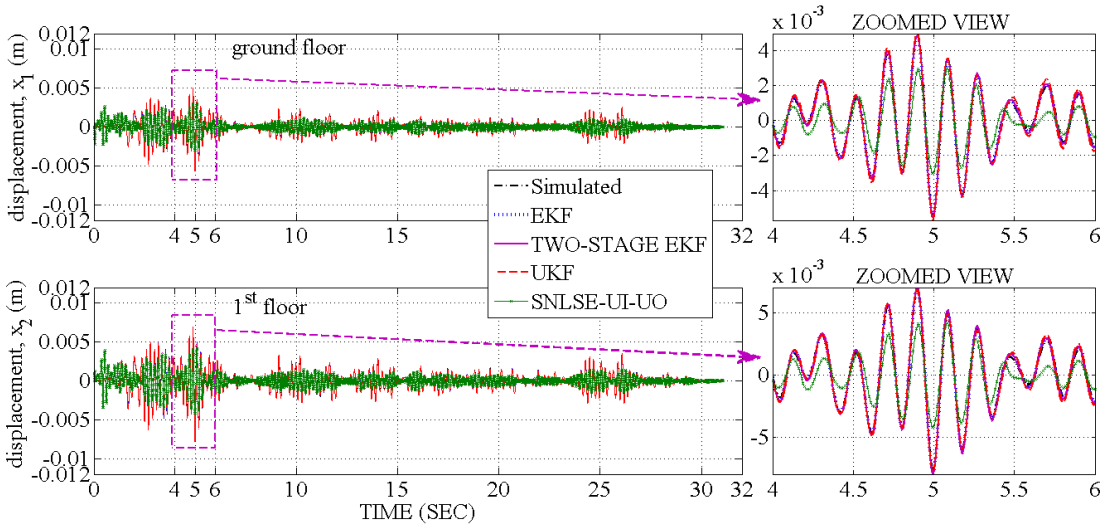

Fig. 4.17: Comparison of identified displacement time-history and simulated displacement time-history at ground floor (x_1) and 1st floor (x_2) level for Problem Type-I (using simulated response with 5% added noise) under excitation El Centro(1940):Comp-180

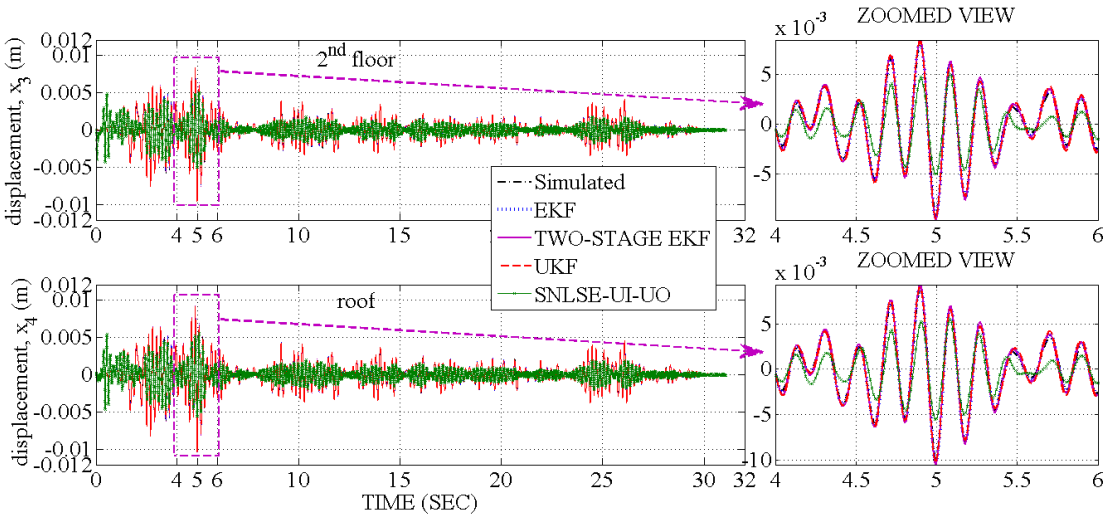

Fig. 4.18: Comparison of identified displacement time-history and simulated displacement time-history at 2nd floor (x_3) and roof (x_4) level for Problem Type-I (using simulated response with 5% added noise) under excitation El Centro (1940): Comp-180

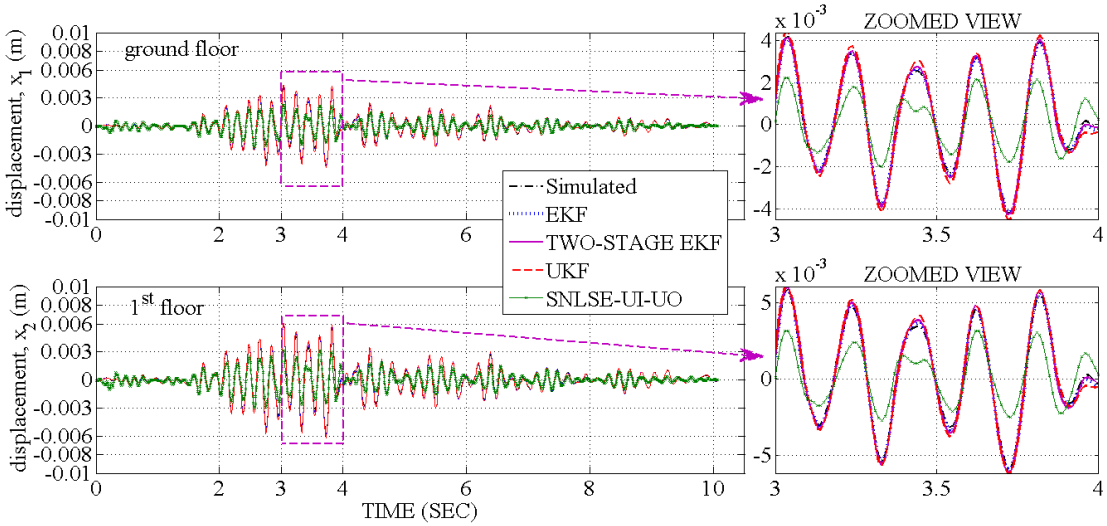

Fig. 4.19: Comparison of identified displacement time-history and simulated displacement time-history at ground floor (x_1) and 1st floor (x_2) level for Problem Type-I (using simulated response with 5% added noise) under excitation Koyna (1967): Comp-Longitudinal

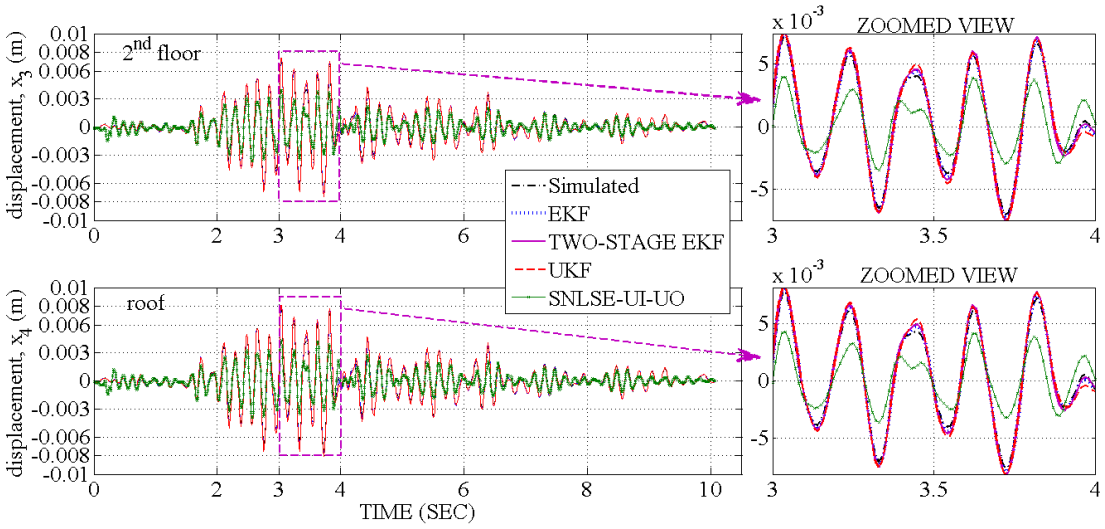

Fig. 4.20: Comparison of identified displacement time-history and simulated displacement time-historyat2ndfloor (x_3) and roof (x_4) level for Problem Type-I (using simulated response with 5% added noise) under excitation Koyna (1967): Comp-Longitudinal

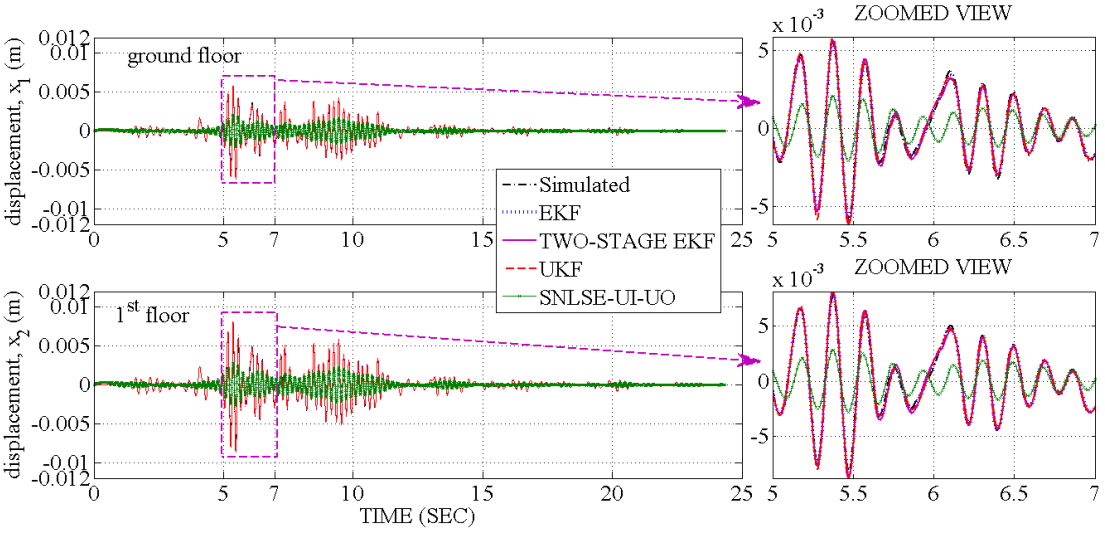

Fig. 4.21: Comparison of identified displacement time-history and simulated displacement time-history at ground floor (x_1) and 1st floor (x_2) level for Problem Type-I (using simulated response with 5% added noise) under excitation Victoria (1980): Comp-CPE045

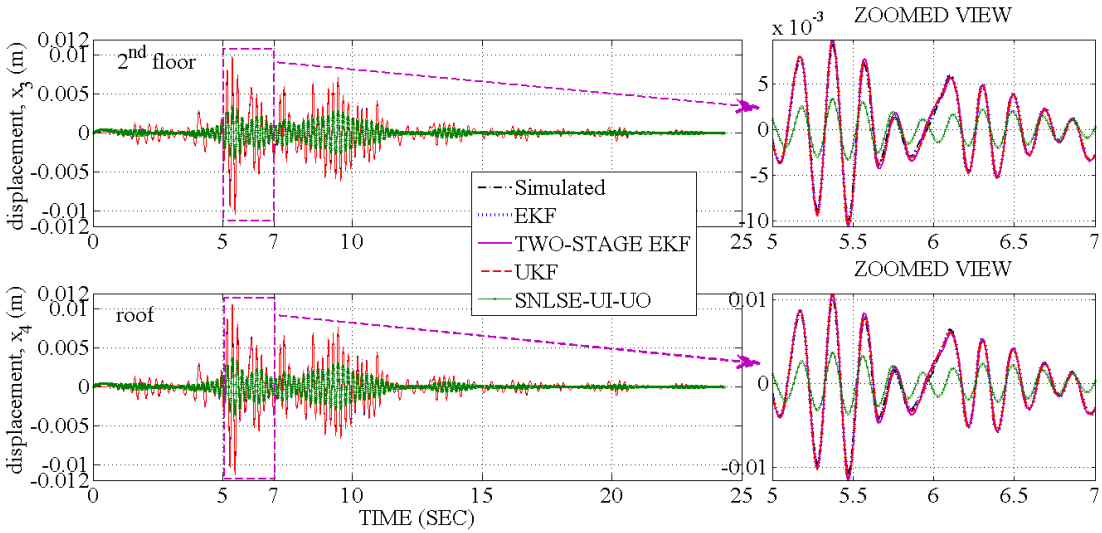

Fig. 4.22: Comparison of identified displacement time-history and simulated displacement time-history at 2nd floor (x_3) and roof (x_4) level for Problem Type-I (using simulated response with 5% added noise) under excitation Victoria (1980): Comp-CPE045

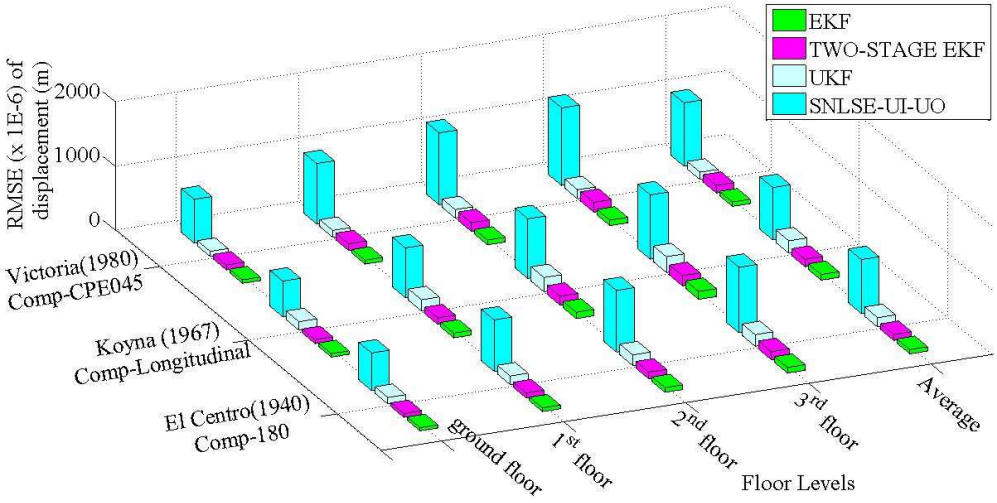

Fig. 4.23: 3D Bar Chart showing RMSE of identified displacement at all floor levels for Problem Type-I (using simulated response with 5% added noise) under all considered earthquake excitations

The results of identified displacement using SNLSE-UI-UO as shown in this section have been obtained by filtering the noisy response prior to its use by the algorithm. A 6th order Butterworth high pass filter has been used to remove low frequency noises from the response. Presence of low frequency noise in acceleration response often causes drift in displacement

[Lin Jeng-Wen *et al.*(2001)]. However, EKF, Two-stage EKF and UKF are self filtering algorithms due to presence of noise covariance matrix [R] in the Kalman gain equation, (Eq.(4.27), (4.70) and (4.75)).

Table 4.9: RMSE of identified displacement for Problem Type-I (using simulated response contaminated with different noise level) under excitation El Centro (1940): Comp-180

Noise level	Floor level	EKF	Two-Stage EKF	UKF	SNLSE-UI-UO
		x 10^{-5} (m)	x 10^{-5} (m)	x 10^{-5} (m)	x 10^{-5} (m)
0%	ground	4	6	7	58
0%	1st	6	8	9	80
0%	2nd	7	9	11	95
0%	roof	8	11	12	102
Average of 0%		6.25	8.5	9.75	83.75
1%	ground	4	6	10	58
1%	1st	5	8	14	79
1%	2nd	7	10	17	94
1%	roof	7	12	19	101
Average of 1%		5.75	9	15	83
2%	ground	6	6	10	60
2%	1st	9	8	13	83
2%	2nd	10	11	16	98
2%	roof	12	12	18	105
Average of 2%		9.25	9.25	14.25	86.5
5%	ground	5	6	10	59
5%	1st	6	8	14	80
5%	2nd	7	11	17	96
5%	roof	9	12	18	102
Average of 5%		6.75	9.25	14.75	84.25

Table 4.10: RMSE of identified displacement for Problem Type-I (using simulated response contaminated with different noise level) under excitation Koyna (1967): Comp-Longitudinal

Noise level	dof	EKF	Two-Stage EKF	UKF	SNLSE-UI-UO
		x 10^{-5} (m)	x 10^{-5} (m)	x 10^{-5} (m)	x 10^{-5} (m)
0%	ground	6	5	5	57
0%	1st	7	8	8	78
0%	2nd	9	9	10	93
0%	roof	10	11	11	101
Average of 0%		8	8.25	8.5	82.25
1%	ground	5	6	7	56
1%	1st	7	10	11	77
1%	2nd	9	13	14	92
1%	roof	10	14	16	100
Average of 1%		7.75	10.75	12	81.25
2%	ground	7	6	8	57
2%	1st	11	10	12	77
2%	2nd	14	14	15	92
2%	roof	15	16	17	100
Average of 2%		11.75	11.5	13	81.5
5%	ground	5	6	13	56
5%	1st	7	10	18	78
5%	2nd	10	14	22	93
5%	roof	12	16	25	100
Average of 5%		8.5	11.5	19.5	81.75

Table 4.11: RMSE of identified displacement for Problem Type-I (using simulated response contaminated with different noise level) under excitation Victoria (1980): Comp-CPE045

Noise level	dof	EKF	Two-Stage EKF	UKF	SNLSE-UI-UO
		x 10^{-5} (m)	x 10^{-5} (m)	x 10^{-5} (m)	x 10^{-5} (m)
0%	ground	8	8	8	65
0%	1st	10	11	11	89
0%	2nd	12	13	13	106
0%	roof	13	14	15	114
Average of 0%		10.75	11.5	11.75	93.5
1%	ground	5	8	8	62
1%	1st	6	11	11	86
1%	2nd	7	14	13	102
1%	roof	8	15	14	109
Average of 1%		6.5	12	11.5	89.75
2%	ground	8	8	8	62
2%	1st	10	11	11	85
2%	2nd	12	14	13	101
2%	roof	14	16	14	109
Average of 2%		11	12.25	11.5	89.25
5%	ground	5	8	8	68
5%	1st	6	11	11	94
5%	2nd	7	14	13	112
5%	roof	9	15	14	121
Average of 5%		6.75	12	11.5	98.75

Table 4.12: Average RMSE of identified displacement for Problem Type-I (using simulated response contaminated with different noise level) under different earthquake excitations

Noise level	EKF	Two-Stage EKF	UKF	SNLSE-UI-UO
	x 10^{-5} (m)	x 10^{-5} (m)	x 10^{-5} (m)	x 10^{-5} (m)
0%	8	9	10	87
1%	7	11	13	85
2%	11	11	13	86
5%	7	11	15	88
Average	8.25	10.5	12.75	86.5

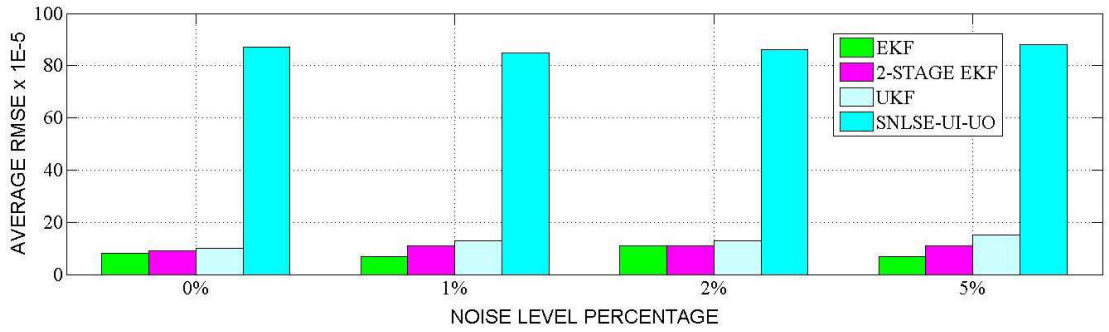

Fig. 4.24: 2D Bar Chart showing average RMSE of identified displacement at different noise level for Problem Type-I, under all considered earthquake excitations

From the entire exercise furnished above, responses with different noise level, different base excitations and different identification algorithms, it is evident that performances of all these algorithms are comparable at all noise levels. It may however be noted that the level of error is quite insignificant, even when the data is contaminated with high level of noise. The performance of SNLSE-UI-UO is really poor when the data is contaminated with noise. It may again be mentioned that external pre-filtering of data has been applied before prior to its use by the SNLSE-UI-UO algorithm, in-spite of which the performance obtained is much poorer that the other three algorithms. Thus, it can be concluded that EKF, Two-Stage EKF as well as UKF are found to be suitable, even when that data are contaminated with high level of noise.

4.6.1.2 Results of state identification for Problem Type-I with missing sensor using SNLSE-UI-UO algorithm

With only one number of missing sensor SNLSE-UI-UO performs somewhat well but with more than one missing sensor, the performance leads to serious errors in identification. Apart from this, the algorithm becomes unstable. The performance of the algorithm with one missing sensor has been demonstrated by Yang Jann N. and Huang Hongwei (2007) while applying it to a simulated model. But the performance of the algorithm with more than one missing sensor is not reported so far. Fig. 4.25 shows the identified displacement at floor levels with missing sensor at 2nd floor level and Fig. 4.26 shows the identified displacement where sensor is missing at 1stand 2nd floor levels. These displacement histories have been plotted along with simulated displacement histories in these figures. A good match is observed between identified and simulated displacement histories.

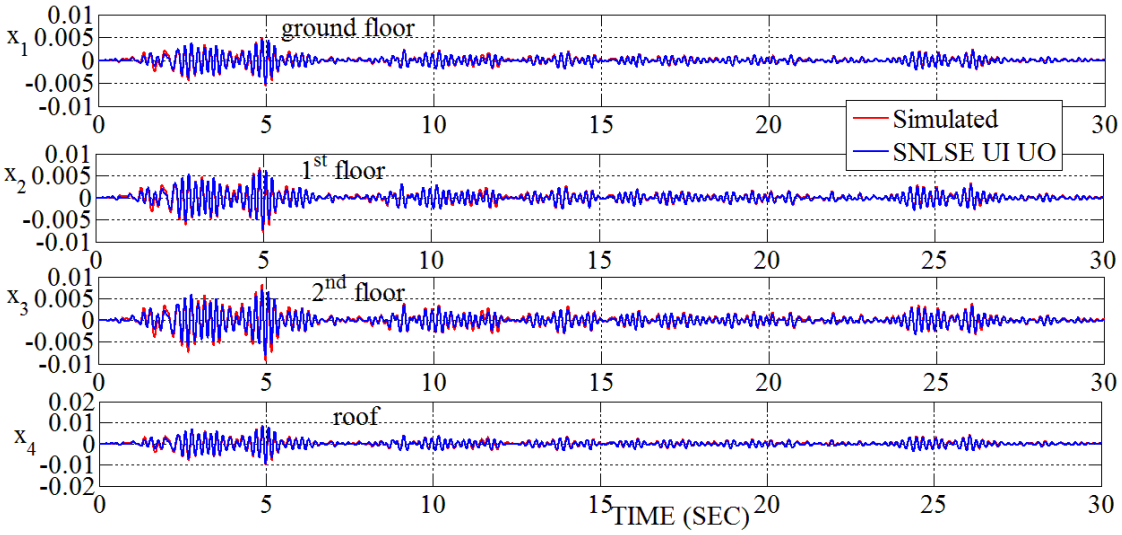

Fig. 4.25: Comparison of identified displacement time-history (using SNLSE-UI-UO algorithm) and simulated displacement time-history for Problem Type-I, under excitation El Centro (1940): Comp-180 (sensor missing at 2nd floor level)

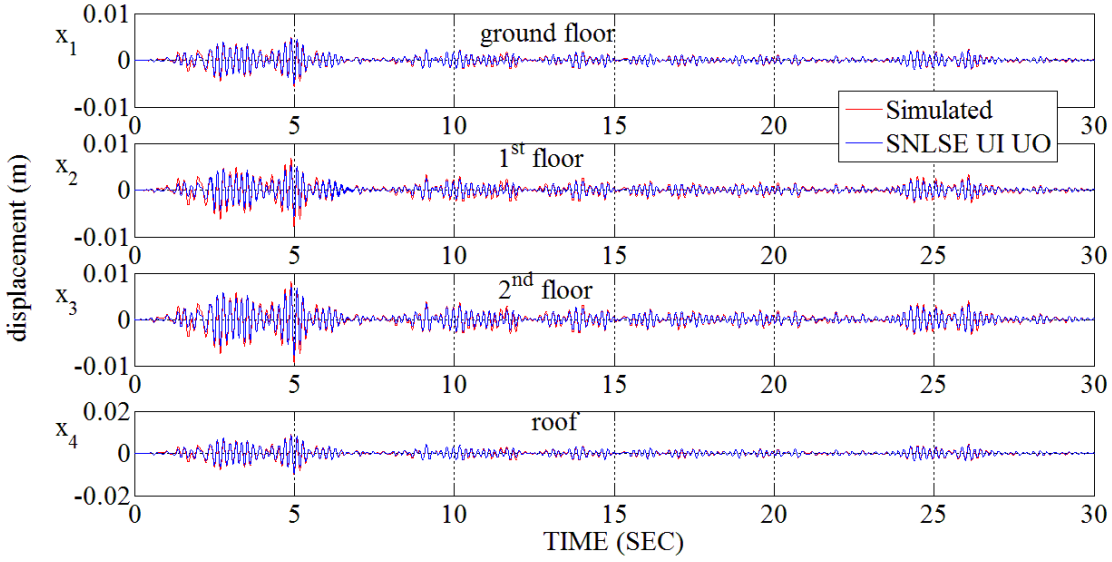

Fig. 4.26: Comparison of identified displacement time-history (using SNLSE-UI-UO algorithm) and simulated displacement time-history for Problem Type-I, under excitation El Centro (1940): Comp-180 (sensor missing at 1stand 2nd floor level)

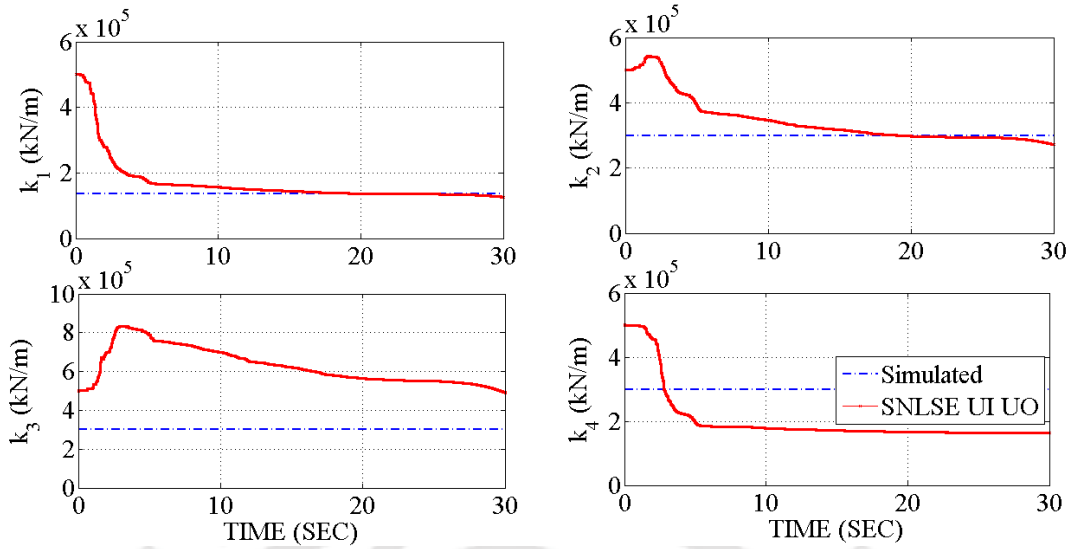

Fig. 4.27: Comparison of identified stiffness (using SNLSE-UI-UO algorithm) with assumed value of stiffness considered for simulated Building, Type-I, under excitation El Centro (1940): Comp-180 (sensor missing at 2nd floor level)

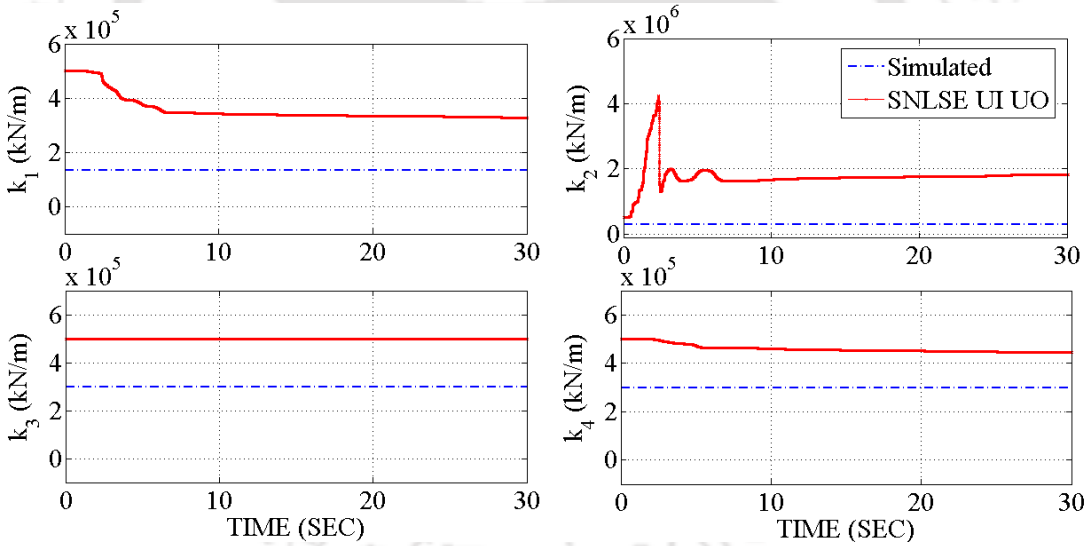

Fig. 4.28: Comparison of identified stiffness (using SNLSE-UI-UO algorithm) with assumed value of stiffness considered for simulated Building, Type-I, under excitation El Centro (1940): Comp-180 (sensor missing at 1st and 2nd floor level)

Fig. 4.27 shows the identified stiffness with missing sensor at 2nd floor level. The identified results are somewhat closer to simulated one. However, from Fig. 4.28, which show the identified stiffness with missing sensor at 1stand 2nd floor level, it is observed that the performance is degraded. Therefore, the SNLSE-UI-UO algorithm is not considered for all the identification cases in the further studies.

4.6.1.3 Results of displacement identification for Problem Type-IIa in transverse direction

In this identification study, the acceleration response at 1st, 3rd, 7th and roof level are considered. Fig. 4.29 to Fig. 4.31 show the plot of identified displacement time-history along with simulated displacement time-history at all the floor levels under excitation NE-EQ-1: Comp-transverse. Fig. 4.32 to Fig. 4.34 show similar results obtained from excitation NE-EQ-2: Comp-transverse. The 3D bar chart plot of Fig. 4.35 provides the RMSE of identified displacement obtained using different algorithms and earthquake excitations under consideration.

Table 4.13 provides the values of RMSE of identified displacement. These data have been used to plot the 3D bar chart shown Fig. 4.35. It is observed that in both the earthquake cases, the performances of EKF as well as Two-Stage EKF are comparable and their performance is much better than UKF.

It is to be noted that in this simulated case, the response used for identification study is noise-free response. As the existing sample building has a lot of missing sensors, this simulation and identification of analytical model provides a guideline for identification of the existing building using field responses.

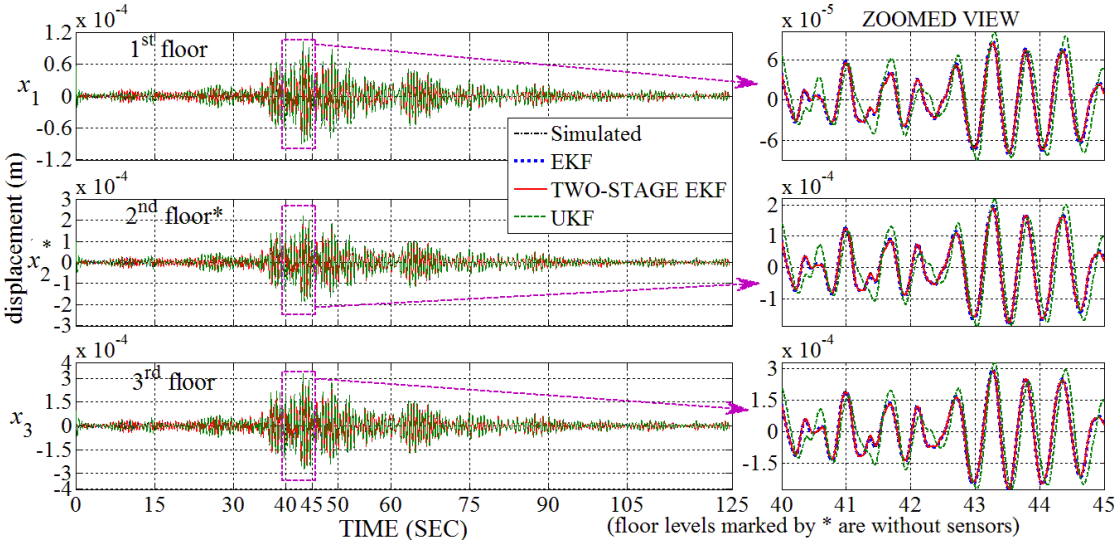

Fig. 4.29: Comparison of identified displacement time-history and simulated displacement time-history at 1st to 3rd floor levels for Problem Type-IIa under excitation NE-EQ-1: Comp-transverse

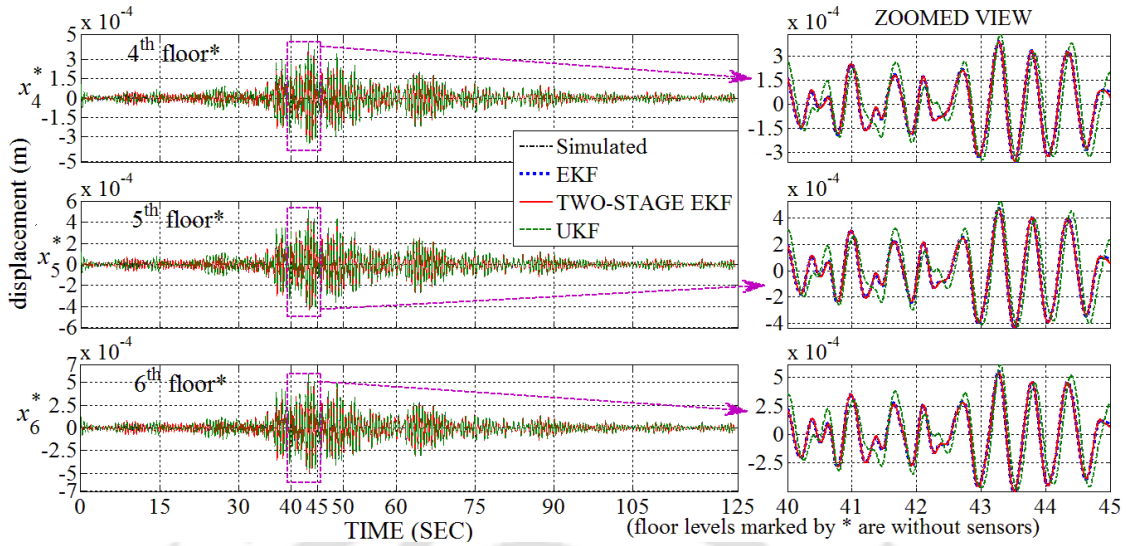

Fig. 4.30: Comparison of identified displacement time-history and simulated displacement time-history at 4th to 6th floor levels for Problem Type-IIa under excitation NE-EQ-1: Comp-transverse

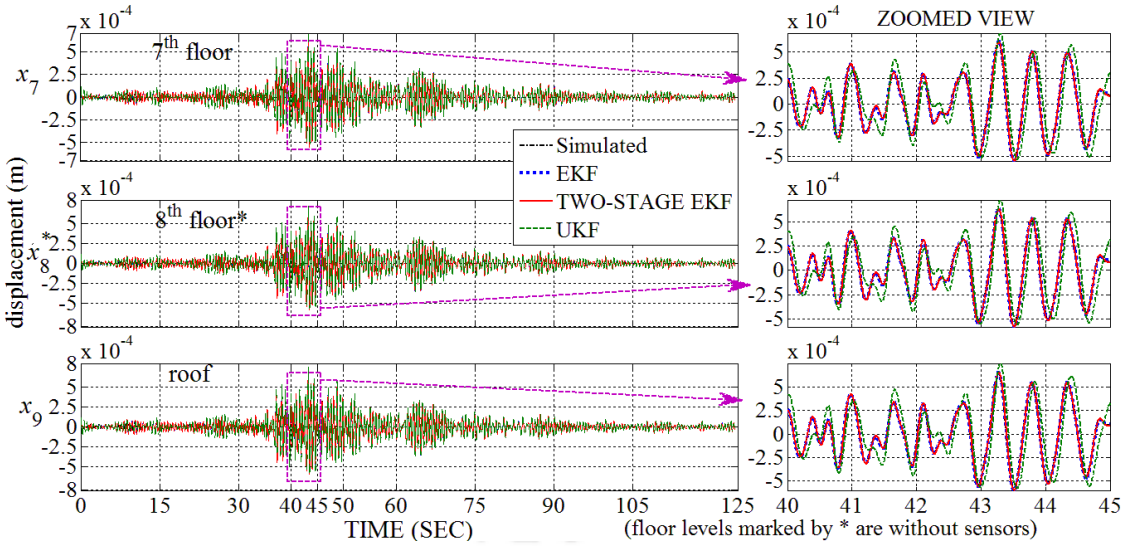

Fig. 4.31: Comparison of identified displacement time-history and simulated displacement time-history at 7th floor to roof level for Problem Type-IIa under excitation NE-EQ-1: Comp-transverse

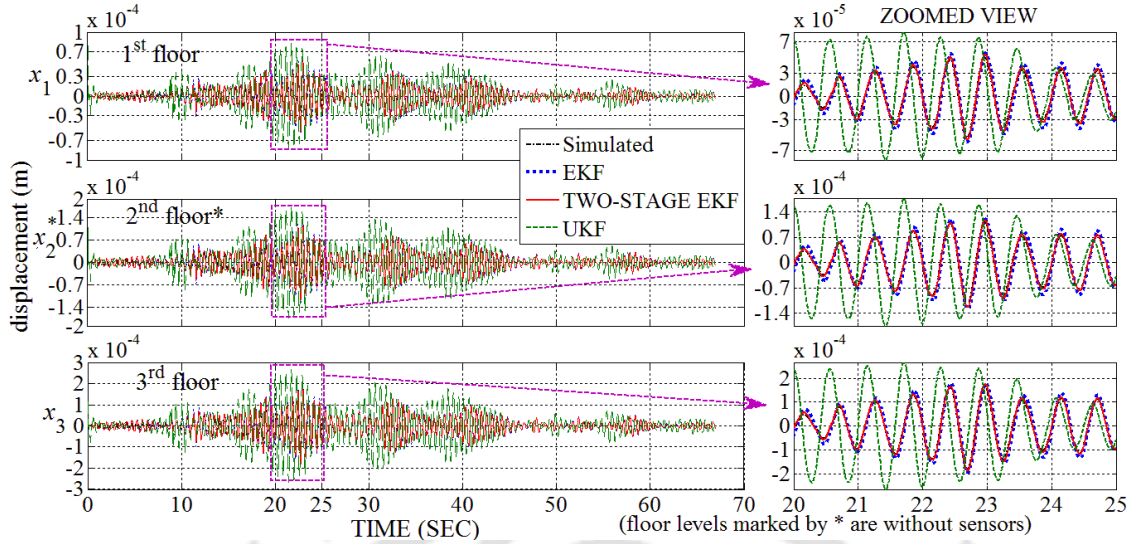

Fig. 4.32: Comparison of identified displacement time-history and simulated displacement time-history at 1st to 3rd floor levels for Problem Type-IIa under excitation NE-EQ-2: Comp-transverse

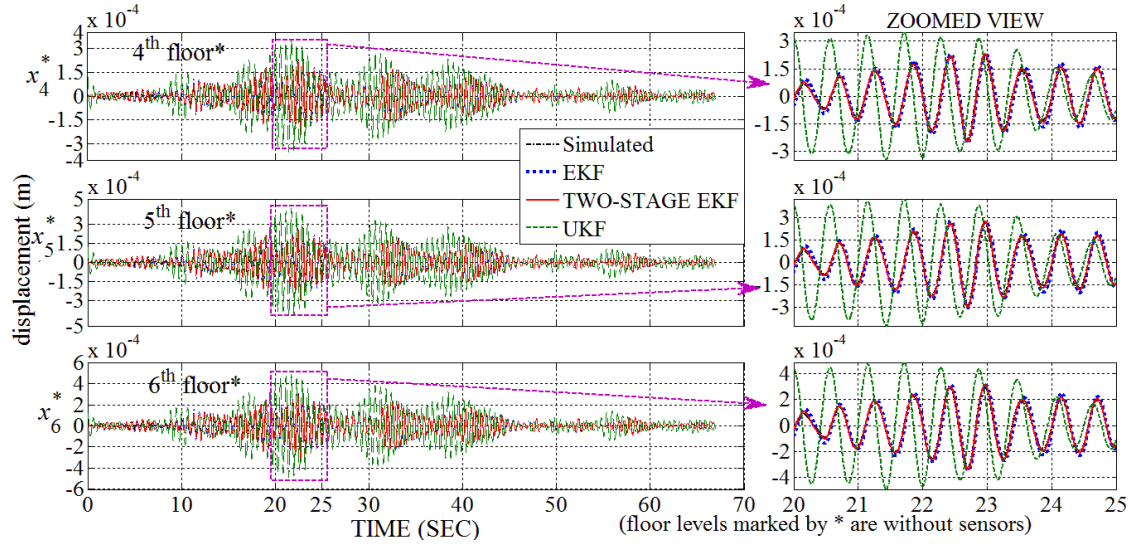

Fig. 4.33: Comparison of identified displacement time-history and simulated displacement time-history at 4th to 6th floor levels for Problem Type-IIa under excitation NE-EQ-2: Comp-transverse

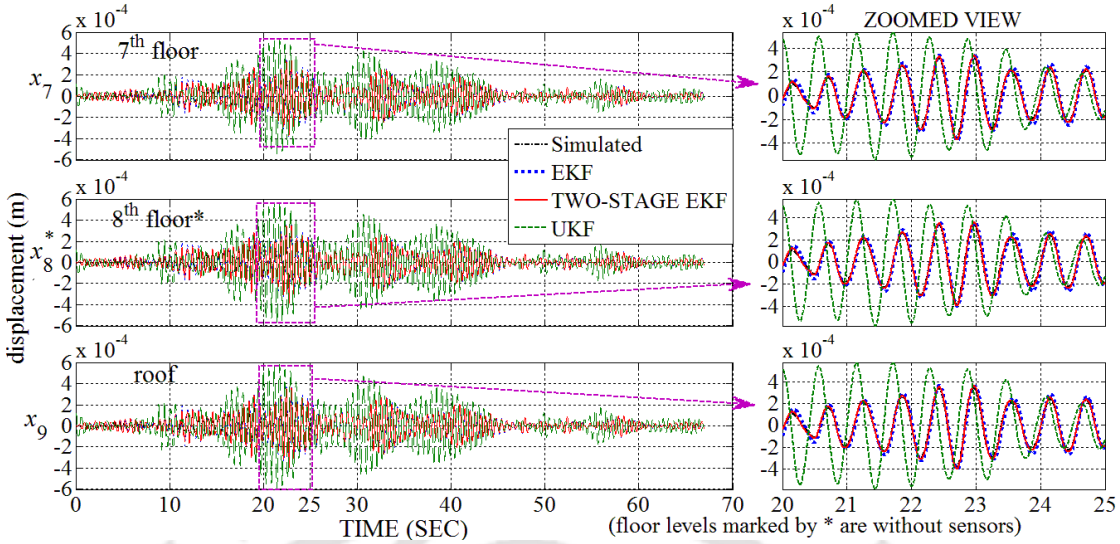

Fig. 4.34: Comparison of identified displacement time-history and simulated displacement time-history at 7th floor to roof level for Problem Type-IIa under excitation NE-EQ-2: Comp-transverse

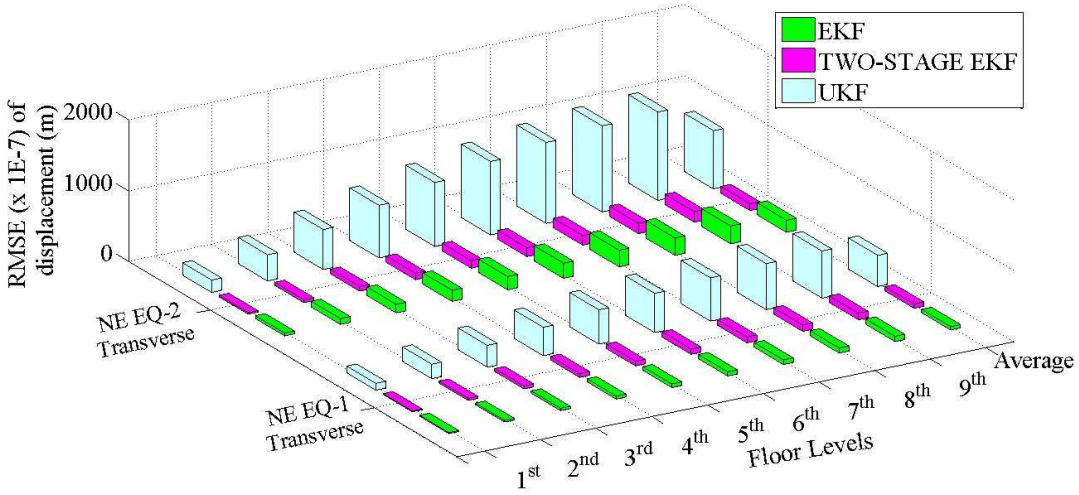

Fig. 4.35: 3D Bar Chart showing RMSE of identified displacement for Problem Type-IIa under excitations NE-EQ-1: Comp-transverse and NE EQ-2: Comp-transverse

Table 4.13: RMSE of identified displacement for Problem Type-IIa under excitations NE EQ-1: Comp-transverse and NE EQ-2: Comp-transverse

Floor level	NE EQ-1 (Comp: transverse)			NE EQ-2 (Comp: transverse)		
	EKF	Two-Stage EKF	UKF	EKF	Two-Stage EKF	UKF
	x10^{-7} (m)	x10^{-7} (m)	x10^{-7} (m)	x10^{-7} (m)	x10^{-7} (m)	x10^{-7} (m)
1st	14	13	96	40	21	175
2nd	23	28	204	81	43	370
3rd	33	42	307	121	66	564
4th	42	54	401	157	90	743
5th	51	64	484	188	106	903
6th	59	75	555	214	124	1037
7th	65	83	611	233	134	1143
8th	70	90	649	246	144	1215
9th	73	92	665	251	148	1247
Average RMSE	48	60	441	170	97	822

4.6.1.4 Results of displacement identification for Problem Type-IIa in longitudinal direction

In the previous sub-section, identification study has been carried out in the transverse direction. In this sub-section, identification is carried out in the longitudinal direction. The acceleration response at 1st, 5th and roof level are considered. Fig. 4.36 to Fig. 4.38 show the plot of identified displacement time-history along with simulated displacement time-history at all the floor levels under excitation NE-EQ-1: Comp-longitudinal. Fig. 4.39 to Fig. 4.41 show similar results obtained from NE-EQ-2: Comp-longitudinal excitation. The 3D bar chart plot of Fig. 4.42 provides the RMSE of identified displacement obtained using different algorithms and earthquake excitations under consideration.

The values of RMSE of identified displacement are furnished in Table 4.14. It is observed that in both the earthquake cases, the performance of EKF and Two-Stage EKF are comparable and their performance is much better than UKF.

From the 2D Bar Chart of Fig. 4.42, showing the average values of RMSEs obtained from both transverse and longitudinal direction under all the considered ground motions, it is observed that the performance of Two-Stage EKF is the best, followed by EKF and then UKF.

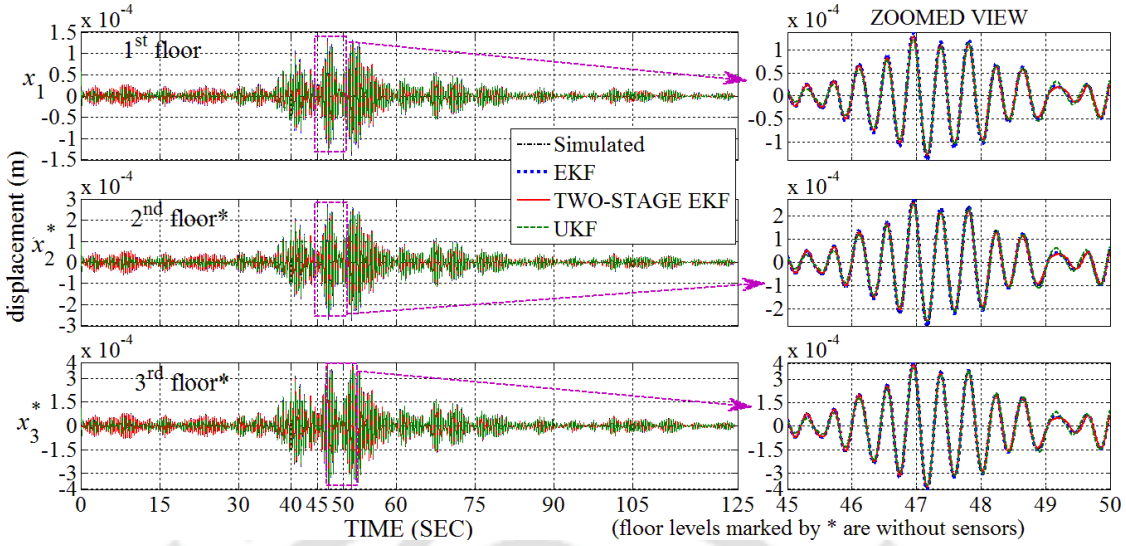

Fig. 4.36: Comparison of identified displacement time-history and simulated displacement time-history at 1st to 3rd floor levels for Problem Type-IIa under excitation NE-EQ-1: Comp-longitudinal

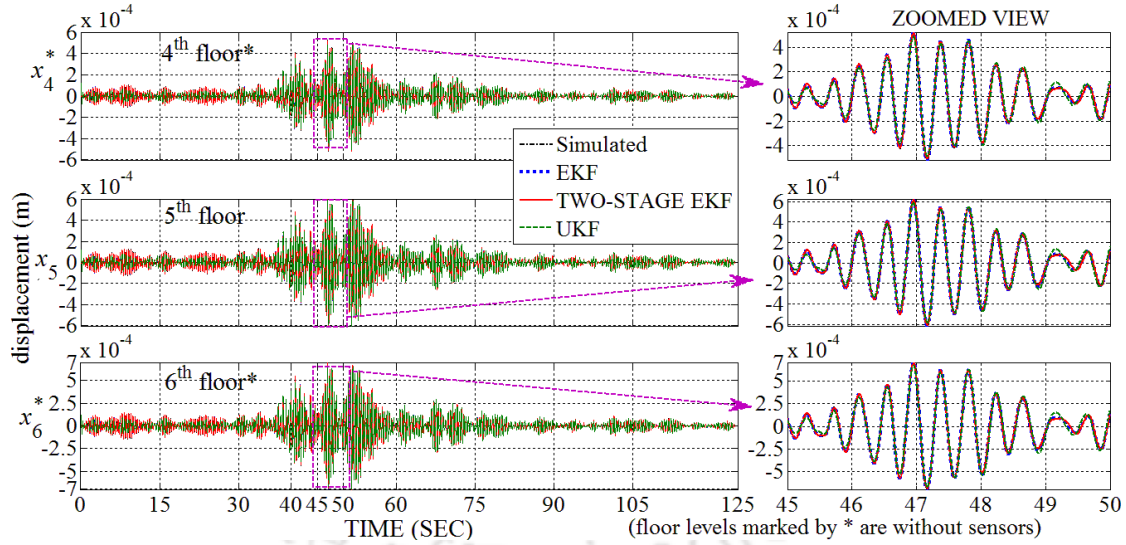

Fig. 4.37: Comparison of identified displacement time-history and simulated displacement time-history at 4th to 6th floor levels for Problem Type-IIa under excitation NE-EQ-1: Comp-longitudinal

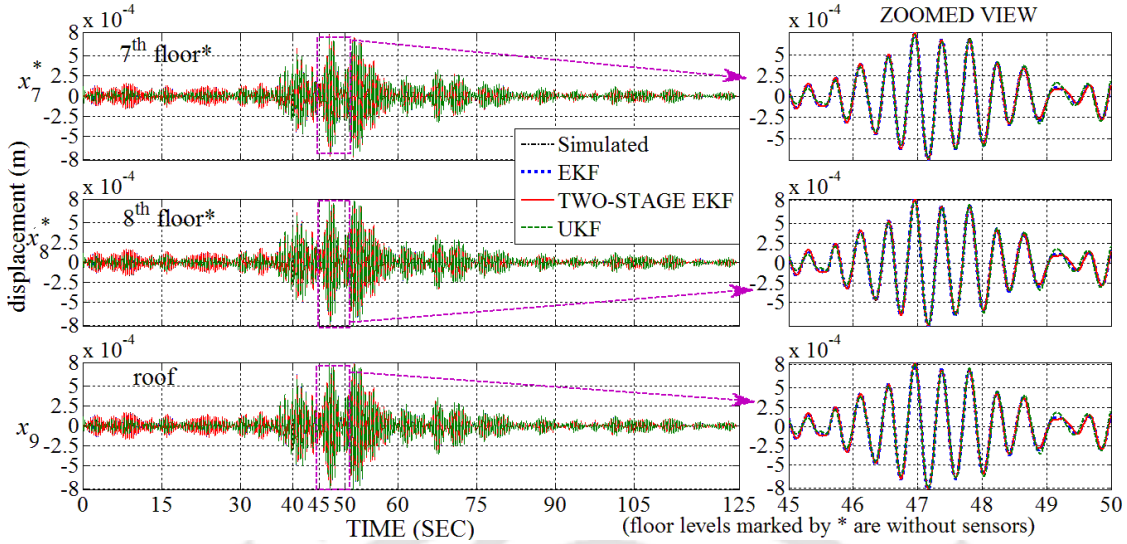

Fig. 4.38: Comparison of identified displacement time-history and simulated displacement time-history at 7th floor to roof level for Problem Type-IIa under excitation NE-EQ-1: Comp-longitudinal

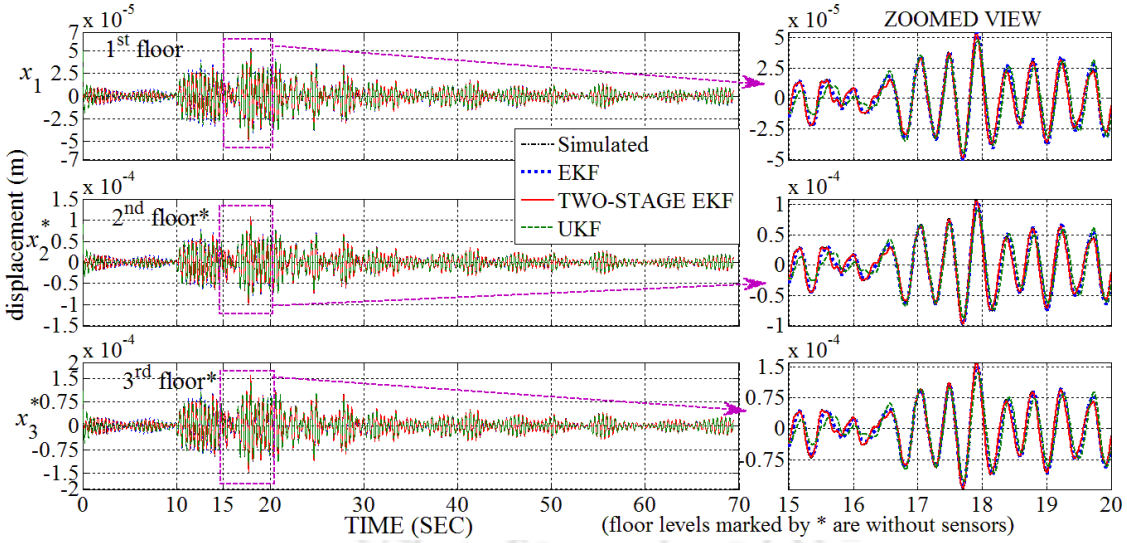

Fig. 4.39: Comparison of identified displacement time-history and simulated displacement time-history at 1st to 3rd floor levels for Problem Type-IIa under excitation NE-EQ-2: Comp-longitudinal

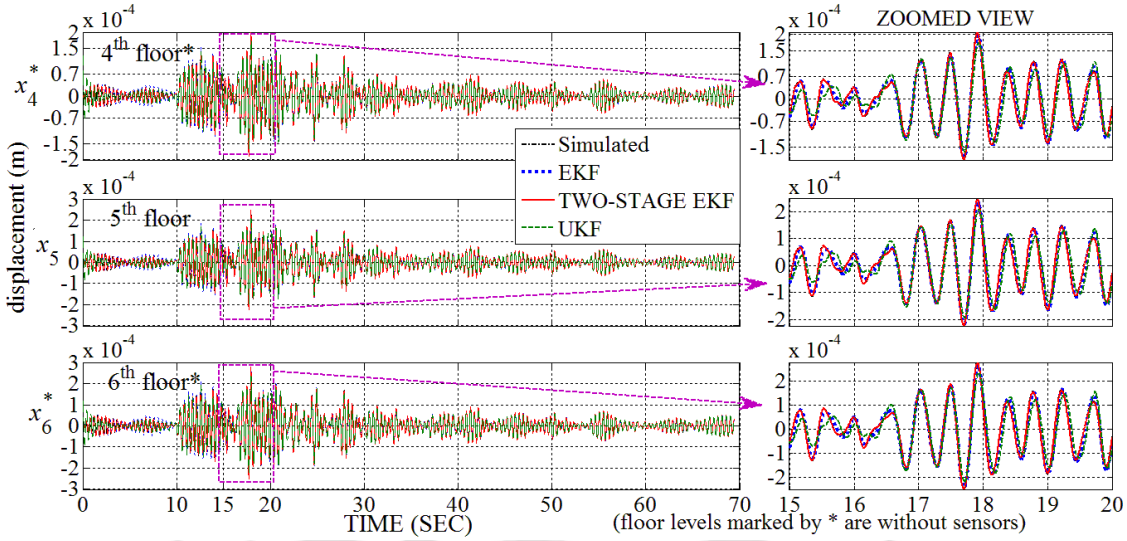

Fig. 4.40: Comparison of identified displacement time-history and simulated displacement time-history at 4th to 6th floor levels for Problem Type-IIa under excitation NE-EQ-2: Comp-longitudinal

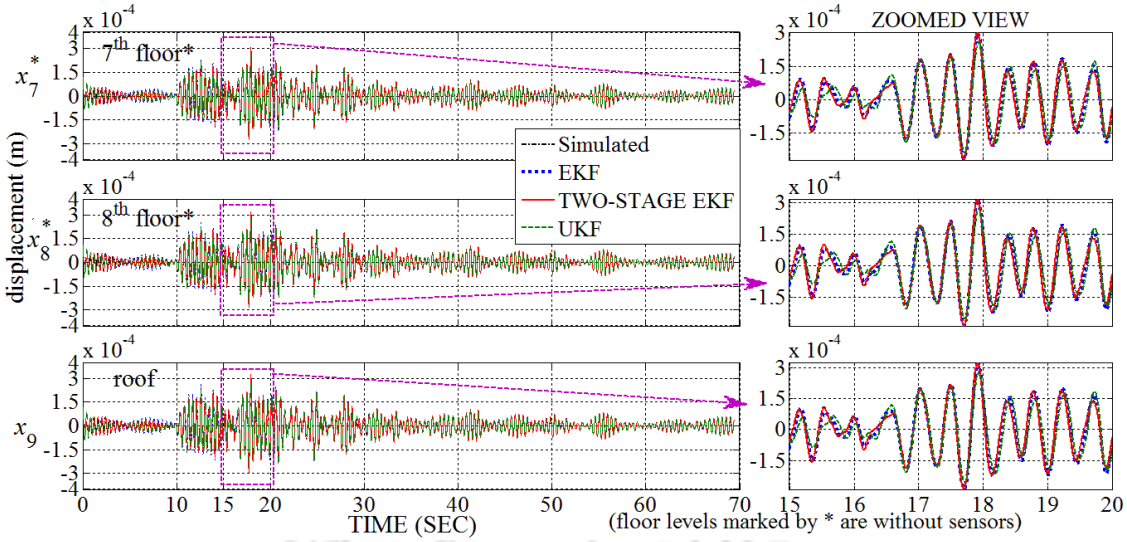

Fig. 4.41: Comparison of identified displacement time-history and simulated displacement time-history at 7th floor to roof level for Problem Type-IIa under excitation NE-EQ-2: Comp-longitudinal

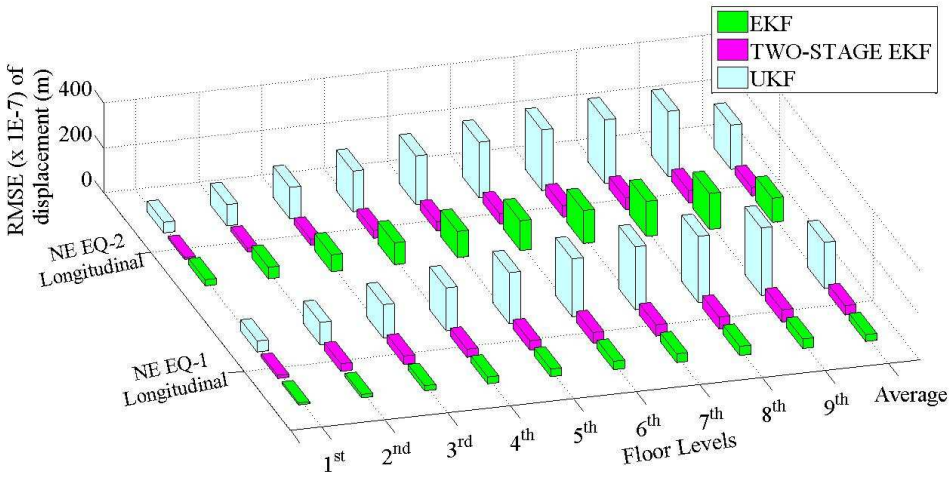

Fig. 4.42: 3D Bar Chart showing RMSE of identified displacement for Problem Type-IIa under excitations NE-EQ-1: Comp-longitudinal and NE-EQ-2: Comp-longitudinal

Table 4.14: RMSE of identified displacement for Problem Type-IIa under excitations NE-EQ-1: Comp-longitudinal and NE-EQ-2: Comp-longitudinal

Floor level	NE EQ-1 (Comp: longitudinal)			NE EQ-2 (Comp: longitudinal)		
	EKF	Two-Stage EKF	UKF	EKF	Two-Stage EKF	UKF
	$x10^{-7}$ (m)	$x10^{-7}$ (m)	$x10^{-7}$ (m)	$x10^{-7}$ (m)	$x10^{-7}$ (m)	$x10^{-7}$ (m)
1st	9	14	49	27	9	47
2nd	15	34	100	51	19	94
3rd	23	37	147	75	27	139
4th	30	36	190	97	34	180
5th	34	42	226	116	41	216
6th	37	47	256	132	46	245
7th	39	50	278	146	50	268
8th	41	53	293	155	53	282
9th	42	54	299	159	54	288
Average RMSE	30	41	204	107	37	196

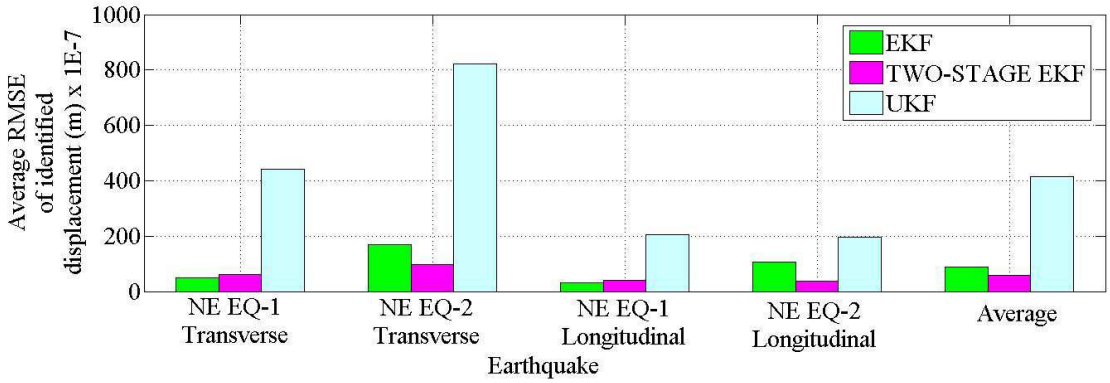

Fig. 4.43: 2D Bar Chart showing Average RMSE of identified displacement for Problem Type-IIa under excitations NE EQ-1: Comp-transverse and NE EQ-2: Comp-transverse

4.6.1.5 Results of displacement identification for Problem Type-IIb in transverse direction

In this sub-section, identifications of displacements have been carried out for the existing building under excitations NE-EQ-1: Comp-transverse and NE-EQ-2: Comp-transverse using field measured responses. Field response data are available for 1st, 3rd, 7th and roof level. Fig. 4.44 to Fig. 4.46 show identified displacement time history at different floor levels for excitation NE-EQ-1: Comp-transverse. Fig. 4.47 to Fig. 4.49 show identified displacement time history at different floor levels for excitation NE-EQ-2: Comp-transverse. From Fig. 4.44 to Fig. 4.49 it is observed that the displacements identified by the different algorithms are in good agreement with each other.

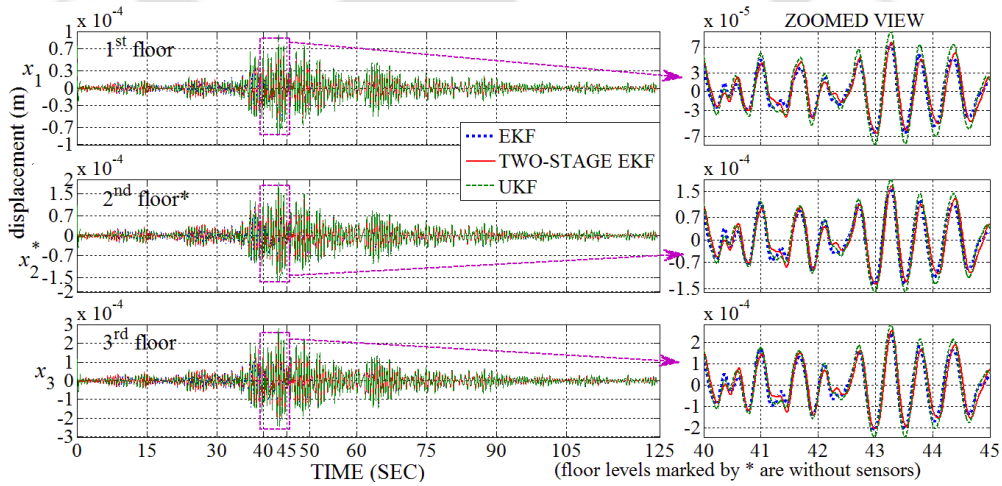

Fig. 4.44: Comparison of identified displacement time-history of 1stto 3rd floor level using different algorithms for Problem Type-IIb under excitation NE EQ-1: Comp-transverse

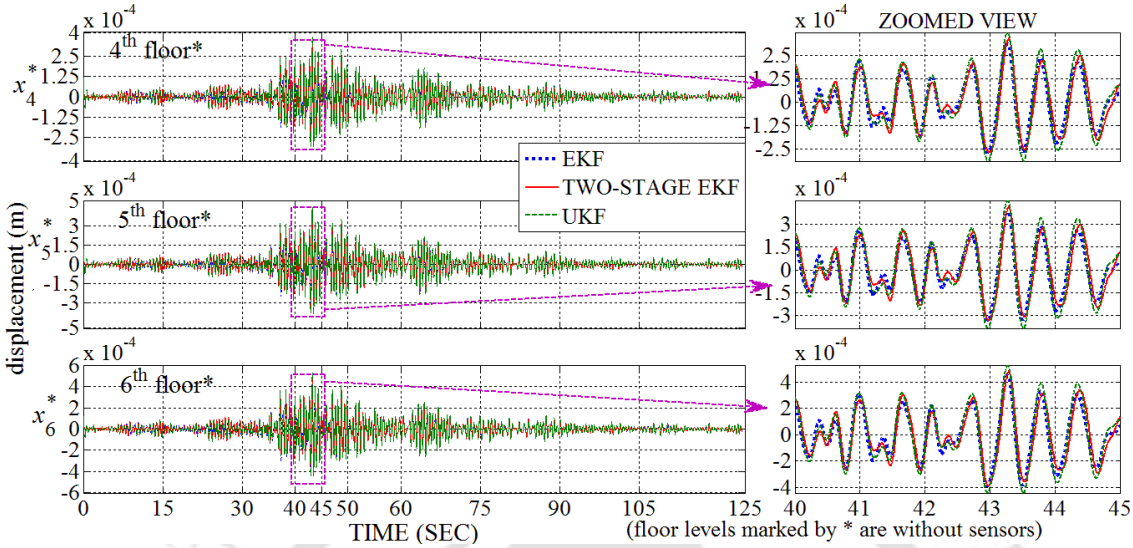

Fig. 4.45: Comparison of identified displacement time-history of 4th to6th floor level using different algorithms for Problem Type-IIb under excitation NE EQ-1: Comp-transverse

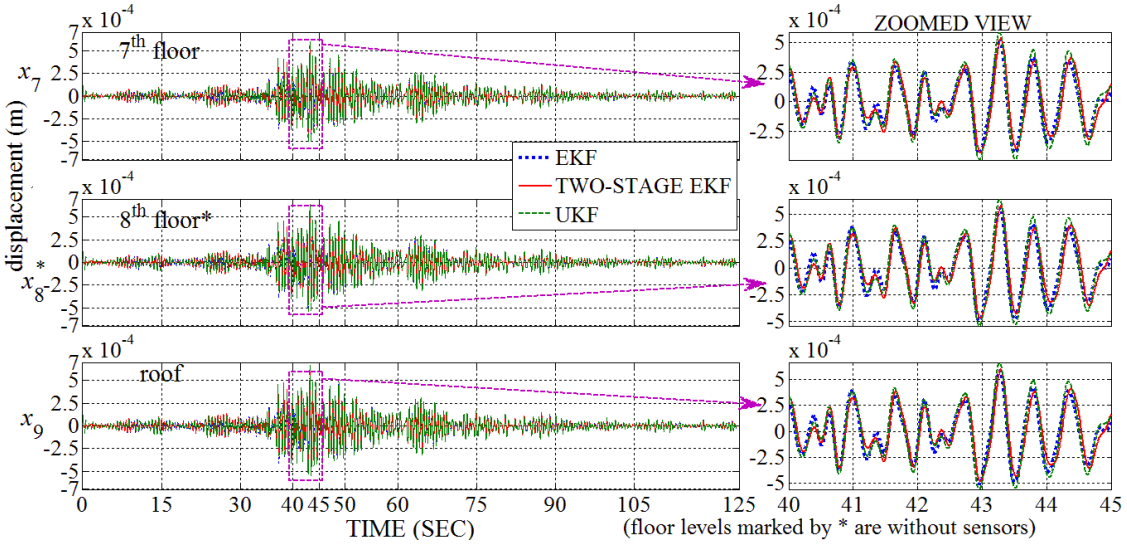

Fig. 4.46: Comparison of identified displacement time-history of 7th floor to roof level using different algorithms for Problem Type-IIb under excitation NE EQ-1: Comp-transverse

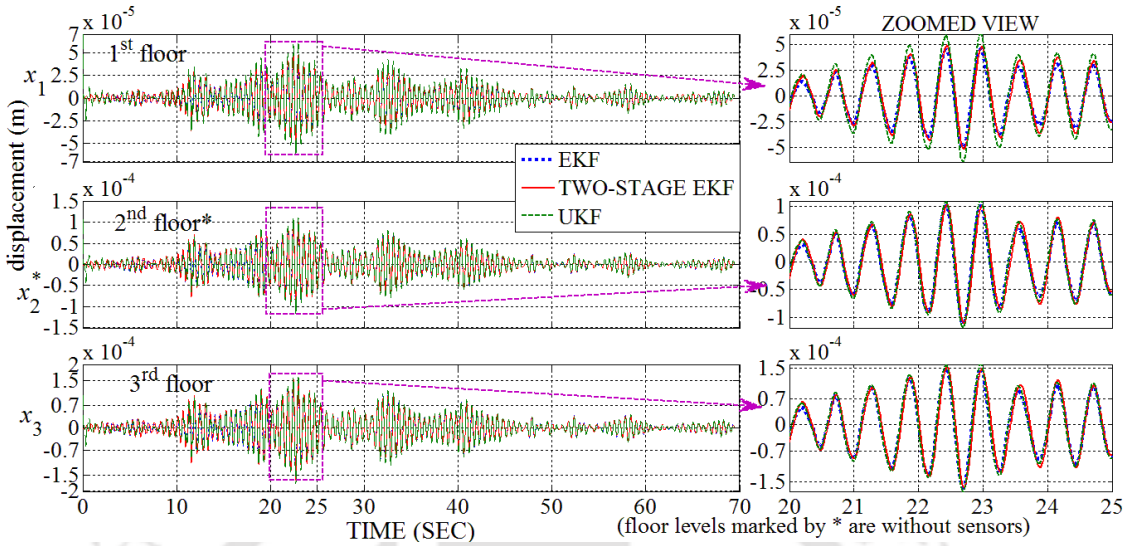

Fig. 4.47: Comparison of identified displacement time-history of 1st to 3rd floor level using different algorithms for Problem Type-IIb under excitation NE EQ-2: Comp-transverse

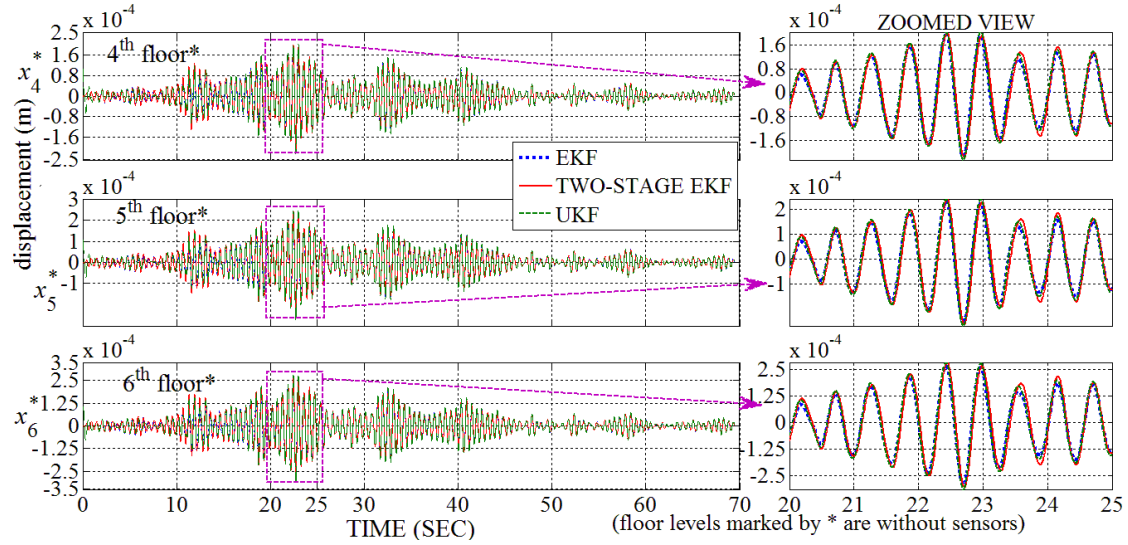

Fig. 4.48: Comparison of identified displacement time-history of 4th to6th floor level using different algorithms for Problem Type-IIb under excitation NE EQ-2: Comp-transverse

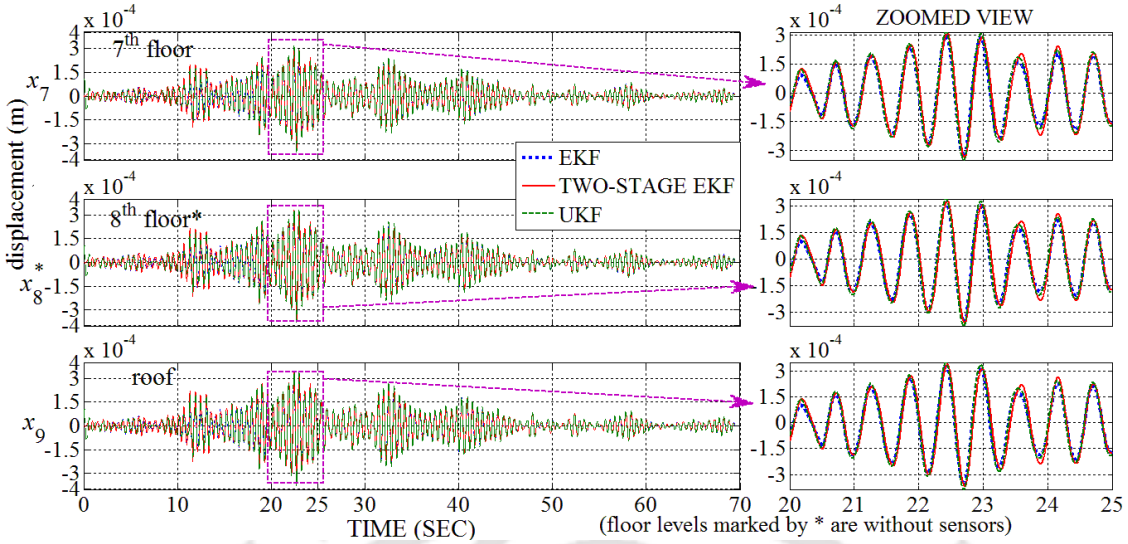

Fig. 4.49: Comparison of identified displacement time-history of 7th floor to roof level using different algorithms for Problem Type-IIb under excitation NE EQ-2: Comp-transverse

4.6.1.6 Results of displacement identification for Problem Type-IIb in longitudinal direction

In this sub-section, identifications of displacements have been carried out for the existing building under excitations NE-EQ-1: Comp-longitudinal and NE-EQ-2: Comp-longitudinal using field measured responses. Field response data are available for 1st, 5th and roof level. Fig. 4.50 to Fig. 4.52 show identified displacement time history at different floor levels for excitation NE-EQ-1: Comp-longitudinal. Fig. 4.53 to Fig. 4.55 show identified displacement time history at different floor levels for excitation NE-EQ-2: Comp-longitudinal. From Fig. 4.50 to Fig. 4.55, it is observed that the displacements identified by the different algorithms are in good agreement with each other.

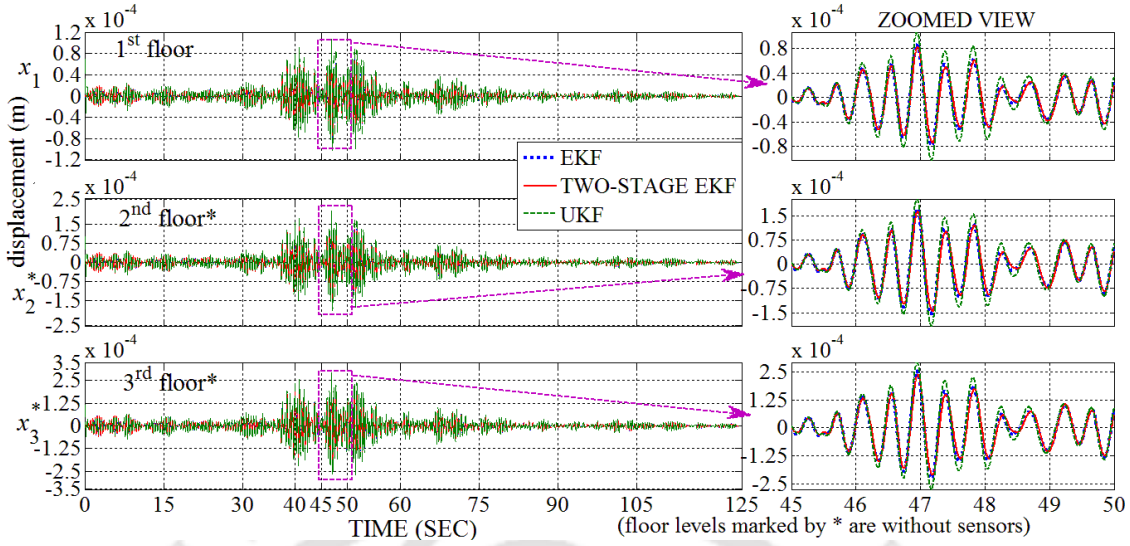

Fig. 4.50: Comparison of identified displacement time-history of 1st to 3rd floor level using different algorithms for Problem Type-IIb under excitation NE EQ-1: Comp-longitudinal

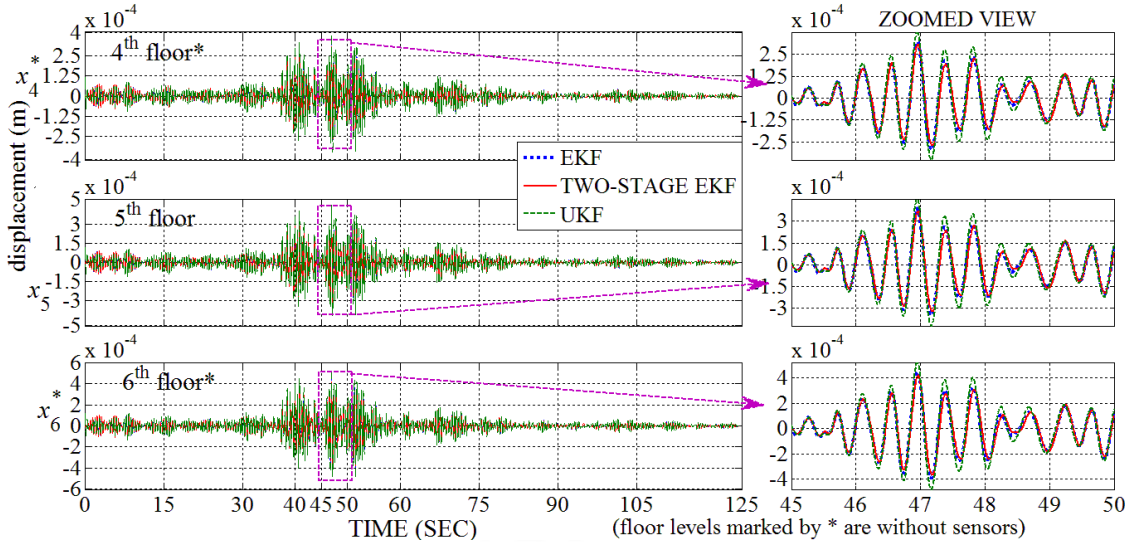

Fig. 4.51: Comparison of identified displacement time-history of 4th to 6th floor level using different algorithms for Problem Type-IIb under excitation NE EQ-1: Comp-longitudinal

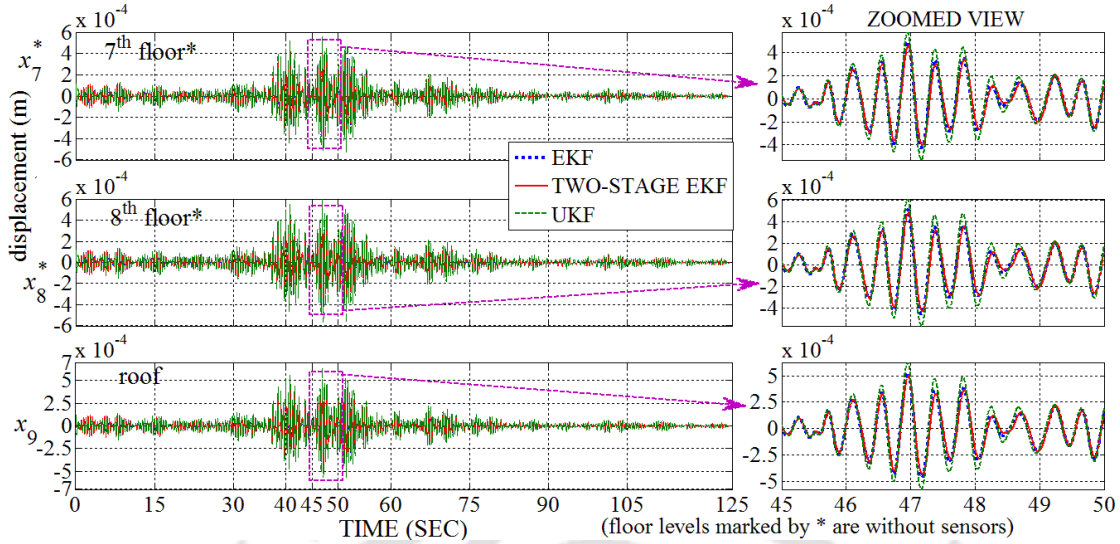

Fig. 4.52: Comparison of identified displacement time-history of 7th floor to roof level using different algorithms for Problem Type-IIb under excitation NE EQ-1: Comp-longitudinal

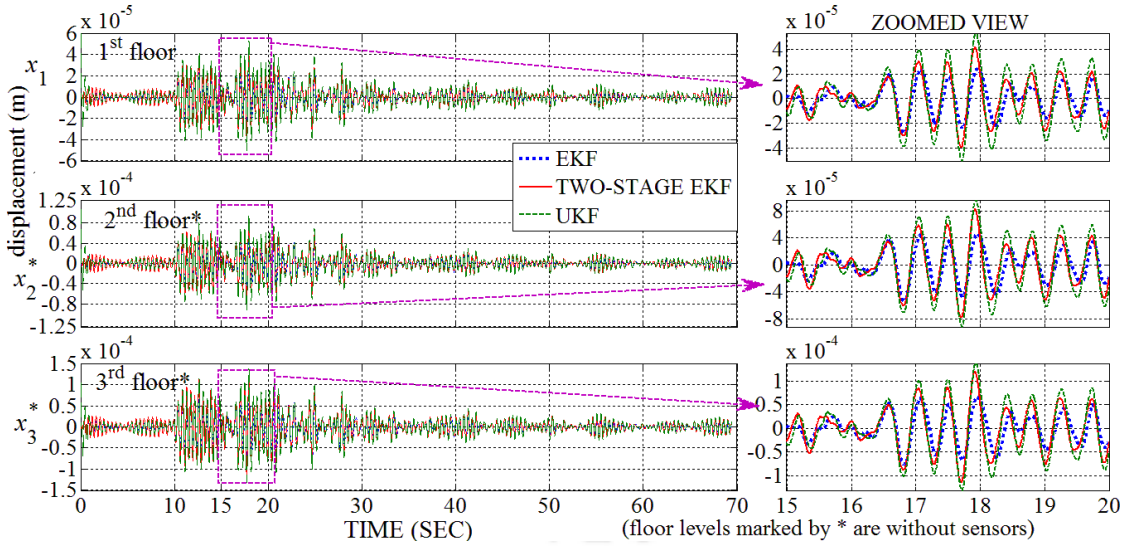

Fig. 4.53: Comparison of identified displacement time-history of 1st to 3rd floor level using different algorithms for Problem Type-IIb under excitation NE EQ-2: Comp-longitudinal

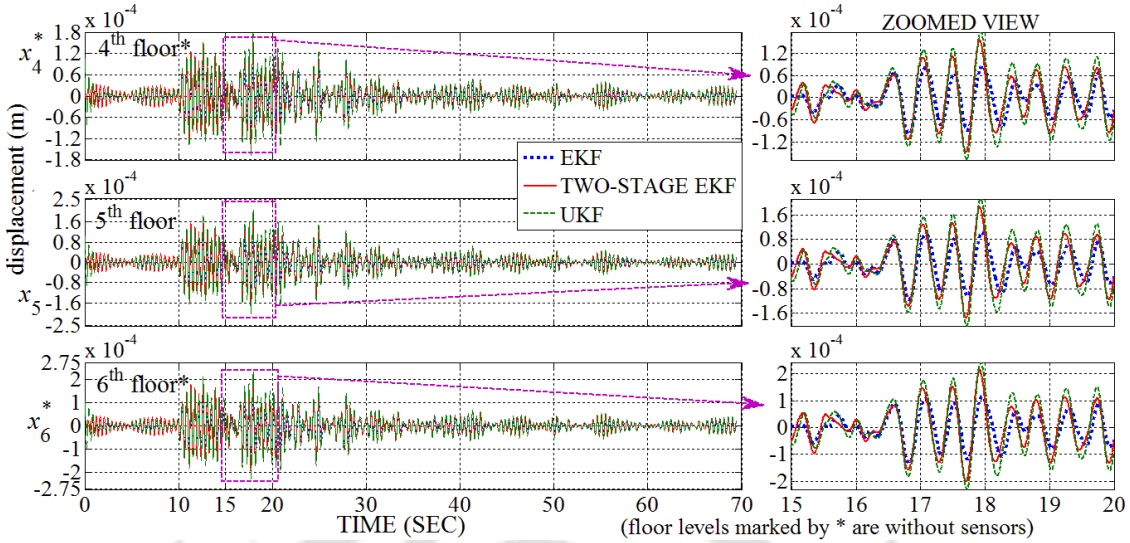

Fig. 4.54: Comparison of identified displacement time-history of 4th to 6th floor level using different algorithms for Problem Type-IIb under excitation NE EQ-2: Comp-longitudinal

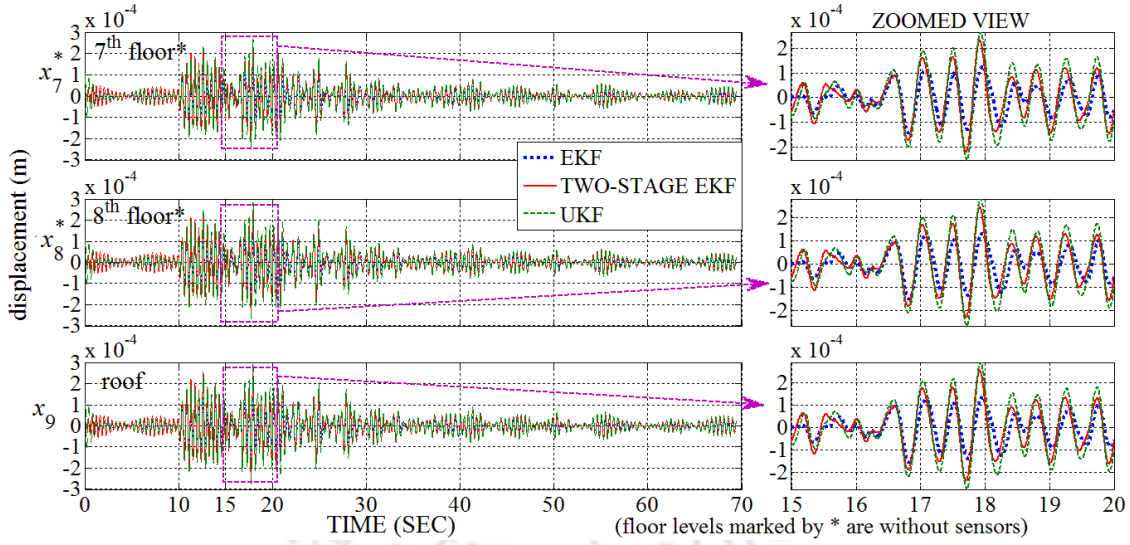

Fig. 4.55: Comparison of identified displacement time-history of 7th to roof level using different algorithms for Problem Type-IIb under excitation NE EQ-2: Comp-longitudinal

4.6.1.7 Results of displacement identification for Problem Type-IIIa and IIIb in transverse direction

In this study, the numbers of floor levels are four, which is much lesser compared to Problem Type-II. The identification of displacement of Problem Type-IIIb has been performed using

field data whereas simulated responses have been used for Problem Type-IIIa. In the existing building, there are missing sensors at two consecutive levels i.e. at 1st floor and 2nd floor levels. In order to replicate the behaviour of existing building, similar sensor arrangement as adopted for field building, is also considered for the simulated building. Therefore, identification of Problem Type-IIIa provides a guideline to carryout the identification of the existing building. Fig. 4.56 and Fig. 4.57 show the plot of identified displacement time-history and simulated displacement time-history using simulated noise-free responses from Problem Type-IIIa under excitation NE EQ-3: Comp-transverse. Similarly, Fig. 4.58 and Fig. 4.59 show identified displacement time-history for Problem Type-IIIb, using field response. Results obtained in case of Problem Type-IIIa using the different algorithms are in very good agreement with that of simulated one. The accuracy of identification of displacement is assessed by evaluating the RMSEs of the identified displacement w.r.t. simulated displacement assumed as base value. Fig. 4.60 shows the 2D plot of RMSEs of identified displacement at all floor levels along with average of all floors. The RMSE values are furnished in Table 4.15. It is observed that the performance of Two-Stage EKF is the best, followed by EKF and then UKF. In the case of identification using field response (Problem Type-IIIb), the comparative plot (Fig. 4.58 and Fig. 4.59) of identified displacement history by different algorithms appears to be in good agreement with each other.

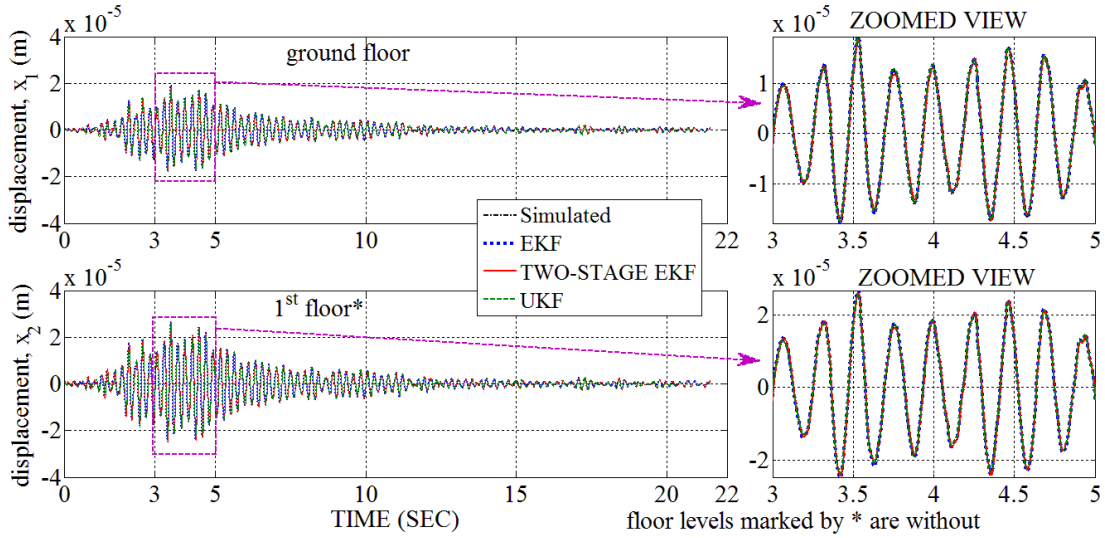

Fig. 4.56: Comparison of identified displacement time-history and simulated displacement time-history of ground floor (x_1) and 1st floor (x_2) level using different algorithms for Problem Type-IIIa under excitation NE EQ-3: Comp- transverse

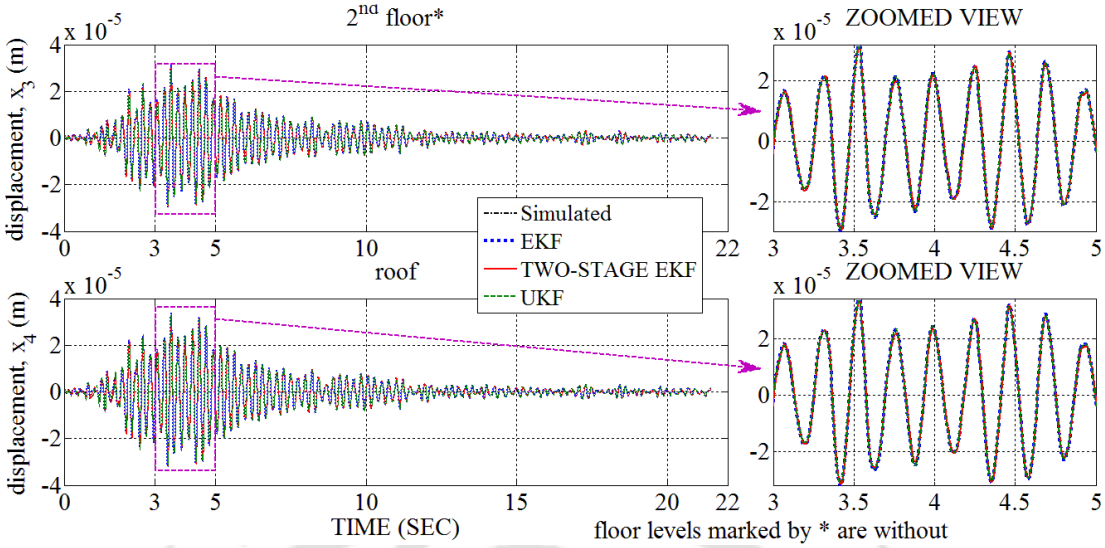

Fig. 4.57: Comparison of identified displacement time-history and simulated displacement time-history of 2nd floor (x_3) and roof (x_4) level using different algorithms for Problem Type-IIIa under excitation NE EQ-3: Comp- transverse

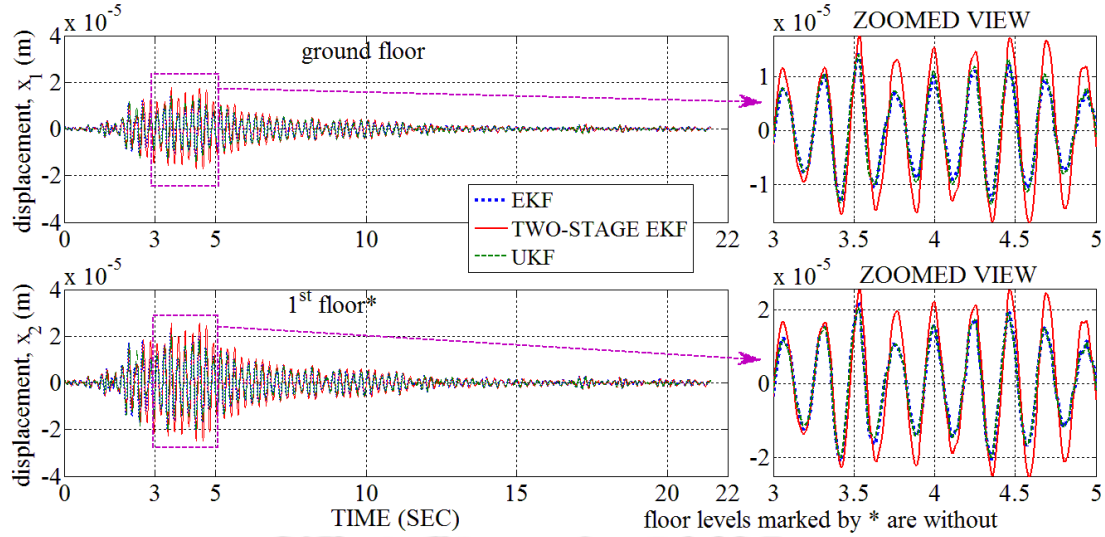

Fig. 4.58: Comparison of identified displacement time-history of ground floor (x_1) and 1st floor (x_2) level using different algorithms for Problem Type-IIIb excitation under NE EQ-3: Comp- transverse

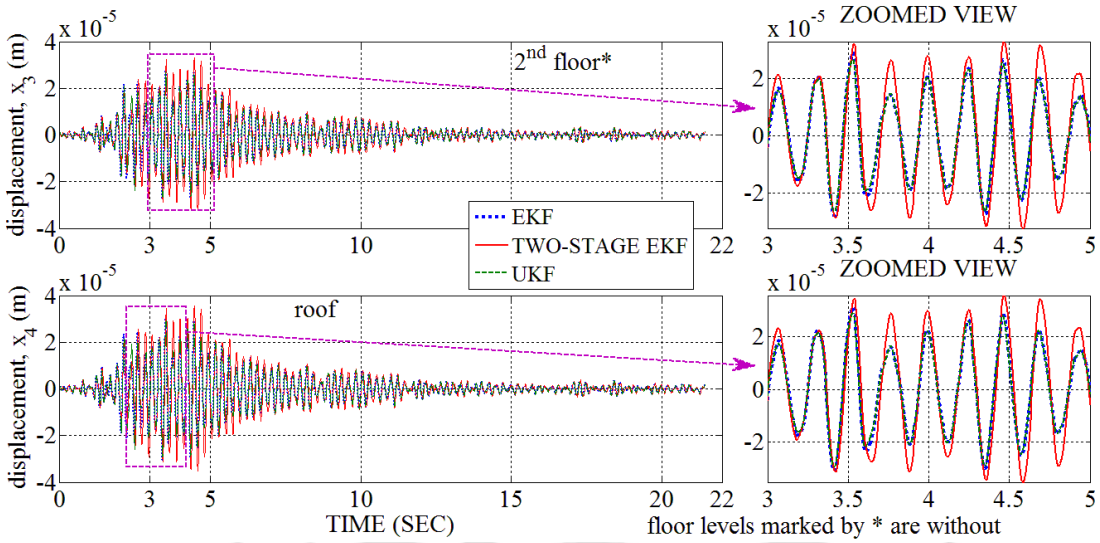

Fig. 4.59: Comparison of identified displacement time-history of 2nd floor (x_3) and roof (x_4) level using different algorithms for Problem Type-IIIb under excitation NE EQ-3: Comp- transverse

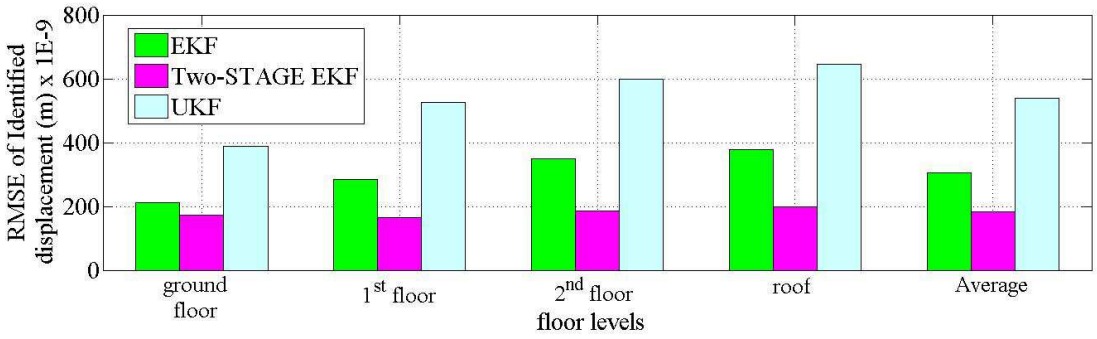

Fig. 4.60: 2D Bar Chart showing RMSE of identified displacement Problem Type-IIIa under excitation NE EQ-3: Comp-transverse

Table 4.15: RMSE of identified displacement Problem Type-IIIa under excitation NE EQ-3: Comp-transverse

Floor level	EKF (x 10^{-9})	Two-Stage EKF (x 10^{-9})	UKF (x 10^{-9})
Ground	211	174	388
1st	285	165	526
2nd	350	187	600
Roof	378	200	646
Average	306	182	540

4.6.2 Results of Parameter identification

4.6.2.1 Results of parameter identification for Problem Type-I

The result of identification of stiffness (parameter) for all the earthquakes under consideration and for noise level of 0% and 5% are plotted as shown in Fig. 4.61 to Fig. 4.63 and Fig. 4.67 to Fig. 4.69 respectively. The result with 1% and 2% has not been shown as performance at higher noise is sufficient to prove performance in lower noise levels. However, performances in the form of percentage error at all noise level are shown in the form of 3D bar chart of Fig. 4.64 to Fig. 4.66 and Fig. 4.70, respectively for 0% to 5% noise level. The values of identified stiffness and its percentage error, calculated from the assumed stiffness of the simulated model are furnished in Table 4.16 to Table 4.21. It is observed that there is some variation in results in different cases under consideration and no conclusion can be arrived at using such results. Therefore, it is difficult to evaluate the performance of the different algorithms w.r.t. accuracy in identification of stiffness by utilising response contaminated with different noise levels and under different earthquake excitation. To overcome this difficulty, average percentage error of identified stiffnesses are evaluated for all floor levels for any particular ground motion and noise levels. 3D plot of percentage error in identified stiffnesses for all floor levels and average of floor levels are presented in Fig. 4.64 to Fig. 4.66 and Fig. 4.70, respectively for 0% to 5% noise level. From these values, again average are evaluated and presented in Fig. 4.71. The average values of percentage error in identified stiffnesses are furnished in Table 4.22. From Fig. 4.71, it is observed that the performance of SNLSE-UI-UO is the worst. Amongst the Kalman Filter based algorithms, the performance of UKF is the best, followed by Two-Stage EKF and then by EKF.

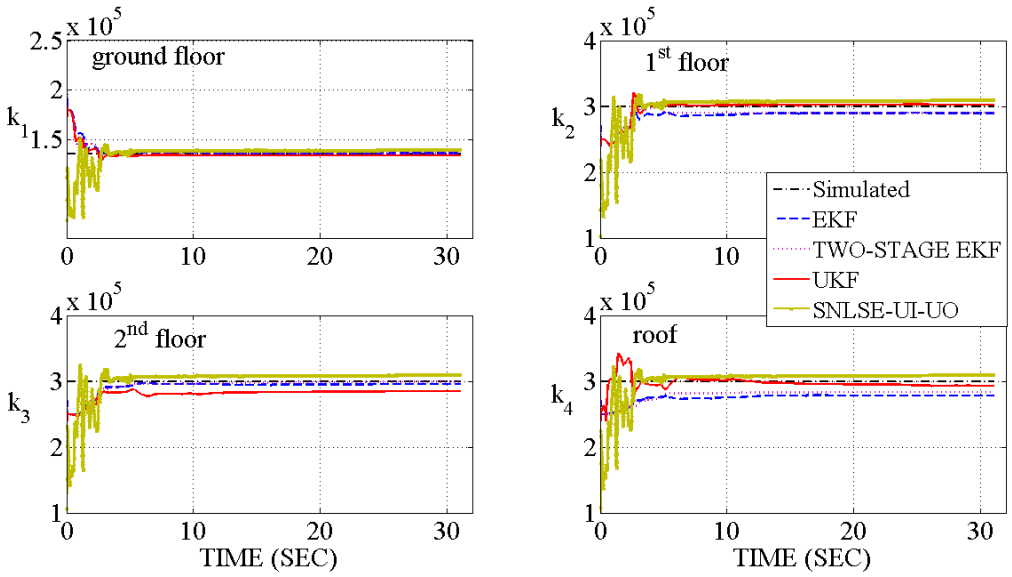

Fig. 4.61: Identified stiffness *vs* simulated stiffness (using simulated response with 0% added noise) for Problem Type-I under excitation El Centro (1940): Comp-180

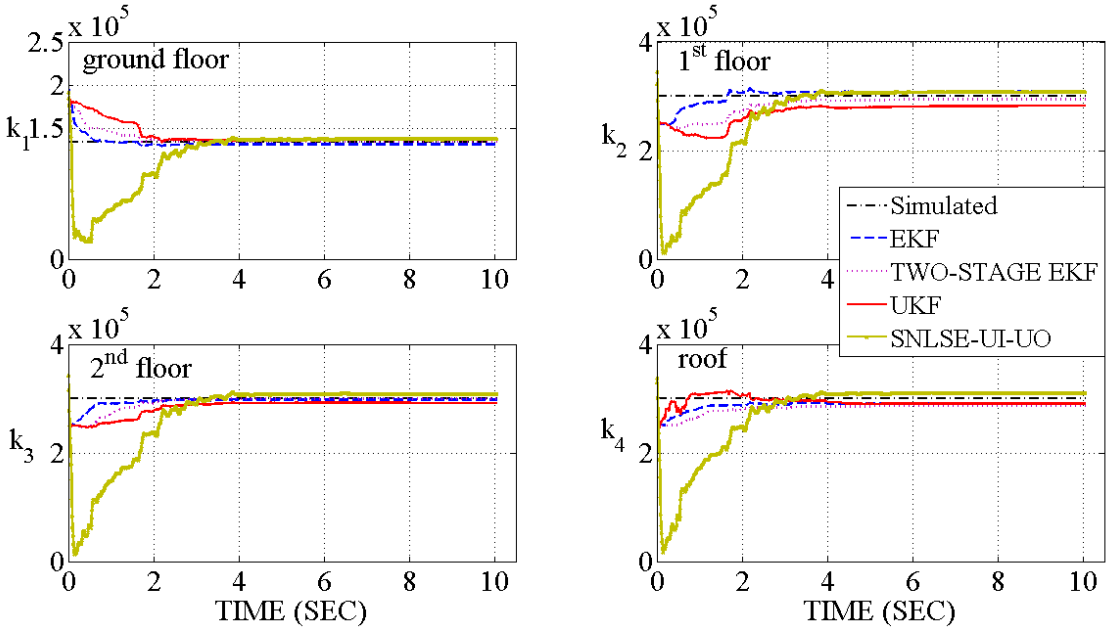

Fig. 4.62: Identified stiffness *vs* simulated stiffness (using simulated response with 0% added noise) for Problem Type-I under excitation Koyna (1967): Comp-Longitudinal

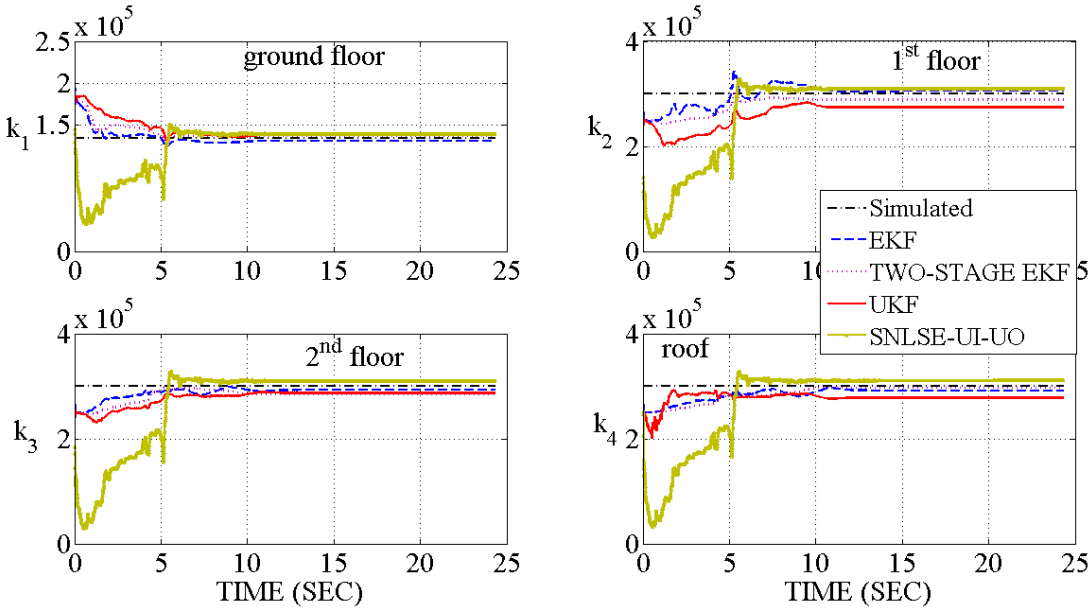

Fig. 4.63: Identified stiffness *vs* simulated stiffness (using simulated response with 0% added noise) for Problem Type-I under excitation Victoria (1980): Comp-CPE045

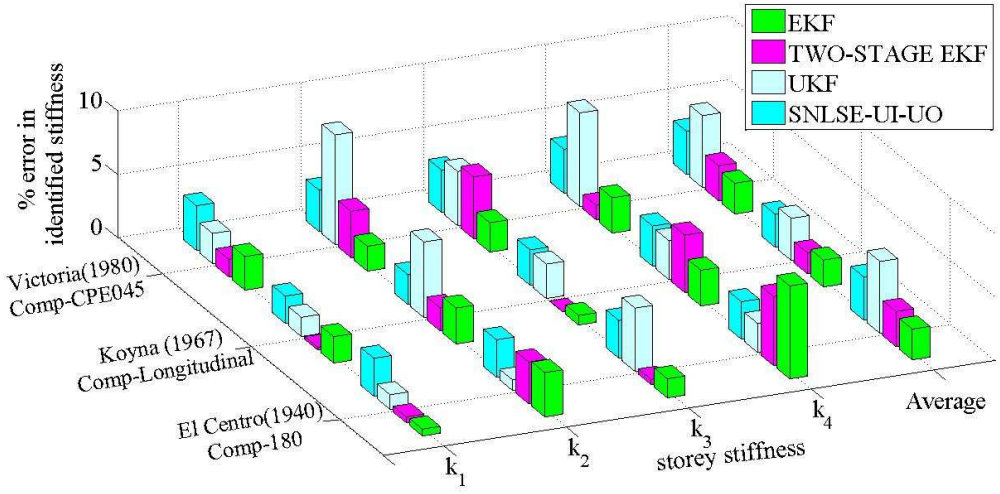

Fig. 4.64: 3D Bar Chart showing percentage error in identified stiffness of Problem Type-I (using simulated response with 0% added noise) under different earthquake excitation

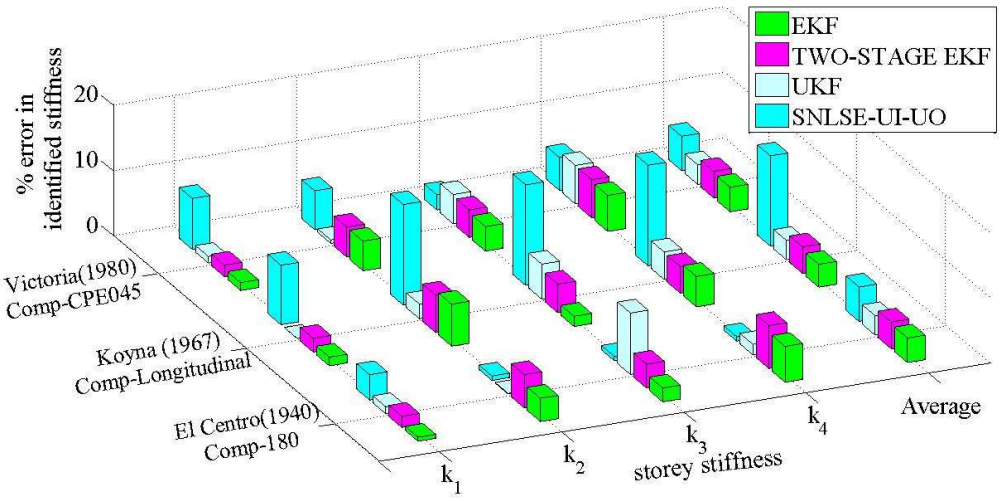

Fig. 4.65: 3D Bar Chart showing percentage error in identified stiffness of Problem Type-I (using simulated response with 1% added noise) under different earthquake excitation

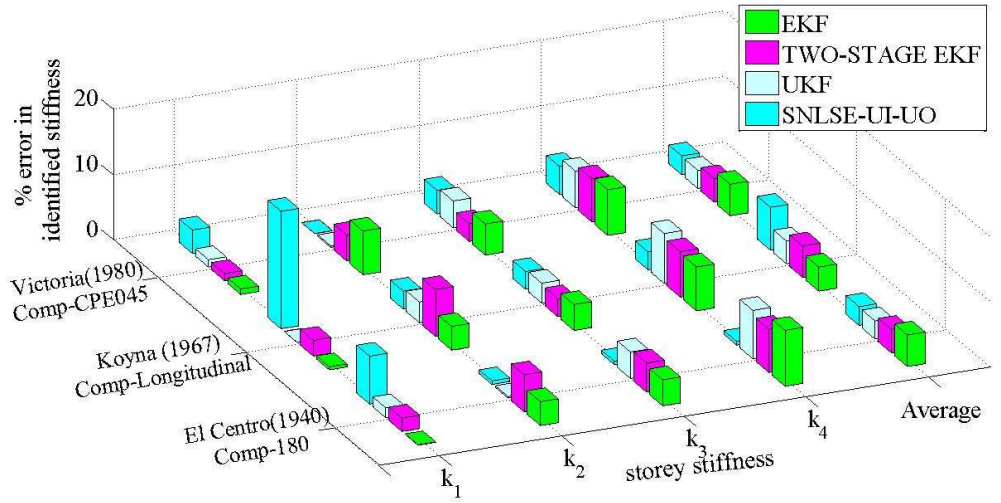

Fig. 4.66: 3D Bar Chart showing percentage error in identified stiffness of Problem Type-I (using simulated response with 2% added noise) under different earthquake excitation

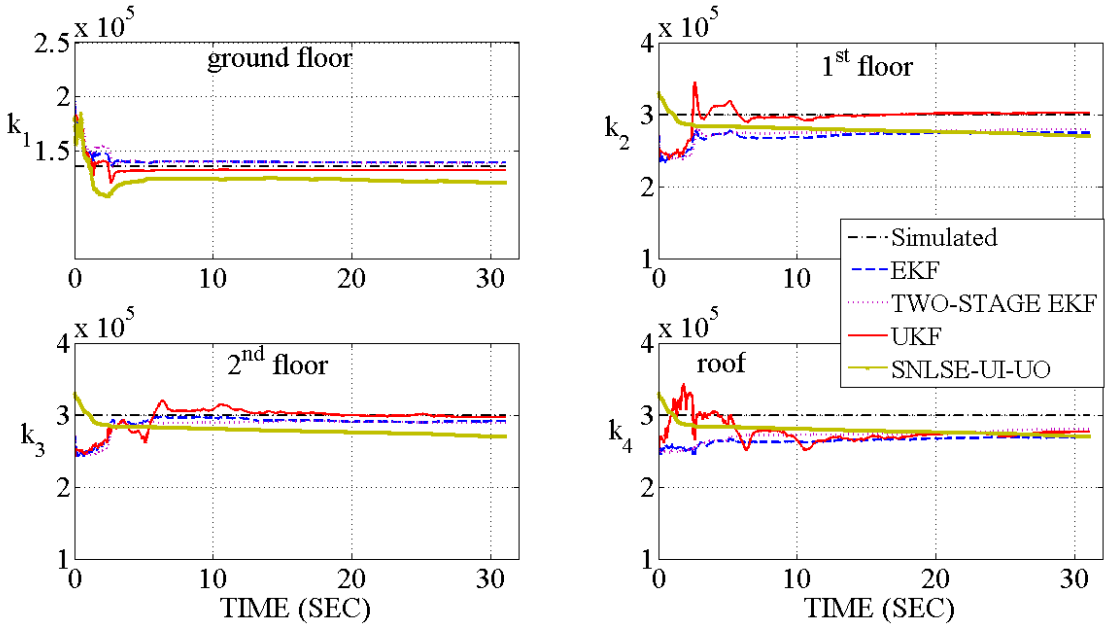

Fig. 4.67: Identified stiffness *vs* simulated stiffness (using simulated response with 5% added noise) for Problem Type-I under excitation El Centro (1940): Comp-180

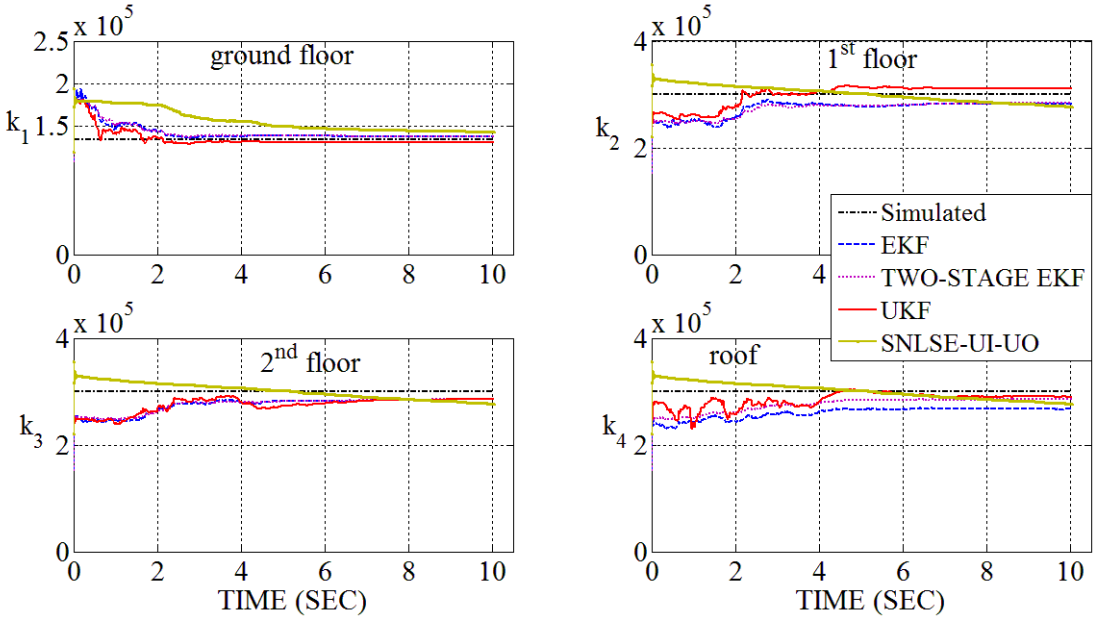

Fig. 4.68: Identified stiffness *vs* simulated stiffness (using simulated response with 5% added noise) for Problem Type-I under excitation Koyna (1967): Comp-Longitudinal

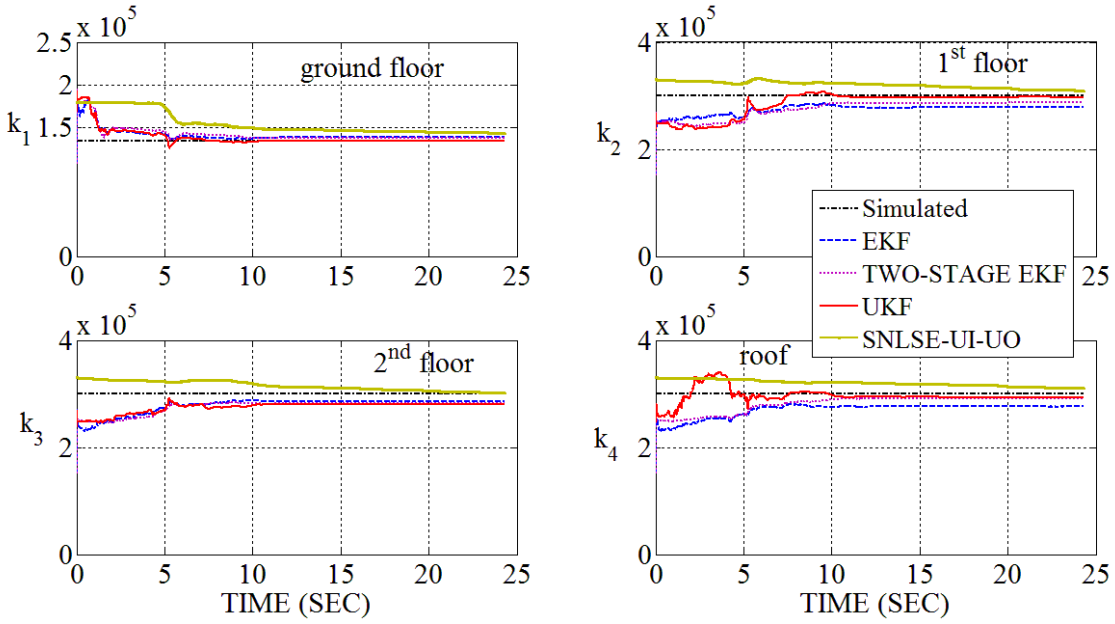

Fig. 4.69: Identified stiffness *vs* simulated stiffness (using simulated response with 5% added noise) for Problem Type-I under excitation Victoria (1980): Comp-CPE045

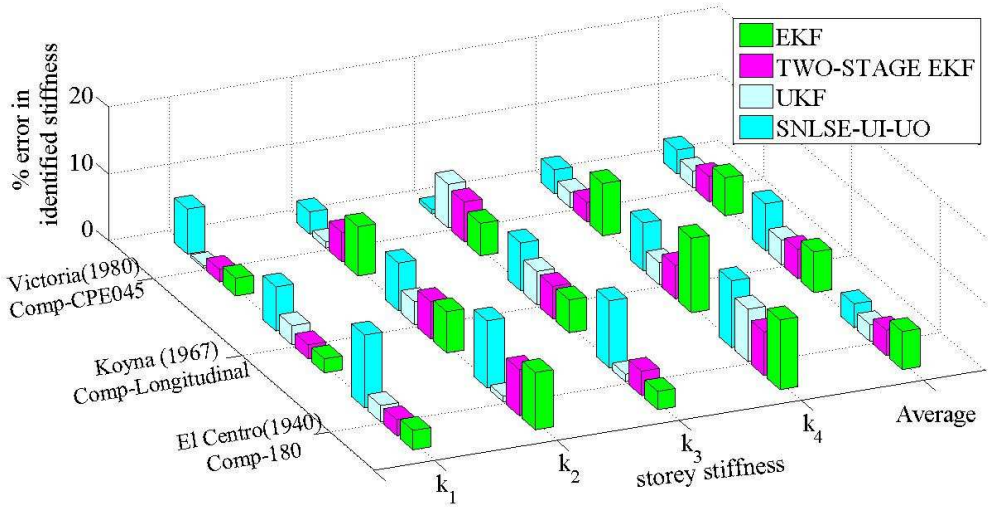

Fig. 4.70: 3D Bar Chart showing percentage error in identified stiffness of Problem Type-I (using simulated response with 5% added noise) under different earthquake excitation

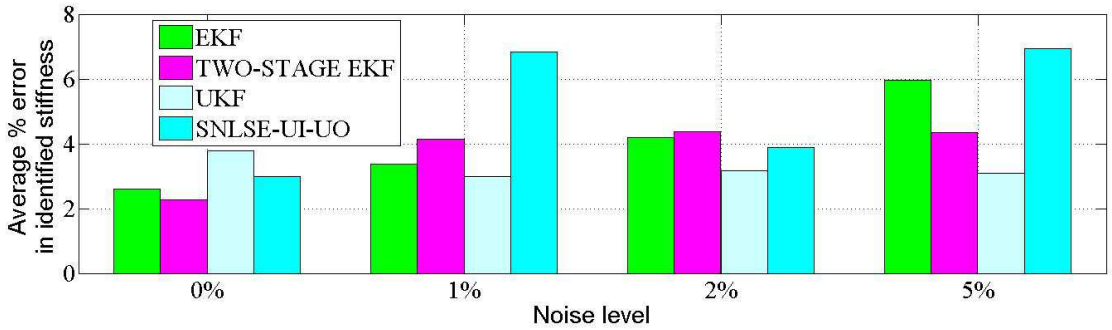

Fig. 4.71: 2D Bar Chart showing average percentage error in identified stiffness of Problem Type-I using simulated response with different noise level and under different earthquake excitation

Table 4.16: Identified stiffness (using simulated response with different added noise levels) for Problem Type-I under excitation El Centro (1940): Comp-180

Noise level	Stiffness (kN/m)	Value used for simulation	EKF	Two-Stage EKF	UKF	SNLSE-UI-UO
		x 10^5	x 10^5	x 10^5	x 10^5	x 10^5
0%	k_1	1.35	1.36	1.36	1.33	1.39
0%	k_2	3.00	2.89	2.90	3.03	3.09
0%	k_3	3.00	2.95	2.99	2.85	3.09
0%	k_4	3.00	2.78	2.84	2.93	3.09
1%	k_1	1.35	1.36	1.37	1.34	1.30
1%	k_2	3.00	2.89	2.85	3.00	3.02
1%	k_3	3.00	2.94	2.89	2.72	3.02
1%	k_4	3.00	2.84	2.80	2.95	3.02
2%	k_1	1.35	1.35	1.38	1.33	1.25
2%	k_2	3.00	2.89	2.83	2.99	2.98
2%	k_3	3.00	2.88	2.87	2.88	2.98
2%	k_4	3.00	2.74	2.80	2.78	2.98
5%	k_1	1.35	1.39	1.38	1.32	1.20
5%	k_2	3.00	2.74	2.79	3.02	2.70
5%	k_3	3.00	2.92	2.89	2.97	2.70
5%	k_4	3.00	2.69	2.80	2.76	2.70

Table 4.17: Percentage error in identified stiffness (using simulated response with different added noise levels) for Problem Type-I under excitation El Centro (1940): Comp-180

Noise level	stiffness	EKF	Two-Stage EKF	UKF	SNLSE-UI-UO
		Error Percentage			
0%	k_1	0.54	0.46	1.16	2.99
0%	k_2	3.50	3.29	0.83	2.95
0%	k_3	1.51	0.41	4.99	2.97
0%	k_4	7.33	5.45	2.29	2.95
1%	k_1	0.60	1.7	1.08	3.89
1%	k_2	3.55	5.07	0.12	0.65
1%	k_3	2.11	3.65	9.37	0.65
1%	k_4	5.46	6.55	1.6	0.65
2%	k_1	0.07	2.05	1.53	7.33
2%	k_2	3.64	5.63	0.23	0.56
2%	k_3	3.98	4.44	4.04	0.56
2%	k_4	8.52	6.58	7.38	0.56
5%	k_1	2.89	2.4	2.42	10.97
5%	k_2	8.55	6.92	0.81	10.06
5%	k_3	2.74	3.66	1.12	10.06
5%	k_4	10.42	6.53	7.85	10.06

Table 4.18: Identified stiffness (using simulated response with different added noise levels) for Problem Type-I under excitation Koyna (1967): Comp-Longitudinal

Noise level	Stiffness (KN/m)	Value used for simulation	EKF	Two-Stage EKF	UKF	SNLSE-UI-UO
		x 10^5	x 10^5	x 10^5	x 10^5	x 10^5
0%	k_1	1.35	1.32	1.35	1.37	1.38
0%	k_2	3.00	3.09	2.95	2.82	3.07
0%	k_3	3.00	2.98	3.00	2.92	3.08
0%	k_4	3.00	2.92	2.86	2.91	3.10
1%	k_1	1.35	1.37	1.38	1.35	1.22
1%	k_2	3.00	2.81	2.83	2.93	2.52
1%	k_3	3.00	2.95	2.87	2.84	2.52
1%	k_4	3.00	2.86	2.88	2.87	2.52
2%	k_1	1.35	1.34	1.38	1.35	1.59
2%	k_2	3.00	2.89	2.79	2.91	3.07
2%	k_3	3.00	2.88	2.92	2.91	3.07
2%	k_4	3.00	2.80	2.79	2.77	3.07
5%	k_1	1.35	1.38	1.38	1.31	1.44
5%	k_2	3.00	2.82	2.83	3.10	2.77
5%	k_3	3.00	2.85	2.85	2.85	2.77
5%	k_4	3.00	2.67	2.85	2.90	2.77

Table 4.19: Percentage error in identified stiffness (using simulated response with different added noise levels) for Problem Type-I under excitation Koyna (1967): Comp-Longitudinal

Noise level	stiffness	EKF	Two-Stage EKF	UKF	SNLSE-UI-UO
		Error Percentage			
0%	k_1	2.07	0.20	1.53	2.16
0%	k_2	2.84	1.83	5.96	2.36
0%	k_3	0.75	0.02	2.71	2.80
0%	k_4	2.82	4.55	3.07	3.19
1%	k_1	1.33	2.10	0.01	9.65
1%	k_2	6.40	5.71	2.24	15.96
1%	k_3	1.55	4.37	5.33	15.96
1%	k_4	4.64	4.05	4.19	15.96
2%	k_1	0.47	2.40	0.02	17.64
2%	k_2	3.61	7.16	3.16	2.19
2%	k_3	3.96	2.74	3.04	2.19
2%	k_4	6.69	6.93	7.61	2.19
5%	k_1	2.10	2.10	2.87	6.30
5%	k_2	6.15	5.58	3.47	7.73
5%	k_3	4.91	4.86	4.99	7.73
5%	k_4	11.14	4.97	3.32	7.73

Table 4.20: Identified stiffness (using simulated response with different added noise levels) for Problem Type-I under excitation Victoria (1980): Comp-CPE045

Noise level	Stiffness (KN/m)	Value used for simulation	EKF	Two-Stage EKF	UKF	SNLSE-UI-UO
		x 10^5	x 10^5	x 10^5	x 10^5	x 10^5
0%	k_1	1.35	1.31	1.37	1.38	1.40
0%	k_2	3.00	3.06	2.89	2.74	3.10
0%	k_3	3.00	2.93	2.85	2.87	3.10
0%	k_4	3.00	2.92	2.97	2.78	3.10
1%	k_1	1.35	1.37	1.37	1.34	1.45
1%	k_2	3.00	2.86	2.86	3.02	3.17
1%	k_3	3.00	2.89	2.87	2.87	3.07
1%	k_4	3.00	2.83	2.83	2.82	3.15
2%	k_1	1.35	1.36	1.36	1.33	1.40
2%	k_2	3.00	2.80	2.88	3.01	2.99
2%	k_3	3.00	2.86	2.92	2.88	2.88
2%	k_4	3.00	2.79	2.80	2.83	2.87
5%	k_1	1.35	1.39	1.38	1.35	1.44
5%	k_2	3.00	2.78	2.87	2.97	3.10
5%	k_3	3.00	2.85	2.82	2.80	3.01
5%	k_4	3.00	2.77	2.91	2.93	3.10

Table 4.21: Percentage error in identified stiffness (using simulated response with different added noise levels) for Problem Type-I under excitation Victoria (1980): Comp-CPE045

Noise level	stiffness	EKF	Two-Stage EKF	UKF	SNLSE-UI-UO
		Error Percentage			
0%	k_1	2.65	1.39	2.39	3.52
0%	k_2	1.96	3.67	8.65	3.25
0%	k_3	2.32	4.88	4.27	3.34
0%	k_4	2.78	1.15	7.39	3.48
1%	k_1	1.20	1.77	1.00	7.67
1%	k_2	4.52	4.57	0.53	5.81
1%	k_3	3.74	4.19	4.45	2.20
1%	k_4	5.50	5.80	5.90	4.94
2%	k_1	0.83	1.10	1.12	3.43
2%	k_2	6.67	3.97	0.24	0.20
2%	k_3	4.74	2.69	4.08	3.86
2%	k_4	6.98	6.57	5.64	4.46
5%	k_1	2.67	1.88	0.35	6.64
5%	k_2	7.36	4.40	0.91	3.20
5%	k_3	4.86	5.97	6.53	0.47
5%	k_4	7.83	2.91	2.29	3.43

Table 4.22: Average percentage error in identified stiffness for Problem Type-I using simulated response with different added noise levels excited under excitation different earthquake

Earthquake	Noise level	EKF	Two-Stage EKF	UKF	SNLSE-UI-UO
		Average Error Percentage			
El Centro	0%	3.22	2.40	2.32	2.97
	1%	2.93	4.24	3.04	1.46
	2%	4.05	4.68	3.30	2.25
	5%	6.15	4.88	3.05	10.29
Koyna	0%	2.12	1.65	3.32	2.63
	1%	3.48	4.06	2.94	14.38
	2%	3.68	4.81	3.46	6.05
	5%	6.08	4.38	3.66	7.37
Victoria	0%	2.43	2.77	5.68	3.40
	1%	3.74	4.08	2.97	5.16
	2%	4.81	3.58	2.77	2.99
	5%	5.68	3.79	2.52	3.44
Average among all Earthquakes	0%	2.59	2.28	3.77	3.00
	1%	3.38	4.13	2.99	7.00
	2%	4.18	4.36	3.17	3.76
	5%	5.97	4.35	3.08	7.03

4.6.2.2 Results of parameter identification Problem Type-IIa (In transverse direction)

In this sub-section, identification study has been carried out using the response from simulated building (Problem Type-IIa) under excitation in transverse direction. To simulate the condition of missing sensors, responses corresponding to particular floor levels are only considered for identification. In the present case of excitation in the transverse direction, sensors are assumed to be available at 1st, 3rd, 7th and roof levels. Similar sensor arrangements are also present in Problem Type-IIb, wherein identification has been carried out using acquired field responses (section-4.6.2.4). Thus numerical model (Problem Type-IIa) replicates the existing building model (Problem Type-IIb). Fig.4.72 and Fig.4.73 show the identified stiffness under NE EQ-1: Comp-transverse excitation and Fig.4.74 and Fig.4.75 show the identified stiffness under NE EQ-2: Comp-transverse excitation. The identified stiffness has been compared with the stiffness of the simulated model. The values of identified stiffness have been furnished in Table 4.23. The percentage error in identified stiffness from that assumed in simulated model is furnished in Table 4.24. A 3D bar chart showing the percentage error in identified stiffness under both the earthquake excitations is shown in Fig. 4.76. From the values of error percentages and its average as furnished in Table 4.24, it is observed that all these algorithms performed quite well. The performance of EKF and Two-Stage EKF are observed to be better than that of UKF's performance. In-spite of large numbers of missing sensors, these algorithms are found to be stable and the identified stiffness shows a good convergence of results.

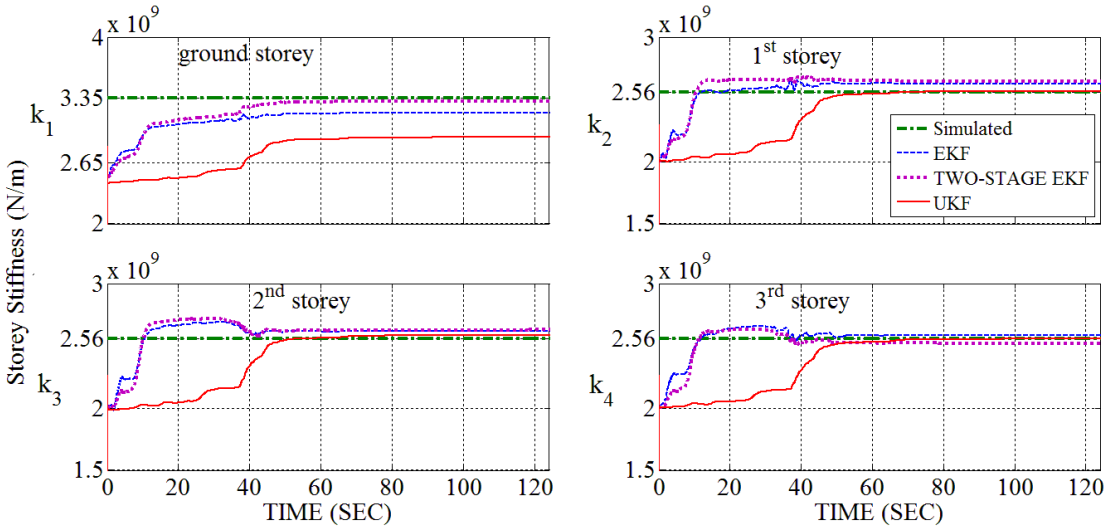

Fig.4.72: Identified stiffness *vs* simulated stiffness (ground storey to 3rd storey) of Problem Type-IIa under excitation NE EQ-1: Comp-transverse

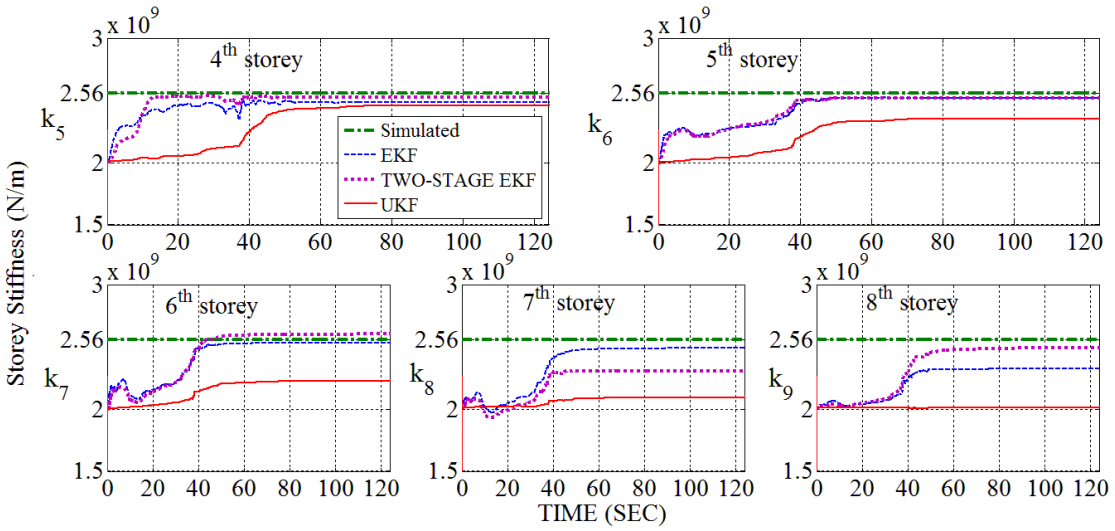

Fig.4.73: Comparison of identified storey stiffness (4th to 8th storey) with simulated storey stiffness for Problem Type-IIa under excitation NE EQ-1: Comp-transverse

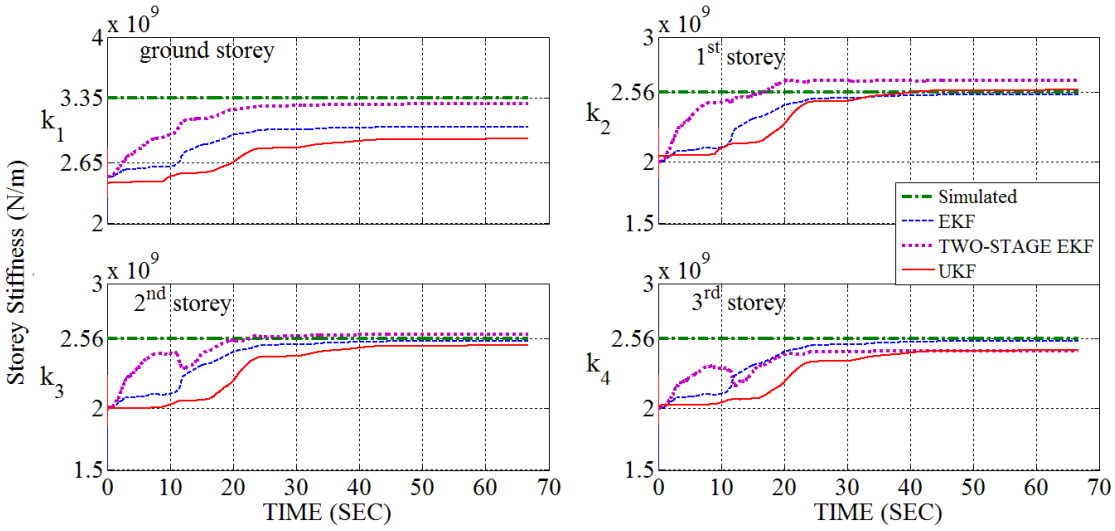

Fig.4.74: Identified stiffness *vs* simulated stiffness (ground storey to 3rd storey) of Problem Type-IIa under excitation NE EQ-2: Comp-transverse

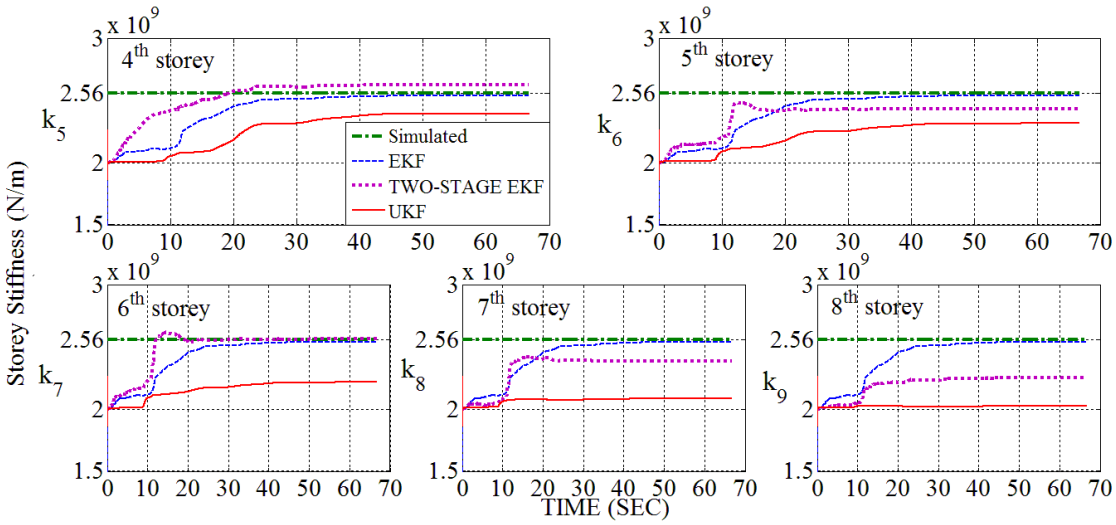

Fig.4.75: Identified stiffness *vs* simulated stiffness (4th to 8th storey) of Problem Type-IIa under excitation NE EQ-2: Comp-transverse

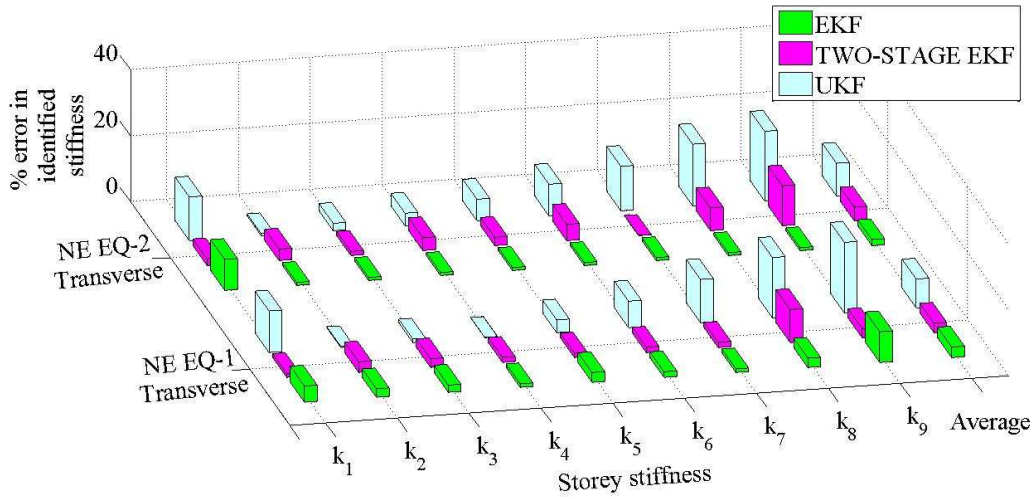

Fig. 4.76: 3D Bar Chart showing percentage error in identified stiffness of Problem Type-IIa using simulated response under excitations NE EQ-1: Comp-transverse and NE EQ-2: Comp-transverse

Table 4.23: Identified stiffness using simulated response of Problem Type-IIa under excitations NE EQ-1: Comp-transverse and NE EQ-2: Comp-transverse

Stiffness (N/m)	Value used for simulation	NE EQ-1 (Comp: Transverse)			NE EQ-2(Comp: Transverse)		
		EKF	Two-Stage EKF	UKF	EKF	Two-Stage EKF	UKF
	x 10^9	x 10^9	x 10^9	x 10^9	x 10^9	x 10^9	x 10^9
k_1	3.35	3.19	3.31	2.93	3.04	3.28	2.91
k_2	2.56	2.63	2.64	2.57	2.54	2.65	2.58
k_3	2.56	2.62	2.63	2.59	2.54	2.59	2.50
k_4	2.56	2.59	2.52	2.56	2.54	2.46	2.46
k_5	2.56	2.48	2.53	2.46	2.54	2.62	2.39
k_6	2.56	2.52	2.52	2.35	2.54	2.43	2.32
k_7	2.56	2.53	2.60	2.23	2.54	2.56	2.22
k_8	2.56	2.49	2.30	2.09	2.54	2.38	2.08
k_9	2.56	2.32	2.49	2.02	2.54	2.25	2.02

Table 4.24: Percentage error of identified stiffness using simulated response of Problem Type-IIa under excitations NE EQ-1: Comp-transverse and NE EQ-2: Comp-transverse

Stiffness	NE EQ-1 (Comp: Transverse)			NE EQ-2(Comp: Transverse)		
	EKF	Two-Stage EKF	UKF	EKF	Two-Stage EKF	UKF
	Error percentage			Error percentage		
k_1	4.90	1.15	12.55	9.35	2.02	13.18
k_2	2.56	3.18	0.29	0.90	3.44	0.59
k_3	2.17	2.64	1.06	0.90	1.25	2.22
k_4	1.07	1.55	0.08	0.90	3.90	3.78
k_5	2.97	1.37	3.84	0.90	2.50	6.50
k_6	1.71	1.62	8.02	0.90	4.93	9.54
k_7	1.07	1.61	13.08	0.90	0.11	13.45
k_8	2.82	10.01	18.21	0.90	6.90	18.63
k_9	9.31	2.75	21.29	0.90	12.10	21.06
Average	3.18	2.87	8.71	1.84	4.13	9.88

4.6.2.3 Results of parameter identification Problem Type-IIa (In longitudinal direction)

In this sub-section, identification study has been carried out using the response from simulated building (Problem Type-IIa) under excitation in longitudinal direction. This study is similar to that carried out in section-4.6.2.2 for excitation in transverse direction with a difference that in the present case sensors are assumed to be available at 1st, 5th and roof levels. Fig.4.77 and Fig.4.78 show the identified stiffness under NE EQ-1: Comp-longitudinal excitation and Fig.4.79 to Fig.4.80 show the identified stiffness under excitation NE EQ-2: Comp-longitudinal. The identified stiffness has been compared with the stiffness of the simulated model. The values of identified stiffness have been furnished in Table 4.25. The percentage error in identified stiffness from that of simulated model is furnished in Table 4.26. A 3D bar chart showing the percentage error in identified stiffness under both the earthquake excitations is given in Fig. 4.81.From the average percentage of errors furnished in Table 4.26, it is observed that the performance of Two-Stage EKF is best, followed by EKF and then by UKF.

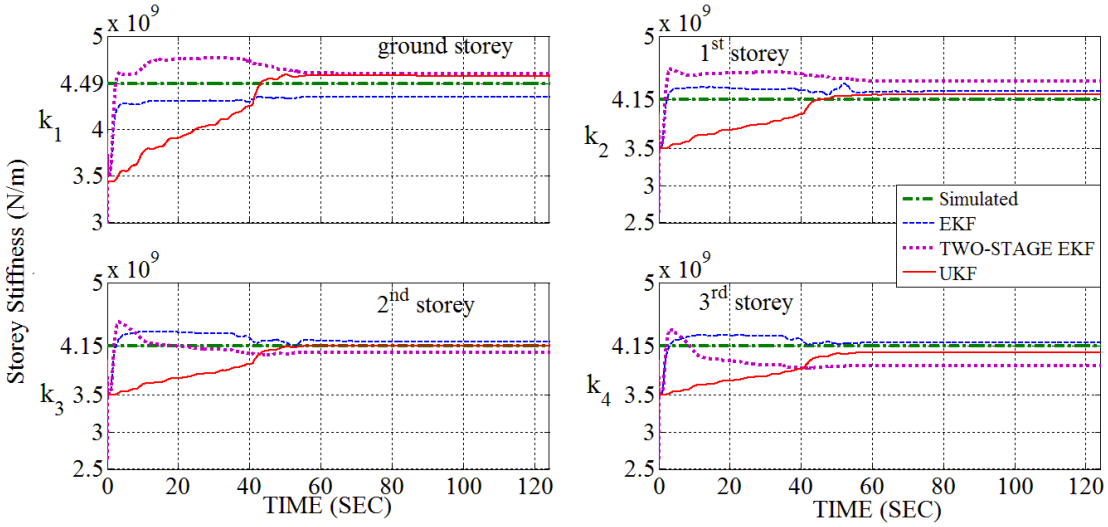

Fig.4.77: Identified stiffness *vs* simulated stiffness (ground storey to 3rd storey) of Problem Type-IIa under excitation NE EQ-1: Comp-longitudinal

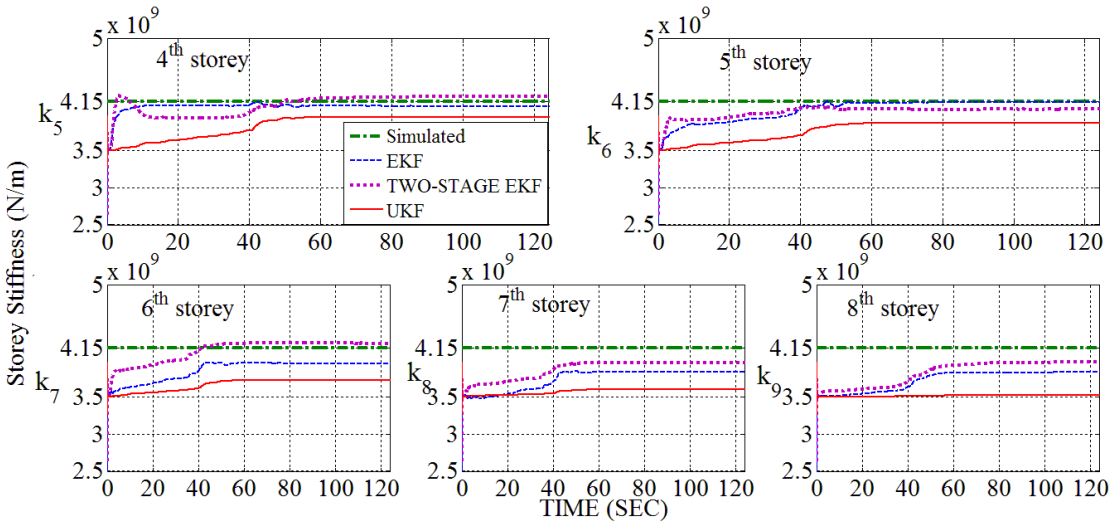

Fig.4.78: Identified stiffness *vs* simulated stiffness (4th to 8th storey) of Problem Type-IIa under excitation NE EQ-1: Comp-longitudinal

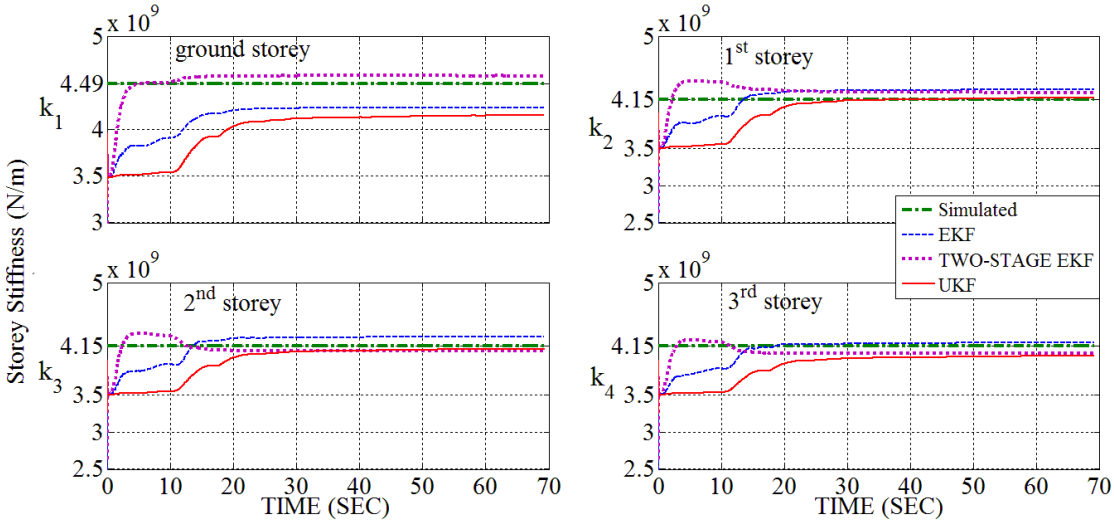

Fig.4.79: Identified stiffness *vs* simulated stiffness (ground storey to 3rd storey) of Problem Type-IIa under excitation NE EQ-2: Comp-longitudinal

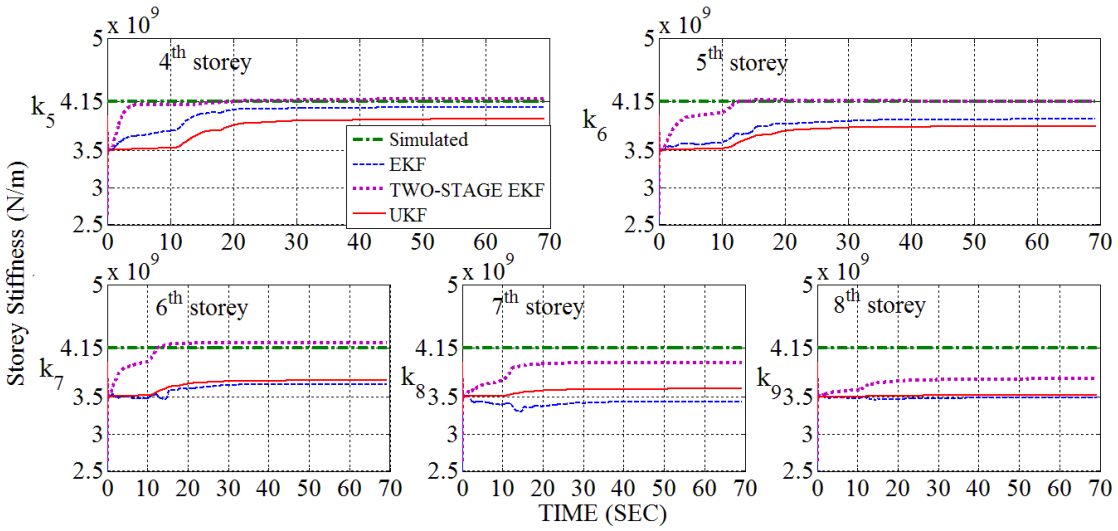

Fig.4.80: Identified stiffness *vs* simulated stiffness (4th to 8th storey) of Problem Type-IIa under excitation NE EQ-2: Comp-longitudinal

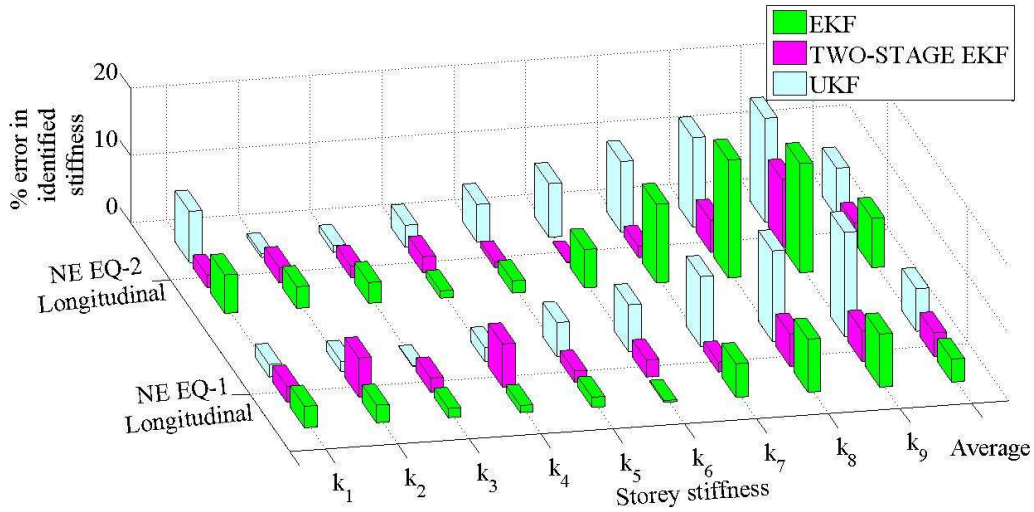

Fig. 4.81: 3D Bar Chart showing percentage error in identified stiffness of Problem Type-IIa using simulated response under excitations NE EQ-1: Comp-longitudinal and NE EQ-2: Comp-longitudinal

Table 4.25: Identified stiffness using simulated response of Problem Type-IIa under excitations NE EQ-1: Comp-longitudinal and NE EQ-2: Comp-longitudinal

Stiffness (N/m)	Value used for simulation	NE EQ-1 (Comp: Longitudinal)			NE EQ-2 (Comp: Longitudinal)		
		EKF	Two-Stage EKF	UKF	EKF	Two-Stage EKF	UKF
	x 10^9	x 10^9	x 10^9	x 10^9	x 10^9	x 10^9	x 10^9
k_1	4.49	4.35	4.60	4.57	4.23	4.57	4.15
k_2	4.15	4.26	4.39	4.21	4.28	4.24	4.17
k_3	4.15	4.21	4.06	4.15	4.28	4.08	4.11
k_4	4.15	4.19	3.88	4.06	4.19	4.05	4.01
k_5	4.15	4.09	4.22	3.94	4.07	4.19	3.92
k_6	4.15	4.14	4.05	3.86	3.91	4.15	3.82
k_7	4.15	3.94	4.21	3.72	3.67	4.22	3.72
k_8	4.15	3.82	3.95	3.59	3.43	3.95	3.60
k_9	4.15	3.82	3.96	3.51	3.48	3.74	3.51

Table 4.26: Percentage error of identified stiffness using simulated response of Problem Type-IIa under excitations NE EQ-1: Comp-longitudinal and NE EQ-2: Comp-longitudinal

Stiffness	NE EQ-1 (Comp: Longitudinal)			NE EQ-2(Comp: Longitudinal)		
	EKF	Two-Stage EKF	UKF	EKF	Two-Stage EKF	UKF
	Error percentage			Error percentage		
k_1	3.18	2.38	1.84	5.69	1.87	7.57
k_2	2.60	5.81	1.54	3.19	2.25	0.52
k_3	1.36	2.09	0.12	3.06	1.71	1.01
k_4	1.05	6.39	2.08	1.08	2.37	3.26
k_5	1.52	1.63	5.04	1.81	0.85	5.59
k_6	0.28	2.51	6.92	5.69	0.09	7.92
k_7	4.97	1.46	10.34	11.64	1.64	10.42
k_8	7.85	4.81	13.39	17.42	4.75	13.20
k_9	7.86	4.56	15.37	16.14	9.96	15.32
Average	3.41	3.52	6.29	7.30	2.83	7.20

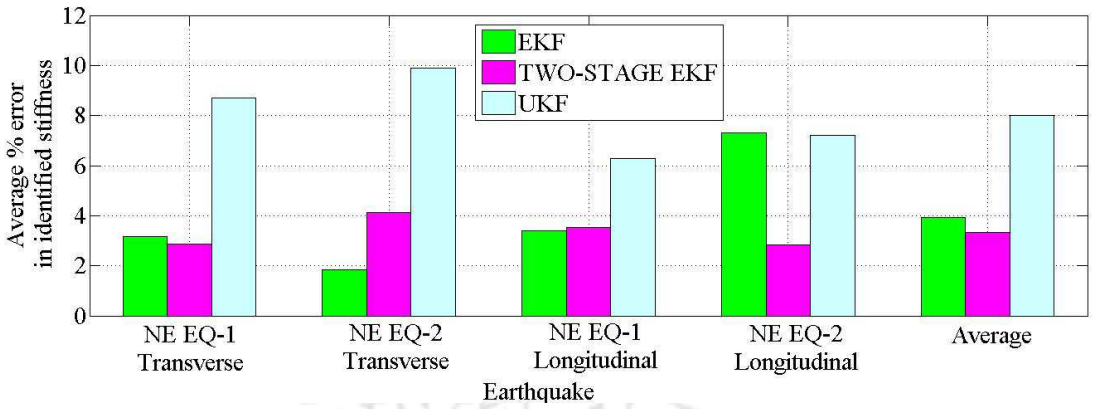

Fig. 4.82: 2D Bar Chart showing average percentage error in identified stiffness of Problem Type-IIa using simulated response under excitations NE EQ-1: Comp-longitudinal and NE EQ-2: Comp-longitudinal

The 2D bar chart of Fig. 4.82, shows the average percentage of errors in identified stiffness for Problem Type-IIa under excitation in both transverse and longitudinal direction. It is concluded that the performance of Two-Stage EKF is the best followed by EKF. The performance of UKF is worst among the three algorithms.

4.6.2.4 Results of parameter identification Problem Type-IIb (In Transverse direction)

The Problem Type-IIb is similar to Problem Type-IIa as described in section-4.6.2.2 with the exception that in Problem Type-IIb, identification has been carried out using acquired field responses. Fig.4.83and Fig.4.84 show the identified stiffness under excitation NE EQ-1: Comp-transverse and Fig.4.85 and Fig.4.86 show the identified stiffness under excitation NE EQ-2: Comp-transverse. The values of identified stiffness have been furnished in Table 4.27. A 3D bar chart showing the percentage error in identified stiffness under both the earthquake excitations is shown in Fig. 4.87. From the identified values of stiffness (Table 4.27), it is observed that the performance of all these algorithms is comparable.

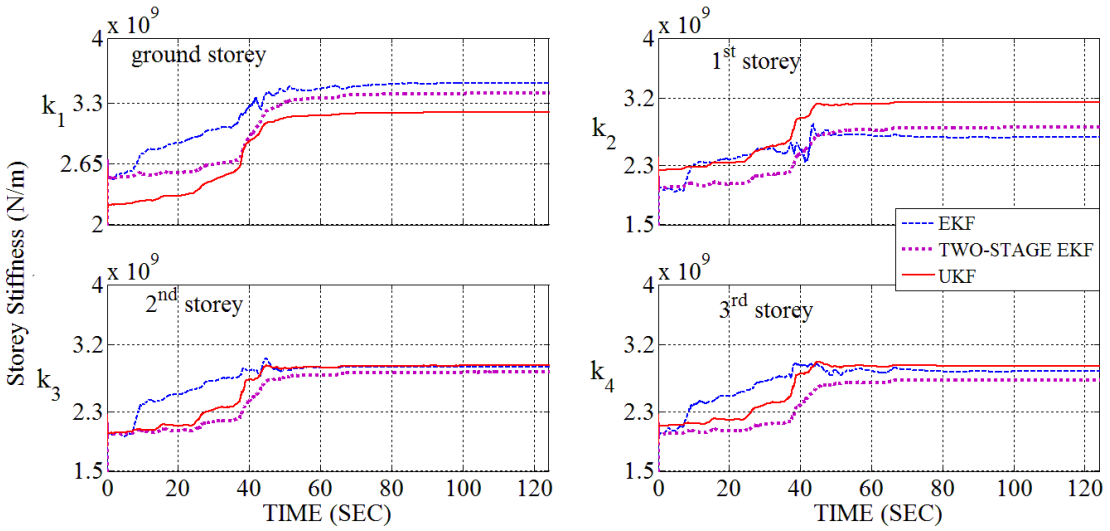

Fig.4.83: Comparison of identified stiffness (ground storey to 3rd storey) obtained using different algorithms, for Problem Type-IIb under excitation NE EQ-1: Comp-transverse

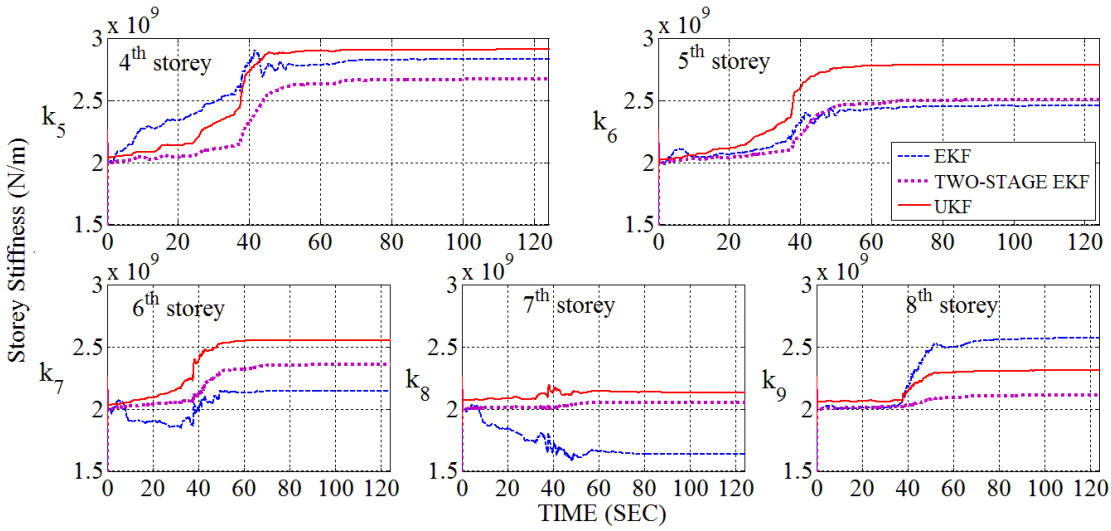

Fig.4.84: Comparison of identified stiffness (4th to 8th storey) obtained using different algorithms, for Problem Type-IIb under excitation NE EQ-1: Comp-transverse

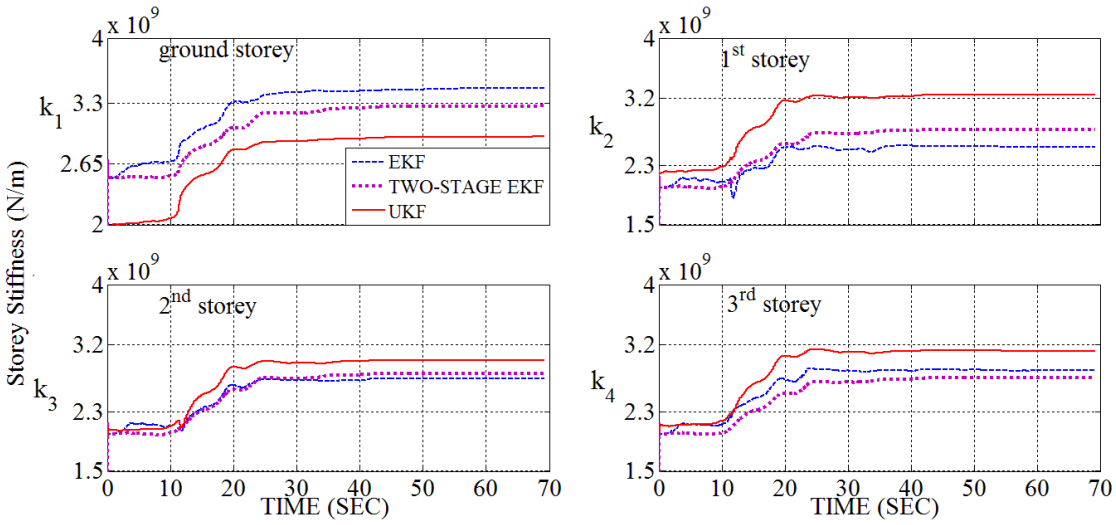

Fig.4.85: Comparison of identified stiffness (ground storey to 3rd storey) obtained using different algorithms, for Problem Type-IIb under excitation NE EQ-2: Comp-transverse

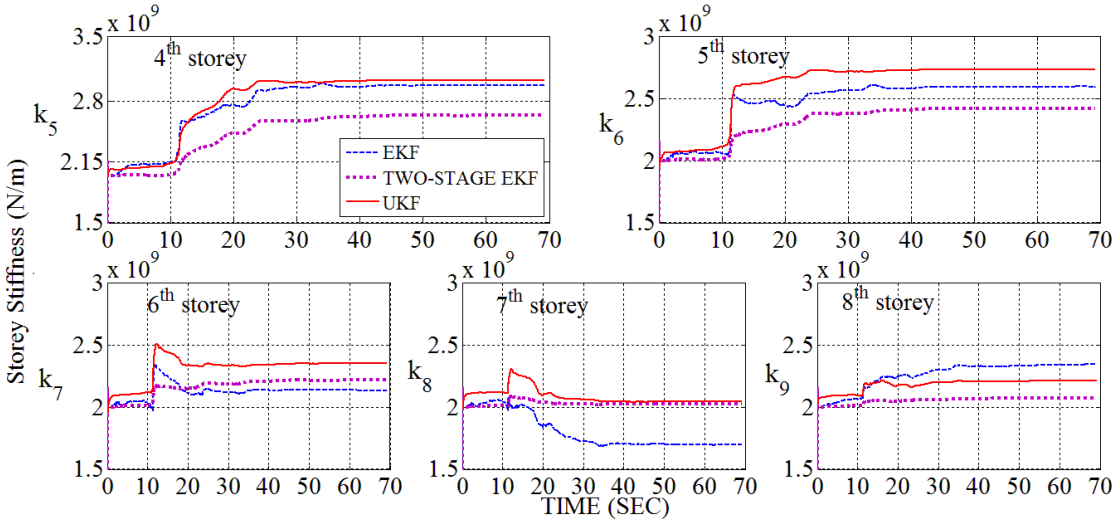

Fig.4.86: Comparison of identified stiffness (4th to 8th storey) obtained using different algorithms, for Problem Type-IIb under excitation NE EQ-2: Comp-transverse

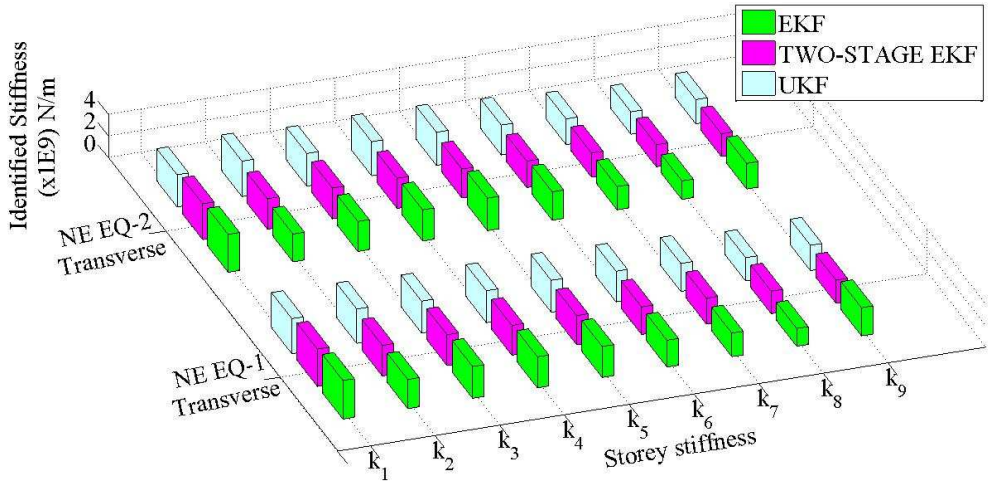

Fig. 4.87: 3D Bar Chart showing identified storey stiffness for Problem Type-IIb under excitations NE EQ-1: Comp-transverse and NE EQ-2: Comp-transverse

Table 4.27: Identified stiffness using field response for Problem Type-IIb under excitations NE EQ-1: Comp-transverse and NE EQ-2: Comp-transverse

Stiffness (N/m)	NE EQ-1 (Comp: Transverse)			NE EQ-2 (Comp: Transverse)		
	EKF	Two-Stage EKF	UKF	EKF	Two-Stage EKF	UKF
	x 10^9	x 10^9	x 10^9	x 10^9	x 10^9	x 10^9
k_1	3.52	3.41	3.21	3.46	3.27	2.94
k_2	2.67	2.80	3.14	2.54	2.78	3.24
k_3	2.90	2.82	2.91	2.74	2.81	2.99
k_4	2.84	2.72	2.91	2.85	2.75	3.11
k_5	2.83	2.67	2.91	2.97	2.65	3.03
k_6	2.45	2.51	2.79	2.59	2.42	2.73
k_7	2.15	2.36	2.55	2.13	2.21	2.35
k_8	1.63	2.05	2.13	1.69	2.02	2.04
k_9	2.57	2.11	2.31	2.34	2.07	2.21

4.6.2.5 Results of parameter identification Problem Type-IIb (In Longitudinal direction)

In this sub-section, identification study using acquired field responses has been carried out for Problem Type-IIb in longitudinal direction. Fig.4.88 and Fig.4.89 show the identified

stiffness under NE EQ-1: Comp-longitudinal excitation and Fig.4.90 and Fig.4.91 show the identified stiffness under excitation NE EQ-2: Comp-longitudinal. The values of identified stiffness have been furnished in Table 4.28. A 3D bar chart showing the percentage error in identified stiffness under both the earthquake excitations is shown in Fig. 4.92. From the identified values of stiffness (Table 4.28), it is observed that the performance of all these algorithms is comparable.

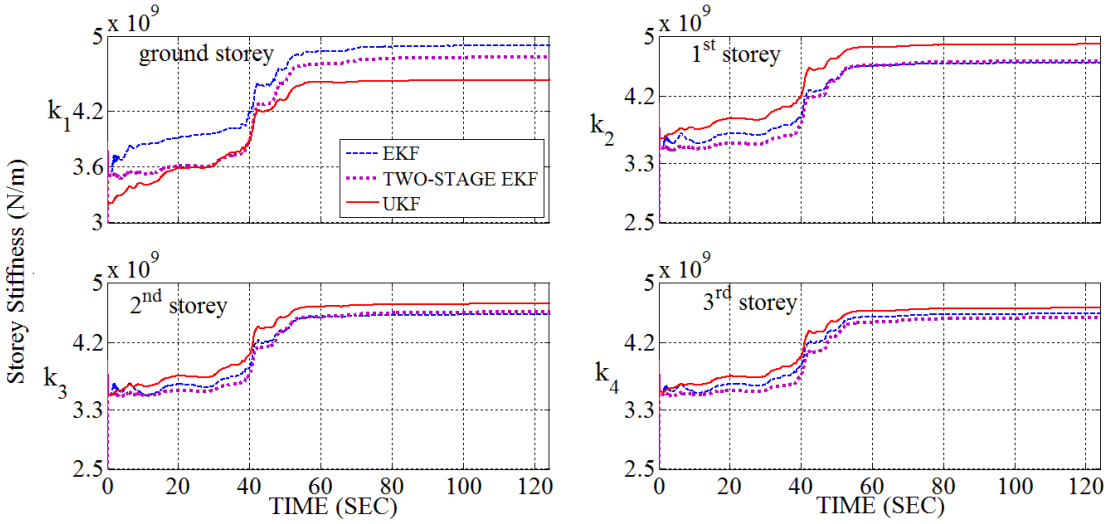

Fig.4.88: Comparison of identified stiffness (ground storey to 3rd storey) obtained using different algorithms, for Problem Type-IIb under excitation NE EQ-1: Comp-longitudinal

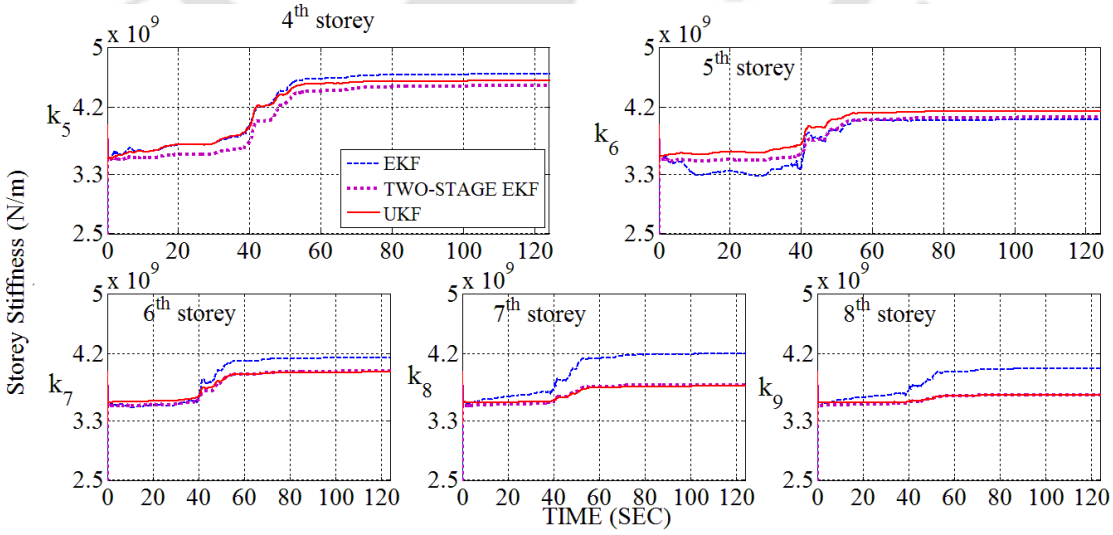

Fig.4.89: Comparison of identified stiffness (4th to 8th storey) obtained using different algorithms, for Problem Type-IIb under excitation NE EQ-1: Comp-longitudinal

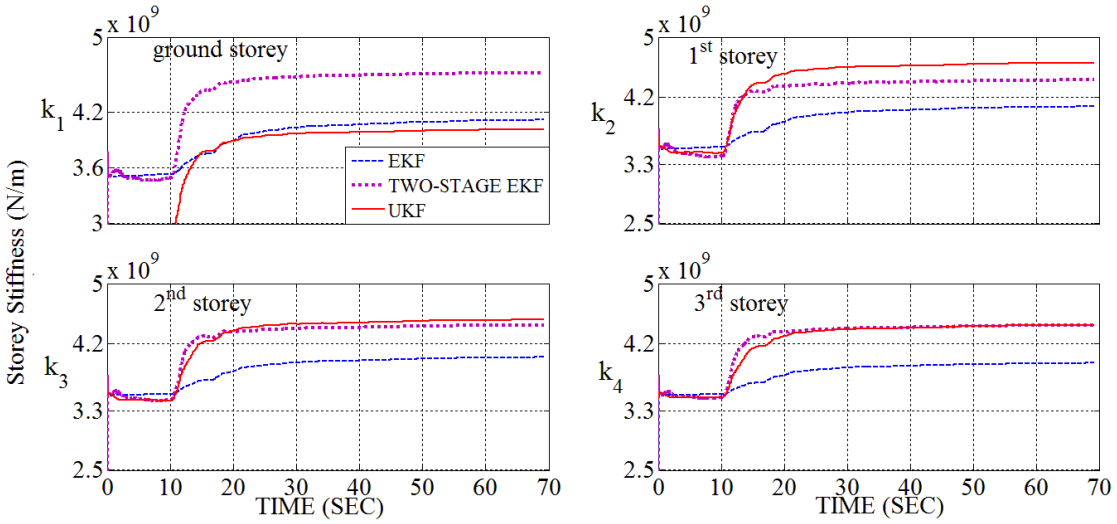

Fig.4.90: Comparison of identified stiffness (ground storey to 3rd storey) obtained using different algorithms, for Problem Type-IIb under excitation NE EQ-2: Comp-longitudinal

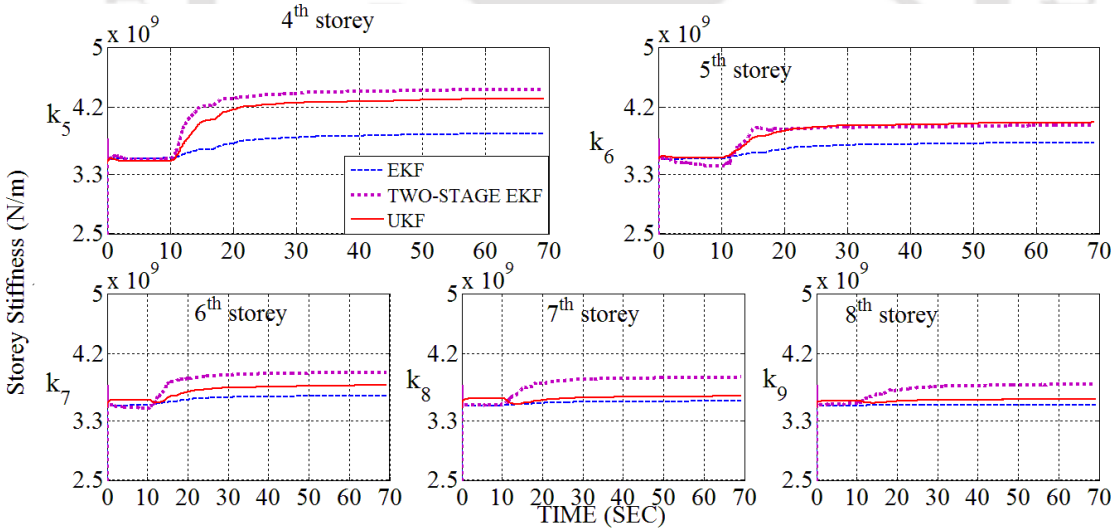

Fig.4.91: Comparison of identified stiffness (4th to 8th storey) obtained using different algorithms, for Problem Type-IIb under excitation NE EQ-2: Comp-longitudinal

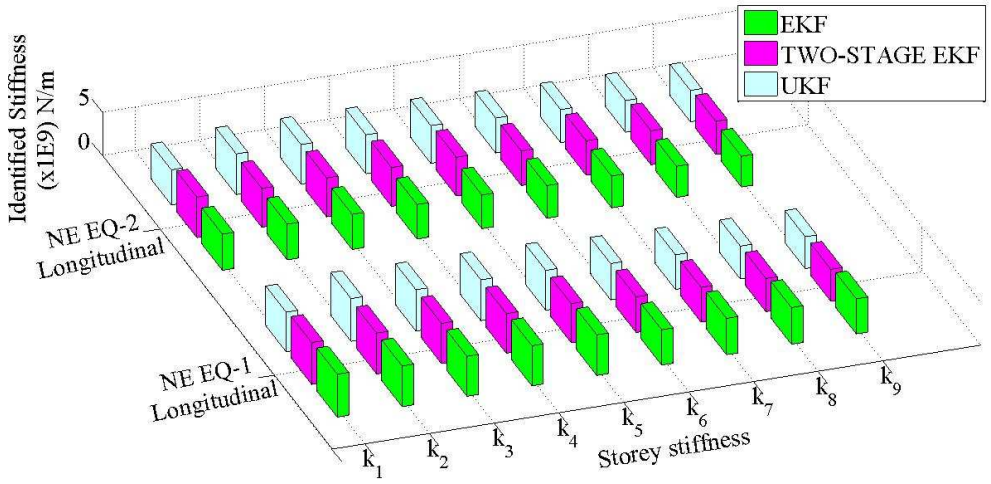

Fig. 4.92: 3D Bar Chart showing identified storey stiffness for Problem Type-IIb under excitations NE EQ-1: Comp-longitudinal and NE EQ-2: Comp-longitudinal

Table 4.28: Identified stiffness using field response for Problem Type-IIb under excitations NE EQ-1: Comp-longitudinal and NE EQ-2: Comp-longitudinal

Stiffness (N/m)	NE EQ-1 (Comp: Longitudinal)			NE EQ-2 (Comp: Longitudinal)		
	EKF	Two-Stage EKF	UKF	EKF	Two-Stage EKF	UKF
	x 10^9	x 10^9	x 10^9	x 10^9	x 10^9	x 10^9
k_1	4.90	4.78	4.53	4.12	4.62	4.01
k_2	4.64	4.67	4.89	4.07	4.43	4.65
k_3	4.57	4.60	4.71	4.01	4.44	4.52
k_4	4.58	4.53	4.66	3.94	4.44	4.45
k_5	4.64	4.48	4.55	3.84	4.43	4.31
k_6	4.03	4.06	4.14	3.72	3.95	3.99
k_7	4.14	3.96	3.95	3.63	3.94	3.77
k_8	4.19	3.78	3.76	3.56	3.88	3.62
k_9	4.00	3.64	3.64	3.51	3.78	3.58

4.6.2.6 Results of parameter identification obtained from simulated and field studies for the case of three-storey conventional (Problem Type-III) with missing sensor(in transverse direction)

In this sub-section, identifications of stiffness of the simulated building (Problem Type-IIIa) and the existing building (Problem Type-IIIb) have been carried out under excitation in transverse direction. In the existing building, sensors are available only at ground floor and roof levels. There are missing sensors at 1st and 2nd floor levels. In the identification study involving Problem Type-IIIa, simulated response at ground floor and roof levels are only considered to replicate the scenario of missing sensors as exists in the field building. Fig.4.93 shows the identified stiffness under excitation NE EQ-3: Comp-transverse for Problem Type-IIIa, where as Fig.4.94 shows the result for Problem Type-IIIb.

For the case of Problem Type-IIIa, the identified stiffness has been compared with the stiffness of the simulated model. The values of identified stiffness and the percentage error in identified stiffness are furnished in Table 4.29.2D Bar Chart showing the percentage error in identified stiffness for all floor levels for Problem Type-IIIa is presented in Fig. 4.30. It is observed that the average percentage error is the least for Two-Stage EKF. Therefore, it can be concluded that the performance of Two-Stage EKF is the best, followed by EKF and then by UKF algorithms.

In case of Problem Type-IIIb, the values of identified stiffness are furnished in Table 4.30. Fig. 4.96 shows the values of identified stiffness of all storeys in form of 2D Bar Chart. From the average values of identified stiffness using different algorithms, it is observed that the performance of these algorithms is comparable.

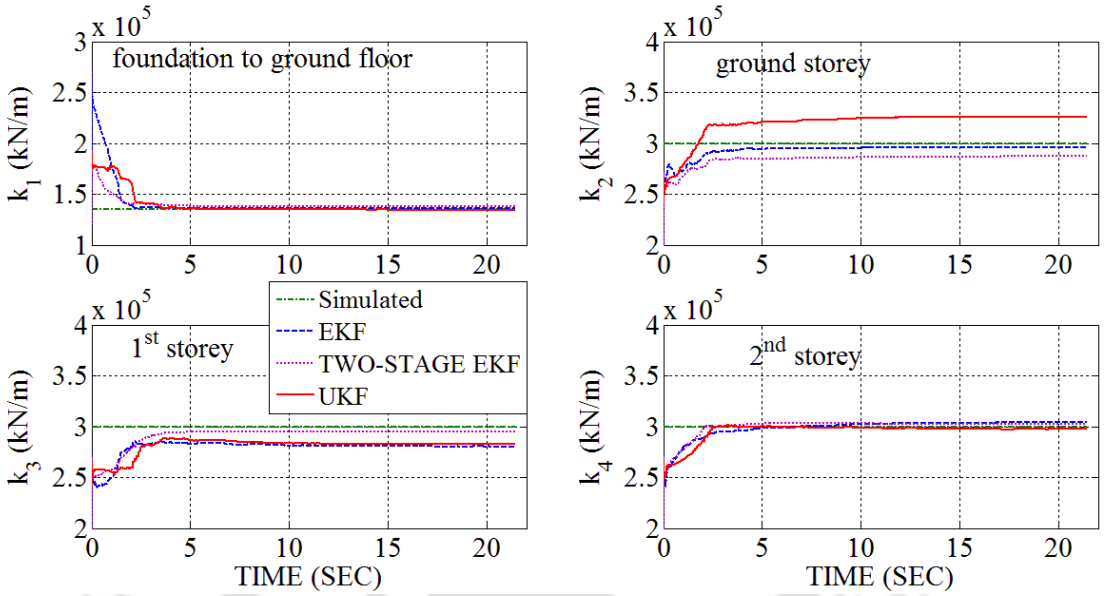

Fig.4.93: Identified stiffness *vs* simulated stiffness of three-storey conventional (Twin building), Problem Type-IIIa under excitation NE EQ-3: Comp-transverse

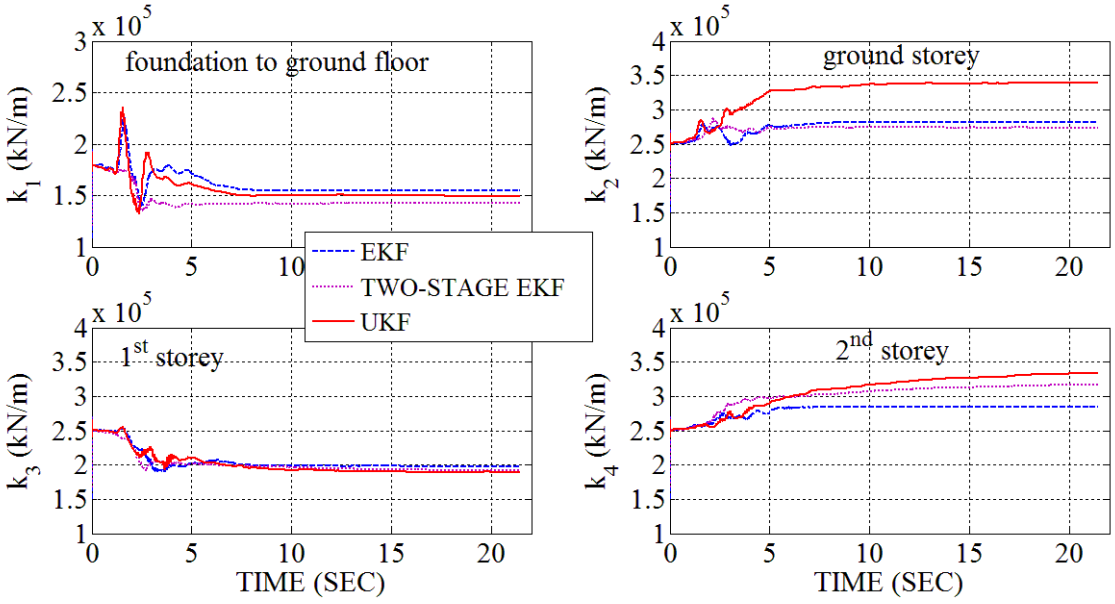

Fig.4.94: Identified stiffness for three-storey conventional (Twin building), Problem Type-IIIb under excitation NE EQ-3: Comp-transverse

Table 4.29: Identified stiffness and percentage error in identification of three-storey conventional (Twin building), Problem Type-IIIa under excitation NE EQ-3: Comp-transverse

Storey Stiffness (kN/m)	Assumed in simulation	Identified Values			% error in identified values		
		EKF	Two-Stage EKF	UKF	EKF	Two-Stage EKF	UKF
	x 10^5	x 10^5	x 10^5	x 10^5			
k_1	1.35	1.36	1.38	1.35	0.94	2.04	0.34
k_2	3.00	2.96	2.87	3.26	1.44	4.30	8.61
k_3	3.00	2.80	2.95	2.83	6.56	1.61	5.77
k_4	3.00	3.05	3.03	2.97	1.53	0.83	0.87
Average= $(k_1+k_2+k_3+k_4)/4$					2.62	2.20	3.90

Table 4.30: Identified stiffness of three-storey conventional (Twin building), Problem Type-IIIb under excitation NE EQ-3: Comp-transverse

Stiffness (kN/m)	EKF	Two-Stage EKF	UKF
	x 10^5	x 10^5	x 10^5
k_1	1.54	1.42	1.49
k_2	2.81	2.73	3.39
k_3	1.98	1.91	1.89
k_4	2.84	3.17	3.34
Average= $(k_1+k_2+k_3)/3$	2.55	2.61	2.87

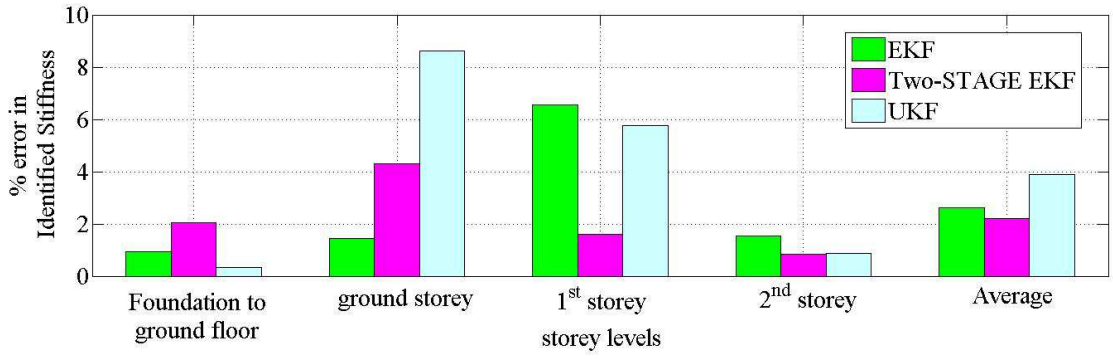

Fig. 4.95: 2D Bar Chart showing percentage error in identified stiffness of three-storey conventional (Twin building), Problem Type-IIIa under excitation NE EQ-3: Comp-transverse

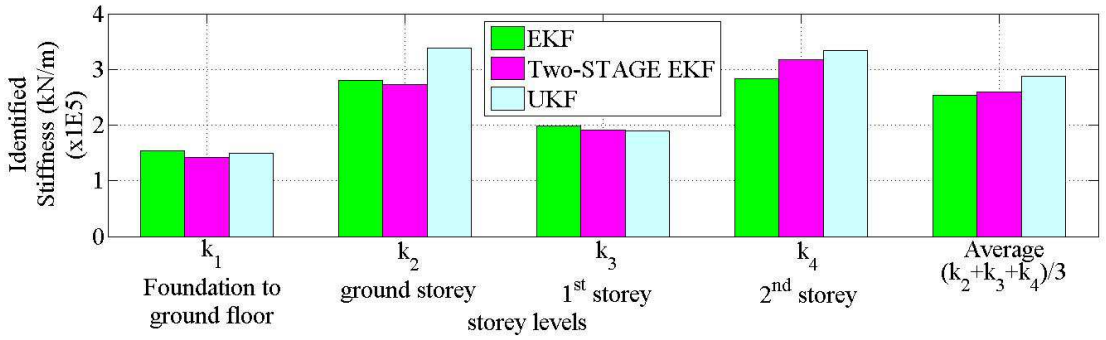

Fig. 4.96: 2D Bar Chart showing identified stiffness of three-storey conventional (Twin building), Problem Type-IIIb under excitation NE EQ-3: Comp-transverse

4.7 Concluding Remarks

In Problem Type-I, SNLSE-UI-UO algorithm has also been used in addition to EKF, Two-Stage EKF and UKF. The performance of SNLSE-UI-UO is relatively poorer than Kalman Filter based algorithms. The identified displacement diverges if SNLSE-UI-UO is used for noise contaminated response. Presence of noisy response is creating this divergence issue. Therefore, filtered response data is used for SNLSE-UI-UO algorithm. In the case of stiffness identification, it is observed that the error in identification of stiffness by all these algorithms is quite comparable. The performances of Two-Stage EKF and UKF are quite consistent at all noise level.

The SNLSE-UI-UO algorithm is found to be not performing well in case of more than one missing sensor and hence it is not continued further for Problem Type-II and III, which are cases of large number of missing sensors.

For state identification of Problem Type-IIa, it is observed from the average RMSE, that the performance of Two-Stage EKF is the best followed by EKF and UKF. In case of parameter identification, the performance of Two-Stage EKF is found to be best considering the average percentage error in identified stiffness. The number of missing sensors in longitudinal direction is more than that of transverse direction. Even with increasing number of missing sensors, the performance of Two-Stage EKF is observed to be best. Similar observations are also found in case of Problem Type-III.

The study on comparative performance of the considered algorithms with respect to identification of state and parameter of fixed base building has been carried out using

Problem Types as defined in Table 4.1. A comprehensive summary of the identification study using the considered algorithms for all the discussed Problem Types are presented in Table 4.31. Rank 1 is defined for best performance, while Rank 4 is for least performance and Rank 2 and Rank 3 stands for intermediate performance level.

Table 4.31: Result of state and parameter identification for different considered problem types showing rank as per their performances

Problem Type	Criteria	State / Parameter	EKF	Two-Stage EKF	UKF	SNLSE-UI-UO
I	Increasing noise level	state	1	2	3	4
		parameter	3	2	1	4
II	Increasing number of missing sensors for a large structure	state	2	1	3	-
		parameter	2	1	3	-
III	Missing sensors in small structure	state	2	1	3	-
		parameter	2	1	3	-

Thus, it can be concluded that

- Kalman Filter based algorithms such as EKF, Two-Stage EKF as well as UKF can handle noise contaminated response data quite well. In case of LSE based algorithms such as SNLSE-UI-UO, noisy response is required to be filtered prior to its use in the identification algorithm.
- Kalman Filter based algorithms can work in an environment of multiple missing sensor. The performance degrades with increasing number of missing sensor. Performance of LSE based algorithms such as SNLSE-UI-UO drastically deteriorates with more than one number of missing sensor.
- For state identification with availability of all sensor data, EKF, Two-Stage EKF as well as UKF are found to be suitable, even when that data are contaminated with high level of noise. The performance of SNLSE-UI-UO algorithm is far more inferior than all the considered Kalman Filter based algorithms.
- For parameter identification with noisy response and with the availability of all sensor measurements, the performance of UKF is consistent for data with all the noise levels.
- For state identification with large number of missing sensors, the performance of Two-Stage EKF is found to be the best. The performance of Two-Stage EKF is 2nd best followed by that of UKF.
- For parameter identification with large number of missing sensors, Two-Stage EKF is found to be performing the best, followed by UKF and finally by EKF algorithm.

Chapter 5

Evaluation of state and structural parameters of multi-storey base-isolated building system

5.1 Introduction

In this chapter, identification of state and structural parameters of a SREI supported base-isolated (BI) building system have been carried out using different identification algorithms such as EKF, Two-Stage EKF and UKF. Identification of state and parameters are carried out on a simulated model of three-storey BI building and then the study is extended to an existing three-storey BI building. Influences of limited sensors on the performance of these algorithms have also been studied. Further, study has been carried out on the simulated model with missing sensor at ground floor level. The floor slab level above the base isolators denotes the ground floor level. Finally, comparative studies on the performances of different identification algorithms have been presented. Identification using SNLSE-UI-UO has not been carried out on BI building system due to the difficulties already pointed out in chapter-4, section 4.6.1.2.

5.2 Modelling the three-storey base-isolated building

In this chapter, a three-storey BI building supported on SREI has been considered. The building is analysed by considering an idealized two dimensional (2D) shear frame model having lumped masses at different floor levels. Only one horizontal dof has been considered at each floor level. The simulation of the numerical model has been carried out in MATLAB. The stiffness and damping parameters of the numerical model have been evaluated from the geometry and material properties of the building and are furnished in Table 4.3. The conventional Bouc-Wen model as given by Eq. **(5.22**) has been adopted to simulate the load-displacement behaviour of the SREI based base isolation system. Depending on the availability of sensors, added noise level in the response from simulated building and source of data, the considered problems for identification are grouped as shown in

Table 5.1. Identification study of the building based on simulated responses corresponding to different cases of sensor availability has been grouped under type-*S* where, *S* defines *Simulation* based model. The same building when identified using recorded responses as obtained from installed sensors is defined as type-*F* where, *F* defines *Field* model. The details of modelling of the BI building system have been taken up in the next sub-section.

Table 5.1: Different types of considered identification problems

Description	Type	Sensor Location	Noise consideration
Simulated three-storey BI building	*S*1	Sensor in all floors	No noise considered
	*S*2	Sensor missing at 1st floor level and 2nd floor level.	No noise considered
	*S*3	Sensor missing at ground floor level and 2nd floor level.	1% added Gaussian white noise
Existing three-storey BI building	*F*	Sensor missing at 1st floor level and 2nd floor level.	Field data used

5.2.1 Description of the base-isolated three-storey simulated building

The structural parameters like mass and stiffness of the simulated building (Type-*S* problems) have been evaluated from the available geometry and material properties. The evaluated parameters (Table 4.3) provide an initial guess for the identification algorithms. The horizontal stiffness of the isolator has been adopted from the available force-displacement test result of the manufacturer.

The simulated responses are generated by utilising the parameters of Table 4.3 and Table 5.3 and using the ground excitation as furnished in Table 5.4**.** The generated acceleration responses are used for identification study by the considered identification algorithms. The detailed study is presented in this chapter.

Table 5.2: Structural parameters considered for the simulation model for excitation in transverse direction.

Storey	Storey Stiffness (kN/m)		Storey Height (m)		Mass (M.T.)	
Ground	k_1	3.0E+005	$\hat{h}_1$	3.00	m_1	22.641
1st	k_2	3.0E+005	$\hat{h}_2$	3.00	m_2	22.641
2nd	k_3	3.0E+005	$\hat{h}_3$	3.00	m_3	20.907

Table 5.3: Parameters considered for the isolator model for excitation in shorter direction.

Parameter	k_b	m_b	α	β	γ
Unit	kN/m	M.T.	Unit less		
Adopted parameter values	7200	15.682	1	2	0.5

Table 5.4: Characteristics of the selected earthquake records for the 3-storey BI building

Earthquake excitations	Date	Peak Ground Acceleration (g)	Frequency Range (rad/sec)
El Centro (1940): Comp - 180	18 May, 1940	0.320	0-65
NE EQ-3: Comp-transverse	10 Sept, 2006	0.003	0-170

5.2.2 Description of the existing base-isolated three-storey building

Two numbers of three-storey prototype reinforced concrete framed buildings located at IIT Guwahati is considered for the present study. One of the buildings is conventional FB building while the other building is supported on four numbers of base isolators. Both the buildings are identical in plan and elevation. The BI building is supported on lead plug bearings, comprising of alternate layers of rubber and steel shims with a central lead core. The details of the buildings along with their photograph are already described in section 4.4 of chapter 4. In chapter 4, FB buildings have been considered for the system identification study. In this chapter, the BI building (Type-*F* problem) is considered for the identification of state and parameters of building.

Sensors were installed at ground floor and roof level of the building. The two consecutive intermediate floors (1stand 2nd floor) had missing sensors. The placement of sensors at different floor levels has already been shown in Fig. 4.4 and 4.5 of chapter 4. The table showing sensor location has been repeated here for convenience and presented in Table 4.7. Instrumentation of the building and acquisition of its acceleration responses, following seismic events were carried out by previous researchers [Nath R.J. *et al.* (2013)]. In the present study, identification of state and parameters of the BI building have been carried out by the considered algorithms using the field measured sensor data.

Table 5.5: Sensor locations at different floor levels of the twin building

Conventional Building			Base-isolated Building	
Floor	Sensor		Floor	Sensor
Ground Floor	*x, y*		Ground Floor	*x, y, z*
1st Floor	No sensor		1st Floor	No sensor
2nd Floor	No sensor		2nd Floor	No sensor
Roof	*x, y*		Roof	*x, y*

where, *x*-direction is the longitudinal direction.

5.2.3 Governing equation of motion of the multi-storey base-isolated building

Naiem and Kelly (1999) provided details of seismic isolation based on two-mass structural model and further extended it for multi-storey BI building systems. In this sub-section, a concise review of the original formulation of Naiem and Kelly (1999) has been carried out. The originally proposed model of BI multi-storey building by Naiem and Kelly (1999) considered linear spring model of base isolation system as well as linear model for the building supported on the isolation system. In the present study, the linear spring model is replaced by the nonlinear hysteretic Bouc-Wen model to represent SREI. This modification has been introduced in line with Nezhad *et al.* (2008a), where nonlinear hysteretic model as proposed by Naiem and Kelly (1999) were incorporated for FREI supported structural system. Therefore, the final model that has been achieved after incorporating the modifications fits into the requirement of the considered identification algorithms. However, if the response of ground floor level is missing, identification cannot be carried out using the present form of the model. Available literature does not speak on this issue of missing sensor at floor slab located just above the isolator. Thus, in order to deal with this problem, further modification has been carried out in the model of seismic isolation system. The complete details of the formulation are presented in the following paragraphs.

The theory based on two-mass structural model is shown in Fig. 5.1. The mass of the superstructure is represented by m and m_b is mass of the base slab above the isolation system. The structural stiffness and damping is represented by k_s and c_s respectively. The stiffness and damping of the isolator are k_b and c_b respectively. Absolute displacements of the two masses are denoted by v_b and v_s, whereas the ground displacement is denoted by x_g. It will be convenient to express the displacements in terms of relative displacements as

$$x_b = v_b - x_g \tag{5.1}$$

$$u_s = v_s - v_b \tag{5.2}$$

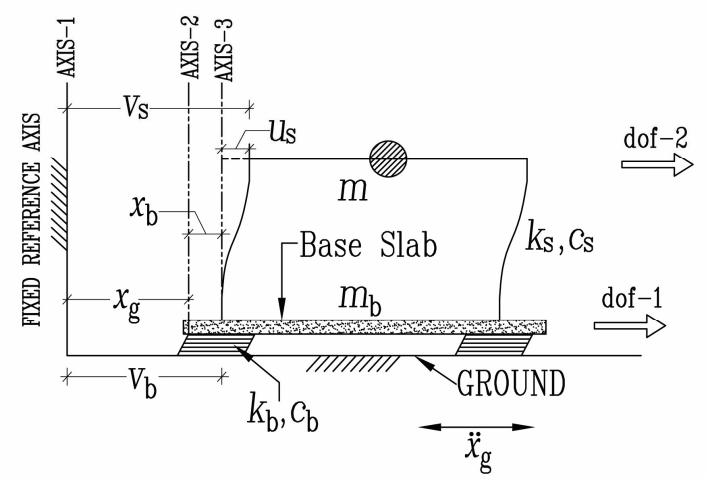

Fig. 5.1: Two degrees of freedom BI building system [Naiem and Kelly (1999)]

The basic equations of motion of 2-dof model are

$$(m+m_b)\ddot{x}_b + m\ddot{u}_s + c_b\dot{x}_b + k_b x_b = -(m+m_b)\ddot{x}_g \tag{5.3}$$

and

$$m\ddot{v}_s + c_s\dot{u}_s + k_s u_s = 0 \tag{5.4}$$

Eq. (5.4) can be expressed using Eq.(5.1), (5.2) and (5.4) as

$$m\left(\ddot{x}_g + \ddot{x}_b + \ddot{u}_s\right) + c_s\dot{u}_s + k_s u_s = 0 \tag{5.5}$$

Further simplification of the above equation gives

$$m\ddot{x}_b + m\ddot{u}_s + c_s\dot{u}_s + k_s u_s = -m\ddot{x}_g \tag{5.6}$$

Eq.(5.3) and (5.6) can be written in matrix notation as

$$\begin{bmatrix} m+m_b & m \\ m & m \end{bmatrix}\begin{Bmatrix} \ddot{x}_b \\ \ddot{u}_s \end{Bmatrix} + \begin{bmatrix} c_b & 0 \\ 0 & c_s \end{bmatrix}\begin{Bmatrix} \dot{x}_b \\ \dot{u}_s \end{Bmatrix} + \begin{bmatrix} k_b & 0 \\ 0 & k_s \end{bmatrix}\begin{Bmatrix} x_b \\ u_s \end{Bmatrix} = -\begin{bmatrix} m+m_b & m \\ m & m \end{bmatrix}\begin{Bmatrix} 1 \\ 0 \end{Bmatrix}\ddot{x}_g \tag{5.7}$$

Eq.(5.7) can be expressed in matrix form as

$$\boldsymbol{M\ddot{u} + C\dot{u} + Ku = -M\eta\ddot{x}_g} \tag{5.8}$$

where, $\boldsymbol{\eta}$ is excitation influence vector.

The 2-dof linear model of Eq.(5.8) can be extended to BI multi-storey building system. Prior to extending the 2-dof model to multi-storey BI model, the equation of motion of

conventional building (Fig. 5.2) has been formulated. The building is modelled as 2D shear building with each floor slab being considered to be behaving like a rigid diaphragm. There is only one horizontal dof at each storey level with lumped masses m_1, m_2 and m_3. The inter-storey stiffness are k_1, k_2 and k_3 and storey heights are $\hat{h}_1, \hat{h}_2 \text{and} \hat{h}_3$.

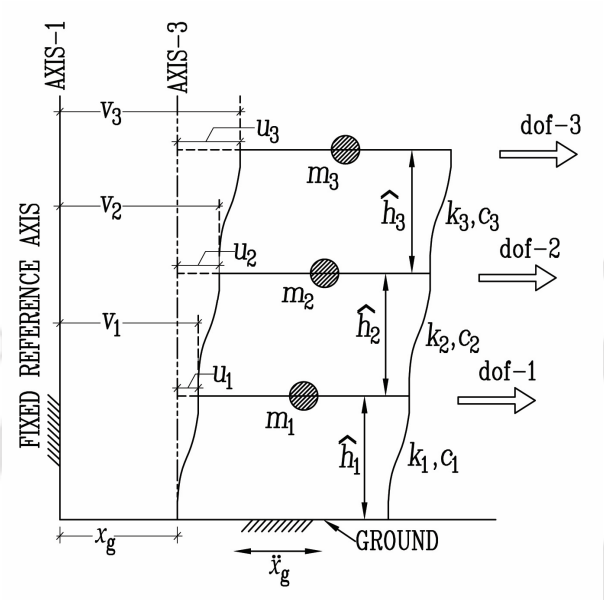

Fig. 5.2: Three storey conventional building

$$\boldsymbol{M\ddot{u} + C\dot{u} + Ku = -\eta' M\ddot{x}_g} \tag{5.9}$$

where, $\boldsymbol{\eta'}$ is excitation influence matrix

$$\boldsymbol{M} = \begin{bmatrix} m_1 & 0 & 0 \\ 0 & m_2 & 0 \\ 0 & 0 & m_3 \end{bmatrix} \tag{5.10}$$

$$\boldsymbol{K} = \begin{bmatrix} k_1 + k_2 & -k_2 & 0 \\ -k_2 & k_2 + k_3 & -k_3 \\ 0 & -k_3 & k_3 \end{bmatrix} \tag{5.11}$$

$$\boldsymbol{C} = \begin{bmatrix} c_1 + c_2 & -c_2 & 0 \\ -c_2 & c_2 + c_3 & -c_3 \\ 0 & -c_3 & c_3 \end{bmatrix} \tag{5.12}$$

$$\boldsymbol{\eta'} = \begin{bmatrix} 1 & 0 & 0 \\ 0 & 1 & 0 \\ 0 & 0 & 1 \end{bmatrix} \tag{5.13}$$

$$\boldsymbol{u} = \{u_1 \quad u_2 \quad u_3\}^T \tag{5.14}$$

$$\dot{\boldsymbol{u}} = \{\dot{u}_1 \quad \dot{u}_2 \quad \dot{u}_3\}^T \tag{5.15}$$

$$\ddot{\boldsymbol{u}} = \{\ddot{u}_1 \quad \ddot{u}_2 \quad \ddot{u}_3\}^T \tag{5.16}$$

To generate the model of multi-storey BI building system, the conventional building as shown in Fig. 5.2 and represented by Eq.(5.9) is superimposed on a base isolation system with horizontal stiffness k_b and damping c_b. The isolator stiffness k_b represents the total horizontal stiffness of the four isolators used in the building. A base slab of mass m_b is placed just above the base isolators. The combined system consisting of the three-storey conventional building superimposed over the base isolation system is shown in Fig. 5.3.

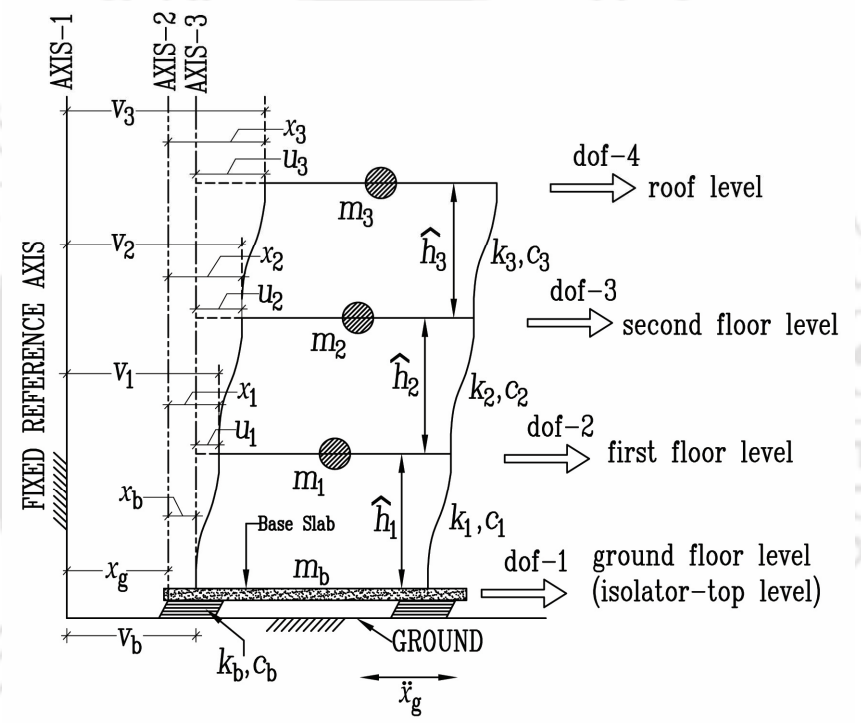

Fig. 5.3: Three storey BI building

The governing equation of motion can be written as

$$\boldsymbol{M}\ddot{\boldsymbol{u}} + \boldsymbol{C}\dot{\boldsymbol{u}} + \boldsymbol{K}\boldsymbol{u} = -\boldsymbol{\eta}'\boldsymbol{M}\left(\ddot{x}_g + \ddot{x}_b\right) \tag{5.17}$$

The equation of motion of the BI building along with the base slab has been derived in a similar manner as has been carried out for 2-dof BI building system Eq.(5.7) and is detailed below.

$$(m_b + m_1 + m_2 + m_3)\ddot{v}_b + m_1\ddot{u}_1 + m_2\ddot{u}_2 + m_3\ddot{u}_3 + c_b\dot{x}_b + k_b x_b = 0$$

or, $(m_b + m_1 + m_2 + m_3)\ddot{x}_b + m_1\ddot{u}_1 + m_2\ddot{u}_2 + m_3\ddot{u}_3 + c_b\dot{x}_b + k_b x_b$

$= -(m_b + m_1 + m_2 + m_3)\ddot{x}_g$

or, $\acute{m}\ddot{x}_b + m_1\ddot{u}_1 + m_2\ddot{u}_2 + m_3\ddot{u}_3 + c_b\dot{x}_b + k_b x_b = -\acute{m}\ddot{x}_g$ (5.18)

where,

$\acute{m} = m_b + m_1 + m_2 + m_3$ (5.19)

Combining Eq.(5.17) and (5.18) gives the equation of the multi-storey BI building as

$$\begin{bmatrix} \acute{m} & \boldsymbol{m}_{ss} \\ \mathbf{0} & \boldsymbol{M} \end{bmatrix} \begin{Bmatrix} \ddot{x}_b \\ \ddot{\boldsymbol{u}} \end{Bmatrix} + \begin{bmatrix} c_b & \mathbf{0} \\ \mathbf{0} & \boldsymbol{C} \end{bmatrix} \begin{Bmatrix} \dot{x}_b \\ \dot{\boldsymbol{u}} \end{Bmatrix} + \begin{bmatrix} k_b & \mathbf{0} \\ \mathbf{0} & \boldsymbol{K} \end{bmatrix} \begin{Bmatrix} x_b \\ \boldsymbol{u} \end{Bmatrix} = -\begin{bmatrix} \acute{m} & \boldsymbol{m}_{ss} \\ \mathbf{0} & \boldsymbol{M} \end{bmatrix} \boldsymbol{\eta}\ddot{x}_g \quad (5.20)$$

where, $\boldsymbol{m}_{ss} = \{m_1 \quad m_2 \quad m_3\}$ and $\boldsymbol{\eta}$ is excitation influence vector.

The above equation, Eq.(5.20) represents the model of multi-storey BI building applicable for linear system. However, in the present study, the isolator has been modelled by nonlinear hysteretic model, while the superstructure is modelled assuming a linear elastic system. To consider the nonlinear model of the isolator, Eq.(5.20) is modified as

$$\begin{bmatrix} \acute{m} & \boldsymbol{m}_{ss} \\ \mathbf{0} & \boldsymbol{M} \end{bmatrix} \begin{Bmatrix} \ddot{x}_b \\ \ddot{\boldsymbol{u}} \end{Bmatrix} + \begin{bmatrix} c_b & \mathbf{0} \\ \mathbf{0} & \boldsymbol{C} \end{bmatrix} \begin{Bmatrix} \dot{x}_b \\ \dot{\boldsymbol{u}} \end{Bmatrix} + \begin{bmatrix} k_b & \mathbf{0} \\ \mathbf{0} & \boldsymbol{K} \end{bmatrix} \begin{Bmatrix} z_b \\ \boldsymbol{u} \end{Bmatrix} = -\begin{bmatrix} \acute{m} & \boldsymbol{m}_{ss} \\ \mathbf{0} & \boldsymbol{M} \end{bmatrix} \boldsymbol{\eta}\ddot{x}_g \quad (5.21)$$

where, $\dot{z}_b$, is the nonlinear Bouc-Wen differential hysteretic parameter [Manzoori and Nezhad (2017)] and is given as

$\dot{z}_b = \dot{x}_b - \beta|\dot{x}_b||z_b|^{(\alpha-1)}z_b - \gamma\dot{x}_b|z_b|^{\alpha}$ (5.22)

If the response from the system such as $\ddot{x}_b$, $\ddot{\boldsymbol{u}}$ and ground acceleration, $\ddot{x}_g$ are available, then the model represented by Eq.(5.21) can be utilised in the identification algorithms for identification of state and parameters of the system. However, in an instrumented building, the accelerometers usually records absolute accelerations such as $\ddot{v}_b, \ddot{v}_1, \ddot{v}_2$ and $\ddot{v}_3$ (Fig. 5.3). The relative acceleration responses $\ddot{x}_b$ and $\ddot{\boldsymbol{u}}$, which are required by the identification algorithms can be obtained from the measured absolute acceleration response using the following relations.

$\ddot{x}_b = \ddot{v}_b - \ddot{x}_g$ (5.23)

$\ddot{u}_1 = \ddot{v}_1 - \ddot{v}_b$ (5.24)

$\ddot{u}_2 = \ddot{v}_2 - \ddot{v}_b$ (5.25)

$\ddot{u}_3 = \ddot{v}_3 - \ddot{v}_b$ (5.26)

To perform the identification using the considered algorithms, at least some responses from the structure are required. However, if the acceleration at the ground floor level ($\ddot{v}_b$) is not available, the relative acceleration response ($\ddot{x}_b, \ddot{u}_1, \ddot{u}_2, \ddot{u}_3$) at the considered levels cannot be evaluated using the relation given in Eq. (5.23) to (5.26). Therefore, identification cannot be carried out in such circumstances. To overcome this problem, some modifications have been carried out in the equation representing the base isolation model of Eq.(5.21) as presented below.

It can be observed from Fig. 5.3and also from Eq.(5.23) to (5.26) that evaluation of relative acceleration responses ($\ddot{\boldsymbol{u}}$) at different floor levels, are dependent on the response of isolator-top level ($\ddot{v}_b$). The relative acceleration responses, $\ddot{\boldsymbol{u}}$ corresponding to different floor level are measured with respect to ground floor level (isolator-top level). If $\ddot{\boldsymbol{u}}$ can be expressed with respect to ground level, defined by $\ddot{\boldsymbol{x}}$, as shown in Fig. 5.3, then $\ddot{\boldsymbol{u}}$ can be decoupled from $\ddot{v}_b$. Thus, the dependency of relative acceleration of different floor levels on ground floor level can be avoided. The transformation can be carried out using the relation as follows.

$$\boldsymbol{x} = \boldsymbol{x}_b + \boldsymbol{u} \tag{5.27}$$

where,

$$\boldsymbol{x} = \{x_1 \quad x_2 \quad x_3\}^T \tag{5.28}$$

$$\boldsymbol{x}_b = \{x_b \quad x_b \quad x_b\}^T \tag{5.29}$$

$$\boldsymbol{u} = \{u_1 \quad u_2 \quad u_3\}^T \tag{5.30}$$

Transforming Eq.(5.17) using the relation given by Eq.(5.27) gives

$$\boldsymbol{M}(\ddot{\boldsymbol{x}} - \ddot{\boldsymbol{x}}_b) + \boldsymbol{K}(\boldsymbol{x} - \boldsymbol{x}_b) + \boldsymbol{C}(\dot{\boldsymbol{x}} - \dot{\boldsymbol{x}}_b) = -\boldsymbol{\eta}'\boldsymbol{M}\left(\ddot{x}_g + \ddot{x}_b\right) \tag{5.31}$$

$$\boldsymbol{M}\ddot{\boldsymbol{x}} + \boldsymbol{K}\boldsymbol{x} - \boldsymbol{K}\boldsymbol{x}_b + \boldsymbol{C}\dot{\boldsymbol{x}} - \boldsymbol{C}\dot{\boldsymbol{x}}_b = -\boldsymbol{\eta}'\boldsymbol{M}\ddot{x}_g \tag{5.32}$$

$$\boldsymbol{M}\begin{Bmatrix}\ddot{x}_1\\ \ddot{x}_2\\ \ddot{x}_3\end{Bmatrix} + \boldsymbol{K}\begin{Bmatrix}x_1\\ x_2\\ x_3\end{Bmatrix} - \boldsymbol{K}\begin{Bmatrix}x_b\\ x_b\\ x_b\end{Bmatrix} + \boldsymbol{C}\begin{Bmatrix}\dot{x}_1\\ \dot{x}_2\\ \dot{x}_3\end{Bmatrix} - \boldsymbol{C}\begin{Bmatrix}\dot{x}_b\\ \dot{x}_b\\ \dot{x}_b\end{Bmatrix} = -\boldsymbol{\eta}'\boldsymbol{M}\ddot{x}_g \tag{5.33}$$

Eq. (5.33) can be expressed in the form as given by

$$\begin{bmatrix}0 & m_1 & 0 & 0\\ 0 & 0 & m_2 & 0\\ 0 & 0 & 0 & m_3\end{bmatrix}\begin{Bmatrix}\ddot{x}_b\\ \ddot{x}_1\\ \ddot{x}_2\\ \ddot{x}_3\end{Bmatrix}+\begin{bmatrix}-k_1 & k_1+k_2 & -k_2 & 0\\ 0 & -k_2 & k_2+k_3 & -k_3\\ 0 & 0 & -k_3 & k_3\end{bmatrix}\begin{Bmatrix}x_b\\ x_1\\ x_2\\ x_3\end{Bmatrix}$$

$$+\begin{bmatrix}-c_1 & c_1+c_2 & -c_2 & 0\\ 0 & -c_2 & c_2+c_3 & -c_3\\ 0 & 0 & -c_3 & c_3\end{bmatrix}\begin{Bmatrix}\dot{x}_b\\ \dot{x}_1\\ \dot{x}_2\\ \dot{x}_3\end{Bmatrix}$$

$$=-\boldsymbol{\eta}''\begin{bmatrix}0 & m_1 & 0 & 0\\ 0 & 0 & m_2 & 0\\ 0 & 0 & 0 & m_3\end{bmatrix}\ddot{x}_g \tag{5.34}$$

It may be observed that if $x_b, \dot{x}_b$ and $\ddot{x}_b$ are replaced by zero in Eq.(5.31) to (5.34), then equations represents the conventional building model given by Eq.(5.9).

Transforming Eq.(5.18) using the relation of Eq.(5.27) and replacing $k_b x_b$ by $k_b z_b$ gives

$$\acute{m}\ddot{x}_b + m_1(\ddot{x}_1 - \ddot{x}_b) + m_2(\ddot{x}_2 - \ddot{x}_b) + m_3(\ddot{x}_3 - \ddot{x}_b) + c_b\dot{x}_b + k_b z_b = -\acute{m}\ddot{x}_g \tag{5.35}$$

Substituting $\acute{m}$ by Eq.(5.19), gives

$$(m_b + m_1 + m_2 + m_3)\ddot{x}_b + m_1(\ddot{x}_1 - \ddot{x}_b) + m_2(\ddot{x}_2 - \ddot{x}_b) + m_3(\ddot{x}_3 - \ddot{x}_b)$$
$$+ c_b\dot{x}_b + k_b z_b = -(m_b + m_1 + m_2 + m_3)\ddot{x}_g \tag{5.36}$$

On simplification,

$$m_b\ddot{x}_b + m_1\ddot{x}_1 + m_2\ddot{x}_2 + m_3\ddot{x}_3 + c_b\dot{x}_b + k_b z_b = -(m_b + m_1 + m_2 + m_3)\ddot{x}_g \tag{5.37}$$

Combining Eq.(5.34) and (5.37) gives

$$\begin{bmatrix}m_b & m_1 & m_2 & m_3\\ 0 & m_1 & 0 & 0\\ 0 & 0 & m_2 & 0\\ 0 & 0 & 0 & m_3\end{bmatrix}\begin{Bmatrix}\ddot{x}_b\\ \ddot{x}_1\\ \ddot{x}_2\\ \ddot{x}_3\end{Bmatrix}+\begin{bmatrix}k_b & 0 & 0 & 0 & 0\\ 0 & -k_1 & k_1+k_2 & -k_2 & 0\\ 0 & 0 & -k_2 & k_2+k_3 & -k_3\\ 0 & 0 & 0 & -k_3 & k_3\end{bmatrix}\begin{Bmatrix}z_b\\ x_b\\ x_1\\ x_2\\ x_3\end{Bmatrix}$$

$$+\begin{bmatrix}c_b & 0 & 0 & 0\\ -c_1 & c_1+c_2 & -c_2 & 0\\ 0 & -c_2 & c_2+c_3 & -c_3\\ 0 & 0 & -c_3 & c_3\end{bmatrix}\begin{Bmatrix}\dot{x}_b\\ \dot{x}_1\\ \dot{x}_2\\ \dot{x}_3\end{Bmatrix}$$

$$=-\boldsymbol{\eta}\begin{bmatrix}m_b & m_1 & m_2 & m_3\\ 0 & m_1 & 0 & 0\\ 0 & 0 & m_2 & 0\\ 0 & 0 & 0 & m_3\end{bmatrix}\ddot{x}_g \tag{5.38}$$

Eq. (5.38) can be written in matrix form as shown by Eq. (5.39) and is the governing equation of motion of the BI multi-storey building system. It can be observed from Eq.(5.38) that there are no terms containing displacement, velocity or acceleration measured with respect to ground level. Therefore, Eq.(5.38) can be easily used to represent BI building model in the considered identification algorithms. Further, the modified model has the capacity to handle missing sensor at ground floor level (the floor slab just above the isolators) as well as missing sensor at any other floor levels. Thus, the modified equation of motion Eq. (5.38) is written in concise form as

$$\boldsymbol{M}_B\ddot{\boldsymbol{x}}_B + \boldsymbol{K}_B\boldsymbol{x}_{ZB} + \boldsymbol{C}_B\dot{\boldsymbol{x}}_B = -\boldsymbol{\eta}\boldsymbol{M}_B\ddot{x}_g \tag{5.39}$$

where, mass and stiffness matrices of the 3-storey (4-dof) BI building are expressed as

$$\boldsymbol{M}_B = \begin{bmatrix} m_b & m_1 & m_2 & m_3 \\ 0 & m_1 & 0 & 0 \\ 0 & 0 & m_2 & 0 \\ 0 & 0 & 0 & m_3 \end{bmatrix}, \quad \boldsymbol{K}_B = \begin{bmatrix} k_b & 0 & 0 & 0 & 0 \\ 0 & -k_1 & k_1+k_2 & -k_2 & 0 \\ 0 & 0 & -k_2 & k_2+k_3 & -k_3 \\ 0 & 0 & 0 & -k_3 & k_3 \end{bmatrix} \tag{5.40}$$

The damping and excitation localization matrices are given as

$$\boldsymbol{C}_B = \begin{bmatrix} c_b & 0 & 0 & 0 \\ -c_1 & c_1+c_2 & -c_2 & 0 \\ 0 & -c_2 & c_2+c_3 & -c_3 \\ 0 & 0 & -c_3 & c_3 \end{bmatrix}, \qquad \boldsymbol{\eta} = \begin{bmatrix} 1 & 0 & 0 & 0 \\ 0 & 1 & 0 & 0 \\ 0 & 0 & 1 & 0 \\ 0 & 0 & 0 & 1 \end{bmatrix} \tag{5.41}$$

The vectors $\ddot{\boldsymbol{x}}_B, \dot{\boldsymbol{x}}_B$ and $\boldsymbol{x}_{ZB}$ are given as

$$\ddot{\boldsymbol{x}}_B = \begin{Bmatrix} \ddot{x}_b \\ \ddot{x}_1 \\ \ddot{x}_2 \\ \ddot{x}_3 \end{Bmatrix}, \quad \boldsymbol{x}_{ZB} = \begin{Bmatrix} z_b \\ x_b \\ x_1 \\ x_2 \\ x_3 \end{Bmatrix} \text{and} \dot{\boldsymbol{x}}_B = \begin{Bmatrix} \dot{x}_b \\ \dot{x}_1 \\ \dot{x}_2 \\ \dot{x}_3 \end{Bmatrix} \tag{5.42}$$

Eq.(5.39) may be represented in state-space form as

$$\begin{Bmatrix} \dot{\boldsymbol{x}}_B \\ \ddot{\boldsymbol{x}}_B \\ \dot{z}_b \end{Bmatrix} = \frac{d}{dt}\begin{Bmatrix} \boldsymbol{x}_B \\ \dot{\boldsymbol{x}}_B \\ z_B \end{Bmatrix} = \begin{Bmatrix} \dot{\boldsymbol{x}}_B \\ -\boldsymbol{\eta}\ddot{x}_g - \boldsymbol{M}_B^{-1}\boldsymbol{K}_B\boldsymbol{x}_{ZB} - \boldsymbol{M}_B^{-1}\boldsymbol{C}_B\dot{\boldsymbol{x}}_B \\ \dot{x}_b - \beta|\dot{x}_b||z_b|^{\alpha}z_b - \gamma\dot{x}_b|z_b|^{\alpha} \end{Bmatrix} \tag{5.43}$$

Eq. (4.2) is of the form $\boldsymbol{y}' = \boldsymbol{f}(x)$, and can be solved by Runga-Kutta4th order integration scheme.

5.3 Evaluation of state and parameter using different algorithms

Three different algorithms EKF, Two-Stage EKF and UKF algorithms are used for evaluation of state and parameters of the considered BI building system. In chapter-3, detailed general description of these algorithms and formulation are given. However, those formulations are in general form and cannot be directly implemented for identification of a BI building system under consideration. Formulations specific to BI system needs to be derived to suit the requirements of each of these algorithms depending on the type and nature of input available from BI building system. The detailed procedures adopted to transform the general equations of these algorithms to fit the considered model of the BI building system are presented in the following sub-sections.

5.3.1 EKF algorithm for identification of base-isolated building

The details of formulation of EKF and its implementation in MATLAB for identification of state and parameters of the three-storey BI building system are described.

5.3.1.1 Formulation of EKF for three-storey base-isolated building

In this sub-section, stiffness, damping and Jacobian matrices of the BI building model required for EKF algorithm have been derived.

The equation of motion as given by Eq. (5.39) is repeated below as Eq. (5.44)

$$\boldsymbol{M}_B\ddot{\boldsymbol{x}}_B + \boldsymbol{K}_B\boldsymbol{x}_{ZB} + \boldsymbol{C}_B\dot{\boldsymbol{x}}_B = -\boldsymbol{\eta}\boldsymbol{M}_B\ddot{x}_g = -\boldsymbol{\eta}\boldsymbol{F} \tag{5.44}$$

The unknown state vector is represented by $\boldsymbol{X}$ and the unknown parametric vector is represented by $\boldsymbol{\theta}$. The extended state vector obtained by extending the state vector to incorporate parametric vector is represented by $\boldsymbol{X}_e$.

$$\boldsymbol{X} = \{z_b \quad x_1 \quad x_2 \quad x_3 \quad \dot{x}_b \quad \dot{x}_1 \quad \dot{x}_2 \quad \dot{x}_3\}^T \tag{5.45}$$

$$\boldsymbol{\theta} = \{k_b \quad k_1 \quad k_2 \quad k_3 \quad c_b \quad c_1 \quad c_2 \quad c_3 \quad \beta \quad \gamma\}^T \tag{5.46}$$

$$\begin{aligned}\boldsymbol{X}_e &= \{\boldsymbol{X}^T \quad \boldsymbol{\theta}^T\}^T \\ &= \{z_b \quad x_b \quad x_1 \quad x_2 \quad x_3 \quad \dot{x}_b \quad \dot{x}_1 \quad \dot{x}_2 \quad \dot{x}_3 \quad k_b \quad k_1 \quad k_2 \quad k_3 \quad c_b \quad c_1 \quad c_2 \quad c_3 \quad \beta \quad \gamma\}^T\end{aligned} \tag{5.47}$$

The state-space form is represented as

$$\dot{\boldsymbol{X}}_e = \frac{d}{dt}\begin{Bmatrix} z_b \\ \{x_b \quad x_1 \quad x_2 \quad x_3\}^T \\ \dot{x}_b \\ \dot{x}_1 \\ \dot{x}_2 \\ \dot{x}_3 \\ \{k_b \quad k_1 \quad k_2 \quad k_3\}^T \\ \{c_b \quad c_1 \quad c_2 \quad c_3\}^T \\ \beta \\ \gamma \end{Bmatrix} = \boldsymbol{g}(\boldsymbol{X}, \boldsymbol{\theta}, \boldsymbol{F}) = \begin{Bmatrix} \dot{z}_b \\ \{\dot{x}_b \quad \dot{x}_1 \quad \dot{x}_2 \quad \dot{x}_3\}^T \\ \ddot{x}_b \\ \ddot{x}_1 \\ \ddot{x}_2 \\ \ddot{x}_3 \\ \{\dot{k}_b \quad \dot{k}_1 \quad \dot{k}_2 \quad \dot{k}_3\}^T \\ \{\dot{c}_b \quad \dot{c}_1 \quad \dot{c}_2 \quad \dot{c}_3\}^T \\ \dot{\beta} \\ \dot{\gamma} \end{Bmatrix}$$

$$\boldsymbol{g}(\boldsymbol{X}, \boldsymbol{\theta}, \boldsymbol{f}) = \begin{bmatrix} \dot{x}_b - \beta|\dot{x}_b||z_b|^{\alpha} z_b - \gamma \dot{x}_b |z_b|^{\alpha} \\ \{\dot{x}_b \quad \dot{x}_1 \quad \dot{x}_2 \quad \dot{x}_3\}^T \\ \begin{Bmatrix} -1 \\ -1 \\ -1 \\ -1 \end{Bmatrix} \ddot{x}_g - [M_B]^{-1} \left[[K_B] \begin{Bmatrix} z_b \\ x_b \\ x_1 \\ x_2 \\ x_3 \end{Bmatrix} + [C_B] \begin{Bmatrix} \dot{x}_b \\ \dot{x}_1 \\ \dot{x}_2 \\ \dot{x}_3 \end{Bmatrix} \right] \\ \{0 \quad 0 \quad 0 \quad 0\}^T \\ \{0 \quad 0 \quad 0 \quad 0\}^T \\ 0 \\ 0 \end{bmatrix} = \begin{Bmatrix} g_1 \\ \{g_2 \quad g_3 \quad g_4 \quad g_5\}^T \\ g_6 \\ g_7 \\ g_8 \\ g_9 \\ \{g_{10} \quad g_{11} \quad g_{12} \quad g_{13}\}^T \\ \{g_{14} \quad g_{15} \quad g_{16} \quad g_{17}\}^T \\ g_{18} \\ g_{19} \end{Bmatrix} \tag{5.48}$$

$$\boldsymbol{K}_B \boldsymbol{x}_{ZB} = \begin{bmatrix} k_b & 0 & 0 & 0 & 0 \\ 0 & -k_1 & k_1 + k_2 & -k_2 & 0 \\ 0 & 0 & -k_2 & k_2 + k_3 & -k_3 \\ 0 & 0 & 0 & -k_3 & k_3 \end{bmatrix} \begin{Bmatrix} z_b \\ x_b \\ x_1 \\ x_2 \\ x_3 \end{Bmatrix} = \begin{Bmatrix} k_b z_b \\ -k_1 x_b + k_1 x_1 + k_2 x_1 - k_2 x_2 \\ -k_2 x_1 + k_2 x_2 + k_3 x_2 - k_3 x_3 \\ -k_3 x_2 + k_3 x_3 \end{Bmatrix} \tag{5.49}$$

Eq. (4.9) is obtained using the expressions given in Eq. (5.40) and Eq. (5.45).

Differentiating $\boldsymbol{K}_B \boldsymbol{x}_{ZB}$ with respect to $\boldsymbol{x}_{ZB}$

$$\frac{\partial}{\partial \boldsymbol{x}_{ZB}} \boldsymbol{K}_B \boldsymbol{x}_{ZB} = [K] \tag{5.50}$$

Differentiating $\boldsymbol{K}_B \boldsymbol{x}_{ZB}$ with respect to $\dot{\boldsymbol{x}}_B$

$$\frac{\partial}{\partial \dot{\boldsymbol{x}}_B} \boldsymbol{K}_B \boldsymbol{x}_{ZB} = \begin{bmatrix} 0 & 0 & 0 & 0 \\ 0 & 0 & 0 & 0 \\ 0 & 0 & 0 & 0 \\ 0 & 0 & 0 & 0 \end{bmatrix} = \boldsymbol{0}_{4x4} \tag{5.51}$$

Differentiating $\boldsymbol{K}_B \boldsymbol{x}_{ZB}$ with respect to $\boldsymbol{\theta}_i$, where, i=1,2,3,4.and $\boldsymbol{\theta}_i = \{k_b \quad k_1 \quad k_2 \quad k_3\}^T$

$$\frac{\partial}{\partial \boldsymbol{\theta}_i}\boldsymbol{K}_B\boldsymbol{x}_{ZB} = \begin{bmatrix} z_b & 0 & 0 & 0 \\ 0 & -(x_b - x_1) & (x_1 - x_2) & 0 \\ 0 & 0 & -(x_1 - x_2) & (x_2 - x_3) \\ 0 & 0 & 0 & -(x_2 - x_3) \end{bmatrix} = [KK_{ZB}] \tag{5.52}$$

Differentiating $\boldsymbol{K}_B\boldsymbol{x}_{ZB}$ with respect to $\boldsymbol{\theta}_j$, where, j=5 to 10 and $\boldsymbol{\theta}_j = \{c_b \quad c_1 \quad c_2 \quad c_3 \quad \beta \quad \gamma\}^T$

$$\frac{\partial}{\partial \boldsymbol{\theta}_j}\boldsymbol{K}_B\boldsymbol{x}_{ZB} = \begin{bmatrix} 0 & 0 & 0 & 0 & 0 & 0 \\ 0 & 0 & 0 & 0 & 0 & 0 \\ 0 & 0 & 0 & 0 & 0 & 0 \\ 0 & 0 & 0 & 0 & 0 & 0 \end{bmatrix} = \boldsymbol{0}_{4x6} \tag{5.53}$$

Therefore, combining Eq. (4.11), (5.51), (5.52) and (5.53), $\frac{\partial}{\partial \boldsymbol{X}_e}(\boldsymbol{K}_B\boldsymbol{x}_{ZB})$ is obtained as

$$\begin{aligned} &\frac{\partial}{\partial \boldsymbol{X}_e}(\boldsymbol{K}_B\boldsymbol{x}_{ZB}) \\ &= \left[\frac{\partial}{\partial \boldsymbol{x}_{ZB}}(\boldsymbol{K}_B\boldsymbol{x}_{ZB}) \quad \frac{\partial}{\partial \dot{\boldsymbol{x}}_B}(\boldsymbol{K}_B\boldsymbol{x}_{ZB}) \quad \frac{\partial}{\partial \boldsymbol{\theta}_i}(\boldsymbol{K}_B\boldsymbol{x}_{ZB}) \quad \frac{\partial}{\partial \boldsymbol{\theta}_j}(\boldsymbol{K}_B\boldsymbol{x}_{ZB})\right] \\ &= [\boldsymbol{K} \quad \boldsymbol{0}_{4x4} \quad \boldsymbol{K}\boldsymbol{K}_{ZB} \quad \boldsymbol{0}_{4x6}] \end{aligned} \tag{5.54}$$

Using the expressions given in Eq. (5.40), (5.41) and (5.42)

$$\begin{aligned} \boldsymbol{C}_B\dot{\boldsymbol{x}}_B &= \begin{bmatrix} c_b & 0 & 0 & 0 \\ -c_1 & c_1 + c_2 & -c_2 & 0 \\ 0 & -c_2 & c_2 + c_3 & -c_3 \\ 0 & 0 & -c_3 & c_3 \end{bmatrix} \begin{Bmatrix} \dot{x}_b \\ \dot{x}_1 \\ \dot{x}_2 \\ \dot{x}_3 \end{Bmatrix} \\ &= \begin{Bmatrix} c_b\dot{x}_b \\ -c_1\dot{x}_b + c_1\dot{x}_1 + c_2\dot{x}_1 - c_2\dot{x}_2 \\ -c_2\dot{x}_1 + c_2\dot{x}_2 + c_3\dot{x}_2 - c_3\dot{x}_3 \\ -c_3\dot{x}_2 + c_3\dot{x}_3 \end{Bmatrix} \end{aligned} \tag{5.55}$$

Eq. (5.55) is obtained using the expression given in Eq. (5.41) and Eq. (5.42).

Differentiating $\boldsymbol{C}_B\dot{\boldsymbol{x}}_B$ with respect to $\boldsymbol{x}_{ZB}$

$$\frac{\partial}{\partial \boldsymbol{x}_{ZB}}\boldsymbol{C}_B\dot{\boldsymbol{x}}_B = \begin{bmatrix} 0 & 0 & 0 & 0 & 0 \\ 0 & 0 & 0 & 0 & 0 \\ 0 & 0 & 0 & 0 & 0 \\ 0 & 0 & 0 & 0 & 0 \end{bmatrix} = \boldsymbol{0}_{4x5} \tag{5.56}$$

Differentiating $\boldsymbol{C}_B\dot{\boldsymbol{x}}_B$ with respect to $\dot{\boldsymbol{x}}_B$

$$\frac{\partial}{\partial \dot{\boldsymbol{x}}_B}\boldsymbol{C}_B\dot{\boldsymbol{x}}_B = [C] \tag{5.57}$$

Differentiating $\boldsymbol{C}_B\dot{\boldsymbol{x}}_B$ with respect to $\boldsymbol{\theta}_i$, where, i=1,2,3,4 and $\boldsymbol{\theta}_i = \{k_b \quad k_1 \quad k_2 \quad k_3\}^T$

$$\frac{\partial}{\partial \boldsymbol{\theta}_i}\boldsymbol{C}_B\dot{\boldsymbol{x}}_B = \begin{bmatrix} 0 & 0 & 0 & 0 \\ 0 & 0 & 0 & 0 \\ 0 & 0 & 0 & 0 \\ 0 & 0 & 0 & 0 \end{bmatrix} = \boldsymbol{0}_{4x4} \tag{5.58}$$

Differentiating $\boldsymbol{C}_B\dot{\boldsymbol{x}}_B$ with respect to $\boldsymbol{\theta}_j$, where, j=5 to8 and $\boldsymbol{\theta}_j = \{c_b \quad c_1 \quad c_2 \quad c_3\}^T$

$$\frac{\partial}{\partial \boldsymbol{\theta}_j}\boldsymbol{C}_B\dot{\boldsymbol{x}}_B = \begin{bmatrix} \dot{x}_b & 0 & 0 & 0 \\ 0 & -(\dot{x}_b - \dot{x}_1) & (\dot{x}_1 - \dot{x}_2) & 0 \\ 0 & 0 & -(\dot{x}_1 - \dot{x}_2) & (\dot{x}_2 - \dot{x}_3) \\ 0 & 0 & 0 & -(\dot{x}_2 - \dot{x}_3) \end{bmatrix} = [CC_B] \tag{5.59}$$

Differentiating $\boldsymbol{C}_B\dot{\boldsymbol{x}}_B$ with respect to $\boldsymbol{\theta}_{\beta,\gamma}$, where,$\boldsymbol{\theta}_{\beta,\gamma} = \{\beta \quad \gamma\}^T$

$$\frac{\partial}{\partial \boldsymbol{\theta}_{\beta,\gamma}}\boldsymbol{C}_B\dot{\boldsymbol{x}}_B = \begin{bmatrix} 0 & 0 \\ 0 & 0 \\ 0 & 0 \\ 0 & 0 \end{bmatrix} = \boldsymbol{0}_{4x2} \tag{5.60}$$

Therefore, combining Eq. (5.56) to (5.60), $\frac{\partial}{\partial \boldsymbol{X}_e}(\boldsymbol{C}_B\dot{\boldsymbol{x}}_B)$ is obtained as

$$\begin{aligned} &\frac{\partial}{\partial \boldsymbol{X}_e}(\boldsymbol{C}_B\dot{\boldsymbol{x}}_B) \\ &= \left[\frac{\partial}{\partial \boldsymbol{x}_{ZB}}(\boldsymbol{C}_B\dot{\boldsymbol{x}}_B) \quad \frac{\partial}{\partial \dot{\boldsymbol{x}}_B}(\boldsymbol{C}_B\dot{\boldsymbol{x}}_B) \quad \frac{\partial}{\partial \boldsymbol{\theta}_i}(\boldsymbol{C}_B\dot{\boldsymbol{x}}_B) \quad \frac{\partial}{\partial \boldsymbol{\theta}_j}(\boldsymbol{C}_B\dot{\boldsymbol{x}}_B) \quad \frac{\partial}{\partial \boldsymbol{\theta}_{\beta,\gamma}}(\boldsymbol{C}_B\dot{\boldsymbol{x}}_B)\right] \\ &= [\boldsymbol{0}_{4x5} \quad \boldsymbol{C} \quad \boldsymbol{0}_{4x4} \quad \boldsymbol{CC}_B \quad \boldsymbol{0}_{4x2}] \end{aligned} \tag{5.61}$$

Differentiating $\dot{z}_b$ as given in Eq. (5.22) with respect to z_b

$$\begin{aligned} \frac{\partial \dot{z}_b}{\partial z_b} &= -(\beta|\dot{x}_b||z_b|^{\alpha})\frac{\partial z_b}{\partial z_b} - (\beta|\dot{x}_b|z_b)\frac{\partial(|z_b|^{\alpha})}{\partial z_b} - \gamma\dot{x}_b\frac{\partial(|z_b|^{\alpha})}{\partial z_b} \\ &= -\beta|\dot{x}_b||z_b|^{(\alpha-1)} - \beta|\dot{x}_b|(\alpha-1)|z_b|^{(\alpha-2)}z_b * sign(z_b) \\ &\quad - \gamma\dot{x}_b\alpha|z_b|^{(\alpha-1)}sign(z_b) \end{aligned} \tag{5.62}$$

Differentiating $\dot{z}_b$ with respect to $\dot{x}_b$

$$\frac{\partial \dot{z}_b}{\partial \dot{x}_b} = 1 - \beta * sign(\dot{x}_b)|z_b|^{(\alpha-1)} z_b - \gamma|z_b|^{\alpha} \tag{5.63}$$

Differentiating $\dot{z}_b$ with respect to β

$$\frac{\partial \dot{z}_b}{\partial \beta} = -|\dot{x}_b||z_b|^{(\alpha-1)} z_b \tag{5.64}$$

Differentiating $\dot{z}_b$ with respect to γ

$$\frac{\partial \dot{z}_b}{\partial \gamma} = -\dot{x}_b|z_b|^{\alpha} \tag{5.65}$$

Jacobian of Matrix $\boldsymbol{g}$ is $\boldsymbol{A} = \frac{\partial \boldsymbol{g}}{\partial \boldsymbol{X}_e}$

$$\frac{\partial \boldsymbol{g}}{\partial}_{e} = \begin{bmatrix} \frac{\partial g_1}{\partial z_b} & \frac{\partial g_1}{\partial x_b} & \cdots & \frac{\partial g_1}{\partial \gamma} \\ \frac{\partial g_2}{\partial z_b} & \frac{\partial g_2}{\partial x_b} & \cdots & \frac{\partial g_2}{\partial \gamma} \\ \vdots & \vdots & \cdots & \vdots \\ \frac{\partial g_{19}}{\partial z_b} & \frac{\partial g_{19}}{\partial x_b} & \cdots & \frac{\partial g_{19}}{\partial \gamma} \end{bmatrix} \tag{5.66}$$

where, the extended unknown state vector is represented by $\boldsymbol{X}_e$ and is given by Eq.(5.47)

If the i^{th} row of matrix [**A**] is denoted as $\boldsymbol{A}_i$, then

$$\boldsymbol{A}_1 = \frac{\partial \boldsymbol{g}_1}{\partial \boldsymbol{X}_e} = \begin{bmatrix} \frac{\partial \dot{z}_b}{\partial z_b} & \boldsymbol{0}_{1x4} & \frac{\partial \dot{z}_b}{\partial \dot{x}_b} & \boldsymbol{0}_{1x11} & \frac{\partial \dot{z}_b}{\partial \beta} & \frac{\partial \dot{z}_b}{\partial \gamma} \end{bmatrix} \tag{5.67}$$

$$\boldsymbol{A}_{2\ to\ 5} = \frac{\partial \boldsymbol{g}_{2\ to\ 5}}{\partial \boldsymbol{X}_e} = [\boldsymbol{0}_{4x5} \quad \boldsymbol{I}_{4x4} \quad \boldsymbol{0}_{1x10}] \tag{5.68}$$

$$\boldsymbol{A}_{6\ to\ 9} = \frac{\partial \boldsymbol{g}_{6\ to\ 9}}{\partial \boldsymbol{X}_e} = \left[-\boldsymbol{M}_B^{-1} \frac{\partial}{\partial \boldsymbol{X}_e}(\boldsymbol{K}_B \boldsymbol{x}_{ZB}) - \boldsymbol{M}_B^{-1} \frac{\partial}{\partial \boldsymbol{X}_e}(\boldsymbol{C}_B \dot{\boldsymbol{x}}_B)\right] \tag{5.69}$$

Substituting $\frac{\partial}{\partial x_e}(\boldsymbol{K}_B \boldsymbol{x}_{ZB})$ and $\frac{\partial}{\partial x_e}(\boldsymbol{C}_B \dot{\boldsymbol{x}}_B)$ from Eq. (5.54) and (5.61) into Eq.(5.69)

$$\begin{aligned} &\boldsymbol{A}_{6\ to\ 9} \\ &= [-\boldsymbol{M}_B^{-1}[\boldsymbol{K} \quad \boldsymbol{0}_{4x4} \quad \boldsymbol{K}\boldsymbol{K}_{ZB} \quad \boldsymbol{0}_{4x6}] \quad -\boldsymbol{M}_B^{-1}([\boldsymbol{0}_{4x5} \quad \boldsymbol{C} \quad \boldsymbol{0}_{4x4} \quad \boldsymbol{C}\boldsymbol{C}_B \quad \boldsymbol{0}_{4x2}])] \\ &= -\boldsymbol{M}_B^{-1}[\boldsymbol{K} \quad \boldsymbol{C} \quad \boldsymbol{K}\boldsymbol{K}_{ZB} \quad \boldsymbol{C}\boldsymbol{C}_B \quad \boldsymbol{0}_{4x2}] \end{aligned} \tag{5.70}$$

The Jacobian matrix from row 10 to row 19 is zero. In the matrix form, it is shown as

$$\boldsymbol{A}_{10\ to\ 19} = \frac{\partial \boldsymbol{g}_{10\ to\ 19}}{\partial \boldsymbol{X}_e} = \boldsymbol{0}_{10x19} \tag{5.71}$$

Assembling the derivatives obtained from the equations, Eq. (5.67) to (5.71), the full Jacobian matrix is given as

$$\boldsymbol{A} = \begin{bmatrix} \left[\frac{\partial \dot{z}_b}{\partial z_b} \quad \mathbf{0}_{1x4}\right] & \left[\frac{\partial \dot{z}_b}{\partial \dot{x}_b} \quad \mathbf{0}_{1x3}\right] & \mathbf{0}_{4x4} & \mathbf{0}_{4x4} & \frac{\partial \dot{z}_b}{\partial \beta} & \frac{\partial \dot{z}_b}{\partial \gamma} \\ \mathbf{0}_{4x5} & \boldsymbol{I}_{4x4} & \mathbf{0}_{4x4} & \mathbf{0}_{4x4} & \mathbf{0}_{4x1} & \mathbf{0}_{4x1} \\ -\boldsymbol{M}_B^{-1}(\boldsymbol{K} & \boldsymbol{C} & \boldsymbol{K}\boldsymbol{K}_{ZB} & \boldsymbol{C}\boldsymbol{C}_B & \mathbf{0}_{4x1} & \mathbf{0}_{4x1}) \\ \mathbf{0}_{10x5} & \mathbf{0}_{10x4} & \mathbf{0}_{10x4} & \mathbf{0}_{10x4} & \mathbf{0}_{10x1} & \mathbf{0}_{10x1} \end{bmatrix} \tag{5.72}$$

Using the above formulations, the EKF algorithm is implemented in MATLAB in the following steps as given below.

5.3.1.2 Implementation procedure of EKF in MATLAB

The algorithm is implemented in four steps which are given below.

Step-1: Initialization Step.

Initialization is done by assuming the initial value of

e) The extended state vector, $\boldsymbol{X}_e$.

f) Error covariance matrix, $\boldsymbol{P}$ of extended state vector $\boldsymbol{X}_e$.

g) Process error covariance matrix, $\boldsymbol{Q}$.

h) Measurement error covariance matrix, $\boldsymbol{R}$.

Step-2: Evaluation of state transfer matrix

The state transition matrix is determined by evaluating the Jacobian of the process equation and is given by Eq.(5.72)

Step-3: Prediction Step

Prediction of unknown extended state vector is carried out for current time-step, using the input information and state information of previous time-step. This is done by integrating Eq. (4.8) by 4th order Runga-Kutta integration scheme.

Upon integration of Eq. (4.8), the predicted value of extended state vector $\boldsymbol{X}_e$ is obtained and is denoted by $\widehat{\boldsymbol{X}}_{k|k}$.The measurement equation is generated using $\widehat{\boldsymbol{X}}_{k|k}$as

$$\ddot{\hat{\boldsymbol{x}}}_i = \boldsymbol{\Lambda}\left(-\boldsymbol{\eta}\ddot{x}_g - \boldsymbol{M}_B^{-1}[\boldsymbol{K}_B + \boldsymbol{C}_B]\widehat{\boldsymbol{X}}_{k|k}\right) \tag{5.73}$$

where, $\boldsymbol{\Lambda}$ is a matrix defining the sensor location. If sensor at 1st floor and 2nd floor level are missing then the sensor location matrix is expressed as

$$\boldsymbol{\Lambda} = \begin{bmatrix} 1 & 0 & 0 & 0 \\ 0 & 0 & 0 & 1 \end{bmatrix} \tag{5.74}$$

If sensor at ground floor and roof level are missing then the sensor location matrix is expressed as

$$\boldsymbol{\Lambda} = \begin{bmatrix} 0 & 1 & 0 & 0 \\ 0 & 0 & 0 & 1 \end{bmatrix} \tag{5.75}$$

When sensors are located at all the floor levels then the sensor location matrix is expressed as

$$\boldsymbol{\Lambda} = \begin{bmatrix} 1 & 0 & 0 & 0 \\ 0 & 1 & 0 & 0 \\ 0 & 0 & 1 & 0 \\ 0 & 0 & 0 & 1 \end{bmatrix} \tag{5.76}$$

The rows denote the sensor numbers and the columns denote the floor levels. The floor level where sensor is present is having a value of unity. In case where sensor data are available for all floor levels, $\boldsymbol{\Lambda}$ is a unit matrix having the dimension of total number of considered dof.

Step-4: Updating Step

The measurement information at current time step is used to correct the estimate to get more accurate state information. This is accomplished by Kalman Filtering, which is described in the following steps.

The state transition matrix $\boldsymbol{\Phi}_{\mathrm{k-1|k-1}}$ is determined as

$$\boldsymbol{\Phi}_{\mathrm{k-1|k-1}} = \boldsymbol{I}_{19x19} + \Delta t.\boldsymbol{A}\left(\widehat{\boldsymbol{X}}_{k-1|k-1}\right) \tag{5.77}$$

Using the state transition matrix, the predicted prior estimate covariance is determined

$$\boldsymbol{P}_{k|k-1} = \boldsymbol{\Phi}_{k-1|k-1}\boldsymbol{P}_{k-1|k-1}\boldsymbol{\Phi}^{\boldsymbol{T}}{}_{k-1|k-1} + \boldsymbol{Q}_k \tag{5.78}$$

The Kalman Gain matrix is determined as

$$\boldsymbol{\mathcal{K}}_k = \frac{\boldsymbol{P}_{k|k-1}\boldsymbol{H}^T}{\boldsymbol{H}\boldsymbol{P}_{k|k-1}\boldsymbol{H}^T + \boldsymbol{R}} \tag{5.79}$$

where, $\boldsymbol{H}$ is the Jacobian of the measurement equation, given by Eq. (5.69)

$$\boldsymbol{H} = \boldsymbol{\Lambda}\boldsymbol{A}_{6\ to\ 9} = \boldsymbol{\Lambda}\frac{\partial \boldsymbol{g}_{6\ to\ 9}}{\partial \boldsymbol{X}_e} = \boldsymbol{\Lambda}\left[-\boldsymbol{M}_B^{-1}\frac{\partial}{\partial \boldsymbol{X}_e}(\boldsymbol{K}_B\boldsymbol{x}_{ZB}) - \boldsymbol{M}_B^{-1}\frac{\partial}{\partial \boldsymbol{X}_e}(\boldsymbol{C}_B\dot{\boldsymbol{x}}_B)\right] \tag{5.80}$$

If the current measured acceleration from the system is denoted as $\ddot{\boldsymbol{x}}_i$, then the difference between current measurement and estimated measurement (Eq.(4.23)), also known as innovation is given as

$$\hat{\boldsymbol{y}}_{\boldsymbol{k}} = \left(\boldsymbol{\Lambda}\ddot{\boldsymbol{x}}_i - \ddot{\hat{\boldsymbol{x}}}_i\right) \tag{5.81}$$

The updated posterior estimate of the extended state vector is given as

$$\hat{\boldsymbol{X}}_{e,k|k} = \hat{\boldsymbol{X}}_{e,k|k-1} + \mathcal{K}_{\mathrm{k}}\hat{\boldsymbol{y}}_{\boldsymbol{k}} \tag{5.82}$$

5.3.2 Two-Stage EKF algorithm for identification of base-isolated building

The details of formulation of Two-Stage EKF and its implementation in MATLAB for identification of state and parameters of the three-storey BI building system are described.

5.3.2.1 Formulation of Two-Stage EKF for three-storey base-isolated building

In this sub-section, stiffness, damping and Jacobian matrices of the BI building model required for Two-Stage EKF algorithm have been derived.

The unknown extended state vector, $\boldsymbol{X_e}$, contains both state vector $\boldsymbol{X}$ and parametric vector $\boldsymbol{\theta}$. The vector $\boldsymbol{X_e}$ is partitioned into state and parametric vector denoted by $\mathbf{X}$ and $\boldsymbol{\theta}$ respectively.

$$\boldsymbol{X_e} = \{\boldsymbol{X^T} \quad \boldsymbol{\theta^T}\}^T \tag{5.83}$$

$$\text{where, } \boldsymbol{X} = \{z_b \quad x_b \quad x_1 \quad x_2 \quad x_3 \quad \dot{x}_b \quad \dot{x}_1 \quad \dot{x}_2 \quad \dot{x}_3\}^T \tag{5.84}$$

$$\text{and, } \boldsymbol{\theta} = \{k_b \quad k_1 \quad k_2 \quad k_3 \quad c_b \quad c_1 \quad c_2 \quad c_3 \quad \beta \quad \gamma\}^T \tag{5.85}$$

For ease of representation, the state vector $\boldsymbol{X}$is further segregated into $\boldsymbol{x}_{ZB}$ and $\dot{\boldsymbol{x}}_B$ as

$$\boldsymbol{X} = \{\boldsymbol{x}_{ZB}^T \quad \dot{\boldsymbol{x}}_{\mathrm{B}}^{\mathrm{T}}\}^T \tag{5.86}$$

$$\boldsymbol{x}_{ZB} = \{z_b \quad x_b \quad x_1 \quad x_2 \quad x_3\}^T = \{z_b \quad \boldsymbol{x}_B^T\}^T \tag{5.87}$$

$$\boldsymbol{x}_B = \{x_b \quad x_1 \quad x_2 \quad x_3\}^T \qquad \dot{\boldsymbol{x}}_B = \{\dot{x}_b \quad \dot{x}_1 \quad \dot{x}_2 \quad \dot{x}_3\}^T \tag{5.88}$$

The state-space form of the governing differential equation is given by

$$\dot{\boldsymbol{X}} = \begin{Bmatrix} \dot{\boldsymbol{x}}_{ZB} \\ \ddot{\boldsymbol{x}}_B \end{Bmatrix} = \frac{d}{dt}\begin{Bmatrix} \boldsymbol{x}_{ZB} \\ \dot{\boldsymbol{x}}_B \end{Bmatrix} = \frac{d\boldsymbol{X}}{dt} = \begin{Bmatrix} \dot{\boldsymbol{x}}_{ZB} \\ -\boldsymbol{\eta}\ddot{x}_g - \boldsymbol{M}_B^{-1}\boldsymbol{K}_B\boldsymbol{x}_{ZB} - \boldsymbol{M}_B^{-1}\boldsymbol{C}_B\dot{\boldsymbol{x}}_B \end{Bmatrix}$$
$$= \begin{Bmatrix} \dot{z}_b \\ \dot{\boldsymbol{x}}_B \\ -\boldsymbol{\eta}\ddot{x}_g - \boldsymbol{M}_B^{-1}[\boldsymbol{K}_B + \boldsymbol{C}_B]\begin{Bmatrix} \boldsymbol{x}_{ZB} \\ \dot{\boldsymbol{x}}_B \end{Bmatrix} \end{Bmatrix}$$
$$= \begin{Bmatrix} \dot{x}_b - \beta|\dot{x}_b||z_b|^{(\alpha-1)}z_b - \gamma\dot{x}_b|z_b|^{\alpha} \\ \dot{\boldsymbol{x}}_B \\ -\boldsymbol{\eta}\ddot{x}_g - \boldsymbol{M}_B^{-1}[\boldsymbol{K}_B + \boldsymbol{C}_B]\{\boldsymbol{X}\} \end{Bmatrix} \tag{5.89}$$

The observation equation is given by

$$\boldsymbol{h} = \boldsymbol{\Lambda}\left(-\boldsymbol{\eta}\ddot{x}_g - \boldsymbol{M}_B^{-1}\boldsymbol{K}_B\boldsymbol{x}_{ZB} - \boldsymbol{M}_B^{-1}\boldsymbol{C}_B\dot{\boldsymbol{x}}_B\right) \tag{5.90}$$

where, $\boldsymbol{\Lambda}$ is the sensor location matrix defined in Eq. (5.74) and (5.75).The observation equation at time $t = k \times \Delta t$ is a nonlinear function of unknown parametric vector $\boldsymbol{\theta}_k$ and can be linearized via Taylor series expansion, that is,

$$\boldsymbol{h}(\boldsymbol{X}_k, \boldsymbol{\theta}_k, \boldsymbol{F}_k) = \boldsymbol{h}\left(\widehat{\boldsymbol{X}}_{k|k-1}, \widehat{\boldsymbol{\theta}}_{k-1}, \boldsymbol{F}_k\right) + \boldsymbol{H}_k\left(\boldsymbol{\theta}_k - \widehat{\boldsymbol{\theta}}_{k-1}\right) \tag{5.91}$$

where, $\boldsymbol{H}_k$ is obtained based on the chain rule of partial differential with respect to the parametric vector $\boldsymbol{\theta}_k$ as follows

$$\boldsymbol{H}_k = \boldsymbol{\Lambda}\left(\boldsymbol{H}_{\theta,k} + \boldsymbol{H}_{X,k}\boldsymbol{X}_{\theta,k}\right) \tag{5.92}$$

In which,

$$\boldsymbol{H}_{\theta,k} = \boldsymbol{\Lambda}\left[\frac{\partial \boldsymbol{h}(\boldsymbol{X}, \boldsymbol{\theta}, \boldsymbol{F})}{\partial \boldsymbol{\theta}}\right]_{\boldsymbol{X}=\widehat{\boldsymbol{X}}_{k|k-1}, \boldsymbol{\theta}=\widehat{\boldsymbol{\theta}}_{k-1}}$$
$$\boldsymbol{H}_{X,k} = \boldsymbol{\Lambda}\left[\frac{\partial \boldsymbol{h}(\boldsymbol{X}, \boldsymbol{\theta}, \boldsymbol{F})}{\partial \boldsymbol{X}}\right]_{\boldsymbol{X}=\widehat{\boldsymbol{X}}_{k|k-1}, \boldsymbol{\theta}=\widehat{\boldsymbol{\theta}}_{k-1}} ; \boldsymbol{X}_{\theta,k} = \left[\frac{\partial \boldsymbol{X}(\boldsymbol{X}, \boldsymbol{\theta}, \boldsymbol{F})}{\partial \boldsymbol{\theta}}\right]_{\boldsymbol{\theta}=\widehat{\boldsymbol{\theta}}_{k-1}} \tag{5.93}$$

The details of Eq.(4.37) to (4.39) are given in Chapter 3.The partial derivative of the observation equation, Eq. (4.33) with respect to state vector $\boldsymbol{X}$ is given by

$$\boldsymbol{H}_{X,k} = \boldsymbol{\Lambda}\frac{\partial \boldsymbol{h}}{\partial \boldsymbol{X}} = \boldsymbol{\Lambda}\frac{\partial}{\partial \boldsymbol{X}}\left(-\boldsymbol{\eta}\ddot{x}_g - \boldsymbol{M}_B^{-1}\boldsymbol{K}_B\boldsymbol{x}_{ZB} - \boldsymbol{M}_B^{-1}\boldsymbol{C}_B\dot{\boldsymbol{x}}_B\right)$$
$$= -\boldsymbol{\Lambda}\boldsymbol{M}_B^{-1}\frac{\partial}{\partial \boldsymbol{X}}[\boldsymbol{K}_B\boldsymbol{x}_{ZB} \quad \boldsymbol{C}_B\dot{\boldsymbol{x}}_B]$$
$$= -\boldsymbol{\Lambda}\boldsymbol{M}_B^{-1}\frac{\partial}{\partial \boldsymbol{X}}[\boldsymbol{K}_B \quad \boldsymbol{C}_B]\begin{Bmatrix}\boldsymbol{x}_{ZB}\\ \dot{\boldsymbol{x}}_B\end{Bmatrix} = -\boldsymbol{\Lambda}\boldsymbol{M}_B^{-1}\frac{\partial}{\partial \boldsymbol{X}}[\boldsymbol{K}_B \quad \boldsymbol{C}_B]\{\boldsymbol{X}\}$$
$$= -\boldsymbol{\Lambda}\boldsymbol{M}_B^{-1}[\boldsymbol{K}_B \quad \boldsymbol{C}_B] \tag{5.94}$$

The partial derivative of the observation equation, Eq. (4.33) with respect to parametric vector $\boldsymbol{\theta}$ is

$$\boldsymbol{H}_{\theta,k} = \boldsymbol{\Lambda}\frac{\partial \boldsymbol{h}}{\partial \boldsymbol{\theta}} = \boldsymbol{\Lambda}\frac{\partial}{\partial \boldsymbol{\theta}}\left(-\boldsymbol{\eta}\ddot{x}_g - \boldsymbol{M}_B^{-1}\boldsymbol{K}_B\boldsymbol{x}_{ZB} - \boldsymbol{M}_B^{-1}\boldsymbol{C}_B\dot{\boldsymbol{x}}_B\right)$$
$$= -\boldsymbol{\Lambda}\boldsymbol{M}_B^{-1}\left[\frac{\partial}{\partial \boldsymbol{\theta}}(\boldsymbol{K}_B\boldsymbol{x}_{ZB}) + \frac{\partial}{\partial \boldsymbol{\theta}}(\boldsymbol{C}_B\dot{\boldsymbol{x}}_B)\right] \tag{5.95}$$

Partitioning the parametric vector $\boldsymbol{\theta}$ into $\boldsymbol{\theta}_i$, $\boldsymbol{\theta}_j$ and$\boldsymbol{\theta}_{\beta,\gamma}$ as

$$\boldsymbol{\theta} = \{k_b \quad k_1 \quad k_2 \quad k_3 \,|\, c_b \quad c_1 \quad c_2 \quad c_3 \,|\, \beta \quad \gamma\}^T = \{\boldsymbol{\theta}_i^T \quad \boldsymbol{\theta}_j^T \quad \boldsymbol{\theta}_{\beta,\gamma}^T\}^T \tag{5.96}$$

where,

$$\boldsymbol{\theta}_i = \{k_b \quad k_1 \quad k_2 \quad k_3\}^T \qquad \boldsymbol{\theta}_j = \{c_b \quad c_1 \quad c_2 \quad c_3\}^T \qquad \boldsymbol{\theta}_{\beta,\gamma} = \{\beta \quad \gamma\}^T \tag{5.97}$$

Evaluating $\frac{\partial}{\partial \boldsymbol{\theta}}(\boldsymbol{K}_B\boldsymbol{x}_{ZB})$ as

$$\frac{\partial}{\partial \boldsymbol{\theta}}(\boldsymbol{K}_B\boldsymbol{x}_{ZB}) = \left[\frac{\partial}{\partial \boldsymbol{\theta}_i}(\boldsymbol{K}_B\boldsymbol{x}_{ZB}) \quad \frac{\partial}{\partial \boldsymbol{\theta}_j}(\boldsymbol{K}_B\boldsymbol{x}_{ZB}) \quad \frac{\partial}{\partial \boldsymbol{\theta}_{\beta,\gamma}}(\boldsymbol{K}_B\boldsymbol{x}_{ZB})\right] \tag{5.98}$$

$$\boldsymbol{K}_B\boldsymbol{x}_{ZB} == \begin{Bmatrix} k_b z_b \\ -k_1x_b + k_1x_1 + k_2x_1 - k_2x_2 \\ -k_2x_1 + k_2x_2 + k_3x_2 - k_3x_3 \\ -k_3x_2 + k_3x_3 \end{Bmatrix} \tag{5.99}$$

Eq. (5.99) is obtained using the expressions given in Eq. (4.9).

$$\frac{\partial}{\partial \boldsymbol{\theta}_i}\boldsymbol{K}_B\boldsymbol{x}_{ZB} = \begin{bmatrix} z_b & 0 & 0 & 0 \\ 0 & -(x_b - x_1) & (x_1 - x_2) & 0 \\ 0 & 0 & -(x_1 - x_2) & (x_2 - x_3) \\ 0 & 0 & 0 & -(x_2 - x_3) \end{bmatrix} = [KK_{ZB}] \tag{5.100}$$

Eq. (5.100) is obtained using the expressions given in Eq. (5.52).

Differentiating $\boldsymbol{K}_B\boldsymbol{x}_{ZB}$ with respect to $\boldsymbol{\theta}_j$

$$\frac{\partial}{\partial \boldsymbol{\theta}_j}(\boldsymbol{K}_B\boldsymbol{x}_{ZB}) = \begin{bmatrix} 0 & 0 & 0 & 0 \\ 0 & 0 & 0 & 0 \\ 0 & 0 & 0 & 0 \\ 0 & 0 & 0 & 0 \end{bmatrix} = \boldsymbol{0}_{4x4} \tag{5.101}$$

Differentiating $\boldsymbol{K}_B\boldsymbol{x}_{ZB}$ with respect to $\boldsymbol{\theta}_{\beta,\gamma}$

$$\frac{\partial}{\partial \boldsymbol{\theta}_{\beta,\gamma}}(\boldsymbol{K}_B\boldsymbol{x}_{ZB}) = \begin{bmatrix} 0 & 0 \\ 0 & 0 \\ 0 & 0 \\ 0 & 0 \end{bmatrix} = \boldsymbol{0}_{4x2} \tag{5.102}$$

The partial derivative of $\boldsymbol{K}_B\boldsymbol{x}_{ZB}$ with respect to $\boldsymbol{\theta}$ is obtained by combining Eq.(5.100), (4.50) and (5.102) as

$$\frac{\partial}{\partial \boldsymbol{\theta}}(\boldsymbol{K}_B\boldsymbol{x}_{ZB}) = [\boldsymbol{K}\boldsymbol{K}_{ZB} \quad \boldsymbol{0}_{4x4} \quad \boldsymbol{0}_{4x2}] \tag{5.103}$$

$$\boldsymbol{C}_B\dot{\boldsymbol{x}}_B = \begin{Bmatrix} c_b\dot{x}_b \\ -c_1\dot{x}_b + c_1\dot{x}_1 + c_2\dot{x}_1 - c_2\dot{x}_2 \\ -c_2\dot{x}_1 + c_2\dot{x}_2 + c_3\dot{x}_2 - c_3\dot{x}_3 \\ -c_3\dot{x}_2 + c_3\dot{x}_3 \end{Bmatrix} \tag{5.104}$$

Eq. (5.104) is obtained using the expressions given in Eq. (5.55).

From Eq. (5.58), $\frac{\partial}{\partial \boldsymbol{\theta}_i}(\boldsymbol{C}_B\dot{\boldsymbol{x}}_B)$ is given as

$$\frac{\partial}{\partial \boldsymbol{\theta}_i}(\boldsymbol{C}_B\dot{\boldsymbol{x}}_B) = \begin{bmatrix} 0 & 0 & 0 & 0 \\ 0 & 0 & 0 & 0 \\ 0 & 0 & 0 & 0 \\ 0 & 0 & 0 & 0 \end{bmatrix} = \boldsymbol{0}_{4x4} \tag{5.105}$$

Differentiating $\boldsymbol{C}_B\dot{\boldsymbol{x}}_B$ with respect to $\boldsymbol{\theta}_j$

$$\frac{\partial}{\partial \boldsymbol{\theta}_j}(\boldsymbol{C}_B\dot{\boldsymbol{x}}_B) = \begin{bmatrix} \dot{x}_b & 0 & 0 & 0 \\ 0 & -(\dot{x}_b - \dot{x}_1) & (\dot{x}_1 - \dot{x}_2) & 0 \\ 0 & 0 & -(\dot{x}_1 - \dot{x}_2) & (\dot{x}_2 - \dot{x}_3) \\ 0 & 0 & 0 & -(\dot{x}_2 - \dot{x}_3) \end{bmatrix} = [CC_B] \tag{5.106}$$

Eq. (5.106) is obtained using the expressions given in Eq. (5.59).

Differentiating $\boldsymbol{C}_B\dot{\boldsymbol{x}}_B$ with respect to $\boldsymbol{\theta}_{\beta,\gamma}$

$$\frac{\partial}{\partial \boldsymbol{\theta}_{\beta,\gamma}}(\boldsymbol{C}_B\dot{\boldsymbol{x}}_B) = \begin{bmatrix} 0 & 0 \\ 0 & 0 \\ 0 & 0 \\ 0 & 0 \end{bmatrix} = \mathbf{0}_{4x2} \tag{5.107}$$

The partial derivative of $\boldsymbol{C}_B\dot{\boldsymbol{x}}_B$ with respect to $\boldsymbol{\theta}$ is obtained by combining Eq.(5.105), (5.106) and (5.107) as

$$\frac{\partial}{\partial \boldsymbol{\theta}}(\boldsymbol{C}_B\dot{\boldsymbol{x}}_B) = [\mathbf{0}_{4x4} \quad \boldsymbol{C}\boldsymbol{C}_B \quad \mathbf{0}_{4x2}] \tag{5.108}$$

Substituting $\frac{\partial}{\partial \boldsymbol{\theta}}(\boldsymbol{K}_B\boldsymbol{x}_{ZB})$ from Eq. (5.103) and $\frac{\partial}{\partial \boldsymbol{\theta}}(\boldsymbol{C}_B\dot{\boldsymbol{x}}_B)$ from Eq. (5.108) into Eq. (4.47)

$$\begin{aligned} \boldsymbol{H}_{\theta,k} = \boldsymbol{\Lambda}\frac{\partial \boldsymbol{h}}{\partial \boldsymbol{\theta}} &= -\boldsymbol{\Lambda}\boldsymbol{M}_B^{-1}\left[\frac{\partial}{\partial \boldsymbol{\theta}}(\boldsymbol{K}_B\boldsymbol{x}_{ZB}) + \frac{\partial}{\partial \boldsymbol{\theta}}(\boldsymbol{C}_B\dot{\boldsymbol{x}}_B)\right] \\ &= -\boldsymbol{\Lambda}\boldsymbol{M}_B^{-1}\left[[\boldsymbol{K}\boldsymbol{K}_{ZB} \quad \mathbf{0}_{4x4} \quad \mathbf{0}_{4x2}] + [\mathbf{0}_{4x4} \quad \boldsymbol{C}\boldsymbol{C}_B \quad \mathbf{0}_{4x2}]\right] \\ &= -\boldsymbol{\Lambda}\boldsymbol{M}_B^{-1}[\boldsymbol{K}\boldsymbol{K}_{ZB} \quad \boldsymbol{C}\boldsymbol{C}_B \quad \mathbf{0}_{4x2}] \end{aligned} \tag{5.109}$$

The state-space form of the governing differential equation is given as

$$\begin{aligned} \dot{\boldsymbol{X}} = \begin{Bmatrix} \dot{\boldsymbol{x}}_{ZB} \\ \ddot{\boldsymbol{x}}_B \end{Bmatrix} = \frac{d\boldsymbol{X}}{dt} = \frac{d}{dt}\begin{Bmatrix} \boldsymbol{x}_{ZB} \\ \dot{\boldsymbol{x}}_B \end{Bmatrix} &= \begin{Bmatrix} \begin{Bmatrix} \dot{z}_b \\ \dot{\boldsymbol{x}}_B \end{Bmatrix} \\ -\boldsymbol{\eta}\ddot{x}_g - \boldsymbol{M}_B^{-1}\boldsymbol{K}_B\boldsymbol{x}_{ZB} - \boldsymbol{M}_B^{-1}\boldsymbol{C}_B\dot{\boldsymbol{x}}_B \end{Bmatrix} \\ &= \begin{Bmatrix} \begin{Bmatrix} \dot{z}_b \\ \dot{\boldsymbol{x}}_B \end{Bmatrix} \\ -\boldsymbol{\eta}\ddot{x}_g - \boldsymbol{M}_B^{-1}\boldsymbol{F}_s(\boldsymbol{x}_{ZB},\boldsymbol{\theta}) - \boldsymbol{M}_B^{-1}\boldsymbol{F}_c(\dot{\boldsymbol{x}}_B,\boldsymbol{\theta}) \end{Bmatrix} \end{aligned} \tag{5.110}$$

where,

$$\dot{\boldsymbol{x}}_{ZB} = \begin{Bmatrix} \dot{z}_b \\ \dot{\boldsymbol{x}}_B \end{Bmatrix} = \begin{Bmatrix} \dot{z}_b \\ \dot{x}_b \\ \dot{x}_1 \\ \dot{x}_2 \\ \dot{x}_3 \end{Bmatrix} \qquad \dot{z}_b = \dot{x}_b - \beta|\dot{x}_b||z_b|^{(\alpha-1)}z_b - \gamma\dot{x}_b|z_b|^{\alpha} \tag{5.111}$$

The expression for $\boldsymbol{X}, \boldsymbol{x}_{zb}, \boldsymbol{x}_B$ and $\dot{\boldsymbol{x}}_B$ are given in Eq. (5.86) to Eq. (5.88)

Differentiating both side of Eq.(5.110) by $\boldsymbol{\theta}$ and denoting $\frac{d\boldsymbol{x}_{ZB}}{d\boldsymbol{\theta}} = \boldsymbol{x}_{ZB,\theta}$ and $\frac{d\boldsymbol{x}_B}{d\boldsymbol{\theta}} = \boldsymbol{x}_{B,\theta}$

$$\frac{d\dot{\boldsymbol{X}}}{d\boldsymbol{\theta}} = \begin{bmatrix} \frac{d\dot{\boldsymbol{x}}_{ZB}}{d\boldsymbol{\theta}} \\ \frac{d\ddot{\boldsymbol{x}}_B}{d\boldsymbol{\theta}} \end{bmatrix} = \begin{bmatrix} \dot{\boldsymbol{x}}_{ZB,\theta} \\ \ddot{\boldsymbol{x}}_{B,\theta} \end{bmatrix} = \dot{\boldsymbol{X}}_\theta = \frac{d}{dt}\begin{bmatrix} \boldsymbol{x}_{ZB,\theta} \\ \dot{\boldsymbol{x}}_{B,\theta} \end{bmatrix}$$

$$= \begin{bmatrix} \dfrac{d\dot{\boldsymbol{x}}_{ZB}}{d\boldsymbol{\theta}} \\ \dfrac{d}{d\boldsymbol{\theta}}\left(-\boldsymbol{\eta}\ddot{x}_g - \boldsymbol{M}_B^{-1}\boldsymbol{F}_s(\boldsymbol{x}_{ZB},\boldsymbol{\theta}) - \boldsymbol{M}_B^{-1}\boldsymbol{F}_c(\dot{\boldsymbol{x}}_B,\boldsymbol{\theta})\right) \end{bmatrix}$$

$$= \begin{bmatrix} \begin{bmatrix} \dfrac{d\dot{z}_b}{d\boldsymbol{\theta}} \\ \dfrac{d\dot{\boldsymbol{x}}_B}{d\boldsymbol{\theta}} \end{bmatrix} \\ -\boldsymbol{M}_B^{-1}\dfrac{d\boldsymbol{F}_s(\boldsymbol{x}_{ZB},\boldsymbol{\theta})}{d\boldsymbol{\theta}} - \boldsymbol{M}_B^{-1}\dfrac{d\boldsymbol{F}_c(\dot{\boldsymbol{x}}_B,\boldsymbol{\theta})}{d\boldsymbol{\theta}} \end{bmatrix} \tag{5.112}$$

Applying chain rule of differentiation into Eq. (4.58)

$$\frac{d\boldsymbol{F}_s(\boldsymbol{x}_{ZB},\boldsymbol{\theta})}{d\boldsymbol{\theta}} = \frac{\partial \boldsymbol{F}_s}{\partial \boldsymbol{x}_{ZB}}\frac{d\boldsymbol{x}_{ZB}}{d\boldsymbol{\theta}} + \frac{\partial \boldsymbol{F}_s}{\partial \boldsymbol{\theta}}\frac{d\boldsymbol{\theta}}{d\boldsymbol{\theta}} = \frac{\partial \boldsymbol{F}_s}{\partial \boldsymbol{x}_{ZB}}\frac{d\boldsymbol{x}_{ZB}}{d\boldsymbol{\theta}} + \frac{\partial \boldsymbol{F}_s}{\partial \boldsymbol{\theta}} \tag{5.113}$$

$$\frac{d\boldsymbol{F}_c(\dot{\boldsymbol{x}}_B,\boldsymbol{\theta})}{d\boldsymbol{\theta}} = \frac{\partial \boldsymbol{F}_c}{\partial \dot{\boldsymbol{x}}_B}\frac{d\dot{\boldsymbol{x}}_B}{d\boldsymbol{\theta}} + \frac{\partial \boldsymbol{F}_c}{\partial \boldsymbol{\theta}}\frac{d\boldsymbol{\theta}}{d\boldsymbol{\theta}} = \frac{\partial \boldsymbol{F}_c}{\partial \dot{\boldsymbol{x}}_B}\frac{d\dot{\boldsymbol{x}}_B}{d\boldsymbol{\theta}} + \frac{\partial \boldsymbol{F}_c}{\partial \boldsymbol{\theta}} \tag{5.114}$$

$$\frac{d\dot{z}_b}{d\boldsymbol{\theta}} = \frac{\partial \dot{z}_b}{\partial \boldsymbol{X}}\frac{d\boldsymbol{X}}{d\boldsymbol{\theta}} + \frac{\partial \dot{z}_b}{\partial \boldsymbol{\theta}}\frac{d\boldsymbol{\theta}}{d\boldsymbol{\theta}} = \frac{\partial \dot{z}_b}{\partial \boldsymbol{X}}\frac{d\boldsymbol{X}}{d\boldsymbol{\theta}} + \frac{\partial \dot{z}_b}{\partial \boldsymbol{\theta}} = \frac{\partial \dot{z}_b}{\partial \boldsymbol{X}}\begin{Bmatrix} \dfrac{d\boldsymbol{x}_{ZB}}{d\boldsymbol{\theta}} \\ \dfrac{d\dot{\boldsymbol{x}}_B}{d\boldsymbol{\theta}} \end{Bmatrix} + \frac{\partial \dot{z}_b}{\partial \boldsymbol{\theta}} \tag{5.115}$$

where, $X = \begin{Bmatrix} \boldsymbol{x}_{ZB} \\ \dot{\boldsymbol{x}}_B \end{Bmatrix}$, therefore, $\frac{dX}{d\boldsymbol{\theta}} = \begin{Bmatrix} \frac{d\boldsymbol{x}_{ZB}}{d\boldsymbol{\theta}} \\ \frac{d\dot{\boldsymbol{x}}_B}{d\boldsymbol{\theta}} \end{Bmatrix}$

Substituting $\frac{d\boldsymbol{F}_s}{d\boldsymbol{\theta}}$, $\frac{d\boldsymbol{F}_c}{d\boldsymbol{\theta}}$ and $\frac{d\dot{z}_b}{d\boldsymbol{\theta}}$ obtained from Eq.(5.113), (4.60) and (5.115) into Eq. (4.58)

$$\frac{d\dot{\boldsymbol{X}}}{d\boldsymbol{\theta}} = \dot{\boldsymbol{X}}_\theta = \begin{bmatrix} \begin{bmatrix} \dfrac{d\dot{z}_b}{d\boldsymbol{\theta}} \\ \dfrac{d\dot{\boldsymbol{x}}_B}{d\boldsymbol{\theta}} \end{bmatrix} \\ -\boldsymbol{M}_B^{-1}\dfrac{d\boldsymbol{F}_s(\boldsymbol{x}_{ZB},\boldsymbol{\theta})}{d\boldsymbol{\theta}} - \boldsymbol{M}_B^{-1}\dfrac{d\boldsymbol{F}_c(\dot{\boldsymbol{x}}_B,\boldsymbol{\theta})}{d\boldsymbol{\theta}} \end{bmatrix} \tag{5.116}$$

$$\dot{\boldsymbol{X}}_\theta = \begin{bmatrix} \begin{bmatrix} \left(\dfrac{\partial \dot{z}_b}{\partial \boldsymbol{X}}\begin{Bmatrix} \dfrac{d\boldsymbol{x}_{ZB}}{d\boldsymbol{\theta}} \\ \dfrac{d\dot{\boldsymbol{x}}_B}{d\boldsymbol{\theta}} \end{Bmatrix} + \dfrac{\partial \dot{z}_b}{\partial \boldsymbol{\theta}}\right) \\ \dfrac{d\dot{\boldsymbol{x}}_B}{d\boldsymbol{\theta}} \end{bmatrix} \\ -\boldsymbol{M}_B^{-1}\left(\dfrac{\partial \boldsymbol{F}_s}{\partial \boldsymbol{x}_{ZB}}\dfrac{d\boldsymbol{x}_{ZB}}{d\boldsymbol{\theta}} + \dfrac{\partial \boldsymbol{F}_s}{\partial \boldsymbol{\theta}}\right) - \boldsymbol{M}_B^{-1}\left(\dfrac{\partial \boldsymbol{F}_c}{\partial \dot{\boldsymbol{x}}_B}\dfrac{d\dot{\boldsymbol{x}}_B}{d\boldsymbol{\theta}} + \dfrac{\partial \boldsymbol{F}_c}{\partial \boldsymbol{\theta}}\right) \end{bmatrix} \tag{5.117}$$

$$\dot{\boldsymbol{X}}_\theta = \begin{bmatrix} \left[\left(\dfrac{\partial \dot{z}_b}{\partial \boldsymbol{X}}\begin{Bmatrix}\dfrac{d\boldsymbol{x}_{ZB}}{d\boldsymbol{\theta}}\\ \dfrac{d\dot{\boldsymbol{x}}_B}{d\boldsymbol{\theta}}\end{Bmatrix}\right)\right] \\ \dfrac{d\dot{\boldsymbol{x}}_B}{d\boldsymbol{\theta}} \\ \left[-\boldsymbol{M}_B^{-1}\dfrac{\partial \boldsymbol{F_s}}{\partial \boldsymbol{x}_{ZB}} - \boldsymbol{M}_B^{-1}\dfrac{\partial \boldsymbol{F_c}}{\partial \dot{\boldsymbol{x}}_B}\right]\begin{Bmatrix}\dfrac{d\boldsymbol{x}_{ZB}}{d\boldsymbol{\theta}}\\ \dfrac{d\dot{\boldsymbol{x}}_B}{d\boldsymbol{\theta}}\end{Bmatrix} \end{bmatrix} + \begin{bmatrix} \dfrac{\partial \dot{z}_b}{\partial \boldsymbol{\theta}} \\ \boldsymbol{0}_{4x10} \\ -\boldsymbol{M}_B^{-1}\left(\dfrac{\partial \boldsymbol{F_s}}{\partial \boldsymbol{\theta}} + \dfrac{\partial \boldsymbol{F_c}}{\partial \boldsymbol{\theta}}\right) \end{bmatrix} \tag{5.118}$$

Replacing $\mathbf{F}_S$, $\mathbf{F}_C$ from the relation given in Eq. (5.110) into Eq.(5.119), gives

$$\dot{\boldsymbol{X}}_\theta = \begin{bmatrix} \dfrac{\partial \dot{z}_b}{\partial \boldsymbol{x}_{ZB}} & \dfrac{\partial \dot{z}_b}{\partial \dot{\boldsymbol{x}}_B} \\ \boldsymbol{0}_{4x5} & \boldsymbol{I}_{4x4} \\ -\boldsymbol{M}_B^{-1}\left[\dfrac{\partial(\boldsymbol{K}_B\boldsymbol{x}_{ZB})}{\partial \boldsymbol{x}_{ZB}} + \dfrac{\partial(\boldsymbol{C}_B\dot{\boldsymbol{x}}_B)}{\partial \dot{\boldsymbol{x}}_B}\right] \end{bmatrix}\begin{Bmatrix}\dfrac{d\boldsymbol{x}_{ZB}}{d\boldsymbol{\theta}}\\ \dfrac{d\dot{\boldsymbol{x}}_B}{d\boldsymbol{\theta}}\end{Bmatrix} + \begin{bmatrix} \dfrac{\partial \dot{z}_b}{\partial \boldsymbol{\theta}} \\ \boldsymbol{0}_{4x10} \\ -\boldsymbol{M}_B^{-1}\left(\dfrac{\partial \boldsymbol{F_s}}{\partial \boldsymbol{\theta}} + \dfrac{\partial \boldsymbol{F_c}}{\partial \boldsymbol{\theta}}\right) \end{bmatrix} \tag{5.119}$$

Substituting, $\boldsymbol{H}_{\theta,k}$ from Eq. (5.109) into Eq. (5.119) gives

$$\dot{\boldsymbol{X}}_\theta = \begin{bmatrix} \dfrac{\partial \dot{z}_b}{\partial \boldsymbol{x}_{ZB}} & \dfrac{\partial \dot{z}_b}{\partial \dot{\boldsymbol{x}}_B} \\ \boldsymbol{0}_{4x5} & \boldsymbol{I}_{4x4} \\ -\boldsymbol{M}_B^{-1}\boldsymbol{K}_B & -\boldsymbol{M}_B^{-1}\boldsymbol{C}_B \end{bmatrix}\begin{Bmatrix}\dfrac{d\boldsymbol{x}_{ZB}}{d\boldsymbol{\theta}}\\ \dfrac{d\dot{\boldsymbol{x}}_B}{d\boldsymbol{\theta}}\end{Bmatrix} + \begin{bmatrix} \dfrac{\partial \dot{z}_b}{\partial \boldsymbol{\theta}} \\ \boldsymbol{0}_{4x10} \\ \boldsymbol{H}_{\theta,k} \end{bmatrix} \tag{5.120}$$

In the equation, Eq. (5.120), the vector $\left\{\frac{d\boldsymbol{x}_{ZB}}{d\boldsymbol{\theta}} \quad \frac{d\dot{\boldsymbol{x}}_B}{d\boldsymbol{\theta}}\right\}^T$ can be expressed as

$$\begin{Bmatrix}\dfrac{d\boldsymbol{x}_{ZB}}{d\boldsymbol{\theta}}\\ \dfrac{d\dot{\boldsymbol{x}}_B}{d\boldsymbol{\theta}}\end{Bmatrix} = \left\{\frac{d\boldsymbol{X}}{d\boldsymbol{\theta}}\right\} = \boldsymbol{X}_\theta \tag{5.121}$$

Simplifying the Eq. Eq. (5.120) by using the relation of Eq. (5.121) gives

$$\dot{\boldsymbol{X}}_\theta = \begin{bmatrix} \dfrac{\partial \dot{z}_b}{\partial \boldsymbol{X}} \\ \boldsymbol{0}_{4x5} \quad \boldsymbol{I}_{4x4} \\ -\boldsymbol{M}_B^{-1}[\boldsymbol{K}_B \quad \boldsymbol{C}_B] \end{bmatrix}\{\boldsymbol{X}_\theta\} + \begin{bmatrix} \dfrac{\partial \dot{z}_b}{\partial \boldsymbol{\theta}} \\ \boldsymbol{0}_{4x10} \\ \boldsymbol{H}_{\theta,k} \end{bmatrix} \tag{5.122}$$

Integrating Eq. (5.122) using 4th order Runga-Kutta integration scheme, give $\boldsymbol{X}_\theta$ or $\frac{d\boldsymbol{X}}{d\boldsymbol{\theta}}$, provided $\frac{\partial \dot{z}_b}{\partial \boldsymbol{X}}$ and $\frac{\partial \dot{z}_b}{\partial \boldsymbol{\theta}}$ are known. The vectors $\frac{\partial \dot{z}_b}{\partial \boldsymbol{X}}$ and $\frac{\partial \dot{z}_b}{\partial \boldsymbol{\theta}}$ are evaluated as shown below.

Evaluation of $\frac{\partial \dot{z}_b}{\partial \boldsymbol{X}}$

From Eq. (5.111)

$$\dot{z}_b = \dot{x}_b - \beta|\dot{x}_b||z_b|^{(\alpha-1)}z_b - \gamma\dot{x}_b|z_b|^{\alpha} \tag{5.123}$$

From Eq. (5.84), the state vector $\boldsymbol{X}$ is given as

$$\boldsymbol{X} = \{z_b \quad x_b \quad x_1 \quad x_2 \quad x_3 \quad \dot{x}_b \quad \dot{x}_1 \quad \dot{x}_2 \quad \dot{x}_3\}^T \tag{5.124}$$

Therefore,

$$\begin{aligned}\frac{\partial \dot{z}_b}{\partial \boldsymbol{X}} &= \left[\frac{\partial \dot{z}_b}{\partial z_b} \quad \frac{\partial \dot{z}_b}{\partial x_b} \quad \frac{\partial \dot{z}_b}{\partial x_1} \quad \frac{\partial \dot{z}_b}{\partial x_2} \quad \frac{\partial \dot{z}_b}{\partial x_3} \quad \frac{\partial \dot{z}_b}{\partial \dot{x}_b} \quad \frac{\partial \dot{z}_b}{\partial \dot{x}_1} \quad \frac{\partial \dot{z}_b}{\partial \dot{x}_2} \quad \frac{\partial \dot{z}_b}{\partial \dot{x}_3}\right] \\ &= \left[\frac{\partial \dot{z}_b}{\partial z_b} \quad 0 \quad 0 \quad 0 \quad 0 \quad \frac{\partial \dot{z}_b}{\partial \dot{x}_b} \quad 0 \quad 0 \quad 0\right]\end{aligned} \tag{5.125}$$

Evaluating $\frac{\partial \dot{z}_b}{\partial z_b}$ as

$$\begin{aligned}\frac{\partial \dot{z}_b}{\partial z_b} &= \frac{\partial}{\partial z_b}\left(\dot{x}_b - \beta|\dot{x}_b||z_b|^{(\alpha-1)}z_b - \gamma\dot{x}_b|z_b|^{\alpha}\right) \\ &= -\beta|\dot{x}_b||z_b|^{(\alpha-1)} - \beta(\alpha-1)|\dot{x}_b||z_b|^{(\alpha-2)}z_b * sign(z_b) \\ &\quad - \gamma\alpha\dot{x}_b|z_b|^{(\alpha-1)} * sign(z_b)\end{aligned} \tag{5.126}$$

Evaluating $\frac{\partial \dot{z}_b}{\partial \dot{x}_b}$ as

$$\begin{aligned}\frac{\partial \dot{z}_b}{\partial \dot{x}_b} &= \frac{\partial}{\partial \dot{x}_b}\left(\dot{x}_b - \beta|\dot{x}_b||z_b|^{(\alpha-1)}z_b - \gamma\dot{x}_b|z_b|^{\alpha}\right) \\ &= 1 - \beta|z_b|^{(\alpha-1)}z_b * sign(\dot{x}_b) - \gamma|z_b|^{\alpha}\end{aligned} \tag{5.127}$$

Evaluation of $\frac{\partial \dot{z}_b}{\partial \boldsymbol{\theta}}$

From Eq. (5.85), the state vector $\boldsymbol{\theta}$is given as

$$\boldsymbol{\theta} = \{k_b \quad k_1 \quad k_2 \quad k_3 \quad c_b \quad c_1 \quad c_2 \quad c_3 \quad \beta \quad \gamma\}^T \tag{5.128}$$

Therefore,

$$\begin{aligned}\frac{\partial \dot{z}_b}{\partial \boldsymbol{\theta}} &= \left[\frac{\partial \dot{z}_b}{\partial k_b} \quad \frac{\partial \dot{z}_b}{\partial k_1} \quad \frac{\partial \dot{z}_b}{\partial k_2} \quad \frac{\partial \dot{z}_b}{\partial k_3} \quad \frac{\partial \dot{z}_b}{\partial c_b} \quad \frac{\partial \dot{z}_b}{\partial c_1} \quad \frac{\partial \dot{z}_b}{\partial c_2} \quad \frac{\partial \dot{z}_b}{\partial c_3} \quad \frac{\partial \dot{z}_b}{\partial \beta} \quad \frac{\partial \dot{z}_b}{\partial \gamma}\right] \\ &= \left[0 \quad 0 \quad 0 \quad 0 \quad 0 \quad 0 \quad 0 \quad 0 \quad \frac{\partial \dot{z}_b}{\partial \beta} \quad \frac{\partial \dot{z}_b}{\partial \gamma}\right]\end{aligned} \tag{5.129}$$

Evaluating $\frac{\partial \dot{z}_b}{\partial \beta}$ as

$$\frac{\partial \dot{z}_b}{\partial \beta} = \frac{\partial}{\partial \beta}\left(\dot{x}_b - \beta|\dot{x}_b||z_b|^{(\alpha-1)}z_b - \gamma\dot{x}_b|z_b|^{\alpha}\right) = -|\dot{x}_b||z_b|^{(\alpha-1)}z_b \tag{5.130}$$

Evaluating $\frac{\partial \dot{z}_b}{\partial \gamma}$ as

$$\frac{\partial \dot{z}_b}{\partial \gamma} = \frac{\partial}{\partial \gamma}\left(\dot{x}_b - \beta|\dot{x}_b||z_b|^{(\alpha-1)}z_b - \gamma\dot{x}_b|z_b|^{\alpha}\right) = -\dot{x}_b|z_b|^{\alpha} \tag{5.131}$$

Therefore, $\dot{\boldsymbol{X}}_\theta$ can be obtained from Eq. (5.122) by using Eq. (5.125) to Eq. (5.131). The linearized observation equation, $\boldsymbol{H}_k$ of Eq. (4.38) is obtained by substituting $\boldsymbol{H}_{\theta,k}, \boldsymbol{H}_{X,k}, \boldsymbol{X}_{\theta,k}$ obtained from Eq. (5.109),(4.40) and integrating Eq.(5.122) respectively. Using the above formulations, the Two-stage EKF algorithm is implemented in MATLAB in the following steps as given below.

5.3.2.2 Implementation procedure of Two-Stage EKF in MATLAB

The algorithm is implemented in MATLAB in four steps which are given below.

Step-1: Initialization Step.

Initialization is done by assuming the initial value of

h) The state vector, $\boldsymbol{X}$.
i) Error covariance matrix of $\boldsymbol{X}$ which is $\boldsymbol{P}_x$.
j) The parametric vector, $\boldsymbol{\theta}$.
k) Error covariance matrix of $\boldsymbol{\theta}$ which is $\boldsymbol{P}_\theta$.
l) The matrix $\boldsymbol{X}_\theta$ which is $\frac{d\boldsymbol{X}}{d\boldsymbol{\theta}}$.
m) Process error covariance matrix, $\boldsymbol{Q}$.
n) Measurement error covariance matrix, $\boldsymbol{R}$.

Step-2: Evaluation of state transfer matrix

The linearized observation equation matrix, $\boldsymbol{H}_k$ is evaluated using Eq. (4.38).

Step-3a: Prediction of State Vector

With the state and parametric vector of previous step, the stiffness and damping matrix of current step is evaluated. The predicted state vector is evaluated by integration of the state space equation, Eq. (4.32), using 4th order Runga-Kutta integration scheme.

Step-3b: Updating State Vector

The measurement information at current time step is used to correct the estimate to get more accurate state information. This is accomplished by Kalman Filtering which is described in the following steps.

The state transition matrix $\boldsymbol{\Phi}_{k-1|k-1}$is determined as

$$\boldsymbol{\Phi}_{\mathrm{k-1|k-1}} = \boldsymbol{I}_{8x8} + \Delta t.\boldsymbol{A2}\left(\widehat{\boldsymbol{X}}_{k-1|k-1}\right) \tag{5.132}$$

where,

$$\boldsymbol{A2}\left(\widehat{\boldsymbol{X}}_{k-1|k-1}\right) = -\boldsymbol{M}_B^{-1}[\boldsymbol{K}_B \quad \boldsymbol{C}_B] \tag{5.133}$$

The Kalman Gain matrix is determined as

$$\boldsymbol{\mathcal{K}}_k = \frac{\boldsymbol{\Phi}_{k-1|k-1}\boldsymbol{P}_{k|k-1}\boldsymbol{H}_{x,k}{}^T}{\boldsymbol{H}_{x,k}\boldsymbol{P}_{k|k-1}\boldsymbol{H}_{x,k}{}^T + \boldsymbol{R}} \tag{5.134}$$

where, $\boldsymbol{H}_{x,k}$is obtained from Eq.(4.40)

From the measurement equation, Eq. (4.71), the predicted measurement (in the present case: acceleration) is evaluated as

$$\ddot{\widehat{\boldsymbol{x}}}_i = -\boldsymbol{\eta}\ddot{x}_g - \boldsymbol{M}_B^{-1}\boldsymbol{K}_B\boldsymbol{x}_{ZB} - \boldsymbol{M}^{-1}\boldsymbol{C}_B\dot{\boldsymbol{x}}_B \tag{5.135}$$

where, the state $\boldsymbol{x}, \dot{\boldsymbol{x}}$ are the predicted states obtained from Eq. (4.32). The predicted stiffness and damping matrices are obtained from the parametric vector of previous step. If the current measured acceleration from the system is denoted as $\ddot{\boldsymbol{x}}_i$, then the difference between current measurement and estimated measurement Eq. (4.71), also known as innovation is given as

$$\widehat{\boldsymbol{y}}_{\boldsymbol{k}} = \left(\boldsymbol{\Lambda}\ddot{\boldsymbol{x}}_i - \ddot{\widehat{\boldsymbol{x}}}_i\right) \tag{5.136}$$

The updated posterior estimate of the state vector is given as

$$\widehat{\boldsymbol{X}}_{k|k} = \widehat{\boldsymbol{X}}_{k|k-1} + \boldsymbol{\mathcal{K}}_{\mathrm{k}}\widehat{\boldsymbol{y}}_{\boldsymbol{k}} \tag{5.137}$$

and the updated error covariance matrix of $\boldsymbol{X}$, which is $\boldsymbol{P}_X$, is obtained as

$$\boldsymbol{P}_{X,k|k+1} = \boldsymbol{\Phi}_{k-1|k-1}\boldsymbol{P}_{X,k|k}\boldsymbol{\Phi}_{k-1|k-1}^{\boldsymbol{T}} - \boldsymbol{\mathcal{K}}_k\boldsymbol{H}_{x,k}\boldsymbol{P}_{X,k|k}\boldsymbol{\Phi}_{k-1|k-1}^{\boldsymbol{T}} \tag{5.138}$$

Step-3c: Updating Parametric Vector

The Kalman Gain matrix is determined as

$$\boldsymbol{\mathcal{K}}_k = \frac{\boldsymbol{I}\ \boldsymbol{P}_{k|k-1}\boldsymbol{H}_k{}^T}{\boldsymbol{H}_k\boldsymbol{P}_{k|k-1}\boldsymbol{H}_k{}^T + \boldsymbol{R}} \tag{5.139}$$

where, $\boldsymbol{H}_k$ is the linearized measurement equation obtained from Eq.(4.38)

The updated posterior estimate of the parametric vector is evaluated as

$$\boldsymbol{\theta}_{k|k} = \boldsymbol{\theta}_{k|k-1} + \mathcal{K}_{\mathrm{k}}\hat{\boldsymbol{y}}_{\boldsymbol{k}} \tag{5.140}$$

and the updated error covariance matrix of $\boldsymbol{\theta}$ which is $\boldsymbol{P}_{\theta}$, is obtained as

$$\boldsymbol{P}_{\theta,k|k+1} = \boldsymbol{I}\boldsymbol{P}_{\theta,k|k}\boldsymbol{I}^{\boldsymbol{T}} - \mathcal{K}_{\mathrm{k}}\mathbf{H}_{\mathrm{k}}\boldsymbol{P}_{\theta,k|k}\boldsymbol{I}^{\boldsymbol{T}} \tag{5.141}$$

Step-4: Prediction Step of matrix $\boldsymbol{X}_{\theta}$ or $\frac{d\boldsymbol{X}}{d\boldsymbol{\theta}}$ *for next time step*

The predicted matrix $\boldsymbol{X}_{\theta}$, which is required for the evaluation of the linearized measurement equation given by Eq. (4.38) is obtained by integration of the differential equation, Eq. (5.122) by using 4th order Runga-Kutta integration scheme.

5.3.3 UKF algorithm for identification of base-isolated building

In UKF, there is no need to evaluate the complex Jacobian matrices. The process of implementation is very simple. The details of formulation are given in chapter 3. In this section, the implementation issues are presented for a sample three storey BI shear building. The implementation procedure is described below.

5.3.3.1 Implementation procedure of UKF in MATLAB for three-storey base-isolated building

The identification of state and parameter of a sample three storey shear building using UKF technique is described in detail in this sub-section. In this case state and parameters are arranged in a single vector or extended state vector similar to EKF identification.

The unknown extended state vector to be identified is

$$\boldsymbol{X}_e = \{x_b \quad x_1 \quad x_2 \quad x_3 \quad \dot{x}_b \quad \dot{x}_1 \quad \dot{x}_2 \quad \dot{x}_3 \quad k_b \quad k_1 \quad k_2 \quad k_3 \quad \beta \quad \alpha\}^T \tag{5.142}$$

The dimension of the extended state vector, L=14.

The process equation is expressed in state-space form as given by Eq. (4.79)

$$\dot{\boldsymbol{X}}_e = \begin{Bmatrix} \dot{\boldsymbol{x}}_i \\ \ddot{\boldsymbol{x}}_i \\ \dot{\boldsymbol{k}}_i \\ \dot{\beta} \\ \dot{\alpha} \end{Bmatrix} = \frac{d}{dt}\begin{Bmatrix} \boldsymbol{x}_i \\ \dot{\boldsymbol{x}}_i \\ \boldsymbol{k}_i \\ \beta \\ \alpha \end{Bmatrix} = \frac{d\boldsymbol{X}_e}{dt} = \begin{Bmatrix} \dot{\boldsymbol{x}}_i \\ -\boldsymbol{\eta}\ddot{x}_g - \boldsymbol{K}\boldsymbol{x}_i/\boldsymbol{M} - \boldsymbol{C}\dot{\boldsymbol{x}}_i/M \\ 0 \\ 0 \\ 0 \end{Bmatrix} \tag{5.143}$$

Step-1: Initialization Step.

Initialization is done by assuming the initial value of

e) The extended state vector, $\boldsymbol{X_e}$ containing both state and parameter.

f) Error covariance matrix of $\boldsymbol{X_e}$ which is $\boldsymbol{P}$.

g) Process error covariance matrix, $\boldsymbol{Q}$.

h) Measurement error covariance matrix, $\boldsymbol{R}$.

Step-2: Generation of Sigma point.

If the total number of elements in the extended state vector is n, then for each element in the extended state vector $(2n+1)$ sigma points are generated. So, a matrix of sigma points of size $nx\ (2n + 1)$ is created.

Step-3: Passing the Sigma Points through Process equation.

The sigma points are passed through the process equation. The process equation is expressed in state-space form. Using the input ground excitation and one set of sigma point vector, the predicted transformed sigma point vector is generated by integration of the process equation using 4^{th} order Runga-Kutta integration scheme. Similarly, other sigma points are passed through the process equation and $(2n+1)$ transformed sigma point vectors are generated. All the $(2n+1)$ sigma point vectors are combined using specified weights to get the predicted transformed sigma point and its error covariance matrix.

Step-4: Passing the Sigma Points through measurement equation.

From the transformed sigma points obtained from step-3 and input ground acceleration, $(2n+1)$ transformed predicted observations are generated. All the $(2n+1)$ sigma point vectors are combined using specified weights to get the predicted transformed observation and its error covariance matrix.

Step-5: Evaluation of cross covariance matrix, Kalman Gain and updated state and parameter.

Cross covariance matrix and Kalman Gain matrix are evaluated. From the Kalman gain and current measurement, the updated extended state vector and its error covariance are evaluated.

5.4 Performance evaluation of identification algorithms for the evaluation of state and parameters of base-isolated multi-storey building system

In thissection a comparative study has been presented based on the results obtained using all the considered algorithms. Four numbers of sample problems have been considered for the present study based on Type-*S* and Type-*F* problems, as defined in

Table 5.1. Detailed description of different considered problems are given below.

1. ProblemType-*S*1: A three-storey BI simulated building is analysed under NE EQ-3: Comp-transverse excitation (Table 5.4).State and parameters identification of the building have been performed with the considered algorithms by utilizing acceleration response. Noise-free acceleration response from all floor levels has been considered. In this sample problem, the intensity of excitation is very low, which invariably produces further lower intensity of responses at upper storey levels due to the presence of base isolator. Occurrence of numerical round off error has been observed during evaluation of Kalman Gain while using such low intensity response. In such case, possibility of error in identification cannot be ruled out. To overcome this problem, a rectification technique has been applied which is detailed in sub-section 5.4.1.1. Such studies using low intensity excitation is a challenging problem and not explored as per the literature survey carried out so far.

2. Problem Type-*S*2: This problem is also concerned with identification using simulated noise-free response under NE EQ-3: Comp-transverse excitation (Table 5.4) similar to Problem Type-*S*1, but with a difference that in the present case there are missing sensors at 1stand 2nd floor levels (Fig. 5.3). This problem provides a guideline to carry out the identification of BI building using limited field measured response (Problem Type-*F*). Thus, this problem is more critical than the Problem Type-*S*1, since in addition to very low intensity excitation there are also missing sensor at two consecutive floor levels.

3. Problem Type-*S*3: This problem deals with identification of state and parameters of the three-storey BI building using simulated response generated from the analytical model. The performance of the considered algorithms has been evaluated using the simulated response contaminated with 1% Gaussian white noise and under the condition of missing sensor at ground floor level (isolator-top level) as well as missing sensor at 2nd floor level. The structure is excited using El Centro (1940): Comp–180 excitation (Table 5.4). The present study addresses the issue of missing sensor at isolator-top level. Sub-section 5.2.3 is devoted to handle this type of case with missing sensor at isolator-top level.

4. Problem Type-*F*: In this problem, identification of state and parameters of the existing BI building have been carried out. The recorded response data from different floors of the building under NE EQ-3: Comp-transverse excitation (Table 5.4), have been used for identification studies. It has been observed that a numerical problem arises due to low

intensity excitation. Such problem has been addressed using the technique presented in sub-section 5.4.1.1.

A detailed discussion about all the four problems is presented in the following sub-sections. State identification is done first followed by parameters identification.

5.4.1 Results of state identification

In the state identification, only displacement identification has been considered. It has been observed that the intensity of floor responses is much lesser than that of ground acceleration as shown in Fig.5.4. The reduced responses are indicative of the effectiveness of the use of base-isolator as seismic isolation device. The reduced amplitude of floor responses however introduces a problem in identification, causing numerical round off errors. In Fig.5.4 peak excitation position has been zoomed for better clarity.

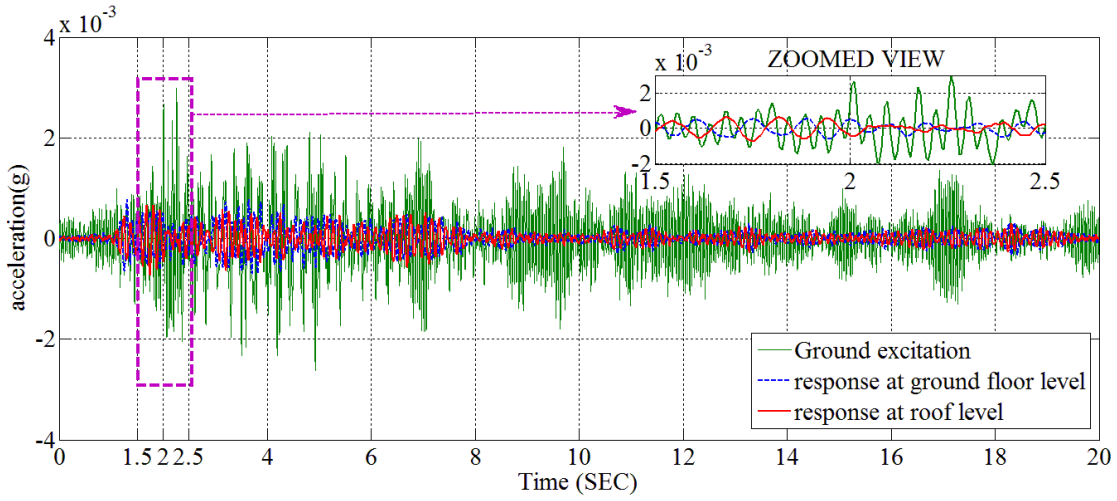

Fig.5.4: Different floor acceleration time-history with ground acceleration time-history (NE EQ-3: Comp-transverse)

The responses of the building under the considered earthquake excitation as well as the ground acceleration data have been used as input for the identification algorithms. The details of the earthquake have been furnished in Table 5.4. Three different identification algorithms such as EKF, Two-Stage EKF and UKF have been used for the comparative study. The comparative performance of these different algorithms in identifying the state of the system has been carried out by evaluating the RMSE of the identified state. The RMSE of the identified displacement has been evaluated by considering the simulated displacement of the numerical model as the reference. The lower the RMSE, the better is the performance of the

algorithm. The comparative performance of these algorithms towards state identification for all the sample problems under consideration is presented in the following paragraphs.

5.4.1.1 Results of the displacement identification for Problem Type-*S*1

A problem has been observed while identifying the state (displacement) using the simulated responses as well as field responses. The simulated model has been excited with NE EQ-3: Comp-transverse excitation. The acceleration responses obtained from all the floor levels have been used in the identification algorithms. However, deviations are observed in the identified displacements either above or below the zero displacement axes as presented in Fig. 5.5 to Fig. 5.7. As per Chatzi and Fuggini (2015), these diverging tendencies or drifts in displacement are generally observed if signals contain very low frequency components. In the present study, rigorous tuning of the filter parameters could not however correct these drifts. Further, this drift could not be corrected even after introducing high-pass filtering to remove low frequency components from the signal using 6^{th} order ButterWorth filter.

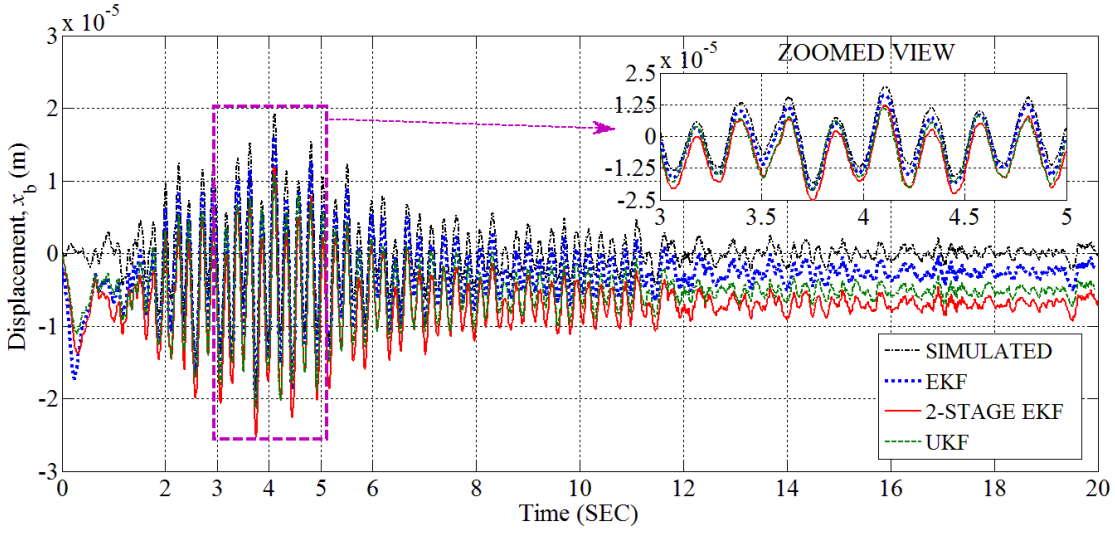

Fig. 5.5: Comparison of identified displacement time-history and simulated displacement time-history at ground floor level for Problem Type-*S*1 under NE EQ-3: Comp-transverse excitation

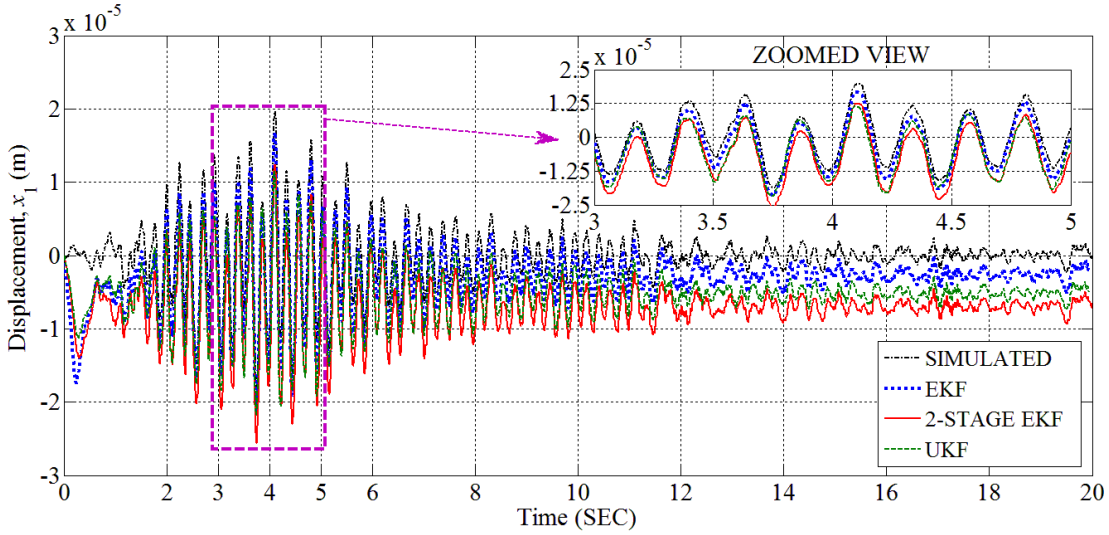

Fig. 5.6: Comparison of identified displacement time-history and simulated displacement time-history at 1st floor level for Problem Type-*S*1 under NE EQ-3: Comp-transverse excitation

However, occurrences of such low excitation earthquakes are not uncommon in practice. Available literature does not speak about this type of problems either for simulated or field studies. To overcome such problem, a different strategy has been applied in the present study. Chatzi and Fuggini (2015) suggested a method for online correction of drift in displacement which arises due to presence of low frequency component in signal. In addition to acceleration data (either measured or from simulated model), an artificial white noise of insignificant amplitude has been used as displacement data to rectify the drift issue.

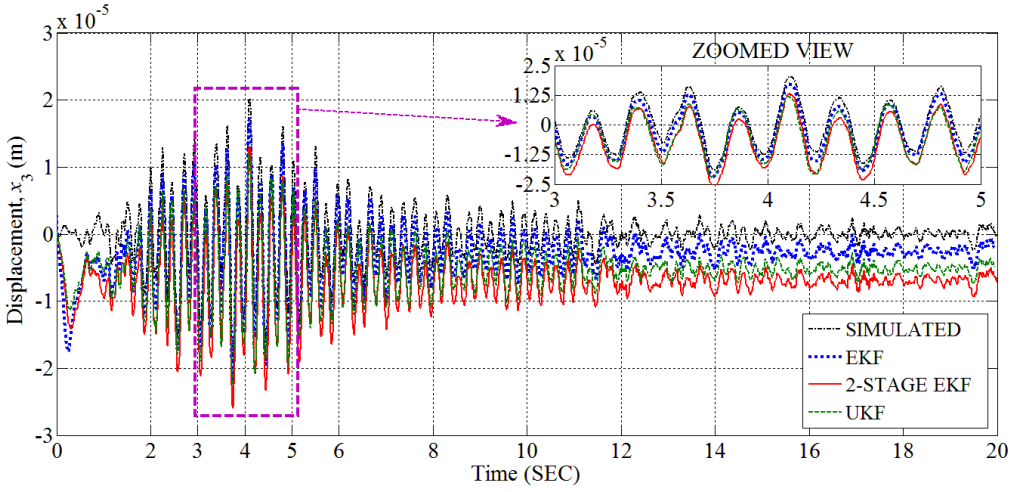

Fig. 5.7: Comparison of identified displacement time-history and simulated displacement time-history at roof level for Problem Type-*S*1 under NE EQ-3: Comp-transverse excitation

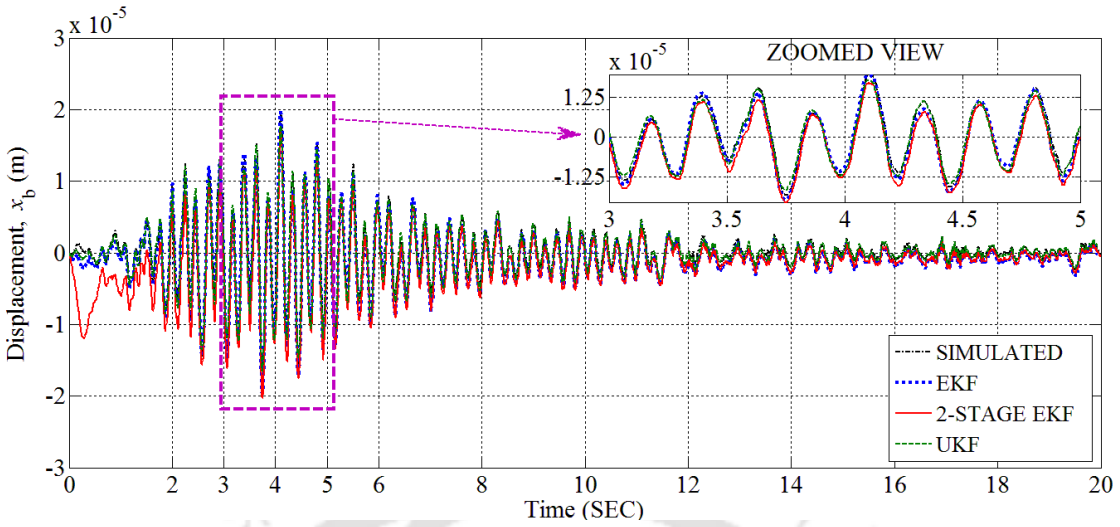

Fig. 5.8: Comparison identified displacement (after drift correction) time-history with simulated displacement time-history at ground floor level for Problem Type-*S*1 under NE EQ-3: Comp-transverse excitation

In line with the technique suggested by Chatzi and Fuggini (2015), low amplitude artificial white noise displacement data with the peak in the range of 10^{-7} to 10^{-9}m has been used as additional input in the observation equation of the considered identification algorithms. Using this technique, drift correction of the identified displacement has been achieved. Fig. 5.8 to Fig. 5.10 show the corrected identified displacement of different floor levels of the BI building. This identification has been carried out using the simulation model problem Type-*S*1 under NE EQ-3: Comp-transverse excitation with sensor data available at all the considered floor levels. Low amplitude artificial white noise has been used as input displacement response at isolator-top level. The displacement response from the isolator-top level along with acceleration response from different considered floor levels have been used as input for the identification algorithms.

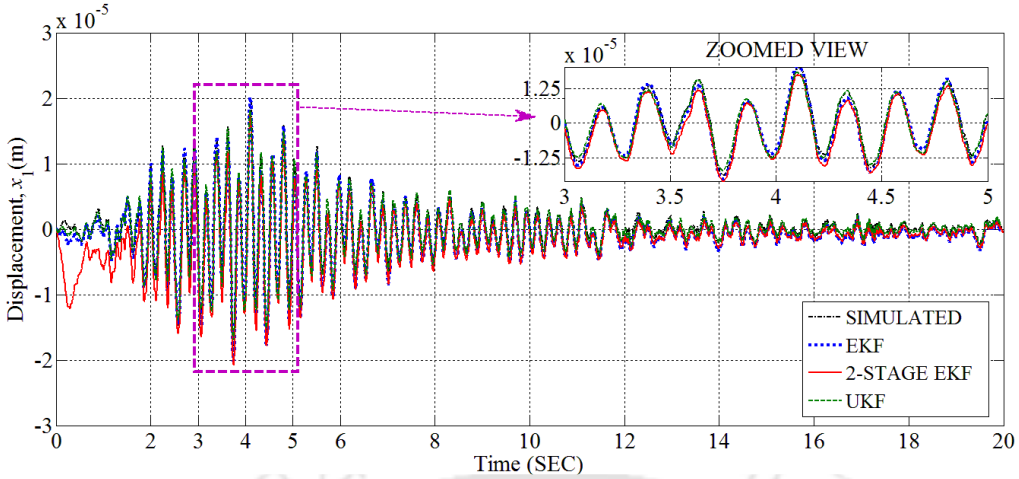

Fig. 5.9: Comparison identified displacement (after drift correction) time-history with simulated displacement time-history at 1st floor level for Problem Type-*S*1 under NE EQ-3: Comp-transverse excitation

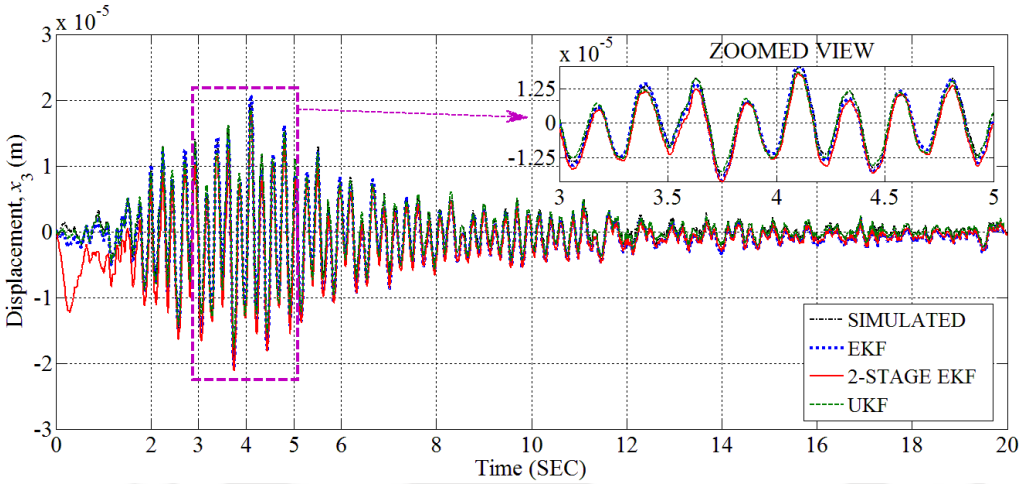

Fig. 5.10: Comparison identified displacement (after drift correction) time-history with simulated displacement time-history at roof level for Problem Type-*S*1 under NE EQ-3: Comp-transverse excitation

5.4.1.2 Results of the displacement identification for Problem Type-*S*2

In this problem, simulation based responses have been considered. The base excitation considered is NE EQ-3: Comp-transverse. Acceleration responses have been generated for all the four different floor levels. During identification using the considered algorithms, the simulated acceleration response of 1stfloor and 2nd floor levels have not been taken into account. This has been done deliberately to simulate a condition of missing sensors at those two floor levels. Therefore, the problem becomes critical, since in combination to low

intensity excitation, there are also missing sensors. Out of the total four floor levels, two numbers of floors have missing sensors. This implies that 50% sensors are missing and that too at two intermediate consecutive levels. Fig. 5.11 to Fig. 5.14 show the identified displacement at different floor levels. To overcome the drift in identified displacement arising out due to low level of excitation, the technique as discussed in sub-section 5.4.1.1has been applied. The results agree well with that of simulated displacements.

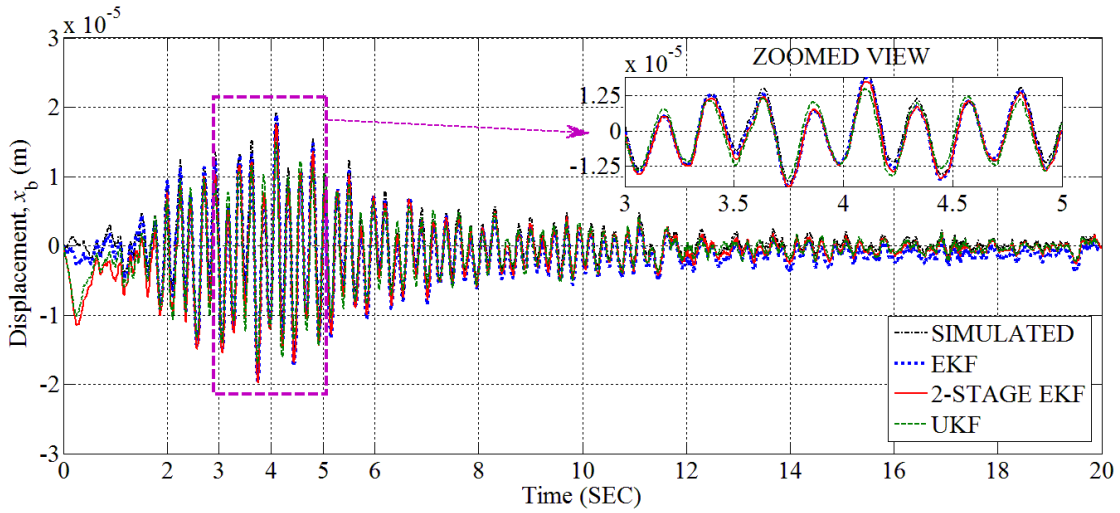

Fig. 5.11: Comparison of identified displacement (after drift correction) time-history with simulated displacement time-history at ground floor level for Problem Type-*S*2 under NE EQ-3: Comp-transverse excitation

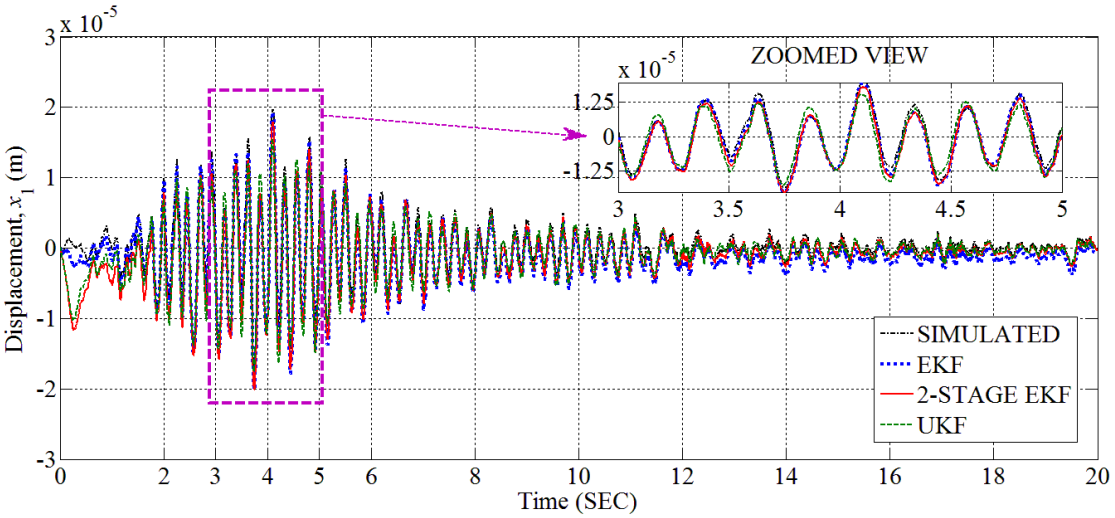

Fig. 5.12: Comparison of identified displacement (after drift correction) time-history with simulated displacement time-history at1st floor level for Problem Type-*S*2 under NE EQ-3: Comp-transverse excitation

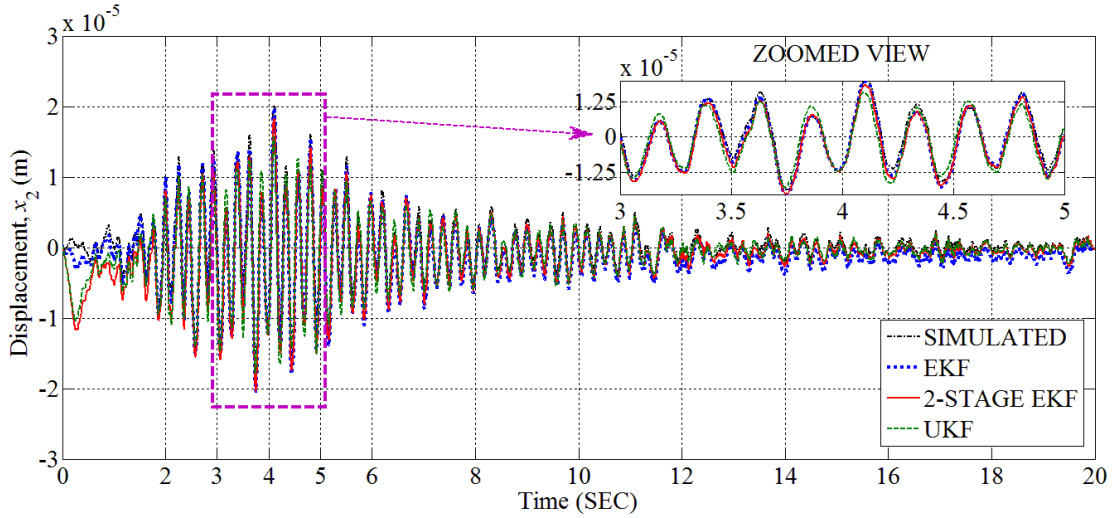

Fig. 5.13: Comparison of identified displacement (after drift correction) time-history with simulated displacement time-history at 2nd floor level for Problem Type-*S*2 under NE EQ-3: Comp-transverse excitation

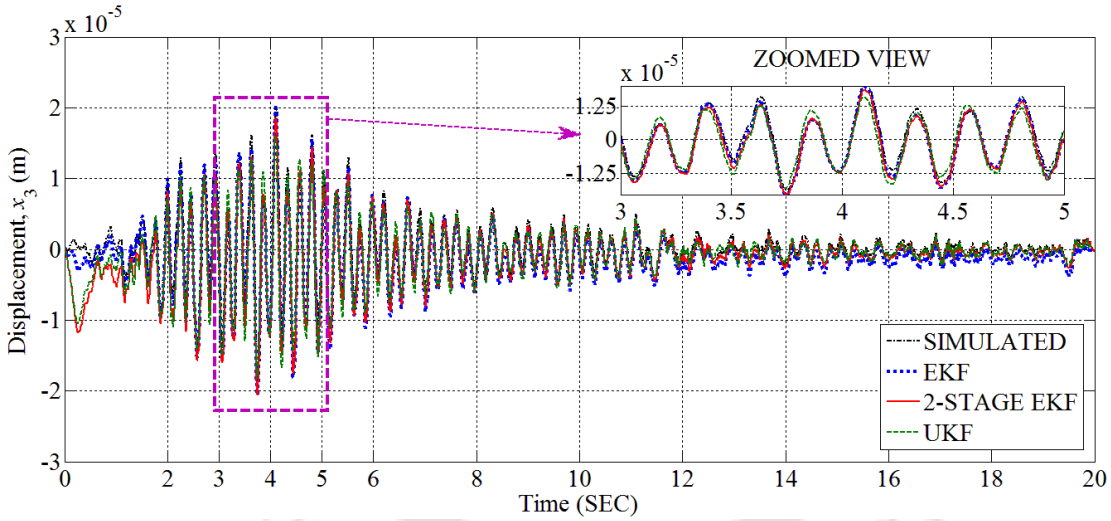

Fig. 5.14: Comparison of identified displacement (after drift correction) time-history with simulated displacement time-history at roof level for Problem Type-*S*2 under NE EQ-3: Comp-transverse excitation

The RMSE of identified displacement is shown in Fig. 5.15 and the values of RMSEs are furnished in Table 5.6. It is observed that the performances of all the three considered algorithms are quite comparable.

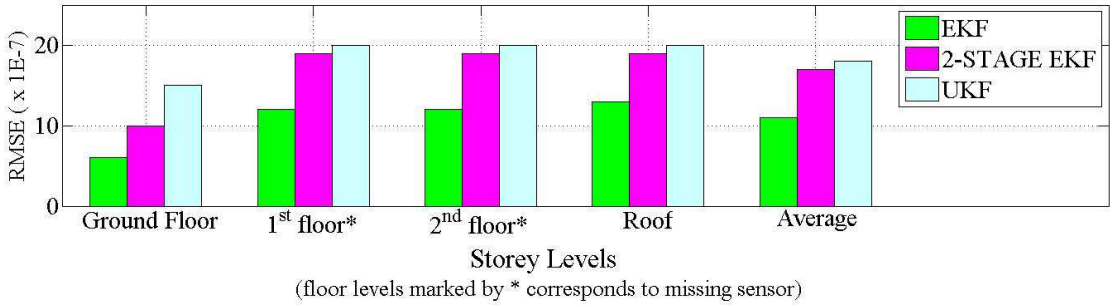

Fig. 5.15: Bar chart showing RMSE of identified displacement of Problem Type-*S*2 under NE EQ-3: Comp-transverse excitation

Table 5.6: RMSE of identified displacement of Problem Type-*S*2 under NE EQ-3: Comp-transverse excitation

Floor level	EKF	Two-Stage EKF	UKF
	From Simulated Response (x 10^{-7})		
1	6	10	15
2	12	19	20
3	12	19	20
4	13	19	20
Average	11	17	18

5.4.1.3 Results of the displacement identification for Problem Type-*S*3

This problem has been undertaken in the present study to compare the performance of all the considered identification algorithms in case of missing sensor at isolator-top level. The system is excited by El Centro (1940): Comp-180. A different excitation of higher intensity is used to show the absence of drift as observed in earlier two cases. The output responses of the structure at 1stfloor and roof levels have been considered for identification study. This has been done to create an environment of missing sensor at isolator-top and 2nd floor levels.

The identified displacements are shown in Fig. 5.16 for all the floor levels. From this figure, it is evident that the state (displacement) has been identified correctly by all the algorithms. Further, occurrence of drift in identified displacement as has been observed in sub-sections 5.4.1.1 and 5.4.1.2 does not appear in the present case. This is due to the fact that the PGA of EL Centro (1940): Comp-180 excitation is much higher that that of NE EQ-3: Comp-transverse earthquake excitation.

To compare the performance of the identification algorithms with respect to state identification, RMSEs of the identified displacements have been evaluated. The Bar charts representing RMSE of identified displacement are shown in Fig. 5.17 and its corresponding

values have been furnished in Table 5.7. The performance of EKF and UKF are comparable and performances of those two algorithms are observed to be better than Two-Stage EKF algorithm.

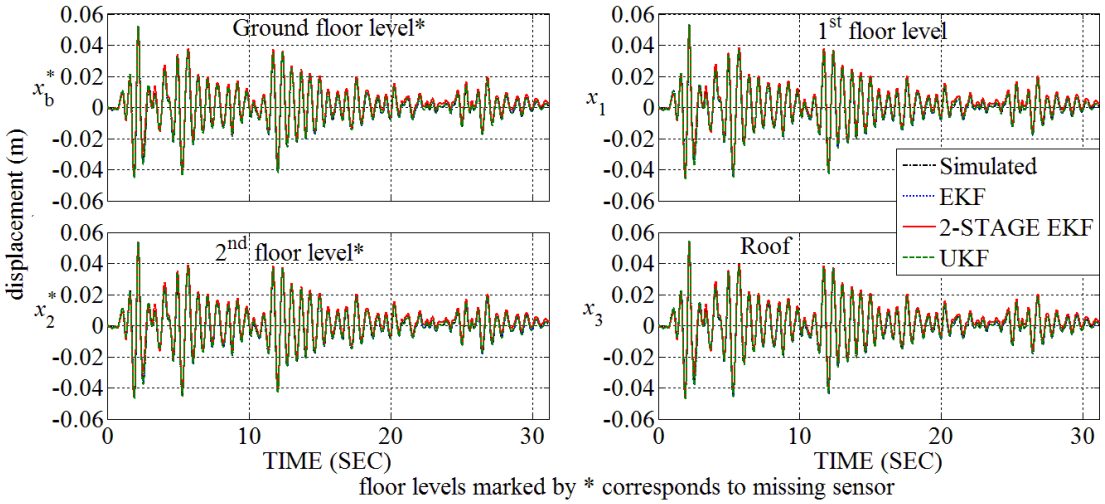

Fig. 5.16: Identified displacement of Type-*S*3 under El Centro (1940): Comp-180 excitation

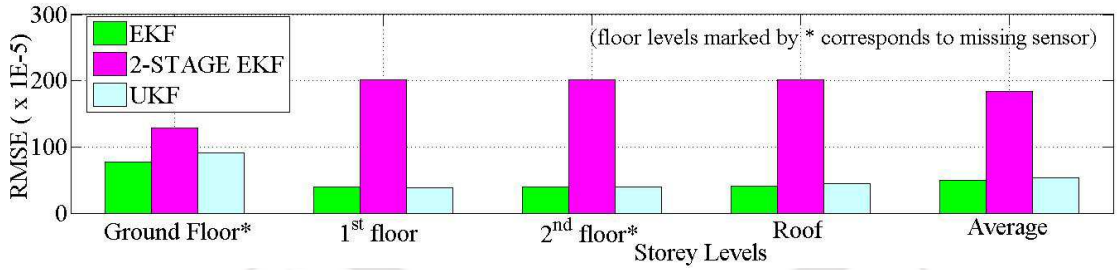

Fig. 5.17: Bar chart showing RMSE of identified displacement of Type-*S*3 under El Centro (1940): Comp-180 excitation

Table 5.7: RMSE of identified displacement of Problem Type-*S3* under El Centro (1940): Comp-180 excitation

Floor level	EKF	Two-Stage EKF	UKF
	From Simulated Response (x 10^{-5})		
1	77	129	91
2	40	202	38
3	39	202	40
4	41	202	44
Average	49	184	53

5.4.1.4 Results of the displacement identification for Problem Type-*F*

In this problem, recorded seismic responses data from an existing BI building have been utilized to evaluate the performance of all the considered identification algorithms. The building was instrumented with sensors located at ground floor and roof level. Acceleration response of the building is available for those two levels. There are missing sensors at 2nd floor and 3rd floor levels. The recorded base excitation is NE EQ-3: Comp-transverse.

Numerical model of the same building, termed as Problem Type-*S* has been generated in MATLAB. The Problem Type-*S*2 has already been discussed in detail in sub-section 5.4.1.2. The sensor arrangement has also been considered similar to the existing building. The basic difference between the two models is that the identification of Problem Type-*S*2 has been carried out using simulated response, while field measured response has been used for Problem Type-*F*. The prime objective of the present study is the identification of state and parameters of the existing BI building. In this context the simulation study using Problem Type-*S*2 provides a guideline towards this aspect. The results obtained from the identification schemes have been discussed in the following paragraphs.

RMSE of identified displacement is used as a measure of accuracy of state identification. RMSE of identified displacement is evaluated by considering a reference displacement time-history. In case of identification using data from simulated model, the simulated displacement time-history acts as a reference displacement for RMSE evaluation. However, in the study involving data from existing building, this is not possible since the reference displacement is not available. Therefore, performance evaluation of these algorithms is not carried out for the case involving data from exiting building. Further, from the identified displacement time-history of all the floor levels using field data as presented in Fig. 5.18 to Fig. 5.21, it can be concluded that these algorithms indeed perform quite well in estimating the state of the BI building.

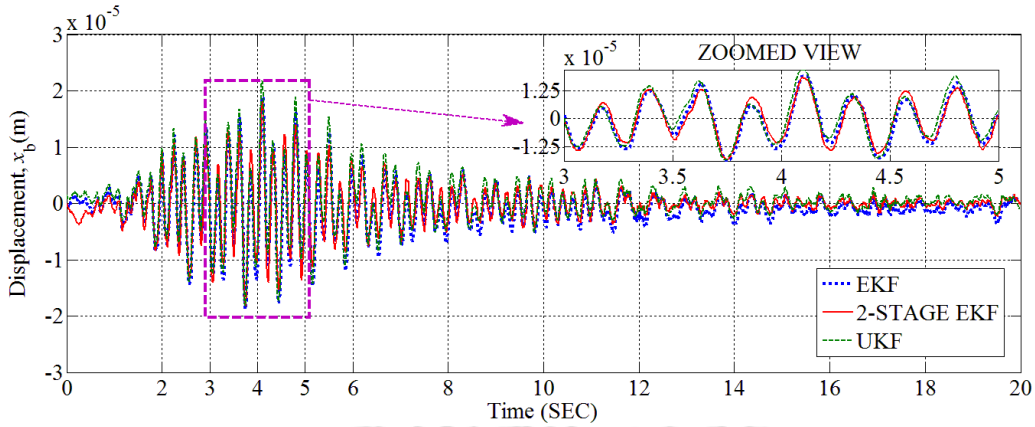

Fig. 5.18: Comparison of identified displacement time-history of ground floor level using different algorithms for Problem Type-*F* under NE EQ-3: Comp-transverse excitation

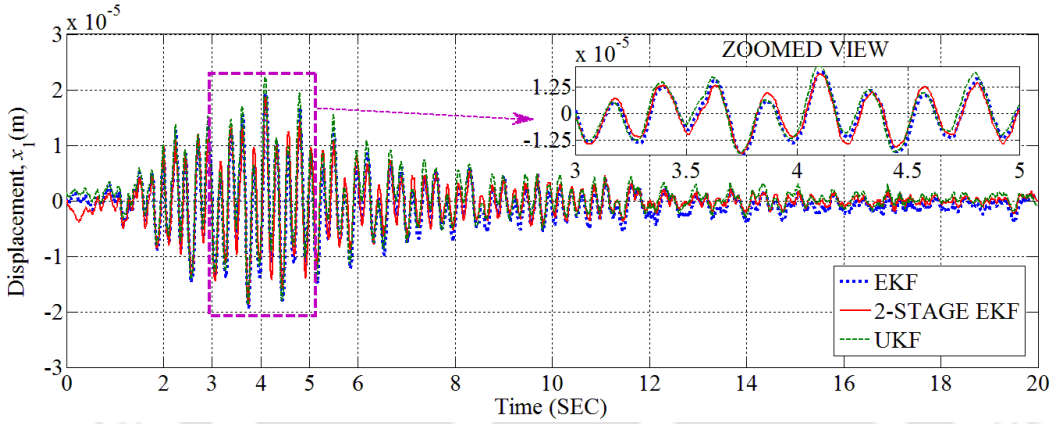

Fig. 5.19: Comparison of identified displacement time-history of 1st floor level using different algorithms for Problem Type-*F* under NE EQ-3: Comp-transverse excitation

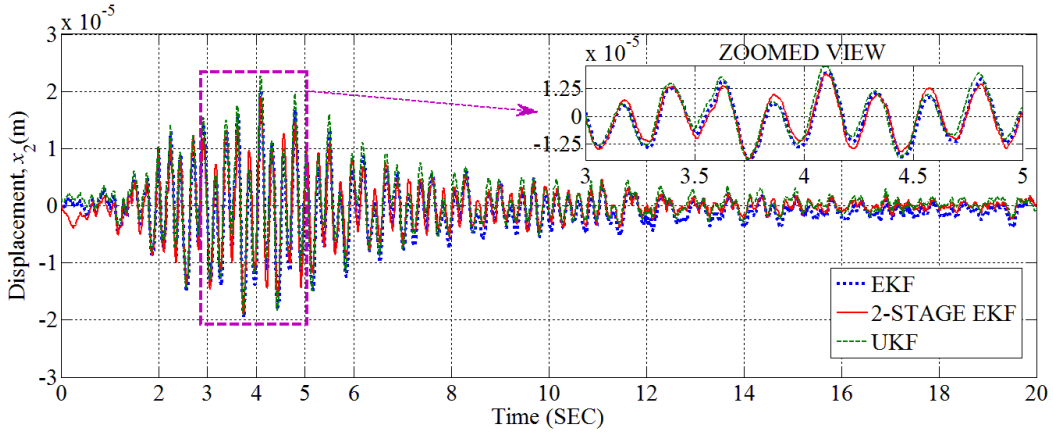

Fig. 5.20: Comparison of identified displacement time-history of 2nd floor level using different algorithms for Problem Type-*F* under NE EQ-3: Comp-transverse excitation

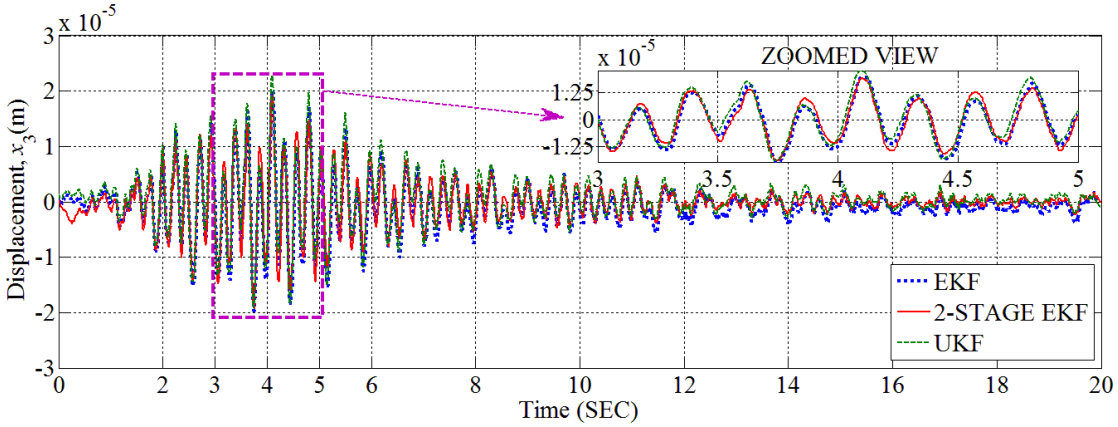

Fig. 5.21: Comparison of identified displacement time-history of roof level using different algorithms for Problem Type-*F* under NE EQ-3: Comp-transverse excitation

5.4.2 Results of parameter identification

Using the considered identification algorithms, the structural parameters (stiffness) of the BI building (Table 5.1) have been identified. Comparative study of the performance of these algorithms with respect to parameter identification has been carried out by evaluating the percentage error of the identified stiffness for the case of Problem Type-*S*2 and *S*3.

The result of parameter identification for Problem Type-*S*1 has not been presented because the problem is primarily concerned with occurrence and rectification of drift in identified displacement. The results obtained for the remaining problems are presented in the following paragraphs.

5.4.2.1 Results of the parameter identification for Problem Type *S*2

This is a problem where identification is carried out using simulated response from a three-storey BI building assuming missing sensors at 1st and 2nd floor level. The sensors are assumed to be available at ground floor and roof level only. The location of sensors assumed in this study is similar to that of field problem Type-*F*. The identified isolator stiffness as well as storey stiffness is presented in Fig. 5.22. A 2D bar chart showing the comparative performance of all the considered algorithms with respect to parameter identification has been presented in Fig. 5.23.The values of the identified parameters and percentage error in identified stiffness are furnished in Table 5.8.

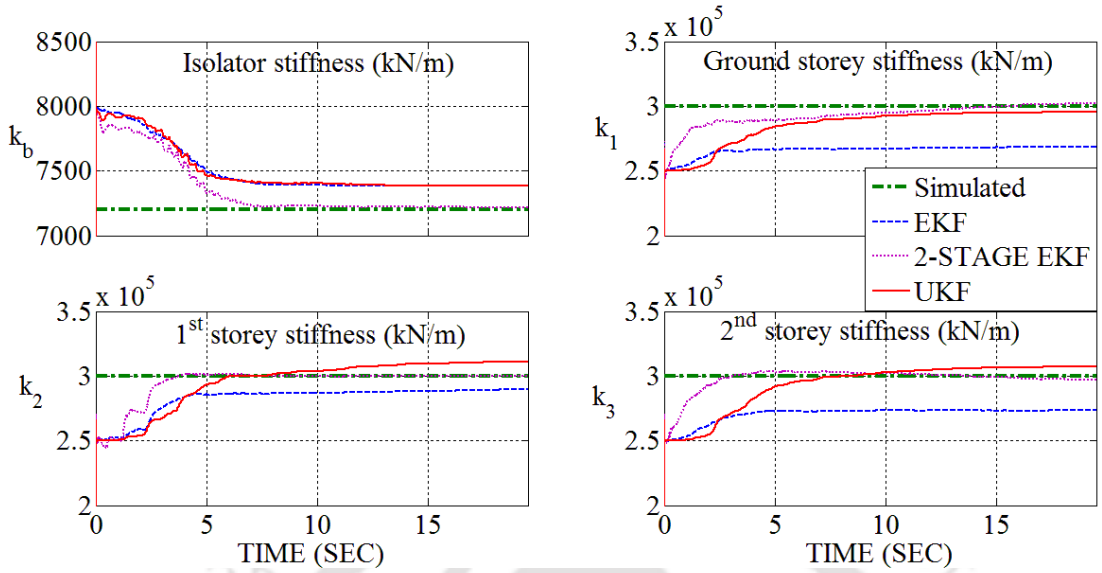

Fig. 5.22: Identified stiffness vs simulated stiffness of Problem Type-*S*2 under NE EQ-3: Comp-transverse excitation

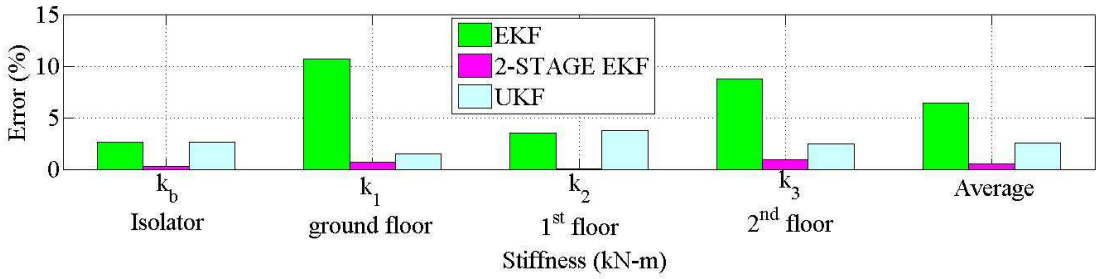

Fig. 5.23: Bar Chart showing percentage error in Identified stiffness for Problem Type-*S*2 under NE EQ-3: Comp-transverse excitation

Table 5.8: Identified stiffness and percentage error of identified stiffness of Problem Type-*S*2 under NE EQ-3: Comp-transverse excitation

Stiffness (kN/m)	Value used in simulation	EKF	Two-Stage EKF	UKF	EKF	Two-Stage EKF	UKF
		Identified stiffness			% error of identified stiffness		
k_b	7200	7390	7220	7390	2.64	0.28	2.64
k_1	3.00E+05	2.68E+05	3.02E+05	2.96E+05	10.69	0.68	1.50
k_2	3.00E+05	2.90E+05	3.00E+05	3.11E+05	3.48	0.08	3.73
k_3	3.00E+05	2.74E+05	2.97E+05	3.07E+05	8.78	0.95	2.50
Overall average percentage error					6.40	0.50	2.59

It is observed from Table 5.8 that the identified values of stiffness are different for each of the floor levels as well as for different algorithms. Therefore, to compare the performance of the algorithms with respect to parameter identification, the average value is considered.

From the average percentage error, it is observed that the performance of Two-Stage EKF is the best, followed by UKF and EKF algorithm.

5.4.2.2 Results of the parameter identification for Problem Type-*S*3

Identification using the considered algorithms has been carried out using simulated response from the building. The simulated response of ground floor and 2nd floor level has not been taken into account in the identification process in order to create a scenario of missing sensors at these two levels. Further, the simulated response from the remaining two floor levels has been contaminated with 1% RMS Gaussian white noise. The noise contaminated response has been utilized for comparative study of state and parameter identification using the considered algorithms. The result of identified stiffness using different considered algorithms has been presented in Fig. 5.24. The comparative performance of different algorithms with respect to parameter identification has been presented in form of bar chart showing the percentage error in identified stiffness. The bar chart has been shown in Fig. 5.25 and the values of percentage error in identified stiffness have been furnished in Table 5.9.

From the average percentage error of the identified stiffness, it is observed that the performance of Two-Stage EKF is the best followed by EKF and then UKF.

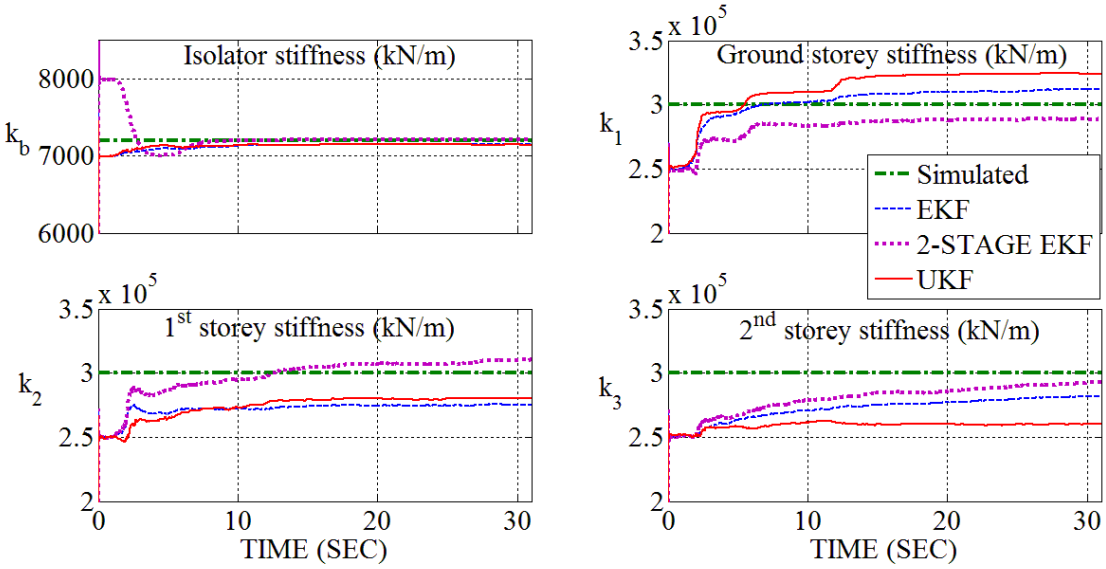

Fig. 5.24: Identified stiffness vs simulated stiffness of Problem Type-*S*3 under El Centro (1940): Comp-180 excitation

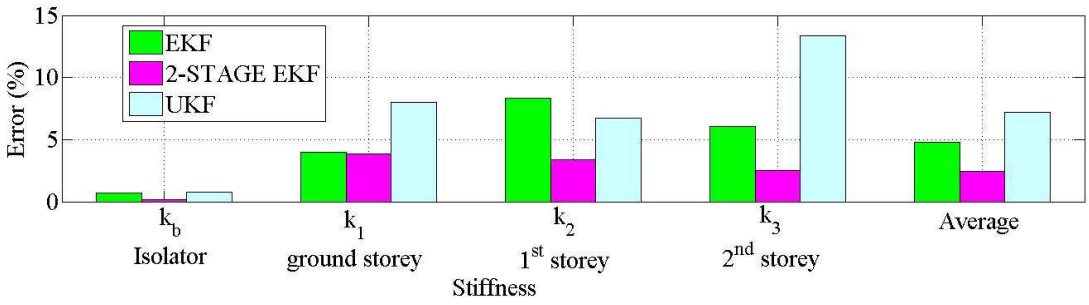

Fig. 5.25: Bar chart showing percentage error in identified stiffness of Problem Type-*S*3 under El Centro (1940): Comp-180 excitation

Table 5.9: Identified stiffness and percentage error of identified stiffness of Problem Type-*S*3 under El Centro (1940): Comp-180 excitation

Stiffness (kN/m)	Value used in simulation	EKF	Two-Stage EKF	UKF	EKF	Two-Stage EKF	UKF
		Identified stiffness			% error of identified stiffness		
k_b	7200	7150	7210	7150	0.69	0.14	0.69
k_1	3.00E+05	3.12E+05	2.89E+05	3.24E+05	3.99	3.83	7.97
k_2	3.00E+05	2.75E+05	3.10E+05	2.80E+05	8.31	3.39	6.70
k_3	3.00E+05	2.82E+05	2.92E+05	2.60E+05	6.07	2.51	13.35
Overall average percentage error					4.77	2.47	7.18

5.4.2.3 Results of the parameter identification for Problem Type *F*

The identified isolator stiffness as well as the storey stiffness is presented in Fig. 5.26. The performance efficiency of the considered algorithms towards parameter identification is presented in form of bar chart (Fig. 5.27), showing the identified stiffness. The results of identified stiffness are furnished in

Table 5.10. The results obtained from all the three algorithms are observed to be quite consistent.

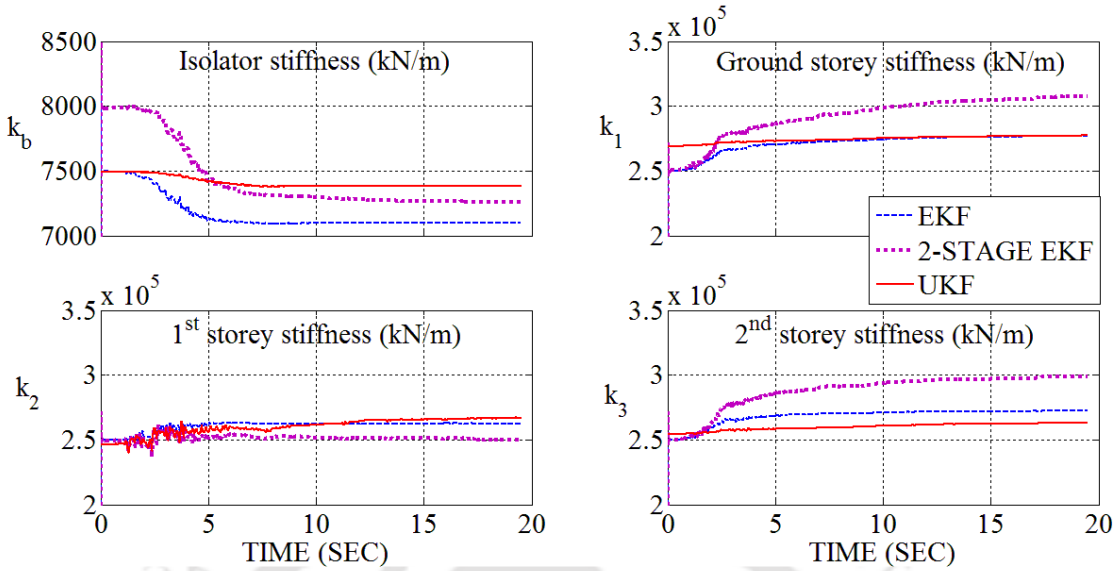

Fig. 5.26: Comparison of identified stiffness using different algorithms for Problem Type-*F* under NE EQ-3: Comp-transverse excitation

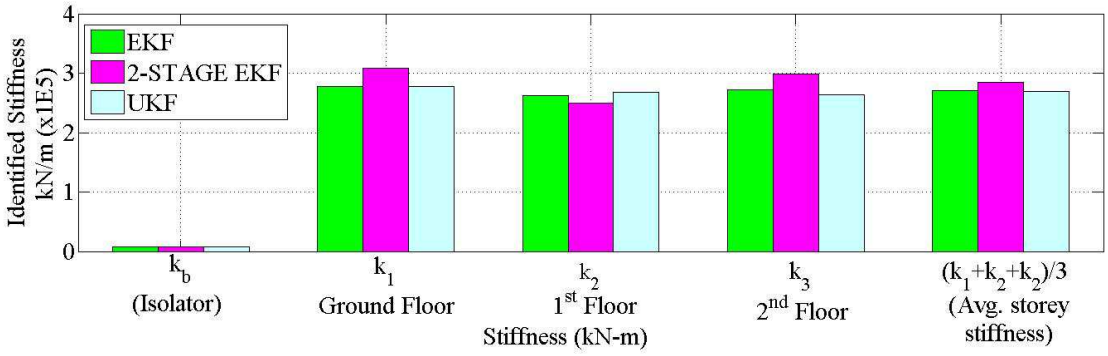

Fig. 5.27: Bar chart showing identified stiffness for Problem Type-*F* under NE EQ-3: Comp-transverse excitation

Table 5.10: Identified stiffness of Problem Type-*F* under NE EQ-3: Comp-transverse excitation

Stiffness (kN/m)	EKF	Two-Stage EKF	UKF
k_b	7097.68	7257.00	7380.98
k_1	2.77E+05	3.08E+05	2.77E+05
k_2	2.62E+05	2.50E+05	2.66E+05
k_3	2.72E+05	2.99E+05	2.63E+05
Average of k_1, k_2 and k_3	2.70E+05	2.85E+05	2.69E+05

5.5 Concluding Remarks

Evaluation of state and parameter of the BI building system have been carried out using three different identification schemes, namely, EKF, Two-Stage EKF and UKF. The SNLSE-UI-UO algorithm has not been considered because it has been observed that the output acceleration response of the structural system requires filtering the noisy response prior to its use in identification. Above all, it has also been observed that performance of SNLSE-UI-UO algorithm is poor in case of more than one missing sensors. The structural system that has been considered in this chapter has more than one missing sensors, therefore the identification using this algorithm is not carried out further. These difficulties using SNLSE-UI-UO algorithm have been already pointed out in chapter-4, under section 4.6.1.2.

The study on comparative performance of the considered algorithms with respect to identification of state and parameter of BI building supported on SREI has been carried out using four numbers of problem Types as defined in Table 5.1. A comprehensive summary of the identification study using the considered algorithms for all the discussed problem types are presented in Table 5.11. Rank 1 is defined for best performance, while Rank 3 is for least performance and rank 2 stands for intermediate performance level.

Table 5.11: Result of state and parameter identification for different considered problem types showing rank as per their performances

Problem type	Criteria	State / Parameter	Identification algorithms		
			EKF	Two-Stage EKF	UKF
*S*1	This study is mainly concerned with occurrence and rectification of drift in identified displacement due to low intensity of response.	State and parameter	Not performed		
*S*2	Impact of missing sensors at two consecutive intermediate floor levels using simulated response from analytical model.	state	1	2	3
		parameter	3	1	2
*S*3	Impact of missing sensors at ground floor level and 2nd floor level using simulated response from analytical model.	state	1	3	2
		parameter	2	1	3
F	Identification using acquired response from field building having sensors located at ground floor level and roof level.	state	Not performed		
		parameter	Identified stiffnesses are quite close to each other.		

Therefore, it can be concluded that

1) The state identification of SREI supported BI building under very low intensity base excitation shows a drift in identified displacement using the KF based algorithms. Drift in identified displacement can be corrected by introducing additional displacement measurements in the form of artificial white noise of very insignificant amplitude.
2) The state and parameter identification can be performed using all the considered KF based algorithms with an appreciable good degree of accuracy even in cases where sensor data is not available at floor level located just above the isolator.
3) In case of state identification of SREI supported BI building with missing sensor at different floor level, the performance of EKF is found to be the best followed by UKF and then Two-Stage EKF.

In case of parameter identification of SREI supported BI building with missing sensor at different floor level, the performance of Two-Stage EKF is found to be the best and the performance of UKF and EKF are closer to each other.

Chapter 6

Evaluation of state and parameter of U-FREI supporting structure

6.1 Introduction

Fibre Reinforced Elastomeric Isolator (FREI) is a recently developed base isolator which has been found to be effective in mitigating seismic effect especially in low-rise masonry building. FREI can be used as bonded or un-bonded as per its application. In bonded application, the top and bottom surface of the isolator are connected to the super-structure at its top and sub-structure at bottom, whereas in un-bonded application, there are no such attachments. Therefore, FREI finds its application as Bonded-FREI (B-FREI) and Unbonded FREI (U-FREI). In U-FREI, there is possibility of full rollover if the excitation is large enough to cause the vertical surface of FREI to rotate and come into contact with top and bottom supporting surfaces. The effective lateral stiffness of the isolator decreases due to rollover deformation. However, when FREIs undergo large displacement resulting in vertical surfaces coming in contact with top and bottom supporting surfaces, the stiffness of FREIs are observed to increase [Manzoori and Nezhad (2017)].

Steel Reinforced Elastomeric Isolators (SREI) have been commonly used for base isolation. The mathematical model generally being used to model the SREI is the classical Bouc-Wen nonlinear hysteresis model give by Eq. (6.6) and (6.7). This model is found to be performing well in representing the load displacement characteristic of SREI and also for degrading hysteretic behaviour of concrete or any deteriorating structure. However, the load displacement characteristic of FREI is somewhat different from that of SREI. Therefore, the Bouc-Wen model which is used to model SREI, cannot be simply adopted for FREI. Some modifications to the standard Bouc-Wen model have been incorporated by researchers so that the model fits the characteristics of FREI more appropriately. The details have been discussed in the modelling portion of U-FREI, wherein emphasis has been given in selection of appropriate model for FREI.

The validation of the selected mathematical model has been carried out using the results of available laboratory based experimental force displacement tests [Das *et al.* (2014)]. Parameters of the model have been obtained by trial and error, so that the hysteresis loop obtained from simulation based studies using the mathematical model fits the hysteresis loop obtained from experiments. The values of all the parameters so obtained are referred to as the base value. In the identification study using the algorithms such as EKF, Two-Stage EKF and

UKF, initial values of these parameters need to be assigned. Some arbitrary values of these parameters, which are somewhat higher or lower than the corresponding base values, are chosen as the initial values of these parameters of the model. Using these initial values of these parameters, the algorithms evaluates the state and parameters of the FREI model using the available responses of shake table based test data of FREI supported test model. The initial values of state are considered zero. The shake table test of FREI supported test model was performed by previous researchers [Das *et al.* (2016a)].

The performance evaluation of different considered algorithms in respect of state identification has been carried out by evaluation of the RMSEs of identified displacements. The experimentally measured displacement time-history has been taken as the base value, based on which RMSEs have been evaluated.

Each of the identified parameters of the extended Bouc-Wen model, evaluated using different algorithms under different earthquake excitations has been found to be different. Therefore, evaluation of the performance of these algorithms with variation of identified parameters is difficult. In order to arrive at a conclusion, sensitivity analysis has been performed by generating *spider diagram. Percentage Error Index* (PEI) has been introduced to compare the performance of the selected algorithms. The PEI is evaluated using the generated *spider diagram*. Detailed description of the procedure to evaluate the PEI has been covered in the relevant section of this chapter. An illustrative example for evaluation of PEI is presented in Appendix-I. From the study, it is observed that among the three considered algorithms, the EKF has the best performance in state identification, while UKF has performed best in identifying the parameters of the isolator. The study is repeated using responses from numerically simulated model, where Gaussian white noise of varying levels is added to the responses. It is observed that the performances of different algorithms have very little influence of artificially added noise. In the state and parameter estimation using all the considered KF based algorithms, the measurement noises are represented by a noise covariance matrix, $\boldsymbol{R}$, which plays an important role. The **R** matrix is thus adjusted to get the best possible results [Bhaiya *et. al.* (2016). As measurement noises are not known accurately, a detailed investigation is conducted to find the influence of $\boldsymbol{R}$ on the performance of the algorithms.

6.2 Modelling of U-FREI

A few models are available in literature which may be considered as feasible working models for FREI. A brief discussion about these models is as follows.

6.2.1 Model as per Chen and Ahmadi (1992)

The basic initial approach towards modelling of FREI may be considered to have been originated long back in the year 1992 by Chen and Ahmadi, who proposed a modified Bouc-Wen model to study the performance of high damping laminated rubber bearing (HD-LRB) for base isolation system. As per Chen and Ahmadi (1992), the horizontal restoring force of the nonlinear base isolator at any instant of time is given by

$$F_r(t) = c\dot{x} + a_1 x + a_2 x^2 + a_3 x^3 + b\left(1 - \frac{\beta}{\mathbb{A}}|z|^{\alpha}\right) z \tag{6.1}$$

where,

$$\dot{z} = \frac{\mathbb{A}\dot{x} - \gamma|\dot{x}||z|^{\alpha-1}z - \beta(\dot{x})|z|^{\alpha}}{Y} \tag{6.2}$$

From Eq. (6.1), it is observed that spring force is represented by a 3rd order polynomial with three coefficients such as a_1, a_2 and a_3. Fig. 6.1 shows the hysteresis loop developed from Eq.(6.1) and Eq.(6.2). The third-order polynomial used in Eq.(6.1) cannot address the issue of stiffening of load-displacement behaviour at very large imposed lateral displacement as it lacks point of inflection.

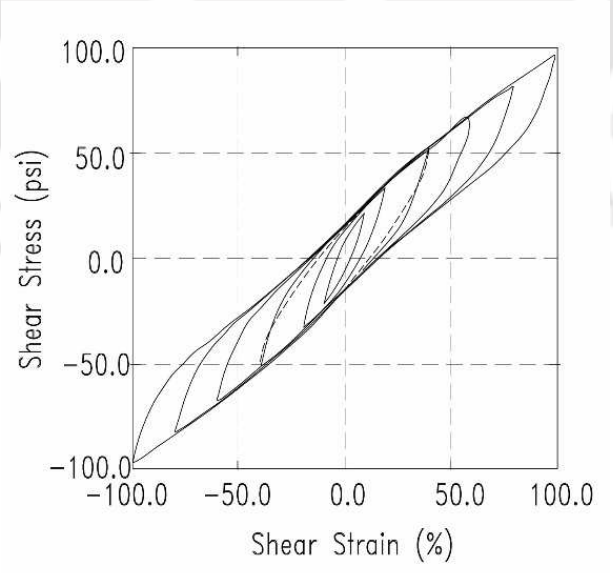

Fig. 6.1: Predicted hysteresis loops of HD-LRB under cyclic loading [Chen and Ahmadi (1992)]

6.2.2 Model as per Manzoori and Nezhad (2017)

This model is a modified Bouc-Wen model with the stiffness part or spring force is represented by 5th order polynomial with 3 unknown coefficients while keeping the equation of the differential form of the Bouc-Wen hysteresis parameter unchanged.

Manzoori and Nezhad (2017) employed a polynomial of order 5 with 3 unknown coefficients only to evaluate the isolator shear force at any instant in time as

$$F_r(t) = c\dot{x} + a_1 x + a_3 x^3 + a_5 x^5 + b\left(1 - \frac{\beta}{\mathbb{A}}|z|^{\alpha}\right) z \tag{6.3}$$

The shear force or hysteretic restoring force, $F_r(t)$ given by Eq.(6.3) can be decomposed into spring force f_s (Eq.(6.4)) and damping force f_d(Eq.(6.5)).

$$f_s(t) = a_1 x + a_3 x^3 + a_5 x^5 \tag{6.4}$$

$$f_d(t) = c\dot{x} + b\left(1 - \frac{\beta}{\mathbb{A}}|z|^{\alpha}\right) z \tag{6.5}$$

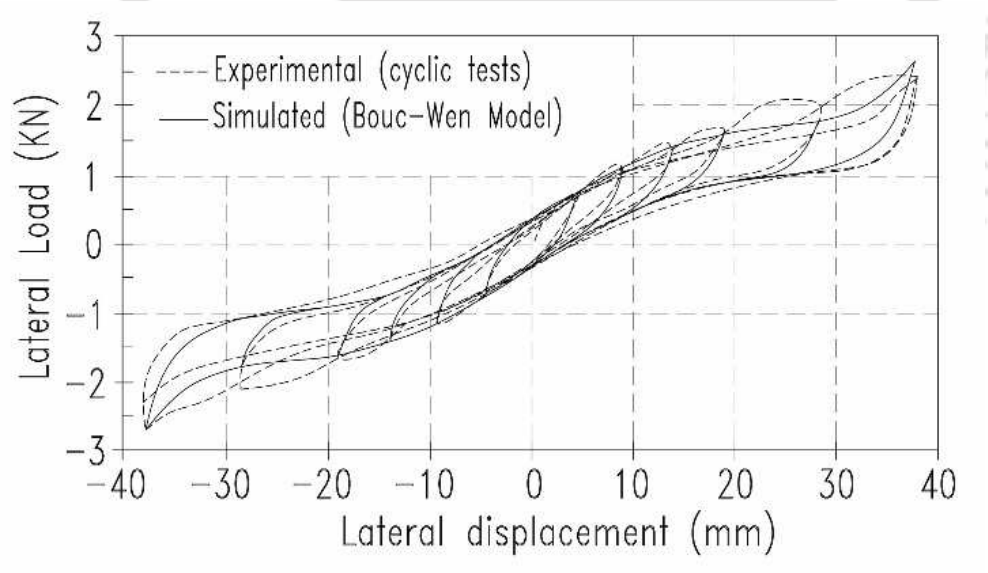

Fig. 6.2: Hysteresis loop of FREI [Manzoori and Nezhad (2017)]

The hysteresis loop presented in Fig. 6.2 has been obtained from Eq.(6.3). From the curve, it is observed that at high displacement, there is a stiffening regime after an initial softening regime.

6.2.3 Model as per Neil *et al.* (2016)

The formulation of the modified or extended Bouc-Wen model for U-FREI was also developed by Neil *et al.* (2016). It is presented here to provide an insight to the transformation of standard Bouc-Wen model to extended Bouc-Wen model and its appropriateness to represent behaviour of U-FREI.

The traditional Bouc-Wen model is given by Eq.(6.6) is based on initial stiffness, k_{ini}, and post-yield stiffness. $F_r(t)$ is the horizontal restoring force where x_y is the yield displacement and α is the ratio of post-yield stiffness to initial stiffness.

$$F_r(t) = \alpha k_{ini} x + (1-\alpha) x_y k_{ini} z \tag{6.6}$$

The hysteretic parameter is determined from the following differential equation

$$\dot{z} = \frac{\dot{x}}{x_y}\{\mathbb{A} - [\beta\, sgn(z\dot{x}) + \gamma]|z|^{\alpha}\} \tag{6.7}$$

where, $\mathbb{A}, \beta, \gamma$ and α are dimensionless quantities that control the shape of the hysteresis loop and *sgn* is the *signum* function.

Modifying the model given by Eq.(6.6) with inclusion of a 5th order polynomial is shown in Eq.(6.8).

$$F_r(t) = a_1 x + a_2 |x| x + a_3 x^3 + a_4 |x| x^3 + a_5 x^5 + Bz \tag{6.8}$$

$$\text{where, } \dot{z} = \frac{\dot{x}}{Y}(\mathbb{A} - [\beta\, sgn(z\dot{x}) + \gamma]|z|^{\alpha}) \tag{6.9}$$

The relationship that exists between k_i, α and x_y as given in Eq. (6.6) is no more present in the transformed restoring force equation [Eq.(6.8)]. This implies that the physical correlation associated with the yield and post-yield stiffness is no longer interpretable in Eq. (6.8). By comparing Eq.(6.7) and Eq.(6.9), it is observed that Y replaces x_y and B in Eq.(6.8) absorbs the coefficient of z of Eq.(6.6). It is also to be noted that the model uses hysteric damping only and viscous damping is thus not included [Neil *et. al.* (2016)].

6.2.4 Selection of appropriate model for FREI

The Bouc-Wen model is a simple analytical model where only one nonlinear differential equation can represent hysteretic behaviour. In SREIs, the hysteretic behaviour is represented by an initial stiffening regime followed by softening regime. This type of behaviour has been found to be successfully represented by classical Bouc-Wen model. However, in FREIs there is initially stiffening, then softening followed by again stiffening regime. The final stiffening

occurs only if there is a rollover deformation caused by large imposed displacements. Therefore, the classical Bouc-Wen model has not been found to be quite adequate in predicting the response of FREIs, wherein there is a stiffening regime followed by initial gradual softening [Sireteanu *et al.*, 2010].

The 5thorder polynomial [Eq. (6.3)] as proposed by Manzoori and Nezhad (2017) is an improvement over 3rd order polynomial [Eq. (6.1)] as suggested by Chen and Ahmadi (1992). One of the characteristics of U-FREIs is their stiffening load-displacement behaviour at extremely large lateral displacements. The 3rdorder polynomial cannot address the issue of stiffening of load-displacement behaviour at very large imposed lateral displacement as it lacks a point of inflection. Therefore, in a Bouc-Wen given by Eq.(6.1), the polynomial has been replaced with a complete fifth order polynomial of five unknown coefficients. The model suggested by Neil *et al.* (2016) and given by Eq. (6.8) and (6.9) can also represent the behaviour of FREI very well. Both the models of Manzoori and Nezhad (2017) and Neil *et al.* (2016) have been observed to represent the behaviour of FREI well. However, the model suggested by Neil *et al.* (2016) has been selected in the present study due to its ease of implementation in simulation and prediction using state space form. The mathematical derivation has been shown in section 6.3.3.

6.3 Evaluation of parameters of the selected mathematical model for U-FREI

Cyclic load test or displacement controlled laboratory force-displacement tests were conducted on U-FREI with constant vertical load [Das *et al.* (2014)]. The recorded data obtained from the experiment are used in this thesis work.

6.3.1 Description of FREI specimen

A typical cross section of the FREI isolator used in the present study is shown in Fig. 6.3.

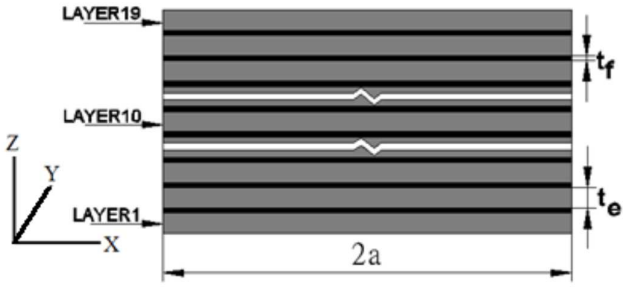

Fig. 6.3: Cross section of FREI, [Das *et al.* (2014)]

The geometric properties of the isolator are furnished in Table 6.1. The material properties of the isolator are furnished in Table 6.2.

Table 6.1: Geometric properties of the FREI, [Das *et al.* (2014)]

Description		Dimension/Number
Plan shape	=	Square
Width (2a)	=	100mm
Thickness of fibre layer (t_f)	=	0.55mm
Number of fibre layer	=	18
Thickness of single rubber layer (t_e)	=	5mm
Number of rubber layer	=	19
Total height of isolator	=	104.9mm

Table 6.2: Material properties of the FREI, [Das *et al.* (2014)]

Hardness IRHD	=	60
Shear modulus of elastomer (G)	=	0.7 MPa
Elongation at break	>	400%
Young's modulus of carbon fibre reinforcement (E_f)	=	220 GPa
Poisson's ratio of carbon fibre reinforcement (ν_f)	=	0.20

6.3.2 Cyclic load test on U-FREI

In this test, sinusoidal displacements of varying amplitude were applied to an assembly of U-FREI with constant vertical load at the top (Fig. 6.4). Details of the experiment are available in Das *et al.* (2014). Horizontal cyclic displacements were applied on the isolator top in the form of push and pull by the actuator, while maintaining a constant vertical load of 12 kN at top of isolator. Three cycles of sinusoidal displacements were applied with constant amplitude of 10mm to 60mm with increment of 10mm after each three cycles. The loading history is shown in Fig. 6.5.

The hysteresis loop as presented in Fig. 6.6 is obtained from the measured restoring force for each of the imposed displacement.

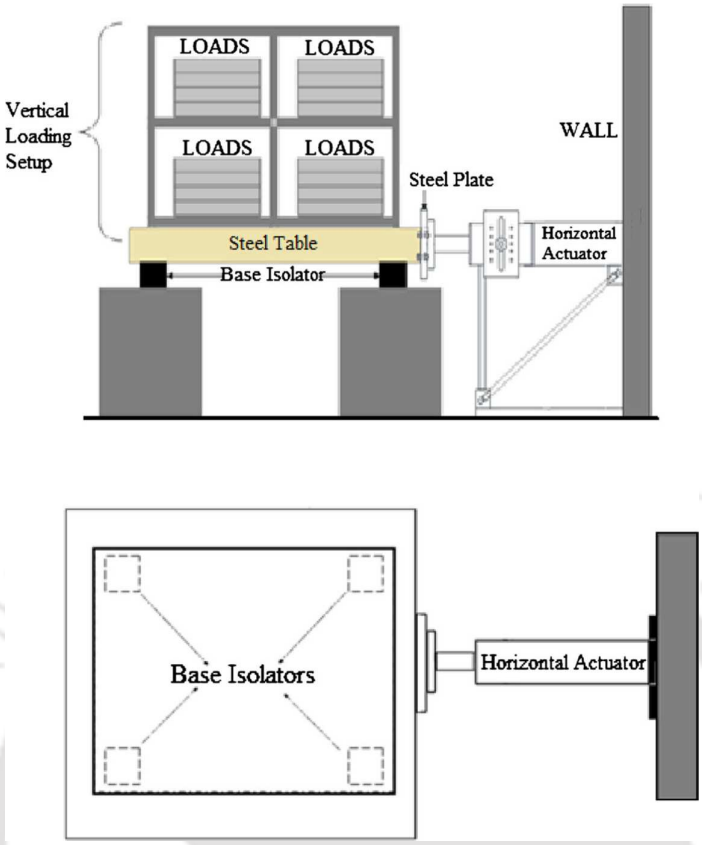

Fig. 6.4: Schematic view of the horizontal cyclic load displacement test on U-FREI assembly system, [Das *et al.* (2014)]

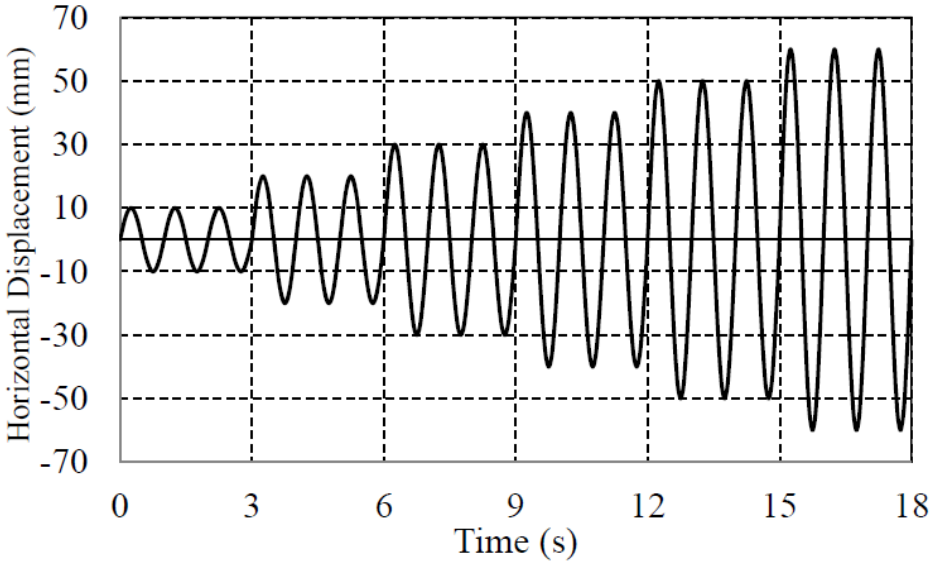

Fig. 6.5: Imposed horizontal displacement *vs* time, [Das *et al.* (2015)]

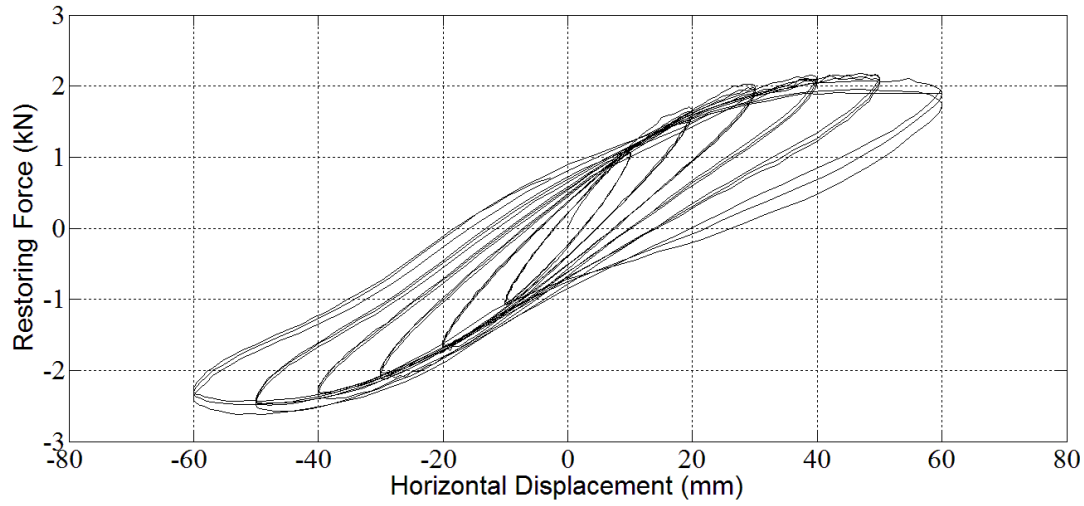

Fig. 6.6: Hysteresis loop of U-FREI obtained experimentally by subjecting the U-FREI to sinusoidal displacement of varying amplitude

The effective horizontal stiffness for each of the displacement cycles is obtained from the hysteresis loop of Fig. 6.6 and the values are furnished in Table 6.3.

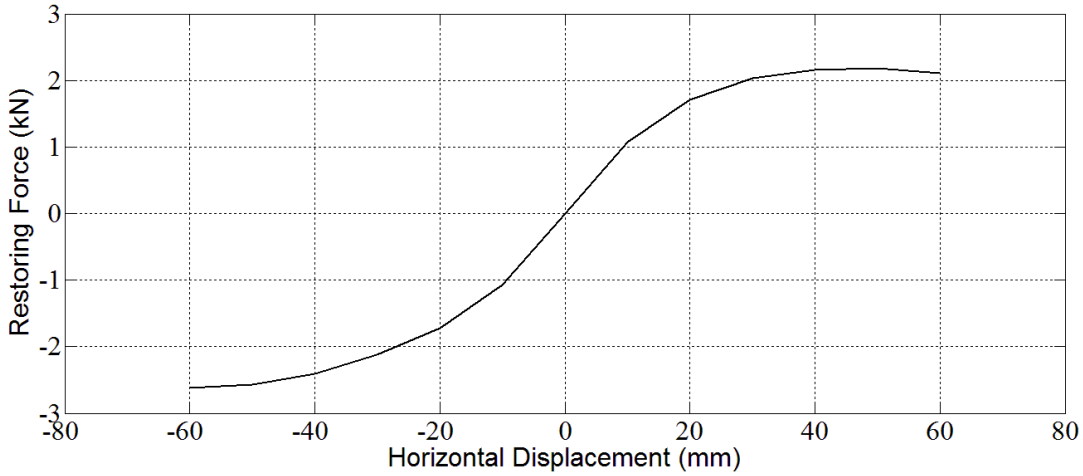

Fig. 6.7: The Back-Bone curve of U-FREI

The backbone curve of the isolator is plotted using the effective horizontal stiffness for each of the displacement amplitude of the applied sinusoidal displacements in the horizontal cyclic load test. The backbone curve is shown in Fig. 6.7. From the backbone curve, it transpires that there is initially a stiffening regime after which there is a gradual softening regime. It may be noted that imposed displacement in the experimental investigation was up to 60mm,

keeping in view the safety of test set-up. The hardening behaviour after softening regime is thus not visible.

Table 6.3: Displacement *vs* Effective horizontal stiffness of U-FREI

Displacement (mm)	Effective Horizontal Stiffness (KN/m)	Damping %
10	98.2	10.1
20	84.3	10.5
30	68.4	11.2
40	56.9	11.6
50	47.5	12.1
60	39.4	12.5

6.3.3 Parameter estimation using force-displacement test result

The selected mathematical model of U-FREI, as described in sub-section 6.2.4, is a modified form of Bouc-Wen model and is also called as an extended Bouc-Wen model. The restoring force equation is re-written here for convenience and is given by Eq. (6.13). In order to estimate the parameters of the model such as a_1 to a_5, B, β and γ etc., some arbitrary values are chosen to simulate the force-displacement hysteresis loop. Simulation is carried out by assuming the FREI supported SDOF system (Fig. 6.8), supporting a mass (m) of 1200 Kg. The system is subjected to a sinusoidal excitation$(\ddot{x}_g)$, having a time period (T) of 1sec and amplitude a_0. The applied acceleration is written as

$$\ddot{x}_g = a_0 \sin\left(\frac{2\pi t}{T}\right) \tag{6.10}$$

For each of the selected amplitude, simulation is performed for 3 seconds or for 3 cycles of oscillations. Simulation is repeated for six different values of amplitude, a_0.

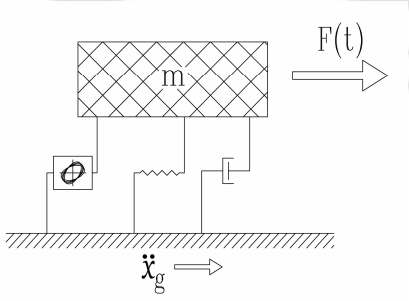

Fig. 6.8: Mechanical representation of FREI supported nonlinear hysteretic SDOF system subjected to base excitation

The governing equation of motion is given by Eq.(6.11).

$$m\ddot{x} + F_r(t) = -m\ddot{x}_g \tag{6.11}$$

The Eq.(6.11) may be represented in the state-space form as

$$\begin{Bmatrix} \dot{x} \\ \ddot{x} \\ \dot{z} \end{Bmatrix} = \frac{d}{dt}\begin{Bmatrix} x \\ \dot{x} \\ z \end{Bmatrix} = \begin{Bmatrix} \dot{x} \\ \left(-m\ddot{x}_g - F_r(t)\right)/m \\ (\mathbb{A}\dot{x} - \beta|\dot{x}||z|^{\alpha-1}z - \gamma\dot{x}|z|^{\alpha})/Y \end{Bmatrix}$$

$$= \begin{Bmatrix} \dot{x} \\ -\ddot{x}_g - (a_1x + a_2|x|x + a_3x^3 + a_4|x|x^3 + a_5x^5 + Bz/m) \\ (\mathbb{A}\dot{x} - \beta|\dot{x}||z|^{\alpha-1}z - \gamma\dot{x}|z|^{\alpha})/Y \end{Bmatrix} \tag{6.12}$$

where, $F_r(t)$ and z are expressed by Eq. (6.13) and (6.14).

Eq.(6.12) is of the form $\boldsymbol{y'=f(x)}$, and can be solved by 4th order Runga-Kutta integration scheme.

$$F_r(t) = a_1x + a_2|x|x + a_3x^3 + a_4|x|x^3 + a_5x^5 + Bz \tag{6.13}$$

$$\dot{z} = \frac{\dot{x}}{Y}(\mathbb{A} - [\beta sgn(z\dot{x}) + \gamma]|z|^{\alpha}) \tag{6.14}$$

Eq.(6.14) is further simplified to get the differential equation as

$$Y\dot{z} = \mathbb{A}\dot{x} - \beta\dot{x}\, sgn(z\dot{x})|z|^{\alpha} - \gamma\dot{x}|z|^{\alpha}$$

$$= \mathbb{A}\dot{x} - \beta\dot{x}\frac{|z\dot{x}|}{z\dot{x}}|z|^{\alpha} - \gamma\dot{x}|z|^{\alpha} \quad = \mathbb{A}\dot{x} - \beta\frac{|z||\dot{x}|}{z}|z|^{\alpha} - \gamma\dot{x}|z|^{\alpha}$$

$$= \mathbb{A}\dot{x} - \beta\frac{z|\dot{x}|}{|z|}|z|^{\alpha} - \gamma\dot{x}|z|^{\alpha} = \mathbb{A}\dot{x} - \beta|\dot{x}||z|^{\alpha-1}z - \gamma\dot{x}|z|^{\alpha}$$

$$\dot{z} = \frac{\mathbb{A}\dot{x} - \beta|\dot{x}||z|^{\alpha-1}z - \gamma\dot{x}|z|^{\alpha}}{Y} \tag{6.15}$$

Assuming the value of amplitude of excitation, a_0 as well as parameters of the model (a_1 to a_5, B, β, γ, Y) and by using Eq.(6.12) to (6.13), the plot of displacement *vs* restoring force is obtained analytically. The analytical plots are superimposed on those obtained from experiments. The parameters are tuned to get the best fit curve. Tuned parameters are furnished in Table 6.4, so that the force-displacement hysteresis loop matches with the experimental hysteresis loop for all considered displacements of 10mm to 60mm.

Table 6.4: Set of control parameters for the hysteresis loop

Parameter	a_1	a_2	a_3	a_4	a_5	B	β	γ	$\mathbb{A}$	Y	α
Values	59	-555	25	0	0	73	95	16	1	1	1

In Fig. 6.9, the experimentally obtained hysteresis loop is superimposed over that of simulated one. The parameters of the selected FREI model are furnished in Table 6.4. Thus, it is observed that by using the selected parameters, there is a good agreement between the experimental and analytical hysteresis loop. Using the same parameters and by changing the amplitude of excitation to achieve a maximum and minimum displacement of 20mm, similar hysteresis loop is obtained as shown in Fig. 6.10. A close agreement between the experimental and analytical hysteresis loops is observed. Similarly, the process is repeated for 30mm to 60mm maximum displacement as presented in Fig. 6.11 to Fig. 6.14 respectively using the same parameters of FREI as furnished in Table 6.4. A close agreement between the experimental and analytical hysteresis loops is observed for all the different displacement cases. Thus, it can be concluded that the selected mathematical model along with all the considered values of parameters adopted for U-FREI suits very well the hysteretic characteristics of the U-FREI and one can proceed with further studies using this model.

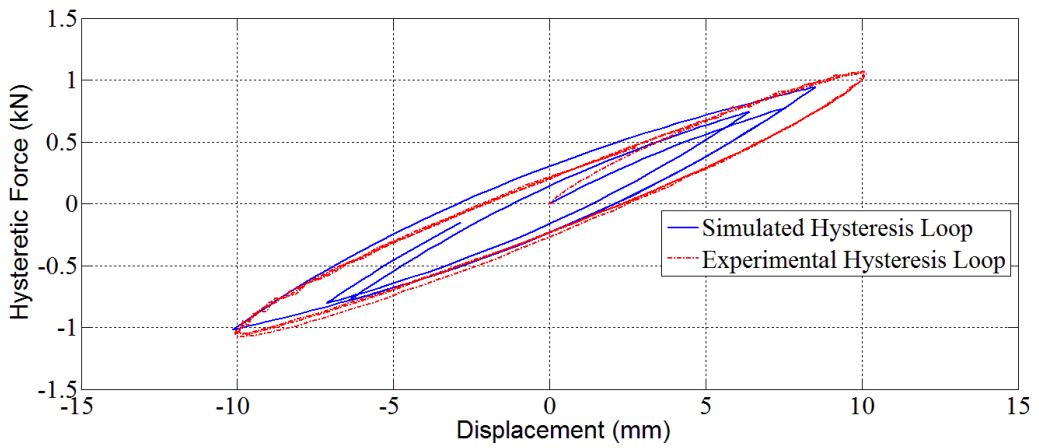

Fig. 6.9: Simulated *vs* Experimental Hysteresis Loop for 10mm max displacement

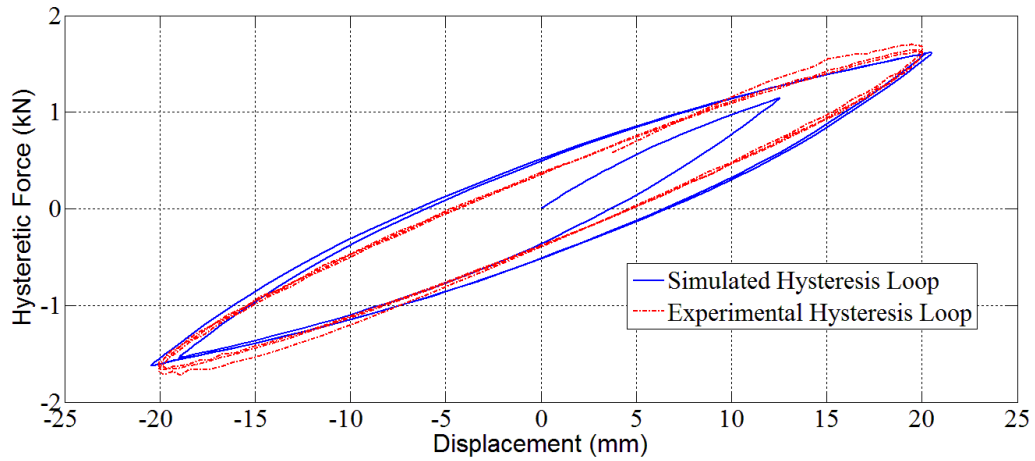

Fig. 6.10: Simulated *vs* Experimental Hysteresis Loop for 20mm max displacement

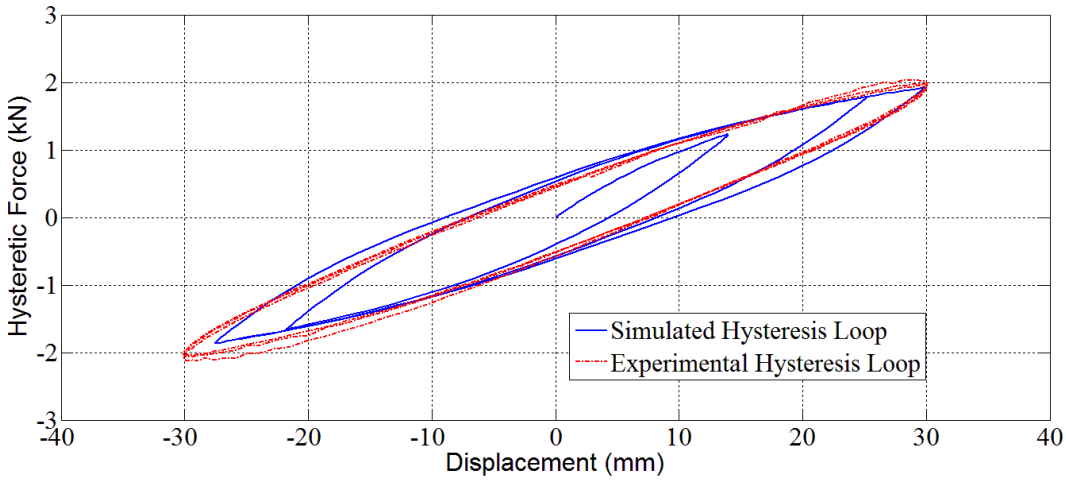

Fig. 6.11: Simulated *vs* Experimental Hysteresis Loop for 30mm max displacement

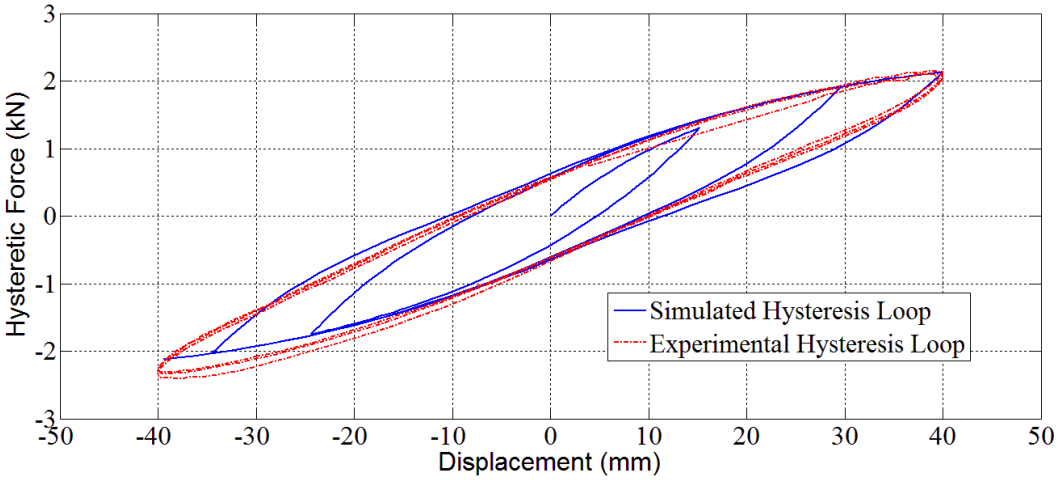

Fig. 6.12: Simulated *vs* Experimental Hysteresis Loop for 40mm max displacement

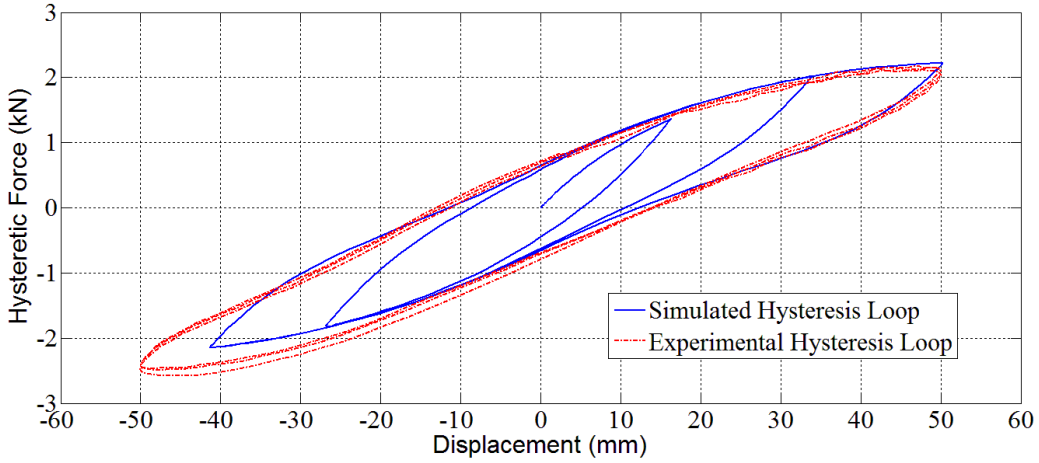

Fig. 6.13: Simulated *vs* Experimental Hysteresis Loop for 50mm max displacement

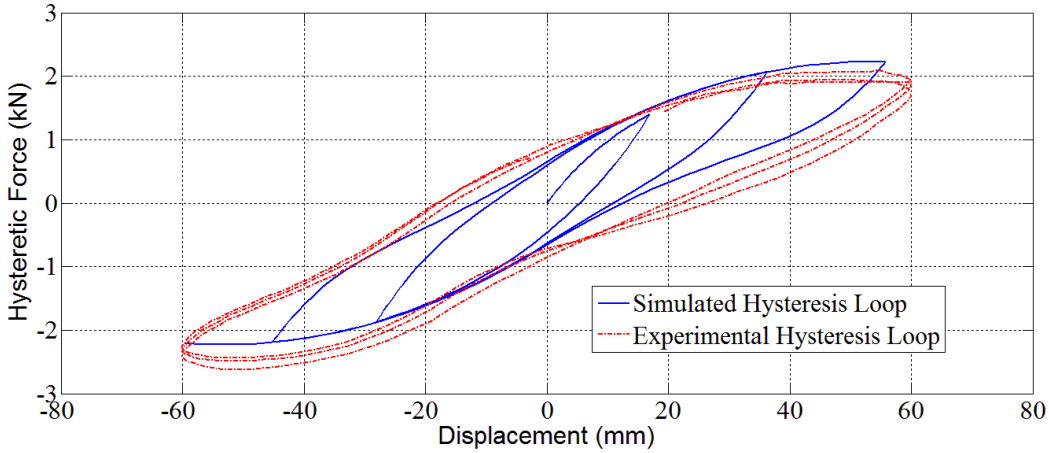

Fig. 6.14: Simulated *vs* Experimental Hysteresis Loop for 60mm max displacement

6.4 Parameter Sensitivity Ranking

In the present study, the extended Bouc-Wen model is used to represent FREI. The base-isolated system supported on FREI is subjected to seismic excitation and different system identification algorithms are used to estimate state and parameters of FREI. However, during the identification of parameters of the adopted model using the three considered identification schemes, it may be observed that the error or deviations in identified parameters from that given in Table 6.4 is not the same for all the algorithms. Further, for any considered algorithm, the error in identification of any particular parameter also may vary for different earthquake excitations. The variations of the identified parameters can thus occur in the following ways.

1) Variation from algorithm to algorithm, wherein input excitation and added noise levels are kept same for all the algorithms.
2) Variation for different ground excitation, wherein algorithm and added noise level are kept same for all the considered ground excitations.
3) Variation due to different noise level, using same algorithm and input excitation.

Therefore, it is understandable that a definite conclusion may not be easily achievable regarding the performance of different considered algorithms. Thus, in order to come to such a conclusion, the steps considered are as follows:

1) Sensitivity analyses of the parameters are performed following Yin *et al.*(2010) and spider diagram is generated for each of the parameters to investigate the influence of variation of each of the parameters on the response of the system.
2) From the spider diagram, equations of curves representing variation in different parameter are derived by polynomial curve fitting method.
3) Parameter weights are calculated using the derived polynomial equation and using the percentage error of the identified parameter.
4) Performance error index (PEI) is introduced to judge the performance of any particular algorithm with respect to its overall ability to identify all the parameters. PEI is calculated using the parameter weights and percentage error of the identified parameter.

6.4.1 Generation of the *Spider Diagram*

In section 6.3.3, simulated hysteresis loop for the FREI were generated for 10mm to 60mm maximum displacement. These simulated hysteresis loops are in close agreement with those obtained from experiments. The values of parameters of the adopted FREI model used to generate these analytical hysteresis loops are furnished in Table 6.4 and these values have been considered as base values for comparison with identified values. Among all the parameters furnished in Table 6.4, the parameters selected for identification are B, β, γ, a_1, a_2, a_3.The coefficients a_4 and a_5 in Eq. (6.8) have been assigned zero in the present study, since it has been observed from Fig. 6.7 that there is no hardening behaviour after softening regime. Additionally, value of unity have been assigned to coefficients $\mathbb{A}, Y$ and α.

The procedure for generating spider diagram is as follows.

1) One of the parameters at a time out of the six considered parameters is varied in the range of ±50% with increment of 10% in each step from its base value, keeping other

five parameters constant. The hysteretic restoring force is calculated for each of the steps.

2) The error in hysteretic force for each 10% variation of these parameters are calculated by finding the difference in values between the hysteretic force obtained from variation of parameters and hysteretic force obtained without the variation of parameters.
3) The root mean-square error (RMSE) is calculated over the total execution time of the analysis and for each step of the parameter variation. The plot of percentage variation of parameter from base value in *x*-axis with that of RMSE in *y*-axis is called the *spider diagram.*
4) Similar procedure has been followed for all the parameters and curves are obtained for all the parameters and corresponding to different displacement amplitudes.

The spider diagram corresponding to 10mm to 60mm maximum displacement are shown in Fig. 6.15 to Fig. 6.20. From Fig. 6.15, it is observed that the parameter B is the most sensitive among all the parameters followed by a_1, β, a_2, γ and the least sensitive is the parameter a_3. However, in order to assign weights against each of these parameters as per its sensitivity, a single working diagram is required. The general tendencies of these parameters are however observed to be similar in all the figures. Therefore, an average spider diagram as shown in Fig. 6.21 has been generated by averaging the RMSE values of all of these parameters as plotted in Fig. 6.15 to Fig. 6.20. The average spider diagram serves the purpose of a single working diagram. Normalised average spider diagram (Fig. 6.22) is obtained by normalising the values with respect to the maximum values obtained from the average spider diagram. From normalised average spider diagram parameter weights are evaluated.

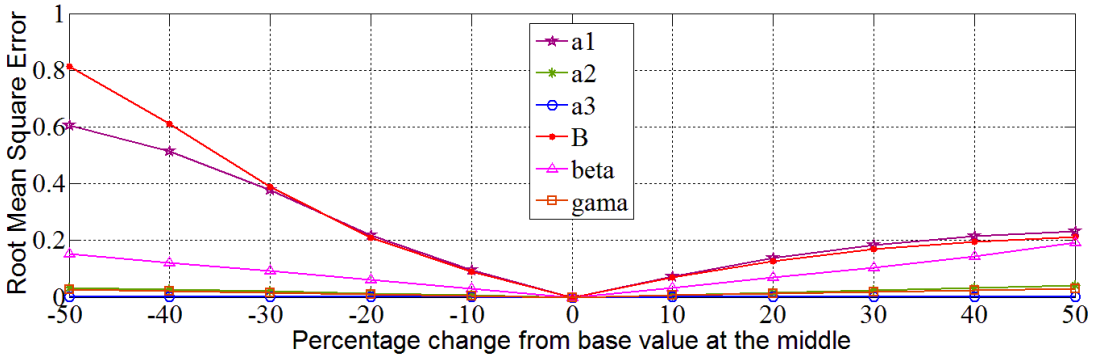

Fig. 6.15: Spider diagram generated by variation of one-factor-at-a-time for maximum displacement of 10mm

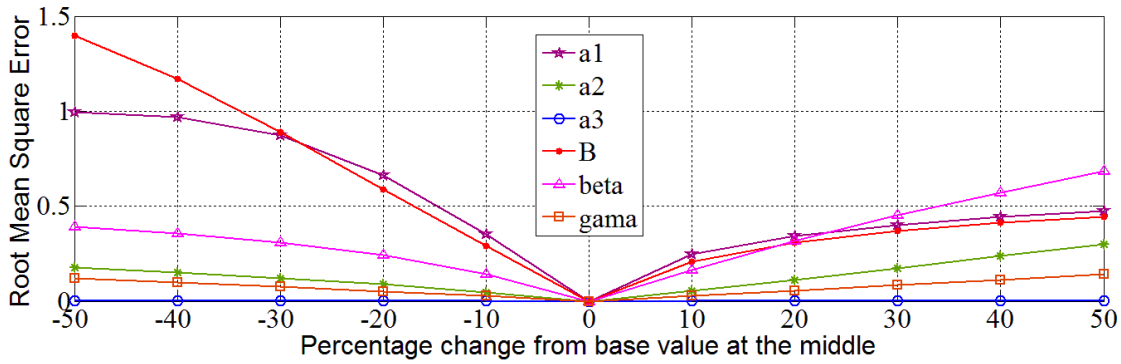

Fig. 6.16: Spider diagram generated by variation of one-factor-at-a-time for maximum displacement of 20mm

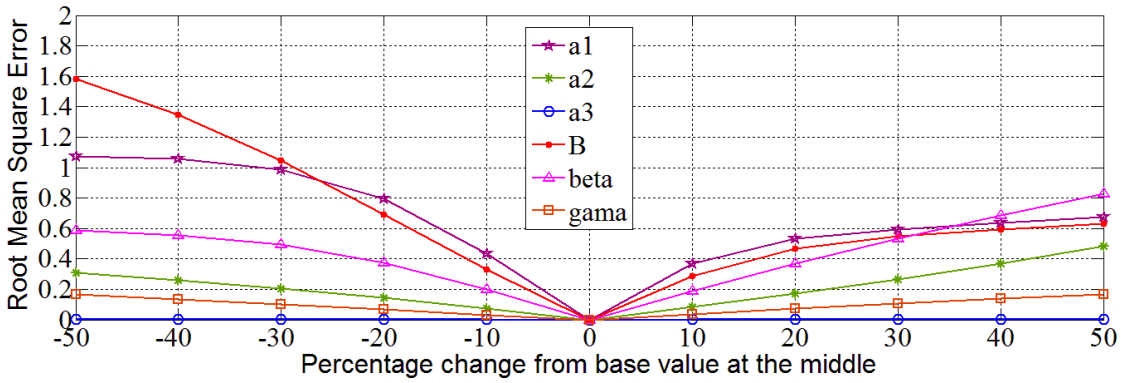

Fig. 6.17: Spider diagram generated by variation of one-factor-at-a-time for maximum displacement of 30mm

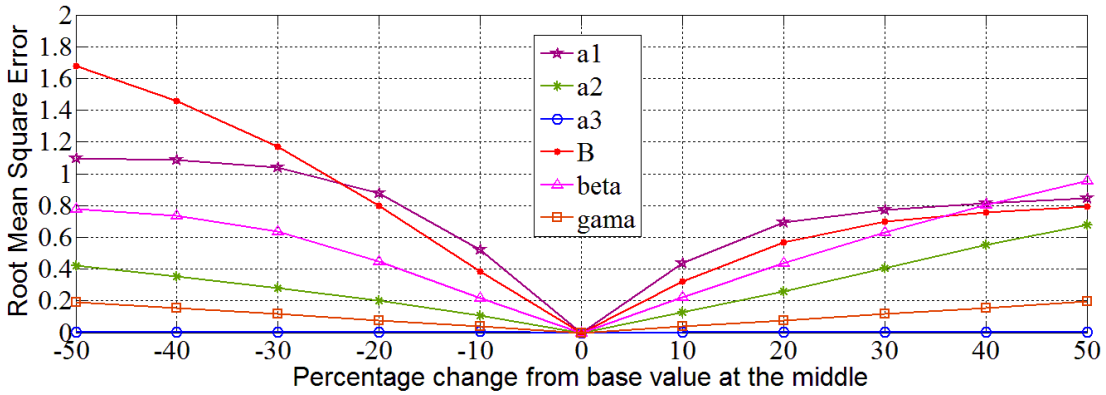

Fig. 6.18: Spider diagram generated by variation of one-factor-at-a-time for maximum displacement of 40mm

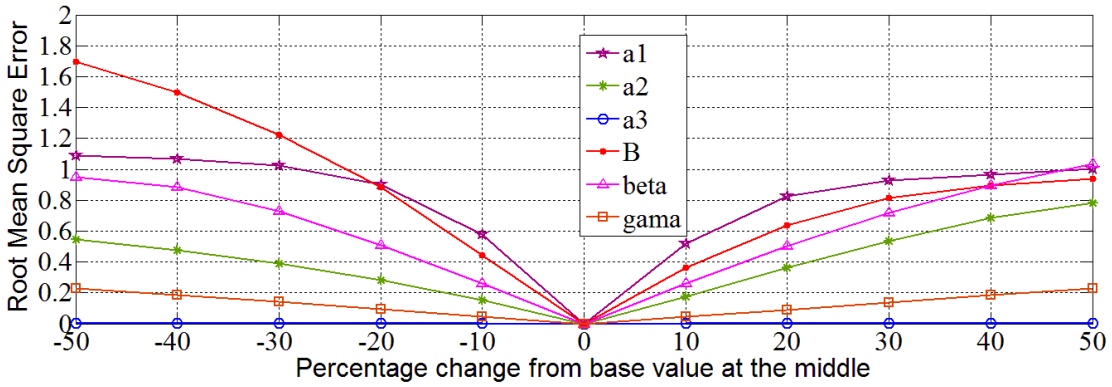

Fig. 6.19: Spider diagram generated by variation of one-factor-at-a-time for maximum displacement of 50mm

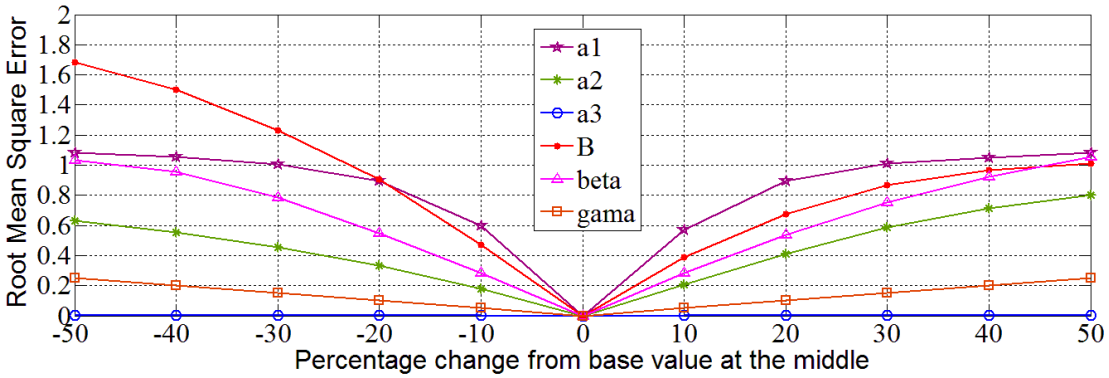

Fig. 6.20: Spider diagram generated by variation of one-factor-at-a-time for maximum displacement of 60mm

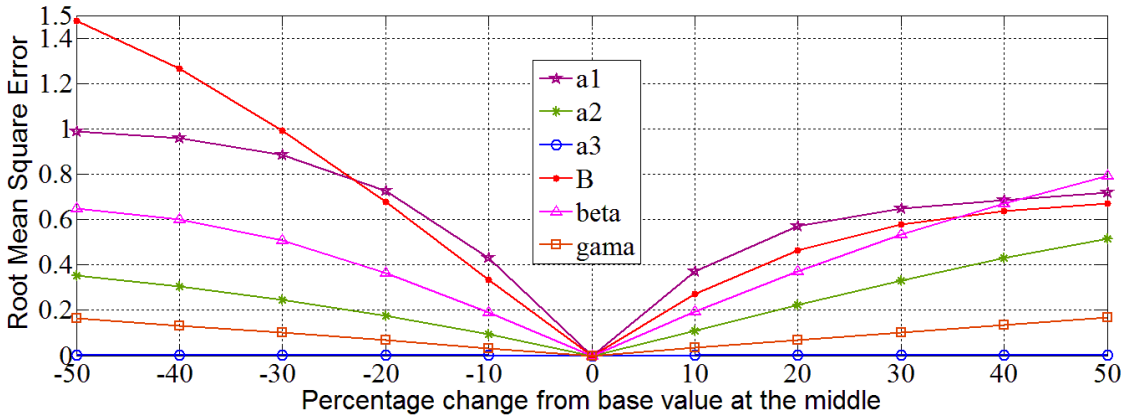

Fig. 6.21: Average diagram generated by variation of one-factor-at-a-time for maximum displacement of 10mm-60mm

Based on the average spider diagram as presented in Fig. 6.21, ranks have been assigned for the parameters and are furnished in Table 6.5 below. Ranks are assigned in order of increasing RMSE, which is considered as indication of sensitivity for any variation in its values. Rank-1 is for maximum sensitivity and Rank-6 for least sensitive parameter.

Table 6.5: Parameter Sensitivity Ranking

Parameter	B	β	γ	a_1	a_2	a_3
RMSE at -50%	1.4758	0.6494	0.1642	0.9899	0.3528	0.0014
Rank	1	3	5	2	4	6

The percentage error of identified parameters may be positive or negative depending on whether it is greater or lesser than base-value. Accordingly, the positive or negative side of the average spider diagram has been followed to finally determine the ranking.

6.4.2 Determination of parameter weights

The weight to be associated with each parameter is determined from the spider diagram, which depicts the relative importance of each parameter in the overall response of the system. To calculate the weights, the average spider diagram is normalized with respect to maximum observed RMSE. The normalized spider diagram is shown in Fig. 6.22. The ordinates of the points forming the curves representing each of the parameters of average spider diagram are furnished in Table 6.6 and Table 6.7. Table 6.6 corresponds to curves on the negative side and Table 6.7 corresponds to curves on the positive side of the horizontal axis. Similarly, Table 6.8 and Table 6.9 show the ordinates of the curves for normalized average spider diagram for negative and positive sides of horizontal axis respectively.

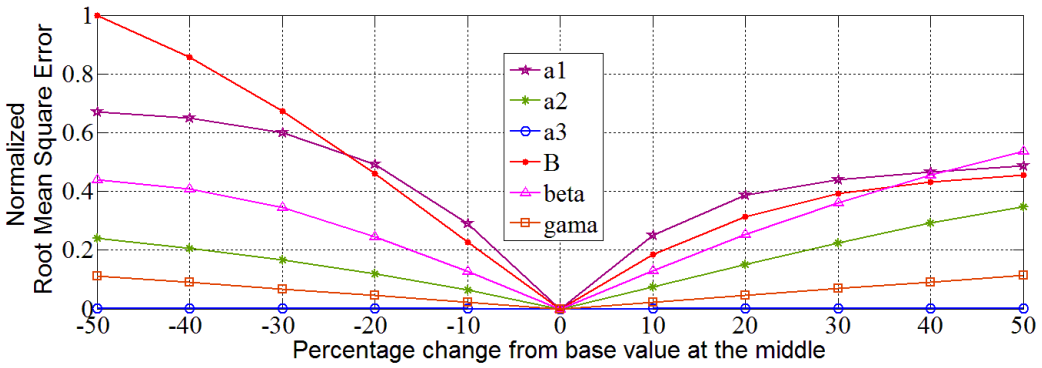

Fig. 6.22: Normalized Spider diagram generated by variation of one-factor-at-a-time for maximum displacement of 10mm-60mm

Table 6.6: Values of root-mean square error obtained from average spider diagram for negative percentage change from base value of parameters

Parameter	Percentage change from base value					
	-50%	-40%	-30%	-20%	-10%	0%
B	1.4758	1.2641	0.9918	0.6792	0.3352	0
β	0.6494	0.6017	0.5082	0.3639	0.1894	0
γ	0.1642	0.1326	0.1005	0.0673	0.0331	0
a_1	0.9899	0.9579	0.8851	0.7249	0.4287	0
a_2	0.3528	0.3030	0.2449	0.1770	0.0947	0
a_3	0.0014	0.0014	0.0014	0.0012	0.0017	0

Table 6.7: Values of root-mean square error obtained from average spider diagram for positive percentage change from base value of parameters

Parameter	Percentage change from base value					
	0%	10%	20%	30%	40%	50%
B	0	0.2718	0.4635	0.5781	0.6368	0.6717
β	0	0.1922	0.3725	0.5322	0.6715	0.7918
γ	0	0.0340	0.0679	0.1024	0.1355	0.1687
a_1	0	0.3698	0.5719	0.6471	0.6867	0.7186
a_2	0	0.1089	0.2217	0.3322	0.4315	0.5143
a_3	0	0.0009	0.0010	0.0011	0.0013	0.0016

Table 6.8: Normalized values of root-mean square error obtained from average spider diagram for negative percentage change from base value of parameters

Parameter	Percentage change from base value					
	-50%	-40%	-30%	-20%	-10%	0%
B	1.0000	0.8566	0.6720	0.4602	0.2271	0
β	0.4401	0.4077	0.3444	0.2466	0.1283	0
γ	0.1113	0.0899	0.0681	0.0456	0.0225	0
a_1	0.6708	0.6490	0.5997	0.4912	0.2905	0
a_2	0.2391	0.2053	0.1660	0.1199	0.0642	0
a_3	0.0009	0.001	0.0010	0.0008	0.0012	0

Table 6.9: Normalized values of root-mean square error obtained from average spider diagram for positive percentage change from base value of parameters

Parameter	Percentage change from base value					
	0%	10%	20%	30%	40%	50%
B	0	0.1842	0.3141	0.3917	0.4315	0.4551
β	0	0.1302	0.2524	0.3606	0.4550	0.5365
γ	0	0.0230	0.0460	0.0694	0.0918	0.1143
a_1	0	0.2505	0.3875	0.4384	0.4653	0.4869
a_2	0	0.0738	0.1502	0.2251	0.2924	0.3485
a_3	0	0.0006	0.0007	0.0007	0.0009	0.0011

Each of the curves as shown in Fig. 6.22 for negative and positive sides of the horizontal axis can be represented by a polynomial of the form shown in Eq. (6.16). A maximum 5th degree polynomial can be fitted as only six numbers of points are available for a single curve. Each parameter has two numbers of curves, one for the negative side and the other for positive side of the percent change in spider diagram. Therefore, each parameter is represented by two numbers of different polynomial for negative side and positive side separately. Thus, parameter weight is evaluated as

$$p(x) = p_1 x'^5 + p_2 x'^4 + p_3 x'^3 + p_4 x'^2 + p_5 x' + p_6 \quad (6.16)$$

where, x'=Normalized value of error in parameter.

The coefficients of the polynomial of Eq.(6.16) are determined by curve fitting technique utilizing the coordinates of normalized average spider diagram as given in Table 6.8 and Table 6.9. The coefficients of the polynomial p_1 to p_6 have been evaluated and furnished in Table 6.10 and Table 6.11.

Table 6.10: Polynomial coefficients for the parameters of the FREI model for the negative side of normalized average spider diagram

Parameter	Coefficients of polynomial for negative side of normalized spider diagram					
	p_1	p_2	p_3	p_4	p_5	p_6
B	24.7801	33.7803	18.643	3.9021	-2.0359	0
β	-17.3805	-18.8647	-5.2434	-1.0174	-1.3498	0
γ	0.7692	1.3203	0.8272	0.202	-0.2114	0
a_1	30.3943	45.0863	19.8462	-1.2361	-3.185	0
a_2	5.0573	6.8157	3.032	0.0862	-0.6572	0
a_3	-2.5551	-3.5859	-1.8333	-0.4114	-0.0377	0

Table 6.11: Polynomial coefficients for the parameters of the FREI model for the positive side of normalized average spider diagram

Parameter	Coefficients of polynomial for positive side of normalized spider diagram					
	p_1	p_2	p_3	p_4	p_5	p_6
B	-4.3743	9.5673	-4.3122	-2.0255	2.0785	0
β	-4.5773	7.1683	-4.1564	0.413	1.2958	0
γ	3.8041	-4.6697	1.9518	-0.3217	0.2474	0
a_1	-64.4834	78.7706	-26.5388	-2.2651	2.925	0
a_2	3.3376	-4.0827	0.9203	0.0901	0.7236	0
a_3	0.2845	-0.4744	0.3014	-0.0877	0.0121	0

6.5 Evaluation of State and parameter of FREI from shake table test of FREI supported test model

Shake table test based data are available from testing of a 1/5th scaled model of masonry building from previous research at IIT Guwahati [Das *et al.*(2015)]. The acceleration data were acquired from different floors and corresponding to different earthquake excitations as input. Using these floor acceleration data as output, EKF, Two-Stage EKF and UKF approaches are applied to identify the state and parameters of FREI supporting the masonry building (test model). The base-isolation system was subjected to different earthquake excitations as input. Like any other online identification scheme, whether it is EKF, UKF, or an optimization based schemes, an initial guess of parameters is essential. The model parameters of any newly manufactured bearing are unknown to begin with. Directly using any online identification schemes without any initial guess may lead to an erroneous result. Thus, the test results under cyclic displacement as mentioned in section 6.3.2 become essential to have some initial guess of parameters.

A schematic representation of the shake table based experimental setup is shown in Fig. 6.23 [Das *et al.* (2015)]. A two storey scaled masonry building (test model) supported on four numbers of FREI was tested. Accelerometers (ACMs) and Linear Variable Differential Transducer (LVDTs) were kept at different floor levels for recording data. As observed from the result of shake table test, the motion of the structure was almost like a rigid body with insignificant difference in displacement and acceleration between base and roof top. Hence, the experimental acceleration response of the building base is used for parameter identification using the EKF, Two-Stage EKF and UKF algorithms. The excitation is taken as those of the recorded acceleration at shake table level. The identified displacement is compared with that of experimentally obtained displacement of LVDT1. The placement of sensors is shown in Fig. 6.23.

The whole structure above the isolation level is considered as a single mass, since rigid body kind of motion was observed from experiments. Acceleration response of the assumed SDOF is taken from sensor ACM2, which is the absolute acceleration at that level. The acceleration data from sensor ACM1 is the shake table acceleration and is treated as input excitation. The displacement response as obtained from LVDT1 is the relative displacement. The experiment was carried out by Das *et al.* (2015). Relative acceleration response at isolator top level (the base slab just above the isolators) is evaluated by deducting table acceleration ACM1 from

absolute acceleration ACM2. The relative acceleration response has been used in the identification algorithms.

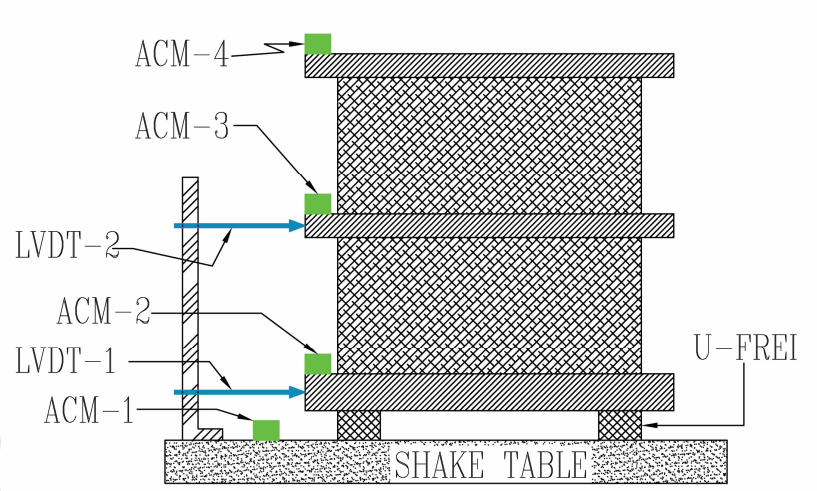

Fig. 6.23: A schematic arrangement the shake table test of U-FREI supported building (test model) [Das *et al.* (2015)]

6.5.1 Implementation of EKF algorithm for identification of state and parameter of U-FREI using Extended Bouc-Wen model

In this sub-section, a detailed derivation is carried out towards EKF implementation of the U-FREI supported SDOF nonlinear hysteretic system subjected to ground excitation.

The hysteretic restoring force, F_r is given by

$$F_r(t) = a_1 x + a_2 |x| x + a_3 x^3 + a_4 |x| x^3 + a_5 x^5 + Bz \tag{6.17}$$

where, z is given by

$$\dot{z} = \frac{\mathbb{A}\dot{x} - \beta|\dot{x}||z|^{\alpha-1}z - \gamma\dot{x}|z|^{\alpha}}{Y} \tag{6.18}$$

The governing equation of motion is given by

$$m\ddot{x} + F_r = \boldsymbol{F} = -m\ddot{x}_g \tag{6.19}$$

Where m is the lumped mass over the isolator, $F_r(t)$ is the restoring force of the system and $\ddot{x}_g$ is the ground acceleration. The process equation is expressed in state-space form and is given by Eq.(6.12), which is re-written here by Eq.(6.20).

$$\dot{\boldsymbol{X}} = \frac{d}{dt}\begin{Bmatrix} x \\ \dot{x} \\ z \end{Bmatrix} = \boldsymbol{g}(\boldsymbol{X}, \boldsymbol{\theta}, \boldsymbol{F}) = \begin{Bmatrix} \dot{x} \\ \ddot{x} \\ \dot{z} \end{Bmatrix}$$

$$= \begin{Bmatrix} \dot{x} \\ -\ddot{x}_g - (a_1 x + a_2|x|x + a_3 x^3 + a_4|x|x^3 + a_5 x^5 + Bz/m) \\ (\mathbb{A}\dot{x} - \beta|\dot{x}||z|^{\alpha-1}z - \gamma\dot{x}|z|^{\alpha})/Y \end{Bmatrix} = \begin{Bmatrix} g_1 \\ g_2 \\ g_3 \end{Bmatrix} \tag{6.20}$$

Jacobian of Matrix$\boldsymbol{g}$ is$\boldsymbol{A} = \frac{\partial \boldsymbol{g}}{\partial \boldsymbol{X_e}}$.

$$\frac{\partial \boldsymbol{g}}{\partial \boldsymbol{X}_e} = \begin{bmatrix} \frac{\partial g_1}{\partial x} & \frac{\partial g_1}{\partial \dot{x}} & \frac{\partial g_1}{\partial z} & \frac{\partial g_1}{\partial B} & \frac{\partial g_1}{\partial \gamma} & \frac{\partial g_1}{\partial \beta} & \frac{g_1}{\partial a_1} & \frac{\partial g_1}{\partial a_2} & \frac{\partial g_1}{\partial a_3} \\ \frac{\partial g_2}{\partial x} & \frac{\partial g_2}{\partial \dot{x}} & \frac{\partial g_2}{\partial z} & \frac{\partial g_2}{\partial B} & \frac{\partial g_2}{\partial \gamma} & \frac{\partial g_2}{\partial \beta} & \frac{\partial g_2}{\partial a_1} & \frac{\partial g_2}{\partial a_2} & \frac{\partial g_2}{\partial a_3} \\ \frac{\partial g_3}{\partial x} & \frac{\partial g_3}{\partial \dot{x}} & \frac{\partial g_3}{\partial z} & \frac{\partial g_3}{\partial B} & \frac{\partial g_3}{\partial \gamma} & \frac{\partial g_3}{\partial \beta} & \frac{\partial g_3}{\partial a_1} & \frac{\partial g_3}{\partial a_2} & \frac{\partial g_3}{\partial a_3} \end{bmatrix} \tag{6.21}$$

where, the extended unknown state vector is represented by $\boldsymbol{X}_e$ and is given by Eq.(6.22).

$$\boldsymbol{X}_e = \{x \quad \dot{x} \quad z \quad B \quad \beta \quad \gamma \quad a_1 \quad a_2 \quad a_3\}^T \tag{6.22}$$

The vector $\boldsymbol{X}_e$ is called the extended state vector, because apart from state vector$\{x, \dot{x}, z\}^T$, the vector $\boldsymbol{X}_e$ is also appended with parameters of the model under consideration called as the parametric vector $\{B, \beta, \gamma, a_1, a_2, a_3\}^T$.

The Jacobian is evaluated as

$$\boldsymbol{A} = \frac{\partial \boldsymbol{g}}{\partial \boldsymbol{X}_e}$$

$$= \begin{bmatrix} 0 & 1 & 0 & 0 & 0 & 0 & 0 & 0 & 0 \\ \frac{\partial g_2}{\partial x} & 0 & -B/m & -z/m & 0 & 0 & -x/m & -|x|x/m & -x^3/m \\ 0 & \frac{\partial g_3}{\partial \dot{x}} & \frac{\partial g_3}{\partial z} & 0 & -|\dot{x}||z|^{\alpha-1}z & -\dot{x}|z|^{\alpha} & 0 & 0 & 0 \end{bmatrix} \tag{6.23}$$

where,

$$\frac{\partial g_2}{\partial x} = -\{a_1 + a_2(|x| + x * sgn(x)) + 3a_3 x^2\}/m$$

$$\frac{\partial g_3}{\partial \dot{x}} = \mathbb{A} - \beta * sgn(\dot{x})|z|^{\alpha-1}z - \gamma|z|^{\alpha}$$

$$\frac{\partial g_3}{\partial z} = -\beta|\dot{x}||z|^{\alpha-1} - \beta|\dot{x}|(\alpha-1)|z|^{\alpha-2} * sgn(z) * z - \gamma\dot{x}\alpha|z|^{\alpha-1} * sgn(z)$$

$$\dot{\boldsymbol{X}}_e = \begin{Bmatrix} \dot{x} \\ \ddot{x} \\ \dot{z} \\ \dot{B} \\ \dot{\beta} \\ \dot{\gamma} \\ \dot{a}_1 \\ \dot{a}_2 \\ \dot{a}_3 \end{Bmatrix} = \frac{d}{dt}\begin{Bmatrix} x \\ \dot{x} \\ z \\ B \\ \beta \\ \gamma \\ a_1 \\ a_2 \\ a_3 \end{Bmatrix} = \frac{d\boldsymbol{X}_e}{dt} = \begin{Bmatrix} \dot{x} \\ \left(-m\ddot{x}_g - F_r\right)/m \\ (\mathbb{A}\dot{x} - \beta|\dot{x}||z|^{\alpha-1}z - \gamma\dot{x}|z|^{\alpha})/Y \\ 0 \\ 0 \\ 0 \\ 0 \\ 0 \\ 0 \end{Bmatrix}$$

$$= \begin{Bmatrix} \dot{x} \\ -\ddot{x}_g - (a_1 x + a_2|x|x + a_3 x^3 + a_4|x|x^3 + a_5 x^5 + Bz/m) \\ (\mathbb{A}\dot{x} - \beta|\dot{x}||z|^{\alpha-1}z - \gamma\dot{x}|z|^{\alpha})/Y \\ 0 \\ 0 \\ 0 \\ 0 \\ 0 \\ 0 \end{Bmatrix} \tag{6.24}$$

Using the above formulations, the identification algorithm is implemented in MATLAB as detailed below.

Implementation procedure in MATLAB

Step-1: Initialization Step.

Initialization is done by assuming the initial value of

i) The extended state vector, $\boldsymbol{X}_e$.

j) Error covariance matrix of extended state vector, $\boldsymbol{P}$.

k) Process error covariance matrix, $\boldsymbol{Q}$.

l) Measurement error covariance matrix, $\boldsymbol{R}$.

Step-2: Evaluation of state transfer matrix

The state transition matrix is determined by evaluating the Jacobian of the process equation and is given by Eq.(6.23).

Step-3: Prediction Step

Prediction of unknown extended state vector is made for current time step using the input information and state information of previous time step. This is done by integrating the

Eq.(6.24) by 4th order Runga-Kutta integration scheme. Using the predicted state vector and predicted parametric vector, the predicted measurement is calculated as given by Eq.(6.25)

$$H = -\ddot{x}_g - (a_1 x + a_2|x|x + a_3 x^3 + a_4|x|x^3 + a_5 x^5 + Bz/m) \tag{6.25}$$

Step-4: Updating Step

The measurement information at current time step is used to correct the estimate to get more accurate state information. This is accomplished by Kalman Filtering.

6.5.2 Implementation of Two-Stage EKF algorithm for identification of state and parameter of U-FREI using Extended Bouc-Wen model

The unknown extended state vector, $\boldsymbol{X}_e$, given by Eq.(6.22) contains both state vector $\boldsymbol{X}$ and parametric vector $\boldsymbol{\theta}$.

$$\boldsymbol{X}_e = \{x \quad \dot{x} \quad z|B \quad \beta \quad \gamma \quad a_1 \quad a_2 \quad a_3\}^T = \{\boldsymbol{X}^T \quad \boldsymbol{\theta}^T\}^T \tag{6.26}$$

where the state vector **X** and the parametric vector $\boldsymbol{\theta}$ are given as

$$\boldsymbol{X} = \{x \quad \dot{x} \quad z\}^T \tag{6.27}$$

$$\boldsymbol{\theta} = \{B \quad \beta \quad \gamma \quad a_1 \quad a_2 \quad a_3\}^T \tag{6.28}$$

The hysteretic restoring force, $F_r(t)$ as given by Eq.(6.17) is re-written here by omitting the 4th and 5th order terms as these terms represent the stiffening part of the hysteresis loop following the gradual softening region. Since, the data used in the present study are from the experimental results of the FREI and represents the gradual softening part only without going into further stiffening region. The polynomial upto the 3rd order suffices the present requirement. The truncated equation of restoring force is written as

$$F_r(t) = a_1 x + a_2|x|x + a_3 x^3 + Bz \tag{6.29}$$

where, z is given by Eq.(6.18).

$$\dot{z} = \frac{\mathbb{A}\dot{x} - \beta|\dot{x}||z|^{\alpha-1}z - \gamma\dot{x}|z|^{\alpha}}{Y} \tag{6.30}$$

The process equation is expressed in state-space form and is given by Eq.(6.35).

$$\dot{\boldsymbol{X}} = \frac{d}{dt}\begin{Bmatrix} x \\ \dot{x} \\ z \end{Bmatrix} = \boldsymbol{g}(\boldsymbol{X}, \boldsymbol{\theta}, \boldsymbol{F}) = \begin{Bmatrix} \dot{x} \\ \ddot{x} \\ \dot{z} \end{Bmatrix}$$

$$= \begin{Bmatrix} \dot{x} \\ -\ddot{x}_g - (a_1 x + a_2 |x| x + a_3 x^3 + Bz/m) \\ (\mathbb{A}\dot{x} - \beta |\dot{x}||z|^{\alpha-1} z - \gamma \dot{x} |z|^{\alpha})/Y \end{Bmatrix} = \begin{Bmatrix} g_1 \\ g_2 \\ g_3 \end{Bmatrix} \tag{6.31}$$

The Jacobian matrix $\boldsymbol{A_2}$ is given by Eq. (6.32)

$$\boldsymbol{A_2} = \frac{\partial \boldsymbol{g}}{\partial \boldsymbol{X}} = \begin{bmatrix} \frac{\partial g_1}{\partial x} & \frac{\partial g_1}{\partial \dot{x}} & \frac{\partial g_1}{\partial z} \\ \frac{\partial g_2}{\partial x} & \frac{\partial g_2}{\partial \dot{x}} & \frac{\partial g_2}{\partial z} \\ \frac{\partial g_3}{\partial x} & \frac{\partial g_3}{\partial \dot{x}} & \frac{\partial g_3}{\partial z} \end{bmatrix} = \begin{bmatrix} 0 & 1 & 0 \\ \frac{\partial g_2}{\partial x} & 0 & -B/m \\ 0 & \frac{\partial g_3}{\partial \dot{x}} & \frac{\partial g_3}{\partial z} \end{bmatrix} \tag{6.32}$$

where,

$$\frac{\partial g_2}{\partial x} = -\left[a_1 + a_2 |x| + a_2 * sgn(x) * x + 3a_3 x^2\right]/m$$

$$\frac{\partial g_3}{\partial \dot{x}} = \mathbb{A} - \beta * sgn(\dot{x}) |z|^{\alpha-1} z - \gamma |z|^{\alpha}$$

$$\frac{\partial g_3}{\partial z} = -\beta |\dot{x}| \{|z|^{\alpha-1} + z(\alpha - 1)|z|^{\alpha-2} * sgn(z)\} - \gamma \dot{x} \alpha |z|^{\alpha-1} * sgn(z)$$

The observation equation is given by Eq.(6.33)

$$h = -\ddot{x}_g - (a_1 x + a_2 |x| x + a_3 x^3 + Bz/m) \tag{6.33}$$

The observation equation at time $t = k \times \Delta t$ is a nonlinear function of unknown parametric vector $\boldsymbol{\theta}_k$ and can be linearized via Taylor series expansion as

$$\boldsymbol{h}(\boldsymbol{X}_k, \boldsymbol{\theta}_k, \boldsymbol{F}_k) = \boldsymbol{h}\left(\widehat{\boldsymbol{X}}_{k|k-1}, \widehat{\boldsymbol{\theta}}_{k-1}, \boldsymbol{F}_k\right) + \boldsymbol{H}_k\left(\boldsymbol{\theta}_k - \widehat{\boldsymbol{\theta}}_{k-1}\right) \tag{6.34}$$

where, $\boldsymbol{H}_{\mathrm{k}}$ is obtained based on the chain rule of partial differential with respect to the parametric vector $\boldsymbol{\theta_k}$as

$$\boldsymbol{H}_k = \boldsymbol{H}_{\theta,k} + \boldsymbol{H}_{X,k} \boldsymbol{X}_{\theta,k} \tag{6.35}$$

In which,

$$\boldsymbol{H}_{\theta,k} = \left[\frac{\partial \boldsymbol{h}(\boldsymbol{X},\boldsymbol{\theta},\boldsymbol{F})}{\partial \boldsymbol{\theta}}\right]_{\boldsymbol{X}=\widehat{\boldsymbol{X}}_{k|k-1},\boldsymbol{\theta}=\widehat{\boldsymbol{\theta}}_{k-1}} \tag{6.36}$$

$$\boldsymbol{H}_{X,k} = \left[\frac{\partial \boldsymbol{h}(\boldsymbol{X},\boldsymbol{\theta},\boldsymbol{F})}{\partial \boldsymbol{X}}\right]_{\boldsymbol{X}=\widehat{\boldsymbol{X}}_{k|k-1},\boldsymbol{\theta}=\widehat{\boldsymbol{\theta}}_{k-1}} \tag{6.37}$$

$$\boldsymbol{X}_{\theta,k} = \left[\frac{\partial \boldsymbol{X}(\boldsymbol{X},\boldsymbol{\theta},\boldsymbol{F})}{\partial \boldsymbol{\theta}}\right]_{\boldsymbol{\theta}=\widehat{\boldsymbol{\theta}}_{k-1}} \tag{6.38}$$

The details of Eq.(6.34), (6.35) and (6.36) are given in Chapter-3 of this thesis.

The partial derivative of the observation equation with respect to state vector $\boldsymbol{X}$ is given by Eq.(6.39)

$$\begin{aligned}\boldsymbol{H}_{X,k} = \frac{\partial h}{\partial \boldsymbol{X}} &= \left[\frac{\partial h}{\partial x} \quad \frac{\partial h}{\partial \dot{x}} \quad \frac{\partial h}{\partial z}\right] \\ &= -\left(\frac{1}{m}\right)\left[\left(a_1 + a_2\left(|x| + x * sgn(x)\right) + 3a_3x^2\right) \quad 0 \quad B\right]\end{aligned} \tag{6.39}$$

The partial derivative of the observation equation with respect to parametric vector $\boldsymbol{\theta}$ is given by Eq.(6.40).

$$\begin{aligned}\boldsymbol{H}_{\theta,k} = \frac{\partial h}{\partial \boldsymbol{\theta}} &= \left[\frac{\partial h}{\partial B} \quad \frac{\partial h}{\partial \beta} \quad \frac{\partial h}{\partial \gamma} \quad \frac{\partial h}{\partial a_1} \quad \frac{\partial h}{\partial a_2} \quad \frac{\partial h}{\partial a_3}\right] \\ &= -\left(\frac{1}{m}\right)\left[z \quad 0 \quad 0 \quad x \quad |x|x \quad x^3\right]\end{aligned} \tag{6.40}$$

Evaluating the matrix $\boldsymbol{X}_{\theta,k}$ as given in Eq. (6.35).

Differentiating both side of Eq. (6.31) with respect to parametric vector $\boldsymbol{\theta}$ and denoting $\frac{d\boldsymbol{X}}{d\boldsymbol{\theta}}$ by $\mathbf{X}_\theta$

$$\frac{d\dot{\boldsymbol{X}}}{d\boldsymbol{\theta}} = \dot{\mathbf{X}}_\theta = \begin{Bmatrix} \frac{d\dot{x}}{d\boldsymbol{\theta}} \\ \frac{d}{d\boldsymbol{\theta}}\{-\ddot{x}_g - (a_1x + a_2|x|x + a_3x^3 + Bz/m)\} \\ \frac{d}{d\boldsymbol{\theta}}\{(\mathbb{A}\dot{x} - \beta|\dot{x}||z|^{\alpha-1}z - \gamma\dot{x}|z|^{\alpha})/Y\} \end{Bmatrix} = \begin{Bmatrix} \frac{d\dot{x}}{d\boldsymbol{\theta}} \\ \frac{dh}{d\boldsymbol{\theta}} \\ \frac{d\dot{z}}{d\boldsymbol{\theta}} \end{Bmatrix} \tag{6.41}$$

Applying chain rule of partial differential to Eq. (6.41).

$$\frac{d\dot{x}}{d\boldsymbol{\theta}} = \frac{\partial \dot{x}}{\partial \boldsymbol{X}}\frac{d\boldsymbol{X}}{d\boldsymbol{\theta}} + \frac{\partial \dot{x}}{\partial \boldsymbol{\theta}}\frac{d\boldsymbol{\theta}}{d\boldsymbol{\theta}} = \frac{\partial \dot{x}}{\partial \boldsymbol{X}}\frac{d\boldsymbol{X}}{d\boldsymbol{\theta}} + \frac{\partial \dot{x}}{\partial \boldsymbol{\theta}} \tag{6.42}$$

$$\frac{dh}{d\boldsymbol{\theta}} = \frac{\partial h}{\partial \boldsymbol{X}}\frac{d\boldsymbol{X}}{d\boldsymbol{\theta}} + \frac{\partial h}{\partial \boldsymbol{\theta}}\frac{d\boldsymbol{\theta}}{d\boldsymbol{\theta}} = \frac{\partial h}{\partial \boldsymbol{X}}\frac{d\boldsymbol{X}}{d\boldsymbol{\theta}} + \frac{\partial h}{\partial \boldsymbol{\theta}} \tag{6.43}$$

$$\frac{d\dot{z}}{d\boldsymbol{\theta}} = \frac{\partial \dot{z}}{\partial \boldsymbol{X}}\frac{d\boldsymbol{X}}{d\boldsymbol{\theta}} + \frac{\partial \dot{z}}{\partial \boldsymbol{\theta}}\frac{d\boldsymbol{\theta}}{d\boldsymbol{\theta}} = \frac{\partial \dot{z}}{\partial \boldsymbol{X}}\frac{d\boldsymbol{X}}{d\boldsymbol{\theta}} + \frac{\partial \dot{z}}{\partial \boldsymbol{\theta}} \tag{6.44}$$

Substituting $\frac{d\dot{x}}{d\boldsymbol{\theta}}, \frac{dh}{d\boldsymbol{\theta}}$ and $\frac{d\dot{z}}{d\boldsymbol{\theta}}$ obtained from Eq. (6.42), (6.43) and (6.44) into Eq. (6.41)

$$\frac{d\dot{\boldsymbol{X}}}{d\boldsymbol{\theta}} = \dot{\mathbf{X}}_{\theta} = \begin{Bmatrix} \frac{d\dot{x}}{d\boldsymbol{\theta}} \\ \frac{dh}{d\boldsymbol{\theta}} \\ \frac{d\dot{z}}{d\boldsymbol{\theta}} \end{Bmatrix} = \begin{Bmatrix} \left(\frac{\partial \dot{x}}{\partial \boldsymbol{X}}\frac{d\boldsymbol{X}}{d\boldsymbol{\theta}} + \frac{\partial \dot{x}}{\partial \boldsymbol{\theta}}\right) \\ \left(\frac{\partial h}{\partial \boldsymbol{X}}\frac{d\boldsymbol{X}}{d\boldsymbol{\theta}} + \frac{\partial h}{\partial \boldsymbol{\theta}}\right) \\ \left(\frac{\partial \dot{z}}{\partial \boldsymbol{X}}\frac{d\boldsymbol{X}}{d\boldsymbol{\theta}} + \frac{\partial \dot{z}}{\partial \boldsymbol{\theta}}\right) \end{Bmatrix} = \begin{Bmatrix} \frac{\partial \dot{x}}{\partial \boldsymbol{X}}\frac{d\boldsymbol{X}}{d\boldsymbol{\theta}} \\ \frac{\partial h}{\partial \boldsymbol{X}}\frac{d\boldsymbol{X}}{d\boldsymbol{\theta}} \\ \frac{\partial \dot{z}}{\partial \boldsymbol{X}}\frac{d\boldsymbol{X}}{d\boldsymbol{\theta}} \end{Bmatrix} + \begin{Bmatrix} \frac{\partial \dot{x}}{\partial \boldsymbol{\theta}} \\ \frac{\partial h}{\partial \boldsymbol{\theta}} \\ \frac{\partial \dot{z}}{\partial \boldsymbol{\theta}} \end{Bmatrix}$$

$$= \begin{Bmatrix} \frac{\partial \dot{x}}{\partial \boldsymbol{X}} \\ \frac{\partial h}{\partial \boldsymbol{X}} \\ \frac{\partial \dot{z}}{\partial \boldsymbol{X}} \end{Bmatrix} \left\{\frac{d\boldsymbol{X}}{d\boldsymbol{\theta}}\right\} + \begin{Bmatrix} \frac{\partial \dot{x}}{\partial \boldsymbol{\theta}} \\ \frac{\partial h}{\partial \boldsymbol{\theta}} \\ \frac{\partial \dot{z}}{\partial \boldsymbol{\theta}} \end{Bmatrix} = \begin{Bmatrix} \frac{\partial \dot{x}}{\partial \boldsymbol{X}} \\ \frac{\partial h}{\partial \boldsymbol{X}} \\ \frac{\partial \dot{z}}{\partial \boldsymbol{X}} \end{Bmatrix} \boldsymbol{X}_{\theta} + \begin{Bmatrix} \frac{\partial \dot{x}}{\partial \boldsymbol{\theta}} \\ \frac{\partial h}{\partial \boldsymbol{\theta}} \\ \frac{\partial \dot{z}}{\partial \boldsymbol{\theta}} \end{Bmatrix} \tag{6.45}$$

Replacing $\frac{\partial h}{\partial \boldsymbol{X}}$ by $\boldsymbol{H}_{X,k}$ and $\frac{\partial h}{\partial \boldsymbol{\theta}}$ by $\boldsymbol{H}_{\theta,k}$ obtained from Eq. (6.39) and (6.40) into Eq.(6.45).

$$\frac{d\dot{\boldsymbol{X}}}{d\boldsymbol{\theta}} = \dot{\mathbf{X}}_{\theta} = \begin{Bmatrix} \frac{\partial \dot{x}}{\partial \boldsymbol{X}} \\ \boldsymbol{H}_{X,k} \\ \frac{\partial \dot{z}}{\partial \boldsymbol{X}} \end{Bmatrix} \boldsymbol{X}_{\theta} + \begin{Bmatrix} \frac{\partial \dot{x}}{\partial \boldsymbol{\theta}} \\ \boldsymbol{H}_{\theta,k} \\ \frac{\partial \dot{z}}{\partial \boldsymbol{\theta}} \end{Bmatrix} \tag{6.46}$$

Eq. (6.46) can be solved using 4th order Runga-Kutta integration scheme to get $\boldsymbol{X}_{\theta}$. Hence, the matrix $\boldsymbol{H}_k$ is determined using Eq. (6.35).

Evaluation of $\frac{\partial \dot{x}}{\partial \boldsymbol{X}}$

$$\frac{\partial \dot{x}}{\partial \boldsymbol{X}} = \begin{bmatrix} \frac{\partial \dot{x}}{\partial x} & \frac{\partial \dot{x}}{\partial \dot{x}} & \frac{\partial \dot{x}}{\partial z} \end{bmatrix} = [0 \quad 1 \quad 0] \tag{6.47}$$

Evaluation of $\frac{\partial \dot{z}}{\partial \boldsymbol{X}}$

$$\frac{\partial \dot{z}}{\partial \boldsymbol{X}} = \begin{bmatrix} \frac{\partial \dot{z}}{\partial x} & \frac{\partial \dot{z}}{\partial \dot{x}} & \frac{\partial \dot{z}}{\partial z} \end{bmatrix} = \begin{bmatrix} 0 & \frac{\partial \dot{z}}{\partial \dot{x}} & \frac{\partial \dot{z}}{\partial z} \end{bmatrix} \tag{6.48}$$

Evaluation of $\frac{\partial \dot{z}}{\partial \dot{x}}$

$$\frac{\partial \dot{z}}{\partial \dot{x}} = \mathbb{A} - \beta|z|^{(\alpha-1)}z * sign(\dot{x}) - \gamma|z|^{\alpha} \tag{6.49}$$

Evaluation of $\frac{\partial \dot{z}}{z}$

$$\frac{\partial \dot{z}}{\partial z} = -\beta|\dot{x}|\left(|z|^{(\alpha-1)} + z(\alpha-1)|z|^{(\alpha-2)} * sign(z)\right) - \gamma\alpha\dot{x}|z|^{(\alpha-1)} * sign(z) \tag{6.50}$$

Evaluation of $\frac{\partial \dot{x}}{\partial \boldsymbol{\theta}}$

$$\frac{\partial \dot{x}}{\partial \boldsymbol{\theta}} = \left[\frac{\partial \dot{x}}{\partial B} \quad \frac{\partial \dot{x}}{\partial \beta} \quad \frac{\partial \dot{x}}{\partial \gamma} \quad \frac{\partial \dot{x}}{\partial a_1} \quad \frac{\partial \dot{x}}{\partial a_2} \quad \frac{\partial \dot{x}}{\partial a_3}\right] = [0 \quad 0 \quad 0 \quad 0 \quad 0 \quad 0] \tag{6.51}$$

Evaluation of $\frac{\partial \dot{z}}{\partial \boldsymbol{\theta}}$

$$\frac{\partial \dot{z}}{\partial \boldsymbol{\theta}} = \left[\frac{\partial \dot{z}}{\partial B} \quad \frac{\partial \dot{z}}{\partial \beta} \quad \frac{\partial \dot{z}}{\partial \gamma} \quad \frac{\partial \dot{z}}{\partial a_1} \quad \frac{\partial \dot{z}}{\partial a_2} \quad \frac{\partial \dot{z}}{\partial a_3}\right] = \left[0 \quad \frac{\partial \dot{z}}{\partial \beta} \quad \frac{\partial \dot{z}}{\partial \gamma} \quad 0 \quad 0 \quad 0\right]$$
$$= \left[0 \quad \left(-|\dot{x}||z|^{(\alpha-1)}z\right) \quad \left(-\dot{x}|z|^{\alpha}\right) \quad 0 \quad 0 \quad 0\right] \tag{6.52}$$

Using the above formulations, the identification algorithm is implemented in MATLAB as detailed below.

Implementation procedure in MATLAB

Step-1: Initialization Step.

Initialization is done by assuming the initial value of

a) The state vector, $\boldsymbol{x}$ and error covariance matrix of $\boldsymbol{x}$, i.e. $\boldsymbol{P_x}$.
b) The parametric vector, $\boldsymbol{\theta}$ and error covariance matrix of $\boldsymbol{\theta}$, which is $\boldsymbol{P_\theta}$.
c) The matrix $\boldsymbol{X_\theta}$.
d) Process error covariance matrix, $\boldsymbol{Q}$.
e) Measurement error covariance matrix, $\boldsymbol{R}$.

Step-2: Kalman Estimation of parametric vector $\boldsymbol{\theta}$.

From initial guess or from previous time step, the state, the parametric vector and the input ground acceleration are utilized to determine the predicted measurement as given by Eq.(6.33). The matrix $\boldsymbol{H_\theta}$ and $\boldsymbol{H_X}$ are evaluated using Eq.(6.36) and (6.37). The matrix $\boldsymbol{H_k}$ is determined using Eq.(6.35) and $\boldsymbol{X_\theta}$, which is obtained from previous time step.

Kalman Filtering is carried out using the current measurement and the predicted measurement to get an updated estimate of parameters, and error covariance matrix of parametric vector.

Step-3: Kalman Estimation of state vector ***X****.*

The Jacobian of the process equation [$\boldsymbol{A_2}$] is evaluated using already estimated parameters in *step-2* and Eq.(6.32). Kalman Filtering is carried out to estimate the state vector.

Step-4: Prediction of matrix $\boldsymbol{X_0}$ for next time step.

The matrix $\boldsymbol{X_0}$ is evaluated by integration of Eq.(6.41) using 4th order Runga-Kutta Integration scheme.

6.5.3 Implementation of UKF algorithm for identification of state and parameter of U-FREI using Extended Bouc-Wen model

In UKF, there is no need to evaluate the complex Jacobian matrix. The process of implementation is rather simple. The details of formulation are given in chapter-3. The step-by-step implementation of the algorithm in MATLAB is similar to that already described under steps-1 to 5 of section-4.5.3.1 in chapter-4.

6.6 Performance evaluation of different identification strategies for the evaluation of state and parameter of U-FREI

In this sub-section, a comparative study has been conducted based on the identification results of EKF, Two-Stage EKF and UKF algorithms. Three different earthquake data have been considered for base excitation of the FREI supported building system. The system identification have been performed using 1) experimentally acquired output responses and 2) simulated output responses corrupted with four different noise levels of 0%, 2%, 5% and 10%. The structural system considered here comprises of a two storey masonry building supported on four numbers of FREIs (Fig. 6.23). The output responses from all the floor levels indicated that the structure was experiencing a rigid body motion [Das *et al.* (2015)]. Therefore, only the response of the base of the structure has been considered. The acceleration response ACM2 is considered as the output response of the system and the displacement response obtained from LVDT1 is used for comparison with the identified displacement (Fig. 6.23). The shake table acceleration obtained from sensor ACM1 is considered as the ground excitation.

All the computer programs related to the considered identification algorithms and simulation algorithms have been developed in MATLAB.

The results of identification have been analysed in three different ways as discussed below.

a) The first part is concerned with identification of state of the system. In the present study, the state of the system refers only to the displacement at the considered level of the structure. In the study following experimental data, displacements obtained from the application of identification algorithms are plotted against time and comparison is done with respect to measured displacement time-history obtained from laboratory tests. The experimentally measured displacement time-history is considered as base value based on which all identified displacement time-history have been compared. Similarly, identification of state has been done using data from simulation, but the comparison is done with the displacement obtained directly from simulation considered as base value. The accuracy of identification is evaluated by determining the RMSE of identified displacement with that of corresponding base values. For comparative study of the performance of the algorithms, a bar chart representation of RMSE has been made.

b) The second part is concerned with the identification of parameters of FREI. Parameter of FREI refers to B, β, γ, a_1, a_2 and a_3. The identified parameters using each of the algorithms and for each of the base excitations are plotted in bar chart format. The errors in identified parameters from the base value are also represented in bar chart format. The base value refers to the selected values of these parameters as presented in Table 6.4. Since, each of the identified parameters varies from algorithm to algorithm and for different ground excitations, it becomes difficult to ascertain the performance of an algorithm for a particular setup and also for assessment of comparative efficiency of all the considered algorithms for the study on FREI supported system. To simplify the evaluation of performance of the algorithms, a performance index has been introduced named as Performance Error Index (PEI) as already discussed in the previous section 6.4. The PEI for each algorithm is determined for each of the cases, whether based on experimental or simulation based data. Smaller value of PEI indicates better accuracy in identification. A comparative study of PEI will indicate the performance accuracy of these algorithms. However, PEI may be considered as effective only if the identified parameters converge with time.

c) The third part is concerned with the study on convergence of identified parameters. Merely finding the PEI will not indicate the performance level of these algorithms. The identified parameters plotted against time should indicate convergence. Only a

qualitative analysis is performed regarding the convergence by plotting the identified parameters against time.

6.6.1 Results of identification of *state* of U-FREI

The states of U-FREI supported isolation system are represented by displacement, velocity and the differential parameter z of the Bouc-Wen model. RMSE has been evaluated to determine the identification accuracy of displacement. Lower value of RMSE suggests greater accuracy in results. Identification of velocity is not undertaken as it can be easily obtained by differentiation of displacement. In all the identification schemes, acceleration responses from the system are used as input for the identification algorithms. The predicted states like displacement and velocity of the system are evaluated by integration procedure. Integration often leads to divergence of identified states and thereby leading to failure of the algorithms. Therefore, accuracy of displacement identification will indirectly indicate accuracy of identification of other states also. The accuracy of identification of z can be ascertained from the plot of simulated or experimentally obtained hysteresis loops. The details of the identified results are given below.

6.6.1.1 Identification of *state* of U-FREI based on Experimental responses

Results of identified displacement *vs.* experimentally measured displacement time-history for different earthquakes are shown in Fig. 6.24 to Fig. 6.26. It is observed that identified displacement using the algorithms are in good agreement with that of measured displacement obtained from experiments.

The efficiency of the algorithms in identifying the state of the system can be assessed very effectively by evaluating the RMSE of the identified displacement. The error in identification at any given time instant is the difference between identified displacement and experimentally measured displacement. The experimentally measured displacement is considered as the base value based on which RMSE is evaluated.

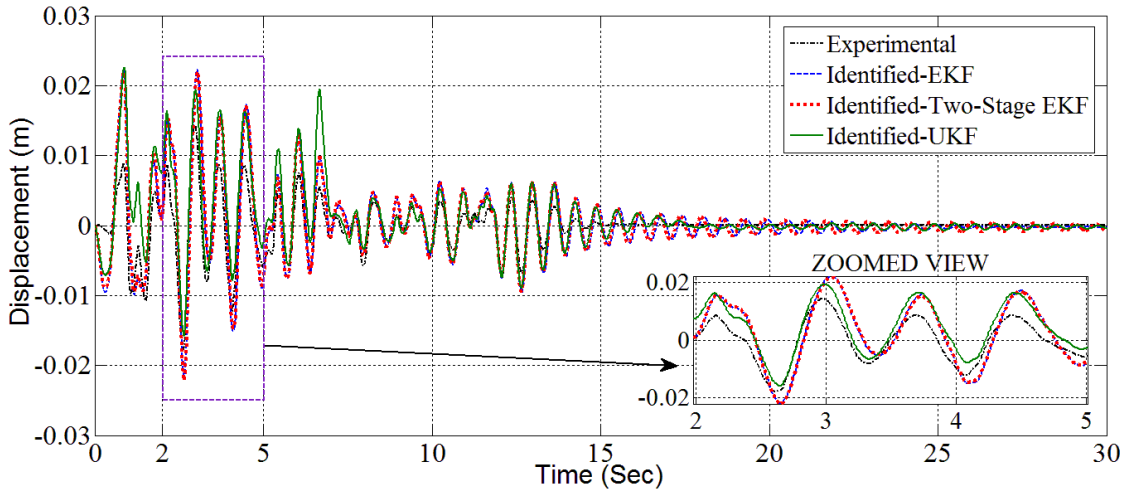

Fig. 6.24: Comparison of identified displacement time-history with experimentally measured displacement time-history using experimental response under excitation El Centro (1940): Comp-180

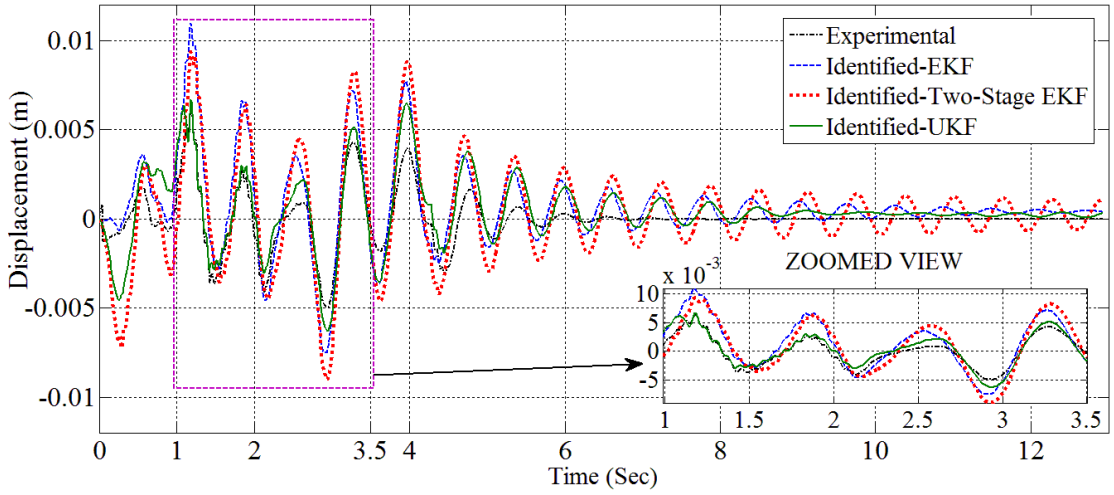

Fig. 6.25: Comparison of identified displacement time-history with experimentally measured displacement time-history using experimental response under excitation Koyna (1967): Comp-Longitudinal

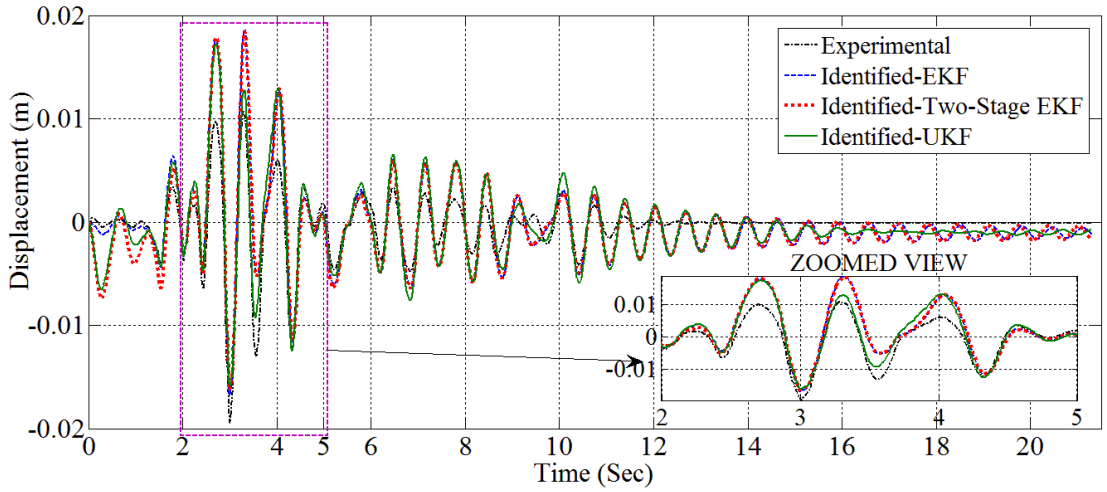

Fig. 6.26: Comparison of identified displacement time-history with experimentally measured displacement time-history using experimental response under excitation Victoria (1980): Comp-CPE045

Fig. 6.24 to Fig. 6.26 shows the identified displacement corresponding to different algorithms and experimentally measured displacements. It is observed that the identified displacement matches well with the experimentally observed displacement. The RMSE has been represented in form of bar chart (Fig. 6.27) and values of RMSE are given in Table 6.12.It is observed that the performances of all the algorithms are quite comparable. The magnitude of RMSE is significantly low for all the three algorithms.

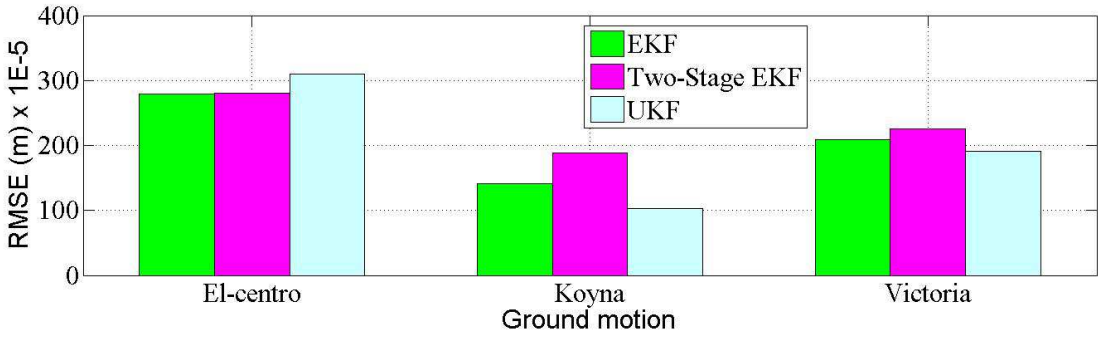

Fig. 6.27: Bar Chart showing RMSE of identified displacement using experimental response and under different earthquake excitation

Table 6.12: RMSE of identified displacement using experimental response and under different earthquake excitation

Earthquake	EKF	Two-Stage EKF	UKF
	(x 1E-5)	(x 1E-5)	(x 1E-5)
El Centro (1940): Comp-180	280	280	310
Koyna (1967): Comp-Longitudinal	142	188	103
Victoria (1980): Comp-CPE045	209	226	191

A plot of hysteresis loop as obtained from the identification using algorithms EKF, Two-Stage EKF and UKF for three different ground motions are shown in Fig. 6.28 to Fig. 6.30. These identification results are obtained using responses from the experimental investigation. These hysteresis plots using different identification schemes show quite good agreement. This indicates that apart from displacement, the other state of the system such as velocity and the hysteresis parameter z [Eq. (6.18)] have also been identified by the algorithms with quite reasonable accuracy.

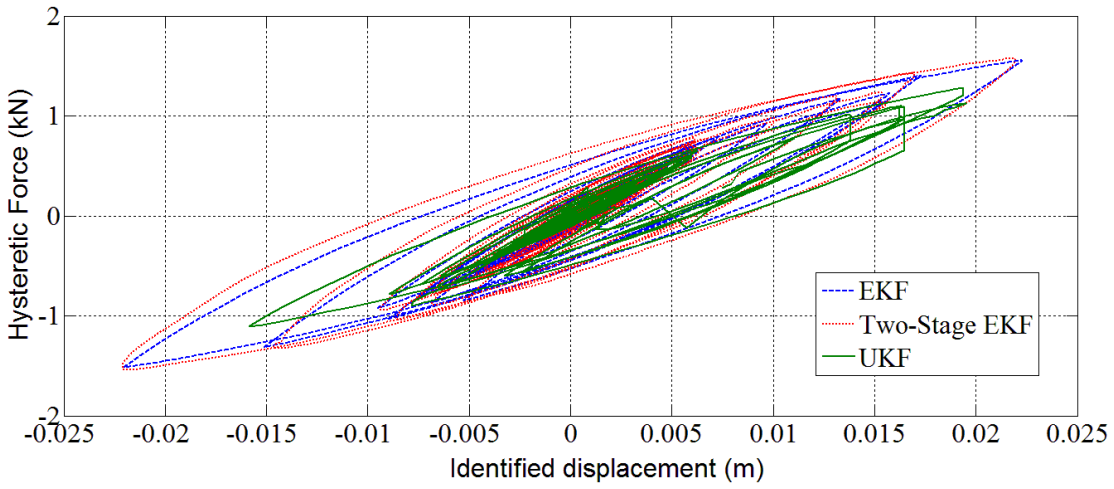

Fig. 6.28: Comparison of identified hysteresis loop with experimental hysteresis loop under excitation El Centro (1940): Comp-180

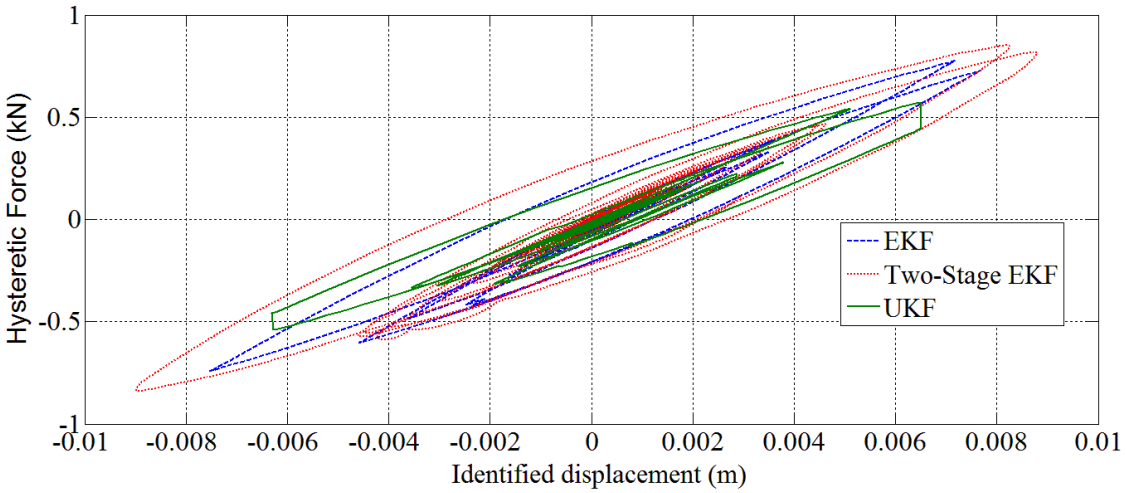

Fig. 6.29: Comparison of identified hysteresis loop with experimental hysteresis loop under excitation Koyna (1967): Comp-Longitudinal

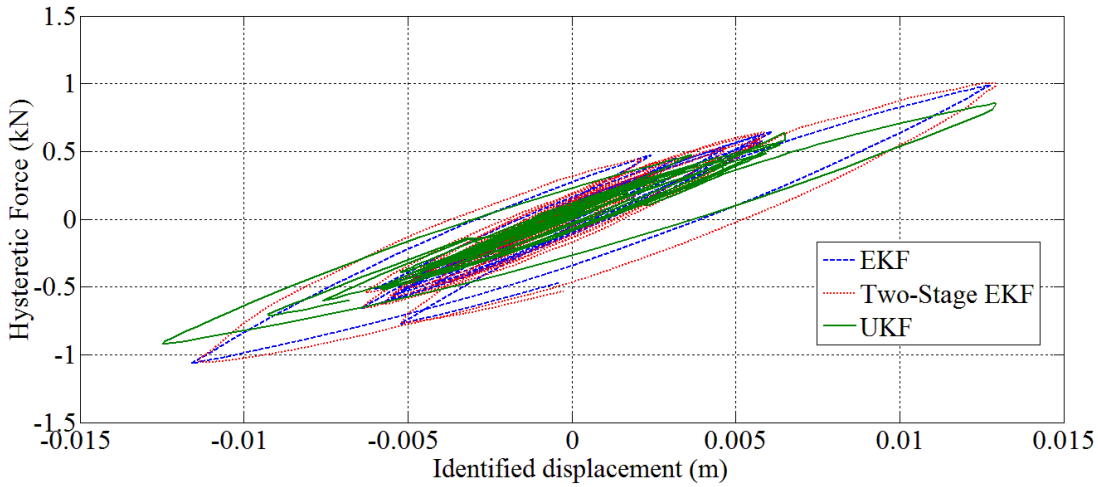

Fig. 6.30: Comparison of identified hysteresis loop with experimental hysteresis loop under excitation Victoria (1980): Comp-CPE045

6.6.1.2 Identification of *state* of U-FREI based on simulation responses with different added noise levels

The values of parameters of FREI model have been selected from Table 6.4 for the purpose of simulation. Gaussian white noise with noise to signal ratio of 0%, 2%, 5% and 10% are added to the simulated output acceleration. These output responses have been used for identification of the state of FREI. A typical plot of identified displacements using simulated response corrupted with 10% noise level is shown in Fig. 6.31 to Fig. 6.33. RMSE of identified displacements for all the cases of noise levels have been represented in the form of bar chart as shown in Fig. 6.34 and values are furnished in Table 6.13.

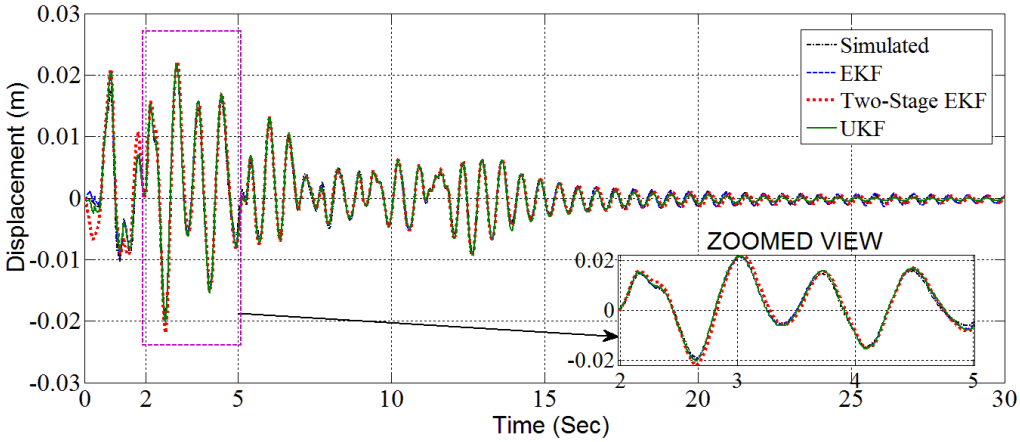

Fig. 6.31: Comparison of identified displacement time-history with experimentally measured displacement time-history using simulated response contaminated with 10% noise and under excitation El Centro (1940): Comp-180

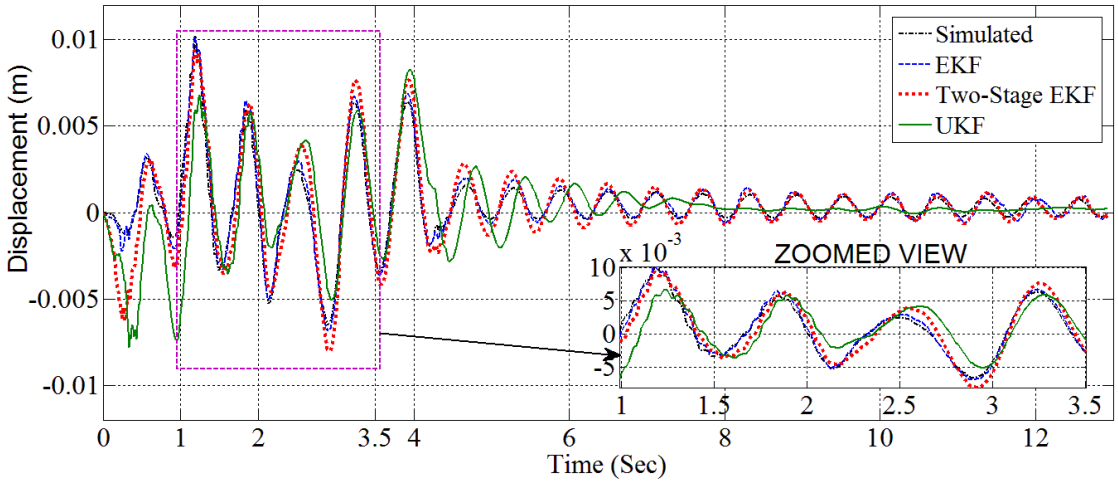

Fig. 6.32: Comparison of identified displacement time-history with experimentally measured displacement time-history using simulated response contaminated with 10% noise and under excitation Koyna (1967): Comp-Longitudinal

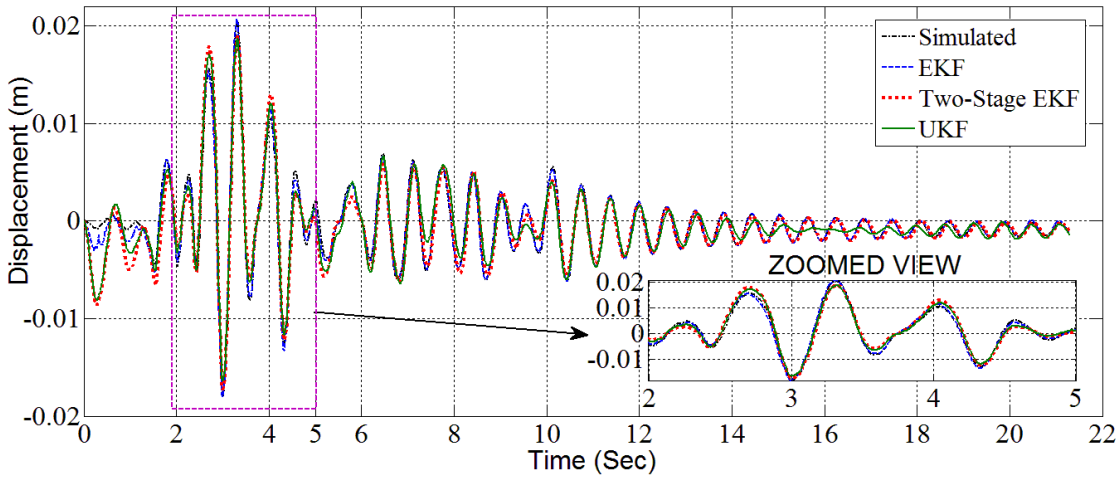

Fig. 6.33: Comparison of identified displacement time-history with experimentally measured displacement time-history using simulated response contaminated with 10% noise and under excitation Victoria (1980): Comp-CPE045

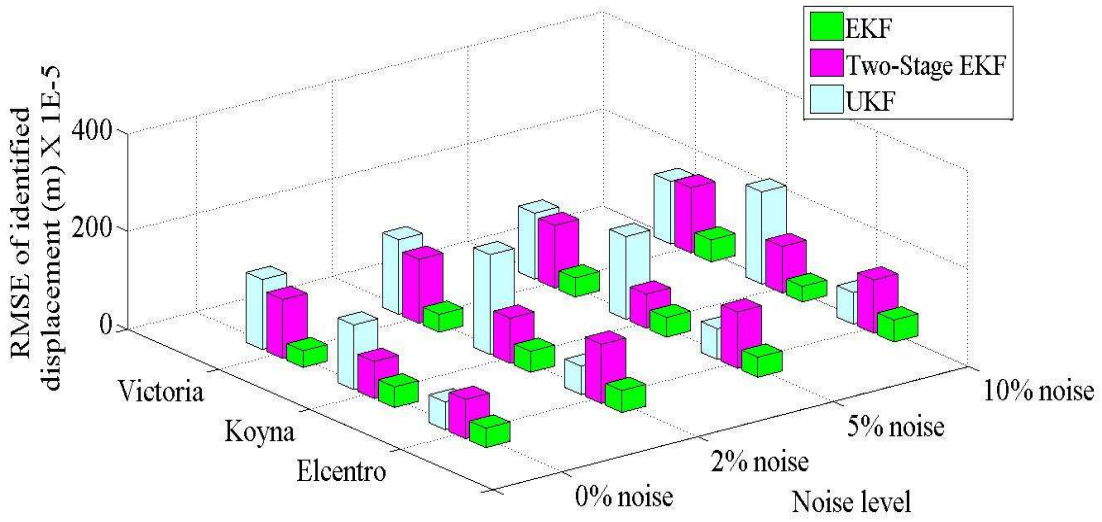

Fig. 6.34: 3D Bar Chart showing RMSE of identified displacement using simulated response contaminated with noise and under different considered earthquake excitation

A noise level of 2% was used by Yang *et al.* (2007) in identification of a three-storey Bouc-Wen hysteretic structure using adaptive EKF. A 10% noise level was used by Yang *et al.* (2006) in system identification using adaptive EKF. Therefore, the study using 0% to 10% noise level in the simulated output response is adopted in the present study.

Typical plots (Fig. 6.31 to Fig. 6.33) show that the identified displacement from different algorithms using 10% added noise to simulated response. The plots show that the identified

displacements agree well with simulated displacements even at high noise level. It is clear that all the algorithms perform reasonably well even if the response is noisy. However, merely looking at these plots one cannot compare the performance efficiency of these algorithms. Therefore, RMSE have been evaluated by considering simulated displacement as base value. A 3D bar chart (Fig. 6.34) shows the RMSE plots of identified displacement for all the considered noise levels and for different earthquakes. The values of RMSE have been furnished in Table 6.13. The performance of EKF is found to be best, while all the considered algorithms performed very well. The performances of these algorithms are also found to be consistent with increasing noise level.

Table 6.13: RMSE of identified displacement using simulated response contaminated with noise and under different considered earthquake excitation

Earthquake (as base excitation)	Noise level	EKF	Two-Stage EKF	UKF
		(x 1E-5)	(x 1E-5)	(x 1E-5)
El Centro (1940): Comp-180	0%	40	80	57
	2%	45	121	58
	5%	41	115	63
	10%	45	109	65
Koyna (1967): Comp-Longitudinal	0%	42	76	132
	2%	43	93	204
	5%	40	70	169
	10%	32	95	189
Victoria (1980): Comp-CPE045	0%	34	121	143
	2%	36	131	153
	5%	39	128	135
	10%	45	133	128

6.6.2 Results of identification of *parameters* of U-FREI

This sub-section is concerned with the identification of parameters of FREI. The identified parameters using each of the algorithms and for the cases of different base excitations are plotted in the form of bar charts. The errors in identified parameters are also represented in bar chart format. The identifications of parameters have been carried out for both experimental and simulated cases as described below. In chapter-5, identification of only parameters of the structure supported on the SREI isolator has been taken into consideration. In the present chapter, the focus is on the identification of parameters of model representing FREI supporting the model masonry building.

6.6.2.1 Identification of *parameters* of U-FREI based on Experimental responses

The results of identified parameters of FREI model for the cases of different ground motion is shown in Fig. 6.35.

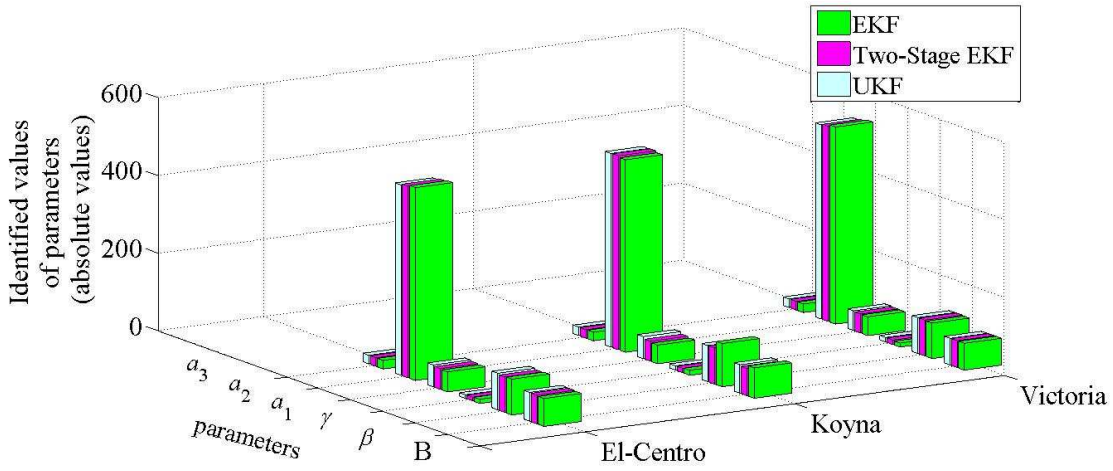

Fig. 6.35: 3D-Bar Chart showing identified parameter (absolute) values using experimental response and under different earthquake excitation

It is observed that identified values of parameters are closer to those of base values, but the identified result for any particular parameter using a particular algorithm fluctuates for different input ground motions. This is more clearly visible in the bar charts showing percentage of error in estimated parameters as shown in Fig. 6.36 and from values presented in Table 6.14 to Table 6.16.

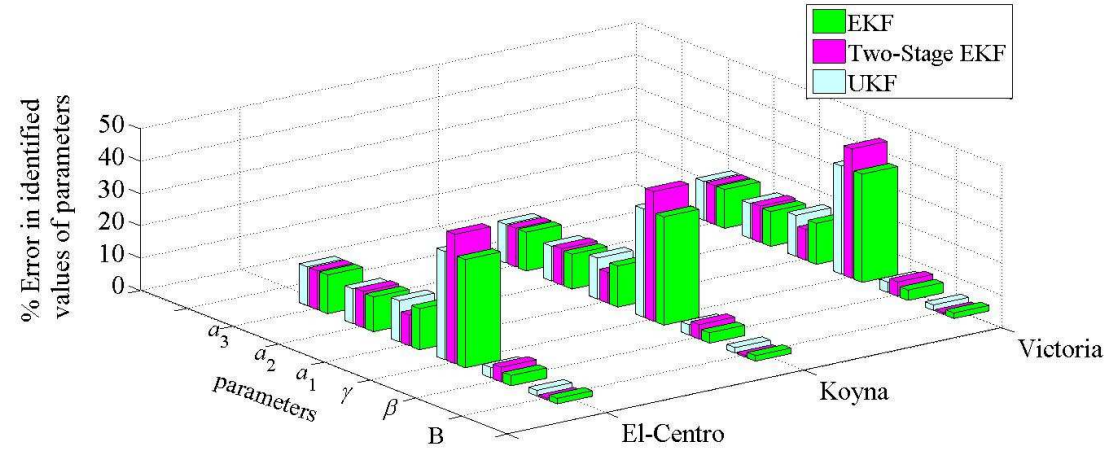

Fig. 6.36: 3D-Bar Chart showing percentage error in identified parameters using experimental response and under different earthquake excitation

Table 6.14: Identified parameter value, percentage error for identification using experimental data and under excitation El Centro (1940): Comp-180

Parameter	Base Value	Identified Value			% Error in Identified Value		
		EKF	Two-Stage EKF	UKF	EKF	Two-Stage EKF	UKF
B	73	71.75	73.40	74.27	-1.71	0.55	-1.71
β	95	91.95	90.74	93.95	-3.21	-4.49	-3.21
γ	16	10.64	9.59	9.17	-33.50	-40.06	-33.50
a_1	59	51.51	53.41	56.26	-12.70	-9.48	-12.70
a_2	-555	-495.26	-492.65	-489.26	-10.76	-11.23	-10.76
a_3	25	22.00	22.00	22.00	-12.00	-12.00	-12.00

Table 6.15: Identified parameter value, percentage error for identification using experimental data and under excitation Koyna (1967): Comp-Longitudinal

Parameter	Base Value	Identified Value			% Error in Identified Value		
		EKF	Two-Stage EKF	UKF	EKF	Two-Stage EKF	UKF
B	73	78.07	70.19	72.89	6.94	-3.85	6.94
β	95	110.84	93.36	92.69	16.68	-1.73	16.68
γ	16	12.84	11.33	11.03	-19.72	-29.20	-19.72
a_1	59	47.94	51.33	56.60	-18.75	-13.00	-18.75
a_2	-555	-494.42	-498.18	-497.51	-10.92	-10.24	-10.92
a_3	25	22.00	22.00	22.00	-12.00	-12.00	-12.00

To assess the performance of these algorithms from such a wide range of data set, PEI values have been evaluated for each algorithm and for different sets of considered ground motions and are represented in the form of bar chart as shown in Fig.6.37 and Table 6.17. The lesser the PEI value, the better is the performance. It is observed that UKF has the least PEI amongst all the three algorithms and for all the considered earthquakes. UKF is followed by Two-Stage EKF and EKF in terms of the performance in the identification of parameters.

Table 6.16: Identified parameter value, percentage error for identification using experimental data and under excitation Victoria (1980): Comp-CPE045

Parameter	Base Value	Identified Value			% Error in Identified Value		
		EKF	Two-Stage EKF	UKF	EKF	Two-Stage EKF	UKF
B	73	68.81	68.97	68.31	-5.73	-5.52	-5.73
β	95	91.10	92.33	92.23	-4.11	-2.81	-4.11
γ	16	10.09	11.43	11.59	-36.96	-28.59	-36.96
a_1	59	48.26	48.92	50.52	-18.20	-17.08	-18.20
a_2	-555	-506.21	-501.49	-498.71	-8.79	-9.64	-8.79
a_3	25	22.00	22.00	22.00	-12.00	-12.00	-12.00

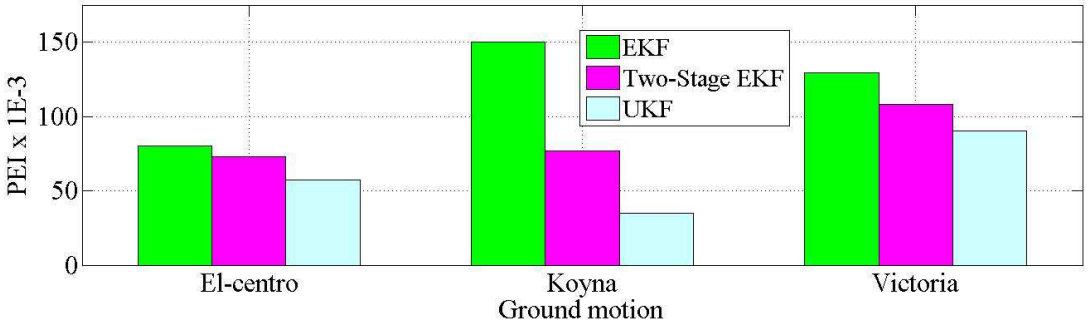

Fig.6.37: Bar Chart showing Percentage Error Index (PEI) of identified Parameters using Experimental data

Table 6.17: PEI values of algorithms using experimental data

Earthquake	Percentage Error Index (PEI)		
	EKF	Two-Stage EKF	UKF
	(x 1E-3)	(x 1E-3)	(x 1E-3)
El Centro (1940): Comp-180	80	73	57
Koyna (1967): Comp-Longitudinal	150	77	35
Victoria (1980): Comp-CPE045	130	108	91

In order to determine the performance of these algorithms for increase in noise level, a simulation based study has been conducted whose details are given in the following sub-section.

6.6.2.2 Identification of *parameters* of U-FREI based on simulation responses with different added noise levels

The variations of error in identifications of parameters due to different noise level and using different base excitation are shown in the form of 3D bar chart in Fig. 6.38 to Fig. 6.40. From these plots one cannot however assess the performance of these algorithms as identified parameters vary randomly across algorithms and base excitations. Hence, PEI of these algorithms have been calculated and shown in Table 6.18 to Table 6.20 for each of the considered earthquake and noise level. 3D plot is shown in Fig. 6.41 for collective representation of the PEI values for all the cases under consideration.

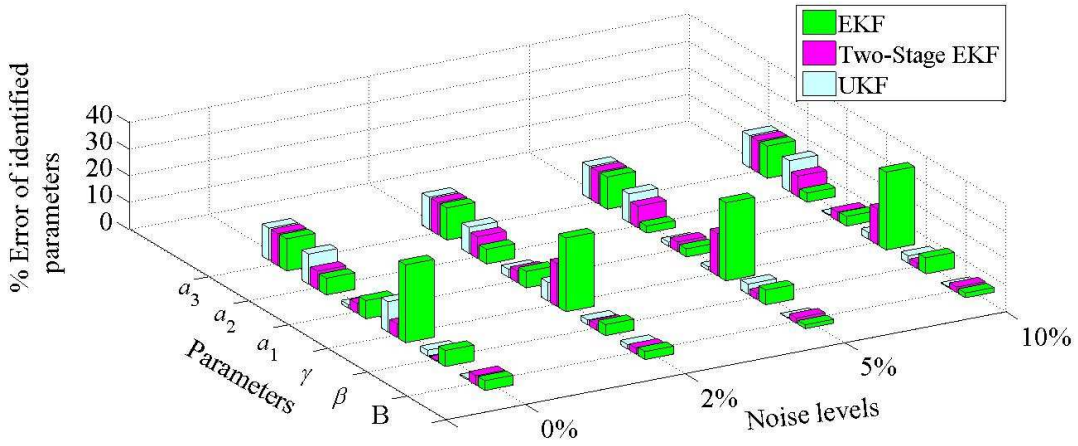

Fig. 6.38: 3D Bar Chart showing the percentage error in identified parameters using simulated response contaminated with different noise level and under excitation El Centro (1940): Comp-180)

Table 6.18: PEI values of algorithms using simulated response contaminated with different noise level and under excitation El Centro (1940): Comp-180

Noise level	EKF	Two-Stage EKF	UKF
	(x 1E-3)	(x 1E-3)	(x 1E-3)
0% Noise	44	11	14
2% Noise	35	18	12
5% Noise	28	16	11
10% Noise	30	13	11

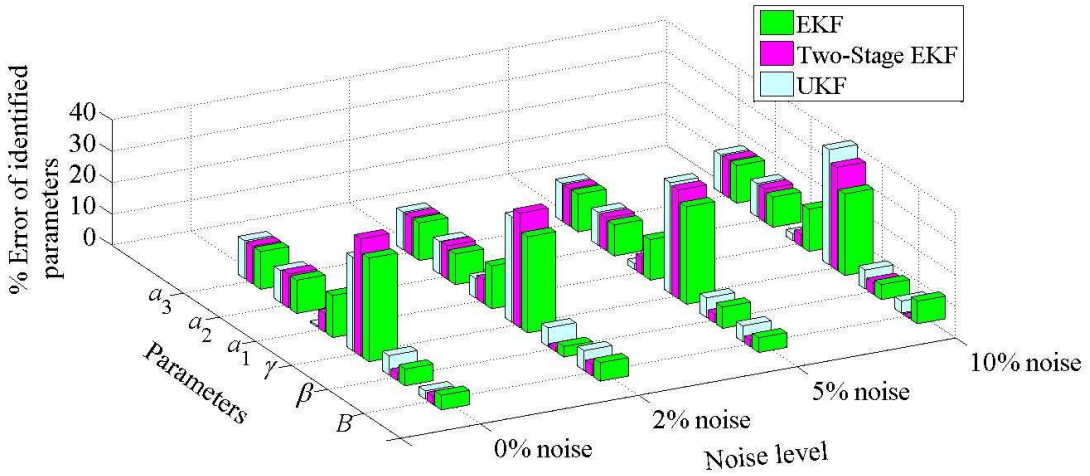

Fig. 6.39: 3D Bar Chart showing the percentage error in identified parameters using simulated response contaminated with different noise level and under excitation Koyna (1967): Comp-Longitudinal)

Table 6.19: PEI values of algorithms using simulated response contaminated with different noise level and under excitation Koyna (1967): Comp-Longitudinal

Noise level	EKF	Two-Stage EKF	UKF
	(x 1E-3)	(x 1E-3)	(x 1E-3)
0% Noise	89	52	33
2% Noise	87	57	58
5% Noise	85	45	47
10% Noise	84	38	47

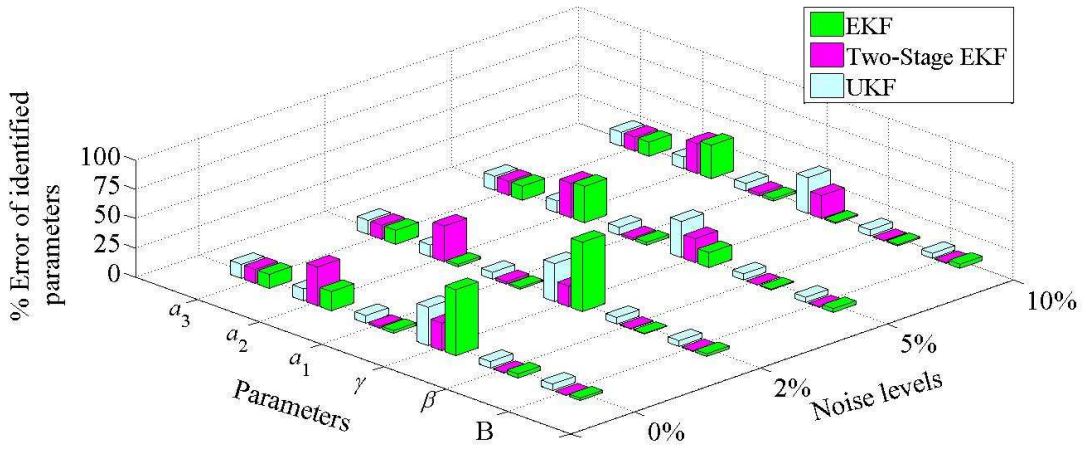

Fig. 6.40: 3D Bar Chart showing the percentage error identified parameters using simulated response contaminated with different noise level and under excitation Victoria (1980): Comp-CPE045

Table 6.20: PEI values of algorithms using simulated response contaminated with different noise level and under excitation Victoria (1980): Comp-CPE045

Noise level	EKF	Two-Stage EKF	UKF
	(x 1E-3)	(x 1E-3)	(x 1E-3)
0%	98	95	55
2%	86	78	50
5%	80	76	50
10%	65	60	48

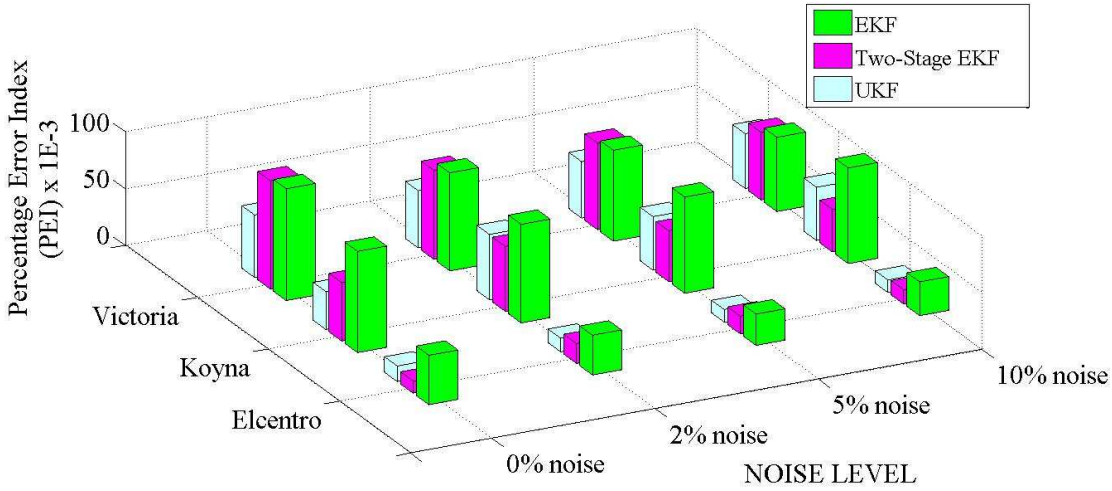

Fig. 6.41: 3D Bar Chart showing the PEI values of parameters for different noise level using simulated response and under different ground excitation

From the observed values of PEI, it is found that UKF is the best performer as it has the least value of PEI for most of the cases, the second best performer is the two-stage EKF followed by EKF.

6.6.3 Discussion on convergence issues in identification of *parameters* of U-FREI

Evaluating the performance of an algorithm by just using the PEI value, without taking due care of convergence of identified parameters may lead to erroneous assessment of PEI. Plots have been made for the variation of identified parameters with time.

6.6.3.1 Convergence of identified *parameters* based on experimental responses

The plot of identified parameter along with time will clearly indicate, although qualitatively, the convergence of the parameters to a specific values. Fluctuations of parameter values

towards the end of identification are not desirable as this would indicate uncertainty in the finally identified value. Fig. 6.42 shows typical plot of identified parameter *vs* time based on experimentally acquired responses under excitation El Centro earthquake.

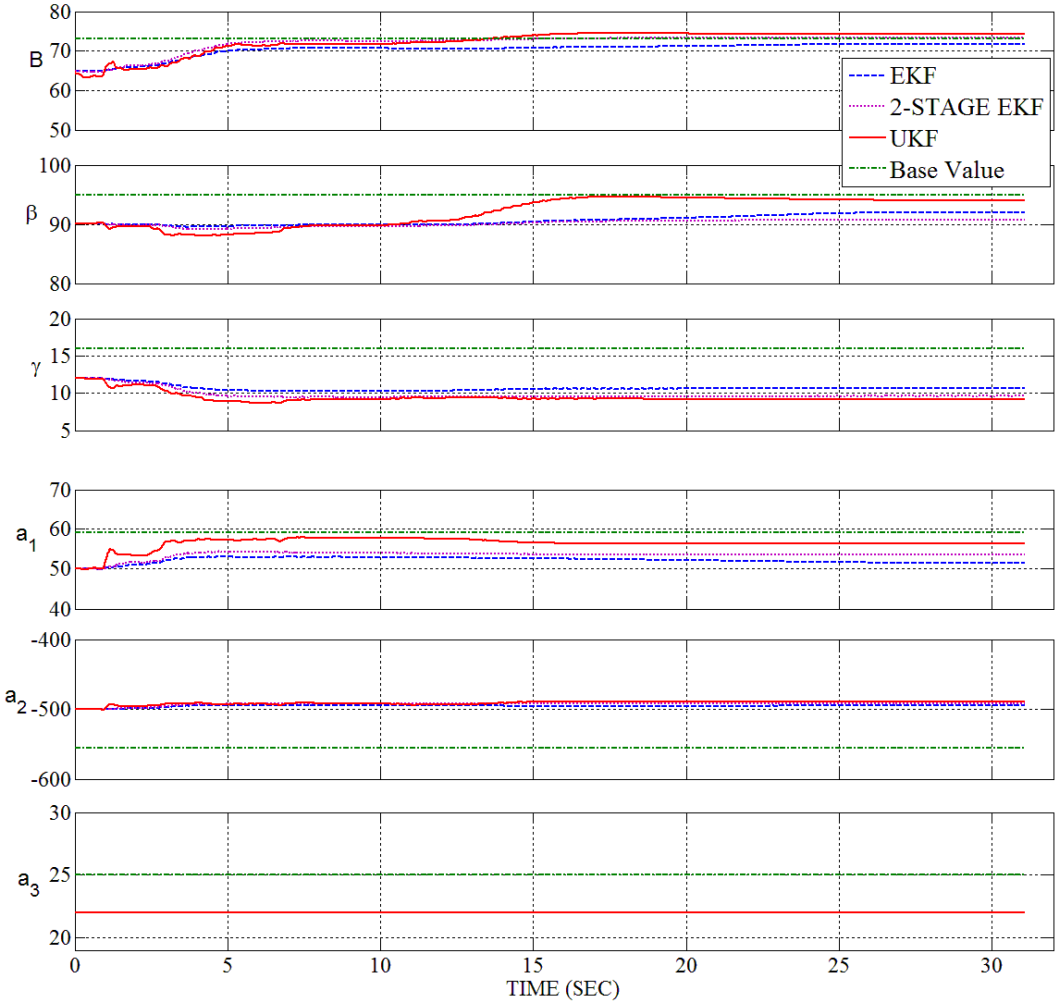

Fig. 6.42: Plot of identified parameters *vs* time based on experimental response and under excitation El Centro (1940): Comp-180

From Fig. 6.42 it is also observed that the identified parameters converge or have stable values towards the end of time history.

6.6.3.2 Convergence of identified *parameters* based on simulation responses

Fig.6.43 to Fig.6.46 show typical plot of identified parameter *vs* time based on response from numerically simulated model corrupted with 0% to 10% added Gaussian white noise under excitation El Centro.

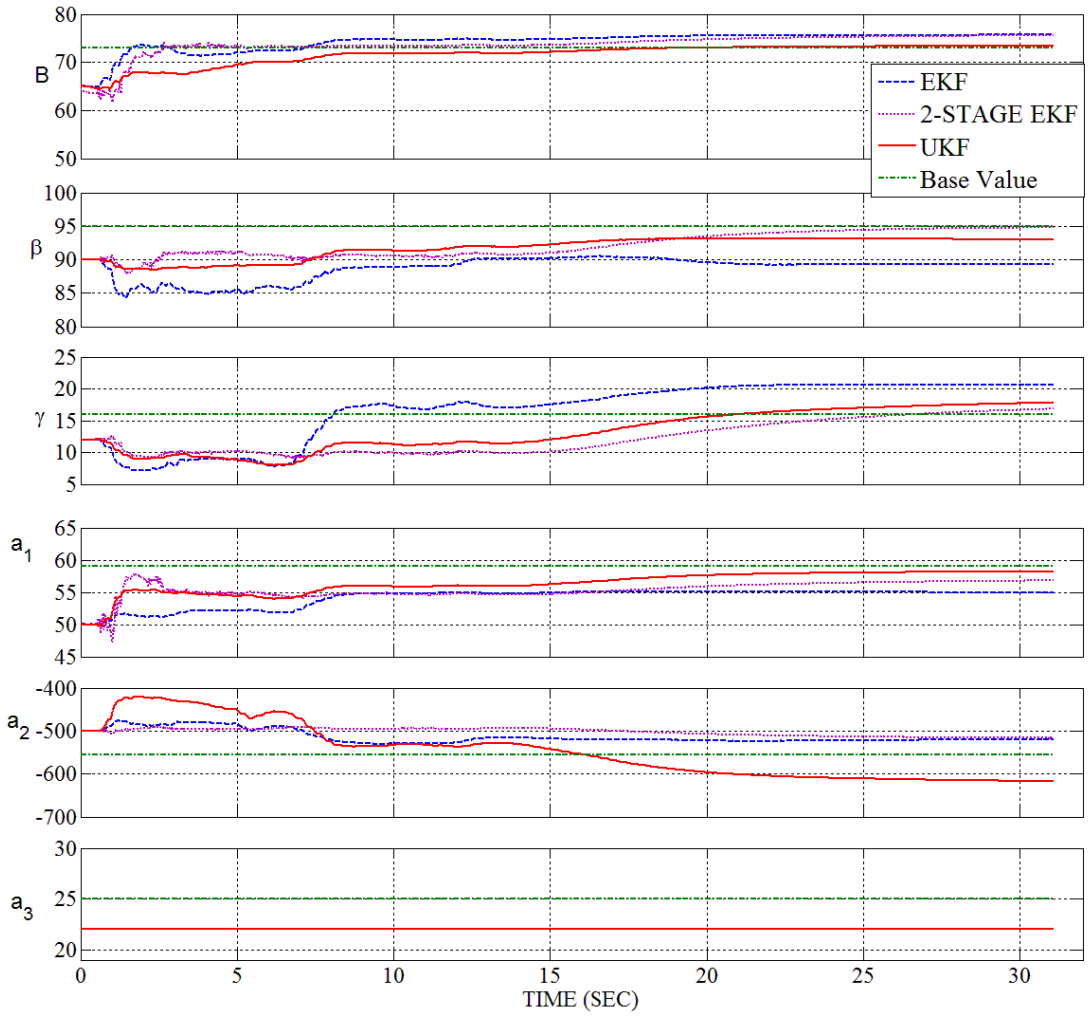

Fig.6.43: Plot of identified parameters *vs* time based on simulated response with no added noise and under excitation El Centro (1940): Comp-180

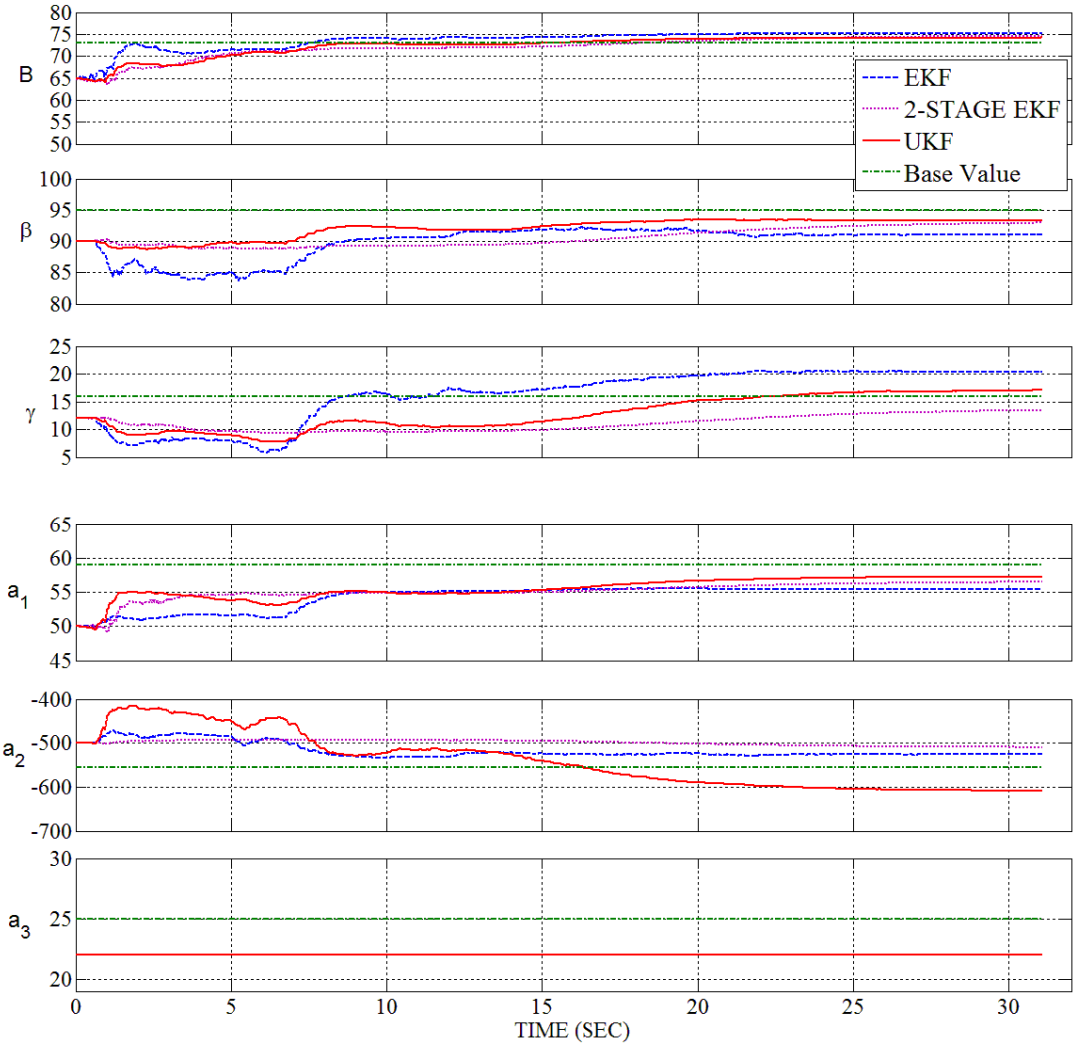

Fig.6.44: Plot of identified parameters *vs* time based on simulated response with 2% added noise and under excitation El Centro (1940): Comp-180

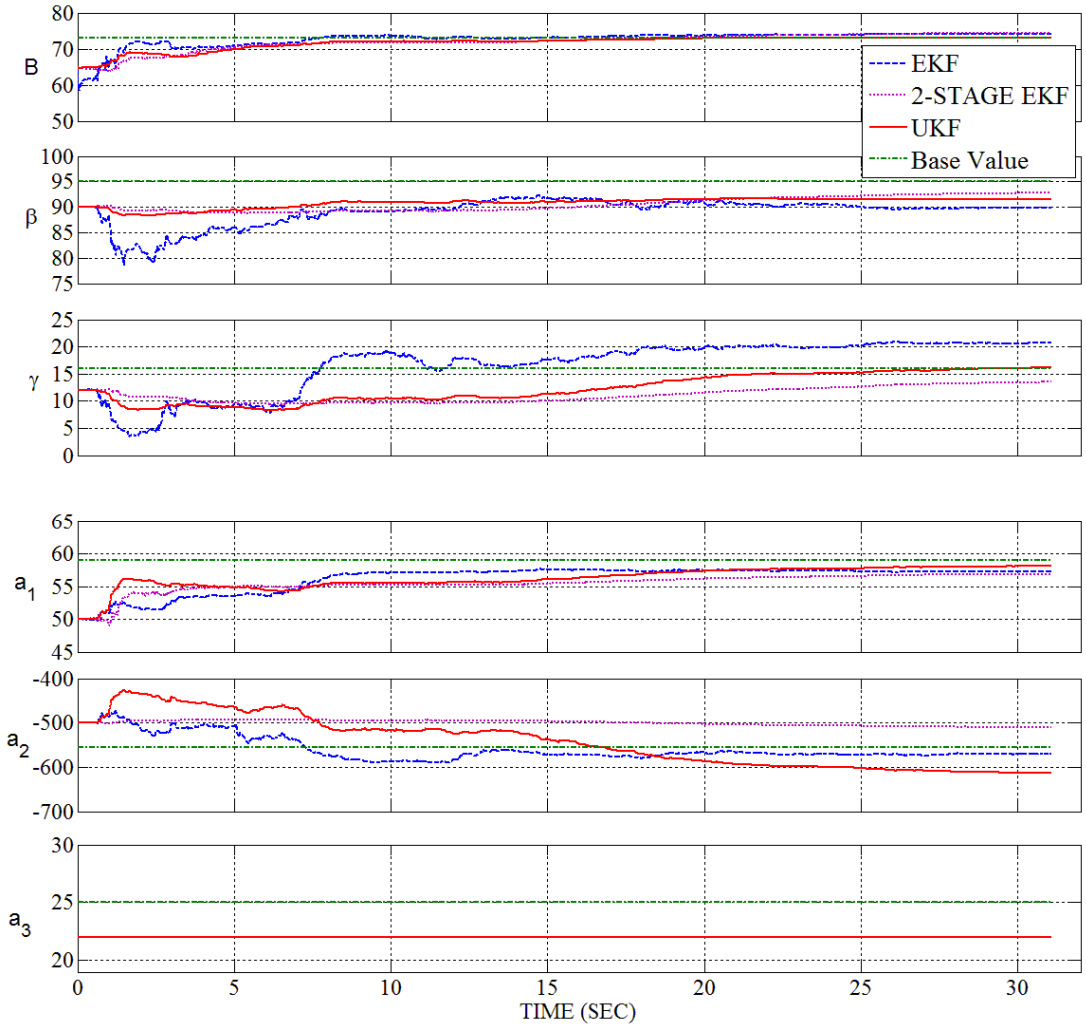

Fig.6.45: Plot of identified parameters *vs* time based on simulated response with 5% added noise and under excitation El Centro (1940): Comp-180

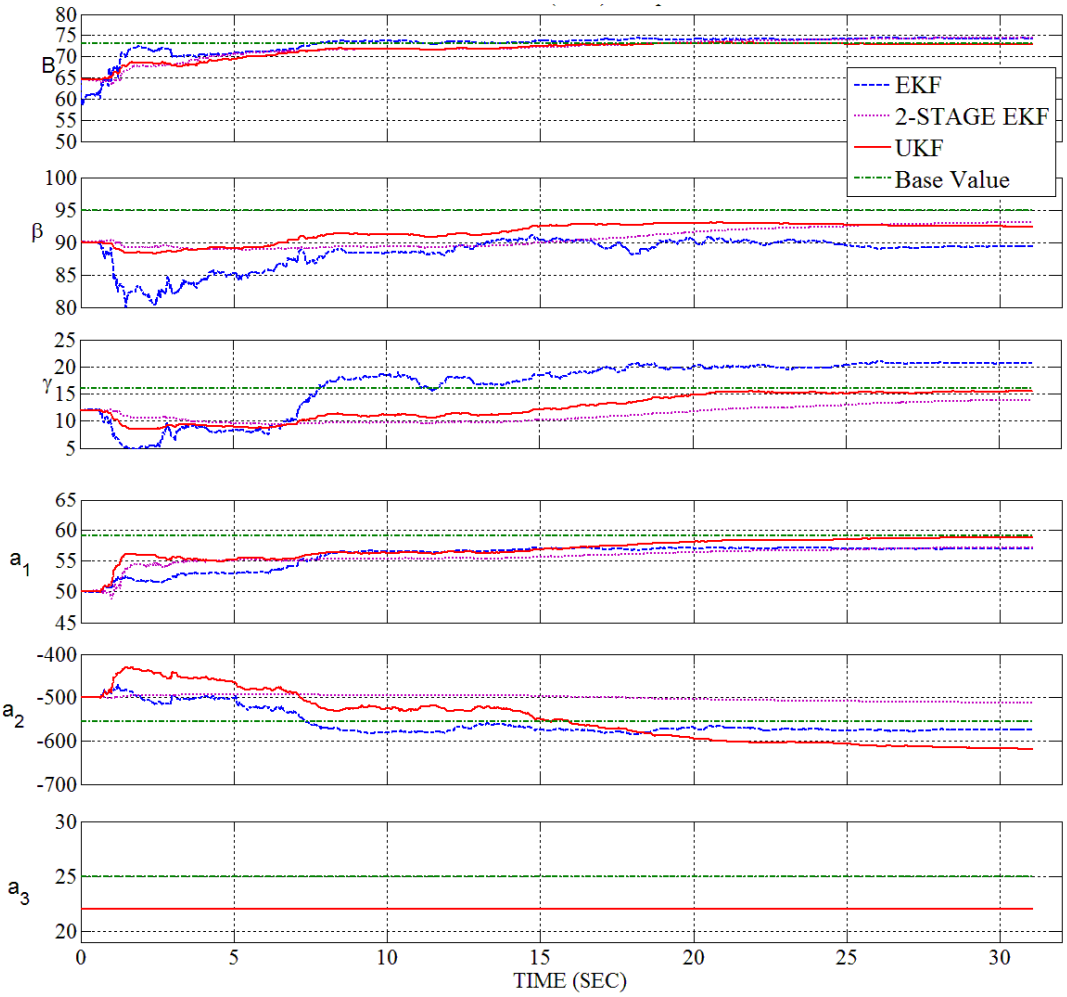

Fig.6.46: Plot of identified parameters *vs* time based on simulated response with 10% added noise and under excitation El Centro (1940): Comp-180

The results obtained from other earthquake motion have not been shown as these plots are only for confirmation of convergence requirement. From all the above figures (Fig.6.43 to Fig.6.46), it is observed that at the end of time-history, the parameters attain a stable value. The finally attained stable values of these parameters may differ from the base values, but the curves of the parameters are almost parallel to the time axis, indicating the attainment of stability.

6.7 Influence of varying measurement noise covariance *R* on the performance of the algorithms in identification of state and parameters of U-FREI

Investigation has been carried out to study the impact of noise covariance matrix, ***R*** on the performance of the algorithms. The influence of ***R*** on the identification of state and parameter has been studied separately as given below.

6.7.1 Influence of different values of *R* on state identification

The performance of these algorithms in identification of state is obtained by evaluating the RMSE of displacement. The RMSEs obtained by adopting different values of measurement noise covariance ***R***, using different level of simulated noisy response, are shown in Fig.6.47. It is observed that there is a gradual performance deterioration as the value of ***R*** is increased for both EKF and Two stage EKF. Whereas, the performance of UKF is erratic after some lower range of selected ***R***. The value of ***R*** which gives best performance by any algorithm is observed to be different for different earthquake excitations but a common similarity among them is that best performance is obtained using lower value of ***R*** in the range of 0.5 to 10. Further, it is observed that noise has no significant effect on the RMSE values.

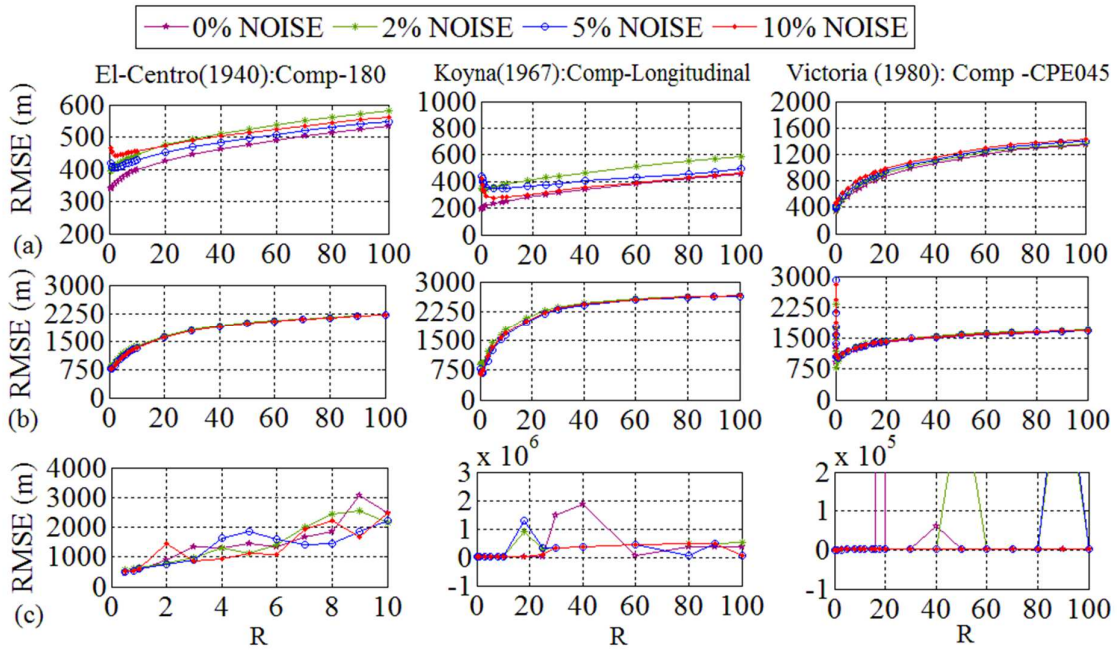

Fig.6.47: Comparison of RMSE of identified displacement, using (a) EKF, (b) Two-Stage EKF and (c) UKF algorithm; with different noise covariance, R and using different level of noisy response under different earthquake excitation

6.7.2 Influence of different values of *R* on parameter identification

The performance of these algorithms in identification of parameters is obtained by evaluating the PEI. The PEIs obtained by adopting different values of measurement noise covariance ***R***, using different level of simulated noisy response are shown in Fig.6.48. In PEI evaluation, it is also observed that there is a gradual performance deterioration as the value of ***R*** is increased for both EKF and Two stage EKF. Whereas, the performance of UKF is erratic after some lower range of selected ***R***. Further it is observed that at very low level of ***R***, there is a sharp increase in value of PEI in most of the cases. The best performance by any algorithms is obtained by selecting a lower value of ***R*** in the range of 0.5 to 10. Therefore, ***R*** needs to be tuned or adjusted to get best result. Further, it is observed that noise has no significant effect on the PEI values.

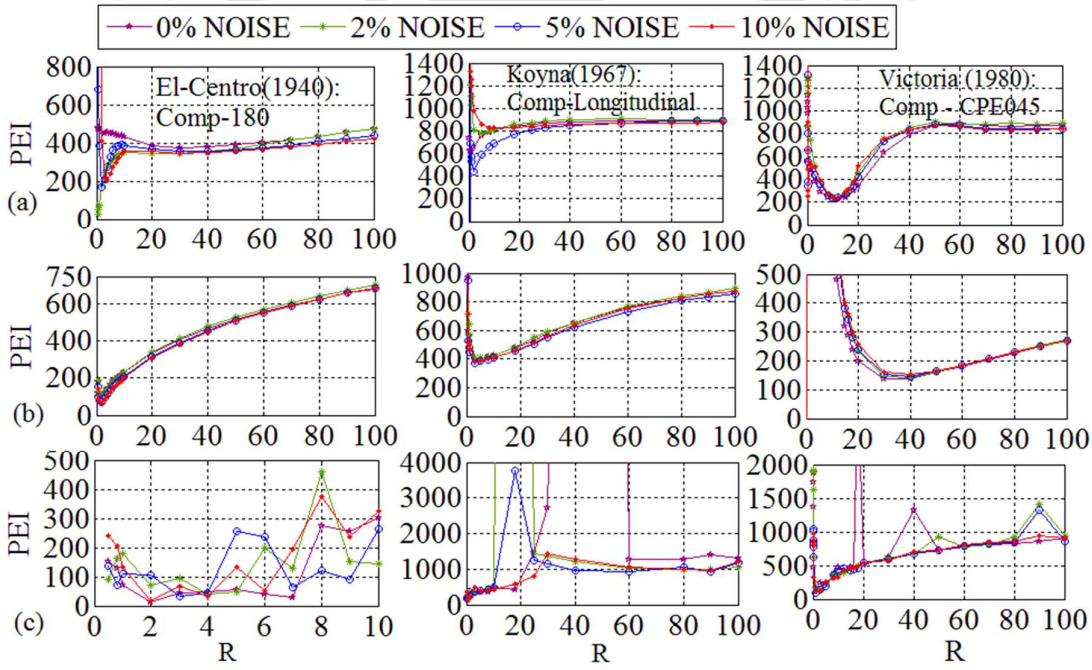

Fig.6.48: Comparison of PEI, evaluated using identified parameters obtained from (a) EKF, (b) Two-Stage EKF and (c) UKF algorithm; with different noise covariance, ***R*** and using different level of noisy response under different earthquake excitation

6.8 Concluding Remarks

A suitable mathematical model has been selected to represent the hysteretic behaviour of U-FREI. Three identification algorithms are considered in the present study namely, EKF, Two-Stage EKF and UKF. The considered identification algorithms require initial guess of parameters. The tuned set of parameters obtained using curve fitting the simulated hysteresis

loop with the experimental hysteresis loop provides a guess of initial parameter values for the identification algorithms. Comparative study on the performance of the considered algorithms towards identification of state and parameter of U-FREI has been carried out. The results obtained from the identification have been analysed with two different perspectives: 1) state identification and 2) parameter identification. The details are discussed in the following paragraphs. The details are discussed in the following paragraphs.

A comprehensive summary of the identification study using the considered algorithms for U-FREI is presented in Table 6.21. Rank 1 is defined for best performance, while Rank 3 is for least performance and rank 2 stands for intermediate performance level.

Table 6.21: Result of state and parameter identification for different considered problem types showing rank as per their performances

Sl. No.	Criteria	State / Parameter	Identification algorithms		
			EKF	Two-Stage EKF	UKF
1	Simulation study using different noise level.	state	1	2	3
		parameter	3	2	1
2	Study using experimental response data	state	2	3	1
		parameter	3	2	1

6.8.1 On State identification

The state refers to the system states comprising of displacement, velocity and the nonlinear Bouc-Wen hysteretic differential parameter *z*. In the state identification, only displacement identification has been considered for comparative study. RMSE of the identified displacement has been used to compare the performance of the considered algorithms. The simulated displacement acts as the reference displacement based on which RMSE has been evaluated in case of simulation based study. In case of study using experimentally acquired response, the measured displacement acts as the reference for evaluation of RMSE of identified displacement. The RMSE seems to be an effective tool to quantify the performance of the algorithms in identification of state (displacement) [Nortey (2012), Konotowski *et al.*(2016)].

The RMSE of the identified displacement is shown in form of a bar chart in Fig. 6.27 and tabulated in Table 6.12. It is observed that the performance of all these algorithms is quite comparable. However, amongst all the algorithms, the UKF is found to be performing better in most of the cases.

The performance of the algorithms for identification of the other two states such as velocity and nonlinear parameter z can be assessed by comparing the hysteresis loops, because the equation of hysteretic restoring force (Eq. (6.15)) involves both velocity and z term. The hysteresis loops shown in Fig. 6.28 to Fig. 6.30 shows quite a good match among these algorithms which evidently proves that the identified states has parity among themselves.

A simulation based study has also been carried out by superimposing the simulated response with 2%, 5% and 10% RMS Gaussian white noise. These noise contaminated responses have been utilised for comparative study of state and parameter identification using the considered algorithms. The main objective is to assess and compare the performance of the algorithms due to noise contaminated response.

It is observed that all the algorithms perform reasonably well even if the response is noisy. A 3D bar chart of Fig. 6.34 shows the RMSE plots of identified displacement for all considered noise level and for different earthquakes. The performance of EKF is found to be best, followed by Two-Stage EKF and then UKF. The performances of these algorithms are also found to be consistent with increasing noise level.

6.8.2 Parameter Identification

There are six different parameters of the model representing FREI, which have been identified by three different algorithms under three different earthquake excitations. Therefore, there is a variation of identified results leading to some complexity in arriving at a definite conclusion regarding the performance of any particular algorithm. To address this issue, PEI has been introduced. PEI is a single number or an index which has the ability to represent the performance of an algorithm according to sensitivity based ranking of the six different parameters of FREI. By comparing the PEI values evaluated for each algorithm for each of the problem cases, the performance of the algorithms can be ascertained with ease.

The values of PEI evaluated using the identified results based on experimental data, are presented in form of bar chart shown in Fig.6.37. It is observed that for all the experimental cases, UKF perform the best followed by Two-Stage EKF and then by EKF. 3D bar chart of PEI obtained from simulation based studies with different noise levels are shown in Fig. 6.41. It is observed that noise has little impact on the identification process. This is due to the fact that the algorithms can be tuned to cancel out the effect of noise. The influence of noisy response on the identification of the system can be reduced by tuning the diagonal elements of the measurement error covariance matrix [$\boldsymbol{R}$]. Since, the Kalman gain matrix is inversely

proportional to [***R***]; increase in [***R***] will decrease the gain, thus the filter will have the tendency to give less preference to the current measurements and more priority to the previous estimate. By proper tuning of **[*R*]**, the effect of noise can be eliminated to desired level. Therefore, it is observed that proper tuning of noise covariance matrix, **[*R*]** has a significant impact on the performance of the algorithms.

6.8.3 Convergence of identified parameters

As already discussed, it is highly desirable that the parameter values should converge towards the end of identification process, so than PEI can be applied successfully. From the observation of Fig.6.43 to Fig.6.46, it is quite apparent that all the parameters converge to a stable value toward the end of the identification process. It is well known fact that filters tuning is required to achieve result within desirable limit. Further, the initial guess of the parameters should be within close limits. A bad guess may lead to erroneous result and ultimately both state and parameter may diverge. The initial guess of state may be started with zero value for all the states, but starting the UKF with the initial value of the nonlinear hysteretic parameter $z=0$ may sometimes stop the algorithm after few cycle of run as it may produce instability in cholesky factorization used for finding the square root of matrix during determination of sigma points. The other tuning factor is the initial error covariance matrix, which is a diagonal matrix and needs to be set a priori. Each state and parameter is associated with their individual covariance, which are assembled in a single matrix named as covariance matrix. Covariance of a parameter can be thought of as the range or search area, within which the parameter value should lie. Setting a too large covariance may lead to instability of the algorithms. It is needless to mention that in the identification process, the mean and covariance gets updated in each cycle. It may so occur, that in order to achieve an optimum parameter values, the algorithm may extend the covariance of a parameter in wrong direction, thus leading to instability of the identification process. Therefore, the initial tuning of the covariance is required. To achieve a good convergence much effort is required to tune EKF than Two-Stage EKF and UKF. In EKF the state and parameter are assembled in a single vector named as extended state vector, which is a large vector, therefore difficult to handle at a time leading too much greater tuning. The two-Stage EKF is much better to handle the issues of convergence and much less tuning is required than its EKF counterpart. This is due to the fact that state and parameter are handled separately in two sequential steps. Tuning the UKF requires much less effort than EKF as it working principle is different wherein evaluations of Jacobians are not required.

Chapter 7

Summary and Conclusions

7.1 Summary

The present work is an effort towards evaluating the efficacy of different system identification algorithms like SNLSE-UI-UO, EKF, Two-Stage EKF and UKF in identifying state and parameters of different structural systems under seismic excitations. The structural systems considered in the study comprises of i) multi-storeyed fixed-base building, ii) multi-storeyed base-isolated building supported on conventional SREI isolators and iii) FREI supported structures. The study is based on data from both experimental and numerical simulation. The main areas of the present study are i) identification of state and parameters of multi-storeyed fixed-base building using simulated responses corrupted with varying amount of Gaussian white noise and comparing the performance of all the chosen algorithms, ii) identification using field recorded responses from existing fixed-base building with limited sensors and comparing the identification accuracy of different algorithms, iii) comparing the identification efficacy of all the considered algorithms for a simulated model of base isolated building supported on conventional SREI. The study is also extended to an existing base isolated building with limited sensor measurement data, iv) mathematical derivation to address the situation when sensor data is missing at isolator level, and its implementation in the system identification algorithms and comparing the efficacy of the considered algorithms towards identification of state and parameters of the system, v) applying a technique of artificial white noise of insignificant amplitude as an additional displacement measurement apart from original acceleration response measurement to tackle the issue of drift in identified displacement arising out due to very low amplitude responses from structure, causing numerical problem in identification algorithms, vi) selection of a suitable mathematical model for appropriate representation of FREI and comparing the model with that of experimentally obtained results, vii) comparing the performance of the algorithms in respect of identification of displacement with that of experimentally measured displacements, viii) to address the issue of difficulties faced in judging the performance of the algorithms due to variation of each of the identified parameters using different base excitation and different algorithms, a Performance Error Index (PEI) has been introduced, ix) parameter sensitivity has been determined by generating *spider diagram*, using which PEI has been evaluated, x) comparison of the parameter identification accuracy of the algorithms have been carried out using this PEI value.

Attempts have been made in formulating and modifying each of the algorithms to suit different structural systems under consideration. Formulations from available literatures have been arranged so that it becomes more presentable. Chapter-3 consists of basic derivations of each of the algorithms. However, implementation of the identification algorithms cannot be straight forwardly done just by using those formulations alone. Problem specific derivations have been shown in each of the chapters corresponding to different problem cases. This involves mainly the derivation of state-space formulation, generation of observation equation and derivation of Jacobians etc.

Both the state and parameters have been identified using the algorithms under consideration for each of the problem cases. Under state identification, only displacement identification has been considered for problem with fixed base building and base-isolated building systems. The other state like velocity is not taken into consideration as velocity can be easily obtained by differentiating displacement. Displacement identification is much more critical as displacement is identified by integrating acceleration twice, which sometime results in drifts and spikes. Therefore, if displacement is identified correctly, velocity identification can also be considered to be correct. The measure of identification accuracy of displacement has been carried out using Root Mean Square Estimate (RMSE) of the identified displacement. The reference value based on which RMSE is calculated is either the measured displacement, wherever available or simulated displacement in case of numerically simulated building. Lower value of RMSE indicates greater accuracy in identification.

The other state in case of isolators of base isolation building systems is the non-linear hysteretic differential parameter z of the standard or extended Bouc-Wen model for SREI or FREI respectively. The hysteresis loop is obtained from the plot of identified displacement versus identified hysteretic force. The parameter z is not a measurable quantity, but it shows it presence in the form of hysteresis force. The experimental hysteresis force is obtained from laboratory force-displacement test. The performance of the algorithms with respect to identification of this hidden state z is compared with the experimental hysteresis loop or simulated hysteresis loop as the case may be.

The accuracy of the parameter identification has been evaluated using the identified parameters under the condition that the identified parameter converges to a stable value. In the case of base-isolated structure supported on FREI, the extended Bouc-Wen model that has been used to model the FREI comprises of six different parameters. The base isolated system

was excited using three different recorded earthquake motions on a shake table. On identification of these six parameters using the considered algorithms, the values of the identified parameters are found to be different for different algorithms and also there are variations of the identified parameters for different considered excitation used in shake table based test. Therefore, it becomes difficult to assess the performance of the algorithms for different cases. To address this issue, the identification efficiency of these algorithms has been judged with respect to (PEI) value. The PEI has been introduced here as a measure of performance efficiency of the algorithms for parameter identification. The PEI value has been evaluated using spider diagram, which is obtained from sensitivity.

7.2 Conclusions

The present work is undertaken to study and compare the performances of different identification techniques applied to different structural types e.g. fixed base building, BI building supported on SREI and FREI. Both experimental responses and simulated responses have been utilized to evaluate the performance of algorithms. Based on the present study, following major conclusions are drawn.

Based on considered algorithms

1) Kalman Filter based algorithms such as EKF, Two-Stage EKF as well as UKF can handle noise contaminated response data quite well. In case of LSE based algorithms such as SNLSE-UI-UO, low frequency component in the response is required to be removed prior to its use in the identification algorithm.
2) Kalman Filter based algorithms can work in an environment of multiple missing sensor. The performance degrades with increasing number of missing sensor. Performance of LSE based algorithms such as SNLSE-UI-UO drastically deteriorates with more than one number of missing sensor.

Based on fixed-base building

3) For state identification with availability of all sensor data, EKF, Two-Stage EKF as well as UKF are found to be suitable, even when that data is contaminated with high level of noise. The performance of SNLSE-UI-UO algorithm is far more inferior than all the considered Kalman Filter based algorithms.
4) For parameter identification with noisy response and with the availability of all sensor measurements, the performance of UKF is consistent for data with all the noise levels. However, the performance of EKF deteriorates with increasing noise level.

5) For state identification with large number of missing sensors, the performance of Two-Stage EKF is found to be performing the best, followed by UKF and finally by EKF algorithm.
6) For parameter identification with large number of missing sensors, Two-Stage EKF is found to be performing the best, followed by UKF and finally by EKF algorithm.

Based on base-isolated building supported on SREI

7) The state identification of SREI supported BI building under very low intensity base excitation shows a drift in identified displacement using the KF based algorithms. Drift in identified displacement can be corrected by introducing additional displacement measurements in the form of artificial white noise of very insignificant amplitude.
8) The state and parameter identification can be performed using all the considered KF based algorithms with an appreciable good degree of accuracy even in cases where sensor data is not available at floor level located just above the isolator.
9) In case of state identification of SREI supported BI building with missing sensor at different floor level, the performance of EKF is found to be the best followed by UKF and then Two-Stage EKF.
10) In case of parameter identification of SREI supported BI building with missing sensor at different floor level, the performance of Two-Stage EKF is found to be the best and the performance of UKF and EKF are closer to each other.

Based on U-FREI of the sample base-isolated test model

11) The Extended Bouc-Wen model is found to be a suitable for modelling U-FREI up to roll-over deformation till the initiation of hardening effect and can be recommended for use in further analysis pertaining to U-FREI of the sample BI test model.
12) In case of state identification of U-FREI, the EKF is a better choice than the Two-Stage EKF and UKF algorithms.
13) The Performance Error Index is a useful tool to measure the efficiency of identification algorithm.
14) For parameter estimation of U-FREI, UKF is a better option even in the case of noise corrupted response of the system and therefore UKF is recommended for parameter identification.

15) Selection of measurement noise covariance plays an important role in performance of the algorithms. The measurement noise covariance matrix should be tuned to get the best performance by an algorithm.
16) Noise corrupted response has no such significant impact on the performance of different variants of KF based algorithms.

7.3 Major contribution of the thesis

The present work is a holistic approach towards comparative study on different types of building structures with fixed base, base-isolated using SREI and FREI, using different existing system identification algorithms. However, while implementing these algorithms on these considered building structures, several problems were encountered. Such problems were overcome by adopting different strategies and are indentified as major contributions of the thesis to the existing literature as summarised below.

1) Resolving the problem of drift in identified displacement, which was observed during implementing the considered algorithms on SREI supported base-isolated building excited by very low amplitude excitation. The issue was solved using Gaussian white noise of insignificant amplitude as additional displacement data in these algorithms.
2) Available formulation found in existing literature towards system identification using these algorithms cannot function with non-availibility of recorded response at the floor level just on top of isolator. In this thesis, the existing formulation has been modified to addresse the above stated problem.
3) Effort has been carried out towards state and parameter identification of FREI supporting a masonry test model. A proper mathematical model has been selected to simulate FREI. The mathematical model has many parameters. The identified parameters vary differently under different excitation. PEI has been introduced as a performance index to assess the performance of these algorithms in identifying the parameters of the model. FREI is comparatively new in the field of base-isolation and system identification study on FREI is a novel approach undertaken in this thesis work.

7.4 Scope for Future Work

Areas on which the present study can be extended through additional research include the following:

1) To study the optimum number of sensor requirement for tall structures, both for fixed base and base isolated systems.
2) To extend the study to torsionally coupled or unsymmetrical buildings.
3) To study the performance of these algorithms in B-FREI.
4) To study the performance of these algorithms for U-FREI isolated system undergoing very large deformation. In such case, the modelling of FREI need higher order terms of Bouc-Wen extended model.

REFERENCES

Bhaiya V, Bharti SD, Shrimali MK, Datta TK. Effect of noises on the active optimal control on partially observed structures for white random ground motion. *Noise control Engineering Journal.* 2016;64(6):789-799. https://doi.org/10.3397/1/376420.

Bisht Saurabh S. and Singh Mahendra P. (2014), "An adaptive unscented Kalman filter for tracking sudden stiffness changes", *Mechanical Systems and Signal Processing*, Vol. 49, pp. 181–195.

Bisht Saurabh S. and Singh Mahendra P. (2018), "Adaptive constrained unscented Kalman filtering for real time nonlinear structural system identification", *Structural Control Health Monitoring.*, Vol. 25: e2084.

Borsakia Arun Ch, Dutta Anjan and Deb S.K. (2010), "System Identification of multistoreyed non-standard shear building using parametric state space modeling", *Structural control and health monitoring*, Vol-18, pp.471-480. DOI: 10.1002/stc.385.

Brown Robert Grover and Hwang Patrick Y.C., "Introduction to Random Signals and applied Kalman Filtering, 4th Edition", *John Wiley & Sons, Inc.* ISBN 978-0-470-60969-9 (hardback)

Chatzi Eleni N. and Smyth Andrew W. (2009), "The unscented Kalman filter and particle filter methods for nonlinear structural system identification with non-collocated heterogeneous sensing", *Structural control and health monitoring*, Vol. 16, pp. 99-123. DOI: 10.1002/stc.290.

Chatzi Eleni N. and Fuggini Clemente (2015), "Online correction of drift in structural identification using artificial white noise observations and an unscented Kalman Filter", *Smart Structures and Systems*, Vol. 16, No. 2, pp. 295-328. DOI: http://dx.doi.org/10.12989/sss.2015. 16.2.295.

Chen Y. and Ahmadi G. (1992), "Wind effects on base-isolated structures", *Journal of Engineering Mechanics*, Vol. 118, pp: 1708-1727.

Chen J. and Li J. (2004), "Simultaneous identification of structural parameters and input time history from output-only measurements", *Computational Mechanics*, Vol-33, pp. 365-374.

Darryl Morrell (1997), "Extended Kalman Filter Lecture Notes", EEE 581-Spring 1997. < https://www.cs.cmu.edu/~motionplanning/papers/sbp_papers/kalman/ekf_lecture_notes.pdf>

Das A., Dutta A. and Deb S.K. (2014), "Performance of fiber-reinforced elastomeric base isolators under cyclic excitation", *Structural Control and Health Monitoring*, DOI: 10.1002/stc.1668.

Das A., Dutta A. and Deb S.K. (2015), "Seismic response control of low-rise buildings using fiber-reinforced elastomeric isolator", *PhD-Thesis*, IIT Guwahati.

Das A., Deb S.K. and Dutta A. (2016a), "Shake table testing of un-reinforced brick masonry building test model isolated by U-FREI", *Earthquake Engineering and Structural Dynamics*, Vol. 45, pp. 253-272, DOI: 10.1002/eqe.2626.

Das A., Deb S.K. and Dutta A. (2016b), "Comparison of numerical and experimental seismic responses of FREI supported on un-reinforced brick masonry model building", *Journal of Earthquake Engineering*, DOI: 10.1080/13632469.2016.1140098.

Engelen Neil C. Van, Konstantinidis Dimitrios and Tait Michael J. (2016), "Structural and nonstructural performance of a seismically isolated building using stable unbonded fiber-reinforced elastomeric isolators", *Earthquake engineering and structural dynamics*, Vol. 45, pp. 421-439. DOI: 10.1002/eqe.2665.

Gelb Arthur (2001), "Applied Optimal Estimation", *MIT press*. ISBN 0-262-20027-9 (hardback) Haykin Simon (2014), "Adaptive Filter Theory", *5th Edition, Pearson Education Limited*. ISBN 13: 978-0-273-76408-3.

Hong-de Dai, Shao-wu Dai, Yuan-cai Cong nad Guang-bin Wu (Nov-2012), "Performance Comparison of EKF/UKF/CKF for the Tracking of Ballistic Target", *Telkomnika*, Vol. 10, No. 7, pp. 1537–1542.

Hoshiya Masaru. and Saito Etsuro (1984), "Structural Identification by Extended Kalman", *Journal of Engineering Mechanics*, pp. 1757-1770.

Hoshiya M. and Sutoh A. (1992), "Extended Kalman Filter-Weighted local iteration method for dynamic structural identification", *Earthquake Engineering, Tenth World Conference, Balkema, Rotterdam*, pp. 3715-3720.

Julier Simon. J. and Uhlmann J. K. (1997a), "A new extension of the Kalman filter to nonlinear systems," *in Proc. AeroSense: 11th Int. Symp.Aerospace/Defense Sensing, Simulation and Controls*, pp.182–193.

Julier Simon J. and Uhlmann Jeffrey K. (1997b), "A consistent, Debaised Method for Converting Between Polar and Cartesian Coordinate System," *In the Proceedings of Aerosense: The 11th International Symposium on Aerospace/Defence sensing, simulation and controls, Orlando, Florida, USA. Acquisition, Tracking and Pointing XI*. Vol. 3086, pp. 110-121, SPIE.

Julier Simon J. (1998), "A Skewed Approach to Filtering," *In the Proceedings of Aerosense: The 12th International Symposium on Aerospace/Defence sensing, simulation and controls, Orlando, Florida, USA. Signal and Data Processing of small Targets*. Vol. 3373, pp. 54-65, SPIE.

Julier Simon. J. and Uhlmann J. K. (2002a), "The scaled unscented transformation," *in Proc. Amer. Control Conf.*, pp. 4555–4559.

Julier Simon. J. and Uhlmann J. K. (2002b), "Reduced sigma point filters for the propagation of means and covariances through nonlinear transformations," *in Proc. Amer. Control Conf.*, pp. *887–892*.

Konatowski Stanislaw, Kaniewski Piotr, Matuszewski Jan (2016), "Comparison of Estimation Accuracy of EKF, UKF and PF Filters", *Annual of Navigation*, Vol. 23, pp. 69–86. DOI: 10.1515/aon-2016-0005.

Lacey A.J. and Thacker N.A. (1998), "Tutorial: Kalman Filter", Imaging science and Biomedical Engineering Division, Medical School, University of Manchester, Stopford Building, Oxford Road, Manchester, M13 9PT.

< http://citeseerx.ist.psu.edu/viewdoc/download?doi=10.1.1.408.5594&rep=rep1&type=pdf>

Lei Y and Jiang Y.Q. (2011), "A Two-Stage Kalman Estimation Approach for the Identification of Nonlinear Structural Parameters", *The Twelfth East Asia-Pacific Conference on Structural Engineering and Construction, Procedia Engineering*, Vol-14, pp. 3088-3094.

Lei Ying, Wu Yan and Li Tao (2012), "An adaptive extended kalman filter for structural damage identification II: unknown inputs", *International Journal of Nonlinear Mechanics*, Vol-47, pp. 1141-1146.

Lei Ying, Chen Feng and Zhou Huan (2015), “An algorithm based on two-step Kalman filter for intelligent structural damage detection”, *Structural control and health monitoring*, Vol-22, pp. 694-706.

Lin Jeng-Wen, Betti Raimondo, Smyth Andrew W. and Longman Richard W. (2001), "On-line identification of non-linear hysteretic structural systems using variable trace approach", *Earthquake Engineering and Structural Dynamics*, Vol-30, pp.1279-1303. DOI: 10.1002/eqe.63

Love, J. S., Tait, M. J., and Toopchi-Nezhad, H. (2011), “A hybrid structural control system using a tuned liquid damper to reduce the wind induced motion of a base isolated structure”, *Engineering Structures*, Vol. 33, pp: 738-746.

Manzoori Ali and Toopchi-Nezhad Hamid (2017), “Application of an Extended Bouc-Wen Model in Seismic Response Prediction of Unbonded Fibre-Reinforced Isolators”, *Journal of Earthquake Engineering*, Vol. 21, pp: 87-104.

Meilian Wu and Andrew W. Smyth (2007), “Application of the unscented Kalman filter for real-time nonlinear structural system identification”, *Structural Control and Health Monitoring*, Vol. 14, pp. 971–990.

Merwe Rudolph vander and Wan Eric A. (2001), “The square-root unscented Kalman filter for state and parameter-estimation,” *in Proc. IEEE Int. Conf. Acoustics, Speech, and Signal Processing (ICASSP)*, vol. 6, pp. 3461–3464.

Naeim, F and Kelly, J.M. (1999) “Design of Seismic Isolated Structures,” *John Willey, New York.*

Nath R. J., Deb S. K., and Dutta A. (2013) “Base isolated RC building – performance evaluation and numerical model updating using recorded earthquake response,” *Earthquakes and Structures,* Vol. 4, No. 5, pp: 471–487. *http://dx.doi.org/10.12989/eas.2013.4.5.471*

Nezhad Toopchi, H., Tait, M. J., and Drysdale, R. G. (2008a) “Testing and modeling of square carbon fiber reinforced elastomeric seismic isolators,” *Structural Control and Health Monitoring,* Vol. 15(6), pp: 876–900.

Ngo Thuyet V., Deb S.K. and Dutta A. (2017a), "Effect of horizontal loading direction on performance of prototype square unbounded fibre reinforced elastomeric isolator ", *Structural control and health monitoring*, DOI:10.1002/stc.2112.

Ngo Thuyet V., Deb S.K. and Dutta A. (2018), " Mitigation of Seismic Vulnerability of Prototype Low-Rise Masonry Building Using U-FREIs ", *ASCE Journal of performance* of *constructed facilities*, DOI: 10.1061/(ASCE)CF.1943-5509.0001136.

Ngo Thuyet V., Dutta A and Deb S.K. (2017b), "Evaluation of horizontal stiffness of fibre-reinforced elastomeric isolators.", *Earthquake engineering and structural dynamics*, DOI: 10.1002/eqe.2879.

Niel C., Van Engelen, Dimitrios Konstantinidis, and Michael J. Tait (2016), "Structural and nonstructural performance of a seismically isolated building using stable unbonded fiber-reinforced elastomeric isolators", *Journal of Earthquake Engineering and Structural Dynamics*, Vol-45, pp.421-439. DOI: 10.1002/eqe.2665

Nortey Andrew Yeboah (2012), "State and Parameter Estimation Using Unscented Kalman Filter", *Master of Philosophy Thesis,* Kwame Nkrumah University of Science and Technology.

Pan Tso-Chien and Yang Guichang (1996), "Nonlinear analysis of base-isolated MDOF structures", *Eleventh conference on earthquake engineering, paper no. 1534*, ISBN: 0 08 042822 3.

Sayed Ali H. and Kailath Thomas (2000), "Recurssive Least-Squares Adaptive Filters", *CRC Press Ltd*, <http://www.engnetbase.com>.

Sireteanu, T., Giuclea, M. and Mitu, A.M. (2010), "Identification of an extended Bouc-Wen model with application to seismic protection through hysteretic devices", *Journal of Engineering Mechanics*, Vol. 45, pp: 431-441.

Tan R.Y. and Chen C.C. (1988), "Structural identification of a nonlinear MDOF system by extended Kalman Filter", *Proceedings of Ninth World Conference on Earthquake Engineering, Tokyo-Kyoto, Japan*, Vol-V, pp. 325-330.

Tait MJ, Toopchi-Nezhad H, Drysdale RG (2008). "Influence of end geometry on fiber reinforced elastomeric isolator bearings". *Proceedings of the 14th World Conference on Earthquake Engineering, October 12-17, Beijing*.

Tenne D. and Singh T. (2003), "The higher order unscented filter," *in Proc. Amer. Control Conf.*, vol. 3, pp. 2441–2446.

Toopchi-Nezhad, H., Tait, M. J., and Drysdale, R. G. (2008b) "A novel elastomeric base isolation system for seismic mitigation of low-rise buildings", *Proc., 14th World Conference on Earthquake Engineering (14 WCEE), Beijing, China.*

Toopchi-Nezhad, H., Tait, M. J., and Drysdale, R. G. (2009). "Shake table study on an ordinary lowrise building seismically isolated with SU-FREIs (stable unbounded fiber reinforced elastomeric isolators)", *Earthquake Engineering & Structural Dynamics* Vol. 38(11), pp: 1335–1357.

Van Engelen NC, Konstantinidis D, Tait MJ (2016). 'Structural and nonstructural performance of a seismically isolated building using stable unbonded fiber reinforced elastomeric isolators", *Earthquake Engineering & Structural Dynamics*, Vol. 45(3), pp: 421-439.

Yang Jann N. and Lin Silian (2004), "On-line identification of non-linear hysteretic structures using an adaptive tracking technique", *International Journal of Non-Linear Mechanics*, Vol. 39, pp. 1481-1491.

Yang Jann N. and Lin Silian (2005), "Identification of Parametric Variations of Structures Based on Least Squares Estimation and Adaptive Tracking Technique", *Journal of Engineering Mechanics*, Vol. 131, pp.290-298.

Yang Jann N, Huang Hongwei and Lin Silian (2006), "Sequential non-linear least-square estimation for damage identification of structures", *International Journal of Non-Linear Mechanics*, Vol. 41, pp. 124-140.

Yang Jann N. and Huang Hongwei (2006), "Damage tracking of Base-Isolated Building using Sequential Nonlinear LSE with Unknown Inputs and Outputs", *Smart Structures and Materials*, Vol. 6174, pp.1-11.

Yang Jann N., Lin Silian, Huang Hongwei and Zhou Li(2006a), "An adaptive extended Kalman filter for structural damage identification", *Structural control and health monitoring*, Vol-13, pp. 849-867.

Yang Jann N and Huang Hongwei (2007), "Sequential non-linear least-square estimation for damage identification of structures with unknown inputs and unknown outputs", *International Journal of Non-Linear Mechanics*, Vol. 42, pp. 789-801.

Yang Jann N., Pan S. and Huang H. (2007a), "An adaptive extended kalman filter for structural damage identification II: unknown inputs", *Structural control and health monitoring*, Vol-14, pp. 497-521.

Yang Jann N., Wu Shinya and Zhou Li (2008), "Experimental Study of an Adaptive Extended Kalman Filter for structural damage identification", *Journal of Infrastructure systems, ASCE*, Vol-14, pp. 42-51.

Yang Jann N., Zhou Li and Mu Tengfei (2014), "Experimental Study of an Adaptive Sequential Nonlinear LSE with Unknown Inputs for Structural Damage Tracking", *Shock and Vibration*, *Hindawi Publishing Corporation,* Vol. 2014, Article ID 294163. *http://dx.doi.org/10.1155/2014/294163.*

Yin Qiang, Zhou Li and Wang Xinming (2010), "Parameter identification of hysteretic model of rubber-bearing based on sequential nonlinear least-square estimation", *Earthquake Engineering and Engineering Vibration*, Vol. 9, pp. 375-383.

Zhang Yigong and Lin Jeen-Shang (1994), "Nonlinear Structural identification using Extended Kalman Filter", *Computers and Structures*, Vol-52, No.4, pp. 757-764.

Zhang H., Ma F., Bockstedte A., Paevere P. and Foliente G.C. (2003), "On Parameter analysis of the differential model of hysteresis", *IUTAM Symposium on Nonlinear Stochastic Dynamics*, pp.257-268.

Zongbo Xie and Jiuchao Feng (2012), "Real-time nonlinear structural system identification via iterated unscented Kalman filter", *Mechanical Systems and Signal Processing*, Vol. 28, pp. 309–322.

List of Publications

(A) Journals:

1. Paul Prodip Kumar, Dutta Anjan and Deb S.K., "Comparison of Performance of EKF, Two-Stage EKF and UKF algorithms for identification of state and parameters of U-FREI", *Structural Control and Health Monitoring*. (Communicated)
2. Paul Prodip Kumar, Deb S.K and Dutta Anjan, "Performance Comparison of EKF, Two-Stage EKF and UKF for identification of state and structural stiffness of base-isolated buildings with missing sensors at different floor levels", (Under preparation)
3. Paul Prodip Kumar, Dutta Anjan and Deb S.K., "Performance Comparison of EKF, Two-Stage EKF and UKF for identification of state and structural stiffness of fixed-base buildings with missing sensors at different floor levels", (Under preparation)

(B) Conferences:

1. Paul Prodip Kumar, Dutta Anjan and Deb S.K., "System Identification and Damage Detection of R.C. Structure", COMPDYN 2015, 5th ECCOMAS Thematic Conference on Computational Methods in Structural Dynamics and Earthquake Engineering, Crete Island, Greece, 25–27 May 2015.

APPENDIX-I

Evaluation of Percentage Error Index (PEI)

The weights associated with each of the parameters are calculated as per the procedure described in section 6.4.2. The implication of this weight on the PEI is demonstrated by an illustrative example shown below. With the help of PEI, the performance of each algorithm can be assessed in terms of its effectiveness in estimation of parameters of model representing FREI.

Illustrative Example for calculation of PEI

Base value of the FREI model parameters are given in Table 6.4. The identified value of the parameters obtained from UKF algorithm under Koyna earthquake is furnished in Table 6.15. The percentage error in identification of parameters with respect to the base values of parameters of FREI are furnished in Table A1. Using these values, the weights of the parameters are evaluated as shown below.

Calculation of weight (w) for parameter B

Identified value = 72.89, base value = 73

% error = (73-72.89) *100/73= -0.156 %

Substituting x= -0.156/100= -0.001506 in Eq.(6.16) and using the coefficients of polynomial from Table 6.10 and Table 6.11, the weight corresponding to parameter B is obtained as 0.003. Similarly, weights of other parameters are calculated and are furnished in Table A1.

The weighted error for parameter B= -0.001506*0.003=4.64E-06. The sum total of the weighted error represents the PEI. PEI=0 corresponds to no error in estimation and the identification is perfect. Increasing value of PEI indicates more error in identified parameter. Thus, for any particular problem, the PEI value for any algorithm which comes out to be least will indicate to be most effective in terms of its performance for parameter estimation.

Table A1: Calculated values for illustrative example-1

Parameters	Base Value	Identified value	% error with respect to base value	Calculated weight (w)	Weighted error (absolute value)
Column No.	C1	C2	C3	C4	C5
			(C2-C1)*100/C1		ABS(C3/100)*C4
B	73	72.89	-0.151	0.003	4.64E-06
β	95	92.69	-2.432	0.032	7.85E-04
γ	16	11.03	-31.063	0.070	2.19E-02
a_1	59	56.6	-4.068	0.126	5.14E-03
a_2	-555	-497.51	-10.359	0.066	6.87E-03
a_3	25	22	-12.000	0.001	1.31E-04
				Total weighted error or PEI=	0.035

The values of PEI obtained using other algorithms and under different earthquake excitations are furnished in Table 6.17.